MOLECULAR INTERACTIONS BETWEEN CROPS AND PHYTOPATHOGENS, VOLUME I: WHEAT AND MAIZE

EDITED BY: Xiaodong Wang, Xiaojie Wang, Lisong Ma, Jin-Ying Gou, Meixiang Zhang, Guotian Li, Jianhui Wu and Xiao-Ren Chen

PUBLISHED IN: Frontiers in Plant Science

frontiers Research Topics

frontiers

ISSN 1664-8714
ISBN 978-2-88976-888-2
DOI 10.3389/978-2-88976-888-2

About Frontiers

Frontiers is more than just an open-access publisher of scholarly articles: it is a pioneering approach to the world of academia, radically improving the way scholarly research is managed. The grand vision of Frontiers is a world where all people have an equal opportunity to seek, share and generate knowledge. Frontiers provides immediate and permanent online open access to all its publications, but this alone is not enough to realize our grand goals.

Frontiers Journal Series

The Frontiers Journal Series is a multi-tier and interdisciplinary set of open-access, online journals, promising a paradigm shift from the current review, selection and dissemination processes in academic publishing. All Frontiers journals are driven by researchers for researchers; therefore, they constitute a service to the scholarly community. At the same time, the Frontiers Journal Series operates on a revolutionary invention, the tiered publishing system, initially addressing specific communities of scholars, and gradually climbing up to broader public understanding, thus serving the interests of the lay society, too.

Dedication to Quality

Each Frontiers article is a landmark of the highest quality, thanks to genuinely collaborative interactions between authors and review editors, who include some of the world's best academicians. Research must be certified by peers before entering a stream of knowledge that may eventually reach the public - and shape society; therefore, Frontiers only applies the most rigorous and unbiased reviews.
Frontiers revolutionizes research publishing by freely delivering the most outstanding research, evaluated with no bias from both the academic and social point of view. By applying the most advanced information technologies, Frontiers is catapulting scholarly publishing into a new generation.

What are Frontiers Research Topics?

Frontiers Research Topics are very popular trademarks of the Frontiers Journals Series: they are collections of at least ten articles, all centered on a particular subject. With their unique mix of varied contributions from Original Research to Review Articles, Frontiers Research Topics unify the most influential researchers, the latest key findings and historical advances in a hot research area! Find out more on how to host your own Frontiers Research Topic or contribute to one as an author by contacting the Frontiers Editorial Office: frontiersin.org/about/contact

MOLECULAR INTERACTIONS BETWEEN CROPS AND PHYTOPATHOGENS, VOLUME I: WHEAT AND MAIZE

Topic Editors:
Xiaodong Wang, Agricultural University of Hebei, China
Xiaojie Wang, Northwest A&F University, China
Lisong Ma, Hebei Agricultural University, China
Jin-Ying Gou, Fudan University, China
Meixiang Zhang, Nanjing Agricultural University, China
Guotian Li, Huazhong Agricultural University, China
Jianhui Wu, Northwest A&F University, China
Xiao-Ren Chen, Yangzhou University, China

Citation: Wang, X., Wang, X., Ma, L., Gou, J.-Y., Zhang, M., Li, G., Wu, J., Chen, X.-R., eds. (2022). Molecular Interactions Between Crops and Phytopathogens, Volume I: Wheat and Maize. Lausanne: Frontiers Media SA. doi: 10.3389/978-2-88976-888-2

Table of Contents

04 ***Editorial: Molecular interactions between crops and phytopathogens, Volume I: Wheat and maize***
Xiaodong Wang, Xiaojie Wang, Xiao-Ren Chen, Jianhui Wu, Jin-Ying Gou, Meixiang Zhang, Guotian Li and Lisong Ma

07 ***Multi-Omics Analyses Reveal the Regulatory Network and the Function of ZmUGTs in Maize Defense Response***
Chunxia Ge, Yi-Ge Wang, Shouping Lu, Xiang Yu Zhao, Bing-Kai Hou, Peter J. Balint-Kurti and Guan-Feng Wang

24 ***Functional Verification of Two Genes Related to Stripe Rust Resistance in the Wheat*-Leymus mollis *Introgression Line M8664-3***
Pengfei Jin, Kaixiang Chao, Juan Li, Zihao Wang, Peng Cheng, Qiang Li and Baotong Wang

38 ***Corrigendum: Functional Verification of Two Genes Related to Stripe Rust Resistance in the Wheat*-Leymus mollis *Introgression Line M8664-3***
Pengfei Jin, Kaixiang Chao, Juan Li, Zihao Wang, Peng Cheng, Qiang Li and Baotong Wang

40 **Trichoderma longibrachiatum *(TG1) Enhances Wheat Seedlings Tolerance to Salt Stress and Resistance to* Fusarium pseudograminearum**
Solomon Boamah, Shuwu Zhang, Bingliang Xu, Tong Li and Alejandro Calderón-Urrea

57 ***Wheat Apoplast-Localized Lipid Transfer Protein* TaLTP3 *Enhances Defense Responses Against* Puccinia triticina**
Jiaojie Zhao, Weishuai Bi, Shuqing Zhao, Jun Su, Mengyu Li, Lisong Ma, Xiumei Yu and Xiaodong Wang

70 ***TaMYB29: A Novel R2R3-MYB Transcription Factor Involved in Wheat Defense Against Stripe Rust***
Xiaoxu Zhu, Xiang Li, Qi He, Dongxiao Guo, Caiqi Liu, Junying Cao, Zhongyi Wu, Zhensheng Kang and Xiaojing Wang

86 ***Silencing of a Wheat Ortholog of Glucan Synthase-Like Gene Reduced Resistance to* Blumeria graminis f. *sp.* tritici**
Peng Cheng, Zihao Wang, Yanyan Ren, Pengfei Jin, Kangjie Ma, Qiang Li and Baotong Wang

96 ***An Aminobutyric Acid Transaminase in* Zea mays *Interacts With* Rhizoctonia solani *Cellulase to Participate in Disease Resistance***
Xiuna Guo, Jinyin Chen, Mengyi Gao and Duochuan Li

109 ***Multi-Omics Analysis Reveals a Regulatory Network of ZmCCT During Maize Resistance to Gibberella Stalk Rot at the Early Stage***
Bozeng Tang, Zhaoheng Zhang, Xinyu Zhao, Yang Xu, Li Wang, Xiao-Lin Chen and Weixiang Wang

128 ***The Black Necrotic Lesion Enhanced* Fusarium graminearum *Resistance in Wheat***
Lanfei Zhao, Peisen Su, Bingqian Hou, Hongyan Wu, Yanhui Fan, Wen Li, Jinxiao Zhao, Wenyang Ge, Shoushen Xu, Shiwen Wu, Xin Ma, Anfei Li, Guihua Bai, Hongwei Wang and Lingrang Kong

frontiers | Frontiers in Plant Science

TYPE Editorial
PUBLISHED 27 July 2022
DOI 10.3389/fpls.2022.979855

OPEN ACCESS

EDITED BY
Youssef Rouphael,
University of Naples Federico II, Italy

REVIEWED BY
Pasquale Tripodi,
Council for Agricultural and Economics Research (CREA), Italy

*CORRESPONDENCE
Xiaodong Wang
zhbwxd@hebau.edu.cn
Xiaojie Wang
wangxiaojie@nwsuaf.edu.cn
Xiao-Ren Chen
xrchen@yzu.edu.cn
Jianhui Wu
wujh@nwafu.edu.cn
Jin-Ying Gou
jygou@fudan.edu.cn
Meixiang Zhang
meixiangzhang@snnu.edu.cn
Guotian Li
li4@mail.hzau.edu.cn
Lisong Ma
lisong.ma@anu.edu.au

SPECIALTY SECTION
This article was submitted to Crop and Product Physiology, a section of the journal Frontiers in Plant Science

RECEIVED 28 June 2022
ACCEPTED 11 July 2022
PUBLISHED 27 July 2022

CITATION
Wang X, Wang X, Chen X-R, Wu J, Gou J-Y, Zhang M, Li G and Ma L (2022) Editorial: Molecular interactions between crops and phytopathogens, Volume I: Wheat and maize. *Front. Plant Sci.* 13:979855. doi: 10.3389/fpls.2022.979855

Editorial: Molecular interactions between crops and phytopathogens, Volume I: Wheat and maize

Xiaodong Wang[1]*, Xiaojie Wang[2]*, Xiao-Ren Chen[3]*, Jianhui Wu[4]*, Jin-Ying Gou[5]*, Meixiang Zhang[6]*, Guotian Li[7]* and Lisong Ma[1,8]*

[1]State Key Laboratory of North China Crop Improvement and Regulation, College of Plant Protection, Hebei Agricultural University, Baoding, China, [2]State Key Laboratory of Crop Stress Biology for Arid Areas, College of Plant Protection, Northwest Agriculture and Forestry University, Xianyang, China, [3]College of Horticulture and Plant Protection, Yangzhou University, Yangzhou, China, [4]College of Agronomy, Northwest Agriculture and Forestry University, Xianyang, China, [5]State Key Laboratory of Genetic Engineering, MOE Key Laboratory for Biodiversity Science and Ecological Engineering, MOE Engineering Research Center of Gene Technology, School of Life Sciences, Institute of Plant Biology, Fudan University, Shanghai, China, [6]National Engineering Laboratory for Endangered Medicinal Resource Development in Northwest China, Key Laboratory of Medicinal Resources and Natural Pharmaceutical Chemistry of Ministry of Education, College of Life Sciences, Shaanxi Normal University, Xi'an, China, [7]State Key Laboratory of Agricultural Microbiology and Provincial Key Laboratory of Plant Pathology of Hubei Province, College of Plant Science and Technology, Huazhong Agricultural University, Wuhan, China, [8]College of Horticulture, Hebei Agricultural University, Baoding, China

KEYWORDS

wheat, maize, fungal pathogen, multiple omics, hypersensitive response

Editorial on the Research Topic
Molecular Interactions between Crops and Phytopathogens, Volume I: Wheat and Maize

Crop disease poses a significant threat to global food security as the world population continues to expand dramatically. Crops have evolved sophisticated strategies to ward off various invading phytopathogens. Accordingly, phytopathogens have evolved intricate virulent mechanisms to facilitate their infection processes. Steady progress has been achieved in understanding plant resistance to phytopathogens in the last two decades. An emerging field of studying the molecular basis of crop-pathogen interactions is gaining more attention.

Wheat and maize are the main food crops cultivated worldwide. The dominant wheat-maize rotation in many areas has remarkably impacted the cultivation environments of these two crops. In addition to traditional fungal diseases such as wheat rust, powdery mildew, and *Fusarium* head blight, soil-borne diseases, including *Fusarium* crown rot, *Gibberella* stalk rot, and sheath blight, have emerged as new threats to the global productions of wheat and maize.

This Research Topic aims to explore the application of multiple omics in understanding the molecular interactions between wheat/maize and phytopathogens; identification of novel genes or genetic loci of wheat/maize conferring resistance to phytopathogens; functional characterization of defense-related genes in wheat/maize; and discovery of pathogenicity-related factors in phytopathogens. In total, it collects nine intriguing articles from international experts in the field and covers a broad range of subjects, which allows us to divide these articles into the following two themes:

Plant basal and induced resistance

The plant cell wall serves as the first barrier against the invasion of phytopathogens. Glucan is involved in the formation of callose, which prevents the initial infection of pathogens at the cell wall. Cheng et al. characterized a wheat glucan synthase-like gene *TaGSL22* during plant resistance to powdery mildew pathogen (*Blumeria graminis* f. sp. *tritici*, *Bgt*). An avirulent *Bgt* pathotype significantly upregulated the expression level of *TaGSL22*. Knocking down of *TaGSL22* by virus-induced gene silencing (VIGS) reduced callose deposition, which resulted in enhanced wheat susceptibility to *Bgt*.

Necrotrophic phytopathogens destroy basal host defense with various cell wall-degrading enzymes (CWDEs) to facilitate their infections. In contrast, host plants evolve corresponding mechanisms to counteract the activities of CWDEs. Guo et al. identified a maize gamma-aminobutyric acid transaminase (GABA-T) that directly interacted with a cellulase from corn sheath blight pathogen (*Rhizoctonia solani*). Furthermore, they demonstrated that the identified maize *GABA-T* gene and its rice homolog (*OsGABA-T*) were sufficient to suppress the cellulase-induced necrosis, while CRISPR/Cas9-mediated *OsGABA-T* knockout rice plants displayed enhanced susceptibility to *R. solani*.

As key downstream of plant defense response, various pathogenesis-related (PR) proteins function in the apoplastic space during the onset of plant-pathogen interaction. Zhao J. et al. revealed that a wheat lipid transfer protein TaLTP3, also known as a homolog of PR14, was positively correlated with plant resistance to leaf rust. Overexpression of the *TaLTP3* gene in the transgenic wheat lines resulted in enhanced rust resistance and higher expression of *TaPR1a* in response to the infection of the model bacterial pathogen *Pseudomonas syringae* pv. *tomato* DC3000. Further investigation indicated that TaLTP3 directly interacted with TaPR1a in the apoplastic space to co-regulate the plant defense response.

Key regulators and components in early responses of plant resistance to phytopathogens may have great potential in interpreting the mechanism of plant defense responses. Using multiple omics techniques, Tang et al. profiled the regulatory network of a maize *Gibberella* stalk rot (GSR)-resistant gene *ZmCCT* at the early infection stage. The *ZmCCT*-mediated maize resistance to *Gibberella* stalk rot caused by *Fusarium graminearum* were associated with activations of pattern-triggered immunity (PTI), phytohormone pathways of salicylic acid (SA) and auxin, and accumulations of phenylalanine metabolites.

Systemic acquired resistance (SAR) was another critical add-on for plant defense response beyond the hypersensitive response (HR). The action of some biocontrol agents was intensively associated with SAR. Boamah et al. reported that a biocontrol fungus *Trichoderma longibrachiatum* (TG1) with positive effects on wheat tolerance to salt stress and resistance to *Fusarium* crown rot caused by *F. pseudograminearum*. Moreover, expression levels of *PR* genes were significantly increased in response to TG1.

Hypersensitive response

Activation of plant major resistance (*R*) genes in response to biotrophic phytopathogens often leads to hypersensitive responses (HR) at the infection site following the gene-for-gene theory. Many *R* genes derived from crop wild relatives are widely used in breeding practice. Jin et al. identified a stripe rust resistance gene *YrM8664-3* in a wheat-*Leymus mollis* introgression line. *YrM8664-3*, located on wheat chromosome 4AL, encoded a protein with plastid lipid-associated proteins (PAP)_fibrillin domain (TaFBN). *TaFBN* conferred high resistance to stripe rust in transgenic wheat lines.

Myeloblastosis (MYB) transcription factors are vital components in plant development and resistance to various stresses. Zhu et al. cloned a member of the R2R3-MYB superfamily in wheat and designated it as *TaMYB29*. Transient expression of *TaMYB29* in tobacco leaves triggered pathogen-independent cell death associated with increased accumulation of reactive oxygen species (ROS). Conversely, silencing of *TaMYB29* by VIGS significantly reduced the wheat resistance to stripe rust with reduced ROS accumulation.

Specific mutations on plant *R* genes that exhibited autoactivated HR are considered as valuable genetic resources to explore the mechanism of cell death in the plant. Ge et al. revealed the transcriptomic and metabolomic profiles of a maize auto-active HR mutant *Rp1-D21*. Further investigation indicated that two maize UDP-dependent glycosyltransferase (*ZmUGTs*) genes partially suppressed the HR triggered by Rp1-D21 in a protein interaction-independent manner.

Interestingly, HR-like black necrotic lesions (HR-BNL) often occur around the leaf infection sites of *Fusarium* head blight (FHB) in resistant wheat cultivars. Zhao L. et al. investigated the HR-BNL response in the leaf samples of a resistant wheat cultivar Sumai 3 inoculated with four disinct *F. graminearum* isolates. Flavonoid metabolites were identified and proved to be

involved in the formation of HR-BNL. SA signaling pathway associated with ROS burst positively regulated FHB resistance in wheat with HR-BNL.

Overall, this Research Topic presents a broad range of articles that describe the application of multi-omics approaches in different wheat/maize-fungus pathosystems and expand our knowledge toward understanding the molecular interactions between wheat/maize and phytopathogens. Notably, several collected articles focusing on the role of HR in crop resistance have provided new insights into the molecular mechanism of crop major resistance genes.

Author contributions

All authors listed have made a substantial, direct, and intellectual contribution to the work and approved it for publication.

Funding

XiaodW was supported by the Provincial Natural Science Foundation of Hebei (C2022204010 and C2021204008) and State Key Laboratory of North China Crop Improvement and Regulation (NCCIR2021ZZ-4). XiaojW was supported by the Shaanxi Innovation Team Project (2018TD-004). X-RC was supported by the National Natural Science Foundation of China (31871907 and 31671971) and Jiangsu Agriculture Science and Technology Innovation Fund (JASTIF) [CX(20)3125]. JW was supported by the Key R&D Program of Shaanxi Province in China (2021ZDLNY0-01). J-YG was supported by the National Natural Science Foundation of China (31972350). MZ was supported by the National Natural Science Foundation of China (32072399 and 31672008) and the Fundamental Research Funds for the Central Universities (GK202201017). GL was supported by the National Natural Science Foundation of China (32172373). LM was supported by the Hundred Talents Program for the introduction of high-level overseas talents in Hebei Province (E2020100004).

Acknowledgments

We thank the Frontiers Editorial Office and reviewers for their assistance in completing this Research Topic.

Conflict of interest

The authors declare that the research was conducted in the absence of any commercial or financial relationships that could be construed as a potential conflict of interest.

Publisher's note

frontiers in Plant Science

ORIGINAL RESEARCH
published: 24 September 2021
doi: 10.3389/fpls.2021.738261

Multi-Omics Analyses Reveal the Regulatory Network and the Function of ZmUGTs in Maize Defense Response

Chunxia Ge[1,2†], Yi-Ge Wang[1†], Shouping Lu[3], Xiang Yu Zhao[4], Bing-Kai Hou[1], Peter J. Balint-Kurti[5,6] and Guan-Feng Wang[1]*

[1] The Key Laboratory of Plant Development and Environmental Adaptation Biology, Ministry of Education, School of Life Sciences, Shandong University, Qingdao, China, [2] School of Public Health and Management, Binzhou Medical University, Yantai, China, [3] Maize Research Institute, Shandong Academy of Agricultural Sciences, Jinan, China, [4] State Key Laboratory of Crop Biology, Shandong Agricultural University, Tai'an, China, [5] Department of Entomology and Plant Pathology, North Carolina State University, Raleigh, NC, United States, [6] US Department of Agriculture-Agricultural Research Service, Plant Science Research Unit, Raleigh, NC, United States

OPEN ACCESS

Edited by:
Meixiang Zhang,
Nanjing Agricultural University, China

Reviewed by:
Qinhu Wang,
Northwest A and F University, China
Li-Hung Chen,
National Chung Hsing University, Taiwan

***Correspondence:**
Guan-Feng Wang
gfwang@sdu.edu.cn

[†] These authors have contributed equally to this work and share first authorship

Specialty section:
This article was submitted to Crop and Product Physiology, a section of the journal Frontiers in Plant Science

Received: 08 July 2021
Accepted: 26 August 2021
Published: 24 September 2021

Citation:
Ge C, Wang Y-G, Lu S, Zhao XY, Hou B-K, Balint-Kurti PJ and Wang G-F (2021) Multi-Omics Analyses Reveal the Regulatory Network and the Function of ZmUGTs in Maize Defense Response. Front. Plant Sci. 12:738261. doi: 10.3389/fpls.2021.738261

Maize is one of the major crops in the world; however, diseases caused by various pathogens seriously affect its yield and quality. The maize *Rp1-D21* mutant (mt) caused by the intragenic recombination between two nucleotide-binding, leucine-rich repeat (NLR) proteins, exhibits autoactive hypersensitive response (HR). In this study, we integrated transcriptomic and metabolomic analyses to identify differentially expressed genes (DEGs) and differentially accumulated metabolites (DAMs) in *Rp1-D21* mt compared to the wild type (WT). Genes involved in pathogen-associated molecular pattern (PAMP)-triggered immunity (PTI) and effector-triggered immunity (ETI) were enriched among the DEGs. The salicylic acid (SA) pathway and the phenylpropanoid biosynthesis pathway were induced at both the transcriptional and metabolic levels. The DAMs identified included lipids, flavones, and phenolic acids, including 2,5-DHBA *O*-hexoside, the production of which is catalyzed by uridinediphosphate (UDP)-dependent glycosyltransferase (UGT). Four maize *UGTs* (*ZmUGTs)* homologous genes were among the DEGs. Functional analysis by transient co-expression in *Nicotiana benthamiana* showed that ZmUGT9250 and ZmUGT5174, but not ZmUGT9256 and ZmUGT8707, partially suppressed the HR triggered by Rp1-D21 or its N-terminal coiled-coil signaling domain (CC_{D21}). None of the four ZmUGTs interacted physically with CC_{D21} in yeast two-hybrid or co-immunoprecipitation assays. We discuss the possibility that ZmUGTs might be involved in defense response by regulating SA homeostasis.

Keywords: disease resistance, ETI, hypersensitive response, maize, NLR, salicylic acid, UGT

INTRODUCTION

To defend against pathogenic microorganisms, plants have evolved a multilayered and sophisticated immune system including pathogen-associated molecular pattern (PAMP)-triggered immunity (PTI) and effector-triggered immunity (ETI; McHale et al., 2006; Cui et al., 2015). The PTI is activated by the recognition of PAMPs *via* the pattern recognition receptors (PRRs)

localized at the surface of plant cells, while ETI is triggered when the intracellular receptors termed nucleotide-binding leucine-rich-repeat (NLR) proteins recognize the specific effector proteins secreted from pathogens. Two recent studies (Ngou et al., 2021; Yuan et al., 2021) suggest that PTI and ETI responses are closely connected with ETI potentiating the PTI response. PRR- and NLR-mediated downstream signaling pathways result in some similar immune outputs, such as increased expression of pathogenesis-related (*PR*) genes and the burst of reactive oxygen species (ROS). A nicotinamide adenine dinucleotide phosphate (NADPH) oxidase called respiratory burst oxidase homolog D (RBOHD) is an indispensable immune component connecting PRR and NLR immune receptors, and the phosphorylation of RBOHD mediates ROS generation and activates disease resistance (Ngou et al., 2021). A distinct feature of NLR-triggered immunity is often accompanied by the hypersensitive response (HR), a form of localized programmed cell death at the pathogen infection sites (Bent and Mackey, 2007; Kourelis and van der Hoorn, 2018; Balint-Kurti, 2019).

Salicylic acid (SA) is a pivotal phytohormone mediating both local and systemic defense responses against biotrophic and semi-biotrophic pathogens (Vlot et al., 2009; Dempsey et al., 2011). The activation of SA biosynthesis, metabolism, and signaling pathways play critical roles for both PTI- and ETI-mediated defense responses (Vlot et al., 2009; Ding et al., 2018). The SA is synthesized by the isochorismate synthase (ICS) and the Phe ammonia-lyase (PAL) pathways which play the major and minor roles in SA biosynthesis, respectively (Dempsey et al., 2011). In Arabidopsis, when the gene *EDS16* in the ICS pathway was mutated, the total SA level was reduced to <10% of the wild-type level after *Erysiphe orontii* infection (Dewdney et al., 2000). Once synthesized, the SA is subject to a number of modifications including glycosylation, hydroxylation, and methylation. Hydroxylated products of SA, including 2,3-dihydroxybenzoic acid (2,3-DHBA) and 2,5-dihydroxybenzoic acid (2,5-DHBA), are the major metabolic forms of SA. The DHBA is cytotoxic and it is generally found in its less toxic glycosylated form in plants (Bartsch et al., 2010). Glycosylation products of DHBA may activate plant defense. DHBA glycoside compounds are increased in Arabidopsis after infection by *Pseudomonas syringae* pv. *tomato* (*Pst*) strain DC3000 or *Hyaloperonospora arabidopsidis* (Bartsch et al., 2010). When overexpressed, the Arabidopsis uridine diphosphate (UDP)-dependent glycosyltransferase UGT76D1, which catalyzes the formation of DHBA glycosides, leads to the induction of HR, a burst of ROS, the increased expression of *PR* genes and enhanced resistance to *Pst* DC3000 (Huang et al., 2018). The UGT76D1 plays important roles in plant immunity by modulating SA homeostasis by glycosylations of DHBA (Huang et al., 2018).

Nucleotide-binding leucine-rich-repeat disease resistance proteins can be divided into two major types depending on their N-terminal domains; the coiled-coil type (CNL) and the Toll/interleukin-1 receptor type (TNL; Monteiro and Nishimura, 2018; Sun et al., 2020). The maize *Rp1* locus on the short arm of chromosome 10 carries multiple tandemly repeated CNL genes (Hulbert, 1997). One of these genes, *Rp1-D*, confers resistance to maize common rust caused by the fungus, *Puccini sorghi* (Hulbert, 1997). The chimeric gene *Rp1-D21* was derived from intragenic recombination between two paralogs, *Rp1-D* and *Rp1-dp2* (Sudupak et al., 1993; Sun et al., 2001; Smith et al., 2010). The *Rp1-D21* confers a spontaneous HR phenotype in the absence of pathogen infection (Sun et al., 2001; Smith et al., 2010; Wang et al., 2015a). The severity of this HR is affected by light, temperature, developmental stage, and genetic background (Chintamanani et al., 2010; Negeri et al., 2013). The *Rp1-D21*-induced HR is entirely suppressed at 30°C and can be activated by reducing the temperature to 22°C (Negeri et al., 2013). The *Rp1-D21* had been used as a tool to identify quantitative trait loci (QTL), genes, and pathways associated with modulation of the severity of HR in maize (Chintamanani et al., 2010; Olukolu et al., 2014). Two key enzymes in lignin biosynthesis pathway, caffeoyl-CoA O-methyltransferase (CCoAOMT) and hydroxycinnamoyl transferase (HCT), have been shown to suppress Rp1-D21-induced HR through physical interaction (Wang et al., 2015b; Wang and Balint-Kurti, 2016). The gene encoding CCoAOMT has also been shown to increase resistance to both southern leaf blight and gray leaf spot in maize (Yang et al., 2017).

In recent years, transcriptome and metabolome analyses have provided a powerful comprehensive approach to assess the relationship of genotype, phenotype, and metabolite changes in plants challenged by abiotic and biotic stresses (Etalo et al., 2013; Mo et al., 2019; Ye et al., 2019; Hong et al., 2020). For example, transcriptional profiling combined with targeted metabolite quantification found that the levels of many genes and several metabolites in phenylpropanoid and shikimate pathways are significantly changed by the expression of WtsE, an effector secreted from *Pantoea stewartii* ssp. *Stewartii* (*Pnss*), which can cause Stewart's wilt and leaf blight in maize (Asselin et al., 2015).

Here, using a similar multi-omics approach, we investigated the gene regulatory network modulating Rp1-D21-mediated HR. We identified a number of different pathways associated with resistance response mediated by *Rp1-D21*, in particular, the SA biosynthesis and metabolism pathway. Four DHBA glucosyltransferase homologs of *ZmUGTs*, were highly induced, two of which we show may have important roles in modulating Rp1-D21-mediated HR.

RESULTS

Transcriptome Sequencing and Quality Assessment

Transcriptional analysis of *Rp1-D21*-induced hypersensitive response (HR) was undertaken in two different temperature regimes (**Supplementary Figure 1**). In the first treatment, here called the temperature shift treatment, plants were grown at 30°C, and then were transferred immediately to 22°C to induce a synchronous systematic HR. For the second temperature regime, the constant temperature treatment, the plants were grown at a constant 22°C. Comparisons of two different pairs of near isogenic F1 hybrids were used for these experiments: B73 × H95-*Rp1-D21* with B73 ×H 95 and Mo17 × H95-*Rp1-D21* with Mo17 × H95.

The *Rp1-D21* HR phenotype in Mo17 × H95-*Rp1-D21* is more severe than in B73 × H95-*Rp1-D21* (Chintamanani et al., 2010). In the temperature shift experiment, *Rp1-D21*-carrying plants displayed HR at 3 days after temperature shift in the Mo17 × H95-*Rp1-D21*, and at 5 days in the B73 × H95-*Rp1-D21* background. For this experiment, samples from near-isogenic wild type (WT) and *Rp1-D21* mutant (mt) plants in each genetic background were collected at 3, 6, 24, and 48 h post the temperature shift (hpts). The HR was not observed in either background at these time points. Therefore, in order to confirm that the defense response had indeed been activated by the temperature shift, we used semi-quantitative reverse transcription polymerase chain reaction (RT-PCR) to monitor the transcript levels of *PR1* and *PR5*, the two plant defense response marker genes. The *PR1* levels were noticeably induced in mutant plants at 6 hpts in Mo17 × H95 background and at 24 hpts in the B73× H95 background, while the *PR5* levels increased in mutant plants at 24 hpts and 48 hpts in B73 × H95 and Mo17 × H95, respectively (**Supplementary Figure 2**). Thus, we chose samples collected at 6 and 48 hpts for RNA sequencing (RNA-seq) experiments to investigate the early response genes involved in *Rp1-D21*-induced HR. These samples are referred to below as B73 × H95-WT-6 hpts, B73 × H95-mt-6 hpts, B73 × H95-WT-48 hpts, B73 × H95-mt-48 hpts, Mo17 × H95-WT-6 hpts, Mo17 × H95-mt-6 hpts, Mo17 × H95-WT-48 hpts, and Mo17 × H95-mt-48 hpts. To investigate whether the expression of *Rp1-D21* was induced after temperature shift which induced HR, we performed semi-quantitative RT-PCR analysis and found that the transcript levels of *Rp1-D21* were increasingly induced from 3 to 48 hpts in both genetic backgrounds (**Supplementary Figure 2**).

We used the constant temperature experiment to explore the late response genes involved in *Rp1-D21*-induced HR. In this case, we sampled plants from near isogenic pairs of each genetic background and the sample names were B73 × H95-WT-22°C, B73 × H95-mt-22°C, Mo17 × H95-WT-22°C, and Mo17 × H95-mt-22°C.

Read numbers for each sample ranged from 21.48 to 44.06 million with an average of 32.36 million. In each case, the read number of WT and mt from the same background at the same time point were quite similar (**Supplementary Table 1**). Hierarchical indexing for spliced alignment of transcripts 2 (HISAT2) was used to map the reads against the B73 reference genome (B73_v4, maizegdb.org). Approximately 87.57–92.92% of the reads were mapped to the reference genome, of which 84.79% were uniquely mapped (**Supplementary Table 1**). Fragments per kilobase of exon per million mapped reads (FPKM) values were calculated to evaluate the gene expression levels and the reproducibility of biological replicates. Raw counts expression data showed an average Pearson's correlation coefficient of 0.87 ranging from 0.65 to 0.96, indicating high correlation between the two biological replicates in each case (**Supplementary Figure 3A**). A multidimensional scaling (MDS) plot was generated to assess the sequencing quality (**Supplementary Figure 3B**). The transcript levels of all the expressed genes were clearly divided into different groups at constant 22°C for WT and *Rp1-D21* mt from B73× H95 and Mo17 × H95 backgrounds, but it was difficult to distinguish for samples at 6 hpts, which might be due to the low number of differentially expressed genes (DEGs) detected at this timepoint.

Identification of DEGs Responsive to *Rp1-D21*-Induced Hypersensitive Response

To facilitate the global identification of genes triggered during *Rp1-D21*-mediated hypersensitive response (HR), uniquely mapped DEGs were identified by comparing the gene expression levels and the abundance of each transcript in *Rp1-D21* mt relative to the WT for each near-isogenic pair at each timepoint. The DEGs were identified with a false discovery rate (FDR) or adjusted *p*-values (padj) < 0.05 and a $|\log2$ (fold-change) $|>1$. Since we want to analyze the most robust DEGs, we detected DEGs using both edgeR and DEseq2 software, and only those DEGs identified by both the methods were used for further analysis. The number of DEGs detected by edgeR/DEseq2 methods at each timepoint/condition is shown in **Figure 1A** and **Supplementary Table 2**. In every case, the large majority of DEGs were identified by both the methods (**Figure 1B**). At 6 hpts, seven common DEGs were identified in B73 × H95 and Mo17 × H95 backgrounds using both the methods (**Figure 1B**). At 48 hpts, 263 and 141 common DEGs were identified in B73 × H95 and Mo17 × H95 backgrounds, respectively, and 116 genes were commonly identified in both the backgrounds (**Figures 1B,C**). In the constant temperature experiment, 4,463 (2,799 induced, 1,664 repressed) and 5,106 (3,156 induced, 1,950 repressed) DEGs were identified in B73 × H95 and Mo17 × H95 backgrounds, respectively (**Figure 1B**). Of these, 3,633 common DEGs were detected in both the backgrounds using two methods (**Figure 1C**).

Many more DEGs were identified in the constant temperature experiment (>5,000) than in the temperature shift experiment (149–316 at 48 hpts) in both the backgrounds. In every case, more DEGs were upregulated than downregulated by the presence or activation of Rp1-D21 (**Figure 1A**). There were some notable differences between the two genetic backgrounds. For example, at 48 hpts, the number of DEGs in the B73 × H95 background was almost twice that in the Mo17 × H95 background. On the other hand, substantially more DEGs, both up- and downregulated, were detected in the Mo17 × H95 background at constant 22°C.

Functional Enrichment for *Rp1-D21*-Mediated DEGs

The maize gene ontology (GO) database was used for the functional annotation of the DEGs identified by both edgeR and DEseq2 in B73 and Mo17 backgrounds. At 6 hpts, 6 out of 7 DEGs were predicted to be involved in adenosine diphosphate (ADP) binding (GO:0043531), and oxidation-reduction process (GO:0055114). At 48 hpts, the DEGs were mainly predicted to be involved in heme binding (GO:0020037), extracellular region (GO:0005576), transmembrane transport (GO:0055085), and defense response (GO:0006952), which included some genes in salicylic acid (SA) biosynthetic process (GO:0080142) (**Figure 2A**). At constant 22°C, the DEGs in the biological process category mainly included transmembrane transport,

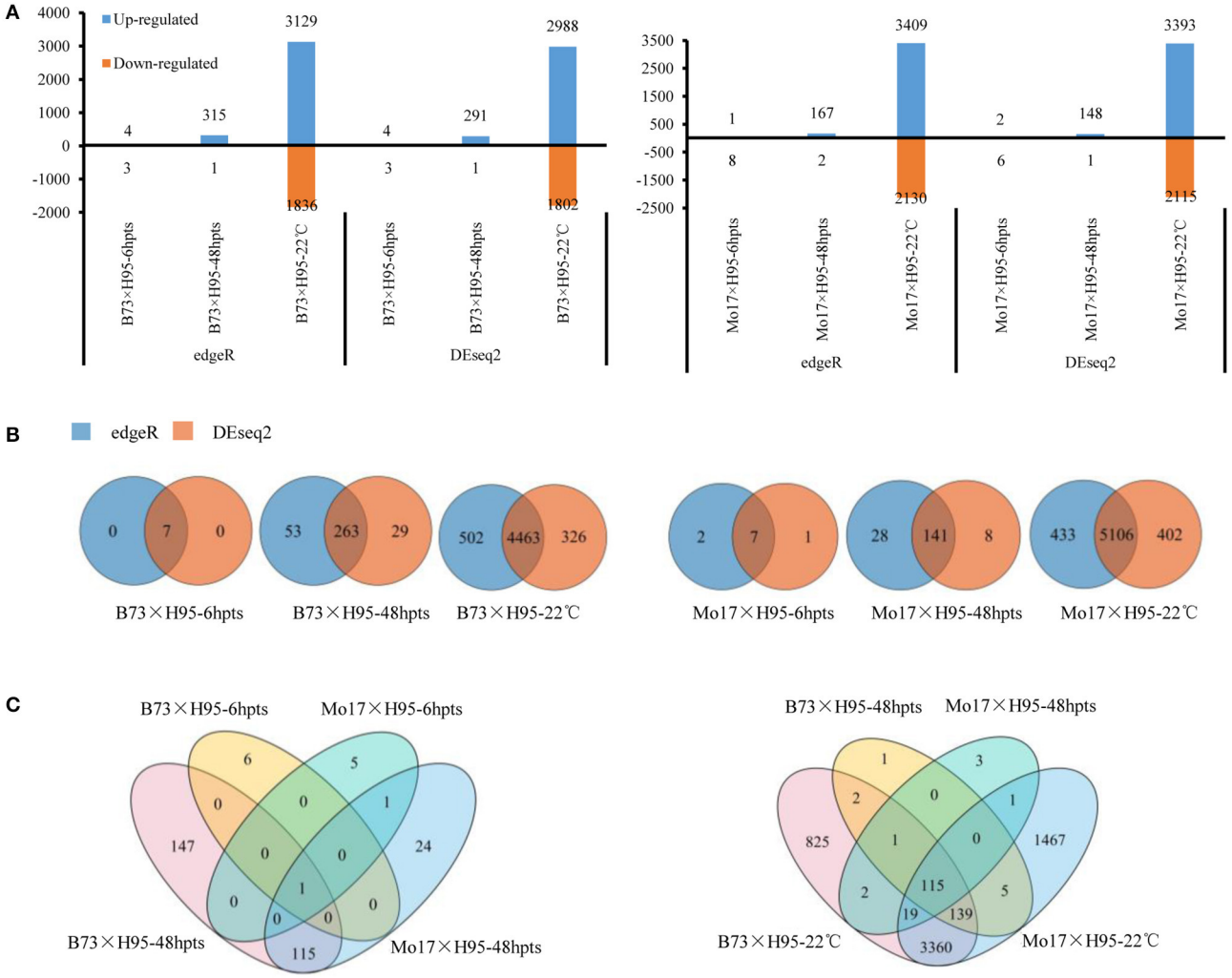

FIGURE 1 | Differentially expressed genes (DEGs) in *Rp1-D21* mutant (mt) compared to the wild type (WT) in B73 × H95 and Mo17 × H95 backgrounds. **(A)** The up and downregulated DEGs in B73 × H95 and Mo17 × H95 backgrounds as calculated by edgeR and DEseq2. **(B)** Numbers of DEGs from edgeR and DEseq2 methods at different treatments. Venn diagrams of DEGs among different time points and temperature treatments from both edgeR and DEseq2. **(C)** The common DEGs between both genotypes at 6 and 48 h post temperature shift (hpts) (left), and at constant 22°C (right), respectively.

protein autophosphorylation, and hormone signaling pathway (**Figure 2B**). For molecular function category, the enriched GO terms mainly contained genes involved in binding (e.g., cofactor and heme binding) and catalytic activity [e.g., uridine diphosphate (UDP)-glycosyltransferase activity] (**Figure 2B**). For cellular component (CC) category, the enriched GO terms included plasmodesma, chloroplast thylakoid membrane, and intracellular component of the plasma membrane (**Figure 2B**).

Upon the initiation of HR, transcriptional activation genes were mainly involved in genes encoding receptor kinases, transcription factors, calcium regulation, and protein degradation (**Supplementary Figure 4**) as analyzed by MapMan software (Usadel et al., 2009). At constant 22°C conditions, a large number of transcription factors (TFs) were differentially expressed in *Rp1-D21* mts from both B73 × H95 and Mo17 × H95 backgrounds, indicating that massive transcription reprogramming occurred at this condition. Most of these genes were related to the establishment of transcriptional reprogramming and the enhancement of immune response for *Rp1-D21*-mediated HR. Gene regulatory networks (GRNs) represent the maps of potential transcriptional regulation between TFs and their target genes. To investigate the GRNs of Rp1-D21-mediated HR, the GRNs of the 3,633 DEGs detected in both B73 and Mo17 backgrounds at constant 22°C were predicted for the regulatory interactions with their upstream TFs based on the existing TF binding motifs and the conservation of TF binding sites (TFBSs) (Zhou et al., 2020). In total, 73 putative TFs were predicted to bind DEGs at constant 22°C condition under cutoff p-value ≤ 0.05 (**Supplementary Table 3**). Of those 73 TFs, the majority are WRKY (16, 21.92%), bZIP (14, 19.18%), MYB (9, 12.33%), and NAC (9, 12.33%). Some TFs were predicted to target themselves (**Supplementary Table 3**). Most

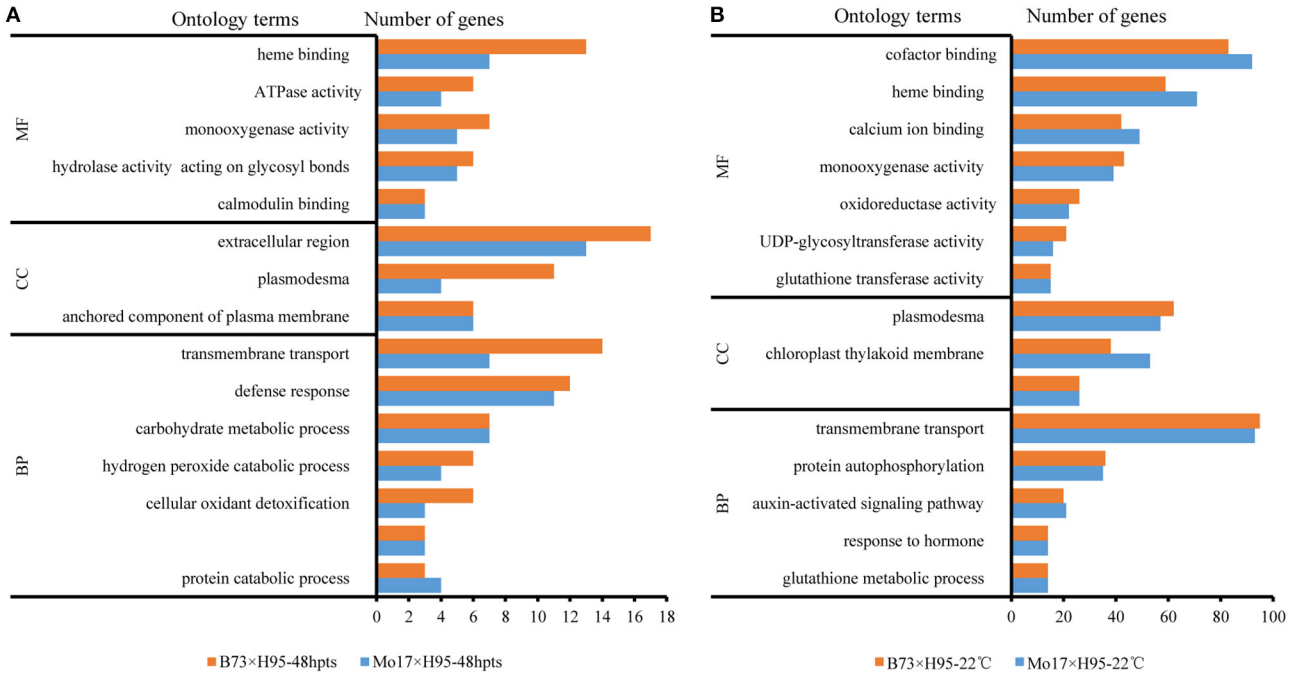

FIGURE 2 | The Gene ontology (GO) enrichment of differentially expressed genes (DEGs) in maize *Rp1-D21* mutant (mt) compared to the wild type (WT) for the indicated times. **(A)** Top 15 GO subcategories of DEGs from *Rp1-D21* mt in B73 × H95 and Mo17 × H95 backgrounds at 48 hours post temperature shift (hpts). **(B)** Top 15 GO subcategories of DEGs from *Rp1-D21* mt in B73× H95 and Mo17 × H95 backgrounds at constant 22°C. MF, molecular function; CC, cellular component; BP, biological process.

of other DEGs which were related to biotic stresses, included genes involved in protein modification, protein degradation, calcium regulation, and hormone biosynthesis. Interestingly, many DEGs encoded receptor kinases, G-proteins, and mitogen activated protein (MAP) kinases, which directly or indirectly regulate the signal perception and activation of immunity, such as SA defense-related pathway.

Many Genes Involved in PTI and SA Pathway Are Differentially Expressed in *Rp1-D21* Mutant

Pathogen-triggered immunity (PTI) and effector-triggered immunity (ETI) can function synergistically to protect plants against pathogens. Interestingly, we found that many genes predicted to be involved in maize PTI were differentially expressed in *Rp1-D21* mt, including the homologs of *BAK1*, *FLS2*, Ca^{2+}-ATPase genes (*CA*s), and *RBOH*s (**Supplementary Figure 5**, **Supplementary Table 4**). Some key components predicted to act in the plant immunity signaling pathway were also differentially expressed, for instance, the mitogen-activated protein kinases (*MAPK*s) cascades and receptor-like cytoplasmic kinase VII (*RLCK VII*) subfamily genes, which act as central players in both PTI and ETI (Liang and Zhou, 2018; Zhou and Zhang, 2020). The SA pathway plays important roles in plant disease resistance and pathogen-induced HR (Zheng et al., 2015; Cui et al., 2017; Zhang et al., 2017). We found that the genes predicted to encode the SA receptors, *nonexpressor of pathogenesis-related genes 1* (*NPR1*) and *NPR4*, and the SA marker genes, *pathogenesis-related 1* (*PR1*) and *PR5* were significantly differentially expressed in *Rp1-D21* mt.

The Differential Accumulated Metabolites and the Association With Transcriptomic Analysis in *Rp1-D21*

To investigate the metabolic changes induced by *Rp1-D21*, widely targeted metabolome analysis (Chen et al., 2013) was conducted by ultra-high-performance liquid chromatography-tandem mass spectroscopy (UPLC-MS). Due to the lack of seeds in B73 × H95 or Mo17 × H95 backgrounds, we used the isogenic hybrids A632 × H95-*Rp1-D21* and A632 × H95 for this experiment. A total of 423 metabolites were detected, including lipid, phenolic acids, flavonoids, and alkaloids. The orthogonal partial least squares discriminant analysis (OPLS-DA) model was performed on the metabolic analysis, and significantly differential accumulated metabolites (DAMs) were selected with $|\log2 \text{ (fold-change)}| > 0.6$ and variable importance for projection (VIP) > 1. Finally, a total of 103 DAMs (76 upregulated and 27 downregulated in the *Rp1-D21* background) were identified (**Supplementary Figure 6A**, **Supplementary Table 5**). Pathway enrichment analysis was conducted using Kyoto encyclopedia of genes and genomes (KEGG). These DAMs were mainly divided into "biosynthesis of secondary metabolites," "biosynthesis of amino acids," and "phenylpropanoid biosynthesis" (**Supplementary Figure 6B**).

To study the association between transcriptomic and metabolic analyses in *Rp1-D21* mt, the conjoint analysis of DAMs and DEGs at constant temperature were conducted by the KEGG pathway. Seven common pathways were enriched in *Rp1-D21* mt (**Figure 3**, **Supplementary Table 5**), with phenylpropanoid biosynthesis (**Supplementary Figure 7**) and α-linolenic acid metabolism as the top two significantly enriched pathways.

SA Pathway Genes and Metabolites Are Differentially Accumulated in *Rp1-D21*

Salicylic acid and its derivatives play important roles in plant disease resistance (Vlot et al., 2009; Ding et al., 2018); therefore, we investigated the DEGs and DAMs in the SA pathway. The SA biosynthesis occurs *via* two pathways, the isochorismate synthase (ICS) pathway and the phenylalanine ammonia-lyase (PAL) pathway, which play the major and minor roles in SA biosynthesis, respectively (**Figure 4A**, Dempsey et al., 2011). Interestingly, most genes encoding enzymes in ICS biosynthesis, including ICS1, EDS5, and PBS3, were downregulated in the late stage of HR induction (22°C), while most genes in the PAL pathway had an opposite expression pattern, including PAL and AIM1 homologs (**Figure 4B**, **Supplementary Table 6**). The level of phenylalanine, the precursor of the PAL pathway was increased to 1.53 fold in *Rp1-D21* mt compared to WT (**Supplementary Table 5**). In addition to the SA biosynthesis, the regulation of genes predicted to be involved in SA modifications were also investigated (**Figure 4B**). The genes associated with SA hydroxylation (S5H and S3H) were highly induced, while the genes related to SA methylation (BSMT), amino acid conjugation (GH3.5), and SA sulfonation (SOT) were downregulated in the late stage of HR (**Figures 4A,B**). In Arabidopsis, AtUGT74F1/2 and AtUGT75B1 modify SA to generate glycosylated SA (Noutoshi et al., 2012; George Thompson et al., 2017). We identified 9 and 4 SA glucosyltransferase (SAGT) homologs when searched the maize genome for sequences homologous to AtUGT74F1/2 and AtUGT75B1, respectively (**Supplementary Figure 8**). Among these 13 genes encoding SAGTs, 5 and 1 were up- and downregulated in *Rp1-D21*, respectively (**Figure 4B**, **Supplementary Figure 8**).

Salicylic acid can be hydroxylated by S5H to form 2,5-dihydroxy benzoic acid (2,5-DHBA), which can be further

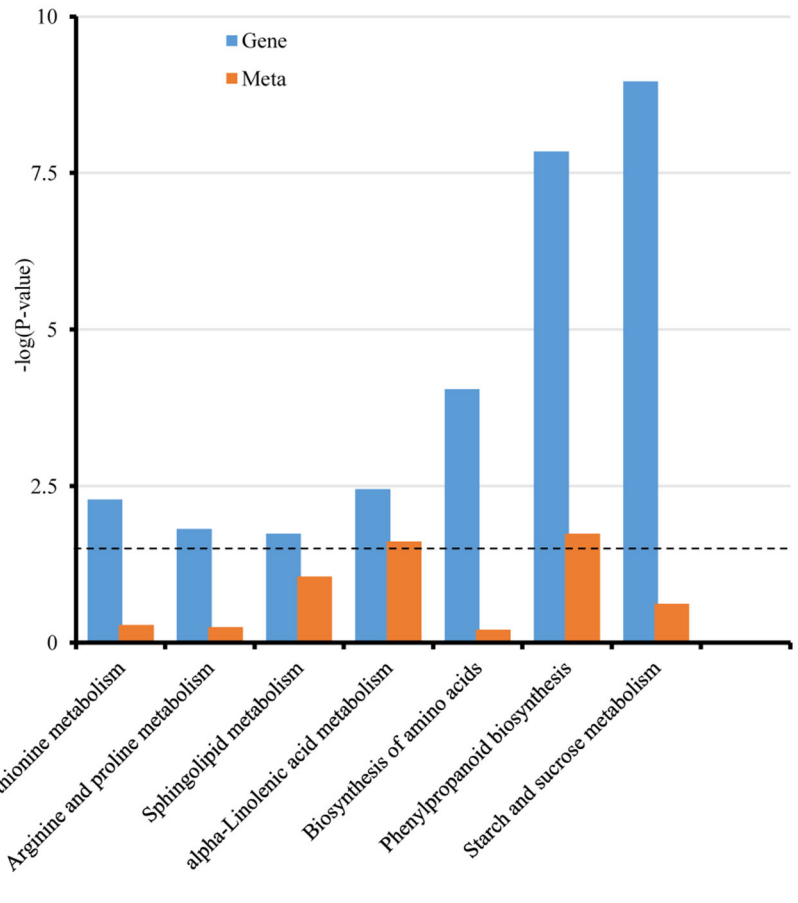

FIGURE 3 | Integrated analyses of transcriptomic and metabonomic results of *Rp1-D21* mutant (mt) compared to the wild type (WT). The Kyoto Encyclopedia of Genes and Genomes (KEGG) enrichment histogram of conjoint analysis of DEGs and differential accumulated metabolites (DAMs). The x-axis represents the metabolic pathways and the y-axis represents the expression as -log (*p*-value). The blue columns represent the enrichment *p*-values of DEGs, and the orange columns represent the enrichment *p*-values of DAMs. The black dotted line represents the threshold for significant enrichment at $p < 0.05$.

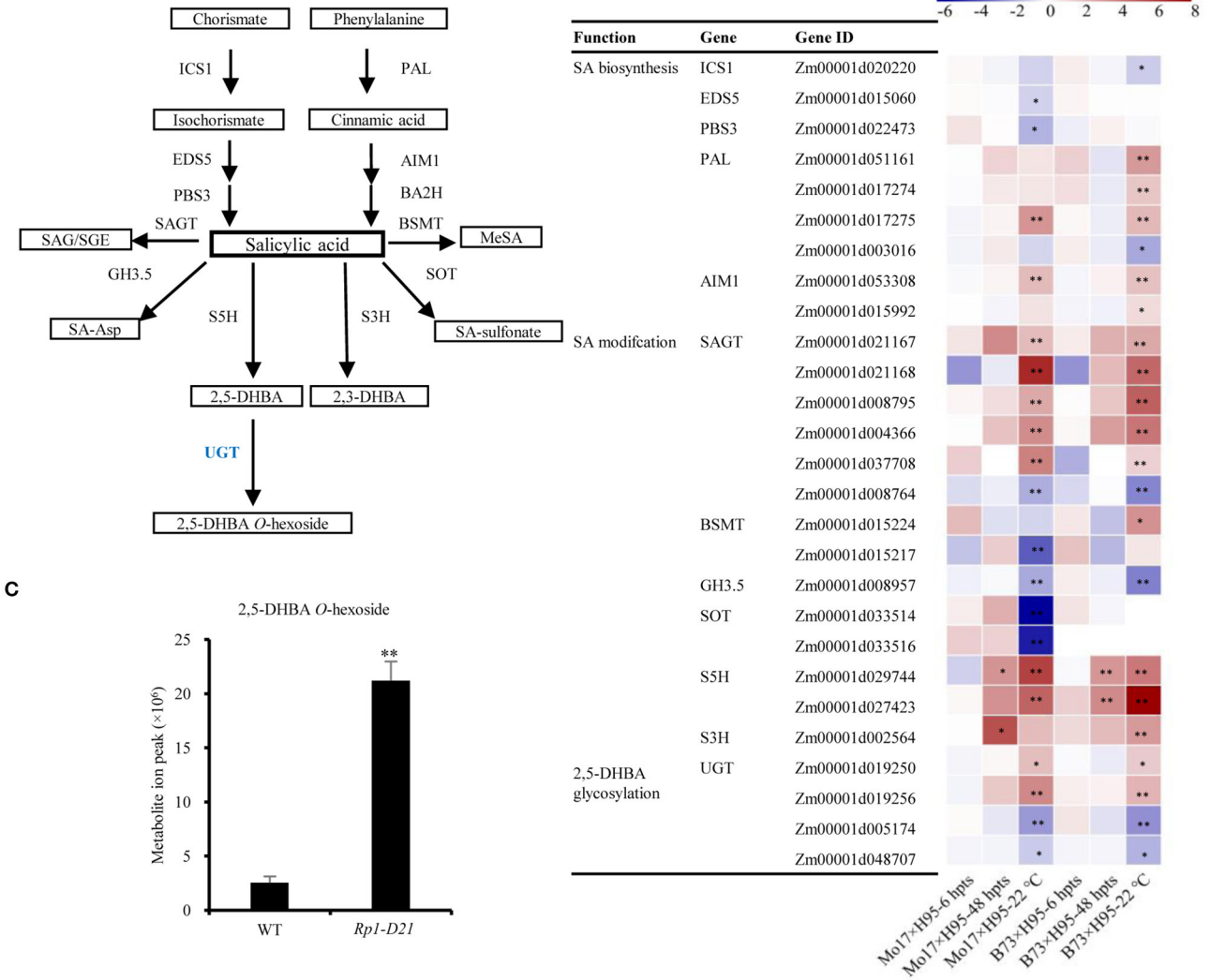

FIGURE 4 | The key enzymes involved in salicylic acid (SA) biosynthesis and modification pathways. **(A)** The SA biosynthesis and modification pathways. ICS1, isochorismate synthase 1; PAL, phenylalanine ammonia-lyase; EDS5, enhanced disease susceptibility 5; PBS3, AvrPphB susceptible3; AIM1, abnormal inflorescence meristem1; BA2H, benzoic acid 2-hydroxylase; UGT, UDP-glucosyltransferases; SAGT, salicylic acid glucosyltransferase; SAG, SA 2-O-β-Dglucoside; SGE, salicylate glucose ester; BSMT, benzoic acid/salicylic acid carboxyl methyltransferase; MeSA, methyl salicyliate; GH3.5, GH3 acyl adenylase family member 3.5; SA-Asp, salicyloyl-L-aspartate; SOT, sulfotransferase; S5H, SA 5-hydroxylase; S3H, SA 3-hydroxylase; 2,5-DHBA, 2,5-dihydroxybenzoic acid; 2,3-DHBA, 2,3-dihydroxybenzoic acid. **(B)** The log2 fold-change of the genes encoding key enzymes in SA biosynthesis and modification pathways. The fold change was normalized with the FPKM value. **(C)** The levels of 2,5-DHBA *O*-hexoside were significantly accumulated in *Rp1-D21* mutant (mt) compared to the wild type (WT). Asterisks indicate significant difference between samples, each sample with three biological replicates.

glycosylated by UGT76D1 to generate 2,5-DHBA glucosides in Arabidopsis (Zhang et al., 2017; Huang et al., 2018). We further measured the total and free SA levels of H95-*Rp1-D21* crossed into different backgrounds when they were grown at 22°C, and the result showed that *Rp1-D21* mt in different backgrounds had more SA accumulation than their corresponding WT (**Figure 5A**). Interestingly, the SA levels were largely positively related with the HR strength in different backgrounds (**Figure 5B**). To investigate whether SA affect Rp1-D21-mediated HR, we grew Mo17x H95-*Rp1-D21* at 30°C for 8 days, and then treated the seedlings with H_2O and 1.2 mM benzothiadiazole S-methyl ester (BTH), an analog of SA, and put the plant at 22°C to induce HR. We found that BTH significantly reduced the severity of *Rp1-D21*-mediated HR compared to H_2O (**Figure 6**). Among the DAMs, 2,5-DHBA *O*-hexoside was identified as one of the top DAMs, which accumulated at 8.34-fold in *Rp1-D21* mt than the WT (**Figure 4C**, **Supplementary Table 5**).

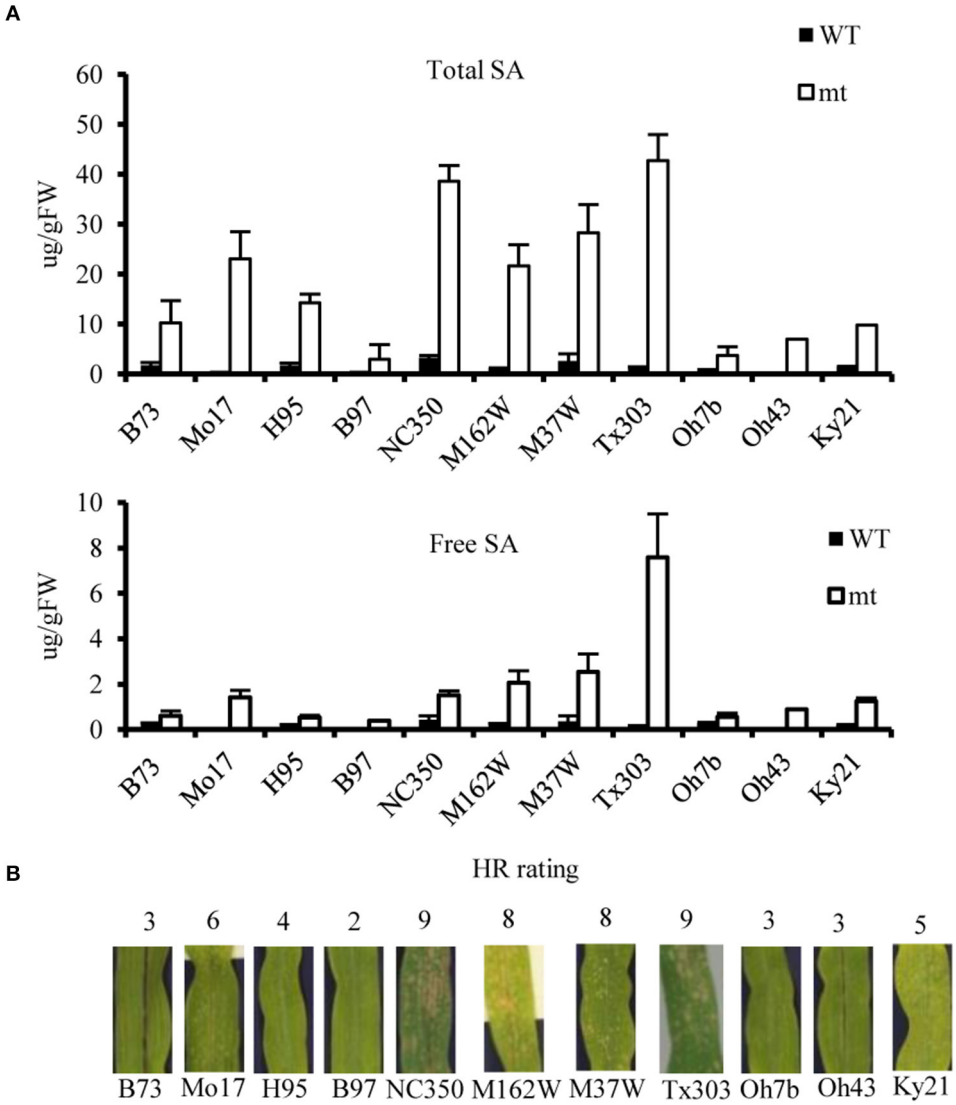

FIGURE 5 | The salicylic acid (SA) levels and hypersensitive response (HR) severity of *Rp1-D21* in different genetic backgrounds. **(A)** The levels of total SA and free SA were significantly accumulated in *Rp1-D21* mutant (mt) compared to the wild type (WT) in different backgrounds crossed with H95-*Rp1-D21* when they were grown at 22°C. **(B)** The HR rating of *Rp1-D21* mt in different backgrounds crossed with H95-*Rp1-D21*grown at 22°C condition.

DHBA Glucosyltransferases (*ZmUGTs*) Are Induced in *Rp1-D21*

In Arabidopsis, AtUGT76D1 (AT2G26480) is responsible for the conversion from 2,5-DHBA to 2,5-DHBA glucoside (Huang et al., 2018). We identified UDP-glucuronosyltransferase (UGT) homologs from maize (ZmUGTs) according to AtUGT76D1 and performed a phylogenetic analysis (**Figure 7A**). Of the nine ZmUGT homologs identified, Zm00001d019250 (ZmUGT9250) and Zm00001d019256 (ZmUGT9256) were upregulated at the late stage of HR induction in the *Rp1-D21* mt compared to the corresponding WT in both B73 and Mo17 backgrounds (**Figure 7A**), while Zm00001d005174 (ZmUGT5174) and Zm00001d048707 (ZmUGT8707) had the opposite expression pattern (**Supplementary Table 7**). Other ZmUGT homologs were not differentially expressed under these conditions (**Supplementary Table 7**).

ZmUGTs Partially Suppress Rp1-D21-Mediated HR in *Nicotiana benthamiana*

To investigate the possible roles of the four differentially regulated ZmUGTs in Rp1-D21-mediated HR, we used the agrobacteria-mediated transient expression in *Nicotiana benthamiana*. The four ZmUGTs were fused with a C-terminal enhanced green fluorescent protein (EGFP) tag. GUS:EGFP and HCT1806:EGFP were used as negative and positive controls,

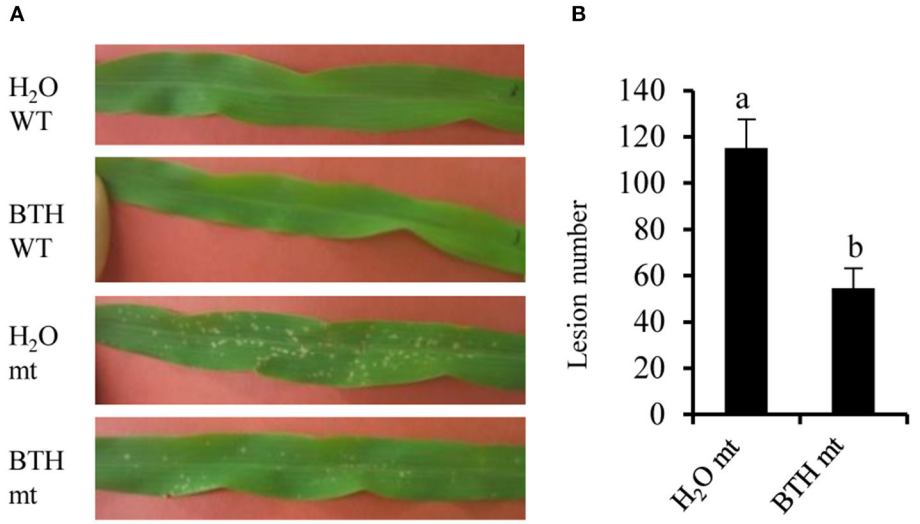

FIGURE 6 | Benzothiadiazole (BTH) treatment reduced Rp1-D21-mediated HR. **(A)** Plants in Mo17 × H95 background were grown at 30°C for 8 days, then the plants were treated by H_2O or 1.2 mM BTH. After treatment, the temperature was dropped to 22°C to induce hypersensitive response (HR), and the pictures of the third leaves were taken at 4 days after temperature shift. **(B)** The lesion number in mutant (mt was calculated after H_2O and BTH treatment. Significant differences ($p < 0.05$) between samples are indicated by different letters (a,b). Wild type (WT) and *Rp1-D21* mutant (mt).

respectively. The HCT1806 had previously been shown to be a strong suppressor of Rp1-D21-mediated HR (Wang et al., 2015b; Wang and Balint-Kurti, 2016; Murphree et al., 2020). When transiently co-expressed with Rp1-D21 fused with C-terminal 3 × hemagglutinin (HA) tag in *N. benthamiana*, ZmUGT9250 and ZmUGT5174 partially suppressed Rp1-D21-induced HR compared to HCT1806, while ZmUGT9256 and ZmUGT8707 did not suppress Rp1-D21-induced HR (**Figure 7B**). Ion leakage conductivity data further verified our visual observations (**Figure 7C**). Co-expression of ZmUGTs did not significantly change the protein accumulation of Rp1-D21 which was expressed at substantial and broadly comparable levels (**Figure 7D**).

The N-terminal coiled-coil (CC) domain of Rp1-D21 protein (CC_{D21}) conferred an obvious autoactive HR when it was fused with EGFP and transiently expressed in *N. benthamiana* (Wang et al., 2015b). To determine whether ZmUGTs can suppress CC_{D21}-mediated HR, we co-expressed them and CC_{D21}:EGFP in *N. benthamiana*. The results showed that ZmUGT9250 suppressed CC_{D21}-mediated HR which was similar to HCT1806, ZmUGT5174 partially suppressed CC_{D21}-mediated HR, and ZmUGT9256 and ZmUGT8707 had no obvious effect (**Supplementary Figure 9**).

ZmUGTs Have No Interaction With CC_{D21}

Several Rp1-D21 regulators we identified previously interact with CC_{D21} and suppress CC_{D21}-mediated HR (Wang et al., 2015b; Wang and Balint-Kurti, 2016; Zhu et al., 2020; Liu et al., 2021; Luan et al., 2021). To investigate whether ZmUGTs can interact with CC_{D21}, we performed yeast two-hybrid assays. We did not detect interaction between any of the four ZmUGTs investigated and CC_{D21} (**Supplementary Figures 10A,B**). A co-immunoprecipitation assay between CC_{D21} and ZmUGT9250, which had the strongest suppression effect on CC_{D21}-mediated HR, also did not detect any interaction (**Supplementary Figure 10C**).

ZmUGTs Have No Obvious Suppression Effect on Other Elicitor-Induced HR

To investigate whether ZmUGTs could suppress HR induced by other nucleotide-binding leucine-rich-repeats (NLRs), we co-expressed them with *Arabidopsis* RPM1(D505V) and barley MLA10(D502V), which confer an autoactive HR when transiently expressed in *N. benthamiana* (Gao et al., 2011; Bai et al., 2012). The results showed that all the four ZmUGTs had no obvious suppression effect on either MLA10(D502V)- or RPM1(D505V)-induced HR (**Supplementary Figure 11**). We further co-expressed ZmUGTs with BAX or INF, the death-promoting protein or cell death elicitor (Kamoun et al., 1998; Lacomme and Santa Cruz, 1999), and found that neither of them substantially suppressed either BAX- or INF-induced HR (**Supplementary Figure 11**).

DISCUSSION

In this study, we used transcriptome and metabolome analyses to investigate the molecular responses of Rp1-D21-mediated hypersensitive response (HR). The conditions used for the transcriptome analysis and metabolome analysis differed substantially in terms of the growth conditions and the genotypes used. Despite this, the salicylic acid (SA) pathway and the phenylpropanoid biosynthesis pathway were induced at both the transcriptional and metabolic levels. Especially, the genes predicted to encode 2,5-DHBA UGTs

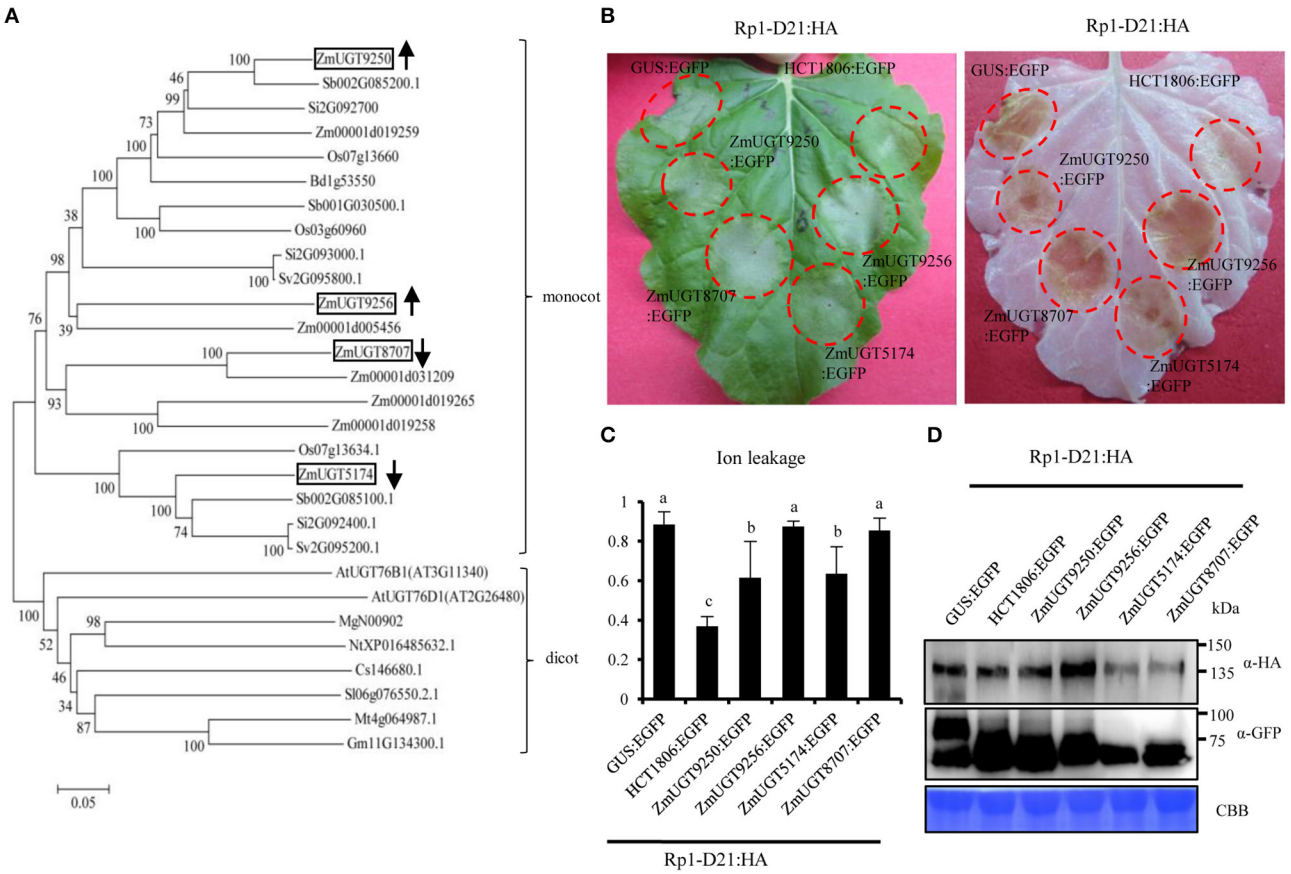

FIGURE 7 | Phylogenetic analysis of UDP-glucuronosyltransferase (UGT) proteins and the function of ZmUDP-glucuronosyltransferases (UGTs) in Rp1-D21-mediated hypersensitive response (HR). **(A)** The phylogenetic tree was constructed using MEGA 6.0 software. At, *Arabidopsis thaliana*; Bd, *Brachypodiumdistachyon*; Cs, *Cucumissativus*; Gm, *Glycine max*; Mg, *Mimulusguttatus*; Mt, *Medicagotruncatula*; Nt, *Nicotianatabacum*; Os, *Oryza sativa*; Sb, *Sorghum bicolor*; Si, *Setaria italica*; Sl, *Solanum lycopersicum*; Sv, *Setaria viridis*; Zm, *Zea mays*. The boxes indicate the UGT homologs of maize which were differentially expressed in *Rp1-D21*. **(B)** ZmUGTs were transiently co-expressed with Rp1-D21 into *Nicotiana benthamiana*. The representative leaf was photographed at 3 days after inoculation (left), and the same leaf was cleared by ethanol (right). **(C)** Ion leakage conductivity [average ± standard error (SE), $n > 5$] was measured at 60 h after co-expression of GUS, HCT1806, or ZmUGTs with Rp1-D21. Significant differences ($p < 0.05$) between samples are indicated by different letters (a–c). **(D)** Total protein was extracted from agro-infiltrated leaves at 40 hour post inoculation (hpi). Anti-HA was used to detect the expression of Rp1-D21, and anti-GFP was used to detect the expression of GUS, HCT1806, and ZmUGTs. Equal loading of protein samples was shown by Coomassie brilliant blue (CBB) staining. The experiments were performed three times with similar results.

were differentially expressed in *Rp1-D21* mutant (mt) and the 2,5-DHBA *O*-hexoside catalyzed by UGTs were high accumulated in *Rp1-D21* mt. We further examined that two Zm UDP-glucuronosyltransferases (UGTs) partially suppress Rp1-D21-mediated HR.

The Autoactive *Rp1-D21* mt Is an Excellent Tool for the Identification of Disease Resistance Genes in Maize

Autoimmune mutants caused by inappropriate activation of nucleotide-binding leucine-rich-repeats (NLRs) are widely used for mechanistic investigation of immune signaling components in different plants, e.g., Arabidopsis *snc1* and *mkk1mkk2* (Kong et al., 2012; Dong et al., 2016; Chakraborty et al., 2018). Rp1-D21 is an NLR protein which confers autoimmunity in maize (Sun et al., 2001; Smith et al., 2010). The transcript levels of *Rp1-D21* were greatly increased over time after temperature dropping from 30 to 22°C, especially at 48 h post the temperature shift (hpts) (**Supplementary Figure 2**). At constant 22°C, the transcript levels of *Rp1-D21* were even much higher (**Supplementary Figure 2**). These data suggested that the onset of HR might be related with the increased expression of *Rp1-D21*. Consistent with the trends of the transcript levels of *Rp1-D21*, more differentially expressed genes (DEGs) were identified at constant 22°C than at 48 and 6 hpts, indicating that these DEGs were induced by the increased levels of *Rp1-D21*. Several transcription factors (TF)s, including WRKY and bZIP which are known to act in plant immunity (Jakoby et al., 2002; Kaminaka et al., 2006; Pandey and Somssich, 2009), were predicted as the major TFs to bind the promoters of DEGs

(**Supplementary Table 3**), indicating that Rp1-D21-mediated HR is under tight transcriptional regulation. We showed that many genes predicted to act in pathogen-triggered immunity (PTI) were differentially expressed in the defense response triggered by the NLR Rp1-D21, including gene homologs encoding FLS2, BAK1, RBOHs, RLCKs, and MAPK cascades (**Supplementary Figure 5**). Consistent with our results, it was recently reported that effector-triggered immunity (ETI) can increase the defense strength through transcriptional induction of PTI signaling components and PTI is required for disease resistance mediated by several NLRs (Ngou et al., 2021; Yuan et al., 2021).

Several studies have used the *Rp1-D21* mt to identify genes or loci associated with modulation of the severity of HR (Chintamanani et al., 2010; Chaikam et al., 2011; Olukolu et al., 2014). We have verified that two homolog genes encoding enzymes of lignin biosynthesis pathway ZmHCT1806 and ZmCCoAOMT2 (Wang et al., 2015b; Wang and Balint-Kurti, 2016), two flavone synthase homologs of ZmFNSIs (Zhu et al., 2020), the nicotinate *N*-methyl transferase ZmNA*N*MT(Liu et al., 2021), and the metacaspase homologs, ZmMC1 and ZmMC2 (Luan et al., 2021), can suppress Rp1-D21-mediated HR likely through physical interaction with the cellular component (CC) signaling domain of Rp1-D21 when transiently expressed in *Nicotiana benthamiana*. Interestingly, ZmCCoAOMT2 was also proved to confer quantitative resistance to both southern leaf blight and gray leaf spot in maize (Yang et al., 2017). The homologs of these genes in different plant species also act in plant immunity (Coll et al., 2010; Senthil-Kumar et al., 2010; Gallego-Giraldo et al., 2011; Zeilmaker et al., 2015), suggesting the functional association between disease resistance and HR regulation. Recently, it was reported that the transcriptional responses triggered by Rp1-D21 are broadly similar to those triggered by its wild type (WT) counterpart Rp1-D, which is activated by *Puccinia sorghi* infection (Kim et al., 2021). The DEGs identified in *Rp1-D21* are highly correlated with disease resistance; therefore, *Rp1-D21* can be used as a quick and effective tool for exploring new HR regulation and disease resistance genes.

Rp1-D21-Mediated HR Related Signal Transduction and Metabolic Pathways in Maize

Except for the SA pathway, we found that the α-linolenic acid pathways and the phenylpropanoid biosynthesis pathway were induced in *Rp1-D21* at both the transcriptional and metabolic levels according to the integrated transcriptome and metabolome analyses (**Figure 3**). The α-linolenic acid is produced by two metabolic pathways, 9-lipoxygenase (9-LOX) pathway, and 13-lipoxygenase (13-LOX) pathway (Wasternack, 2007). LOX-derived oxylipins have been implicated in plant growth and development, senescence, and resistance to pathogens (Blée, 2002; Mosblech et al., 2009). When infected by different pathogens, the transcript levels and the related metabolites in 9-LOX pathway were increased in tobacco, potato, and maize with the occurrence of HR (Gobel et al., 2001, 2003; Davoine et al., 2006; Gao et al., 2009). The 9-hydroxyoctadecatrienoic acid (9-HOT) and 9,10-epoxyoctadecenoic acid (9,10-EOT) in the 9-LOX pathways were among the most active oxylipins (Prost et al., 2005; Vicente et al., 2012). The mutant insensitive to 9-HOT displays enhanced susceptibility to *Pseudomonas* infection (Vellosillo et al., 2007). In our metabolites analysis, we found that the transcript levels of genes and metabolite products in the α-linolenic acid metabolism pathway were increased in the *Rp1-D21* mutant (**Figure 3**, **Supplementary Table 5**). In particular, we observed a massive accumulation of 9-HOT and 9,10-EOToxylipins derived from the 9-LOX pathway suggested that they play pivotal roles in Rp1-D21-mediated HR and plant disease resistance.

The phenylpropaniod biosynthesis pathway, mainly including lignin intermediates, anthocyanins, isoflavonoidphytoalexins, and phenolic compounds, has been implicated as one of the major pathways for defense against pathogens (Ranjan et al., 2019). As displayed in **Figure 3**, transcriptome and metabolome conjoint analysis indicated that differentially expressed genes (DEGs) and differential accumulated metabolites (DAMs) associated with the phenylpropaniod pathway were significantly enriched (**Supplementary Table 5**). Many DEGs in the lignin biosynthesis pathway, including *PAL*, cinnamoyl-CoA reductase (*CCR*), *CCoAOMT,* and *HCT* play important roles in plant defense response (Kawasaki et al., 2006; Gallego-Giraldo et al., 2011; Wang and Balint-Kurti, 2016; He et al., 2020). Many genes involved in phenylpropanoid pathway are differentially expressed after inoculation with the pathogen *Fusarium graminearum* (Liu et al., 2016). These results suggest that the phenylpropaniod biosynthesis pathway constituted a key class of enzymes and metabolites associated with modulating the HR induced by Rp1-D21 and disease resistance in maize defense response.

SA and Glycosylation of SA Derivatives May Play a Role in Defense Response

We have previously shown that several regulators interact with CC_{D21} and modulate Rp1-D21-mediated HR (Wang et al., 2015b; Wang and Balint-Kurti, 2016; Zhu et al., 2020; Liu et al., 2021; Luan et al., 2021). Here we found that ZmUGTs suppressed Rp1-D21- and CC_{D21}-mediated HR, but they did not interact with CC_{D21} (**Supplementary Figure 10**). These data suggested that the regulation of Rp1-D21-mediated HR by ZmUGTs might not be through the formation of a protein complex with Rp1-D21.

The plant hormone, SA has profound importance in both local resistance against biotrophic and hemi-biotrophic pathogens and systemic acquired resistance (Vlot et al., 2009). In local pathogen infection, high levels of SA induce defense gene expression by activating the transcriptional activator NPR1 and lead to cell death (Fu and Dong, 2013). In the maize lesion mimic mutant, *Les4*, the free and total SA levels were significantly increased at the lesion-developed stage compared to the prelesion stage (Morris et al., 1998). In this study, many gene homologs in SA biosynthesis and metabolism pathways were differentially expressed in *Rp1-D21* (**Figure 4B**). Interestingly, the genes in the isochorismate synthase 1 (ICS1) and phenylalanine ammonia-lyase (PAL) pathways were

mostly down- and upregulated in *Rp1-D21* mt compared to WT at the late stage, respectively (**Figure 4B**). The level of phenylalanine was also increased in *Rp1-D21* mt compared to WT (**Supplementary Table 5**). However, cinnamic acid, chorismate, and isochorismate were not identified under our conditions. The levels of total SA and free SA were significantly elevated in *Rp1-D21* mts compared to the corresponding WT and there was a positive correlation between SA levels and the HR strength in different backgrounds (**Figure 5**). These data suggested that the activation of the SA pathway might be associated with the formation of HR lesions in plants carrying *Rp1-D21*. The upregulation of genes in the PAL pathway might act to keep the SA level at an appropriate level to trigger HR while the downregulation of genes in the ICS1 pathway might act to prevent the over-accumulation of SA at the late stage. On the other hand, the exogenous application of SA or SA analogs suppresses ETI-mediated HR in Arabidopsis (Zavaliev et al., 2020). Similarly, we found that exogenous application of benzothiadiazole (BTH), an analog of SA, also suppressed Rp1-D21-mediated HR in maize (**Figure 6**). These studies suggest that SA plays important roles in suppressing NLR-mediated HR. Therefore, SA plays dual roles in HR regulation, likely through the induction of positive defense regulators to activate HR or induction of negative regulators to suppress HR (Radojicic et al., 2018; Peng et al., 2021).

Excessive levels of SA can be toxic to plants; therefore SA can be modified by different conjugations to less toxic derivatives (Dempsey et al., 2011). In Arabidopsis, two SAGTs, UGT74F1, and UGT76B1 can glycosylate SA to produce SAG (Noutoshi et al., 2012). Loss of UGT74F1 and UGT76B1 confers resistance to both *Pst* DC3000 and a strain which can be recognized by the NLR protein RPM1 (Noutoshi et al., 2012). Here we found that several maize SAGT homologs were upregulated in *Rp1-D21* and the total SA levels were increased in *Rp1-D21* (**Figures 4**, **5**), suggesting that these SAGT homologs might play a role in Rp1-D21-mediated HR.

2,5-dihydroxybenzoic acid (2,5-DHBA) and 2,3-DHBA are two major catabolic products of SA and they are catalyzed by hydroxylating SA *via* S5H and S3H, respectively (**Figure 4B**, Zhang et al., 2017). 2,5-DHBA is widely distributed in planta and is induced by the pathogen, *Pst*DC3000 in *Arabidopsis* (Zhang et al., 2017). In a previous study (Zhu et al., 2020), we found that the transcript levels of *ZmFNSI*s (also known as *ZmS5H*s) and *ZmS3H* were upregulated in *Rp1-D21* mt (**Figure 4B**), and ZmS5Hs but ZmS3H does not suppress Rp1-D21- and CC_{D21}-mediated HR (Zhu et al., 2020), indicating that ZmS5Hs play important roles in maize defense response. The 2,5-DHBA and 2,3-DHBA can be further glycosylated by a unique UDP-glycosyltransferase UGT76D1 in Arabidopsis (Huang et al., 2018). Expression of the *AtUGT76D1* is induced by *Pst* DC3000. Overexpression of *AtUGT76D1* leads to high SA accumulation, upregulation of defense genes and the autoactive HR phenotype, while the immune responses were compromised when *AtUGT76D1* is knocked out implying that AtUGT76D1 is a positive regulator in plant innate immunity (Huang et al., 2018). Interestingly, AtUGT76B1, a close homolog which had 38.8% similarity of amino acid with AtUGT76D1, was recently found to use *N*-hydroxy-pipecolic acid (NHP) as substrate and act in systemic-acquired resistance (Bauer et al., 2021; Holmes et al., 2021; Mohnike et al., 2021). Loss-of-function mts of *AtUGT76B1* confer a dwarf phenotype and constitutive defense response, with high NHP and SA accumulation and enhanced disease resistance to *Pst*DC3000 (Bauer et al., 2021; Mohnike et al., 2021). The 2,5-DHBA glucosides were also accumulated in tomato and cucumber after infection with the pathogen, citrus exocortis viroid (CEVd) and prunus necrotic ringspot virus (PNRSV) (isolate NCM1), respectively (Fayos et al., 2006). In maize, 147 UGTs belonging to 17 groups were identified (Li et al., 2014), and none of them have been functionally investigated in disease resistance. Here we also found that the transcript levels of four DHBA-glycosyltransferase *ZmUGT* homologs of AtUGT76D1 were significantly differentially expressed and higher levels of SA and 2,5-DHBA *O*-hexoside were accumulated in *Rp1-D21* mt compared to WT (**Figures 4**, **5**, **7**). We further showed that the two ZmUGTs, ZmUGT9250 and ZmUGT5174, suppressed Rp1-D21-mediated HR. These results indicated that ZmUGTs play negative roles in NLR protein Rp1-D21-mediated defense response, which is different from the positive role of AtUGT76D1 in plant immunity. Interestingly, ZmUGT9250 and ZmUGT5174 have opposite expression patterns in the lines harboring Rp1-D21 (**Figures 4**, **7**). The transcript level of ZmUGT9250 was increased in Rp1-D21, suggesting that it might mainly act to inhibit the further spreading of HR when Rp1-D21 is activated, while the transcript level of ZmUGT5174 was decreased in Rp1-D21, suggesting that it might mainly act to keep NLR protein in the inhibited state in WT. The two ZmUGTs had no obvious effects on RPM1 (D505V), MLA (D502V), INF1, or Bax-mediated cell death (**Supplementary Figure 11**), indicating that they are not general cell death suppressors and they might have different mechanisms with Rp1-D21 for triggering cell death. It was reported that DHBA glycosyltransferases play important roles in the innate immune response through regulating the SA homeostasis (Huang et al., 2018). In this way, we hypothesized that the accumulation of DHBA glycosides which might act as an endogenous modulator of SA levels to switch the activity of enzymes in SA-mediated signaling pathways, thus regulating the HR phenotype in *Rp1-D21*. Since the enzyme activity of the four ZmUGThomologs has not been investigated yet, it is not clear which member has the DHBA glycosyltransferase activity. Since these ZmUGTs were homologous to both AtUGT76D1 and AtUGT76B1 (**Figure 7A**), it will be interesting to further investigate whether these ZmUGTs are also functionally similar to AtUGT76B1.

In summary, we used transcriptomic and metabolomic analyses to identify DEGs and DAMs involved in Rp1-D21-meidiated HR, which provides a useful resource for exploring maize disease resistance genes. The SA metabolic pathway and the phenylpropanoid biosynthesis pathway were induced at both the transcriptional and metabolic levels. We further demonstrated that two of four *ZmUGTs* partially suppressed the HR triggered by Rp1-D21 or its N-terminal CC_{D21} domain, which forms the basis for further investigating their roles in plant immunity.

EXPERIMENTAL PROCEDURES

Plant Materials and Growth Conditions

Maize (*Zea mays*) line B73 was used for isolating *ZmUGTs*. The *Rp1-D21*-H95 line was generated by repeatedly backcrossing a line carrying Rp1-D21 as a female to the H95 inbred. As previously reported (Chaikam et al., 2011), *Rp1-D21* mutant is maintained in the heterozygous state in H95 background (H95-*Rp1-D21*) due to its sterile nature in the homozygous state. The H95-*Rp1-D21* line was then crossed as female to B73 and Mo17 to produce the isogenic hybrid pairs, B73 × H95 and B73 × H95-*Rp1-D21* and the isogenic pair, Mo17 ×H95 and Mo17 × H95-*Rp1-D21*, respectively. The only substantial genetic difference between the components of each isogenic pair was at the *Rp1-D21* locus (Chaikam et al., 2011). A632 × H95-*Rp1-D21* used for the metabolic analysis and other lines used for SA assays were generated similarly. For the RNA sequencing (RNA-seq) analysis, plants were grown in the growth chamber in the North Carolina State University (NCSU) Phytotron at temperatures of 22 or 30°C in a 12 h light/12 h dark cycle. The experiments have two temperature treatments: (1) Plants were grown at constant 22°C for 18 days, and the fourth leaves were collected for RNA-seq analysis. (2) Plants were grown at 30°C for 14 days; then the temperature was dropped to 22°C to induce HR, and the fourth leaves were collected at 3, 6, 24, and 48 h post the temperature shift (hpts). Each sample was composed of pooled fourth leaves from five randomly chosen plants with two biological replicates. For the metabolic analysis, the isogenic hybrid pairs, A632 × H95 and A632 ×H 95-*Rp1-D21* were grown in the field (Qingdao, China) and the fifth leaves at the V7 stage were collected with three biological replicates. For SA assays, the isogenic hybrid pairs in different genetic backgrounds were grown in the growth chamber for 18 days at a constant 22°C, and the fourth leaves were collected for SA measurement with three biological replicates.

Wild type *Nicotiana benthamiana* was grown at 24°C with a cycle of 16 h light and 8 h dark.

Semi-quantitative RT-PCR

All primers used in this study are listed in **Supplementary Table 8**. Semi-quantitative RT-PCR was used to measure the gene expression as reported in our previous study (Negeri et al., 2013). Total RNA was extracted from the maize leaf tissue using Trizol (Life Technologies, Carlsbad, CA, USA) according to the instructions of the manufacturer. For complementary DNA (cDNA) synthesis, 1 μg of total RNA was reverse-transcribed using M-MLV (Life Technologies Corporation, Carlsbad, USA) following standard protocols. The amplification conditions for PCR consisted of 32 cycles of 94°C for 30 s, 57°C for 30 s, and 72°C for 30 s, using 250 μM of each primer and 1–2 μL of the 5 × diluted cDNA per reaction.

RNA-Seq Library Construction and Transcriptome Sequencing

Total RNA was extracted from the fourth leaves pooled from five individuals collected from *Rp1-D21* mt and corresponding WT in B73 and Mo17 backgrounds at two treatments. The procedures for RNA sequencing (RNA-seq) analysis were performed according to our previous studies (Olukolu et al., 2014; Wang et al., 2015b). The quality and quantity of RNA were monitored by a NanoDrop 2000c spectrophotometer (Thermo Scientifc, Wilmington, DE, USA) and agarose gel electrophoresis. The messenger RNA (mRNA) was isolated from the total RNA by Dynabeadsoligo (dT25) (Invitrogen Life Technologies, MA, USA). The RNA-seq libraries were constructed according to the TruSeq RNA Sample Prep v2 LS as per the instructions of the manufacturer (Illumina Inc., CA, USA). The normalized libraries with individual index were loaded onto IlluminaHiSeq 2000 platform (Illumina Inc., San Diego, CA, USA) for cluster generation and sequencing. The data from two biological replicates were obtained by single end and paired-end reads (100-bp), respectively.

Bioinformatic and Statistical Analyses

The sequencing reads were aligned to the maize B73 reference genome (ZmB73_RefGen_v38, ftp://ftp.ensemblgenomes.org) using hierarchical indexing for spliced alignment of transcripts 2 (HISAT2) (Kim et al., 2015) by the default parameter settings. Fragments per kilobase of exon model per million mapped reads (FPKM) and Pearson's correlation test were used for the estimation of gene transcription levels and the correlation between different biological replicates, respectively. To avoid taking the log of a number <1, all FPKM values were increased by 1. Differentially expressed genes (DEGs) were identified using the software package, edgeR, and DESeq2 from the Bioconductorsuite (Robinson et al., 2010; Love et al., 2014). The common DEGs were identified by both the methods with a false discovery rate (FDR) or adjusted *p*-values (padj) < 0.05 and a | Log2 (fold-change) | ≥1. Functional enrichment analysis of DEGs was performed based on Gene ontology (GO) Consortium database (http://www.geneontology.org). Network of DEGs and differentially accumulated metabolites (DAMs) were constructed based on Kyoto Encyclopedia of Genes and Genomes (KEGG) pathways (Kanehisa et al., 2017). A regulation overview of DEGs was accomplished using the MapMantool (Usadel et al., 2009). The common DEGs from 48 hpts and at 22°C grown condition treatments were selected to infer the gene regulatory networks (GRNs) using PlantTFDB v5.0 (http://plantregmap.cbi.pku.edu.cn; Zhou et al., 2020). The functional assignment of predicted transcription factors was done based on the functional classification information from the MapMan Toolkit.

Metabolome Analysis

The fifth leaves of maize seedlings at V7 stage were collected with three replications for widely targeted metabolites analysis by ultra-performance liquid chromatography-mass spectrometry/Mass spectrometry (UPLC-MS/MS) (Chen et al., 2013). As described previously (Li et al., 2018; Mo et al., 2019), ∼100 mg of freeze-dried leaf powder was dissolved in 0.6 mL of 70% methanol at 4°C overnight. Supernatant after centrifugation at 10, 000 g for 10 min was filtrated with a 0.22 μm pore size membrane for UPLC-MS/MS analysis using an LC-ESI-MS/MS system (HPLC, Shim-pack UFLC SHIMADZU

CBM30A system, https://www.shimadzu.com.cn/; MS, Applied Biosystems 4500 Q TRAP, http://www.appliedbiosystems.com.cn/). Metabolite quantification is acquired with triple quadrupole scans using multi-reaction monitoring (MRM) model. The DAMs were identified by orthogonal partial least squares-discriminant analysis (OPLS-DA) according to the criteria of |fold-change| $\geq$ 1.5 and the variable importance in project (VIP) $\geq$1.

SA Measurement

Salicylic acid was extracted as described previously (Wang et al., 2011). Briefly, 200 mg of each sample with three replications was ground into powder and extracted with 1.5 mL of 90% methanol followed by extraction with 1.5 mL of 100% methanol. 500 ng of *o*-anisic acid (Sigma, 169978) was added in each sample as the internal control. For each sample, 40 units of β-glucosidase (Sigma, G-0395) were added to digest glucosyl-conjugated SA (total SA) for 1.5 h at 37°C, and then were treated with an equal volume of 10% trichloroacetic acid (TCA) and centrifuged at 10,000 g for 10 min. A Dionex AS50 HPLC instrument with an Acclaim 120 C18 reverse column (4.6 3 250 mm) was used to detect the SA contents.

UGTs Sequence Alignment and Phylogenetic Analysis

For phylogenetic analysis, the protein sequences from UDP-glucuronosyltransferase (UGT) family were aligned using Clustal X v2.1. Based on this alignment, a neighbor-joining tree was constructed using MEGA 6.0 software with 1,000 bootstrap replicates (Tamura et al., 2007). The neighbor-joining and *p*-distance methods were used with the pairwise deletion option to deal with gaps in the amino acid sequences.

Plasmid Construction

Rp1-D21:HA, GUS:EGFP, and CC_{D21}:EGFP were generated previously (Wang et al., 2015b). The cDNA sequences of ZmUGTs were isolated from B73 line and cloned into pENTR directional TOPO cloning vector (D-TOPO, Invitrogen, MA, USA). After sequencing, they were constructed into pSITEII-N1-EGFP vector (Martin et al., 2009) by LR reactions.

Agrobacterium tumefaciens-Mediated Transient Expression

The *Agrobacterium tumefaciens* strain, GV3101 (pMP90) transformed with binary vector constructs was grown at 28°C overnight in 10 mL of L-broth medium supplemented with appropriate antibiotics. The detailed procedures were performed according to our previous study (Wang et al., 2015b). Unless otherwise indicated, all the experiments were repeated three times with similar results.

Ion Leakage Measurement

Ion leakage conductivity was measured with a conductivity meter (METTLER TOLEDO, Zurich, Switzerland) according to our previous studies (Wang and Balint-Kurti, 2016; Zhu et al., 2020).

Yeast Two-Hybrid Assay

ZmUGTs and CC_{D21} were respectively cloned into the pGADT7 (AD) and pGBKT7 (BD) vectors (Clontech, Mountain View, CA, USA) through LR reactions. The different combinations of AD- and BD-derived constructs were co-transformed into the yeast strain, Y2HGold. The Y2H assay was performed according to the protocol provided by the protocol of the manufacturer (Clontech, Mountain View, CA, USA).

Protein Analysis and Co-immunoprecipitation (Co-IP) Assay

For protein analysis as described in our previous study, Myc-, EGFP- and HA-tagged constructs were transiently co-expressed in *Nicotiana benthamiana* and three leaf disk (~1.2 cm in diameter) from different *N. benthamiana* plants were collected at 30 h post inoculation (hpi). Total input protein was extracted in 150 µl extraction buffer (Wang et al., 2015b). Proteins for Co-IP assay were extracted from 0.6 g of leaf tissue collected at 40 hpi in 2.4 ml extraction buffer (Wang et al., 2015a; Wang and Balint-Kurti, 2016). The Western blot assays were performed according to our previous studies (Wang and Balint-Kurti, 2016; Zhu et al., 2020).

DATA AVAILABILITY STATEMENT

The original contributions presented in the study are publicly available. This data can be found at: National Center for Biotechnology Information (NCBI) BioProject database under accession number PRJNA288794 (https://www.ncbi.nlm.nih.gov/bioproject/PRJNA288794).

AUTHOR CONTRIBUTIONS

G-FW conceived the original research plans and supervised and designed the experiments. CG, Y-GW, and G-FW performed the experiments. CG, Y-GW, SL, XZ, B-KH, PB-K, and G-FW analyzed the data. CG and G-FW wrote the manuscript. PB-K revised the manuscript. All authors contributed to the article and approved the submitted version.

FUNDING

This research was supported by grants from the National Natural Science Foundation of China (31871944, 31571263, and 32072405), Qilu Scholarship from Shandong University of China (11200086963061), Agricultural Variety Improvement Project of Shandong Province (2017LZN034), Natural Science Foundation of the USA Plant Genome grants (0822495 and 1444503), and the China Postdoctoral Science Foundation (2019M652391).

SUPPLEMENTARY MATERIAL

The Supplementary Material for this article can be found online at: https://www.frontiersin.org/articles/10.3389/fpls.2021.738261/full#supplementary-material

REFERENCES

Asselin, J. E., Lin, J., Perez-Quintero, A. L., Gentzel, I., Majerczak, D., Opiyo, S. O., et al. (2015). Perturbation of maize phenylpropanoid metabolism by an AvrE family type III effector from *Pantoeastewartii*. *Plant Physiol.* 167, 1117–1135. doi: 10.1104/pp.114.253120

Bai, S., Liu, J., Chang, C., Zhang, L., Maekawa, T., Wang, Q., et al. (2012). Structure-function analysis of barley NLR immune receptor MLA10 reveals its cell compartment specific activity in cell death and disease resistance. *PLoS Pathog.* 8:e1002752. doi: 10.1371/journal.ppat.1002752

Balint-Kurti, P. (2019). The plant hypersensitive response, concepts, control and consequences. *Mol. Plant Pathol.* 20, 1163–1178. doi: 10.1111/mpp.12821

Bartsch, M., Bednarek, P., Vivancos, P. D., Schneider, B., von RoepenackLahaye, E., Foyer, C. H., et al. (2010). Accumulation of isochorismate-derived 2, 3-dihydroxybenzoic 3-O-b-D-xyloside in Arabidopsis resistance to pathogens and ageing of leaves. *J. Biol. Chem.* 285, 25654–25665. doi: 10.1074/jbc.M109.092569

Bauer, S., Mekonnen, D. W., Hartmann, M., Yildiz, I., Janowski, R., Lange, B., et al. (2021). UGT76B1, a promiscuous hub of small molecule-based immune signaling, glucosylates N-hydroxypipecolic acid and controls basal pathogen defense. *Plant Cell* 33, 714–734. doi: 10.1093/plcell/koaa044

Bent, A. F., and Mackey, D. (2007). Elicitors, effectors, and R genes, the new paradigm and a lifetime supply of questions. *Ann. Rev. Phytopathol.* 45, 399–436. doi: 10.1146/annurev.phyto.45.062806.094427

Blée, E. (2002). Impact of phyto-oxylipins in plant defense. *Trends Plant Sci.* 7, 315–322. doi: 10.1016/S1360-1385(02)02290-2

Chaikam, V., Negeri, A., Dhawan, R., Puchaka, B., Ji, J., Chintamanani, S., et al. (2011). Use of mutant-assisted gene identification and characterization (MAGIC) to identify novel genetic loci that modify the maize hypersensitive response. *Theoret. Appl. Genet.* 123, 985–997. doi: 10.1007/s00122-011-1641-5

Chakraborty, J., Ghosh, P., and Das, S. (2018). Autoimmunity in plants. *Planta* 248, 751–767. doi: 10.1007/s00425-018-2956-0

Chen, W., Gong, L., Guo, Z., Wang, W., Zhang, H., Liu, X., et al. (2013). A novel integrated method for large-scale detection, identification, and quantification of widely targeted metabolites, application in the study of rice metabolomics. *Mol. Plant* 6, 1769–1780. doi: 10.1093/mp/sst080

Chintamanani, S., Hulbert, S. H., Johal, G. S., and Balint-Kurti, P. J. (2010). Identification of a maize locus that modulates the hypersensitive defense response, using mutant-assisted gene identification and characterization. *Genetics* 184, 813–825. doi: 10.1534/genetics.109.111880

Coll, N. S., Vercammen, D., Smidler, A., Clover, C., Van Breusegem, F., Dangl, J. L., et al. (2010). Arabidopsis type I metacaspases control cell death. *Science* 330, 1393–1397. doi: 10.1126/science.1194980

Cui, H., Gobbato, E., Kracher, B., Qiu, J., Bautor, J., and Parker, J. E. (2017). A core function of EDS1 with PAD4 is to protect the salicylic acid defense sector in Arabidopsis immunity. *New Phytol.* 213, 1802–1817. doi: 10.1111/nph.14302

Cui, H., Tsuda, K., and Parker, J. E. (2015). Effector-triggered immunity, from pathogen perception to robust defense. *Ann. Rev. Plant Biol.* 66, 487–511. doi: 10.1146/annurev-arplant-050213-040012

Davoine, C., Falletti, O., Douki, T., Iacazio, G., Ennar, N., Montillet, J. L., et al. (2006). Adducts of oxylipin electrophiles to glutathione reflect a 13 specificity of the downstream lipoxygenase pathway in the tobacco hypersensitive response. *Plant Physiol.* 140, 1484–1493. doi: 10.1104/pp.105.074690

Dempsey, D. M. A., Vlot, A. C., Wildermuth, M. C., and Klessig, D. F. (2011). Salicylic acid biosynthesis and metabolism. *Arabidopsis Book* 9:e0156. doi: 10.1199/tab.0156

Dewdney, J., Reuber, T. L., Wildermuth, M. C., Devoto, A., Cui, J., Stutius, L. M., et al. (2000). Three unique mutants of Arabidopsis identify eds loci required for limiting growth of a biotrophic fungal pathogen. *Plant J.* 24, 205–218. doi: 10.1046/j.1365-313x.2000.00870.x

Ding, Y., Sun, T., Ao, K., Peng, Y., Zhang, Y., Li, X., et al. (2018). Oppositeroles of salicylic acid receptors NPR1 and NPR3/NPR4 in transcriptional regulation of plant immunity. *Cell* 173, 1454–1467. doi: 10.1016/j.cell.2018.03.044

Dong, O. X., Meteignier, L. V., Plourde, M. B., Ahmed, B., Wang, M., Jensen, C., et al. (2016). Arabidopsis TAF15b localizes to RNA processing bodies and contributes to *snc1*-mediated autoimmunity. *Mol. Plant Microbe Interact.* 29, 247–257. doi: 10.1094/MPMI-11-15-0246-R

Etalo, D. W., Stulemeijer, I. J., van Esse, H. P., de Vos, R. C., Bouwmeester, H. J., and Joosten, M. H. (2013). System-wide hypersensitive response-associated transcriptome and metabolome reprogramming in tomato. *Plant Physiol.* 162, 1599–1617. doi: 10.1104/pp.113.217471

Fayos, J., Bellés, J. M., López-Gresa, M. P., Primo, J., and Conejero, V. (2006). Induction of gentisic acid 5-O-beta-D-xylopyranoside in tomato and cucumber plants infected by different pathogens. *Phytochemistry* 67, 142–148. doi: 10.1016/j.phytochem.2005.10.014

Fu, Z. Q., and Dong, X. (2013). Systemic acquired resistance, turning local infection into global defense. *Ann. Rev. Plant Biol.* 64, 839–863. doi: 10.1146/annurev-arplant-042811-105606

Gallego-Giraldo, L., Escamilla-Trevino, L., Jackson, L. A., and Dixon, R. A. (2011). Salicylic acid mediates the reduced growth of lignin down-regulated plants. *Proc. Natl. Acad. Sci. U. S. A.* 108, 20814–20819. doi: 10.1073/pnas.1117873108

Gao, X., Brodhagen, M., Isakeit, T., Brown, S. H., Göbel, C., Betran, J., et al. (2009). Inactivation of the lipoxygenase ZmLOX3 increases susceptibility of maize to *Aspergillus* spp. *Mol. Plant Microbe Interact.* 22, 222–231. doi: 10.1094/MPMI-22-2-0222

Gao, Z., Chung, E. H., Eitas, T. K., and Dangl, J. L. (2011). Plant intracellular innate immune receptor resistance to *Pseudomonas syringae*pv. *maculicola*1 (RPM1) is activated at, and functions on, the plasma membrane. *Proc. Natl. Acad. Sci. U. S. A.* 108, 7619–7624. doi: 10.1073/pnas.1104410108

George Thompson, A. M., Iancu, C. V., Neet, K. E., Dean, J. V., and Choe, J. Y. (2017). Differences in salicylic acid glucose conjugations by UGT74F1 and UGT74F2 from *Arabidopsis thaliana*. *Sci. Rep.* 7:46629. doi: 10.1038/srep46629

Gobel, C., Feussner, I., and Rosahl, S. (2003). Lipid peroxidation during the hypersensitive response in potato in the absence of 9-lipoxygenases. *J. Biol. Chem.* 278, 52834–52840. doi: 10.1074/jbc.M310833200

Gobel, C., Feussner, I., Schmidt, A., Scheel, D., Sanchez-Serrano, J., Hamberg, M., et al. (2001). Oxylipin profiling reveals the preferential stimulation of the 9-Lipoxygenase pathway in elicitor-treated potato cells. *J. Biol. Chem.* 276, 6267–6273. doi: 10.1074/jbc.M008606200

He, J., Liu, Y., Yuan, D., Duan, M., Liu, Y., Shen, Z., et al. (2020). An R2R3 MYB transcription factor confers brown planthopper resistance by regulating the phenylalanine ammonia-lyase pathway in rice. *Proc. Natl. Acad. Sci. U. S. A.* 117, 271–277. doi: 10.1073/pnas.1902771116

Holmes, E. C., Chen, Y. C., Mudgett, M. B., and Sattely, E. S. (2021). Arabidopsis UGT76B1 glycosylates N-hydroxy-pipecolic acid andinactivates systemic acquired resistance in tomato. *Plant Cell* 33, 75–765. doi: 10.1093/plcell/koaa052

Hong, Y., Ni, S. J., and Zhang, G. P. (2020). Transcriptome and metabolome analysis reveals regulatory networks and key genes controlling barley malting quality in responses to drought stress. *J. Biol. Chem.* 152, 1–11. doi: 10.1016/j.plaphy.2020.04.029

Huang, X. X., Zhu, G. Q., Liu, Q., Chen, L., Li, Y. J., and Hou, B. K. (2018). Modulation of plant salicylic acid-associated immune responses *via* glycosylation of dihydroxybenzoicacids. *Plant Physiol.* 176, 3103–3119. doi: 10.1104/pp.17.01530

Hulbert, S. H. (1997). Structure and evolution of the rp1 complex conferring rust resistance in maize. *Ann. Rev. Phytopathol.* 35, 293–310. doi: 10.1146/annurev.phyto.35.1.293

Jakoby, M., Weisshaar, B., Droge-Laser, W., Vicente-Carbajosa, J., Tiedemann, J., Kroj, T., et al. (2002). bZIP transcription factors in Arabidopsis. *Trends Plant Sci.* 7, 106–111. doi: 10.1016/S1360-1385(01)02223-3

Kaminaka, H., Nake, C., Epple, P., Dittgen, J., Schutze, K., Chaban, C., et al. (2006). bZIP10-LSD1 antagonism modulates basal defense and cell death in Arabidopsis following infection. *EMBO J.* 25, 4400–4411. doi: 10.1038/sj.emboj.7601312

Kamoun, S., van West, P., Vleeshouwers, V. G., de Groot, K. E., and Govers, F. (1998). Resistance of *nicotianabenthamiana* to phytophthorainfestans is mediated by the recognition of the elicitor protein INF1. *Plant Cell* 10, 1413–1426. doi: 10.1105/tpc.10.9.1413

Kanehisa, M., Furumichi, M., Tanabe, M., Sato, Y., and Morishima, K. (2017). KEGG, new perspectives on genomes, pathways, diseases and drugs. *Nucl. Acids Res.* 45, D353–D361. doi: 10.1093/nar/gkw1092

Kawasaki, T., Koita, H., Nakatsubo, T., Hasegawa, K., Wakabayashi, K., Takahashi, H., et al. (2006). Cinnamoyl-CoA reductase, a key enzyme in lignin

biosynthesis, is an effector of small GTPaseRac in defense signaling in rice. *Proc. Natl. Acad. Sci. U. S. A*. 103, 230–235. doi: 10.1073/pnas.0509875103

Kim, D., Langmead, B., and Salzberg, S. L. (2015). HISAT, a fast-spliced aligner with low memory requirements. *Nat. Method*. 12, 357–360. doi: 10.1038/nmeth.3317

Kim, S. B., Van den, B. L., Karre, S., Choi, H., Christensen, S. A., Wang, G.-F., et al. (2021). Analysis of the transcriptomic, metabolomic and gene-regulatoryresponses to *Pucciniasorghi* in maize. *Mol. Plant Pathol*. 22, 465–479. doi: 10.1111/mpp.13040

Kong, Q., Qu, N., Gao, M., Zhang, Z., Ding, X., Yang, F., et al. (2012). TheMEKK1-MKK1/MKK2-MPK4 kinase cascade negatively regulates immunity mediated by a mitogen-activated protein kinasekinasekinase in Arabidopsis. *Plant Cell* 24, 2225–2236. doi: 10.1105/tpc.112.097253

Kourelis, J., and van der Hoorn, R. A. L. (2018). Defended to the nines, 25 years of resistance gene cloning identifies nine mechanisms for R protein function. *Plant Cell* 30, 285–299. doi: 10.1105/tpc.17.00579

Lacomme, C., and Santa Cruz, S. (1999). Bax-induced cell death in tobacco is similar to the hypersensitive response. *Proc. Natl. Acad. Sci. U. S. A*. 96, 7956–7961. doi: 10.1073/pnas.96.14.7956

Li, S., Dong, X., Fan, G., Yang, Q., Shi, J., Wei, W., et al. (2018). Comprehensive profiling and inheritance patterns of metabolites in foxtail millet. *Front. Plant Sci*. 9:1716. doi: 10.3389/fpls.2018.01716

Li, Y., Li, P., Wang, Y., Dong, R., Yu, H., and Hou, B. (2014). Genome-wide identification and phylogenetic analysis of Family-1 UDP glycosyltransferases in maize (*Zea mays*). *Planta* 239, 1265–1279. doi: 10.1007/s00425-014-2050-1

Liang, X., and Zhou, J. M. (2018). Receptor-like cytoplasmic kinases,central players in plant receptor kinase-mediated signaling. *Ann. Rev. Plant Biol*. 69, 267–299. doi: 10.1146/annurev-arplant-042817-040540

Liu, M., Li, Y.-J., Zhu, Y.-X., Sun, Y., and Wang, G.-F. (2021). Maize nicotinate N-methyltransferase interacts with the NLR protein Rp1-D21 and modulates the hypersensitive response. *Mol. Plant Pathol.* 22,564–579. doi: 10.1111/mpp.13044

Liu,.Y., Guo, Y., Ma, C., Zhang, D., Wang, C., and Yang,.Q. (2016). Transcriptome analysis of maize resistance to *Fusariumgraminearum*. *BMC Genom*. 17:477. doi: 10.1186/s12864-016-2780-5

Love, M. I., Huber, W., and Anders, S. (2014). Moderated estimation of fold change and dispersion for RNA-seq data with DESeq2. *Genome Biol*. 15:550. doi: 10.1186/s13059-014-0550-8

Luan, Q.-L., Zhu, Y.-X., Ma, S., Sun, Y., Liu, X. Y., Liu, M., et al. (2021). Maize metacaspases modulate the defense response mediated by the NLR protein Rp1-D21 likely by affecting its subcellular localization. *Plant J*. 105, 151–166. doi: 10.1111/tpj.15047

Martin, K., Kopperud, K., Chakrabarty, R., Banerjee, R., Brooks, R., and Goodin, M. M. (2009). Transient expression in *Nicotianabenthamiana* fluorescent marker lines provides enhanced definition of protein localization, movement andinteractions in planta. *Plant J*. 59, 150–162. doi: 10.1111/j.1365-313X.2009.03850.x

McHale, L., Tan, X., Koehl, P., and Michelmore, R. W. (2006). Plant NBS-LRR proteins, adaptable guards. *Genome Biol*. 7:212. doi: 10.1186/gb-2006-7-4-212

Mo, X., Zhang, M., Liang, C., Cai, L., and Tian, J. (2019). Integration of metabolome and transcriptome analyses highlights soybean roots responding to phosphorus deficiency by modulating phosphorylated metabolite processes. *J. Biol. Chem*. 139, 697–706. doi: 10.1016/j.plaphy.2019.04.033

Mohnike, L., Rekhter, D., Huang, W., Feussner, K., Tian, H., Herrfurth, C., et al. (2021). Theglycosyltransferase UGT76B1 modulates N-hydroxy-pipecolic acid homeostasis andplant immunity. *Plant Cell* 33, 735–749. doi: 10.1093/plcell/koaa045

Monteiro, F., and Nishimura, M. T. (2018). Structural, functional, and genomic diversity of plant NLR proteins,An evolved resource for rational engineering of plant immunity. *Ann. Rev. Phytopathol*. 56, 243–267. doi: 10.1146/annurev-phyto-080417-045817

Morris, S. W., Vernooij, B., Titatarn, S., Starrett, M., Thomas, S., Wiltse, C. C., et al. (1998). Induced resistance responses in maize. *Mol. Plant Microbe Interact*. 11, 643–658. doi: 10.1094/MPMI.1998.11.7.643

Mosblech, A., Feussner, I., and Heilmann, I. (2009). Oxylipins, structurally diverse metabolites from fatty acid oxidation. *Plant Physiol. Biochem*. 47, 511–517. doi: 10.1016/j.plaphy.2008.12.011

Murphree, C., Kim, S. B., Karre, S., Samira, R., and Balint-Kurti, P. (2020). Use of virus-induced gene silencing to characterize genes involved in modulating hypersensitive cell death in maize. *Mol. Plant Pathol*. 21, 1662–1676. doi: 10.1111/mpp.12999

Negeri, A., Wang, G. F., Benavente, L., Kibiti, C. M., Chaikam, V., Johal, G., et al. (2013). Characterization of temperature and light effects on the defense response phenotypes associated with the maize Rp1-D21 autoactive resistance gene. *BMC Plant Biol*. 13:106. doi: 10.1186/1471-2229-13-106

Ngou, B. P. M., Ahn, H.-K., Ding, P., and Jones, J. D. G. (2021). Mutual potentiation of plant immunity by cell-surface and intracellular receptors. *Nature* 592, 110–115. doi: 10.1038/s41586-021-03315-7

Noutoshi, Y., Okazaki, M., Kida, T., Nishina, Y., Morishita, Y., Ogawa, T., et al. (2012). Novel plant immune-priming compounds identified *via* high-throughput chemical screening target salicylic acid glucosyltransferases in Arabidopsis. *Plant Cell* 24, 3795–3804. doi: 10.1105/tpc.112.098343

Olukolu, B. A., Wang, G.-F., Vontimitta, V., Venkata, B. P., Marla, S., Ji, J., et al. (2014). A genome-wide association study of the maize hypersensitive defense response identifies genes that cluster in related pathways. *PLoS Genet*. 10:e1004562. doi: 10.1371/journal.pgen.1004562

Pandey, S. P., and Somssich, I. E. (2009). The role of WRKY transcription factors in plant immunity. *Plant Physiol*. 150, 1648–1655. doi: 10.1104/pp.109.138990

Peng, Y., Yang, J., Li, X., and Zhang, Y. (2021). Salicylic acid: biosynthesis and signaling. *Annu. Rev. Plant Biol.* 72, 761–791. doi: 10.1146/annurev-arplant-081320-092855

Prost, I., Dhondt, S., Rothe, G., Vicente, J., Rodriguez, M. J., Kift, N., et al. (2005). Evaluation of the antimicrobial activities of plant oxylipins supports theirinvolvement in defense against pathogens. *Plant Physiol*. 139, 1902–1913. doi: 10.1104/pp.105.066274

Radojicic, A., Li, X., and Zhang, Y. (2018). Salicylic acid: a double-edged sword for programed cell death in plants. *Front. Plant Sci.* 9:1133. doi: 10.3389/fpls.2018.01133

Ranjan, A., Westrick, N. M., Jain, S., Piotrowski, J. S., Ranjan, M., Kessens, R., et al. (2019). Resistance against *Sclerotiniasclerotiorum* in soybean involves a reprogramming of the phenylpropanoid pathway and up-regulation of antifungal activity targeting ergosterol biosynthesis. *Plant Biotechnol. J*. 17, 1567–1581. doi: 10.1111/pbi.13082

Robinson, M. D., McCarthy, D. J., and Smyth, G. K. (2010). edgeR, a Bioconductor package for differential expression analysis of digital gene expression data. *Biogeosciences* 26, 139–140. doi: 10.1093/bioinformatics/btp616

Senthil-Kumar, M., Hema, R., Suryachandra, T. R., Ramegowda, H. V., Gopalakrishna,.R., Rama, N., et al. (2010). Functional characterization of three water deficit stress-induced genes in tobacco and Arabidopsis, an approach based on gene down regulation. *J. Biol. Chem*. 48, 35–44. doi: 10.1016/j.plaphy.2009.09.005

Smith, S., Steinau, M., Trick, H., and Hulbert, S. (2010). Recombinant Rp1 genes confer necrotic or nonspecific resistance phenotypes. *Mol. Genet. Genom*. 283, 591–602. doi: 10.1007/s00438-010-0536-5

Sudupak, M. A., Bennetzen, J. L., and Hulbert, S. H. (1993). Unequal exchange and meiotic instability of disease-resistance genes in the Rp1 region of maize. *Genetics* 133, 119–125. doi: 10.1093/genetics/133.1.119

Sun, Q., Collins, N., Ayliffe, M., Smith, S. M., Drake, J., Pryor, T., et al. (2001). Recombination between paralogues at the rp1 rust resistance locus in maize. *Genetics* 158, 423–438. doi: 10.1093/genetics/158.1.423

Sun, Y., Zhu, Y. X., Balint-Kurti, P. J., and Wang, G.-F. (2020). Fine-tuning immunity, players and regulators for plant NLRs. *Trends Plant Sci*. 25, 695–713. doi: 10.1016/j.tplants.2020.02.008

Tamura, K., Stecher, G., Paterson, D., Filipski, A., and Kumar, S. (2007). Mega6, molecular evolutionary genetics analysis software version 6.0. *Mol. Biol. Evol*. 24, 1596–1599. doi: 10.1093/molbev/msm092

Usadel, B., Poree, F., Nagel, A., Lohse, M., Czedik-Eysenberg, A., and Stitt, M. (2009). A guide to using MapMan to visualize and compare omics data in plants, a case study in the crop species, Maize. *Plant Cell Environ*. 32, 1211–1229. doi: 10.1111/j.1365-3040.2009.01978.x

Vellosillo, T., Martinez, M., Lopez, M., Vicente, J., Cascon, T., Dolan, L., et al. (2007). Oxylipins produced by the 9-lipoxygenase pathway in Arabidopsis regulate lateral root development and defense responses through a specific signaling cascade. *Plant Cell* 19, 831–846. doi: 10.1105/tpc.106.046052

Vicente, J., Cascón, T., Vicedo, B., García-Agustín, P., Hamberg, M., and Castresana, C. (2012). Role of 9-Lipoxygenase and α-Dioxygenaseoxylipin

pathways as modulators of local and systemic defense. *Mol. Plant* 5, 914–928. doi: 10.1093/mp/ssr105

Vlot, A. C., Dempsey, D. M. A., and Klessig, D. F. (2009). Salicylic acid, a multifacetedhormone to combat disease. *Ann. Rev. Phytopathol.* 47, 177–206. doi: 10.1146/annurev.phyto.050908.135202

Wang, G.-F., He, Y., Strauch, R., Olukolu, B. A., Nielsen, D., Li, X., et al. (2015b). Maize homologs of hydroxycinnamoyltransferase, a key enzyme in lignin biosynthesis, bind the nucleotide binding leucine-rich repeat Rp1 proteins to modulate the defense response. *Plant Physiol.* 169, 2230–2243. doi: 10.1104/pp.15.00703

Wang, G.-F., Ji, J., Ei-Kasmi, F., Dangl, J. L., Johal, G., and Balint-Kurti, P. J. (2015a). Molecular and functional analyses of a maize autoactive NB-LRR protein identify precise structural requirements for activity. *PLoS Pathog.* 11:e1004674. doi: 10.1371/journal.ppat.1004674

Wang, G. F., and Balint-Kurti, P. J. (2016). Maize homologs of CCoAOMT and HCT, two key enzymes in lignin biosynthesis, form complexes with the NLR Rp1 protein to modulate the defense response. *Plant Physiol.* 171, 2166–2177. doi: 10.1104/pp.16.00224

Wang, G. F., Seabolt, S., Hamdoun, S., Ng, G., Park, J., and Lu, H. (2011). Multiple roles of WIN3 in regulating disease resistance, cell death, and flowering time in Arabidopsis. *Plant Physiol.* 156, 1508–1519. doi: 10.1104/pp.111.176776

Wasternack, C. (2007). Jasmonates, an update on biosynthesis, signal transduction and action in plant stress response, growth and development. *Ann. Bot.* 4, 681–697. doi: 10.1093/aob/mcm079

Yang, Q., He, Y., Kabahuma, M., Chaya, T., Kelly, A., Borrego, E., et al. (2017). A gene encoding maize caffeoyl-CoA O-methyltransferase confers quantitative resistance to multiple pathogens. *Nat. Genet.* 49, 1364–1372. doi: 10.1038/ng.3919

Ye, W., Liu, T., Zhang, W., Li, S., Zhu, M., Li, H., et al. (2019). Disclosure of the molecular mechanism of wheat leaf spot disease caused by bipolarissorokiniana through comparative transcriptome and metabolomics analysis. *Int. J. Mol. Sci.* 20:6090. doi: 10.3390/ijms20236090

Yuan, M., Jiang, Z., Bi, G., Nomura, K., Liu, M., Wang, Y., et al. (2021). Pattern-recognition receptors are required for NLR-mediatedplant immunity. *Nature* 592, 105–109. doi: 10.1038/s41586-021-03316-6

Zavaliev, R., Mohan, R., Chen, T., and Dong, X. (2020). Formation of NPR1 condensates promotes cell survival during the plant immune response. *Cell* 182, 1093–1108 e1018. doi: 10.1016/j.cell.2020.07.016

Zeilmaker, T., Ludwig, N. R., Elberse, J., Seidl, M. F., Berke, L., Van Doorn, A., et al. (2015). Downy Mildew Resistant 6 and DMR6-Like Oxygenase 1 are partially redundant but distinct suppressors of immunity in Arabidopsis. *Plant J.* 81, 210–222. doi: 10.1111/tpj.12719

Zhang, Y., Zhao, L., Zhao, J., Li, Y., Wang, J., Guo, R., et al. (2017). S5H/DMR6 encodes a salicylic acid 5-hydroxylase that fine-tunes salicylic acid homeostasis. *Plant Physiol.* 175, 1082–1093. doi: 10.1104/pp.17.00695

Zheng, X., Zhou, M., Yoo, H., Pruneda-Paz, J., Spivey, N., Kay, S., et al. (2015). Spatial and temporal regulation of biosynthesis of the plant immune signal salicylic acid. *Proc. Natl. Acad. Sci. U. S. A.* 112, 9166–9173. doi: 10.1073/pnas.1511182112

Zhou, J. M., and Zhang, Y. (2020). Plant immunity, danger perception and signaling. *Cell* 181, 978–989. doi: 10.1016/j.cell.2020.04.028

Zhou, P., Li, Z., Magnusson, E., Gomez Cano, F., Crisp, P. A., Noshay, J. M., et al. (2020). Meta gene regulatory networks in maize highlight functionally relevant regulatory interactions. *Plant Cell* 32, 1377–1396. doi: 10.1105/tpc.20.00080

Zhu, Y. X., Ge, C., Ma, S., Liu, X. Y., Liu, M., Sun, Y., et al. (2020). Maize ZmFNSI homologs interact with an NLR protein to modulate hypersensitive response. *Int. J. Mol. Sci.* 21:2529. doi: 10.3390/ijms21072529

Conflict of Interest: The authors declare that the research was conducted in the absence of any commercial or financial relationships that could be construed as a potential conflict of interest.

Publisher's Note: All claims expressed in this article are solely those of the authors and do not necessarily represent those of their affiliated organizations, or those of the publisher, the editors and the reviewers. Any product that may be evaluated in this article, or claim that may be made by its manufacturer, is not guaranteed or endorsed by the publisher.

frontiers in Plant Science

ORIGINAL RESEARCH
published: 25 October 2021
doi: 10.3389/fpls.2021.754823

Functional Verification of Two Genes Related to Stripe Rust Resistance in the Wheat-*Leymus mollis* Introgression Line M8664-3

Pengfei Jin[1†], *Kaixiang Chao*[1,2†], *Juan Li*[1,3], *Zihao Wang*[1], *Peng Cheng*[1], *Qiang Li*[1*] and *Baotong Wang*[1*]

[1] State Key Laboratory of Crop Stress Biology for Arid Areas, College of Plant Protection, Northwest A&F University, Yangling, China, [2] College of Chemistry, Biology and Environment, Yuxi Normal University, Yuxi, China, [3] Dingxi Plant Protection and Quarantine Station, Dingxi, China

OPEN ACCESS

Edited by:
Xiaodong Wang,
Agricultural University of Hebei, China

Reviewed by:
Yuheng Yang,
Southwest University, China
Meinan Wang,
Washington State University, United States

***Correspondence:**
Baotong Wang
wangbt@nwsuaf.edu.cn
Qiang Li
qiangli@nwsuaf.edu.cn

[†]These authors have contributed equally to this work and share first authorship

Specialty section:
This article was submitted to Plant Pathogen Interactions, a section of the journal Frontiers in Plant Science

Received: 07 August 2021
Accepted: 24 September 2021
Published: 25 October 2021

Citation:
Jin P, Chao K, Li J, Wang Z, Cheng P, Li Q and Wang B (2021) Functional Verification of Two Genes Related to Stripe Rust Resistance in the Wheat-Leymus mollis Introgression Line M8664-3. Front. Plant Sci. 12:754823. doi: 10.3389/fpls.2021.754823

Stripe rust, caused by *Puccinia striiformis* f. sp. *tritici* (*Pst*), is one of the most widespread and destructive fungal diseases of wheat worldwide. The cultivation and growth of resistant wheat varieties are the most economical, effective, and environmental friendly methods to control stripe rust. Therefore, it is necessary to use new resistance genes to breed resistant wheat varieties. A single dominant gene temporarily designated as *YrM8664-3*, from a wheat-*Leymus mollis* introgression line M8664-3 highly resistant to Chinese predominant *Pst* races, is a potentially valuable source of stripe rust resistance for breeding. Herein, based on previous *YrM8664-3* chromosome location results (bin 4AL13-0.59-0.66 close to 4AL12-0.43-0.59) and expression change information of candidate genes and bioinformatics analysis, several candidate genes with significantly different expression changes were then selected and verified by virus-induced gene silencing (VIGS). Two of the candidate genes temporarily designated as *TaFBN* [containing plastid lipid-associated proteins (PAP)_fibrillin domain in its protein] and *Ta_Pes_BRCT* [containing Pescadillo and breast cancer tumour suppressor protein C-terminus (BRCT) domain in its protein], produced the most significant resistance changes in the wheat-*Pst* interaction system after silencing. These two genes were further verified by *Agrobacterium*-mediated wheat genetic transformation technology. According to the identification of disease resistance, the resistance function of the candidate gene *TaFBN* was further verified. Then, the expression of *TaFBN* under hormone treatment indicated that *TaFBN* may be related to the salicylic acid (SA) and abscisic acid (ABA) signaling pathways. Combined with the expression of *TaFBN* in response to environmental stress stimulation, it can be reasonably speculated that *TaFBN* plays an important role in the resistance of wheat to *Pst* and is involved in abiotic stress pathways.

Keywords: functional verification, stripe rust, resistance, wheat-*Leymus mollis*, *YrM8664-3*

INTRODUCTION

Wheat (*Triticum aestivum* L.) is one of the most important food crops in the world. Wheat stripe rust, caused by *Pst*, is one of the most important diseases that affects wheat production. It has the characteristics of rapid outbreaks that cause regional epidemics and subsequent extensive and severe harm to wheat crops, and it has been found in almost all major wheat-producing areas in the world. When wheat is susceptible to *Pst* infection, the yield loss is ∼10–20%, but it can exceed 50% or even result in no harvest in severe cases (Wan et al., 2007). Since the 1950s, several nationwide stripe rust epidemics have been recorded in China, among which, a yield loss of 6, 3.2, 2.65, and 1.3 billion kg of wheat occurred in 1950, 1964, 1990, and 2002, respectively (Wan et al., 2004). In 2017, wheat stripe rust was once again epidemic throughout China, affecting an area of 5.56 million hm^2, which was the largest annual occurrence since 2002 (Huang et al., 2018). The most effective, economical, and environmental friendly method to control stripe rust is to breed and grow disease-resistant wheat varieties.

Disease resistance in wheat varieties, like all plants, often depends on pattern-triggered immunity (PTI) brought about by microbial patterns *via* pattern-recognition receptors (PRRs) localized on cell surfaces, and effector-triggered immunity (ETI) activated by pathogen effector proteins *via* predominantly intracellular localized receptors called nucleotide-binding, leucine-rich repeat receptors (NLRs) (Jones and Dangl, 2006; Cui et al., 2015; Yu et al., 2017; Yuan et al., 2021). The disease resistance reaction produced by plants is a complex and orderly process, and is also regulated by multiple genes, especially resistance (R) genes (Jia et al., 2000; Dodds et al., 2006; Luo et al., 2011).

By analyzing protein sequences encoded by cloned R genes, it was found that R genes targeted at different sources and pathogens possessed similar characteristic domains, such as nucleotide binding site (NBS), leucine-rich repeat (LRR), toll-interleukin-1 receptor (TIR), coiled-coil (CC), protein kinase (PK), and the transmembrane domain (TM) (Jones et al., 2016; Monteiro and Nishimura, 2018; Ma et al., 2020). In addition, plant disease resistance is closely related to hormone signal transduction and environmental stress stimulation (Denance et al., 2013; Derksen et al., 2013). At present, salicylic acid (SA), jasmonic acid (JA), ethylene (ET), abscisic acid (ABA), and other signaling molecules involved in plant disease resistance have been extensively studied (Schenk et al., 2000; Denance et al., 2013; Derksen et al., 2013). Therefore, studies on plant disease resistance genes will assist in expanding our understanding of the mechanism of resistance at a deeper level, and will provide some reference for disease control.

Histopathological studies on the interaction between wheat and *Pst* are the basis for revealing the detailed process of *Pst* infection and host resistance. Kang et al. (2002) found that the growth of a pathogenic fungus was inhibited in resistant varieties compared with that in susceptible varieties. Reactive oxygen species (ROS) bursting is one of the fastest and most effective disease resistance reactions in the interaction between plants and their pathogens. By dyeing leaf tissues with diaminobenzidine (DAB), Wang et al. (2007) found that ROS were produced in guard cells of both compatible and incompatible combinations after the interaction. In terms of biochemistry, the resistance of wheat varieties to *Pst* is mainly reflected in protective enzymes, such as superoxide dismutase (SOD) and phenylalanine ammonia-lyase (PAL), as well as the increase in activities of defensive enzymes, such as antimicrobial hydrolase and chitinase, and the increase in resistant proteins and lignin in host cell walls (Asthir et al., 2011; Zheng et al., 2020).

Virus-induced gene silencing is an RNA interference-based technology that transiently knocks down a target gene expression using modified plant viral genomes. When a targeted gene is inserted into a viral genome and a plant is inoculated with viruses, plant cells recognize the threat of the invading viruses and use protective defense mechanisms to destroy any foreign genes carried by viruses and viral vectors. Loss of function phenotype or decreased expression activity of the target gene occurs, and then the function of the target gene can be identified according to phenotypic changes (Scofield et al., 2005; Feng et al., 2015).

The identification of wheat disease-resistance genes and studies on disease-resistance mechanisms are the basis of wheat disease-resistance breeding and disease control. M8664-3 is the hybrid offspring of common wheat cultivar 7182 and wheat-related species *Leymus mollis* (Trin) Hara. Our previous studies have shown that the dominant gene *YrM8664-3* in M8664-3 confers all-stage resistance to Chinese prevalent *Pst* race CYR33. *YrM8664-3* was located in bin 4AL13-0.59-0.66 close to 4AL12-0.43-0.59 on chromosome 4AL and flanked by single-nucleotide polymorphism markers *AX111655681* and *AX109496237* with genetic distances of 5.3 and 2.3 centimorgans, respectively (Chao et al., 2018). However, because of the alien chromosome fragment that may exist in the *YrM8664-3* region, it is difficult to further finely map and clone the gene. The sequencing of the entire genome of wheat variety Chinese Spring has been completed, making it possible to identify candidate genes and perform functional verification analysis of *YrM8664-3* in the reference genome region corresponding to the located chromosome interval.

To identify the candidate genes involved in stripe rust resistance in M8664-3, in this study, the resistance of M8664-3 to CYR33 was investigated and then analyzed. Combined with histological and histochemical techniques, the invasion and infection processes of CYR33 on M8664-3 were studied in detail, and the resistance process of M8664-3 to CYR33 was comprehensively analyzed. Based on the physical location of *YrM8664-3*, the genes related to disease resistance were selected from the annotated database of the Chinese Spring genome according to the structure domains related to disease resistance and function prediction information. Then, a functional validation analysis was carried out to identify the disease-resistant genes. The finding in this study could provide a basis for wheat stripe rust resistance breeding.

MATERIALS AND METHODS

Plants and Pathogens

The wheat-*Leymus mollis* introgression line M8664-3 used in this study was provided by Professor Jie Fu, College of Agronomy, Northwest A&F University, Yangling, China.

Chinese predominate *Pst* race CYR33 was used for seedling tests. After the identification on differential hosts of Chinese *Pst*, CYR33 was increased in susceptible variety Mingxian169.

Seedling Tests, RNA Extraction

Seedling tests were conducted under controlled greenhouse conditions according to Wan et al. (2007) and Bansal et al. (2017). M8664-3 and Mingxian 169 were planted in 7 7 7 cm pots with 15–20 seeds per pots. When the first leaves fully expanded, fresh CYR33 urediniospores were inoculated onto wheat leaves by the smear method, and sterile water was used as MOCK-inoculation control (Roelfs et al., 1992). Approximately 14–16 days post inoculation (dpi), when obvious uredinia were observed on the leaves of Mingxian169, the types of infection types were recorded according to a 0–9 scale. Also, leaf samples were collected at 0, 12, 24, 48, 72, and 96 h post inoculation (hpi). RNA extraction was performed using a Magen plant total RNA extraction kit (Magen Biotech, Guangzhou, China). The concentration and purity of each RNA sample were evaluated using a micro-ultraviolet spectrophotometer (NanoDrop 2000; Thermo Fisher Scientific, Wilmington, DE, United States), and the integrity was determined by 1% agarose gel electrophoresis. The first strand of DNA was synthesized with HiScript II Q-RT SuperMix for qPCR (+ gDNA wiper) (Vazyme Biotech, Nanjing, China).

Candidate Gene Selection and Quantitative Real-Time PCR (Qrt-PCR) Analysis

The sequence of the linked markers of *YrM8664-3* was blasted against the genome sequence of Chinese Spring IWGSC RefSeq v1.0 Genome (IWGSC et al., 2018) (https://wheat-urgi.versailles.inra.fr/Seq-Repository/Assemblies), and the gene was located in the range of 41.6×10^7-63.9×10^7 bp (base pair) on wheat chromosome 4AL (Chao et al., 2018). Referring to the IWGSC RefSeq v1.0 annotation (https://urgi.versailles.inra.fr/download/iwgsc/IWGSC_RefSeq_Annotations/v1.0/), genes near the linked markers containing conserved domains of disease resistance, such as NBS, LRR, and PK, or genes hit by the linked markers were selected.

To measure the transcriptional expression level of selected genes by qRT-PCR, specific primers (**Supplementary Table 1**) were designed using the Primer Premier 5.0 software (Li et al., 2011). Using *TaEF-1α* (GenBank accession number Q03033) as an internal reference gene, the relative transcription expression level of target genes was determined. All the qRT-PCR reactions were performed in a 20-μl reaction mixture containing 10 μl Cham Q™ SYBR® qPCR Master Mix (Vazyme Biotech, Nanjing, China), 0.2 μl each of the forward and reverse gene-specific primers (10 μM), and 2 μl of diluted cDNA (1:10). A Bio-Rad iQ5 Real Time PCR (Bio-Rad, Hercules, CA, United States) system was used to generate cycle threshold (CT) values for the quantification of relative gene expression using the comparative $2^{-\Delta\Delta Ct}$ method (Livak and Schmittgen, 2001). All the samples were analyzed in three biological replications, and all the PCR analyses were replicated three times.

Sequence Amplification, Identification, and Bioinformatics Analysis

According to the primers (**Supplementary Table 2**) at the positive and negative ends of the open reading frame (ORF) region, the cDNA of M8664-3 was used as the template for amplification with gene-specific primers as follows: pre-denaturation at 94°C for 2 min, followed by 35 cycles of 94°C for 30 s, 60°C for 30 s, and 72°C for 1 min, with a final incubation at 72°C for 2 min. The PCR-amplified products were examined by 1.2% agarose gel electrophoresis. The specific target bands were recovered and sequenced by Tsingke (Xi'an, China).

The online BLAST[1] program from the National Center for Biotechnology Information (NCBI) was used to analyze the cDNA sequence. The amino acid sequence was analyzed with ProtParam[2] and TMPred[3] to detect the primary structure and position information of the polypeptide transmembrane region, respectively. TargetP-2.0[4] and Plant-mPLoc[5] in Cell-PLoc 2.0 were used to predict the subcellular location of the possible protein structure of the amino acid sequence. The conserved domain was identified by Pfam[6] and simple modular architecture research tool (SMART[7]). Multiple sequence alignments were performed using DNAMAN8.0 (Lynnon BioSoft, San Ramon, CA, United States). To reveal phylogenetic relationships and potential functional characteristics of targeted proteins from different species, corresponding proteins were collected from different species according to the domain, namely *Arabidopsis thaliana*, *Oryza sativa*, *Zea mays*, *Brachypodium virgatum*, and *Hordeum vulgare*. The phylogenetic relationship was inferred with the neighbor-joining (NJ) method, and a midpoint rooted base tree was drawn in MEGA 7.0 with 1,000 bootstrap iterations (Kumar et al., 2016).

Virus-Induced Gene Silencing in Wheat

Virus-induced gene silencing, mediated by barley stripe mosaic virus (BSMV), was performed to reveal the function of nine candidate genes during the interaction between wheat M8664-3 and CYR33 (Fitzmaurice et al., 2002; Scofield et al., 2005). The fragment of target gene with *Pac*I and *Not*I was derived from its coding sequence and amplified by RT-PCR (**Supplementary Table 1**) to construct the BSMV:γ plasmid for gene silencing. After amplification of the target gene fragment and vector linearization, the target gene and linearized vector were recombined, connected, linearized with a restriction enzyme, and transcribed *in vitro* (RiboMAX TM Large-Scale RNA Production System-T7 and Ribo m7G Cap Analog; Promega, Madison, WI, United States) to form a recombinant virus containing the target gene (Petty and Jackson, 1990). BSMV:γ was used as a blank control and γ-PDS as a positive control by friction inoculation, and the second leaf of wheat

[1]https://blast.ncbi.nlm.nih.gov/Blast.cgi
[2]https://web.expasy.org/protparam/
[3]http://sbcb.bioch.ox.ac.uk/TM_noj/TM_noj.html
[4]http://www.cbs.dtu.dk/services/TargetP-2.0/
[5]http://www.csbio.sjtu.edu.cn/bioinf/plant-multi/
[6]http://pfam.xfam.org/
[7]http://smart.embl-heidelberg.de/

seedlings was infected with BSMV, with three biological replicates for each gene.

After 24-h incubation in the dark in an artificial climate incubator, the seedlings were placed in a growth chamber at 25°C with 60–80% humidity. When the photo-bleaching phenotype was observed on the BSMV: γ-PDS plants at ∼10 dpi, the fourth leaves of γ-gene silencing plants were inoculated with CYR33. Leaf samples were collected at 0, 24, 48, 96, and 120 hpi for qRT-PCR analysis and histological observation (Li et al., 2011). The infection phenotype of *Pst* was observed at ∼14 dpi.

Histological Observation and Statistical Analysis

Inoculated and control leaves of both *Pst* seedling test and VIGS-induced gene silencing were sampled at different time points for histological observation. For each time point, ∼15 blades were sampled (Ayliffe et al., 2011). The H_2O_2 burst for ROS was observed by DAB (MP Biomedicals, Solon, OH, United States) staining (Xiao et al., 2003; Zou et al., 2018). WGA-Alexa 488 (Invitrogen, Carlsbad, CA, United States) was used to fluorescently stain the *Pst* infestation structure in wheat leaf tissue. The infestation site was determined by the production of germ tubes by *Pst* and the formation of substomatal vesicle in the stomata. For each treatment, 50 infection sites were randomly examined using an Olympus BX-53 microscope (Olympus Corporation, Tokyo, Japan), and the area of ROS, hypha branches, hypha length, and necrotic areas were observed and measured.

The standard error of deviation was calculated using Microsoft Excel. The statistical significance was evaluated by Student's *t* test ($P < 0.05$) using the SPSS software (SPSS, Inc., Chicago, IL, United States).

Wheat Transformation and Functional Verification

Agrobacterium tumefaciens strain EHA105 harboring binary vector, pCAMBIA3301, was used to optimize the transformation system, with ubiquitin promoter and targeted gene replacing cauliflower mosaic virus *35S* promoter and *GUS* gene encoding β-glucuronidase. The ORF of *TaFBN* and *Ta_Pes_BRCT* was amplified separately and inserted into the frame of an expression cassette within the T-DNA region of the pCAMBIA3301 vector digested with *BamHI* and *SpeI*. The construct was verified by DNA sequencing and introduced into *Agrobacterium* EHA105. Then, the *Agrobacterium*-mediated transformation method was applied to genetically transform the target gene (Li et al., 2019). The seeds of 14-day-pollinated immature wheat variety Fielder (scutellum size 1 mm) were treated with 75% alcohol for 30 s and 0.1% HgCl for 10 min, and the immature embryos were then removed with a dissecting needle on an aseptic work table. The immature embryos were infected with the obtained *Agrobacterium*, and then placed on the screening medium and co-cultured in darkness at 23°C for 3 days. Under a microscope, hypocotyls were excised from the contact between the hypocotyl and scutellum of the seeds, and the obtained scutellums were cultured on the screening medium for 14 days. After cutting the callus, a second selection was performed, and the tissue was cultured for 14 days. The healthy callus was transferred to a regeneration medium, and regenerated plantlets were obtained after 7 days. The 786-bp genomic fragment of *TaFBN* and the 1,791-bp genomic fragment of *Ta_Pes_BRCT* were introduced into wheat cultivar Fielder, and the T_0 generation plants were screened with gene-specific primers by PCR amplification under the follow conditions: 1 min pre-denaturation at 94°C, followed by 30 cycles of denaturation at 94°C for 1 min, annealing at 60°C for 1 min, elongation at 72°C for 45 s, and a final extension step of 10 min at 72°C. Then, the T_2 generation plants derived from the positive T_0 plant progeny were inoculated with CYR33 for functional analysis of the target genes.

Abiotic and Hormone Stress Treatments

In order to evaluate the expression level of *TaFBN* in wheat M8664-3 under hormone perception and environmental stress conditions, seedlings of M8664-3 were divided into eight groups. The first four groups were sprayed with methyl jasmonate (MeJA), ethylene (ET), salicylic acid (SA), or abscisic acid (ABA), at 100 mM each as a hormone treatment and cultivated at 16°C. The last four groups were treated with low temperature (4°C), high temperature (37°C), salt (200 mM NaCl), and drought (15% PEG6000) to experience environmental stress, and sterile water was sprayed at 16°C as a blank control. Leaf samples were collected for the expression level analysis of *TaFBN* 0, 1, 3, 6, 12, and 24 h after the different stimulus treatments.

RESULTS

ROS Is Involved in Wheat Cultivar M8664-3 Resistance Against CYR33

The infection type (IT) of wheat M8664-3 to CYR33 was 2 with large areas of necrosis on the leaves, whereas the IT of susceptible wheat Mingxian169 was 9 with fully expanded uredinium covered on the leaves at 15 dpi (**Figure 1A**).

Histological observation showed that significant DAB staining appeared at the leaf infection sites at 12 and 96 hpi (**Figure 1B**). At 12 hpi, strong DAB staining appeared in the guard cells directly contacted by the substomatal vesicle, and there was a significant difference in the H_2O_2 staining area of the infestation sites between M8664-3 and Mingxian 169. Between 24 and 48 hpi, the H_2O_2 staining area of the M8664-3 and Mingxian169 infection sites continuously increased. Between 72 and 96 hpi, the staining area of the M8664-3 infection site expanded to include guard cells and surrounding areas. In the mesophyll cells of Mingxian169, the DAB staining expansion area was far smaller than that of M8664-3 (**Figure 1**).

Expression Analysis of Selected Candidate Genes

Through annotation analysis, 19 genes near the linked markers and containing disease resistance-related domains, or hit by the linked markers of *YrM8664-3* were selected (**Supplementary Figure 1**; **Supplementary Table 2**). Among these, nine genes were significantly upregulated after inoculation with CYR33, as determined by qRT-PCR (**Figure 2**), namely,

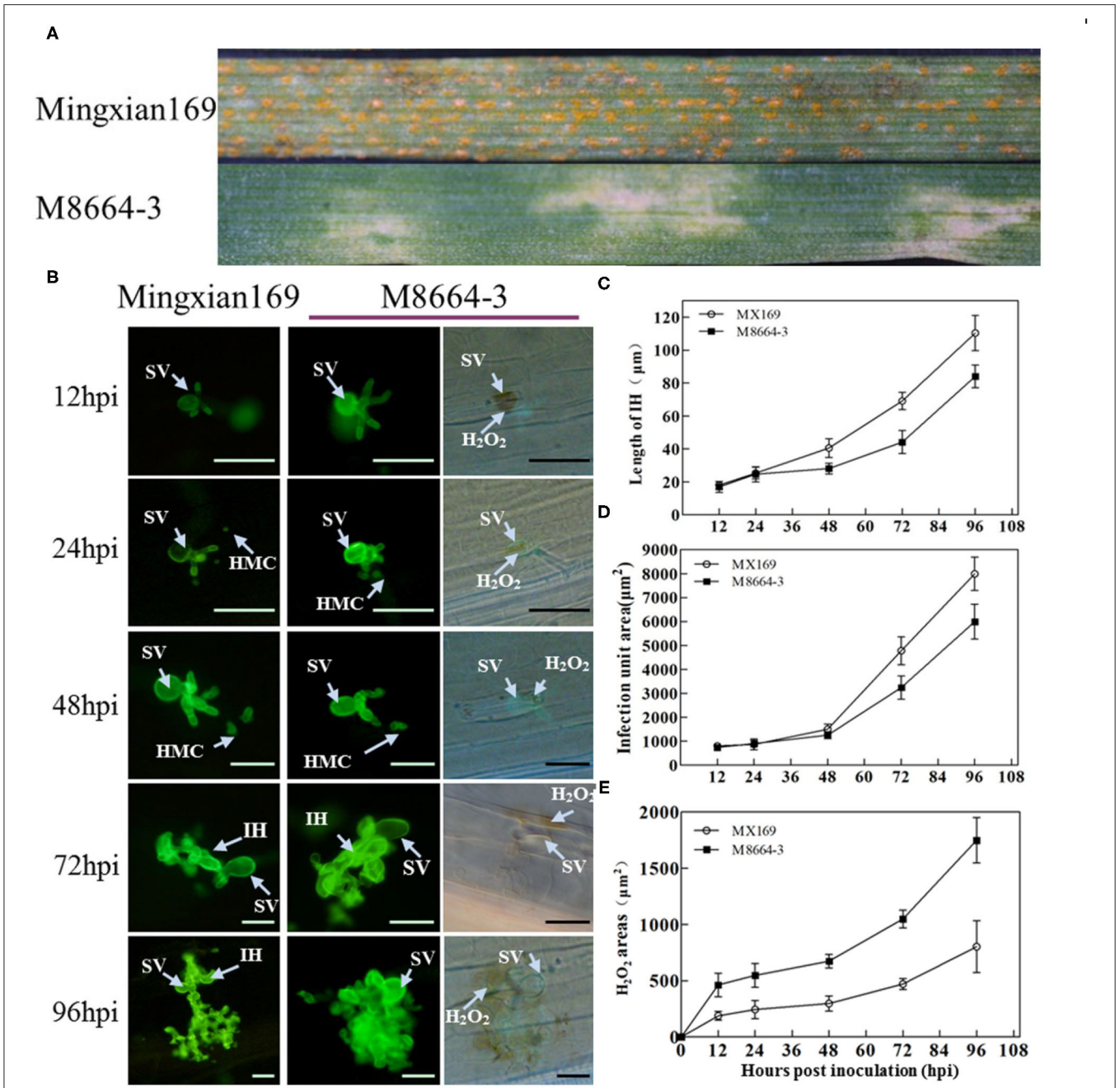

FIGURE 1 | (A) Symptoms of wheat-*Leymusmollis* introgression line M8664-3 and susceptible control cultivar Mingxian169 after inoculation with *Puccinia striiformis* f. sp. *tritici* (*Pst*) *race* CYR33. **(B)** Wheat germ agglutinin (WGA) was used to stain the leaves to visualize pathogens. SV, substomatal vesicle; IH, infection hyphae; HMC, haustorial mother cell; ROS, reactive oxygen species. **(C)** Hyphal lengths were measured at different hpi. **(D)** Infection unit area at different hpi. **(E)** H_2O_2 area at different hpi. Error bars represent the standard deviations of three independent samples. Bar, 50 μm.

TraesCS4A01G305600 (Leucine-rich repeat receptor-like protein kinase family protein), *TraesCS4A01G319000* (PGR5-like protein 1A, chloroplastic), *TraesCS4A01G319300* (disease-resistance protein (NBS-LRR class) family), *TraesCS4A01G365200* (Sn1-specific diacylglycerol lipase alpha), *TraesCS4A01G272000* (plastid-lipid associated protein PAP/fibrillin family protein, which encodes *TaFBN*), *TraesCS4A01G272900* (beta-glucosidase, which encodes *Ta_Pes_BRCT*), *TraesCS4A01G276400* (Pescadillo homolog), *TraesCS4A01G298300* (nonspecific phospholipase C), and *TraesCS4A01G181300* (AP2-like ethylene-responsive transcription factor) (**Table 1**).

Silencing of *TaFBN* and *Ta_Pes_BRCT* Weakens Wheat Resistance Against CYR33

Unique fragments were designed to knock down these nine candidate genes using primers specified in

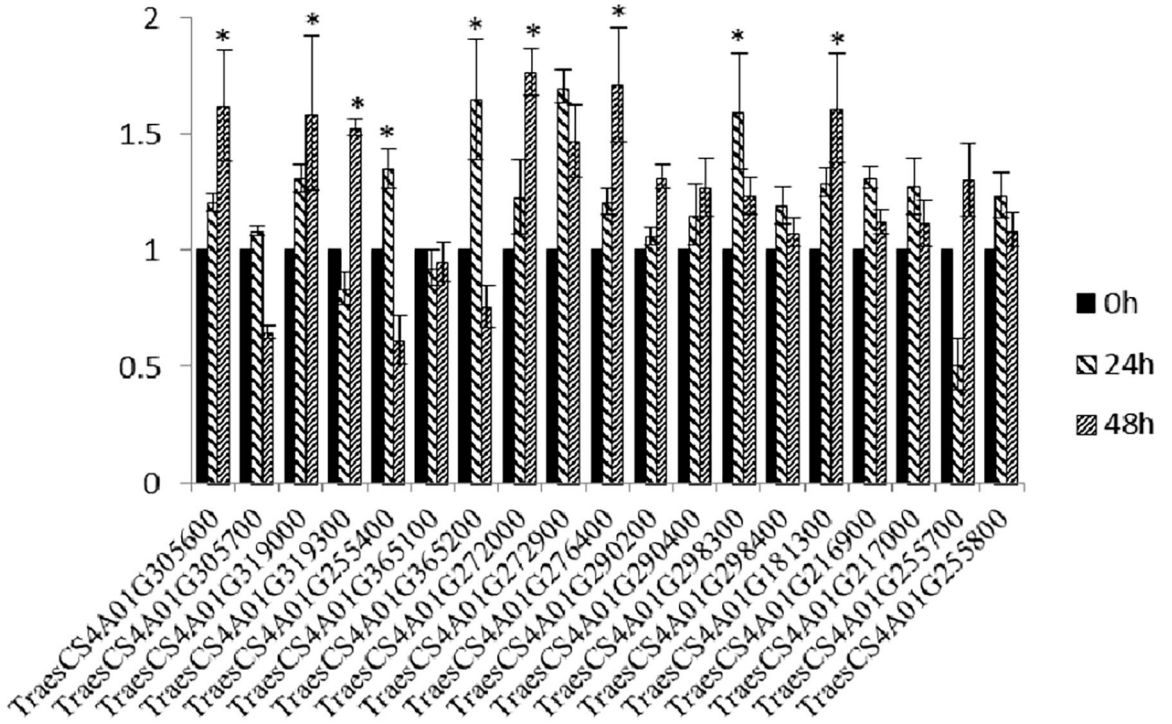

FIGURE 2 | Relative expression levels of 19 candidate genes at 24 and 48 h in M8664-3 after inoculation with *Pst* race CYR33. The data were normalized to the wheat *TaEF-1α* gene. Wheat leaves treated with distilled water were included as a control. Error bars represent the standard deviations of three independent samples. The significance of differences is indicated by asterisks and tested using Student's *t*-test ($P < 0.05$).

Supplementary Table 1. All of the BSMV-inoculated plants displayed chlorotic mosaic symptoms at 10 dpi, but there were no obvious defects in further leaf growth, while the leaves inoculated with BSMV: TaPDS exhibited photobleaching (**Figure 3A**), indicating that the BSMV induced gene silencing system functions well. After knocking down these genes with the VIGS method, M8664-3 became susceptible in the *TaFBN*- and *Ta_Pes_BRCT*-silenced system (**Figure 3B**), which indicated that these two genes may be involved in the resistance of M8664-3 to *Pst*. To determine the efficiency of VIGS, qRT-PCR was performed to examine the relative transcript levels of *TaFBN* and *Ta_Pes_BRCT* in the fourth leaves of infected plants. Compared with control inoculations, transcript levels of *TaFBN*-knockdown plants were reduced by 49, 39, 42, 43, and 42% at 0, 24, 48, 96, and 120 hpi, and *Ta_Pes_BRCT* knockdown plants also showed a stable efficiency by reducing to 49, 44, 36, 44, and 44% at 0, 24, 48, 96, and 120 hpi with CYR33, respectively (**Figure 3C**).

Histological observations showed that the number of haustorial mother cells, hypha length, and *Pst* growth area in *TaFBN*- and *Ta_Pes_BRCT*-silenced leaves all slightly increased as compared with that of the unsilenced treatment 48 hpi, but the DAB-reactive oxygen staining area did not significantly change, and no necrotic cells were found. At 120 hpi, the area of *Pst* growth, length of hyphae, and number of hyphae branches, haustorial mother cells, and haustorium in *TaFBN*- and *Ta_Pes_BRCT*-silenced leaves were all increased, and the difference was extremely significant. DAB-reactive oxygen staining decreased to 0, and the area of necrotic cells also significantly decreased compared with the unsilenced treatment at 120 hpi (**Figure 4**). In summary, the silencing of *TaFBN* and *Ta_Pes_BRCT* reduced disease resistance and made plants more susceptible to *Pst*.

TaFBN or *Ta_Pes_BRCT* Encodes Proteins Related to Defense Response

TaFBN encodes a protein composed of 261 amino acids, with a molecular weight of 28.59 kDa, an isoelectric point (PI) of 9.34, and an average hydrophobicity of −0.330, which suggested that it may be a hydrophilic protein. There was a PAP_fibrillin domain at positions 90–251 of the amino acid; therefore, it was temporarily named *TaFBN*. The phylogenetic analysis of *TaFBN* with *H. vulgare* (*HvFBN4*, KAE8820120), *Brachypodium distachyon* (*BdFBN4*, XP_003560711), *O. sativa* (*OsFBN4*, XP_015632312), *A. thaliana* (*AtFBN3a*, NM_113511; *AtFBN3b*, BT020596), and *Z. mays* (*ZmFBN4*, ACG27798) resulted in the clustering of *TaFBN* with *HvFBN4*, *BdFBN4*, *OsFBN4*, and Zm*FBN4*, all of which are members of FBN4 proteins in monocotyledons (**Figure 5A**). A nucleic acid sequence analysis revealed that *TaFBN* shared 96.55% identity with *HvFBN4* from *H. vulgare*. Multiple amino acid sequence alignments of *TaFBN* with *HvFBN4*,

TABLE 1 | Nineteen candidate genes and markers linked to resistance gene *YrM86664-3* on chromosome 4AL.

Position (bp)	No. of selected genes/Markers of *YrM8664-3*	Gene accession	Annotation
415683496–415683891	*BE446584*		
456290064–456292784	C15	TraesCS4A01G181300	AP2-like ethylene-responsive transcription factor
456292321–456292391	*AX111655681*		
515779130–515782750	C16	TraesCS4A01G216900	ABC transporter G family member
516343042–516343722	C17	TraesCS4A01G217000	Late embryogenesis abundant (LEA) hydroxyproline-rich glycoprotein
567479603–567482101	C5	TraesCS4A01G255400	Serine/threonine-protein kinase
567493169–567495275	C18	TraesCS4A01G255700	Ethylene-dependent gravitropism-deficient and yellow-green-like 2
567646583–567646825	*AX109496237*		
567650074–567650374	*AX109001562*		
567650160–567654340	C19	TraesCS4A01G255800	Basic helix-loop-helix (bHLH) DNA-binding superfamily protein
583754800–583757140	C8	TraesCS4A01G272000	Plastid-lipid associated protein PAP / fibrillin family protein
583756221–583756371	*BE403251*		
583949402–583953409	C9	TraesCS4A01G272900	Beta-glucosidase
583949552–583949670	*BE403721*		
584817688–584823187	C10	TraesCS4A01G276400	Pescadillo homolog
584818692–584818992	*AX86179210*		
594162606–594167272	C11	TraesCS4A01G290200	Ankyrin repeat protein-like
594165370–594165403	*BE406959*		
594212051–594212608	*BE591356*		
594213511–594217122	C12	TraesCS4A01G290400	Phosphomethylpyrimidine synthase
597023208–597024827	C13	TraesCS4A01G298300	Non specific phospholipase C
597024543–597025097	*BE637642*		
597052406–597054154	C14	TraesCS4A01G298400	Cation calcium exchanger
600913413–600914954	C1	TraesCS4A01G305600	Leucine-rich repeat receptor-like protein kinase family protein
600917368–600917668	*AX109895154*		
600918067–600918777	C2	TraesCS4A01G305700	Leucine-rich repeat receptor-like protein kinase family protein
607633308–607635652	C3	TraesCS4A01G319000	PGR5-like protein 1A, chloroplastic
607888036–607888131	*BV211529*		
608267651–608271046	C4	TraesCS4A01G319300	Disease resistance protein (NBS-LRR class) family
638240325–638241099	C6	TraesCS4A01G365100	SHAGGY-like kinase
638661695–638661817	*Xgpw2331*		
638791957–638796803	C7	TraesCS4A01G365200	Sn1-specific diacylglycerol lipase alpha

BdFBN4, *OsFBN4*, and *ZmFBN4* showed that *TaFBN4* is predicted to encode proteins with the unique conserved domains of PAP complex FBN4 (**Figure 5B**). Therefore, it was determined that *TaFBN* and FBN4 were clustered together, and that the functional annotations of the latter on the UniProt website were related to resistance to bacterial diseases and ozone.

Ta_Pes_BRCT encodes a protein composed of 596 amino acids, with a molecular weight of 68.32 kDa, PI of 7.68, and an average hydrophobicity of −0.615, which indicated that it may be a hydrophilic protein. The amino acid coded *by Ta_Pes_BRCT* has a Pescadillo (PES) domain at positions 9–277, and the 339–417 amino acids contain a BRCT domain. The predicted function may be related to ribosomes; therefore, it was temporarily named *Ta_Pes_BRCT*. The phylogenetic analysis and multiple amino acid sequence alignment of Pes_BRCT proteins indicated that *Ta_Pes_BRCT* is predicted to encode proteins with conserved domains of the Pes_BRCT complex (**Supplementary Figure 2**). The functional annotations of BRCT on the UniProt website were related to DNA repair under stress. As predicted by the TMpred program, *TaFBN* and *Ta_Pes_BRCT* have no transmembrane domain. As predicted by TargetP-2.0 and Plant-mPLoc, the location of the protein encoded by *Ta_FBN* was predicted in Chloroplast; the

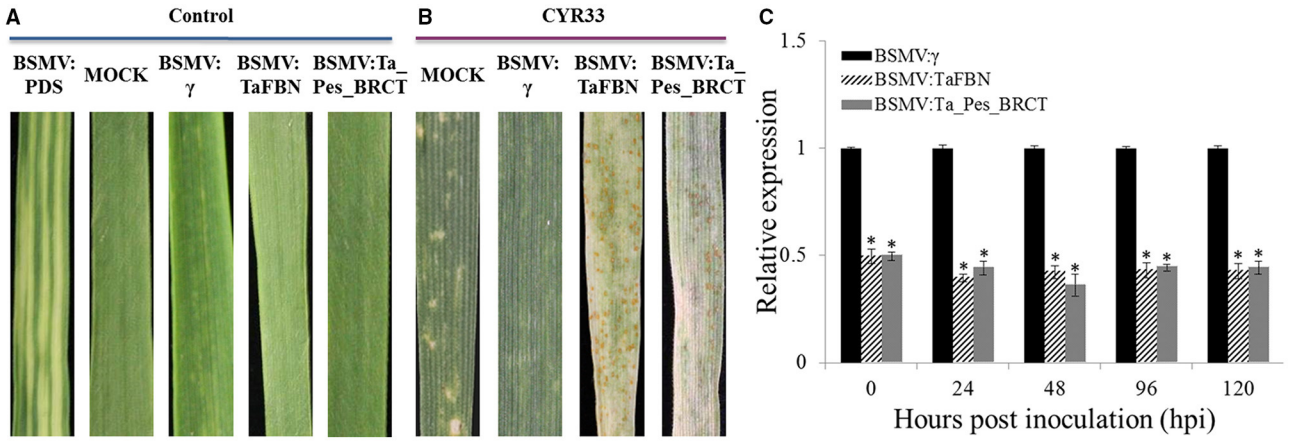

FIGURE 3 | Transient silencing of *TaFBN* and *Ta_Pes_BRCT* with the BSMV-VIGS method. **(A)** Wheat leaves treated with 1× Fes buffer (MOCK) show no phenotypic changes. Mild chlorotic mosaic symptoms were detected on the plants inoculated with BSMV:γ, BSMV:PDS, BSMV:TaFBN, or BSMV:Ta_Pes_BRCT. **(B)** Phenotypes of the fourth leaves infected with uredospores of *Pst* race CYR33 at 10 days post inoculation. **(C)** Silencing efficiency assessment of *TaFBN* in the TaFBN-knockdown plants and *Ta_Pes_BRCT* in the Ta_Pes_BRCT-knockdown plants. Error bars represent the standard deviations of three independent samples. The significance of differences is indicated by asterisks and tested using Student's *t*-test ($P < 0.05$).

location of the protein encoded by *Ta_Pes_BRCT* was predicted in Nucleus.

Functional Verification of Transgenic Plants

In order to further analyze the function of *TaFBN* and *Ta_Pes_BRCT* in stripe rust resistance, the two genes were introduced into the susceptible bread wheat variety Fielder by an *Agrobacterium*-mediated transformation method. The individuals of T_0 generation were identified by PCR analysis (**Figure 6A**), and seven independent T_2 lines obtained from the positive T_0 progeny were further used to conduct disease resistance tests and PCR detection procedures. Three replicates were tested for each line. The T_2 generation of *TaFBN* transgenic plants was resistant to CYR33, while all of the *Ta_Pes_BRCT* transgenic plants were susceptible to CYR33 (**Figure 6B**), which indicated that *TaFBN* confers more important resistance to CYR33.

TaFBN Responds to Abiotic Stress and Hormone Treatments

Under different hormone treatments (MeJA, ET, SA, and ABA), the transcription level of *TaFBN* in the leaves of M8664-3 wheat seedlings was determined (**Figure 7**). The expression level of *TaFBN* significantly increased under SA and ABA treatments, and peaked (more than twice) at 6 and 12 hpi, respectively. The expression of *TaFBN* also slightly increased after MeJA and ET treatment. Under abiotic stress, the expression of *TaFBN* significantly increased after NaCl, PEG6000, and 4°C treatment, but its expression in 37°C-high temperature treatment did not significantly increase. In summary, *TaFBN* might be induced by SA, ABA, high salt, drought, and low temperature to increase its expression.

DISCUSSION

In our previous study, *YrM8644-3* was located in bin 4AL13-0.59-0.66 near 4AL12-0.43-0.59 on wheat chromosome 4A. However, it was challenging to clone this gene because of *YrM8664-3* derived from the wheat-*L. mollis* introgression line M8664-3 and the complexity of the wheat hexaploid genome. Fortunately, the continuous improvement in the whole genome sequencing of wheat "Chinese Spring" provided great convenience for gene cloning and functional analysis (Avni et al., 2017; IWGSC et al., 2018).

In this study, based on the chromosome location of *YrM8664-3* in our previous study, the sequences of the linked markers of *YrM8664-3* were assigned against the Chinese Spring IWGSC RefSeq V1.0 Reference Genome (IWGSC et al., 2018), and then qRT-PCR was performed to analyze the expression level of candidate genes under *Pst* infection. Among the 19 selected genes that are near the linked markers and containing resistance domains or just hit by linked markers of *YrM8664-3*, the expression level of nine genes were significantly enhanced after inoculation with CYR33. The VIGS system was used to characterize gene function, and only two candidate genes, *TaFBN* and *Ta_Pes_BRCT*, silencing plants were found to be significantly weakened in disease resistance to CYR33. VIGS is a technique for rapid gene function analysis based on the principle of specific degradation of endogenous mRNA sequences caused by post-transcriptional gene silencing (PTGS). BSMV-VIGS is widely used in the rapid analysis of gene function of monocotyledonous plants, particularly barley and wheat. Feng et al. (2015) selected six unigenes from transcriptome analysis and achieved transient silencing of the six unigenes individually through VIGS using the BSMV vector. The results showed that the six unigenes

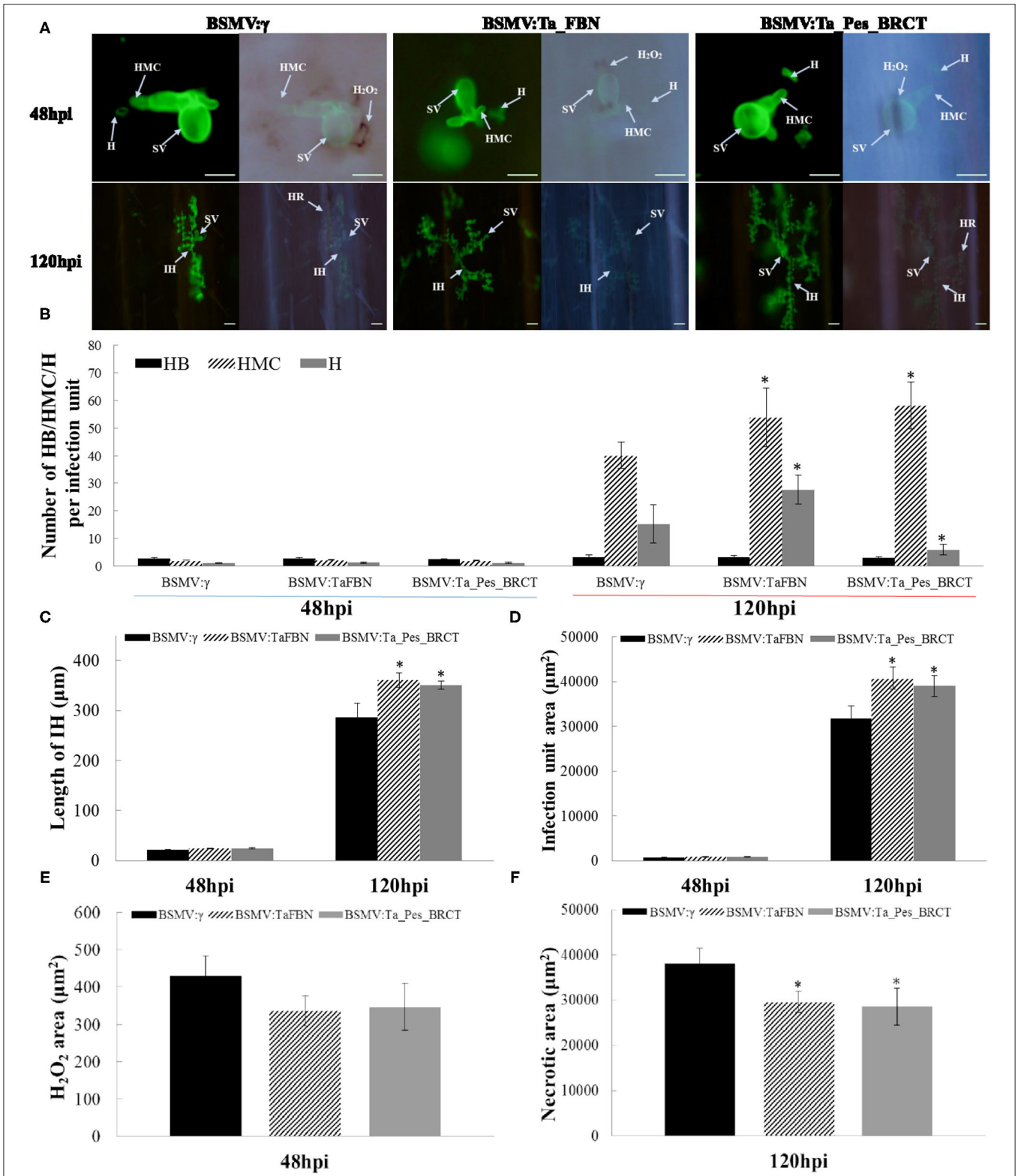

FIGURE 4 | Histological observations of *Pst* race CYR33 infection in TaFBN-knockdown and Ta_Pes_BRCT-knockdown wheat plants. **(A)** WGA was used to stain the leaves to visualize pathogens. **(B)** Number of HB/HMC/H; **(C)** length of IH; **(D)** infection unit area; **(E)** H_2O_2 area; and **(F)** necrotic area staining by 3,3′-diaminobenzidine (DAB) were measured with DP-BSW software in *TaFBN*-knockdown plants at 48 and 120 hpi after inoculation. SV, substomatal vesicle; IH, initial hyphae; HMC, haustorial mother cell; SH, secondary hyphae. Error bars represent the standard deviations of three independent samples. The significance of differences is indicated by asterisks and tested using Student's *t*-test ($P < 0.05$). Bar, 50 μm.

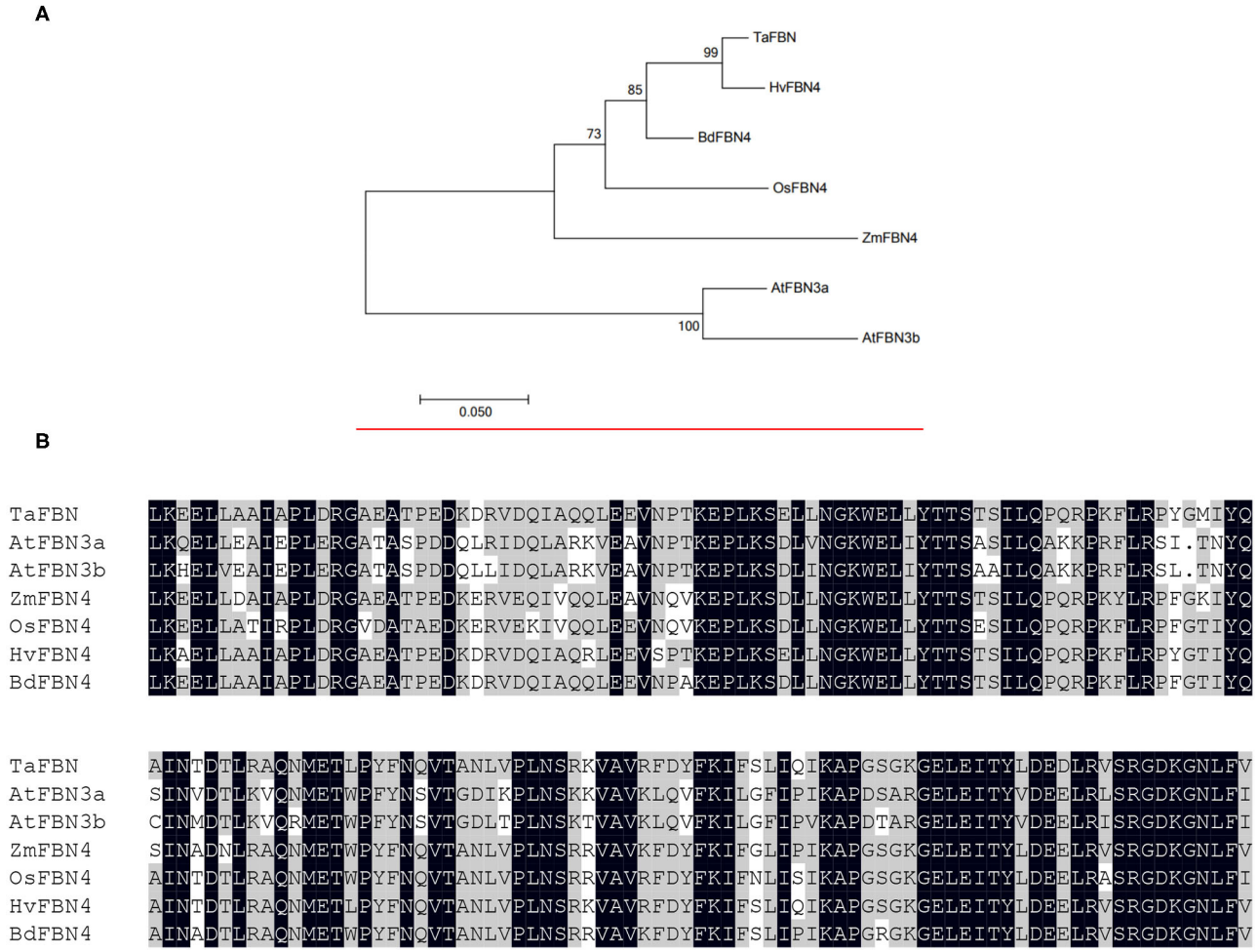

FIGURE 5 | (A) Phylogenetic analysis of fibrillin (FBN) proteins. A neighbor-joining tree of FBN in *Triticuma estivum* (TaFBN, KAF7095220), *Hordeum vulgare* (HvFBN4, KAE8820120), *Brachypodium distachyon* (BdFBN4, XP_003560711), *Oryza sativa* (OsFBN4, XP_015632312), *Arabidopsis thaliana* (AtFBN3a/AT3G26070, NM_113511; AtFBN3b/At3g26080, BT020596), and *Zea mays* (ZmFBN4, ACG27798). **(B)** Multiple amino acid sequence alignments of TaFBN with OsFBN4, ZmFBN4, AtFBN3a, AtFBN3b, and HvFBN4. Amino acid identity (black boxes) and similarity (gray boxes) are shown within the protein kinase domain.

inhibited the vernalization of wheat, and that during silencing or down-regulation, the genes promoted flower development in wheat. Liu et al. (2020) used transient expression and BSMV-mediated *TabHLH49* gene silencing, and discovered that *TabHLH49* positively regulated WZY2 dehydrogenase expression and increased the resistance of wheat to drought.

The most direct and effective verification method for gene function is transgenic technology. By transferring the *HvBADH1* gene from *H. vulgare* into *T. aestivum via* traditional *Agrobacterium tumefaciens*-mediated transformation, Li et al. (2019) found that the overall salt tolerance of target plants was significantly improved, and that the damaging effect of high salt was significantly reduced after overexpression of the *HvBADH1* gene. In cereals, *Agrobacterium*-mediated transgenic sites are generally considered to be cleaner, with fewer copies and rearrangements than biologically generated transgenic sites (Wu et al., 2006). Horvath et al. (2003) subjected the stem-rust-susceptible barley cv. Golden Promise to *Agrobacterium*-mediated transformation with the *Rpg1* gene, and characterized their seedling infection response to pathotype *Pgt*-MCC of the stem rust fungus. This demonstrated that susceptible barley can become resistant by transformation with a cloned resistant gene. In this study, the *TaFBN* and *Ta_Pes_BRCT* genes were transformed into the susceptible variety Fielder by *Agrobacterium*-mediated transformation. The *TaFBN* transgenic plants exhibited obvious resistance after inoculation with CYR33, which indicates that *TaFBN* may be involved in stripe rust resistance in M8664-3.

TaFBN has a conserved fibrillin (FBN) domain that was named fibrils, because those related proteins were first detected in fibrils in the chromoplasts of *Rosa rugosa* and *Capsicum annuum* fruit (Newman et al., 1989; Deruere et al., 1994; Kim et al., 2015). FBN proteins participate in a variety of important biological functions, in addition to photosynthesis and

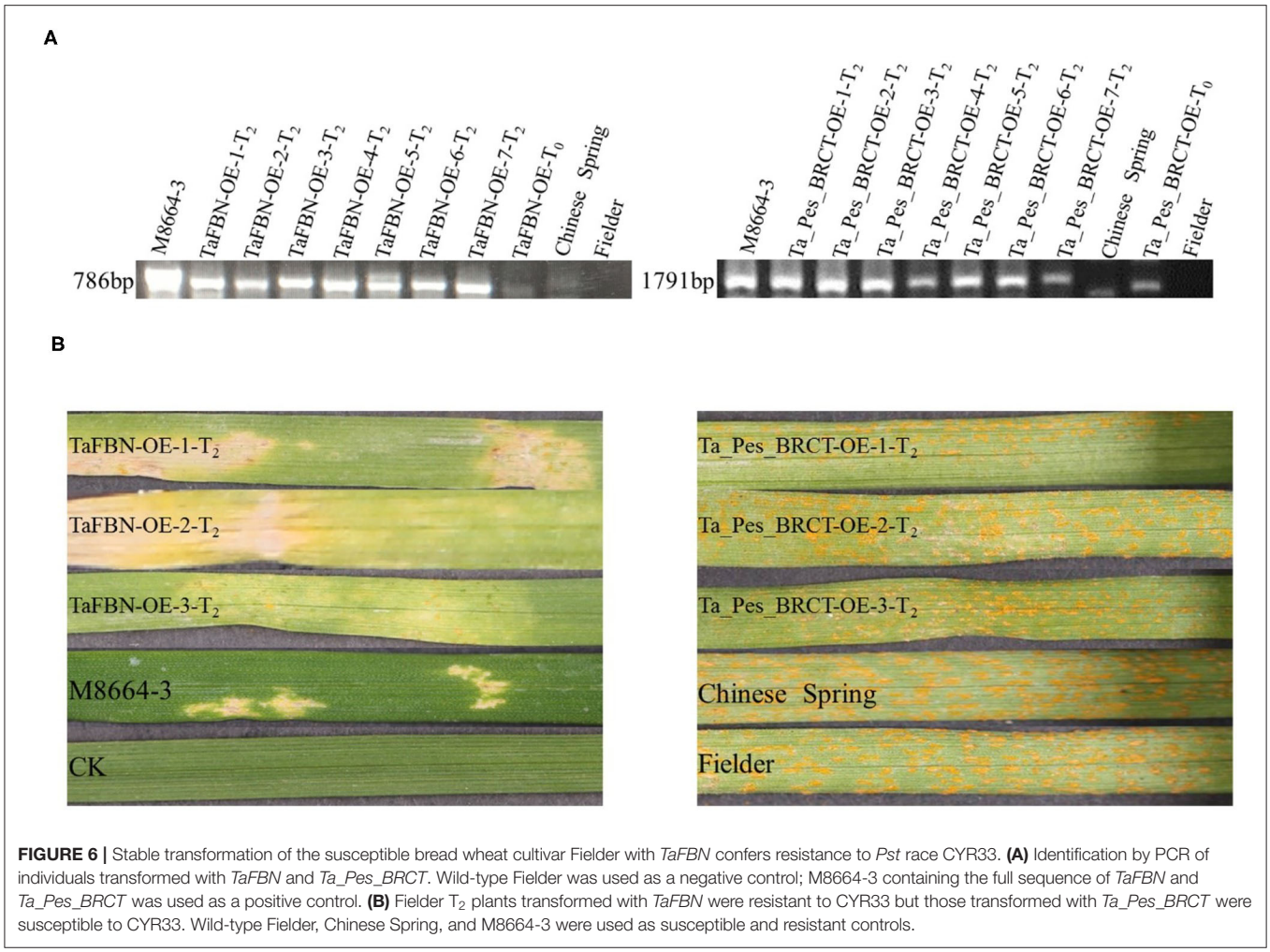

FIGURE 6 | Stable transformation of the susceptible bread wheat cultivar Fielder with *TaFBN* confers resistance to *Pst* race CYR33. **(A)** Identification by PCR of individuals transformed with *TaFBN* and *Ta_Pes_BRCT*. Wild-type Fielder was used as a negative control; M8664-3 containing the full sequence of *TaFBN* and *Ta_Pes_BRCT* was used as a positive control. **(B)** Fielder T_2 plants transformed with *TaFBN* were resistant to CYR33 but those transformed with *Ta_Pes_BRCT* were susceptible to CYR33. Wild-type Fielder, Chinese Spring, and M8664-3 were used as susceptible and resistant controls.

structural roles, which also respond to numerous abiotic and biotic stresses, especially oxidative stress (Youssef et al., 2010; Kim et al., 2015). Leitner-Dagan et al. (2006) showed that the Chrc (FBN1) in cucumber leaves was induced by *Sphaerotheca fuliginea* and *LeChrc* (FBN1) in tomato plants infected with *Botrytis cinerea*. *LeChrc* expression is a necessary condition for resistance to *B. cinerea*. Using the tomato plant system, transgenic plants with *LeChrc* inhibition were more susceptible to infection both *in vitro* with isolated leaves and in growth chambers with intact leaves and stems (Cooper et al., 2003; Leitner-Dagan et al., 2006). Similarly, studies (Singh et al., 2010; Jiang et al., 2020) have shown that both Arabidopsis and apple *FBN4* gene T-DNA insertion mutants are more sensitive to bacterial infections *Pseudomonas syringae* pathovar tomato and *Erwinia amylovora*, respectively. In Arabidopsis, pathogen-associated molecular pattern (PAMP) induces the phosphorylation of *FBN4*, and it is speculated that *FBN4* may be involved in plant disease resistance response.

During plant growth and development stages, when plants are under abiotic stresses (such as drought, cold, heat, bright light, and wound management) or hormone induction (with gibberellin, jasmonic acid, and abscisic acid), the expression of fibrillins is varied and complex (Pruvot et al., 1996; Kuntz et al., 1998; Langenkamper et al., 2001; Leitner-Dagan et al., 2006; Simkin et al., 2008). When red pepper fruits were treated with gibberellic acid, FBN1 mRNA and protein levels decreased (Deruere et al., 1994). Conversely, the FBN1 and FBN2 proteins are involved in the jasmonate biosynthesis pathway in Arabidopsis in response to light and cold stress (Youssef et al., 2010). In addition, when tomato flacca mutant plants were subjected to drought stress, ABA biosynthesis was defective, and FBN protein accumulation decreased, because ABA treatment can induce FBN protein levels (Gillet et al., 1998). Herein, we observed an induction of *TaFBN* upon SA and ABA treatment, suggesting that *TaFBN* may be an effector associated with the SA and ABA signaling pathways. Taken together with our observation of enhancement of *TaFBN* expression in response to environmental stress stimuli (high salt, drought, cold, heat), it is reasonable to hypothesize that *TaFBN* functions at the nexus of biotic and abiotic stress pathways.

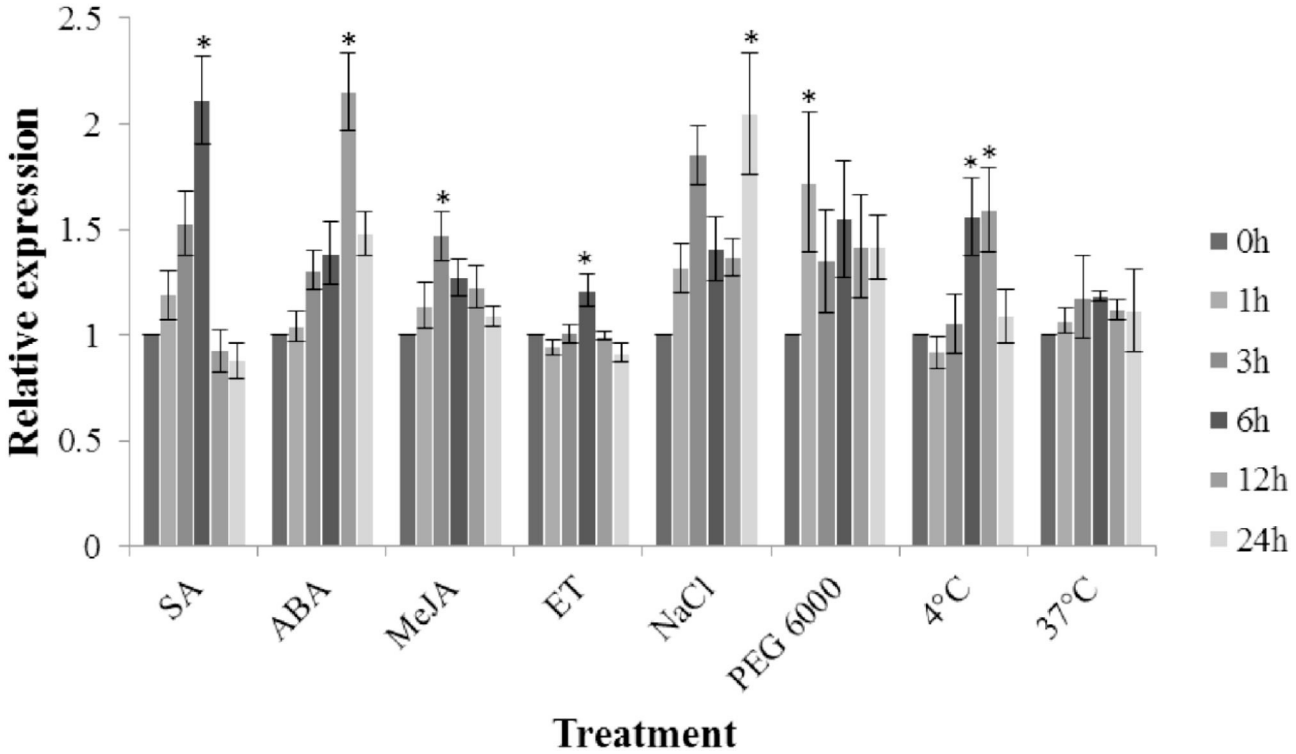

FIGURE 7 | Expression analysis of *TaFBN* under different hormones and abiotic stresses. SA, salicylic acid; ABA, abscisic acid; MeJA, methyl jasmonate; ET, ethylene. Error bars represent the variations among three independent replicates. The data were normalized to the TaEF-1α gene. Wheat leaves treated with distilled water were included as a control. Error bars represent the standard deviations of three independent samples. The significance of differences is indicated by asterisks and tested using Student's *t*-test ($P < 0.05$).

BRCT motifs were originally identified in the breast cancer tumor suppressor protein BRCA1 by Koonin et al. (1996), and now have been identified in numerous proteins involved in DNA repair and cell cycle checkpoints (Mathilde et al., 2003). Roy et al. (2015) indicated the importance of BRCT in regulating the stability of proteins under genotoxic stress in plants. *Pst*-infected wheat may produce oxygen-free radicals, such as O^{2-} and H_2O_2, that damage cells, which subsequently produce metabolic byproducts that cause DNA base damage. *Ta_Pes_BRCT* is a BRCT-domain-containing protein that may be involved in DNA repair and that could be induced to up-regulate by *Pst*. However, after transgenic verification, it was found that *Ta_Pes_BRCT* is a related gene in the process of wheat resistance to *Pst* that plays less important role than *TaFBN*.

In summary, this study selected candidate genes of *YrM8664-3* by bioinformatics analysis, and verified the resistant function of the candidate genes *TaFBN* and *Ta_Pes_BRCT* by qRT-PCR, BSMV-VIGS, and genetic transformation. Finally, it was validated that *TaFBN* may be involved in *YrM8664-3* stripe rust resistance as an important gene *via* the SA and ABA signaling pathways.

DATA AVAILABILITY STATEMENT

The original contributions presented in the study are included in the article/**Supplementary Materials**, further inquiries can be directed to the corresponding author/s.

AUTHOR CONTRIBUTIONS

BW and QL designed the experiments. PJ, KC, JL, and ZW performed the experiments and analyzed the data. PJ, JL, KC, ZW, PC, QL, and BW wrote the manuscript. All authors contributed to the article and approved the submitted version.

FUNDING

This research was supported by the National Key R&D Program of China (Grant Nos: 2018YFD0200403 and 2018YFD0200501), the Open Project Program of State Key Laboratory of Crop Stress Biology for Arid Areas, NWAFU, Yangling, Shaanxi, 712100, China (CSBAA2019007), the Technical Guidance Project of Shaanxi Province (Grant No: 2017CGZH-HJ-01), the National Science Foundation of China (Grant No: 31501620), and the China Ministry of Education 111 Project (Grant No: B07049).

ACKNOWLEDGMENTS

The authors thank the reviewers for helpful comments and valuable suggestions during the revision of the early version of the manuscript.

SUPPLEMENTARY MATERIAL

The Supplementary Material for this article can be found online at: https://www.frontiersin.org/articles/10.3389/fpls.2021.754823/full#supplementary-material

REFERENCES

Asthir, B., Koundal, A., and Bains, N. S. (2011). Kinetic properties of cell wall bound superoxide dismutase in leaves of wheat (*Triticum aestivum L.*) following stripe rust (*Puccinia striiformis*) infection. *Indian J. Biochem. Biophys.* 48, 341–345. doi: 10.1016/j.plrev.2011.07.013

Avni, R., Nave, M., Barad, O., Baruch, K., Twardziok, S. O., Gundlach, H., et al. (2017). Wild emmer genome architecture and diversity elucidate wheat evolution and domestication. *Science* 357, 93–97. doi: 10.1126/science.aan0032

Ayliffe, M., Devilla, R., Mago, R., White, R., Talbot, M., Pryor, A., et al. (2011). Nonhost resistance of rice to rust pathogens. *Mol. Plant Microbe Interact.* 24, 1143–1155. doi: 10.1094/MPMI-04-11-0100

Bansal, M., Kaur, S., Dhaliwal, H. S., Bains, N. S., Bariana, H. S., Chhuneja, P., et al. (2017). Mapping of *Aegilops umbellulata*-derived leaf rust and stripe rust resistance loci in wheat. *Plant Pathol.* 66, 38–44. doi: 10.1111/ppa.12549

Chao, K. X., Yang, J. Y., Liu, H., Jing, J. X., Li, Q., Wang, B. T., et al. (2018). Genetic and physical mapping of a putative *Leymus mollis*-derived stripe rust resistance gene on wheat chromosome 4A. *Plant Dis.* 102, 1001–1007. doi: 10.1094/PDIS-05-17-0671-RE

Cooper, B., Clarke, J. D., Budworth, P., Kreps, J., Hutchison, D., Park, S., et al. (2003). A network of rice genes associated with stress response and seed development. *Proc. Natl. Acad. Sci. USA.* 100, 4945–4950. doi: 10.1073/pnas.0737574100

Cui, H. T., Tsuda, K., and Parker, J. E. (2015). Effector-triggered immunity: from pathogen perception to robust defense. *Annu. Rev. Plant Biol.* 66, 487–511. doi: 10.1146/annurev-arplant-050213-0400

Denance, N., Sanchez-Vallet, A., Goffner, D., and Molina, A. (2013). Disease resistance or growth: the role of plant hormones in balancing immune responses and fitness costs. *Front. Plant Sci.* 4:155. doi: 10.3389/fpls.2013.00155

Derksen, H., Rampitsch, C., and Daayf, F. (2013). Signaling cross-talk in plant disease resistance. *Plant Sci.* 207, 79–87. doi: 10.1016/j.plantsci.2013.03.004

Deruere, J., Romer, S., d'Harlingue, A., Backhaus, R. A., Kuntz, M., and Camara, B. (1994). Fibril assembly and carotenoid overaccumulation in chromoplasts: a model for supramolecular lipoprotein structures. *Plant Cell* 6, 119–133. doi: 10.1105/tpc.6.1.119

Dodds, P. N., Lawrence, G. J., Catanzariti, A. M., Teh, T., Wang, C. I., Ayliffe, M. A., et al. (2006). Direct protein interaction underlies gene-for-gene specificity and coevolution of the flax resistance genes and flax rust avirulence genes. *Proc. Natl. Acad. Sci. USA.* 103, 8888–8893. doi: 10.1073/pnas.0602577103

Feng, Y. L., Wang, K. T., Ma, C., Zhao, Y. Y., and Yin, J. (2015). Virus-induced gene silencing-based functional verification of six genes associated with vernalization in wheat. *Biochem. Bioph. Res. Commun.* 458, 928–933. doi: 10.1016/j.bbrc.2015.02.064

Fitzmaurice, W. P., Holzberg, S., Lindbo, J. A., Padgett, H. S., Palmer, K. E., Wolfe, G. M., et al. (2002). Epigenetic modification of plants with systemic RNA viruses. *OMICS* 6, 137–151. doi: 10.1089/153623102760092742

Gillet, B., Beyly, A., Peltier, G., and Rey, P. (1998). Molecular characterization of CDSP 34, a chloroplastic protein induced by water deficit in *Solanum tuberosum L.* plants, and regulation of CDSP 34 expression by ABA and high illumination. *Plant J.* 16, 257–262. doi: 10.1046/j.1365-313x.1998.00292.x

Horvath, H., Rostoks, N., Brueggeman, R., Steffenson, B., von Wettstein, D., and Kleinhofs, A. (2003). Genetically engineered stem rust resistance in barley using the *Rpg1* gene. *Proc. Natl. Acad. Sci. USA.* 100, 364–369. doi: 10.1073/pnas.0136911100

Huang, S. Y., Steffenson, B. J., Sela, H., and Stinebaugh, K. (2018). Resistance of *Aegilops longissima* to the rusts of wheat. *Plant Dis.* 102, 1124–1135. doi: 10.1094/PDIS-06-17-0880-RE

IWGSC, Appels, R., Eversole, K., Stein, N., Feuillet, C., Keller, B., et al. (2018). Shifting the limits in wheat research and breeding using a fully annotated reference genome. *Science* 361, 10–1126. doi: 10.1126/science.aar7191

Jia, Y., McAdams, S. A., Bryan, G. T., Hershey, H. P., and Valent, B. (2000). Direct interaction of resistance gene and avirulence gene products confers rice blast resistance. *EMBO J.* 19, 4004–4014. doi: 10.1093/emboj/19.15.4004

Jiang, Y. Y., Hu, H. C., Ma, Y. H., an Zhou, J. L. (2020). Genome-wide identification and characterization of the fibrillin gene family in *Triticum aestivum*. *PeerJ* 8:9225. doi: 10.7717/peerj.9225

Jones, J. D., Vance, R. E., and Dangl, J. L. (2016). Intracellular innate immune surveillance devices in plants and animals. *Science* 354:6316. doi: 10.1126/science.aaf6395

Jones, J. D. G., and Dangl, J. L. (2006). The plant immune system. *Nature* 444, 323–329. doi: 10.1038/nature05286

Kang, Z., Huang, L. L., and Buchenauer, H. (2002). Ultrastructural changes and localization of lignin and callose in compatible and incompatible interactions between wheat and *Puccinia striiformis*. *J. Plant Dis. Protect.* 109, 25–37.

Kim, E. H., Lee, Y., and Kim, H. U. (2015). Fibrillin 5 is essential for plastoquinone-9 biosynthesis by binding to solanesyl diphosphate synthases in *Arabidopsis*. *Plant Cell* 27, 2956–2971. doi: 10.1105/tpc.15.00707

Koonin, E. V., Altschul, S. F., and Bork, P. (1996). Functional motifs. *Nat. Genet* 13, 266–268. doi: 10.1038/ng0796-266

Kumar, S., Stecher, G., and Tamura, K. (2016). MEGA7: molecular evolutionary genetics analysis version 7.0 for bigger datasets. *Mol. Biol. Evol.* 33, 1870–1874. doi: 10.1093/molbev/msw054

Kuntz, M., Chen, H. C., Simkin, A. J., Romer, S., Shipton, C. A., Drake, R., et al. (1998). Upregulation of two ripening-related genes from a nonclimacteric plant (pepper) in a transgenic climacteric plant (tomato). *Plant J.* 13, 351–361. doi: 10.1046/j.1365-313X.1998.00032.x

Langenkamper, G., Manac'h, N., Broin, M., Cuine, S., Becuwe, N., Kuntz, M., et al. (2001). Accumulation of plastid lipid-associated proteins (fibrillin/CDSP34) upon oxidative stress, ageing and biotic stress in *Solanaceae* and in response to drought in other species. *J. Exp. Bot.* 52, 1545–1554. doi: 10.1093/jexbot/52.360.1545

Leitner-Dagan, Y., Ovadis, M., Shklarman, E., Elad, Y., David, D. R., and Vainstein, A. (2006). Expression and functional analyses of the plastid lipid-associated protein CHRC suggest its role in chromoplastogenesis and stress. *Plant Physiol.* 142, 233–244. doi: 10.1104/pp.106.082404

Li, P. F., Cai, J., Luo, X., Chang, T. L., Li, J. X., Zhao, Y. W., et al. (2019). Transformation of wheat *Triticum aestivum* with the *HvBADH1* transgene from hulless barley improves salinity-stress tolerance. *Acta Physiol. Plant* 41, 1–14. doi: 10.1007/s11738-019-2940-8

Li, X. Y., Wang, X., Zhang, S. P., Liu, D. W., Duan, Y. X., and Dong, W. (2011). Comparative profiling of the transcriptional response to soybean cyst nematode infection of soybean roots by deep sequencing. *Chin. Sci. Bull.* 56, 1904–1911. doi: 10.1007/s11434-011-4510-3

Liu, H., Yang, Y., Liu, D. D., Wang, X. Y., and Zhang, L. S. (2020). Transcription factor TabHLH49 positively regulates dehydrin *WZY2* gene expression and enhances drought stress tolerance in wheat. *BMC Plant Biol.* 20, 1–10. doi: 10.1186/s12870-020-02474-5

Livak, K. J., and Schmittgen, T. D. (2001). Analysis of relative gene expression data using real-time quantitative PCR and the 2(T)(-Delta Delta C) method. *Methods* 25, 402–408. doi: 10.1006/meth.2001.1262

Luo, S., Peng, J., Li, K., Wang, M., and Kuang, H. (2011). Contrasting evolutionary patterns of the *Rp1* resistance gene family in different species of Poaceae. *Mol. Biol. Evol.* 28, 313–325. doi: 10.1093/molbev/msq216

Ma, S., Lapin, D., Liu, L., Sun, Y., Song, W., Zhang, X., et al. (2020). Direct pathogen-induced assembly of an NLR immune receptor complex to form a holoenzyme. *Science* 370:6521. doi: 10.1126/science.abe3069

Mathilde, G., Ghislaine, G., Daniel, V., and Georges, P. (2003). The Arabidopsis MEI1 gene encodes a protein with five BRCT domains that is involved in meiosis-specific DNA repair events independent of SPO11-induced DSBs. *Plant J.* 35, 465–475. doi: 10.1046/j.1365-313X.2003.01820.x

Monteiro, F., and Nishimura, M. T. (2018). Structural, functional, and genomic diversity of plant NLR proteins: an evolved resource for rational engineering of plant immunity. *Annu. Rev. Phytopathol.* 56, 243–267. doi: 10.1146/annurev-phyto-080417-045817

Newman, L. A., Hadjeb, N., and Price, C. A. (1989). Synthesis of two chromoplast-specific proteins during fruit development in *Capsicum annuum*. *Plant Physiol.* 91, 455–458. doi: 10.1104/pp.91.2.455

Petty, I. T., and Jackson, A. O. (1990). Mutational analysis of barley stripe mosaic virus RNA beta. *Virology* 179, 712–718. doi: 10.1016/0042-6822(90)90138-h

Pruvot, G., Cuine, S., Peltier, G., and Rey, P. (1996). Characterization of a novel drought-induced 34-kDa protein located in the thylakoids of *Solanum tuberosum L.* plants. *Planta* 198, 471–479. doi: 10.1007/BF00620065

Roelfs, A. P., Huertaespino, J., and Marshall, D. (1992). Barley stripe rust in Texas. *Plant Dis.* 76, 538–538. doi: 10.1094/PD-76-0538C

Roy, S., Banerjee, V., and Das, K. P. (2015). Understanding the physical and molecular basis of stability of Arabidopsis DNA Pol lambda under UV-B and high NaCl stress. *PLoS ONE* 10:e0133843. doi: 10.1371/journal.pone.0133843

Schenk, P. M., Kazan, K., Wilson, I., Anderson, J. P., Richmond, T., Somerville, S. C., et al. (2000). Coordinated plant defense responses in *Arabidopsis* revealed by microarray analysis. *Proc. Natl. Acad. Sci. USA*. 97, 11655–11660. doi: 10.1073/pnas.97.21.11655

Scofield, S. R., Huang, L., Brandt, A. S., and Gill, B. S. (2005). Development of a virus-induced gene-silencing system for hexaploid wheat and its use in functional analysis of the *Lr21*-mediated leaf rust resistance pathway. *Plant Physiol.* 138, 2165–2173. doi: 10.1104/pp.105.061861

Simkin, A. J., Moreau, H., Kuntz, M., Pagny, G., Lin, C. W., Tanksley, S., et al. (2008). An investigation of carotenoid biosynthesis in *Coffea canephora* and *Coffea arabica*. *J. Plant Physiol.* 165, 1087–1106. doi: 10.1016/j.jplph.2007.06.016

Singh, D. K., Maximova, S. N., Jensen, P. J., Lehman, B. L., Ngugi, H. K., and McNellis, T. W. (2010). *FIBRILLIN4* is required for plastoglobule development and stress resistance in Apple and Arabidopsis. *Plant Physiol.* 154, 1281–1293. doi: 10.1104/pp.110.164095

Wan, A. M., Chen, X. M., and He, Z. H. (2007). Wheat stripe rust in China. *Aust. J. Agric. Res.* 58, 607–619. doi: 10.1071/AR06142

Wan, A. M., Zhao, Z. H., Chen, X. M., He, Z. H., Jin, S. L., Jia, Q. Z., et al. (2004). Wheat stripe rust epidemic and virulence of *Puccinia striiformis* f. sp. *tritici* in China in 2002. *Plant Dis.* 88, 896–904. doi: 10.1094/PDIS.2004.88.8.896

Wang, C. F., Huang, L. L., Buchenauer, H., Han, Q. M., Zhang, H. C., and Kang, Z. S. (2007). Histochemical studies on the accumulation of reactive oxygen species (O^{2-} and H_2O_2) in the incompatible and compatible interaction of wheat-*Puccinia striiformis* f. sp. tritici. *Physiol. Mol. Plant* 71, 230–239. doi: 10.1016/j.pmpp.2008.02.006

Wu, H. X., Sparks, C. A., and Jones, H. D. (2006). Characterisation of T-DNA loci and vector backbone sequences in transgenic wheat produced by *Agrobacterium*-mediated transformation. *Mol. Breed.* 18, 195–208. doi: 10.1007/s11032-007-9090-1

Xiao, S., Brown, S., Patrick, E., Brearley, C., and Turner, J. G. (2003). Enhanced transcription of the Arabidopsis disease resistance genes *RPW8.1* and *RPW8.2* via a salicylic acid-dependent amplification circuit is required for hypersensitive cell death. *Plant Cell* 15, 33–45. doi: 10.1105/tpc.006940

Youssef, A., Laizet, Y., Block, M. A., Marechal, E., Alcaraz, J. P., Larson, T. R., et al. (2010). Plant lipid-associated fibrillin proteins condition jasmonate production under photosynthetic stress. *Plant J.* 61, 436–445. doi: 10.1111/j.1365-313X.2009.04067.x

Yu, X., Feng, B. M., He, P., and Shan, L. B. (2017). From chaos to harmony: responses and signaling upon microbial pattern recognition. *Annu. Rev. Phytopathol.* 55, 109–137. doi: 10.1146/annurev-phyto-080516-035649

Yuan, M., Jiang, Z., Bi, G., Nomura, K., Liu, M., Wang, Y., et al. (2021). Pattern-recognition receptors are required for NLR-mediated plant immunity. *Nature* 592, 105–109. doi: 10.1038/s41586-021-03316-6

Zheng, P., Chen, L., Zhong, S., Wei, X., Zhao, Q., Pan, Q., et al. (2020). A Cu-only superoxide dismutase from stripe rust fungi functions as a virulence factor deployed for counter defense against host-derived oxidative stress. *Environ. Microbiol.* 22, 5309–5326. doi: 10.1111/1462-2920.15236

Zou, S., Wang, H., Li, Y., Kong, Z., and Tang, D. (2018). The NB-LRR gene *Pm60* confers powdery mildew resistance in wheat. *New Phytol.* 218, 298–309. doi: 10.1111/nph.14964

Conflict of Interest: The authors declare that the research was conducted in the absence of any commercial or financial relationships that could be construed as a potential conflict of interest.

Publisher's Note: All claims expressed in this article are solely those of the authors and do not necessarily represent those of their affiliated organizations, or those of the publisher, the editors and the reviewers. Any product that may be evaluated in this article, or claim that may be made by its manufacturer, is not guaranteed or endorsed by the publisher.

frontiers in Plant Science

CORRECTION
published: 19 November 2021
doi: 10.3389/fpls.2021.803911

Corrigendum: Functional Verification of Two Genes Related to Stripe Rust Resistance in the Wheat-*Leymus mollis* Introgression Line M8664-3

Pengfei Jin[1†], *Kaixiang Chao*[1,2†], *Juan Li*[1,3], *Zihao Wang*[1], *Peng Cheng*[1], *Qiang Li*[1*] and *Baotong Wang*[1*]

[1] State Key Laboratory of Crop Stress Biology for Arid Areas, College of Plant Protection, Northwest A&F University, Yangling, China, [2] College of Chemistry, Biology and Environment, Yuxi Normal University, Yuxi, China, [3] Dingxi Plant Protection and Quarantine Station, Dingxi, China

Keywords: functional verification, stripe rust, resistance, wheat-*Leymus mollis*, *YrM8664-3*

OPEN ACCESS

Edited and reviewed by:
Xiaodong Wang,
Agricultural University of Hebei, China

***Correspondence:**
Baotong Wang
wangbt@nwsuaf.edu.cn
Qiang Li
qiangli@nwsuaf.edu.cn

†These authors have contributed equally to this work and share first authorship

Specialty section:
This article was submitted to Plant Pathogen Interactions, a section of the journal Frontiers in Plant Science

Received: *28 October 2021*
Accepted: *01 November 2021*
Published: *19 November 2021*

Citation:
Jin P, Chao K, Li J, Wang Z, Cheng P, Li Q and Wang B (2021) Corrigendum: Functional Verification of Two Genes Related to Stripe Rust Resistance in the Wheat-Leymus mollis Introgression Line M8664-3. Front. Plant Sci. 12:803911. doi: 10.3389/fpls.2021.803911

A Corrigendum on

Functional Verification of Two Genes Related to Stripe Rust Resistance in the Wheat-*Leymus mollis* Introgression Line M8664-3

by Jin, P., Chao, K., Li, J., Wang, Z., Cheng, P., Li, Q., and Wang, B. (2021). Front. Plant Sci. 12:754823. doi: 10.3389/fpls.2021.754823

In the original article, the fourth image in **Figure 3B** (BSMV:Ta_Pes_BRCT) was incorrect when published. The corrected version of **Figure 3** appears below.

The authors apologize for this error and state that this does not change the scientific conclusions of the article in any way. The original article has been updated.

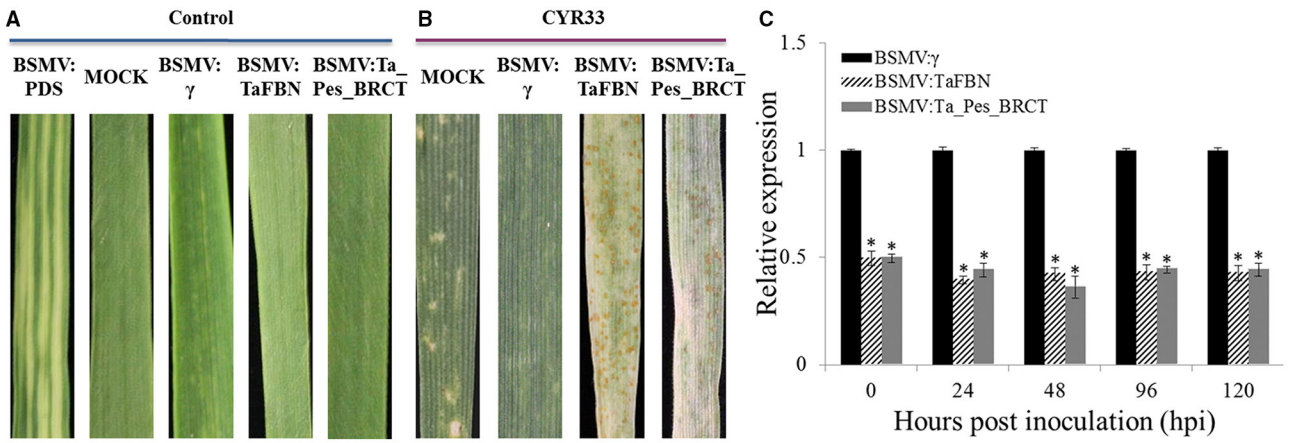

FIGURE 3 | Transient silencing of *TaFBN* and *Ta_Pes_BRCT* with the BSMV-VIGS method. **(A)** Wheat leaves treated with 1× Fes buffer (MOCK) show no phenotypic changes. Mild chlorotic mosaic symptoms were detected on the plants inoculated with BSMV:γ, BSMV:PDS, BSMV:TaFBN, or BSMV:Ta_Pes_BRCT. **(B)** Phenotypes of the fourth leaves infected with uredospores of *Pst* race CYR33 at 10 days post inoculation. **(C)** Silencing efficiency assessment of *TaFBN* in the TaFBN-knockdown plants and *Ta_Pes_BRCT* in the Ta_Pes_BRCT-knockdown plants. Error bars represent the standard deviations of three independent samples. The significance of differences is indicated by asterisks and tested using Student's *t*-test ($P < 0.05$).

frontiers in Plant Science

ORIGINAL RESEARCH
published: 16 November 2021
doi: 10.3389/fpls.2021.741231

Trichoderma longibrachiatum (TG1) Enhances Wheat Seedlings Tolerance to Salt Stress and Resistance to *Fusarium pseudograminearum*

Solomon Boamah[1,2,3], Shuwu Zhang[1,2,3], Bingliang Xu[1,2,3]*, Tong Li[2,3] and Alejandro Calderón-Urrea[2,3]*

[1] Gansu Provincial Key Laboratory of Arid Land Crop Science, Gansu Agricultural University, Lanzhou, China, [2] College of Plant Protection, Lanzhou, China, [3] Biocontrol Engineering Laboratory of Crop Diseases and Pests of Gansu Province, Lanzhou, China

Salinity is abiotic stress that inhibits seed germination and suppresses plant growth and root development in a dose-dependent manner. *Fusarium pseudograminearum* (Fg) is a plant pathogen that causes wheat crown rot. Chemical control methods against Fg are toxic to the environment and resistance has been observed in wheat crops. Therefore, an alternative approach is needed to manage this devastating disease and the effects of salinity. Our research focused on the mycoparasitic mechanisms of *Trichoderma longibrachiatum* (TG1) on Fg and the induction of defenses in wheat seedlings under salt and Fg stress at physiological, biochemical and molecular levels. The average inhibition rate of TG1 against Fg was 33.86%, 36.32%, 44.59%, and 46.62%, respectively, in the four NaCl treatments (0, 50, 100, and 150 mM). The mycoparasitic mechanisms of TG1 against Fg were coiling, penetration, and wrapping of Fg hyphae. In response to inoculation of TG1 with Fg, significant upregulation of cell wall degrading enzymes (CWDEs) was observed. The expression of β-1, 6-glucan synthase (PP4), endochitinase precursor (PH-1), and chitinase (chi18-15) increased by 1. 6, 1. 9, and 1.3-fold on day 14 compared with day 3. Wheat seedlings with combined TG1 + Fg treatments under different NaCl stress levels decreased disease index by an average of 51.89%; increased the superoxide dismutase (SOD), peroxidase (POD), and catalase (CAT) activity by an average of 38%, 61%, and 24.96%, respectively; and decreased malondialdehyde (MDA) and hydrogen peroxide (H_2O_2) content by an average of 44.07% and 41.75% respectively, compared with Fg treated seedlings. The combined TG1 + Fg treatment induced the transcription level of plant defense-related genes resulting in an increase in tyrosin-protein kinase (PR2), chitinase class I (CHIA1), and pathogenesis-related protein (PR1-2) by an average of 1.15, 1.35, and 1.37-fold, respectively compared to Fg treatment. However, the expression levels of phenylalanine ammonia-lyase (PAL) increased 3.40-fold under various NaCl stresses. Our results suggest that TG1 enhances wheat seedling growth and controls wheat crown rot disease by strengthening the plant defense system and upregulating the expression of pathogenesis-related genes under both Fg and salt stress.

Keywords: biocontrol microbes, salinity stress, *Fusarium*, *Trichoderma*, mycoparasitism, antioxidative defense system

OPEN ACCESS

Edited by:
Xiaojie Wang,
Northwest A&F University, China

Reviewed by:
Javier Plasencia,
National Autonomous University of Mexico, Mexico
Ágnes Szepesi,
University of Szeged, Hungary

***Correspondence:**
Shuwu Zhang
zhangsw704@126.com
Bingliang Xu
1592661139@qq.com

Specialty section:
This article was submitted to Plant Pathogen Interactions, a section of the journal Frontiers in Plant Science

Received: *14 July 2021*
Accepted: *23 August 2021*
Published: *16 November 2021*

Citation:
Boamah S, Zhang S, Xu B, Li T and Calderón-Urrea A (2021) Trichoderma longibrachiatum (TG1) Enhances Wheat Seedlings Tolerance to Salt Stress and Resistance to Fusarium pseudograminearum. Front. Plant Sci. 12:741231. doi: 10.3389/fpls.2021.741231

INTRODUCTION

Wheat (*Triticum aestivum* L.) is one of the most important cereals grown in arid and semi-arid regions, providing 20% of the total dietary calorie and proteins intake that promotes human nutrition and healthy living (Shiferaw et al., 2013). Drought, soil nutrient deficiency, salinity stress, and disease-causing phytopathogens are all factors that limit wheat development. *Fusarium pseudograminearum* is one of the wheat pathogens that cause catastrophic yield losses by causing crown and root rots in wheat and barley crops (Pasquali et al., 2016). Infected seedlings can experience pre-emergence and post-emergence damping-off as a result of this pathogen (Kazan and Gardiner, 2018). Plants that survive damping-off may exhibit stunted growth and unfilled kernels due to blockage of water and nutrient transfer in the plants. Due to the rot, infected seedlings have dark brown to black crowns. *Fusarium* infections, including *Fusarium* foot rot (FFR) and *Fusarium* root rot (FRR), are responsible for outbreaks of seedling blight, epidemic scab, and *Fusarium* head blight (FHB) in the United States (Subedi et al., 2007). They directly or indirectly cause millions of dollars of losses in wheat and barley production (El-Allaf et al., 2001). The effects of *F. pseudograminearum* on most cereals are often due to the accumulation of deoxynivalenol (DON), an internationally regulated mycotoxin (Bolanos-Carriel et al., 2020). One of the most important methods for controlling plant diseases is chemical control. However, fungicide control of *F. pseudograminearum* in wheat is minimal and does not provide year-round protection against the pathogen (Moya-Elizondo and Jacobsen, 2016; Alahmad et al., 2018) and may pose a risk to human health. Therefore, an alternative for the use of environmentally-friendly and plant-growth-promoting fungi is urgently needed in recent years. Plant-growth-promoting microbes (PGPM) have several potentials that enable them to enhance plant growth. These include ability to fix atmospheric nitrogen and dissolve phosphate in soil, production of siderophores for iron extraction, ACC deaminase that contributes to stress tolerance, and production of indole-3-acetic acid (IAA). They also indirectly promote plant growth by the combating pathogens through nutrient and space competition, secretion of antibiotic substances and induction of defense systems in the plant.

Soil salinization is considered one of the major threats to agricultural production (Isayenkov and Maathuis, 2019), and affects over 1 billion hectares of arable land worldwide (Ivushkin et al., 2019). Increasing salinization is expected to affect 50% of arable land by 2050 (Wang et al., 2003). Salt stress suppresses plant growth, impedes germination and root development in a dose-dependent manner by blocking auxin signaling (Contreras-Cornejo et al., 2014) and triggering dehydration, nutrient deficiency, membrane dysfunction, and oxidative stress, leading to tissue damage or early senescence (Wu and Wang, 2012; Hossain et al., 2017). The accumulation of reactive oxygen species (ROS) is a well-known consequence of stress (Saghafi et al., 2018). Plants evolve scavenging mechanisms that include both enzymatic and non-enzymatic antioxidants to effectively mitigate ROS damage. The major enzymatic systems for ROS scavenging mechanisms, such as SOD, POD, and CAT are important parameters for assessing plant stress resistance. These ROS scavenging mechanisms mediated by antioxidant enzymes are the first line of defense against stress and directly reflect the effects of stress on plants. To maintain the balance between ROS development and interception and to mitigate the negative effects of stress on physiological metabolism and growth of plants, effective antioxidant capacity is essential (Saghafi et al., 2018). Plant responses to combined biotic and abiotic stresses are complex due to the multiple interactions between plants, pathogens and abiotic stresses. It is well known that the physiological and molecular responses of plants to combined abiotic-pathogen stresses differ significantly from their responses to individual stresses (Lin et al., 2015; Ramegowda and Senthil-Kumar, 2015).

Salicylic acid (SA) plays an important role in regulating plant growth, production, maturation, and defense responses (Miura and Tada, 2014). For instance, SA significantly increased seedling size and mass compared to the untreated (control) when applied exogenously to wheat seedlings (Purcărea et al., 2010), and high salt tolerance of wheat seedlings was observed when treated with the SA solution (Cornelia et al., 2011). The application of SA as a soil drench stimulates antioxidant protective responses that may lead to systemic acquired resistance (SAR) resulting in *F. pseudograminearum* (Sorahinobar et al., 2016). These findings shed light on the physiological and molecular function of SA in plant resistance to hemibiotrophic pathogens. Therefore, an alternative method of using plant-growth-promoting fungi that can increase SA in plants instead of exogenous SA application is more beneficial to the current agricultural system.

Trichoderma species are plant-growth-promoting fungi that play an important role in alleviating abiotic and biotic stresses due to their antimicrobial, mycoparasitic, competitive and secondary metabolic potentials, antioxidant enzyme activity and gene expression and synthesis of phytohormones such as IAA and ACC-deaminase (Qiu et al., 2012; Fu et al., 2017; Rubio et al., 2017). Previous studies reported by Pereira et al. (2014) showed that *T. harzianum* ALL-42 enhanced the response of field bean to *Rhizoctonia solani* by increasing the expression of β-1–3-glucanase and peroxidase genes compared to the host response when exposed to the pathogen alone. Similarly, cucumber roots colonized by *T. harzianum* T-203 showed increased activity of chitinase, β-1,3-glucanase, cellulase and peroxidase at 72 h after inoculation (Chatterton, 2010) which also supports the molecular mechanism of biocontrol- fungi in response to biotic stress.

However, there are fewer reports on the application of *Trichoderma* as biocontrol agent (BCA) in controlling wheat crown rot caused by *F. pseudograminearum* (Fg) and inducing salinity tolerance in wheat seedlings. Thus, the objectives of the present study were (i) to clarify the mycoparasitic mechanisms of

Abbreviations: IAA, indole-3-acetic acid; ROS, reactive oxygen species; MDA, malondialdehyde; H_2O_2, hydrogen peroxide; PGPR, plant growth-promoting rhizobacteria; RNA, ribonucleic acid; ACC, 1-aminocyclopropane-1-carboxylate; SOD, superoxide dismutase; POD, peroxidase; CAT, catalase; DNA, deoxyribonucleic acid; ER, emergence rate; EI, emergence index; EP, emergence potential; NaCl, sodium chloride; Fg, *Fusarium pseudograminearum*; SEM, scanning electron microscopy.

TG1 against Fg by morphological and molecular techniques, (ii) to determine the mechanisms of TG1 in controlling wheat crown rot disease under salinity and Fg stress.

MATERIALS AND METHODS

Fungal Inoculum Preparation

The salt tolerance strain of TG1 and Fg were obtained from the Laboratory of Plant Pathology, Gansu Agricultural University. TG1 and Fg were cultured on potato dextrose agar (PDA) in Petri dishes for 7 and 14 days at 25°C, respectively. The conidia suspensions of TG1 and Fg were prepared according to the method of Zhang et al. (2014). The conidial suspensions of TG1 (1.0×10^8 spores per ml) and Fg (5×10^8 spores per ml) were quantified and stored at 4°C.

Salt Concentration Preparation

Salt tolerance was tested according to Zhang S. et al. (2016) where one liter of liquid medium PDA was prepared and NaCl concentrations of 0, 50, 100, and 150 mM (0, 2.922, 5.844, and 8.766 g) were added and autoclaved at 121°C. The solutions were then poured into 8.5 cm Petri dishes.

Determination of the Activity of TG1 Against *F. pseudograminearum* Under Salinity Stress

The antagonistic activity of TG1 against *F. pseudograminearum* was tested *in vitro* with modified settings using a dual culture approach by Rahman et al. (2009). The salinity tolerance test was performed using a colony diameter growth approach in PDA media supplemented with 0–150 mM NaCl. In the dual culture approach, mycelial plugs (5 mm diameter) of Fg (7-day-old culture) and TG1 (3-day-old culture) were transferred in parallel to opposite sides of a PDA plate at a distance (1.5 cm) from the outer edge of the plate. The experimental design was completely randomized with two controls, positive control (medium inoculated with Fg and salt), negative control (medium inoculated with Fg without salt), and treatment (medium inoculated with TG1, Fg, and salt). Each of these groups consisted of six replicates. Plates were incubated after inoculation at 25 ± 1°C with intermittent light. Fg colony diameters and percentage of Fg colony growth inhibition (CGI) were determined from the first to the fourth day after incubation and calculated. CGI (%) = $[(C - T)/(C - 5)] \times 100$, where C = growth of colony in control, T = growth of diameter in treatment and the 5 are the mycelial plugs.

Observation of the Mycoparasitic Effect of TG1 on *F. pseudograminearum* Using Microscope

The physical interactions between TG1 and *F. pseudograminearum* were monitored using a dual plate assay similar to that mentioned above at 150 mM salt stress. Cellophane fragments were removed from the interaction zone after contact (overgrowth), according to the protocols by Yassin et al. (2019). Using S-3400N Fully Automated VP Scanning Electron Microscope (Hitachi High Technologies America, Inc.) at Gansu Agricultural University, Lanzhou, China, imaging of the <2 mm of the interaction zone was achieved. Samples were dehydrated in 100% ethanol for 1 h, dried with carbon dioxide using a samdri®-790 critical point dryer (Tousimis, Rockville, MD, United States), and mounted in aluminum stubs with double-sided tape. The samples were then coated with a tiny layer of gold to make the surface electrically conductive using a Denton DESK II (JMB-3500VA). The electron scans showed the surface structure of the material. The beam settings for surface analysis were 5.0 kV and 1.5 nA, with a spot size of 150. For light microscopy, a wet-mounted glass slide was prepared and viewed under an inverted microscope (Accu Scope, Commack, NY) EXI-410.

Assessment of TG1 Mycoparasitism Genes

A dual plate assay was performed between TG1 and *F. pseudograminearum*. In a Petri plate containing PDA media with salt (150 mM salt stress) and covered with parafilm, 5 mm mycelial plugs of the pathogen and TG1 were equally spaced following the approach of Lopes et al. (2012). The plates were incubated in the dark at 25 ± 1°C. TG1 mycelia were harvested at three-time points: before contact with *F. pseudograminearum* mycelia (T1), on contact (T2), and after contact (overgrowth) (T3), as defined (Atanasova et al., 2013). The control consisted of TG1 facing itself in a salt medium. Following the method of Pimentel et al. (2020), the induction of mycoparasitism-related genes in TG1 was investigated by quantitative RT-PCR. The selected genes were β-1, 6-glucan synthase (PP4), endochitinase precursor (PH-1), and chitinase (chi18-15). The α-tubulin gene was used as a reference gene. The primers used in the experiments were designed according to the NCBI candidate protein sequences of *Trichoderma* EST. The primer sequences and NCBI genes ID are listed in the **Supplementary Table 1**. Total ribonucleic acid (RNA) was extracted from the collected samples according to the instructions of the manufacturer of the fungal RNA kit (OMEGA Bio-Tek). The quantity and purity of the isolated RNA were analyzed using a Nanophotometer™ (IMPLEN, Schatzbogen, Germany). The A_{260}/A_{280} ratio indicated that the RNA was free from protein contamination. First-strand cDNA (Tiangen Biotechnology, Beijing, China) was synthesized using Revert Aid™ First Strand cDNA Synthesis Kit. qRT-PCR was performed using 2× M5 HiPer Real-time PCR Supermix with Low Rox (Mei5 Biotechnology, Co., Ltd., Beijing, China). According to the manufacturer's instructions, the 20 μl reaction mixture contained 0.5 μl of each primer, 1.0 μl of cDNA, 10 μl of 2× M5 HiPer Realtime PCR Super mix with Low Rox and 8.0 μl of ddH_2O qRT-PCR was performed using the following thermal profile: 95°C for 30 s, 40 cycles of 95°C for 15 s, 65°C for 15 s, and 72°C for 30 s. Three technical replicates were used for each gene. The $2^{-\Delta\Delta Ct}$ method (Livak and Schmittgen, 2001) was used to measure the relative expression of each target gene.

Plant Material and Treatment Conditions

The wheat (*Triticum aestivum* L.) cultivar 'Yongliang 4' provided by Gansu Academy of Agricultural Sciences (Lanzhou, China) was used in all the experiments. The cultivar has been well adapted to the major wheat-growing areas of northwest China. The biocontrol potential of TG1 against *F. pseudograminearum* inoculum was tested in artificial saline soil according to the method of Gond et al. (2015). Wheat seeds of equal sizes were surface sterilized with 1% (v/v) NaOCl for 5 min and were rinsed with sterile water six to ten times after disinfection. Thereafter, wheat seeds were soaked in (i) TG1 suspension (1.0×10^8 spores per ml) only, (ii) TG1 suspension plus Fg suspension (5×10^8 spores per ml), (iii) Fg suspension only, and (iv) sterile water only for 12 h. Seeds were air-dried overnight under aseptic conditions before sowing, according to Zhang et al. (2019b).

Effect of TG1 on Wheat Seeds Emergence Under *F. pseudograminearum* and Salt Stress

Fungi-treated wheat seeds and control seeds were exposed to artificial saline soil at 0, 50, 100, and 150 mM NaCl. The soil used for the study was collected from an agricultural crop field in Lanzhou, China (36.061°N, 103.834°E, and 1,518 m above sea level) had a sandy loam texture. Then completely randomized experimental design with two factorial arrangements having inoculation of TG1 and Fg (plus or minus) as the main variable and salinity as the second variable. For each procedure, 6 plastic pots were used (9 cm in diameter and 10.5 cm in depth), each containing 1 kg of air-dried sterile saline soil. Twenty uniform seeds were sown 1 cm deep in the soil and lightly covered. Plants were irrigated every 24 h with non-saline water and maintained at a constant temperature of 25°C ± 0.5, with supplemental day/night lighting of 16/8 h and relative humidity of 65%. Seedling emergence was counted according to the method Oluwaranti et al. (2015) and the percentage of seed emergence potential (EP%) was determined as follows:

$$\mathrm{EP}(\%) = [(seedlingsemergedafter3\ days)/seedplanted] \times 100$$

Based on the formulation of Niu et al. (2013) with minor modification, emergence index [EI (%) = NESi/Ti × 100], where NESi is the number of emerged seeds in a given time and Ti is the incubation time, and emergence rate [ER (%) = (NSE/TNS) × 100], where NSE is the number of emerged seeds 5 days after sowing and TNS is the total number of seeds in each pot.

Growth Parameters

After 28 days of NaCl treatment, the wheat seedlings were harvested. The shoots and roots of wheat seedlings were removed, washed three times with distilled water, dried, and weighed. Root length and weight were measured with the meter rule and weighing balance. To determine the dry weight, all samples of wheat shoots and roots were oven-dried at 105°C for 30 min and then held at 80°C to maintain a constant weight before being weighed. Each preservation and control was performed six times. The relative water content (RWC) of the shoots and roots was measured according to Tian and Philpot (2015). RWC (%) = [(FW − DW)/FW] × 100, where RWC represents relative water content, FW represents fresh weight, and DW represents dry weight.

Disease Assessment

Wheat crown rot disease index was recorded 28 days after sowing. A disease index (DI) based on crown rot, yellowing, and chlorosis of cotyledons and leaves at 28 days was used to classify disease symptoms. The degree of the disease was graded using one of five scales adapted from Zhang et al. (2015) where; 0 indicates that there is no disease; 1 = trace to 10% discoloration of the first leaf sheath; 2 = 11 percent −25 percent discolored first leaf sheath; 3 = 26 percent −50 percent discolored first leaf sheath; 4 = 50 percent discolored first leaf sheath or necrotic second leaf sheath; 5 = third leaf sheath necrotic or entire plant badly to entirely rotten.

Chlorophyll Content Determination

Following the procedure of Miazek and Ledakowicz (2013), chlorophyll was extracted with methanol. A new 0.2 g wheat seedling leaves was homogenized with 10 ml of methanol. At 665 and 652 nm absorbance, the content of chlorophyll was evaluated in a dual-wavelength spectrophotometer (EPOCH2 Plate Reader, BioTek, United States). This was repeated six times.

Lipid Peroxidation and H_2O_2 Measurements

At 28 days after wheat seeds treatments, the root samples were used for oxidants investigations. Oxidants activity such as MDA and H_2O_2 were investigated according to the manufacturer's protocol using the assay kits provided (Solarbio, China). The absorbance of the MDA sample was measured at three different wavelengths 450, 532, and 600 nm, and H_2O_2 at 415 nm using a spectrophotometer (EPOCH2 Plate Reader, BioTek, United States). The content of MDA and H_2O_2 were expressed as $\mu mol\ g^{-1}$ FW. This was repeated six times.

Antioxidant Enzymes Activities

At 28 days after wheat seeds treatments, the root samples were used for antioxidants investigations. The antioxidants activity of SOD (EC 1.15.1.1), POD (EC 1.11.1.7), PAL (EC 4.3.1.5), and CAT (EC 1.11.1.6) were measured according to the manufacturer's protocol using the assay kits provided (Solarbio, China). SOD was measured at 560 nm, POD at 470 nm, PAL at 290 nm, and CAT at 240 nm, respectively, using a spectrophotometer (EPOCH2 Plate Reader, BioTek, United States). This was repeated six times.

Determination of Endogenous SA in Wheat Seedlings

Free SA determination in wheat leaves was performed by high-pressure-liquid chromatography (HPLC) (Shimadzu Prominence LC System, France) following the method of Allasia et al. (2018) with slight modification where 0.1 g of the leaf sample was homogenized using liquid nitrogen. Separations

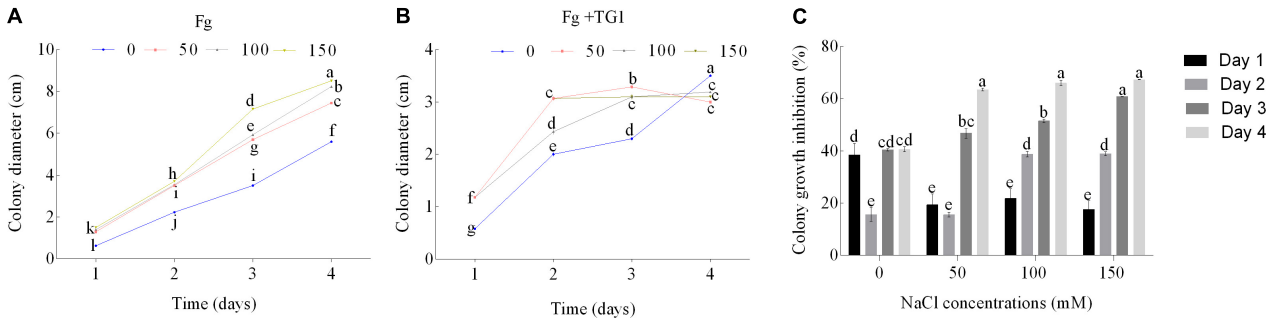

FIGURE 1 | Effect of *T. longibrachiatum* (TG1) and salt stress on *F. pseudograminearum* (Fg) growth. **(A)** colony diameter of Fg only, **(B)** colony diameter of Fg after inoculation with TG1, and **(C)** colony growth inhibition of TG1 against Fg under different salt stresses (0, 50, 100, and 150 mM NaCl) at different days. Different lower case letters indicate significant differences at $P < 0.05$ in Duncan's multiple range test using two-way ANOVA.

by HPLC were performed on a C18 column (250 × 4.6 mm, 5 μm) using a linear aqueous MeOH gradient from 10 to 82% (v/v), at a flow rate of 1 ml min^{-1}, over 30.4 min. Quantify with fluorimetric detection (measured at 305 nm; emission at 407 nm) and determine areas under the corresponding peaks of the standard [2-Methoxybenzoic acid (o-Anisic acid, OAA; internal standard)]. Briefly, stock solution of 152 mg OAA in 10 ml 70% aqueous EtOH (v/v) and diluted 1:1, 000 in ultra-pure water. Using the peak area, the standard curve and linear equation were used to determine the amount of free SA.

Extraction of Total RNA and Analysis of Gene Expression by Quantitative Real-Time Reverse Transcriptase (qRT-PCR)

Total RNA extraction and analysis of 100 mg wheat seedlings root exposed to different levels of NaCl stress and pathogen infection were performed using the E.Z.N.A.® plant RNA kit (OMEGA Bio-Tek, China) (White et al., 2008; Xie et al., 2013). The quantity and quality of isolated RNA and qRT-PCR were analyzed by the same procedure previously used in the analysis of mycoparasitic gene expression. Following the methodology of Zhang S. et al. (2016), unique primers for the bread wheat genes SOD, POD, and CAT and the internal control actin were used to amplify amplicons specific to wheat seedlings. The above genes were selected based on their role in wheat seedlings under stress in previous studies (Asthir et al., 2011). Primers used in the experiments were designed using Primer Express 3.0 software, which amplifies target genes according to the sequences of candidate proteins available in NCBI wheat EST (Wang et al., 2014). Using the previously described method for mycoparasitic gene expression, the relative expression of antioxidant genes (SOD, POD, and CAT) and the expression level of plant defense-related genes [tyrosine-protein kinase (PR2), PR1-2 pathogenesis-related protein, phenylalanine ammonia-lyase (PAL), and chitinase class I (CHIA1)] were assessed by quantitative qRT-PCR. Primer sequences and NCBI gene IDs for all genes can be found in the **Supplementary Table 1**.

Statistical Analysis

The data were tested in each experiment included TG1 strain on controlling *F. pseudograminearum* and inducing salinity tolerance in wheat seedlings. Data were analyzed using two-way ANOVA in SPSS Version 16.0 (SPSS Inc., Chicago, IL, United States), and mean comparisons were made using Duncan's new multiple range test and the significance was considered at $P < 0.05$.

RESULTS

Salinity Tolerance and *in vitro* Colony Growth Inhibition

Salt stress and TG1 significantly ($p < 0.05$) affected the colony growth of Fg at different days after incubation (**Figures 1A,B**). The average inhibitory rate of TG1 against Fg was 33.86%, 36.32%, 44.59%, and 46.62%, respectively, for the four NaCl treatments (0, 50, 100, and 150 mM NaCl) (**Figure 1C**). Additionally, an increase in NaCl concentration increased the inhibitory rate of TG1 against the Fg colony growth at 4 days under different concentrations of salt stress (**Figures 1C**, **2A,B**).

Microscopic Observations of Mycoparasitism

Light microscopy revealed that TG1 wrapped around the host hyphae of Fg and formed appressoria and hook-like structures that allowed firm attachment to the fungal host (**Figure 3A**). Growth of TG1 conidia was observed in the fungal host indicating the use of the fungal host as a nutrient source (**Figures 3B,C**). Visible disruption and decomposition of Fg hyphae by TG1 was observed coupled with a parallel growth in close hyphal association, also suggesting mycoparasitism. Germinating spore tubes of TG1 were found in the hyphae of Fg (**Figures 3D,E**). Again, the strain TG1 showed a mycoparasitic mechanism by invading the hyphae of Fg (**Figures 3F–J**).

Mycoparasitism Genes

In response to inoculation of TG1 with and Fg, significant ($p < 0.05$) upregulation of CWDEs was observed in TG1 at

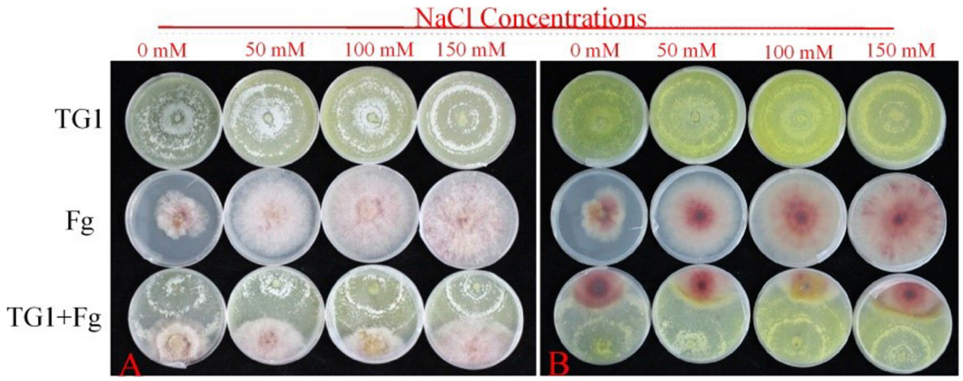

FIGURE 2 | Effect of different NaCl concentrations on colony growth and inhibition between *T. longibrachiatum* (TG1) and *F. pseudograminearum* (Fg) at 4 days after inoculation using dual plate assay (0–150 mM of NaCl concentrations). **(A)** front colony, and **(B)** reverse colony.

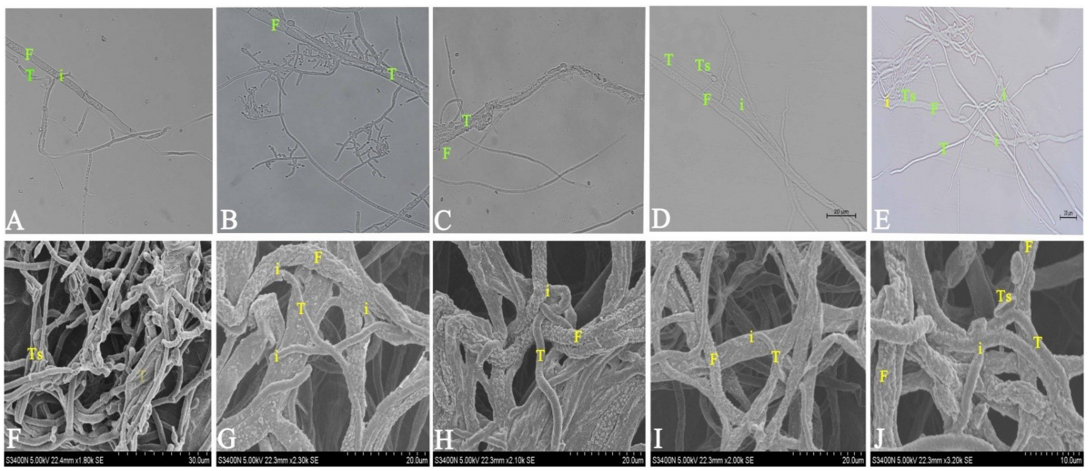

FIGURE 3 | Mycoparasitism of *T. longibrachiatum* (TG1) (T) against *F. pseudograminearum* (Fg) (F) observed under light microscopy at 40× magnification and scanning electron microscopy (SEM) at 4 days after inoculation using dual plate assay at 150 mM NaCl concentration. **(A)** TG1wrapped around *F. pseudograminearum* hyphae with obvious degradation of *F. pseudograminearum* cell wall. **(B)** TG1 conidial growth internally and externally on *F. pseudograminearum* hyphae. **(C)** TG1 hyphal disruption, penetration and breakage of *F. pseudograminearum* hyphae. **(D)** TG1 spore germ tube (Ts) growing on *F. pseudograminearum* hyphae. **(E)** *F. pseudograminearum* hyphae looped by TG1 hyphae and TG1 hyphae extending parallel to *F. pseudograminearum* showing hyphal depression. **(F–H)** SEM images of TG1 (T) coiling the hyphae of *F. pseudograminearum*. **(I,J)** SEM images of TG1 coiling and invading the hyphae of *F. pseudograminearum.* Ts represent *Trichoderma* spore and (i) represent the point of interaction.

150 mM salt stress. The expression of β-1, 6-glucan synthase (PP4) (**Figure 4A**), endochitinase precursor (PH-1) (**Figure 4B**), and chitinase (chi18-15) (**Figure 4C**) genes increased by 1.6, 1.9, and 1.3-fold, respectively, at T3 compared to T1. In appressoria and fast-growing biotrophic hyphae, CWDEs are required for cell wall stiffness, and their rigorous upregulation during biocontrol activity represents a strategy to enhance immunity and mycoparasitism.

Effect of TG1 on Wheat Seed Growth Under *F. pseudograminearum* and Different Salt Stresses

Compared to the treatments with sterile water (control), the seeds treated with TG1 increased emergence rate (ER) (**Figure 5A**) by an average of 8.71%, emergence potential (EP) (**Figure 5B**) by 11.39%, and emergence index (EI) (**Figure 5C**) by 13.19%, in the four NaCl treatments (0, 50, 100, and 150 mM). However, seeds treated with the combination TG1 + Fg increased ER by an average of 15.10%, EP by 15.32%, and EI by 19.15% in all four NaCl treatments compared to the Fg treatment alone. Without TG1 treatment, ER, EP, and EI of the control decreased significantly with increasing NaCl concentration.

Plant Biomass Accumulations and Relative Water Content

Salt and pathogenic stress significantly ($p < 0.05$) affected fresh weight (FW), dry weight (DW), and relative water content (RWC) of shoot and root of wheat seedlings (**Table 1**). Compared with the control, TG1-treated seedlings increased FW and DW

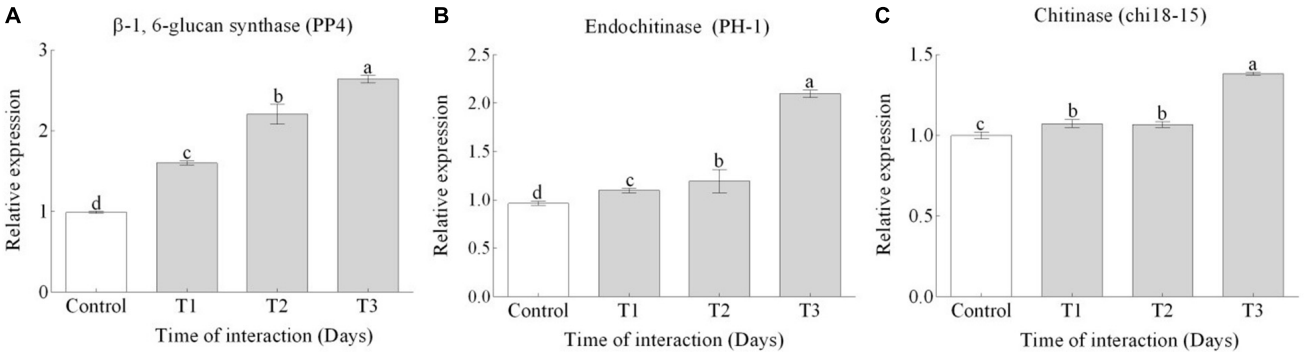

FIGURE 4 | Relative expression levels of **(A)** β-1, 6-glucan synthase (PP4), **(B)** endochitinase (PH-1), and **(C)** endochitinase (chi18-15) genes were measured by qRT-PCR during the interaction of *T. longibrachiatum* (TG1) and *F. pseudograminearum* (Fg) in a dual plate assay at 150 mM salt stress. Gene expression was evaluated at three different interaction time points at Days 3 (T1), 7 (T2), and 14 (T3) after the interaction. The $2^{-\Delta\Delta ct}$ method was used for the relative expression of each target gene using the control and α-tubulin as the reference gene. Small bars represent the standard errors of the means. Different lower case letters indicate significant differences at $P < 0.05$ in Duncan's multiple range test using two-way ANOVA.

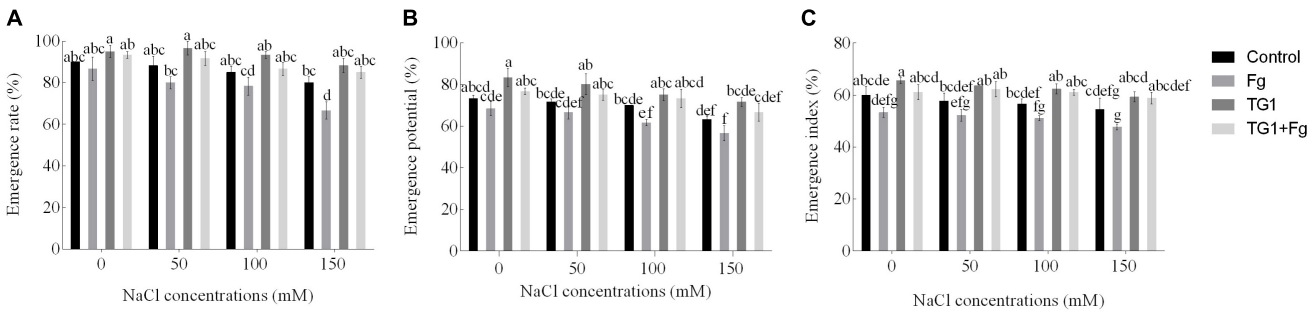

FIGURE 5 | Effect of *T. longibrachiatum* (TG1) on wheat seeds **(A)** emergence rate, **(B)** emergence potential, and **(C)** emergence index under *F. pseudograminearum* (Fg) and salt stress. Different lower case letters indicate significant differences at $P < 0.05$ in Duncan's multiple range test using two-way ANOVA. Emergence rate, potential, and index were determined after treatment, respectively. Control treatments represent wheat seedlings pretreated with distilled water only; TG1 represents wheat seeds pretreated with the suspension of *T. longibrachiatum* (TG1); TG1 + Fg represents wheat seeds pretreated with *T. longibrachiatum* (TG1) and *F. pseudograminearum* (Fg); and Fg represents wheat seeds pretreated with *F. pseudograminearum* (Fg) for 12 h before planting with different NaCl treatments (0, 50, 100, and 150 mM).

of the shoot by an average of 36.53% and 20%; the root FW, DW, and RWC by 25.59%, 6.35%, and 11.16%, respectively, across the four NaCl treatments levels (from 0 to 50, 100, and 150 mM). However, TG1 + Fg-treated seedlings increased FW and DW of the shoot by an average of 63.37% and 43.47%; the root FW, DW, and RWC by 56.20%, 35.89%, and 12.05%, respectively, across the four NaCl treatment levels, compared with Fg treatment alone. Increasing NaCl concentration along with pathogen infection without treatment with strain TG1 decreased seedling FW, DW, and RWC.

Effect of TG1 on Wheat Seedlings Growth, Chlorophyll Content and ROS Accumulation Under *F. pseudograminearum* (Fg) and Different Salt Stresses

Salt and pathogenic stress significantly ($p < 0.05$) affected shoot height and root length of wheat seedlings (**Table 2**). Increasing NaCl concentration along with pathogen stress decreased shoot height and root length. However, TG1 treatment increased shoot height and root length of wheat seedlings irrespectively of the presence of the pathogen or different NaCl concentrations (from 0 to 50, 100, and 150 mM). Compared with the control, shoot height and root length increased by an average of 22.76% and 21.35%, respectively, in the seedlings treated with the strain TG1 at the different NaCl concentrations. However, the seedlings treated with TG1 + Fg showed an average increase of 27.21% and 25.21% in shoot height and root length, respectively, at the different NaCl concentrations compared to the seedlings treated with Fg alone.

Compared to seedlings treated with Fg alone, TG1 treatment increased chlorophyll content by an average of 55.39% at the four NaCl stresses. However, the combined TG1 + Fg treatment increased the chlorophyll content of wheat seedlings by 37.14% and 85.38% at 100 and 150 mM NaCl stress, respectively (**Table 2**).

TABLE 1 | Effect of *T. longibrachiatum* (TG1) on wheat seedling biomass and relative water content under *F. pseudograminearum* (Fg) and different salt stresses.

NaCl (mM)	Treatment	Wheat shoot			Wheat root		
		Fresh weight (g plant^{-1})	Dry weight (g plant^{-1})	Relative water content (%)	Fresh weight (g plant^{-1})	Dry weight (g plant^{-1})	Relative water content (%)
0	Control	0.60 ± 0.03bcd	0.10 ± 0.00c	83.33 ± 0.24abcd	0.25 ± 0.04c	0.09 ± 0.00b	64.00 ± 1.03abcd
	Fg	0.50 ± 0.05fg	0.09 ± 0.00d	82.00 ± 1.52bcde	0.21 ± 0.00de	0.08 ± 0.00c	61.90 ± 0.05abcd
	TG1	0.76 ± 0.03a	0.12 ± 0.01a	84.21 ± 0.032abcd	0.30 ± 0.00a	0.10 ± 0.01a	66.67 ± 0.03ab
	TG1 + Fg	0.67 ± 0.02b	0.11 ± 0.00b	83.58 ± 0.46abcd	0.28 ± 0.03b	0.10 ± 0.00a	64.29 ± 0.02abc
50	Control	0.58 ± 0.02cdef	0.10 ± 0.00c	82.76 ± 0.44abcde	0.22 ± 0.06d	0.09 ± 0.03b	59.09 ± 1.01cde
	Fg	0.43 ± 0.03h	0.08 ± 0.01e	81.40 ± 1.57cde	0.18 ± 0.00gh	0.07 ± 0.00d	61.11 ± 0.15bcd
	TG1	0.75 ± 0.00a	0.11 ± 0.01b	85.33 ± 0.85a	0.27 ± 0.00b	0.09 ± 0.03b	67.67 ± 0.23a
	TG1 + Fg	0.64 ± 0.02bc	0.10 ± 0.01c	84.38 ± 0.90abc	0.24 ± 0.03c	0.09 ± 0.02b	62.50 ± 0.12abcd
100	Control	0.52 ± 0.05efg	0.09 ± 0.00d	82.69 ± 0.78abcde	0.19 ± 0.04fg	0.08 ± 0.00c	57.89 ± 0.09de
	Fg	0.32 ± 0.01i	0.06 ± 0.01f	81.25 ± 0.69de	0.13 ± 0.00j	0.06 ± 0.01e	53.85 ± 0.32e
	TG1	0.59 ± 0.02cde	0.09 ± 0.00d	84.75 ± 0.89ab	0.24 ± 0.00c	0.08 ± 0.02c	66.67 ± 0.21ab
	TG1 + Fg	0.56 ± 0.03cdef	0.10 ± 0.01c	82.14 ± 1.13bcde	0.22 ± 0.03d	0.09 ± 0.01b	59.09 ± 0.03cde
150	Control	0.30 ± 0.01i	0.06 ± 0.00f	80.00 ± 2.28ef	0.15 ± 0.00i	0.07 ± 0.01d	53.33 ± 0.15e
	Fg	0.23 ± 0.02j	0.05 ± 0.00g	78.26 ± 1.90f	0.09 ± 0.00k	0.05 ± 0.00f	44.44 ± 0.05f
	TG1	0.53 ± 0.06def	0.09 ± 0.00d	83.02 ± 1.38abcde	0.20 ± 0.00ef	0.08 ± 0.00c	60.00 ± 0.01cd
	TG1 + Fg	0.45 ± 0.01gh	0.08 ± 0.00e	82.22 ± 0.30bcde	0.17 ± 0.03h	0.07 ± 0.01d	58.82 ± 0.02cde

Data are mean ± standard error of replicates in a column followed by different letters are significantly different at $P < 0.05$ based on Duncan's multiple range test using two-way ANOVA. The treatments are detailed in the footnote of ***Figure 5****.*

TABLE 2 | Effect of *T. longibrachiatum* (TG1) on wheat seedlings growth, chlorophyll content and ROS accumulation under *F. pseudograminearum* (Fg) and different salt stresses.

NaCl concentration (mM)	Treatment	Shoot length (cm)	Root length (cm)	Chlorophyll content (mg g^{-1})	MDA content in root (μmol g^{-1} FW)	H_2O_2 content in root (μmol g^{-1} FW)
0	Control	27.13 ± 1.89bc	14.87 ± 0.38bc	1.37 ± 0.11bcd	0.86 ± 0.02ghi	0.99 ± 0.01fg
	Fg	26.10 ± 0.06cd	13.27 ± 1.13def	1.33 ± 0.10bcde	1.01 ± 0.01fg	1.16 ± 0.11f
	TG1	31.83 ± 0.77a	18.03 ± 0.62a	1.72 ± 0.13a	0.70 ± 0.05i	0.55 ± 0.01h
	TG1 + Fg	29.77 ± 0.18ab	15.27 ± 0.49bc	1.63 ± 0.02ab	0.74 ± 0.08hi	0.63 ± 0.10h
50	Control	25.67 ± 0.64cd	14.20 ± 0.06bcde	1.32 ± 0.09bcd	1.10 ± 0.05f	1.17 ± 0.00f
	Fg	25.03 ± 0.33cd	13.17 ± 0.07def	1.26 ± 0.06cdef	1.65 ± 0.05d	1.58 ± 0.04e
	TG1	31.90 ± 1.47a	17.57 ± 0.03a	1.63 ± 0.05ab	0.86 ± 0.01ghi	0.75 ± 0.00gh
	TG1 + Fg	30.87 ± 1.69b	15.13 ± 0.03bc	1.54 ± 0.13abc	0.89 ± 0.01gh	0.84 ± 0.03gh
100	Control	23.97 ± 1.05cde	12.70 ± 0.45efg	1.14 ± 0.07def	1.67 ± 0.06d	1.89 ± 0.04d
	Fg	23.20 ± 0.74de	11.30 ± 0.06g	0.99 ± 0.03f	2.52 ± 0.03b	2.35 ± 0.27c
	TG1	31.73 ± 1.13a	15.57 ± 0.14b	1.51 ± 0.03abc	1.36 ± 0.11e	1.25 ± 0.02f
	TG1 + Fg	30.63 ± 1.62a	13.97 ± 0.27cde	1.36 ± 0.16bcd	1.41 ± 0.08e	1.28 ± 0.02f
150	Control	21.13 ± 1.25e	12.17 ± 0.19fg	1.06 ± 0.05ef	2.21 ± 0.07c	3.82 ± 0.07b
	Fg	16.87 ± 1.49f	8.97 ± 1.02h	0.68 ± 0.06g	4.04 ± 0.02a	5.22 ± 0.03a
	TG1	24.73 ± 0.28cd	14.33 ± 0.22bcd	1.43 ± 0.04abcd	1.34 ± 0.02e	2.11 ± 0.21cd
	TG1 + Fg	23.03 ± 0.23de	13.20 ± 0.25def	1.25 ± 0.14cdef	1.65 ± 0.03d	3.71 ± 0.03b

Data are mean ± standard error of replicates in a column followed by different letters are significantly different at $P < 0.05$, based on Duncan's multiple range test using two-way ANOVA. The treatments are detailed in the footnote of ***Figure 5****.*

MDA and H_2O_2 content in wheat seedlings treated with control and Fg increased significantly with the increase in NaCl concentration. Averaged over the four NaCl concentration treatments (from 0 to 50, 100, and 150 mM), seedlings treated with strain TG1 decreased MDA and H_2O_2 content in roots by 24.28% and 39.79%, respectively, compared to the control; similarly, the combination of TG1 + Fg treated seedlings decreased MDA and H_2O_2 content by 44.07% and 41.75%, respectively, compared to seedlings treated with Fg alone. The extent of MDA and H_2O_2 content was greater in seedlings treated with Fg at 150 mM NaCl concentration than at 50 and 100 mM NaCl concentrations. Strain TG1 decreased both MDA and H_2O_2 content with or without the pathogen and NaCl stress (**Table 2**).

Crown Rot, Seedling Blight, and Seedling Death

The positive effect of TG1 on reducing the disease index of crown rot was observed when the seeds were treated with BCA. However, the severity of *F. pseudograminearum* increased significantly ($p < 0.05$) in saline soils compared to non-saline soils (**Figure 6E**). The combined treatment with the antagonist and the pathogen (TG1 + Fg) reduced disease index in wheat seedlings by 64%, 52.78%, 47.92%, and 42.86%, respectively, compared to the pathogen alone across the four NaCl concentrations. The conidiospores of the pathogen germinated and invaded the xylem and pith of both the crown and root, developed a reddish-brown or white discoloration (**Figure 6B**). Salinity and pathogen stress caused the crown to turn from green to dull yellow, causing dysfunction, and reducing water and nutrient uptake (**Figure 6D**). Seedling death, root rot and crown rot were observed under pathogen and salinity stress at 150 mM NaCl compared to 0 mM NaCl concentration (**Figures 6A,C**).

Endogenous SA Content and PAL Activity

NaCl and Fg stress significantly ($p < 0.05$) affected SA content and PAL activity in wheat seedlings (**Figures 7A,B**). Compared to the control, seeds treated with strain TG1 increased SA by 47.96% at 0 mM NaCl. However, TG1 + Fg treated seedlings increased SA content by an average of 40.56% compared to Fg treated seedlings (**Figure 7A**).

Fg and NaCl stress significantly affected the activity of PAL. Fg-treated seedlings increased the activity of PAL compared with the control with or without NaCl stress. Averaged over the four levels of NaCl concentration treatment, seeds treated with TG1 + Fg increased the activity of PAL by 11% compared to seedlings treated with Fg alone. Similarly, an increase in NaCl concentration increased the PAL activity of TG1 compared with the control. Across the four NaCl concentration treatments, seedlings treated with TG1 increased the activity of PAL by an average of 28% compared with the control (**Figure 7B**).

Antioxidant Enzymes Activities and Gene Expression

The combined biotic and abiotic stressors had effects on antioxidant enzyme activity. At all four NaCl concentrations (from 0 to 50, 100, and 150 mM), antioxidant enzyme activity increased with an increasing NaCl concentration. Compared with the control, wheat seedlings treated with TG1 increased SOD activity by 32% and 24% at 100 and 150 mM NaCl concentrations, respectively. However, wheat seedlings treated with TG1 increased POD and CAT at all four NaCl concentrations by an average of 38% and 17%, respectively, compared to the control. Similarly, wheat seedlings treated with the combination TG1 + Fg increased the activity of SOD, POD, and CAT by an average of 38%, 61%, and 24.96%, respectively, compared with Fg treatment alone at the four NaCl concentrations (**Figures 8A–C**).

Fg and NaCl stress-induced higher transcript levels of the genes SOD, POD, and CAT compared with control. Significant upregulation of the genes SOD, POD, and CAT was observed in response to TG1 treatment (**Figures 8D–F**). An increase in NaCl concentration along with Fg increased the expression levels of the genes compared with the house-keeping gene. Wheat seedlings treated with TG1 increased the transcript levels of SOD by 1.11 and 1.22-fold at 100 and 150 mM NaCl concentration, respectively, compared with 0 mM NaCl concentration in TG1 treatment. Similarly, the transcript level of POD increased by 1.76-fold in TG1-treated seedlings at 150 mM NaCl concentration compared to 0 mM NaCl concentration. At NaCl concentrations of 50, 100, and 150 mM, TG1-treated seedlings increased the transcription level of the gene CAT by an average of 1.24-fold compared to 0 mM NaCl concentration in TG1 treatment. The combined TG1 + Fg-treated wheat seedlings with 150 mM NaCl-stress increased the expression levels of SOD, POD, and CAT by 1.61, 2.07, and 1.81-fold, respectively, compared to 0 mM NaCl concentration in TG1+Fg treatment.

Plant Defense-Related Genes Expression

NaCl and Fg stress significantly ($p < 0.05$) affected the expression of the proteins associated with pathogenesis (**Figures 9A–C**). The wheat seedlings treated with strain TG1 increased the transcript levels of the tyrosine-protein kinase (PR2) by 1.15 and 1.17-fold at 100 and 150 mM NaCl concentration, respectively, compared to 0 mM NaCl concentration in TG1 treatment. Similarly, transcription of pathogenesis-related protein (PR1-2) increased by 1.24 and 1.44-fold at 100 and 150 mM of NaCl concentration, respectively, under TG1 treatment. Likewise, the transcript level of chitinase class I (CHIA1) in TG1-treated wheat seedlings increased by 1.08-fold at 150 mM NaCl concentration compared to 0 mM NaCl concentration in TG1 treatment. However, the PAL transcript level of TG1-treated wheat seedlings increased by 1.87 and 1.58-fold at 50 and 100 mM NaCl compared with 0 mM of NaCl concentration, respectively (**Figure 9D**). The combined TG1 + Fg treatment induced the transcription level of plant defense-related genes resulting in an increase in PR2, CHIA1, PR1-2, and PAL gene expression by an average of 1.15, 1.35, 1.37, and 3.40-fold, respectively, compared to Fg treatment.

DISCUSSION

High NaCl stress affected colony color and sporulation of both the antagonist and the pathogen. Previous studies found that salt stress decreased colony diameter growth, spore germination, morphology, conidial sporulation and environmental sensitivity of the fungus (Paulitz and Bélanger, 2001). Other studies revealed that *F. solani* was the most resistant among the *Furarium* to an increase in NaCl and temperature (Mandeel, 2006). The NaCl tolerance of the species was followed by the development of massive thick-walled, drought-resistant chlamydospores, indicating that the species is predominantly thermo-osmotolerant (Mandeel, 2006). Similarly, in this study, both the antagonist and the pathogen tolerated 150 mM NaCl stress. *Furarium pseudograminearum* tolerated high sodium chloride stress with slow growth

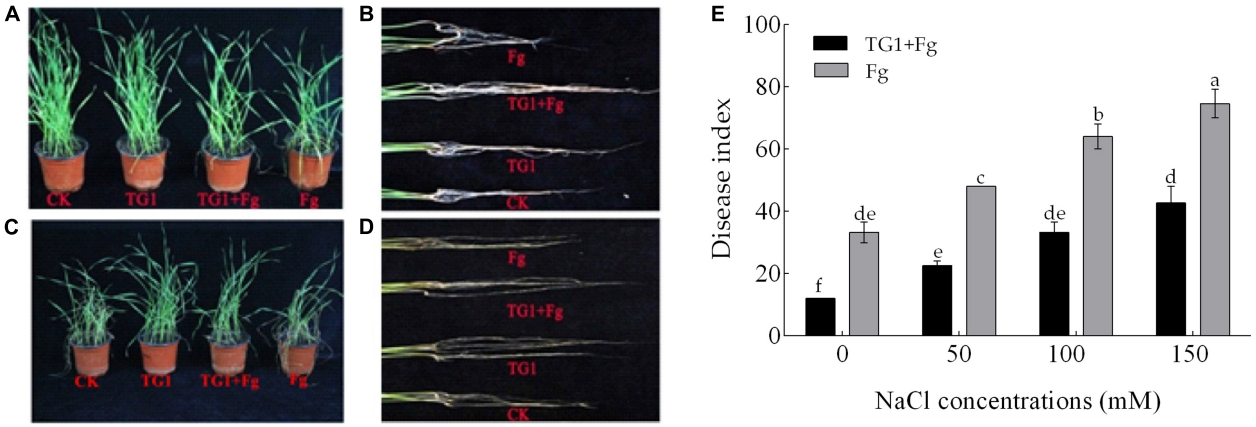

FIGURE 6 | Effect of *T. longibrachiatum* (TG1) on wheat seedling disease index at 28 days after inoculation under *F. pseudograminearum* (Fg) and different NaCl stress. Panels **(A,B)** represent treatments without NaCl; **(C,D)** represent treatments with 150 mM of NaCl stress; and **(E)** represents the disease index across the four NaCl concentrations (0, 50, 100, and 150 mM). Small bars represent the standard errors of the means. Different lower case letters indicate significant differences at $P < 0.05$ in Duncan's multiple range test using two-way ANOVA. The treatments are detailed in the footnote of **Figure 5**.

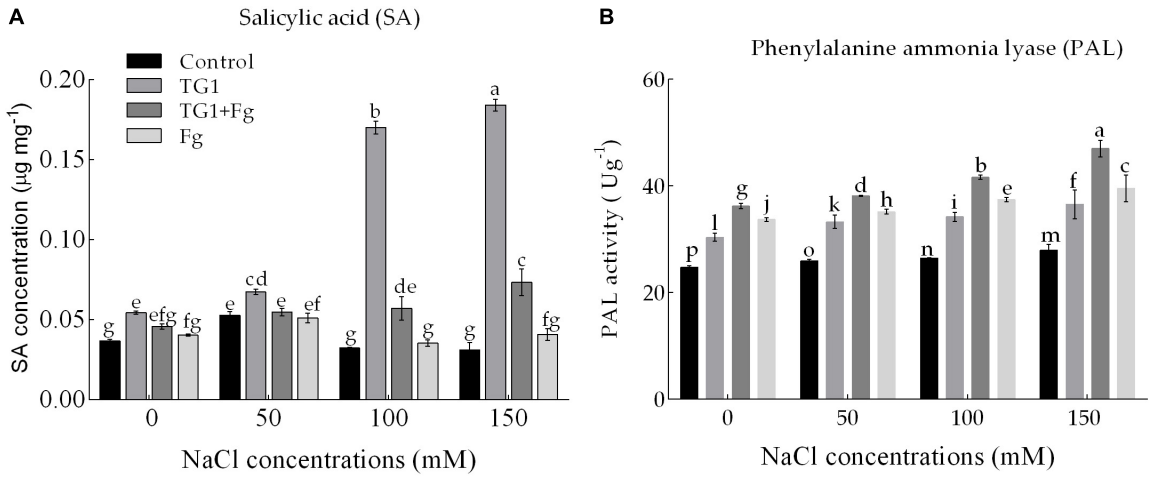

FIGURE 7 | Effect of *T. longibrachiatum* (TG1) on **(A)** salicylic acid content and **(B)** phenylalanine ammonia-lyase (PAL) activity of wheat seedlings subjected to *F. pseudograminearum* (Fg) and different salinity stress at 28 days after inoculation. Small bars represent the standard errors of the means. Different lower case letters indicate significant differences at $P < 0.05$ in Duncan's multiple range test using two-way ANOVA. Treatments are detailed in the footnote of **Figure 5**.

compared to the antagonist. Both fungi developed salt-resistant hyphae, thick-walled conidia and chlamydospores. Interestingly, the antagonist *T. longibrachiatum* TG1 inhibited the growth of the pathogen under both normal and NaCl stress, which is helpful for its activity as a BCA. This result is in agreement with the findings of Narayan et al. (2017) whose study showed that *T. viride* and *Trichoderma* spp. significantly inhibited the mycelial growth of *Fusarium*.

In the present study, the microscopic analysis showed that TG1 wraps around the hyphae of *F. pseudograminearum* and grows parallel with the tight hyphae association, indicating mycoparasitism (Monteiro et al., 2010). Previous studies have shown that during mycoparasitism, *Trichoderma* wraps around the hyphae of the fungal host and forms appressoria and hook-like structures that allow firm attachment to the fungal host (Sachdev and Singh, 2020). Also in this study, during the interaction between *T. longibrachiatum* TG1 and *F. pseudograminearum,* coiling, disintegration of host hyphae, formation of appressoria and hook-like structures and penetration into the hyphae were observed. This suggests that the mechanisms of host recognition and lysis by *Trichoderma* may be different in different *Trichoderma*-host interactions. In addition, a possible CWDEs activity was detected with the degradation of *F. pseudograminearum* cell walls and hyphal deepening in the area infested by *T. longibrachiatum* TG1. These results were confirmed by the findings of Vinale et al. (2008) who reported that CWDEs can degrade or hydrolyze the cell wall of host pathogens and inhibit their growth.

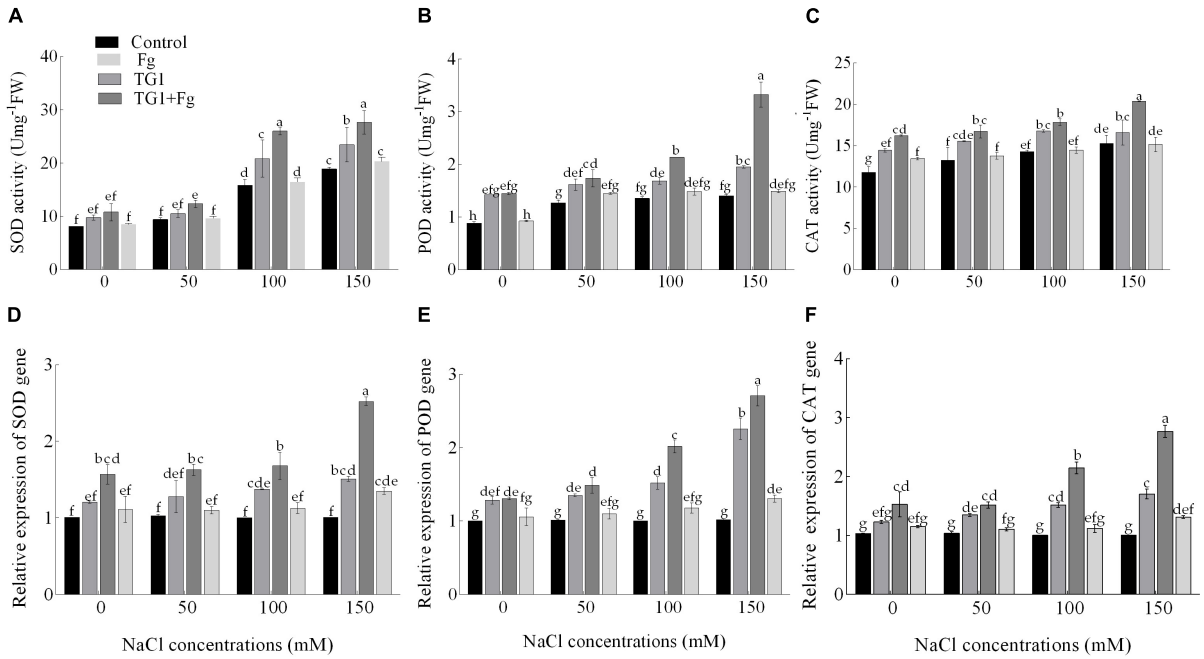

FIGURE 8 | Effect of *T. longibrachiatum* (TG1) on SOD **(A)**, POD **(B)**, and CAT **(C)** activities and relative expressions of SOD **(D)**, POD **(E)**, and CAT **(F)** genes in the root of wheat seedlings under *F. pseudograminearum* (Fg) and different salt stress at 28 days after inoculation. Small bars represent the standard errors of the means. Different lower case letters indicate significant differences at $P < 0.05$ in Duncan's multiple range test using two-way ANOVA. The treatments are detailed in the footnote of **Figure 5**.

Trichoderma spp. are well-known BCA with demonstrated activity against a range of pathogenic fungi (Harman and Uphoff, 2019). CWDEs, such as chitinases and glucanases, have been reported to be directly involved in the mycoparasitic activity of *Trichoderma* by facilitating lysis of the fungal host cell wall during parasitism, thus enabling invasion of the fungal host (Jaroszuk-Ściseł et al., 2019; Pimentel et al., 2020). *Trichoderma longibrachiatum* TG1 showed an increase in the expression level of CWDEs upon interaction with *F. pseudograminearum*. Significant expression of β-1, 6-glucan synthase (PP4), endochitinase (PH-1), and chitinase (chi 18-15) was conspicuous after contact between the two fungi, at a time when *T. longibrachiatum* TG1 overgrew *F. pseudograminearum*. The significant increase in expression of genes during the interaction of TG1 with *F. pseudograminearum* suggests that these enzymes are involved in the mycoparasitic activity of BCA against *F. pseudograminearum*. Previous studies have shown that genomic studies of mycoparasitic *Trichoderma* species have revealed higher numbers of chitinases and glucanases (Karlsson et al., 2017). In other studies, induction and secretion of β-1,3-glucanase and chitinase have been shown to play a role in the mycoparasitism of *F. oxysporum* by *Trichoderma* species (Rashad and Moussa, 2020) and mycoparasitism of *Sclerotinia sclerotiorum* by *T. harzianum* T-aloe (Zhang F. et al., 2016). Consistent with this study, other secondary metabolites produced by *T. longibrachiatum* TG1 species include these CWDEs (Lorito et al., 1994). In biocontrol, these enzymes are often assigned to both parasitism and antibiosis. CWDEs such as chitinase, β-1,3-glucanases, and cellulase, for example, were not only essential features of the mycoparasitism for colonizing the pathogen but also had a significant antifungal effect on the pathogen. This result is in agreement with that of Yuef et al. (2018) where the chitinase and glucanase activities of *T. asperellum*, *T. virens*, *T. gamsii*, and *T. logibrachiatum* inhibited 15% of mycelia growth of *Phytophthora parasitica* and 45% of *F. oxysporum*. The identification of biological control mechanisms that are highly effective against plant pathogens represents a tool that can be explored for plant disease management, especially in the case of important phytopathogens that are difficult to control, such as *F. pseudograminearum*.

In the pot experiment, the different NaCl concentrations and the pathogen decreased the emergence parameters of wheat seeds, which is clearly in accordance with the hypothesis of the study. Several previous studies have reported the adverse effects of salinity on germination and growth of plant seeds both *in vitro* and in the greenhouse (Azooz et al., 2013). Similarly, sodium chloride treatment was reported to inhibit root hair growth (Dey et al., 2004). Previous studies also showed that *F. pseudograminearum* infection increased from less than 20% 10 days after anthesis to more than 98% at maturity under significant environmental stress in both resistant and susceptible wheat cultivars, resulting in unacceptable standard germination and seed vigor (Argyris et al., 2003).

In the present study, the interaction of pathogen and salt stress resulted in poor seed germination and seed vigor.

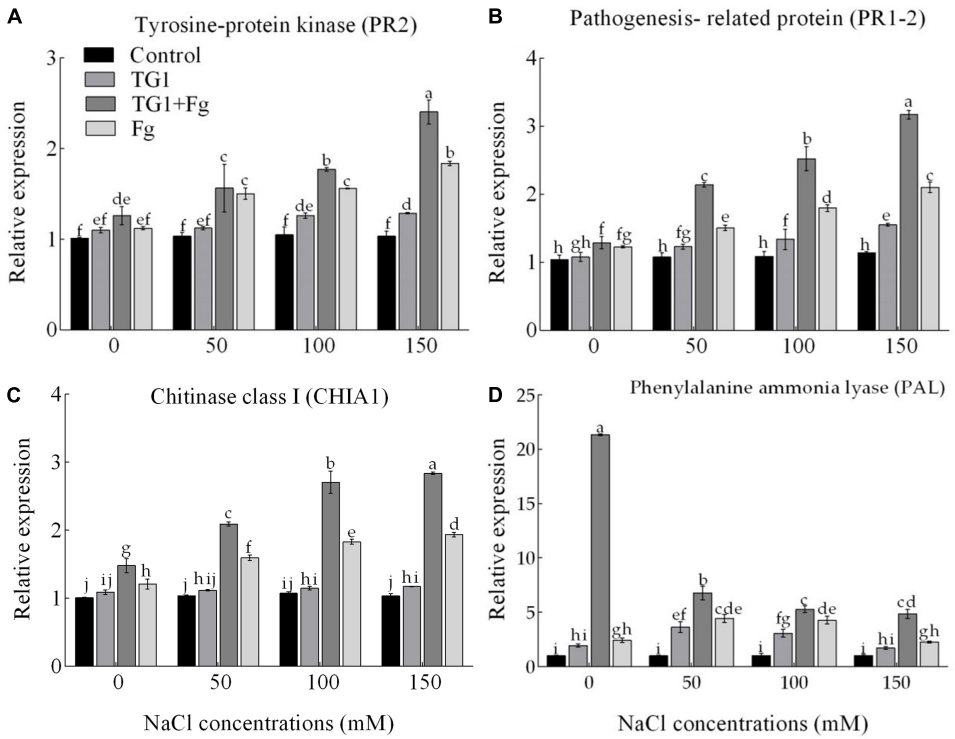

FIGURE 9 | Effect of *T. longibrachiatum* (TG1) on relative expressions of tyrosine-protein kinase PR2 **(A)**, pathogenesis-related protein PR 1-2 **(B)**, chitinase class I CHIA1 **(C)**, and phenylalanine ammonia-lyase **(D)** genes in the root of wheat seedlings under *F. pseudograminearum* (Fg) and different salinity stress at 28 days after inoculation. Small bars represent the standard errors of the means. Different lower case letters indicate significant differences at $P < 0.05$ in Duncan's multiple range test using two-way ANOVA. Treatments are detailed in the footnote of **Figure 5**.

However, the combined treatment (TG1 + Fg) improved seedling emergence and vigor compared with the pathogen alone treatment. Moreover, the application of *T. longibrachiatum* TG1 reduced the deleterious effects of NaCl stress and the pathogen on wheat seedling growth, increasing shoot and root length and enhancing root hair formation, which is beneficial for stressed plants. These results were supported by Mastouri et al. (2012) who reported that application of *T. harzianum* T22 improved germination of tomato (*Lycopersicum esculentum* L.) seeds under abiotic and biotic stress conditions. Similarly, *T. longibrachiatum* T6 promoted the growth of wheat seedlings (*T. aestivum* L.) under NaCl stress by increasing shoot and root length (Zhang et al., 2019b). These results and the general observation show that *Trichoderma* treatments benefit plants most when they are stressed, support the theory that these beneficial fungi alleviate both biotic and abiotic plant stress.

In this study, *T. longibrachiatum* TG1 induced salt tolerance and reduced disease incidence (e.g., seedling blight, crown rot caused by *F. pseudograminearum* on wheat seedlings). In previous studies, *Trichoderma* was shown to promote plant root growth and nutrient solubilization (Contreras-Cornejo et al., 2009). The adverse effects of *Fusarium* wilt are caused by the blockage of xylem vessels leading to leaf senescence and reduced photosynthesis which in turn leads to lower crop yields as previously reported (Singh et al., 2017). The antagonist was an endophytic fungus that increased the relative water content and membrane protection. Infection with a pathogen usually triggers systemic acquired resistance (SAR), a general defense response, first in infected host cells, then in uninfected neighboring tissues. Similarly, the interaction of pathogen and salt stress increased the disease index of wheat seedlings due to the salt tolerance potential of the pathogen. The antagonistic effect of *T. longibrachiatum* TG1 against salinity and the pathogen seems to be related not only to direct competition and mycoparasitism but also to activation of plant defenses through the activation of SA, the synthesis of phytohormones and an increased number of ROS scavenging antioxidant enzymes and the maintenance of osmotic balance and metabolic homeostasis in wheat seedlings. This result was supported by Hasan et al. (2014) who found that the production of lytic enzymes by antagonists has been shown to control pathogenic fungi by competing for tissue nutrients, thus suppressing plant pathogens caused by *Trichoderma* spp.

The abiotic and biotic stresses in this study affected the chlorophyll of the seedlings and decreased the relative water content. Chlorophyll is an important molecule in photosynthesis, and plant bioregulators help to increase the quality of chlorophyll by maintaining cellular osmotic reactions (Burman et al., 2004; Seckin et al., 2009). The decrease in chlorophyll content in wheat under pathogen and salt stress may be due to increased chlorophyll degradation or decreased activity of chlorophyll biosynthesis enzymes (Singh et al., 2016; Mann et al., 2019).

Larger decreases in chlorophyll concentration have also been associated with exacerbation of stress symptoms (Kumar et al., 2018). Previous studies have shown that salinity and *F. pseudograminearum* are known to affect photosynthetic processes in most plants by altering organelle ultrastructure, the concentration of various pigments, metabolites and enzymatic activities (Akram et al., 2018). However, under both stress conditions, the antagonist *T. longibrachiatum* TG1 maintained cells at an optimal hydration level by accumulating osmolytes, which maintained water uptake and increased tissue RWC (Yadav et al., 2020). Other studies have also shown that enhancement of gas exchange properties by endogenous SA through the application of *T. longibrachiatum* helps to improve photosynthetic efficiency and chlorophyll fluorescence, which enables plants to withstand environmental stress (Wang and Li, 2005). Osmolytes are stress tolerance systems that plants use to protect themselves from abiotic stress (Li and Dami, 2016). Similar to the current study, chlorophyll content increased when *T. longibrachiatum* TG1 and the pathogen were applied together, with the antagonist causing rapid root colonization due to its rapid growth and high salt tolerance. This was due to the delay of pathogenic stress and promotion of root development for water and nutrient uptake. In seedlings exposed to salt and pathogen stress, RWC in the plant decreased and photosynthetic structures were damaged due to reduced nutrient uptake.

Endogenous SA which enhances osmotic changes serves as a stress indicator that stabilizes macromolecules and protects against the effects of ROS (Ahmad et al., 2012; Lata et al., 2019). In both treatments, higher endogenous SA content correlated with higher stress intensity as shown by the results of this study (Khan et al., 2013). Previous studies have shown that abiotic and biotic stresses trigger the oxidation of acids in the lipid bilayer leading to a shift in the cell membrane (Carrasco-Ríos et al., 2013). In this study, MDA levels increased in wheat seedlings under saline conditions, while pathogen infection doubled the effects. Higher MDA levels were associated with increased electrolyte loss and H_2O_2 accumulation (Nandwal et al., 2007), which has long been used as a marker of stress tolerance due to lipid peroxidation. However, *T. longibrachiatum* TG1 induced SA to decrease fatty acid degradation, increase antioxidant enzyme activity and decrease MDA and H_2O_2 levels (Abdelkader et al., 2012). Moreover, wheat seedlings treated with the antagonist and pathogen with or without NaCl accumulated low H_2O_2 and MDA levels by increasing the activities of scavenging ROS antioxidant enzymes (SOD, POD, and CAT), compared to what was reported by Zhang et al. (2019a) where *T. harzianum* T-soybean increased scavenging antioxidant enzymes for ROS in cucumber under salt stress.

The expression levels of antioxidant genes were upregulated at all stress levels, which stimulated stress response signaling, increased shoot height and root length, and further increased biomass content in the seedlings treated with the antagonist and the pathogen (TG1 + Fg) compared seedlings treated with the pathogen alone and mock seedlings. This result is similar to that of Zhang et al. (2019c) where *T. longibrachiatum* T6 promoted the growth of wheat seedlings under salt stress through an antioxidant defense system. However, this study involves a different BCA strain that combats both salt and pathogen stress through enzymatic antioxidants, expression of protein enzymes associated with pathogenesis and induction of endogenous SA content of seedlings. Previous studies have shown that exogenous SA treatment increases the transcripts of genes encoding ascorbate and glutathione cycle enzymes (Chen et al., 2016), and overexpression of these genes conferred increased resistance to salt and chilling stress. SA, a phenolic phytohormone, regulates plant growth and production, photosynthesis, transpiration, ion absorption, and transport (Khan et al., 2014), and thus SA has shown positive responses in mitigating both pathogenic and osmotic stress (Chini et al., 2004). Similarly, the increase of endogenous SA by TG1 played an important role in the improvement of the root system, which allowed correction of salt-induced growth and improved biomass production by inducing the expression of enzymatic antioxidants and plant protective genes in plants. Our results are in agreement with those of Luan et al. (2020), who showed that *Trichoderma* isolates ThTrx5 confers salt tolerance to *Arabidopsis* by activating stress response signals and overexpressing of SOD, POD, and CAT, and increase root length and fresh weight of ThTrx5 transgenic plants.

Salicylic acid regulates the activities of various enzymes, such as enzymatic antioxidants and PAL, which are the main components of induced plant protection against biotic and abiotic stresses. In this study, the salicylic acid pathway was determined by the activity of PAL. Previous studies reported that PAL plays a central role in the hypersensitive response (HR) and SAR is associated with early signaling events in response to pathogens, such as activation of PR genes (Dong, 2001; Gruner et al., 2013). By catalyzing cell wall lignification, these enzymes play an important role in protecting plants from pathogens. Other studies have shown that rapid SAR-activation through the expression of various PR genes leads to a significant increase in resistance to pathogen infection (Qi et al., 2019). Pretreatment of wheat seedlings with *T. longibrachiatum* TG1 increased endogenous SA-content and stimulated cell wall degrading enzymes and plant cell wall lignification to reduce pathogen infection. Previous studies by Valifard et al. (2015) showed that salt stress could induce PAL expression (12 to 18 times) and subsequently increase PAL activity (42%–45%) and total phenolic accumulation (35%–43%) in the early hours after stress treatment. Again, Cuong et al. (2020) revealed that, treatment with various concentrations of NaCl (50, 100, and 200 mM) resulted in increased epicatechin levels but decreased accumulation of benzoic acid (TaPAL) in wheat sprouts compared with the control (0 mM). Upregulation of PAL and the enzymes PR1, PR1-2, and chitinase reduced the number of certain mycotoxin forms that accumulated in seedlings and induced salt tolerance. The current study results are in agreement with those of Pereira et al. (2014) who reported that *T. harzianum* ALL-42 appears to enhance the response of field beans to *R. solani* by increasing the expression of β-1–3-glucanase (glu1) and peroxidase (pod3) genes, compared to the host response when exposed to the pathogen alone.

Similarly, cucumber roots colonized by *T. harzianum* T-203 showed increased activity of chitinase, β-1,3-glucanase, cellulase, and peroxidase 72 h after inoculation (Chatterton, 2010) which also supports the current result. Therefore, another mechanism by which *T. longibrachiatum* TG1 increases seedling salt tolerance and resistance to pathogen attack could be realized via the SAR pathway. These results are supported by those of Ali et al. (2018) who found that genes related to pathogenesis (PR) show basal expression under control conditions but increase dramatically after fungal infection both at the locally infected site and in uninfected parts of the host, triggering the SAR pathway.

CONCLUSION

Our results suggest that *T. longibrachiatum* TG1 is a plant growth-promoting fungus that can tolerate salt stress and control *F. pseudograminearum in vitro* and *in vivo*, and induce salinity tolerance of wheat seedlings by attenuating the negative effects of pathogen and salt stress. Rigorous physiological, biochemical, and molecular assays used in the study allowed us to explore the possible mechanisms and pathways in which TG1 attenuates the suppressive effects of pathogen and salt stress. The mechanism involves are; (i) mycoparasitism (ii) overgrowth and space competition (iii) antioxidant defense system and expression and increase of endogenous SA in stressed plants. The identification of biological control agents that are highly effective against salt stress and plant pathogens represents a tool that can be explored for plant disease management, especially in the case of important phytopathogens that are difficult to control, such as *F. pseudograminearum*. These results and the repeated observation show that the greatest benefit of *Trichoderma* treatments to plants occurs when they are under stress, lend credence to the concept that these beneficial fungi alleviate both biotic and abiotic plant stress. Our results provide a basis for future incorporation of biological control agents into strategies to control seedling blight, crown rot, and root rot of plants under salt stress.

DATA AVAILABILITY STATEMENT

The raw data supporting the conclusions of this article will be made available by the authors, without undue reservation, to any qualified researcher.

AUTHOR CONTRIBUTIONS

SB and TL performed the experiments, analyzed data, and wrote and edited the manuscript. SZ, BX, and AC-U conceived the idea and revised the manuscript. SZ designed the experiments, conceived the idea, and revised the manuscript. All authors have read and agreed to the published version of the manuscript.

FUNDING

This study was funded by Gansu Provincial Key Laboratory of Aridland Crop Science, Gansu Agricultural University (project GSCS-2017-1); Fuxi Outstanding Talent Cultivation Program, Gansu Agricultural University (Project Gaufx-03J03); Scientific Research Start-up Funds for Openly recruited Doctors (project 2017RCZX-07); National Natural Science Foundation of China (project 31860526); and Gansu Provincial Science Fund for Distinguished Young Scholars (project 18JR3RA161).

ACKNOWLEDGMENTS

The authors would like to thank the College of Plant Protection research team, Gansu Agricultural University, China.

SUPPLEMENTARY MATERIAL

The Supplementary Material for this article can be found online at: https://www.frontiersin.org/articles/10.3389/fpls.2021.741231/full#supplementary-material

REFERENCES

Abdelkader, A. F., Hassanein, R. A., and Ali, H. (2012). Studies on effects of salicylic acid and thiourea on biochemical activities and yield production in wheat (*Triticum aestivum* var. *Gimaza* 9) plants grown under drought stress. *Afri. J. Biotechnol.* 11, 12728–12739.

Ahmad, P., Kumar, A., Ashraf, M., and Akram, N. A. (2012). Salt-induced changes in photosynthetic activity and oxidative defense system of three cultivars of mustard (*Brassica juncea* L.). *Afri. J. Biotechnol.* 11, 2694–2703.

Akram, N. A., Iqbal, M., Muhammad, A., Ashraf, M., Al-Qurainy, F., and Shafiq, S. (2018). Aminolevulinic acid and nitric oxide regulate oxidative defense and secondary metabolisms in canola (*Brassica napus* L.) under drought stress. *Protoplasma* 255, 163–174. doi: 10.1007/s00709-017-1140-x

Alahmad, S., Simpfendorfer, S., Bentley, A., and Hickey, L. (2018). Crown rot of wheat in Australia: *Fusarium pseudograminearum* taxonomy, population biology and disease management. *Australasian Plant Pathol.* 47, 285–299. doi: 10.1007/s13313-018-0554-z

Ali, S., Ganai, B. A., Kamili, A. N., Bhat, A. A., Mir, Z. A., Bhat, J. A., et al. (2018). Pathogenesis-related proteins and peptides as promising tools for engineering plants with multiple stress tolerance. *Microbiol. Res.* 212, 29–37. doi: 10.1016/j.micres.2018.04.008

Allasia, V., Ponchet, M., Quentin, M., Favery, B., and Keller, H. (2018). Quantification of salicylic acid (SA) and SA-glucosides in *Arabidopsis thaliana*. *Bio-protocol* 8:e2844.

Argyris, J., Van Sanford, D., and Tekrony, D. (2003). *Fusarium graminearum* infection during wheat seed development and its effect on seed quality. *Crop Sci.* 43, 1782–1788. doi: 10.2135/cropsci2003.1782

Asthir, B., Koundal, A., and Bains, N. (2011). Kinetic properties of cell wall bound superoxide dismutase in leaves of wheat (*Triticum aestivum* L.) following stripe rust (*Puccinia striiformis*) infection. *Indian J. Biochem. Bio.* 48, 341–345.

Atanasova, L., Le Crom, S., Gruber, S., Coulpier, F., Seidl-Seiboth, V., Kubicek, C. P., et al. (2013). Comparative transcriptomics reveals different strategies of *Trichoderma* mycoparasitism. *BMC Genomics* 14:121. doi: 10.1186/1471-2164-14-121

Azooz, M. M., Alzahrani, A. M., and Youssef, M. M. (2013). The potential role of seed priming with ascorbic acid and nicotinamide and their interactions to enhance salt tolerance in broad bean ('*Vicia faba*'L.). *Australian J. Crop Sci.* 7, 2091–2100.

Bolanos-Carriel, C., Wegulo, S. N., Baenziger, P. S., Eskridge, K. M., Funnell-Harris, D., Mcmaster, N., et al. (2020). Tri5 gene expression analysis during postharvest storage of wheat grain from field plots treated with a triazole and a strobilurin fungicide. *Can. J. Plant Pathol.* 42, 547–559. doi: 10.1080/07060661.2019.1700169

Burman, U., Garg, B., and Kathju, S. (2004). Interactive effects of thiourea and phosphorus on clusterbean under water stress. *Biol. Plant.* 48, 61–65. doi: 10.1023/b:biop.0000024276.03834.8d

Carrasco-Ríos, L., Rojas, C., and Pinto, M. (2013). Contrasting physiological responses to high salinity between two varieties of corn 'Lluteño'(salt tolerant) and 'Jubilee'(salt sensitive). *Chilean J. Agric. Res.* 73, 205–212. doi: 10.4067/s0718-58392013000300001

Chatterton, S. G. D. (2010). *Mechanisms of biological control of Fusarium root and stem rot of greenhouse cucumber by Gliocladium catenulatum.* Ph.D. Thesis. Burnaby, BC: Biological Sciences Department-Simon Fraser University.

Chen, S. C., Zhao, H. J., Wang, Z. H., Zheng, C. X., Zhao, P. Y., Guan, Z. H., et al. (2016). *Trichoderma harzianum*-induced resistance against *Fusarium oxysporum* involves regulation of nuclear DNA content, cell viability and cell cycle-related genes expression in cucumber roots. *Eur. J. Plant Pathol.* 147, 43–53. doi: 10.1007/s10658-016-0978-7

Chini, A., Grant, J. J., Seki, M., Shinozaki, K., and Loake, G. J. (2004). Drought tolerance established by enhanced expression of the CC–NBS–LRR gene, ADR1, requires salicylic acid, EDS1 and ABI1. *The Plant J.* 38, 810–822. doi: 10.1111/j.1365-313x.2004.02086.x

Contreras-Cornejo, H. A., Macías-Rodríguez, L., Alfaro-Cuevas, R., and López-Bucio, J. (2014). *Trichoderma* spp. improve growth of *Arabidopsis* seedlings under salt stress through enhanced root development, osmolite production, and Na^+ elimination through root exudates. *Mol. Plant Microbe Interact.* 27, 503–514.

Contreras-Cornejo, H. A., Macías-Rodríguez, L., Cortes-Penagos, C., and López-Bucio, J. (2009). *Trichoderma virens*, a plant beneficial fungus, enhances biomass production and promotes lateral root growth through an auxin-dependent mechanism in *Arabidopsis*. *Plant Physiol.* 149, 1579–1592. doi: 10.1104/pp.108.130369

Cornelia, P., Bogdan, A. T., Ipate, L., Chis, A., and Borbely, M. (2011). Exogenous salicylic acid involvement in ameliorating the negative effect of salt stress in wheat (*Triticum aestivum* cv. *crisana*) plants in vegetative stage. *J. Anal. Univ. din Oradea Fascicula Protecñ. Med.* 7, 137–146.

Cuong, D. M., Kwon, S. J., Nguyen, B. V., Chun, S. W., Kim, J. K., and Park, S. U. (2020). Effect of salinity stress on phenylpropanoid genes expression and related gene expression in wheat sprout. *Agronomy* 10:390. doi: 10.3390/agronomy10030390

Dey, R., Pal, K., Bhatt, D., and Chauhan, S. (2004). Growth promotion and yield enhancement of peanut (*Arachis hypogaea* L.) by application of plant growth-promoting rhizobacteria. *Microbiol. Res.* 159, 371–394. doi: 10.1016/j.micres.2004.08.004

Dong, X. (2001). Genetic dissection of systemic acquired resistance. *Curr. Opin. Plant Biol.* 4, 309–314. doi: 10.1016/s1369-5266(00)00178-3

El-Allaf, S., Lipps, P., Madden, L., and Johnston, A. (2001). "Effect of foliar fungicides and biocontrol agents on *Fusarium* head blight development and control in Ohio," in *Proceedings of the 2001 National Fusarium Head Blight Forum: Citeseer, Michigan State University, United States (US)*, (Kinkos, MI: Okemos Press), 49–53.

Fu, J., Liu, Z., Li, Z., Wang, Y., and Yang, K. (2017). Alleviation of the effects of saline-alkaline stress on maize seedlings by regulation of active oxygen metabolism by *Trichoderma asperellum*. *PLoS One* 12:e0179617. doi: 10.1371/journal.pone.0179617

Gond, S. K., Bergen, M. S., Torres, M. S., and White, Jr, J. F. (2015). Endophytic *Bacillus* spp. produce antifungal lipopeptides and induce host defence gene expression in maize. *Microbiol. Res.* 172, 79–87. doi: 10.1016/j.micres.2014.11.004

Gruner, K., Griebel, T., Návarová, H., Attaran, E., and Zeier, J. (2013). Reprogramming of plants during systemic acquired resistance. *Front. Plant Sci.* 4:252. doi: 10.3389/fpls.2013.00252

Harman, G. E., and Uphoff, N. (2019). Symbiotic root-endophytic soil microbes improve crop productivity and provide environmental benefits. *Scientifica* 2019:9106395.

Hasan, S., Gupta, G., and Anand, S. (2014). Lytic enzymes of *Trichoderma*: their role in plant defense. *Int. J. App. Res. Stud.* 3, 2–5.

Hossain, M. S., Elsayed, A. I., Moore, M., and Dietz, K. J. (2017). Redox and reactive oxygen species network in acclimation for salinity tolerance in sugar beet. *J. Exp. Bot.* 68, 1283–1298. doi: 10.1093/jxb/erx019

Isayenkov, S. V., and Maathuis, F. J. (2019). Plant salinity stress: many unanswered questions remain. *Front. Plant Sci.* 10:80. doi: 10.3389/fpls.2019.00080

Ivushkin, K., Bartholomeus, H., Bregt, A. K., Pulatov, A., Kempen, B., and De Sousa, L. (2019). Global mapping of soil salinity change. *Remote Sens. Environ.* 231:111260. doi: 10.1016/j.rse.2019.111260

Jaroszuk-Ściseł, J., Tyśkiewicz, R., Nowak, A., Ozimek, E., Majewska, M., Hanaka, A., et al. (2019). Phytohormones (auxin, gibberellin) and ACC deaminase in vitro synthesized by the mycoparasitic *Trichoderma* DEMTkZ3A0 strain and changes in the level of auxin and plant resistance markers in wheat seedlings inoculated with this strain conidia. *Int. J. Mol. Sci.* 20:4923. doi: 10.3390/ijms20194923

Karlsson, M., Atanasova, L., Jensen, D. F., and Zeilinger, S. (2017). "Necrotrophic mycoparasites and their genomes," in *The Fungal Kingdom*, eds J. Heitman, B. J. Howlett, P. W. Crous, E. H. Stukenbrock, T. Y. James, and N. A. R. Gow (Washington, DC: ASM Press), 1005–1026. doi: 10.1128/9781555819583.ch50

Kazan, K., and Gardiner, D. M. (2018). *Fusarium* crown rot caused by *Fusarium pseudograminearum* in cereal crops: recent progress and future prospects. *Mol. Plant Pathol.* 19, 1547–1562. doi: 10.1111/mpp.12639

Khan, M. I. R., Asgher, M., and Khan, N. A. (2014). Alleviation of salt-induced photosynthesis and growth inhibition by salicylic acid involves glycinebetaine and ethylene in mungbean (*Vigna radiata* L.). *Plant Physiol. Biochem.* 80, 67–74. doi: 10.1016/j.plaphy.2014.03.026

Khan, M. I. R., Iqbal, N., Masood, A., Per, T. S., and Khan, N. A. (2013). Salicylic acid alleviates adverse effects of heat stress on photosynthesis through changes in proline production and ethylene formation. *Plant Signal. Behav.* 8:e26374. doi: 10.4161/psb.26374

Kumar, A., Sharma, S. K., Lata, C., Devi, R., Kulshrestha, N., Krishnamurthy, S., et al. (2018). Impact of water deficit (salt and drought) stress on physiological, biochemical and yield attributes on wheat (*Triticum aestivum*) varieties. *Indian J. Agric. Sci.* 88, 1624–1632.

Lata, C., Soni, S., Kumar, N., Kumar, A., Pooja, Mann, A., et al. (2019). Adaptive mechanism of stress tolerance in *Urochondra* (grass halophyte) using roots study. *Indian J. Agric. Sci.* 89, 1050–1053.

Li, S., and Dami, I. E. (2016). Responses of *Vitis vinifera* 'Pinot gris' grapevines to exogenous abscisic acid (ABA): I. Yield, fruit quality, dormancy, and freezing tolerance. *J. Plant Growth Regul.* 35, 245–255. doi: 10.1007/s00344-015-9529-2

Lin, Y., Liu, T., Liu, J., Liu, X., Ou, Y., Zhang, H., et al. (2015). Subtle regulation of potato acid invertase activity by a protein complex of invertase, invertase inhibitor, and sucrose nonfermenting1-related protein kinase. *Plant Physiol.* 168, 1807–1819. doi: 10.1104/pp.15.00664

Livak, K. J., and Schmittgen, T. D. (2001). Analysis of relative gene expression data using real-time quantitative PCR and the $2^{-\Delta\Delta CT}$ method. *Methods* 25, 402–408. doi: 10.1006/meth.2001.1262

Lopes, F. A. C., Steindorff, A. S., Geraldine, A. M., Brandão, R. S., Monteiro, V. N., Júnior, M. L., et al. (2012). Biochemical and metabolic profiles of *Trichoderma* strains isolated from common bean crops in the Brazilian Cerrado, and potential antagonism against *Sclerotinia sclerotiorum*. *Fungal Biol.* 116, 815–824. doi: 10.1016/j.funbio.2012.04.015

Lorito, M., Hayes, C., Di Pietro, A., Woo, S., and Harman, G. (1994). Purification, characterization, and synergistic activity of a glucan 1, 3-beta-glucosidase and an N-acetyl-beta-glucosaminidase from *Trichoderma harzianum*. *Phytopathology* 84, 398–405. doi: 10.1094/phyto-84-398

Luan, J., Dong, J., Song, X., Jiang, J., and Li, H. (2020). Overexpression of *Tamarix hispida* ThTrx5 confers salt tolerance to *Arabidopsis* by activating stress response signals. *Int. J. Mol. Sci.* 21:1165. doi: 10.3390/ijms21031165

Mandeel, Q. A. (2006). Biodiversity of the genus *Fusarium* in saline soil habitats. *Basic J. Microbiol.* 46, 480–494. doi: 10.1002/jobm.200510128

Mann, A., Kaur, G., Kumar, A., Sanwal, S. K., Singh, J., and Sharma, P. (2019). Physiological response of chickpea (*Cicer arietinum* L.) at early seedling stage under salt stress conditions. *Leg. Res.* 42, 625–632.

Mastouri, F., Björkman, T., and Harman, G. E. (2012). *Trichoderma harzianum* enhances antioxidant defense of tomato seedlings and resistance to water

deficit. *Mol. Plant Microbe Interact.* 25, 1264–1271. doi: 10.1094/mpmi-09-11-0240

Miazek, K., and Ledakowicz, S. (2013). Chlorophyll extraction from leaves, needles and microalgae: a kinetic approach. *Int. J. Agric. Biol. Eng.* 6, 107–115.

Miura, K., and Tada, Y. (2014). Regulation of water, salinity, and cold stress responses by salicylic acid. *Front. Plant Sci.* 5:4. doi: 10.3389/fpls.2014.00004

Monteiro, V. N., Do Nascimento Silva, R., Steindorff, A. S., Costa, F. T., Noronha, E. F., Ricart, C. A. O., et al. (2010). New insights in *Trichoderma harzianum* antagonism of fungal plant pathogens by secreted protein analysis. *Curr. Microbiol.* 61, 298–305.

Moya-Elizondo, E. A., and Jacobsen, B. J. (2016). Integrated management of *Fusarium* crown rot of wheat using fungicide seed treatment, cultivar resistance, and induction of systemic acquired resistance (SAR). *Biol. Control* 92, 153–163. doi: 10.1016/j.biocontrol.2015.10.006

Nandwal, A. S., Kukreja, S., Kumar, N., Sharma, P. K., Jain, M., Mann, A., et al. (2007). Plant water status, ethylene evolution, N_2-fixing efficiency, antioxidant activity and lipid peroxidation in *Cicer arietinum* L. nodules as affected by short-term salinization and desalinization. *J. Plant Physiol.* 164, 1161–1169. doi: 10.1016/j.jplph.2006.05.017

Narayan, O. P., Verma, N., Singh, A. K., Oelmüller, R., Kumar, M., Prasad, D., et al. (2017). Antioxidant enzymes in chickpea colonized by *Piriformospora indica* participate in defense against the pathogen *Botrytis cinerea*. *Sci. Reports* 7, 1–11. doi: 10.1038/s41598-017-12944-w

Niu, X., Mi, L., Li, Y., Wei, A., Yang, Z., Wu, J., et al. (2013). Physiological and biochemical responses of rice seeds to phosphine exposure during germination. *Chemosphere* 93, 2239–2244. doi: 10.1016/j.chemosphere.2013.07.074

Oluwaranti, A., Fakorede, M., and Adeboye, F. (2015). Maturity groups and phenology of maize in a rainforest location. *Int. Agric. Innov. Res.* 4, 124–127.

Pasquali, M., Beyer, M., Logrieco, A., Audenaert, K., Balmas, V., Basler, R., et al. (2016). A European database of *Fusarium graminearum* and *F. culmorum* trichothecene genotypes. *Front. Microbiol.* 7:406. doi: 10.3389/fmicb.2016.00406

Paulitz, T. C., and Bélanger, R. R. (2001). Biological control in greenhouse systems. *Annu. Rev. Phytopathol.* 39, 103–133.

Pereira, J. L., Queiroz, R. M., Charneau, S. O., Felix, C. R., Ricart, C. A., Da Silva, F. L., et al. (2014). Analysis of *Phaseolus vulgaris* response to its association with *Trichoderma harzianum* (ALL-42) in the presence or absence of the phytopathogenic fungi *Rhizoctonia solani* and *Fusarium solani*. *PLoS One* 9:e98234. doi: 10.1371/journal.pone.0098234

Pimentel, M. F., Arnão, E., Warner, A. J., Subedi, A., Rocha, L. F., Srour, A., et al. (2020). *Trichoderma* isolates inhibit *Fusarium virguliforme* growth, reduce root rot, and induce defense-related genes on soybean seedlings. *Plant Dis.* 104, 1949–1959. doi: 10.1094/pdis-08-19-1676-re

Purcărea, C., Cachită, D., Petrus, A., Pop, L., and Chis, A. (2010). Exogenous salicylic acid treatments enhance tolerance to salinity of wheat (*Triticum aestivum*) plantlets. *J. Acta Agraria Debreceniensis* 5, 34–38. doi: 10.34101/actaagrar/i/8371

Qi, P.-F., Zhang, Y. Z., Liu, C. H., Chen, Q., Guo, Z. R., Wang, Y., et al. (2019). Functional analysis of FgNahG clarifies the contribution of salicylic acid to wheat (*Triticum aestivum*) resistance against *Fusarium* head blight. *Toxins* 11:59. doi: 10.3390/toxins11020059

Qiu, M., Zhang, R., Xue, C., Zhang, S., Li, S., Zhang, N., et al. (2012). Application of bio-organic fertilizer can control *Fusarium* wilt of cucumber plants by regulating microbial community of rhizosphere soil. *Biol. Fert. Soils* 48, 807–816. doi: 10.1007/s00374-012-0675-4

Rahman, M., Begum, M., and Alam, M. (2009). Screening of *Trichoderma* isolates as a biological control agent against *Ceratocystis paradoxa* causing pineapple disease of sugarcane. *Microbiology* 37, 277–285. doi: 10.4489/myco.2009.37.4.277

Ramegowda, V., and Senthil-Kumar, M. (2015). The interactive effects of simultaneous biotic and abiotic stresses on plants: mechanistic understanding from drought and pathogen combination. *J. Plant Physiol.* 176, 47–54. doi: 10.1016/j.jplph.2014.11.008

Rashad, Y. M., and Moussa, T. A. (2020). "Biocontrol agents for fungal plant diseases management," in *Cottage Industry of Biocontrol Agents and Their Applications*, eds M. Saleh, M. Abu-hashim, and N. El-Wakeil (Cham: Springer), 337–363. doi: 10.1007/978-3-030-33161-0_11

Rubio, M. B., Hermosa, R., Vicente, R., Gómez-Acosta, F. A., Morcuende, R., Monte, E., et al. (2017). The combination of *Trichoderma harzianum* and chemical fertilization leads to the deregulation of phytohormone networking, preventing the adaptive responses of tomato plants to salt stress. *Front. Plant Sci.* 8:294. doi: 10.3389/fpls.2017.00294

Sachdev, S., and Singh, R. P. (2020). "*Trichoderma*: a multifaceted fungus for sustainable agriculture," in *Ecological and Practical Applications for Sustainable Agriculture*, eds J. Korstad, K. Bauddh, R. P. Singh, and S. Kumar (Singapore: Springer), 261–304. doi: 10.1007/978-981-15-3372-3_13

Saghafi, D., Ghorbanpour, M., and Lajayer, B. A. (2018). Efficiency of *Rhizobium* strains as plant growth promoting rhizobacteria on morpho-physiological properties of *Brassica napus* L. under salinity stress. *J. Soil Sci. Plant Nutrit.* 18, 253–268.

Seckin, B., Sekmen, A. H., and Türkan, I. (2009). An enhancing effect of exogenous mannitol on the antioxidant enzyme activities in roots of wheat under salt stress. *J. Plant Growth Regul.* 28, 12–20. doi: 10.1007/s00344-008-9068-1

Shiferaw, B., Smale, M., Braun, H. J., Duveiller, E., Reynolds, M., and Muricho, G. (2013). Crops that feed the world 10. Past successes and future challenges to the role played by wheat in global food security. *Food Secur.* 5, 291–317. doi: 10.1007/s12571-013-0263-y

Singh, A., Sharma, P., Meena, M., Kumar, A., Mishra, A., Kumar, P., et al. (2016). Effect of salinity on gas exchange parameters and ionic relations in bael (*Aegle marmelos* Correa). *Indian J. Hort.* 73, 48–53.

Singh, R., Mahmoudpour, A., Rajkumar, M., and Narayana, R. (2017). A review on stripe rust of wheat, its spread, identification and management at field level. *Res. Crops* 18, 528–533. doi: 10.5958/2348-7542.2017.00091.2

Sorahinobar, M., Niknam, V., Ebrahimzadeh, H., Soltanloo, H., Behmanesh, M., and Enferadi, S. T. (2016). Central role of salicylic acid in resistance of wheat against *Fusarium graminearum*. *J. Plant Growth Regul.* 35, 477–491. doi: 10.1007/s00344-015-9554-1

Subedi, K., Ma, B., and Xue, A. (2007). Planting date and nitrogen effects on *Fusarium* head blight and leaf spotting diseases in spring wheat. *Agron. J.* 99, 113–121. doi: 10.2134/agronj2006.0171

Tian, J., and Philpot, W. D. (2015). Relationship between surface soil water content, evaporation rate, and water absorption band depths in SWIR reflectance spectra. *Remote Sens. Environ.* 169, 280–289. doi: 10.1016/j.rse.2015.08.007

Valifard, M., Mohsenzadeh, S., Niazi, A., and Moghadam, A. (2015). Phenylalanine ammonia lyase isolation and functional analysis of phenylpropanoid pathway under salinity stress in *Salvia* species. *Aust. J. Crop Sci.* 9, 656–665.

Vinale, F., Sivasithamparam, K., Ghisalberti, E. L., Marra, R., Woo, S. L., and Lorito, M. (2008). *Trichoderma*–plant–pathogen interactions. *Soil Biol. Biochem.* 40, 1–10. doi: 10.1079/9780851995120.0001

Wang, L., and Li, S. (2005). "The effects of salicylic acid on distribution of 14C-assimilation and photosynthesis in young grape plants under heat stress," in *Proceedings of the International Symposium on Biotechnology of Temperate Fruit Crops and Tropical Species*, Vol. 738, Daytona Beach, FL, 779–785. doi: 10.17660/actahortic.2007.738.104

Wang, L., Shi, Z. M., Jiang, C. F., Liu, X., Chen, Q. D., Qian, X., et al. (2014). MiR-143 acts as a tumor suppressor by targeting N-RAS and enhances temozolomide-induced apoptosis in glioma. *Oncotarget* 5, 5416–5427. doi: 10.18632/oncotarget.2116

Wang, W., Vinocur, B., and Altman, A. (2003). Plant responses to drought, salinity and extreme temperatures: towards genetic engineering for stress tolerance. *Planta* 218, 1–14. doi: 10.1007/s00425-003-1105-5

White, E. J., Venter, M., Hiten, N. F., and Burger, J. T. (2008). Modified Cetyltrimethylammonium bromide method improves robustness and versatility: the benchmark for plant RNA extraction. *Biotechnol. J.* 3, 1424–1428. doi: 10.1002/biot.200800207

Wu, G., and Wang, S. (2012). Calcium regulates K^+/Na^+ homeostasis in rice (*Oryza sativa* L.) under saline conditions. *Plant Soil Environ.* 58, 121–127. doi: 10.17221/374/2011-pse

Xie, C., Wang, C., Wang, X., and Yang, X. (2013). Two modified RNA extraction methods compatible with transcript profiling and gene expression analysis for cotton roots. *Prep. Biochem. Biotechnol.* 43, 500–511. doi: 10.1080/10826068.2012.759967

Yadav, T., Kumar, A., Yadav, R., Yadav, G., Kumar, R., and Kushwaha, M. (2020). Salicylic acid and thiourea mitigate the salinity and drought stress on physiological traits governing yield in pearl millet-wheat. *Saudi J. Biol. Sci.* 27, 2010–2017. doi: 10.1016/j.sjbs.2020.06.030

Yassin, S. M., Aly, A., Abdel-Kader, D. A., Morsy, K., and Atallah, O. J. Z. (2019). Antagonistic potential of rhizospheric biocontrol agents against soybean root rot-wilt disease complex syndrome. *Agric. Res.* 46, 1395–1418. doi: 10.21608/zjar.2019.48159

Yuef, M. I., Ariel, T. J., ul, R. I., Alberto, L., Benigno, E., and Eduardo, O. A. (2018). Identification and evaluation of secondary metabolites by gas chromatography-mass spectrometry (GC-MS) in native strains of *Trichoderma* species. *Afri. J. Biotechnol.* 17, 1162–1171. doi: 10.5897/ajb2018.16546

Zhang, F., Ge, H., Zhang, F., Guo, N., Wang, Y., Chen, L., et al. (2016). Biocontrol potential of *Trichoderma harzianum* isolate T-aloe against *Sclerotinia sclerotiorum* in soybean. *Plant Physiol. Biochem.* 100, 64–74.

Zhang, F., Wang, Y., Liu, C., Chen, F., Ge, H., Tian, F., et al. (2019a). *Trichoderma harzianum* mitigates salt stress in cucumber via multiple responses. *Ecotoxicol. Environ. Saf.* 170, 436–445. doi: 10.1016/j.ecoenv.2018.11.084

Zhang, S., Gan, Y., and Xu, B. (2016). Application of plant-growth-promoting fungi *Trichoderma longibrachiatum* T6 enhances tolerance of wheat to salt stress through improvement of antioxidative defense system and gene expression. *Front Plant Sci.* 7:1405. doi: 10.3389/fpls.2016.01405

Zhang, S., Gan, Y., and Xu, B. (2019b). Mechanisms of the IAA and ACC-deaminase producing strain of *Trichoderma longibrachiatum* T6 in enhancing wheat seedling tolerance to NaCl stress. *BMC Plant Biol.* 19:22. doi: 10.1186/s12870-018-1618-5

Zhang, S., Gan, Y., Xu, B., and Xue, Y. (2014). The parasitic and lethal effects of *Trichoderma longibrachiatum* against *Heterodera avenae*. *Biol. Control* 72, 1–8. doi: 10.1016/j.biocontrol.2014.01.009

Zhang, S., Xu, B., and Gan, Y. (2019c). Seed treatment with *Trichoderma longibrachiatum* T6 promotes wheat seedling growth under NaCl stress through activating the enzymatic and nonenzymatic antioxidant defense systems. *Int. J. Mol. Sci.* 20:3729. doi: 10.3390/ijms20153729

Zhang, X.-X., Sun, H. Y., Shen, C. M., Li, W., Yu, H. S., and Chen, H. G. (2015). Survey of *Fusarium* spp. causing wheat crown rot in major winter wheat growing regions of China. *Plant Dis.* 99, 1610–1615. doi: 10.1094/pdis-04-14-0422-re

Conflict of Interest: The authors declare that the research was conducted in the absence of any commercial or financial relationships that could be construed as a potential conflict of interest.

Publisher's Note: All claims expressed in this article are solely those of the authors and do not necessarily represent those of their affiliated organizations, or those of the publisher, the editors and the reviewers. Any product that may be evaluated in this article, or claim that may be made by its manufacturer, is not guaranteed or endorsed by the publisher.

frontiers in Plant Science

ORIGINAL RESEARCH
published: 25 November 2021
doi: 10.3389/fpls.2021.771806

Wheat Apoplast-Localized Lipid Transfer Protein *TaLTP3* Enhances Defense Responses Against *Puccinia triticina*

Jiaojie Zhao[1†], Weishuai Bi[1†], Shuqing Zhao[1], Jun Su[1], Mengyu Li[1], Lisong Ma[1,2], Xiumei Yu[3] and Xiaodong Wang[1*]*

[1] State Key Laboratory of North China Crop Improvement and Regulation, College of Plant Protection, Hebei Agricultural University, Baoding, China, [2] College of Horticulture, Hebei Agricultural University, Baoding, China, [3] College of Life Sciences, Hebei Agricultural University, Baoding, China

Plant apoplast serves as the frontier battlefield of plant defense in response to different types of pathogens. Many pathogenesis-related (PR) proteins are accumulated in apoplastic space during the onset of plant–pathogen interaction, where they act to suppress pathogen infection. In this study, we found the expression of *Triticum aestivum* lipid transfer protein 3 (*TaLTP3*) gene was unregulated during incompatible interaction mediated by leaf rust resistance genes *Lr39/41* at the early infection stage. Stable transgenic wheat lines overexpressing *TaLTP3* exhibited enhanced resistance to leaf rust pathogen *Puccinia triticina*. Transcriptome analysis revealed that overexpression of *TaLTP3* specifically activated the transcription of pathogenesis-related protein 1a (TaPR1a) and multiple plant hormone pathways, including salicylic acid (SA), jasmonic acid (JA), and auxin, in response to the infection of the model bacterial pathogen *Pseudomonas syringae* pv. *tomato* DC3000. Further investigation indicated that *TaLTP3* physically associated with wheat *TaPR1a* protein in the apoplast. Transgenic wheat lines overexpressing *TaLTP3* and *TaPR1a* showed higher accumulations of reactive oxygen species (ROS) during plant defense responses. All these findings suggested that *TaLTP3* is involved in wheat resistance against leaf rust pathogen infection and forming a *TaLTP3-TaPR1a* complex in apoplast against this pathogen, which provides new insights into the functional roles of PR proteins.

Keywords: wheat, pathogenesis-related protein, lipid transfer protein, apoplastic, resistance

OPEN ACCESS

Edited by:
Wen-Ming Wang, Sichuan Agricultural University, China

Reviewed by:
Zhonglin Mou, University of Florida, United States
Pramod Prasad, Indian Institute of Wheat and Barley Research (ICAR), India

****Correspondence:***
Xiaodong Wang
zhbwxd@hebau.edu.cn
Lisong Ma
lisong.ma@anu.edu.au

[†] These authors have contributed equally to this work

Specialty section:
This article was submitted to Plant Pathogen Interactions, a section of the journal Frontiers in Plant Science

Received: *07 September 2021*
Accepted: *19 October 2021*
Published: *25 November 2021*

Citation:
Zhao J, Bi W, Zhao S, Su J, Li M, Ma L, Yu X and Wang X (2021) Wheat Apoplast-Localized Lipid Transfer Protein TaLTP3 Enhances Defense Responses Against Puccinia triticina. Front. Plant Sci. 12:771806. doi: 10.3389/fpls.2021.771806

INTRODUCTION

Plants utilize complex defense mechanisms to fight against pathogen infections. Apoplastic space represents an essential site for pathogen infection and the frontier battlefield of plant defense response, where either plant-secreted proteins, such as proteases and pathogenesis-related (PR) proteins, directly interact with pathogens or cell surface-localized pattern recognition receptors (PRRs) perceive pathogen-associated molecular patterns (PAMPs) to initiate PAMP-triggered immunity (PTI) (Jashni et al., 2015; Qi et al., 2017). PR protein-encoding genes are highly induced by pathogen infections, leading to the enrichment of PR proteins in the apoplast that participate in various plant defense responses (Van Loon et al., 2006; Wang et al., 2018). It has been documented that induction

of *PR* genes expression is considered as the indicator of the activation of phytohormone signaling pathways such as salicylic acid (SA) and jasmonic acid (JA) (Van Loon et al., 2006). PR proteins and peptides have also been utilized as promising tools for engineering plants with multiple stress tolerance (Ali et al., 2018).

Among all the designated PR proteins, *PR1* can be induced by various stresses and considered as a hallmark of plant defense responses with multiple functions (Breen et al., 2017). A quantitative peptidomics study revealed that the CAP-derived peptide 1 (CAPE1) peptide cleavage from C-terminus of *PR1* protein acts as a damage-associated molecular pattern (DAMP) triggering plant defense responses such as the burst of reactive oxygen species (ROS) and expression of other *PR* genes (Chen et al., 2014). More recently, a study showed that *TaPR1*-mediated host defense in wheat against septoria nodorum blotch (SNB) (caused by *Parastagonospora nodorum*) requires the cleavage of the C-terminal region, while toxin 3 (SnTox3) effector suppresses *TaPR1*-mediated plant defense by preventing the cleavage of the C-terminal region via direct interaction with overexpression of pathogenesis-related protein 1a (TaPR1a) (Sung et al., 2021). Interestingly, a recent investigation demonstrated that wheat *TaPR1* associates with thaumatin-like protein TaTLP1 [also known as pathogenesis-related protein 5 (TaPR5)] in the apoplastic space and exerts enhanced antifungal activities (Wang et al., 2020). Overexpression of wheat homolog of *PR1* gene (*TaPR1a*) in transgenic wheat line resulted in significantly enhanced resistance against both stripe rust and leaf rust fungi (Bi et al., 2020). Interestingly, they found that the model bacterial pathogen *Pseudomonas syringae* (*P. syringae*) pv. *tomato* DC3000 was sufficient to activate the transcriptional response of *TaPR1a*-mediated plant defense.

Lipid transfer proteins (LTP) belonging to PR14 family constitute a large protein family that exist in all the land plants and they are involved in various biological processes (Salminen et al., 2016). A growing body of evidence showed that LTPs are involved in plant defense against biotic stress. An *Arabidopsis* apoplastic LTP protein encoded by *defective in induced resistance 1* (*DIR1*) is proposed to interact with a lipid-derived molecule to trigger long-distance signaling (Maldonado et al., 2002). The expression of *Arabidopsis LTP3* is directly regulated by the transcription factor MYB96 (Guo et al., 2013), the latter which serves as a key transcriptional regulator bridging signal pathways of abscisic acid (ABA) and SA (Seo et al., 2009; Seo and Park, 2010). Barley lipid transfer protein 4 (*HvLTP4*), firstly designated as *PR14*, is highly induced by infection of powdery mildew (Molina and García-Olmedo, 1993). Several *Pichia pastoris*-expressed wheat *LTPs* showed direct antifungal activities against multiple pathogens (Sun et al., 2008). Wheat non-specific LTPs exhibit differential inhibition to wheat and non-wheat pathogens *in vitro* (Sun et al., 2008). Overexpression of wheat LTP gene *TaLTP5* results in increased resisance against *Cochliobous sativus* and *Fusarium graminearum* (Zhu et al., 2012). Wang et al. showed that overexpression of *Triticum aestivum* lipid transfer protein (*TaLTP3*) in *Arabidopsis* confers heat stress tolerance (Wang et al., 2014). More recently, heterologous overexpression of *Arabidopsis AtLTP4.4* in transgenic wheat results in enhanced resistance to *Fusarium* head blight and detoxification of mycotoxin deoxynivalenol (DON) (McLaughlin et al., 2020). Although wheat LTPs have been widely studied, the molecular mechanism underlying LTP-mediated defense response in apoplast remains unclear.

Our previous studies showed that *TaLTP3* protein was targeted by a wheat rust effector PNPi (Puccinia NPR1 interactor) (Bi et al., 2020). Therefore, we hypothesized that *TaLTP3* might play an important role in wheat resistance against rust infections. In this study, we generated transgenic wheat lines overexpressing *TaLTP3* to explore its fuctions during wheat defense responses and found transgenic lines exhibited enhanced resistance to leaf rust. Resistance mechanism of *TaLTP3* was further investigated by transcriptome sequencing. *TaLTP3* localized to the apoplast and interacted with *TaPR1a* suggesting that a *TaLTP3-TaPR1a* protein complex is involved in wheat resistance against leaf rust pathogen.

MATERIALS AND METHODS

Gene Cloning, Generation of Wheat Transgenic Lines, and Pathogen Inoculation

The complete coding region of *TaLTP3* (GenBank accession AY226580.1) was amplified from complementary DNA (cDNA) synthesized from RNA extracted from the seedlings of wheat line "Chinese Spring." The complete coding region of *TaLTP3* was constructed to binary T-DNA vector pLGY-02 (*Ubi:gene*, T-DNA). Transgenic wheat line overexpressing *TaLTP3* gene was generated in the genetic background of spring common wheat cultivar "JW1" (selected from a segregating population of the cross of spring common wheat cultivars "Fielder" and "NB1") with technique support from Bangdi Ltd. Company, Shandong, China. Transgenic wheat lines overexpressing *TaPR1a* in the same genetic background were derived from a previous study (Bi et al., 2020).

Seedlings of the wheat isogenic line carrying leaf rust resistance gene *Lr39/41* in background of common wheat cultivar "Thatcher" were inoculated with *Puccinia triticina* (*Pt*), a virulent pathotype THTT following previously described procedure (Li et al., 2018). A high-resistant phenotype with the hypersensitive response (HR) was observed in *Lr39/41* isogenic line after inoculation with *Pt* pathotype THTT. RNA samples for quantitative PCR (qPCR) were collected from wheat leaves inoculated with leaf rust or water control at 0, 1, 2, 5, and 8 days postinoculation (dpi). Four independent biological replicates were included for each time point and treatment. Seedlings of transgenic wheat line *TaLTP3-OE* and wild-type plants were inoculated with *Pt* virulent pathotype FHJQ following a similar procedure. The wild-type plant "JW1" showed a moderate susceptible phenotype (rust sporulation with necrotic spots on wheat leaf) toward most of the collected *Pt* pathotypes including FHJQ and THTT. The disease symptoms were photographed at 14 dpi. An image analysis software ASSESS version 2.0 (American Phytopathological Society, St. Paul, Minisota, MN, United States) was employed to evaluate the percentage of *Pt* sporulation area for each inoculated leaf (Lamari, 2008; Bi et al.,

2020). Two independent transgenic lines of *TaLTP3-OE* with 9–13 biological replicates were included for the *Pt* inoculation. The Dunnett's test was conducted by using statistical analysis software SAS version 9.4.

Model bacterial pathogen *P. syringae* DC3000 was inoculated in second leaves of wheat seedlings according to the previously described method (Bi et al., 2020). *P. syringae* DC3000 was cultivated in low-salt Luria-Bertani (LS-LB) medium with 50 μg/mL rifampicin (Rif) antibiotics for 48 h (Jacob et al., 2017) and then diluted to optical density (OD) 600 = 0.6 in distilled water. Second leaves of transgenic wheat line *TaLTP3-OE* were infiltrated with bacterial suspensions by using a 1-ml needless syringe through the abaxial surface. Each transgenic line consisted of 6–8 independent biological replicates. Seedlings of wild-type plants and water-infiltration served as controls. The infiltration region was marked by using a marker pen. RNA samples for qPCR and RNA-sequencing (RNA-seq) assays were collected from the infiltration region at 6 h post-inoculation (hpi).

Ribonucleic Acid-Sequencing

Ribonucleic acid samples were sent to Novogene Corporation Ltd. for KAPA library construction and transcriptome sequencing following the default procedure. The Illumina HiSeq 1000 System was employed for the 12-Gb sequencing for each RNA sample. Transcriptome was assembled with reference genome of *Triticum aestivum* (common wheat "Chinese Spring" TGACv1 version) (Appels et al., 2018) by using the HISAT2 FDR and StringTie software (Kim et al., 2019). Assembled transcripts that could not be found in the gene models of the reference genome were annotated as "novel" transcripts. Gene expressions were profiled by using the HTSeq version 0.9.1 software (Trapnell et al., 2010). The expected number of fragments per kilobase of transcript sequence per million base pairs (FPKM) for each gene was used to evaluate the expression of assembled genes. FPKM-based heatmaps were generated by the MeV software. Differentially expressed genes (DEGs) were filtered the expression levels of genes between different groups for an false discover rate (FDR)-adjusted p-value < 0.05 and $|\log2\text{-fold change}| > 1$ by using the DESeq2 software (Love et al., 2014). The Gene Ontology (GO) annotations were assigned to each DEGs with the GO sequencing (Young et al., 2010). The KEGG (Kyoto Encyclopedia of Genes and Genomes) annotations were employed to profile the regulatory pathways enriched with DEGs (Kanehisa and Goto, 2000).

Quantitative Real Time-PCR Assay

Ribonucleic acids were prepared by using the RNA Extraction Kit (QIAGEN, Hilden, Germany, United Kingdom) and the first-strand cDNA was synthesized by using the Reverse Transcription Kit (Takara, Dalian, China). Primers for qRT-PCR assay were designed (**Supplementary Table 1**) and a preliminary test was performed on the Roche LightCycler 96 qRT-PCR machine by using a series of 2-fold diluted cDNA templates (1:1, 1:2, 1:4, 1:8, and 1:32) to evaluate the amplification efficiency for each pair of primers. Melting curves were generated to ensure the specificity of the amplification. The wheat reference gene *TaActin* (GenBank accession AB181991) was used as the endogenous control (Paolacci et al., 2009). The transcript level was expressed relative to that of *TaActin* based on the $2^{-\Delta Ct}$ method as described in a previous study (Wu et al., 2019). Mean and SE were calculated by using the Microsoft Excel software. The two-sample t-test and the generalized linear model (GLM) ANOVA were performed by using the SAS software version 9.4.

Subcellular Localization

Full-length open reading frame (ORF) of *TaLTP3* was cloned into transient expression vectors of pGWB5 (*35S:gene-GFP*, T-DNA) and pGWB454 (*35S:gene-RFP*, T-DNA), respectively. The recombinant vectors were transformed into *Agrobacterium* strain GV3101 and then used for infiltration of *Nicotiana benthamiana* (*N. benthamiana*). Corresponding empty vectors expressing only green fluorescent protein (GFP) and red fluorescent protein (RFP) served as controls. Green or red fluorescence was checked 48 hpi by using a Nikon Ti-2 microscope with a GFP or RFP filter, respectively. Epidermal peels of tobacco leaves were prepared from the infiltration region and soaked in 800 mM mannitol for 6 min to induce the plasmolysis (Ma et al., 2012).

Yeast Two-Hybrid Assay

Primers that were used to amplify the full-length ORF of *TaLTP3* and five other plant defense-related *LTP* genes from cDNA synthesized from RNA isolated from the common wheat line "Chinese Spring" are listed in **Supplementary Table 1**. A neighbor-joint tree including all the LTP proteins in this study was generated by using the MEGA software version 7.0. The signal peptides of wheat LTPs were predicted by SignalP 5.0 server.[1] The amplified DNA fragment lacking the sequence encoding the signal peptide was cloned into a Gateway yeast two-hybrid (Y2H) vector pLAW10 bait domain (BD). Recombined Y2H activation domain (AD) vectors carrying different regions of the *TaPR1a* gene were derived from a previous study (Bi et al., 2020). The coding regions of $\text{TaPR1a}_{(25-93\text{aa})}$ and $\text{TaPR1a}_{(25-128\text{aa})}$ were cloned into a Gateway Y2H vector pLAW11 (AD). Yeast transformation was performed by using lithium acetate and polyethylene glycol 3350 as previously described (Gietz and Schiestl, 2007). Cotransformed yeast strains were spotted on SD-Leu-Trp-His-Ade selective medium.

Bimolecular Fluorescence Complementation Assay

Full-length ORF of *TaLTP3* with signal peptide was constructed to pDEST-^{GW}VYNE (*35S:gene-YFP^N*, T-DNA). The recombinant construct of *TaPR1a*-pDEST-^{GW}VYCE carrying complete coding region of *TaPR1a* was derived from our previous study (Bi et al., 2020). The fusion genes were coexpressed in tobacco leaves by *Agrobacterium* infiltration. Yellow fluorescence was checked 48 hpi by using a Nikon Ti-2 microscope with a yellow fluorescent protein (YFP) filter. Coexpression of *AvrLm1*-pDEST-^{GW}VYNE and *BnMPK9*-pDEST-^{GW}VYCE in the same vectors was used as a positive control (Ma et al., 2018). Signal peptide-fused empty

[1] http://www.cbs.dtu.dk/services/SignalP/

vectors of $SP_{(TaPR1a)}$-pDEST-^{GW}VYNE and $SP_{(TaPR1a)}$-pDEST-^{GW}VYCE were derived from our previous study (Bi et al., 2020) and coexpressed with *TaPR1a*-pDEST-^{GW}VYCE and *TaLTP3*-pDEST-^{GW}VYNE, respectively, as negative controls.

Co-immunoprecipitation Assay

Deoxyribonucleic acid fragment encoding the signal peptide-truncated *TaLTP3* protein was cloned into pGWB5 as $35S{:}TaLTP3_{(30-122)}$-*GFP*. A specific reverse primer of *TaPR1a* with stop codon and sequence encoding cMYC tag was designed and used to amplify the DNA fragment encoding the signal peptide-truncated *TaPR1a* protein. The resulting DNA segment was constructed into pGWB5 as $35S{:}TaPR1a_{(25-164)}$-*cMYC*. Recombinant pGWB5:$TaLTP3_{(30-122)}$-*GFP* and pGWB5: $TaPR1a_{(25-164)}$-*cMYC* were coexpressed in tobacco leaves by using *Agrobacterium*. Coexpression of *GFP* and $TaPR1a_{(25-164)}$-*cMYC* served as a negative control. Total proteins were extracted from *Agrobacterium*-infiltrated tobacco leaves at 3 dpi and a portion of the total protein was reserved as an input sample. α-GFP IP samples were prepared by using GFP-trap beads (LABLEAD, Beijing,China). Input and IP samples were separated by sodium dodecyl sulphate-polyacrylamide gel electrophoresis (SDS-PAGE) and then transferred onto membranes made of polyvinylidene difluoride (PVDF). Immunoblots were performed by using α-GFP or α-cMYC antibody (Solarbio, Beijing, China).

Reactive Oxygen Species Staining

To visualize the accumulation of ROS in wheat leaves infiltrated with *P. syringae* DC3000, two chemical reagents, nitroblue tetrazolium (NBT) and 3,3-diaminobenzidine (DAB), were applied to stain the superoxide anion (O_2^-) and hydrogen peroxide (H_2O_2), respectively. The staining protocols were modified from a previous study (Wang et al., 2007). Leaf regions infiltrated with *P. syringae* DC3000 were collected at 2, 4, and 8 hpi. For O_2^- visualization, samples were soaked in 10 mM sodium azide (NaN_3) and 10 mM potassium phosphate buffer (pH 7.8) with 0.1% NBT (w/v) for 24 h. For H_2O_2 staining, samples were incubated in hydrochloric acid (HCl)-acidified solution (pH 3.8) containing 1 mg/mL of DAB for 24 h. Thereafter, samples were decolored in boiling 95% ethanol for 10 min. The percentage of stained area in each leaf was determined by using the ASSESS software (Lamari, 2008). The whole experiment was repeated twice with two independent transgenic lines and each repeat consisted of 6–10 biological replicates. The Dunnett's test was conducted by using the SAS software version 9.4.

RESULTS

Stable Overexpression of *TaLTP3* in Transgenic Wheat Line Results in Enhanced Resistance to Leaf Rust Pathogen *Puccinia triticina*

To determine the role of *TaLTP3* in plant resistance, we first quantified the expression change of this gene in leaf rust resistance mediated by *Lr39/41* gene. Interestingly, *TaLTP3* was significantly upregulated at the wheat early-stage resistance toward leaf rust (**Figure 1A**). To further explore the function of *TaLTP3*, transgenic wheat lines overexpressing *TaLTP3* (*TaLTP3-OE*) were generated in the genetic background of commonspring wheat line "JW1." The expression levels of *TaLTP3* in *TaLTP3-OE* reached 1.7- to 2.8-fold of those in the wild-type (**Figure 1B**). The third leaves of *TaLTP3-OE* and wild-type plants were inoculated with urediniospores of the *Pt* pathotype FHJQ and FHJQ exhibited high virulence on wild-type plants (**Figure 1C**). The sporulation of leaf rust pathogen was observed in both the *TaLTP3-OE* and wild-type plants. The percentage of *Pt* sporulation area for each inoculated leaf was evaluated by using the ASSESS software. Compared with wild-type plants, significantly enhanced resistance to *Pt* was observed in *TaLTP3-OE* as evidenced by decreased sporulation area ($^{**}p < 0.01$, $^{***}p < 0.0001$, 9–30 biological replicates) (**Figure 1C** and **Supplementary Table 2**). We further investigated several agronomic traits of transgenic wheat line *TaLTP3-OE* including plant height, spike length, spikelet number per spike, and seed number per spike under greenhouse conditions. We did not observe any significant difference in these agronomic traits between *TaLTP3-OE* and wild-type plants (**Figure 1D**). However, when we checked the seed size and thousand grain weight, we found smaller and lighter seeds harvested from *TaLTP3-OE* than wild-type plants (**Figure 1E**), indicating overexpression of *TaLTP3* might have influence on wheat production.

Overexpression of *TaLTP3* Positively Regulates Multiple Signaling Pathways Mediated by Plant Hormones of Auxin, Jasmonic Acid, and Salicylic Acid

To reveal the mechanism of *TaLTP3* during plant resistance, we have used model bacterial pathogen *P. syringae* pv. *tomato* DC3000 to trigger the immune response in wheat leaves. Although *P. syringae* DC3000 is not a wheat pathogen under a natural environment, a typical cell death was observed in wheat leaf infiltrated with *P. syringae* DC3000 at 48 hpi (**Figure 2A**), indicating a successful induction of non-host resistance. We applied RNA-seq on samples collected from *P. syringae* DC3000-infiltrated third leaves of wheat transgenic line *TaLTP3-OE* and wild-type plants at 6 hpi. Samples from the water-infiltrated leaves served as a control. Each of the treatments included three biological replicates and, in total, 12 samples were subjected to a 12-Gb Illumina sequencing (**Supplementary Table 3**). The reference genome of *Triticum astivum* from the Ensembl Genomes (TGACv1 version) was used to assemble the transcriptome. A total of 122,130 transcripts were mapped to the genome sequence (**Supplementary Table 4**). Significant ($R^2 > 0.92$) correlations of the overall gene expressions among biological replicates were detected (**Supplementary Table 5**). We used the FPKM value to predict the expression levels of transcripts. Raw reads from the RNA-seq were deposited at the National Center for Biotechnology Information (NCBI) BioProject PRJNA746113.

The expression levels of all 18 *PR* gene families were displayed in the heat map based on their FPKM values derived from the transcriptome data (**Figure 2B**). Most of the *PR*

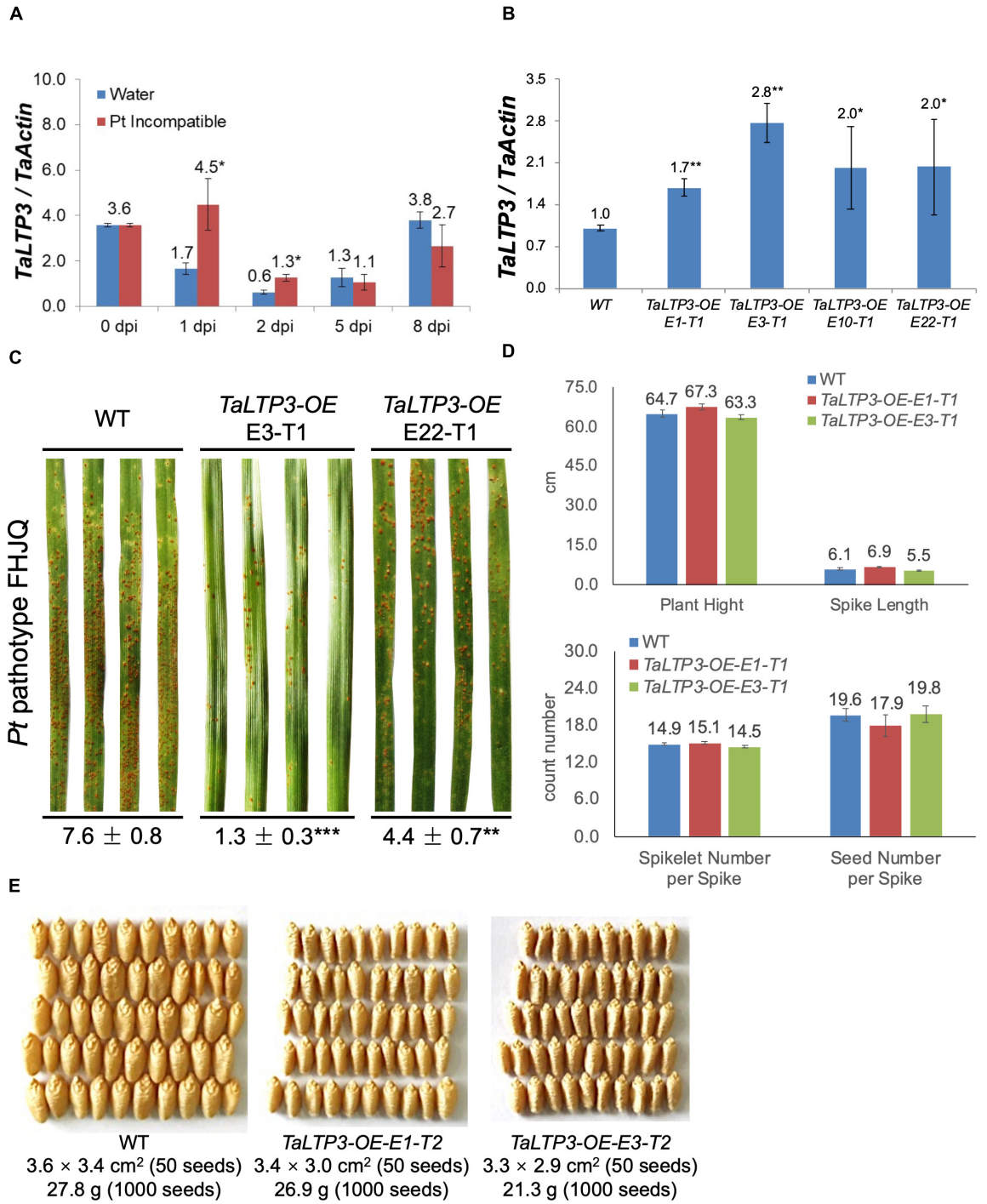

FIGURE 1 | *TaLTP3* was involved in wheat resistance to leaf rust. **(A)** Expression levels of *TaLTP3* during *Lr39/41*-mediated wheat resistance toward leaf rust were evaluated by quantitative PCR (qPCR) assay. Leaf samples were collected at 0, 1, 2, 5, and 8 days postinoculation (dpi) with water (control) and avirulent *Pt* pathotype THTT. The transcript levels for all the genes were expressed as linearized fold-*TaActin* levels, which were calculated based on the formula $2^{(\text{Actin Ct} - \text{Target Ct})}$. Data were expressed as mean ± SE from four biological replicates. The asterisk indicated a significant difference ($p < 0.05$) between the water control and *Pt*-inoculated samples by using the *t*-test. **(B)** The transcript level of *TaLTP3* in transgenic wheat line overexpressing *TaLTP3* and wild-type plants were evaluated by qPCR assay. **(C)** The susceptibility phenotypes of *TaLTP3-OE* and wild-type plants to the *Pt* pathotype FHJQ. The numbers below the images of the *Pt*-infected wheat leaves represent the average percentages of the rust sporulation area in each leaf. The asterisks (**$p < 0.01$, ***$p < 0.0001$) were annotated based on the comparison between the transgenic line and wild-type plants by the Dunnett's test. **(D)** Agronomic traits of transgenic wheat line *TaLTP3-OE* and wild-type plants were investigated in greenhouse condition. **(E)** Seeds harvested from transgenic wheat line *TaLTP3-OE* and wild-type plants were compared in size and thousand grain weight.

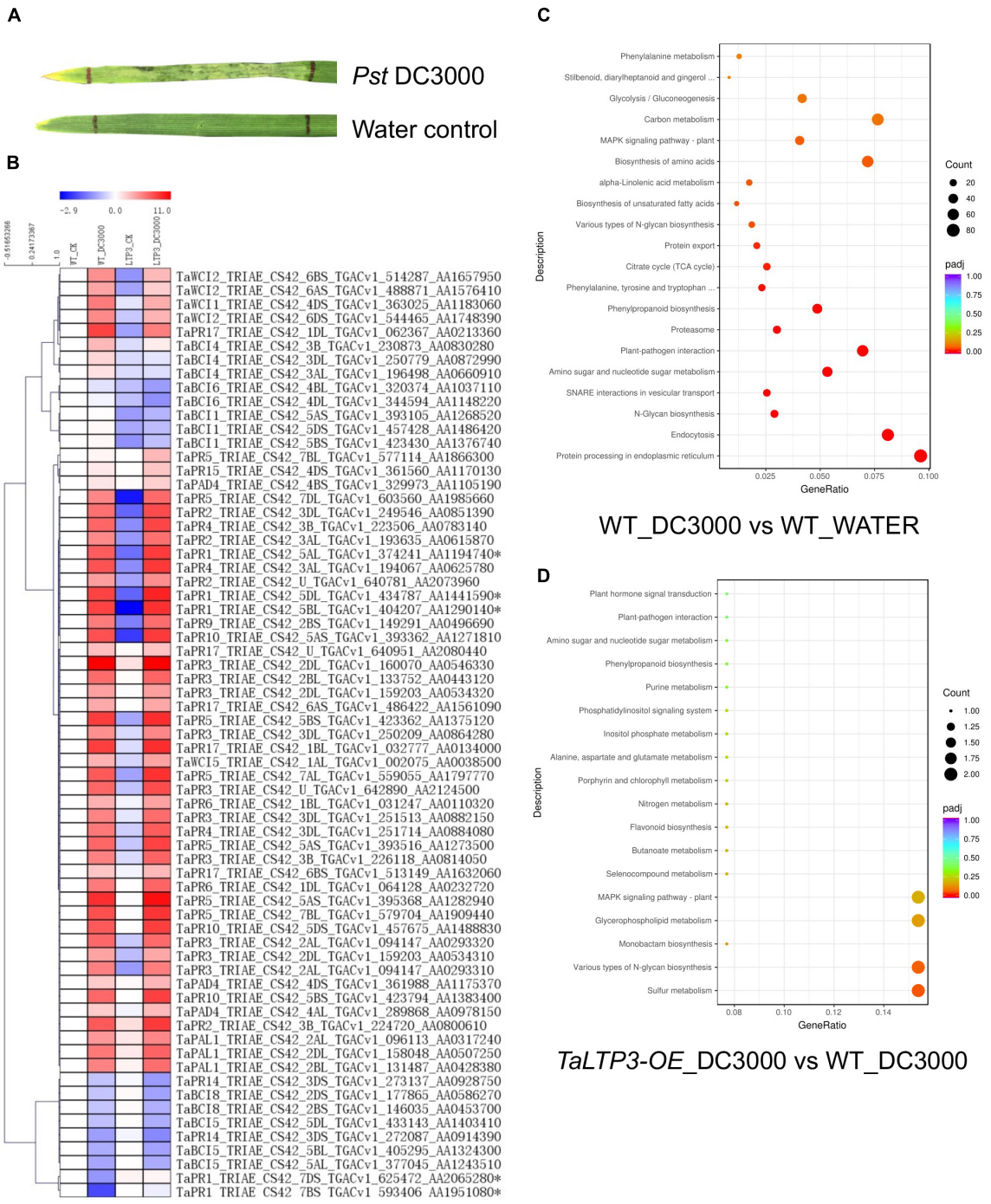

FIGURE 2 | Transcriptome analysis revealed the regulatory network of *TaLTP3* during plant defense. **(A)** A typical cell death was observed in wheat leaf infiltrated with *P. syringae* DC3000 at 48 h postinfiltration. **(B)** Expression profile of *PR* genes upon *P. syringae* DC3000 infection in *TaLTP3-OE* transgenic wheat line. FPKM values of WT_DC3000, LTP_CK, and LTP_DC3000 were relative to that of WT_CK. Data were calculated as log2-fold change format by using the Microsoft Excel software. Heatmap was generated by using the MeV software. Genes with similar expression patterns were clustered. **(C,D)** The Gene Ontology (GO) annotations for upregulated differentially expressed genes (DEGs) in comparisons of "WT_DC3000 vs. WT_WATER"and "*TaLTP3-OE*_DC3000 vs. WT_DC3000." DEGs were classified based on their GO annotations into three main categories including biological process, cellular component, and molecular function.

genes were highly induced by the infection of *P. syringae* DC3000, indicating an activation of a broad-range plant defense response by this model pathogen. Compared with the wild-type plants, *TaPR1a*, *TaPR5*, and *TaPR15* showed higher levels of expression in *TaLTP3-OE*. DEGs in comparison of "WT_DC3000 vs. WT_WATER" were identified (|$\log_2$-fold

change| > 1 and *q*-value < 0.01) by using DESeq2. In the wild-type plants, we found 9,178 genes were significantly upregulated upon *P. syringae* DC3000 infection. The KEGG annotations of these *P. syringae* DC3000-sensitive genes indicated the activation of a broad-range plant defense responses including Ca^{2+}-dependent ROS induction, mitogen-activated protein kinase (MAPK) signaling, and effector-triggered immunity (**Supplementary Figure 1** and **Supplementary Table 6**). The GO annotations for these DEGs enriched in "plant–pathogen interaction" and "protein processing in endoplasmic reticulum" (**Figure 2C**).

From the comparison between "*TaLTP3-OE*_DC3000" and "WT_DC3000," only 214 genes were significantly higher expressed (log_2-fold change > 1 and *q*-value < 0.01) in *TaLTP3-OE* transgenic upon *P. syringae* DC3000 infection. The GO annotations of these upregulated DEGs enriched in "Various types of N-glycan biosynthesis" and "Glycerophospholipid metabolism" (**Figure 2D**). Among all these *TaLTP3*-responsive upregulated DEGs, *TaPR1a* was the only gene annotated into the KEGG pathway of "plant–pathogen interaction" (**Table 1**). Furthermore, we found 173 genes with significantly lower (log2-fold change < -1 and *q*-value < 0.01) expressions in *TaLTP3-OE* transgenic line upon *P. syringae* DC3000 infection. Several key regulators in the hormone pathway of auxin and JA, including *auxin response factor 9* (*ARF9*), *A-type Arabidopsis response regulator* (*A-ARR*), and *protein TIFY 6a* [*JAZ* (jasmonate ZIM-domain)], were downregulated in the KEGG pathway of "plant hormone signal transduction" (**Table 1** and **Supplementary Figure 2**).

We further evaluated the expression levels of two SA synthesis genes, *TaPAL* and *TaPAD4*, during *P. syringae* DC3000 infection in *TaLTP3-OE* transgenic line by using qRT-PCR assay (**Figure 3**). qPCR showed that the expression levels of both the *TaPAL* and *TaPAD4* were elevated upon *P. syringae* DC3000 infection in *TaLTP3-OE* transgenic line, which was consistent with those in RNA-seq (**Figure 2B**), suggesting that our RNA-seq data are reliable.

TaLTP3 Interacts With Pathogenesis-Related Protein 1a in the Apoplastic Space

As overexpression of *TaLTP3* affected *TaPR1a* expression during plant defense response (**Figure 2B**, **Supplementary Figure 2**, and **Table 1**) and both *TaLTP3* and *TaPR1a* are predicted as secreted proteins by signal P, we hypothesized that *TaLTP3* might function through physical interaction with *TaPR1a* in the apoplastic space. The apoplast localization of *TaPR1a* has been validated in our previous study (Bi et al., 2020). GFP- and RFP-tagged *TaLTP3* were generated, respectively. The recombinant constructs *TaLTP3-GFP* and *TaLTP3-RFP* were transientlyexpressed in *N. benthamiana* by agroinfiltration. Plasmolysis was induced by treatment with 800 mM mannitol. Pronounced green and red fluorescent signals for *TaLTP3-GFP* and *TaLTP3-RFP* were visualized in the apoplastic space, respectively (**Figure 4**), but not for the empty vector (EV-GFP and EV-RFP) controls (**Figure 4**), suggesting that *TaLTP3* localizes in the apoplastic space.

To examine the interaction between *TaLTP3* and *TaPR1a*, a Y2H assay was performed by using a signal peptide-truncated version of these two proteins. Strong interaction was observed between $TaPR1a_{(25-164)}$ and $TaLTP3_{(30-122)}$ as yeast transformed with both the constructs was able to grow on the stringent synthetic dropout (SD) selective media lacking leucine, tryptophan, histidine, and adenine (SD-Leu-Trp-His-Ade) (**Figure 5A**). Because the C-terminal region of *TaPR1a* contains the conserved CAPE1 peptide in most PR1 proteins that might act as a DAMP in triggering plant defense response, we generated several truncated versions of *TaPR1a* protein, in which different C-terminal regions were deleted (**Figure 5B**). As shown in **Figure 5A**, an N-terminal region of TaPR1a ranging from 25 to 93 aa was sufficient to mediate the interaction with *TaLTP3*. However, we did not observe any interaction between TaPR1a (94–164 aa) and *TaLTP3*. As many wheat *LTP* genes, including *TaLTP2*, *TaLTP3F1*, *TaLTP4.3*, *TaLTP4.1*, and *TaPR14*, have been previously reported in wheat resistance to various pathogens, we also checked the interaction of *TaPR1a* with these LTP proteins and found that *TaPR1a* interacts with all these LTP proteins (**Supplementary Figure 3**). Collectively, these initial Y2H results indicated a conserved physical interaction between *TaPR1a* and LTP proteins.

To validate the *in-planta* interaction between *TaLTP3* and *TaPR1a*, a bimolecular fluorescence complementation (BiFC) assay was performed in *N. benthamiana*. Strong yellow fluorescence signals in the apoplast were observed in *N. benthamiana* leaves coexpressing *TaLTP3-YFP*^{N} and *TaPR1a-YFP*^{C} (**Figure 5C**), whereas fluorescence in cytoplasm and nucleus was found in positive control coexpressing *AvrLm1-YFP*^{N} and *BnMPK9-YFP*^{C} (Ma et al., 2018). No YFP signals were observed in the *N. benthamiana* leaves coexpressing the negative controls: *TaLTP3-YFP*^{N} and $SP_{(TaPR1a)}$-*YFP*^{C} nor $SP_{(TaPR1a)}$-*YFP*^{N} and *TaPR1a-YFP*^{C}.

To further confirm the interaction *in vivo*, a co-immunoprecipitation (co-IP) assay was performed following transient expression of $TaPR1a_{(25-164)}$-*cMYC* and $TaLTP3_{(30-122)}$-*GFP* constructs in *N. benthamiana*. GFP was used as a negative control. cMYC-tagged TaPR1a co-immunoprecipitated with GFP-tagged TaLTP3, but not with GFP (**Figure 5D** and **Supplementary Figure 4**), indicating that *TaLTP3* physically interacts with *TaPR1a*.

Overexpression of Pathogenesis-Related Protein 1a and *TaLTP3* in Wheat Increases Accumulation of Reactive Oxygen Species Triggered by *P. syringae* DC3000

To explore the coeffects of *TaLTP3* and *TaPR1a* during plant defense response, we evaluate the accumulation of H_2O_2 and O_2^- in the transgenic wheat lines *TaLTP3-OE* and *TaPR1a-OE* during *P. syringae* DC3000 infection. Leaf samples were collected at 2, 4, and 8 h after *P. syringae* DC3000 inoculation and stained with DAB and NBT to visualize H_2O_2 and O_2^-,

TABLE 1 | DEGs of "LTP3_DC vs. WT_DC" annotated in the KEGG pathway of "plant–pathogen interaction" and "plant hormone signal transduction."

KEGG annotation	Gene ID	WT_DC FPKM	LTP3_DC FPKM	LTP3_DC vs WT_DC *p*-adjust value	Gene annotation
PR-1	TRIAE_CS42_7BS_TGACv1_593406_AA1951080	17.26	63.11	4.34×10^{-7}	Pathogenesis-related protein PRB1-2
ARF	novel.6352	1.21	0.03	1.01×10^{-2}	Auxin response factor 9
A-ARR	TRIAE_CS42_2AL_TGACv1_093101_AA0272020	19.57	11.16	2.72×10^{-2}	Two-component response regulator ORR6
	TRIAE_CS42_2BL_TGACv1_132162_AA0435700	3.14	0.71	6.55×10^{-5}	Two-component response regulator ORR1
JAZ	TRIAE_CS42_5AL_TGACv1_375081_AA1215750	2.74	0.66	1.13×10^{-3}	Protein TIFY 6a

LTP, lipid transfer protein; CK, mock inoculation with water; DC, P. syringae DC3000 infection; DEGs, differentially expressed genes.

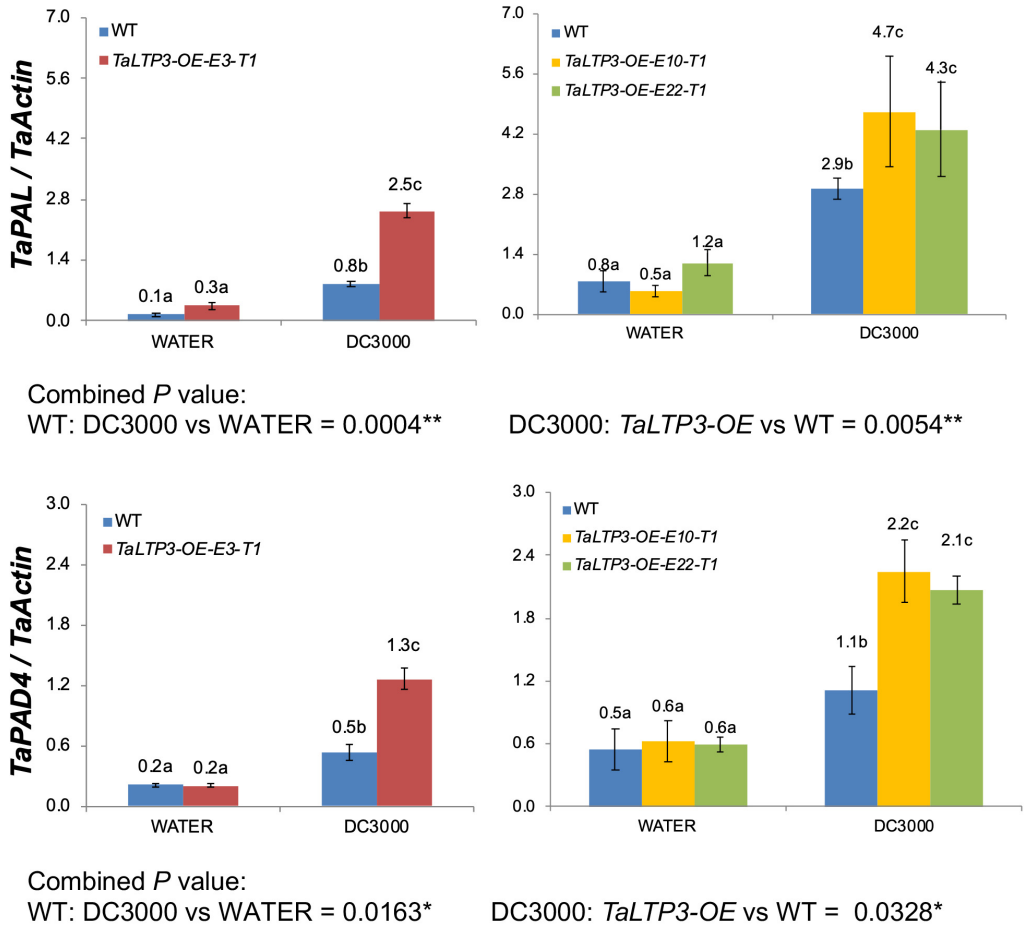

FIGURE 3 | The transcriptional levels of *TaPAL* and *TaPAD4* were determined by qPCR in transgenic line *TaLTP3-OE* upon *P. syringae* DC3000 infection. The transcript levels for all the genes were expressed as linearized fold-*TaActin* levels, which were calculated based on the formula $2^{(\text{Actin Ct} - \text{Target Ct})}$. Three independent transgenic lines of *TaLTP3-OE* were tested. Each experiment, consisting of 4–9 biological replicates, was considered as a block. Calculations of the mean and SE were performed by using the Microsoft Excel software. Generalized linear model (GLM) ANOVA (*$p < 0.05$, **$p < 0.01$) was conducted by using the SAS software version 9.4.

respectively. Percentage of the stained area in each infiltrated leaf was calculated by using the ASSESS software. Compared with the wild-type plants, we observed significantly higher (*$p < 0.05$, **$p < 0.01$, 6–10 biological replicates) accumulation of H_2O_2 in the transgenic wheat lines *TaPR1a-OE* and *TaLTP3-OE* at 4 and 8 hpi (**Figure 6A** and **Supplementary Table 7**). For the NBT staining, the transgenic wheat line *TaPR1a-OE* showed a fast and higher accumulation of O_2^- at 2 and 4 hpi, whereas the transgenic wheat line *TaLTP3-OE* accumulated more O_2^- only at 4 hpi (**Figure 6B** and **Supplementary Table 8**). These results

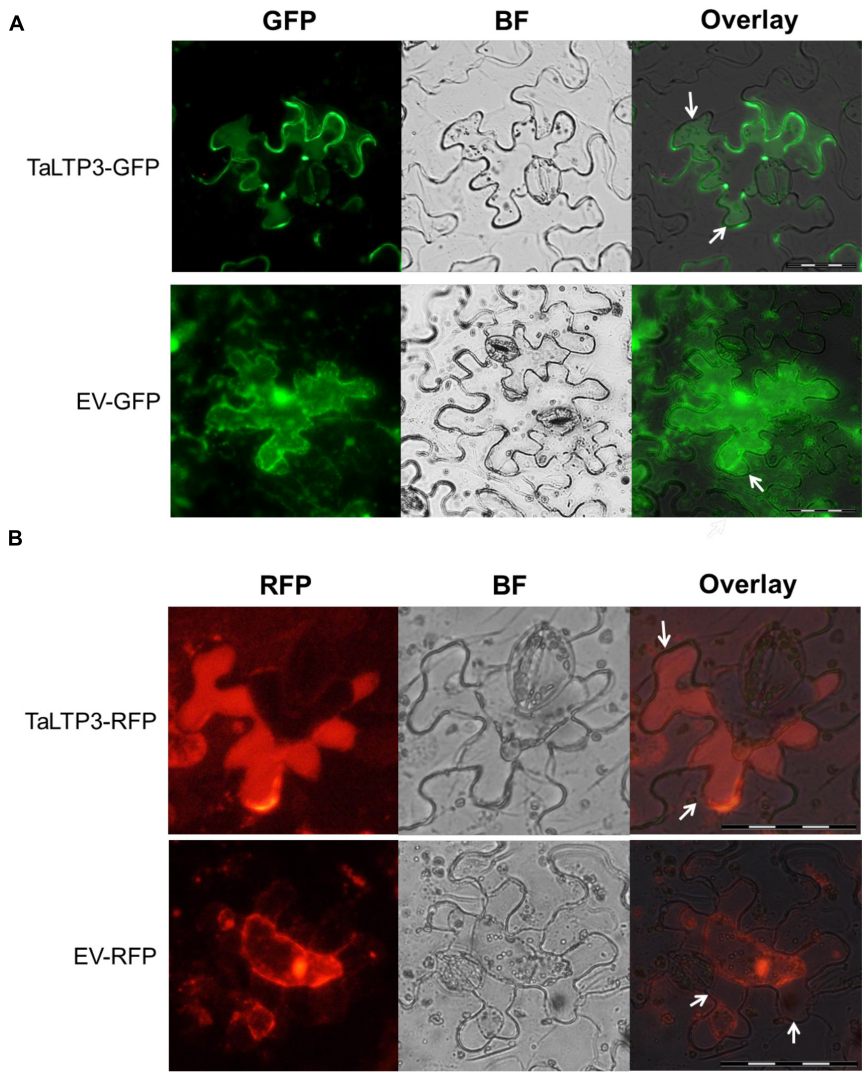

FIGURE 4 | *TaLTP3* protein was localized in the apoplastic space. The *TaLTP3-GFP* **(A)** and *TaLTP3-RFP* **(B)** Recombinant proteins were transiently expressed in *N. benthamiana* leaves by agroinfiltration. GFP or RFP alone was used as a control. Leaf epidermal peels were plasmolyzed by incubation in 800 mM mannitol for 6 min. White arrows indicating the separation between the plant cell wall and plasma membrane during plasmolysis. Scale bar = 100 μm. BF, bright field; EV, empty vector; GFP, green fluorescent protein; RFP, red fluorescent protein.

indicated that both the *TaLTP3* and *TaPR1a* might function through a ROS-dependent plant defense response.

DISCUSSION

Many designated PR proteins are secreted into the apoplastic space to function. Therefore, apoplast represents the initial battlefield between plant and phytopathogens interaction and apoplastic immunity plays an important role in plant defense responses. *TaLTP3*, a member of the *PR14* gene family, was upregulated during wheat resistance to leaf rust infections (**Figure 1A**). Our studies showed that both the *TaLTP3* and *TaPR1a* are secreted into the apoplastic space (**Figure 4**; Bi et al., 2020). PR1 protein functions in multiple ways during plant defense response including direct antimicrobe activity, triggering DAMP-triggered immunity, and targeting pathogen effectors (Chen et al., 2014; Gamir et al., 2017; Sung et al., 2021). LTP also has antifungal and antioxidant activities (McLaughlin et al., 2020). In *Arabidopsis*, LTP was reported as upstream of SA-mediated resistance to biotic and abiotic stresses (Maldonado et al., 2002; Guo et al., 2013). Previous studies showed that PR1 interacts with pathogenesis-related proteins from plants and effectors from pathogens (Breen et al., 2017), suggesting that PR1 has a broad-spectrum interactors in plant–pathogen interaction. Therefore, we speculated that PR1 might form different complexes with various plant defense-related proteins targeting phytopathogens. In this study, we identified and validated a direct interaction between *TaLTP3* and *TaPR1a* in the apoplastic space (**Figure 5**). Further study

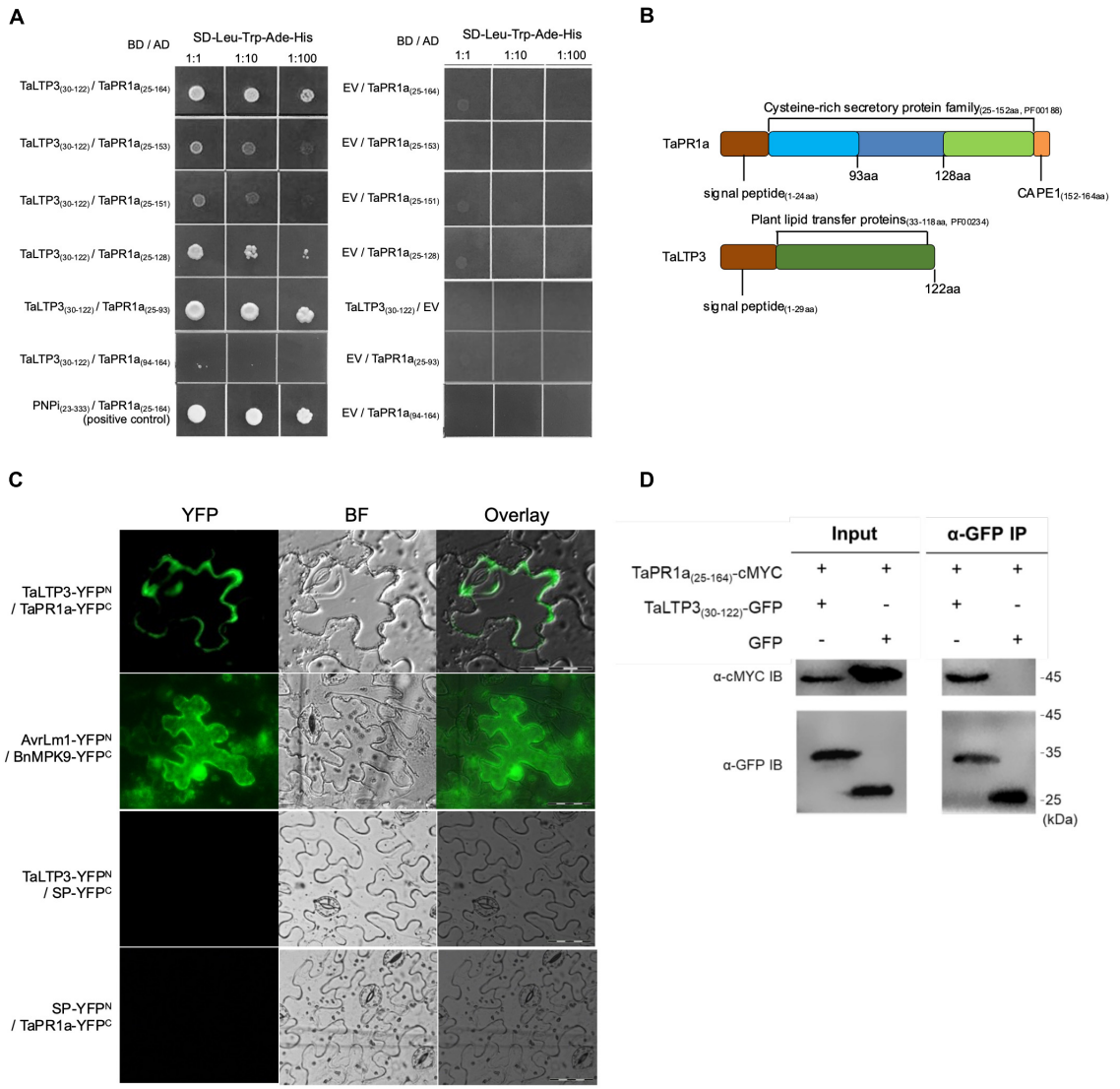

FIGURE 5 | *TaLTP3* physically associated with *TaPR1a in vitro* and *in vivo*. **(A)** Interaction of *TaLTP3* and *TaPR1a* was detected by Y2H. Yeast transformants coexpressing different bait and prey recombinant constructs were tested on selective medium of SD-Leu-Trp-His-Ade, EV, and empty vector. **(B)** Signal peptide and conserved domain for *TaPR1a* and *TaLTP3* proteins were schematically presented. **(C)** Bimolecular fluorescence complementation (BiFC) assay showed that the interaction between TaPR1a and TaLTP3 occurred in the apoplastic space. YFP signals were observed in the tobacco leaves coexpressing *TaLTP3-YFP*^{N} and *TaPR1a-YFP*^{C}. Recombinant constructs of AvrLm1-YFP^N and BnMPK9-YFP^C were coexpressed as a positive control. Segment encoding signal peptide of *TaPR1a* was cloned into BiFC vectors as SP-YFP^N and SP-YFP^C as negative controls. Scale bar = 100 μm. Due to the fixed microscopy settings for visualizing yellow and green fluorescent signals, the yellow fluorescent signals were presented in green color. **(D)** Validation of the interaction between *TaPR1a* and *TaLTP3* by co-immunoprecipitation (Co-IP) assay. Total proteins from tobacco leaves transiently expressing *TaPR1a*$_{(25-164)}$-cMYC and *TaLTP3*$_{(30-122)}$-GFP were extracted and immunoprecipitated with an α-GFP antibody (α-GFP IP). Input and bound proteins were immunoblotted with α-GFP and α-cMYC antibodies, respectively. Original, uncropped blots for the Co-IP assay were displayed as **Supplementary Figure 4**. BF, bright field; EV, empty vector; YFP, yellow fluorescent protein; BiFC, bimolecular fluorescence complementation; Y2H, yeast-two hybrid.

showed that this interaction was conserved among *TaPR1a* and other plant-defense-related LTP proteins (**Supplementary Figure 3**). The CAPE1 peptide in the C-terminal region of PR1 is conserved and acts as a DAMP-triggered plant defense-related transcriptional change (Chen et al., 2014). However, our studies showed the N-terminal region of *TaPR1a*, excluding the CAPE1 peptide, is required for the interaction between *TaLTP3* and *TaPR1a* (**Figures 5A,B**). We also found that the interaction of *TaLTP3* and *TaPR1a* occurs in the apoplast (**Figure 5C**). These observations implicated that TaLTP3 protein forms a complex with *TaPR1a* in the apoplast without occupying the CAPE1 peptide region of TaPR1a, suggesting that *TaLTP3* might stabilize *TaPR1a* via physical interaction to potentiate the CAPE1-triggered plant immune response. Further studies to determine our hypothesis are needed.

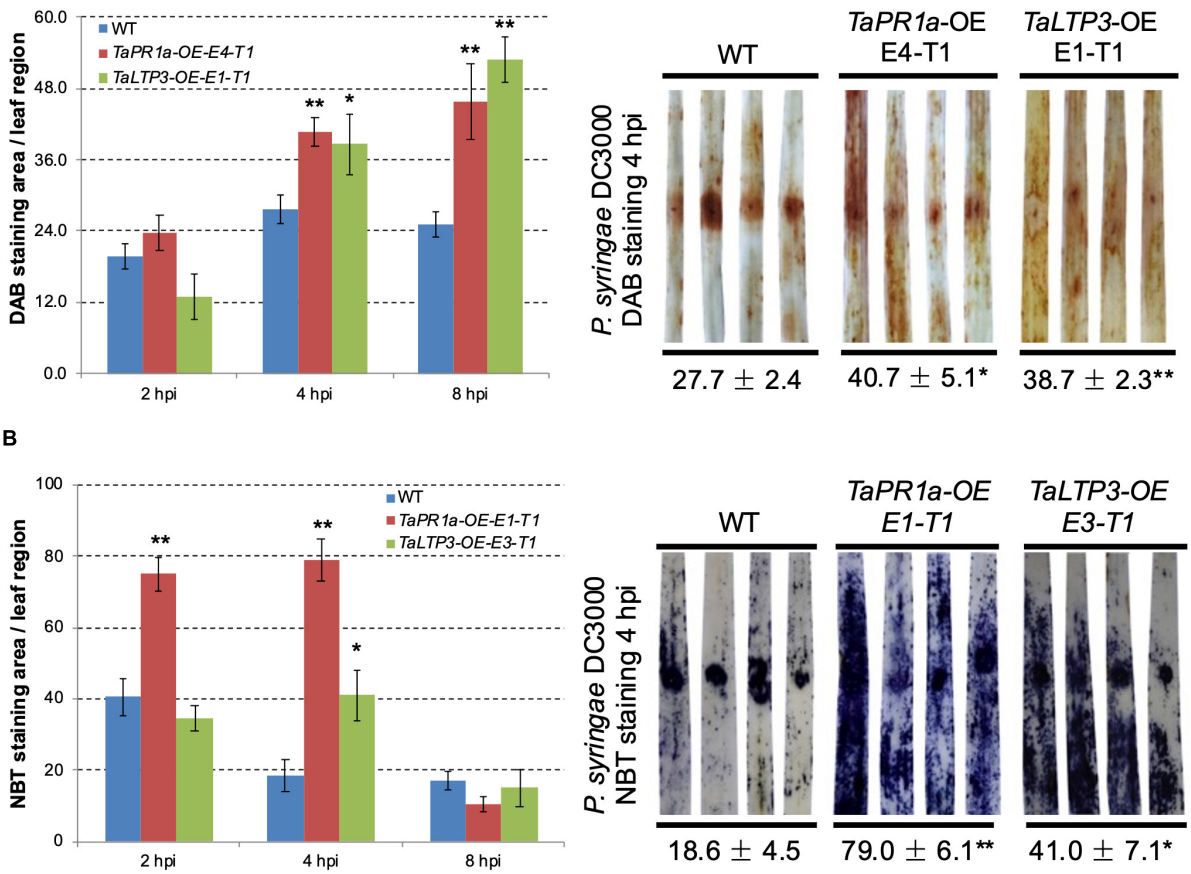

FIGURE 6 | Transgenic wheat lines *TaPR1a-OE* and *TaLTP3-OE* showed higher accumulation of reactive oxygen species (ROS) upon infection of model bacterial pathogen *P. syringae* DC3000. **(A)** Samples from the infiltrated region were collected at 2, 4, and 8 hours postinoculation (hpi) and further stained with 3,3-diaminobenzidine (DAB). **(B)** Corresponding samples were stained with nitroblue tetrazolium (NBT) to visualize the accumulation of superoxide anion (O_2^-). The percentage of stained area in the infiltrated region was calculated By using the ASSESS software. Asterisk indicates the significance of the differences between the transgenic lines and wild-type plants established by using the Dunnett's test (*$p < 0.05$, **$p < 0.01$, **Supplementary Tables 7**, **8**).

Our findings showed that transgenic lines *TaLTP3-OE* and *TaPR1a-OE* exhibited improved resistance to leaf rust (**Figure 1C**; Bi et al., 2020) and increased accumulation of ROS upon *P. syringae* DC3000 infection (**Figure 6** and **Supplementary Tables 7**, **8**). ROS has been widely reported to have a direct antimicrobial effect and can be involved in cell wall stiffening. Moreover, ROS acts as local and systemic signal molecules triggering plant defense response (Waszczak et al., 2018). Our results indicated that both the *TaPR1a* and *TaLTP3* may promote ROS accumulation during pathogen infection. A total of 330 *LTP* genes were identified from hexaploid genome of wheat and many of which were highly induced by abiotic stresses of drought and salinity (Fang et al., 2020). Close homologs in the *LTP* and *PR1* gene families might also have functional redundancy. Future studies focusing on dissecting the redundant functions between *LTP* and *PR1* genes are required.

In our previous study, we noticed that infection of model bacterial pathogen *P. syringae* DC3000 in wheat was sufficient to induce the expression of CAPE1-responsive genes *TaAdi3* and *TaPR7* (Bi et al., 2020). Therefore, we challenged the *TaLTP3-OE* line with model bacterial *P. syringae* for RNA-seq analysis. A specific upregulation of *TaPR1a* was detected in the transcriptome database by the KEGG annotation in *TaLTP3-OE* line compared to that in the WT plant (**Table 1**), suggesting that overexpression of *TaLTP3* can affact the expression of *TaPR1a* that may explain the earlier induction of *TaLTP3* than *TaPR1a* during wheat resistance to leaf rust mediated by the *Lr39/41* gene (**Figure 1A**; Li et al., 2018). Furthermore, we found suppressions of key regulator genes in auxin and JA pathways (*ARF9*, *A-ARR*, and *JAZ*) in *TaLTP3-OE* transgenic line (**Table 1**). Both the *ARF9* and *A-ARR* are negative regulators suppressing transcription of specific auxin-responsive genes (Leyser, 2006). JAZ proteins are repressors of JA signaling and inhibit the expression of JA-responsive genes by interaction with jasmonate-insensitive 1 (JIN1) transcription factor transcription factor (Chini et al., 2007). In addition, gene expressions of *TaPAL* and *TaPAD4* in upstream of SA pathway were highlyinduced in *TaLTP3-OE* transgenic line (**Figures 2B** and **3**). Taken together,

we speculated that *TaLTP3* acts as a positive regulator in the activation of crosstalk among SA, JA, and auxin. Although SA and JA are normally considered to control antagonistic pathways (Pieterse et al., 2009; Li et al., 2019), wheat plants seem to have a unique mechanism of hormone-mediated regulation of disease resistance. For instance, infection of spot blotch in resistance wheat genotype "Yangmai#6" elicited both the SA and JA signaling (Sahu et al., 2016). Spray treatments of both the SA and JA, but not ABA, on wheat leaves improved resistance to leaf rust (Kim et al., 2020).

CONCLUSION

We validated a positive role of *TaLTP3* in plant defense response. Stable expression of *TaLTP3* in transgenic wheat line improved resistance to leaf rust infection. Overexpression of *TaLTP3* elevates the expression of *TaPR1a* and activates multiple plant defense-related hormone pathways including SA, JA, and auxin. A novel interaction between *TaLTP3* and *TaPR1a* in the apoplast was identified and confirmed. TaLTP3 might play multiple roles in plant defense response, such as functioning with antimicrobe activities, forming a *TaLTP3-TaPR1a* complex in apoplast against pathogen and activating defense signaling. The presented findings have greatly expanded our knowledge on the molecular mechanism of *PR* genes during wheat resistance to pathogen infections. The generated transgenic wheat lines with enhanced defense responses may also serve as valuable resources for the genetic improvement of wheat resistance.

DATA AVAILABILITY STATEMENT

The original contributions presented in the study are publicly available. This data can be found here: National Center for Biotechnology Information (NCBI) BioProject database under accession number PRJNA746113.

AUTHOR CONTRIBUTIONS

XW and LM designed the experiment. JZ and WB conducted most of the experiments. SZ, JS, and ML worked on the RT-qPCR validation and rust inoculation. XW drafted the manuscript with contributions from LM and XY. All the authors read and approved the final manuscript.

FUNDING

XW was supported by the Provincial Natural Science Foundation of Hebei (C2021204008), Independent Project of State Key Laboratory of North China Crop Improvement and Regulation (NCCIR2021ZZ-4), the Provincial Supporting Program of Hebei for the Returned Oversea Scholars (C20190180), and the Modern Agricultural Industry System Wheat Innovation Team in Hebei Province (HBCT2018010204). LM was supported by the "Hundred Talents Program" for the introduction of high-level overseas talents in Hebei Province (E2020100004). XY was supported by the Natural Science Foundation of Hebei Province (C2020204050) and the Scientific and Technological Research Projects of Higher Education of Hebei Province (ZD2019086).

ACKNOWLEDGMENTS

We would like to thank Professor Genying Li (Shandong Academy of Agricultural Sciences, China) for the excellent support in generating transgenic wheat materials.

SUPPLEMENTARY MATERIAL

The Supplementary Material for this article can be found online at: https://www.frontiersin.org/articles/10.3389/fpls.2021.771806/full#supplementary-material

REFERENCES

Ali, S., Ganai, B. A., Kamili, A. N., Bhat, A. A., Mir, Z. A., Bhat, J. A., et al. (2018). Pathogenesis-related proteins and peptides as promising tools for engineering plants with multiple stress tolerance. *Microbiol. Res.* 212, 29–37. doi: 10.1016/j.micres.2018.04.008

Appels, R., Eversole, K., Feuillet, C., Keller, B., Rogers, J., Stein, N., et al. (2018). Shifting the limits in wheat research and breeding using a fully annotated reference genome. *Science* 361:eaar7191. doi: 10.1126/science.aar7191

Bi, W., Zhao, S., Zhao, J., Su, J., Yu, X., Liu, D., et al. (2020). Rust effector PNPi interacting with wheat TaPR1a attenuates plant defense response. *Phytopathol. Res.* 2, 1–14.

Breen, S., Williams, S. J., Outram, M., Kobe, B., and Solomon, P. S. (2017). Emerging insights into the functions of pathogenesis-related protein 1. *Trends Plant Sci.* 22, 871–879. doi: 10.1016/j.tplants.2017.06.013

Chen, Y. L., Lee, C. Y., Cheng, K. T., Chang, W. H., Huang, R. N., Nam, H. G., et al. (2014). Quantitative peptidomics study reveals that a wound-induced peptide from PR-1 regulates immune signaling in tomato. *Plant Cell* 26, 4135–4148. doi: 10.1105/tpc.114.131185

Chini, A., Fonseca, S., Fernández, G., Adie, B., Chico, J. M., Lorenzo, O., et al. (2007). The JAZ family of repressors is the missing link in jasmonate signalling. *Nature* 448, 666–671. doi: 10.1038/nature06006

Fang, Z., He, Y., Liu, Y., Jiang, W., Song, J., Wang, S., et al. (2020). Bioinformatic identification and analyses of the non-specific lipid transfer proteins in wheat. *J. Integr. Agr.* 19, 1170–1185. doi: 10.1186/1471-2164-9-86

Gamir, J., Darwiche, R., Van't Hof, P., Choudhary, V., Stumpe, M., Schneiter, R., et al. (2017). The sterol-binding activity of PATHOGENESIS-RELATED PROTEIN 1 reveals the mode of action of an antimicrobial protein. *Plant J.* 89, 502–509. doi: 10.1111/tpj.13398

Gietz, R. D., and Schiestl, R. H. (2007). High-efficiency yeast transformation using the LiAc/SS carrier DNA/PEG method. *Nat. Protoc.* 2, 31–34. doi: 10.1038/nprot.2007.13

Guo, L., Yang, H., Zhang, X., and Yang, S. (2013). Lipid transfer protein 3 as a target of MYB96 mediates freezing and drought stress in Arabidopsis. *J. Exp. Bot.* 64, 1755–1767. doi: 10.1093/jxb/ert040

Jacob, C., Panchal, S., and Melotto, M. (2017). Surface inoculation and quantification of *Pseudomonas* syringae population in the Arabidopsis leaf apoplast. *Bio. Protoc.* 7:e2167. doi: 10.21769/BioProtoc.2167

Jashni, M. K., Mehrabi, R., Collemare, J., Mesarich, C. H., and De Wit, P. J. (2015). The battle in the apoplast: further insights into the roles of proteases and their inhibitors in plant–pathogen interactions. *Front. Plant. Sci.* 6:584. doi: 10.3389/fpls.2015.00584

Kanehisa, M., and Goto, S. (2000). KEGG: kyoto encyclopedia of genes and genomes. *Nucleic Acids Res.* 28, 27–30.

Kim, D., Paggi, J. M., Park, C., Bennett, C., and Salzberg, S. L. (2019). Graph-based genome alignment and genotyping with HISAT2 and HISAT-genotype. *Nat. Biotechnol.* 37, 907–915. doi: 10.1038/s41587-019-0201-4

Kim, M., Lee, A., Roh, Y. J., Lee, H. M., Jo, Y., Cho, H., et al. (2020). Gene Expression and Metabolomics Profiling of the Common Wheat Obtaining Leaf Rust Resistance by Salicylic or Jasmonic Acid through a Novel Detached Leaf Rust Assay. *Agronomy* 10:1668. doi: 10.3390/agronomy10111668

Lamari, L. (2008). *Assess 2.0: image analysis software for plant disease quantification*. St Paul: The American Phytopathological Society (APS).

Leyser, O. (2006). Dynamic Integration of Auxin Transport and Signalling. *Curr. Biol.* 16, R424–R433.

Li, N., Han, X., Feng, D., Yuan, D., and Huang, L.-J. (2019). Signaling Crosstalk between Salicylic Acid and Ethylene/Jasmonate in Plant Defense: Do We Understand What They Are Whispering? *Int. J. Mol. Sci.* 20:671. doi: 10.3390/ijms20030671

Li, X., Wang, X., Kang, Z., Ren, Z., Bi, W., Yang, W., et al. (2018). Suppression subtractive hybridization and microarray analysis reveal differentially expressed genes in the Lr39/41 -mediated wheat resistance to Puccinia triticina. *Eur. J. Plant Pathol.* 152, 479–492.

Love, M. I., Huber, W., and Anders, S. (2014). Moderated estimation of fold change and dispersion for RNA-seq data with DESeq2. *Genome Biol.* 15, 1–21. doi: 10.1186/s13059-014-0550-8

Ma, L., Djavaheri, M., Wang, H., Larkan, N. J., Haddadi, P., Beynon, E., et al. (2018). *Leptosphaeria maculans* effector protein AvrLm1 modulates plant immunity by enhancing MAP kinase 9 phosphorylation. *iScience* 3, 177–191. doi: 10.1016/j.isci.2018.04.015

Ma, L., Lukasik, E., Gawehns, F., and Takken, F. L. (2012). The use of agroinfiltration for transient expression of plant resistance and fungal effector proteins in Nicotiana benthamiana leaves. *Plant Fungal Pathogens* 2012, 61–74.

Maldonado, A. M., Doerner, P., Dixon, R. A., Lamb, C. J., and Cameron, R. K. (2002). A putative lipid transfer protein involved in systemic resistance signalling in Arabidopsis. *Nature* 419, 399–403. doi: 10.1038/nature00962

McLaughlin, J. E., Al Darwish, N., Garcia-Sanchez, J., Tyagi, N., Trick, H. N., Mccormick, S., et al. (2020). A lipid transfer protein has antifungal and antioxidant activity and suppresses Fusarium head blight disease and DON accumulation in transgenic wheat. *Phytopathology* 111, 671–683. doi: 10.1094/PHYTO-04-20-0153-R

Molina, A., and García-Olmedo, F. (1993). Developmental and pathogen-induced expression of three barley genes encoding lipid transfer proteins. *Plant J.* 4:983. doi: 10.1046/j.1365-313x.1993.04060983.x

Paolacci, A. R., Tanzarella, O. A., Porceddu, E., and Ciaffi, M. (2009). Identification and validation of reference genes for quantitative RT-PCR normalization in wheat. *BMC Mol. Biol.* 10:11. doi: 10.1186/1471-2199-10-11

Pieterse, C. M. J., Leon-Reyes, A., Van Der Ent, S., and Van Wees, S. C. M. (2009). Networking by small-molecule hormones in plant immunity. *Nat. Chem. Biol.* 5, 308–316. doi: 10.1038/nchembio.164

Qi, J., Wang, J., Gong, Z., and Zhou, J.-M. (2017). Apoplastic ROS signaling in plant immunity. *Curr. Opin. Plant Biol.* 38, 92–100. doi: 10.1016/j.pbi.2017.04.022

Sahu, R., Sharaff, M., Pradhan, M., Sethi, A., Bandyopadhyay, T., Mishra, V. K., et al. (2016). Elucidation of defense-related signaling responses to spot blotch infection in bread wheat (Triticum aestivum L.). *Plant J.* 86, 35–49. doi: 10.1111/tpj.13149

Salminen, T. A., Blomqvist, K., and Edqvist, J. (2016). Lipid transfer proteins: classification, nomenclature, structure, and function. *Planta* 244, 971–997.

Seo, P. J., and Park, C. M. (2010). MYB96-mediated abscisic acid signals induce pathogen resistance response by promoting salicylic acid biosynthesis in Arabidopsis. *New Phytol.* 186, 471–483. doi: 10.1111/j.1469-8137.2010.03183.x

Seo, P. J., Xiang, F., Qiao, M., Park, J.-Y., Lee, Y. N., Kim, S.-G., et al. (2009). The MYB96 transcription factor mediates abscisic acid signaling during drought stress response in Arabidopsis. *Plant Physiol.* 151, 275–289. doi: 10.1104/pp.109.144220

Sun, J.-Y., Gaudet, D. A., Lu, Z.-X., Frick, M., Puchalski, B., and Laroche, A. (2008). Characterization and antifungal properties of wheat nonspecific lipid transfer proteins. *Mol. Plant Microbe Interact.* 21, 346–360. doi: 10.1094/MPMI-21-3-0346

Sung, Y.-C., Outram, M. A., Breen, S., Wang, C., Dagvadorj, B., Winterberg, B., et al. (2021). PR1-mediated defence *via* C-terminal peptide release is targeted by a fungal pathogen effector. *New Phytol.* 229, 3467–3480. doi: 10.1111/nph.17128

Trapnell, C., Williams, B. A., Pertea, G., Mortazavi, A., Kwan, G., Van Baren, M. J., et al. (2010). Transcript assembly and quantification by RNA-Seq reveals unannotated transcripts and isoform switching during cell differentiation. *Nat. Biotechnol.* 28, 511–515. doi: 10.1038/nbt.1621

Van Loon, L. C., Rep, M., and Pieterse, C. M. (2006). Significance of inducible defense-related proteins in infected plants. *Annu. Rev. Phytopathol.* 44, 135–162. doi: 10.1146/annurev.phyto.44.070505.143425

Wang, C., Huang, L., Buchenauer, H., Han, Q., Zhang, H., and Kang, Z. (2007). Histochemical studies on the accumulation of reactive oxygen species (O^{2-} and H_2O_2) in the incompatible and compatible interaction of wheat-Puccinia striiformis f. sp. tritici. *Physiol. Mol. Plant Pathol.* 71, 230–239. doi: 10.1016/j.pmpp.2008.02.006

Wang, F., Yuan, S., Wu, W., Yang, Y., Cui, Z., Wang, H., et al. (2020). TaTLP1 interacts with TaPR1 to contribute to wheat defense responses to leaf rust fungus. *PLoS Genet.* 16:e1008713. doi: 10.1371/journal.pgen.1008713

Wang, F., Zang, X.-S., Kabir, M. R., Liu, K.-L., Liu, Z.-S., Ni, Z.-F., et al. (2014). A wheat lipid transfer protein 3 could enhance the basal thermotolerance and oxidative stress resistance of Arabidopsis. *Gene* 550, 18–26. doi: 10.1016/j.gene.2014.08.007

Wang, X., Bi, W., Gao, J., Yu, X., Wang, H., and Liu, D. (2018). Systemic acquired resistance, *NPR1*, and pathogenesis-related genes in wheat and barley. *J. Integr. Agr.* 17, 2468–2477. doi: 10.1016/s2095-3119(17)61852-5

Waszczak, C., Carmody, M., and Kangasjärvi, J. (2018). Reactive Oxygen Species in Plant Signaling. *Annu. Rev. Plant Biol.* 69, 209–236.

Wu, J., Gao, J., Bi, W., Zhao, J., Yu, X., Li, Z., et al. (2019). Genome-wide expression profiling of genes associated with the *Lr47*-mediated wheat resistance to leaf rust (*Puccinia triticina*). *Int. J. Mol. Sci.* 20:4498. doi: 10.3390/ijms20184498

Young, M. D., Wakefield, M. J., Smyth, G. K., and Oshlack, A. (2010). Gene ontology analysis for RNA-seq: accounting for selection bias. *Genome Biol.* 11, 1–12.

Zhu, X., Li, Z., Xu, H., Zhou, M., Du, L., and Zhang, Z. (2012). Overexpression of wheat lipid transfer protein gene TaLTP5 increases resistances to Cochliobolus sativus and Fusarium graminearum in transgenic wheat. *Funct. Integr. Genomic.* 12, 481–488. doi: 10.1007/s10142-012-0286-z

Conflict of Interest: The authors declare that the research was conducted in the absence of any commercial or financial relationships that could be construed as a potential conflict of interest.

Publisher's Note: All claims expressed in this article are solely those of the authors and do not necessarily represent those of their affiliated organizations, or those of the publisher, the editors and the reviewers. Any product that may be evaluated in this article, or claim that may be made by its manufacturer, is not guaranteed or endorsed by the publisher.

frontiers in Plant Science

ORIGINAL RESEARCH
published: 29 November 2021
doi: 10.3389/fpls.2021.783388

TaMYB29: A Novel R2R3-MYB Transcription Factor Involved in Wheat Defense Against Stripe Rust

Xiaoxu Zhu[1,2†], Xiang Li[3†], Qi He[1], Dongxiao Guo[1], Caiqi Liu[3], Junying Cao[1], Zhongyi Wu[1], Zhensheng Kang[2] and Xiaojing Wang[1]**

[1]State Key Laboratory of Crop Stress Biology for Arid Areas, College of Life Sciences, Northwest A&F University, Yangling, China, [2]State Key Laboratory of Crop Stress Biology for Arid Areas, College of Plant Protection, Northwest A&F University, Yangling, China, [3]State Key Laboratory of Crop Stress Biology for Arid Areas, College of Innovation and Experiment, Northwest A&F University, Yangling, China

OPEN ACCESS

Edited by:
Meixiang Zhang,
Nanjing Agricultural University, China

Reviewed by:
Zhao Zhang,
China Agricultural University, China
Guan-Feng Wang,
Shandong University, China
Qiong Zhang,
University of California, Berkeley, United States

***Correspondence:**
Zhensheng Kang
kangzs@nwsuaf.edu.cn
Xiaojing Wang
wangxiaojing@nwsuaf.edu.cn

†These authors have contributed equally to this work

Specialty section:
This article was submitted to Plant Pathogen Interactions, a section of the journal Frontiers in Plant Science

Received: *26 September 2021*
Accepted: *04 November 2021*
Published: *29 November 2021*

Citation:
Zhu X, Li X, He Q, Guo D, Liu C, Cao J, Wu Z, Kang Z and Wang X (2021) TaMYB29: A Novel R2R3-MYB Transcription Factor Involved in Wheat Defense Against Stripe Rust. Front. Plant Sci. 12:783388. doi: 10.3389/fpls.2021.783388

Members of the R2R3-MYB transcription factor superfamily have been implicated in plant development, improved disease resistance, and defense responses to several types of stresses. To study the function of TaMYB29 transcription factor—a member of the R2R3-MYB superfamily—in response to an avirulent race of stripe rust pathogen, *Puccinia striiformis* f. sp. *tritici* (*Pst*), we identified and cloned the *TaMYB29* gene from wheat cultivar (cv.) AvS+*Yr10* following infection with *Pst*. The TaMYB29 protein, comprising 261 amino acids, contains two highly conserved MYB domains. We first showed that TaMYB29 is a transcription factor, whose transcriptional levels are significantly induced by salicylic acid (SA), abscisic acid (ABA), jasmonic acid (JA), ethylene (ET), and *Pst*. The results showed that TaMYB29 is involved in the wheat response to stipe rust. The overexpression of the *TaMYB29* gene resulted in the accumulation of reactive oxygen species (ROS) and pathogen-independent cell death in *Nicotiana benthamiana* leaves. The silencing of *TaMYB29* gene in wheat cv. AvS+*Yr10*, containing the stripe rust resistance gene *Yr10*, promoted hyphae growth, significantly downregulated the expression of pathogenesis-related (*PR*) genes, and substantially reduced the wheat resistance to *Pst* compared with the non-silenced control. In addition, the accumulation of hydrogen peroxide (H_2O_2) significantly decreased, and the activity of catalase, an enzyme required for H_2O_2 scavenging, was elevated. Altogether, TaMYB29 positively regulates the defense response against stripe rust in wheat AvS+*Yr10* by enhancing H_2O_2 accumulation, *PR* gene expression, and SA signaling pathway-induced cell death. These results provide new insights into the contribution of TaMYB29 to the defense response against rust pathogens in wheat.

Keywords: TaMYB29, transcription factor, reactive oxygen species, hypersensitive response, stripe rust, VIGS

INTRODUCTION

Wheat is an important food crop grown worldwide and the second most consumed crop in China (Tian et al., 2012). *Puccinia striiformis* f. sp. *tritici* (*Pst*), a fungal pathogen and causative agent of stripe rust disease, has severely affected the annual yield of wheat (Park et al., 2007; Chen et al., 2014). Several control measures have been implemented worldwide to control this

pathogen; these aim at enhancing the tolerance of wheat to the infection (Seo and Park, 2010; Zhang et al., 2012a). The members of the Myeloblastosis (*MYB*) gene superfamily have been reported to actively participate in the developmental processes and defense responses of plants, attracting the worldwide attention of several plant scientists (Fujita et al., 2006; Wang et al., 2015).

Being one of the largest superfamilies of transcription factors in plants, several *MYB* genes have been isolated and identified from different plants (Dubos et al., 2010). The MYB protein contains a protein domain, typically 50 to 53-amino acid long, located near its N-terminus. MYB protein is divided into four categories, namely, 4R-MYB, R1R2R3-MYB, R2R3-MYB, and MYB-related, based on the number of repeats in this domain (Li et al., 2017; Zhang et al., 2018). The majority of MYB proteins belong to the R2R3-MYB gene subfamily. The R2R3-MYB proteins contain three uniformly spaced tryptophan residues within the MYB domain regions, except for R3, in which the first tryptophan residue is replaced by phenylalanine. The MYB repeat has a helix-turn-helix conformation, which forms a hydrophobic core and binds to DNA major grooves to exert their effects during transcription (Ogata and Nishimura, 1995). The first plant *MYB* gene *COLORED1* was cloned and identified from maize (*Zea mays*) and is involved in anthocyanin biosynthesis (Paz-Ares et al., 1987). Since then, functions of several *R2R3-MYB* genes have been discovered and reported in different plant species, including fundamental metabolism, plant growth, cell apoptosis, defense response to abiotic and biotic stresses, and signal transduction (Kranz et al., 1998; Cedroni et al., 2003; Zheng et al., 2017).

The *MYB* gene supports a wide range of signaling crosstalks between biotic and abiotic stress signals (Grant et al., 2003; Chini et al., 2010). For example, the AtMYB96 transcription factor is involved in abscisic acid (ABA)-mediated drought response. It enhances the pathogen resistance of plants by promoting the biosynthesis of salicylic acid (SA), implying that the *MYB* gene affects the ABA–SA signaling crosstalk (Seo and Park, 2010). Similarly, *AtMYB102* responds to salt stress, JA, ABA, wounds, and defense against herbivore attacks (De Vos et al., 2006). *AtMYB108* is involved in biotic and abiotic stress crosstalks and regulated by JA (Mengiste et al., 2003). *AtMYB15* is known to improve drought and salt tolerance in *Arabidopsis*, possibly by the ABA signaling pathway (Ding et al., 2009). TaPIMP1, an R2R3 MYB transcription factor in wheat, positively modulates defense responses to *Bipolaris sorokiniana* and drought stress *via* the ABA–SA signaling pathways in wheat (Zhang et al., 2012b). These findings indicate that several *MYB* genes execute their functions in a highly coordinated manner through a complex signaling network.

At the level of plant–pathogen interaction, a lot of previous studies demonstrated that the transcriptional products of *MYB* genes regulate plant disease resistance. In this regard, *AtMYB30* is identified as a positive regulator during a hypersensitive response (HR) to pathogen attacks in plants (Vailleau et al., 2002; Raffaele et al., 2006). *AtMYB46* modulates the disease susceptibility of *Arabidopsis* to the fungal pathogen *Botrytis cinerea* (Ramirez et al., 2011). Similarly, *AtMYB73* of *Arabidopsis thaliana* is implicated in *NPR1*-mediated SA and JA signaling pathways against necrotrophic fungal pathogen *Bipolaris oryzae* (Jia et al., 2011). *AtMYB108* confers plant resistance to the necrotrophic fungal pathogen *Alternaria brassicicola* (Mengiste et al., 2003). The tobacco *MYB1* gene induced by *Tobacco mosaic virus* infection participates in HR reactions and systemic acquired resistance (SAR). It is located downstream of the SA regulatory pathway and regulates the expression of *PR1* and other disease-related genes (Yang and Klessig, 1996). The overexpression of R2R3-MYB gene *TiMYB2R*-1 from *Thinopyrum intermedium* is known to significantly improve the resistance of transgenic wheat to the take-all disease (Liu et al., 2013). The barley MYB transcription factor gene *HvMYB6* confers resistance in barley to powdery mildew. Silencing of this gene increases the sensitivity of barley to *Blumeria graminis*, the causative agent of powdery mildew, whereas its overexpression enhances the disease resistance of transgenic barley (Chang et al., 2013). In wheat, the overexpression of *TaMYB86* significantly enhances the root rot resistance of transgenic wheat (Shan et al., 2016). *TaMYB4* shows a high similarity to certain R2R3-MYB transcription factors and is implicated in the signaling pathways activated by ABA, ET, and SA hormones to induce stress defense response. In addition, it can promote programmed cell death and increase wheat tolerance to *Pst* in the infection phase (Ma et al., 2011; Al-Attala et al., 2014). Overexpression and underexpression experiments of the wheat R2R3 *MYB* gene *TaPIMP1* show that *TaPIMP1* provides defense against *B. sorokiniana* (Zhang et al., 2012b).

Although several MYB transcription factors in wheat have been functionally studied, more in-depth studies are needed to reveal the function of the *MYB* genes in the complex hexaploid wheat. Zhang et al. (2012a) isolated 60 wheat *MYB* genes containing full-length gene sequences, of which 20 genes were reported to participate in defense response to multiple abiotic stresses involving complicated signaling pathways. Although MYB is the largest transcription factor family in plants, the literature on its functions related to wheat disease resistance is scarce. To elucidate the molecular regulatory mechanisms involved in wheat–*Pst* interaction, we isolated a highly induced *MYB* gene from wheat cultivar (cv.) AvS+*Yr10* after inoculating it with stripe rust fungus. The gene showed a sequence similar to that of the Chinese Spring *TaMYB29*. The *TaMYB29* gene was induced by high salt and exogenous ABA (Zhang et al., 2012a). In addition, *TaMYB29* along with *TaMYB19* and *TaMYB44* can co-regulate wheat plant phloem-based defense (PBD) against phloem-feeding insects; this function is executed through crosstalk with the ET signaling pathway (Zhai et al., 2017). These results imply the ability of *TaMYB29* to respond to biotic and abiotic stresses and suggest that its function is mediated *via* different plant signaling pathways. Therefore, we further wanted to characterize the function of TaMYB29 during the wheat defense response against stripe rust. In this study, we characterized three *TaMYB29* homologous genes, *TaMYB29-5A*, *TaMYB29-5B*, and *TaMYB29-5D* from wheat cv. AvS+*Yr10* and investigated the subcellular localization and transcription activation properties of the TaMYB29-5B protein.

The transcript abundance of *TaMYB29* was studied using quantitative real-time PCR (qRT-PCR) in AvS and its near-isogenic lines (NILs) AvS+*Yr10* seedlings inoculated with *Pst* pathotype CYR32, and in response to different exogenous hormone treatments. The transient expression of *TaMYB29-5B* confers auto active HR response to tobacco. Furthermore, we used barley stripe mosaic virus-induced gene silencing (BSMV-VIGS) to show that *TaMYB29* is involved in defense against *Pst*. The relationships between *TaMYB29* silencing and SA concentration, accumulation of reactive oxygen species (ROS), and the expression of pathogenesis-related (*PR*) genes were studied. In addition, we evaluated the pathogen growth and cell death. Our results suggest that TaMYB29 is a positive regulator of resistance to *Pst* in wheat and executes this function through the accumulation of SA and ROS. We believe that the results of this study contribute to an increased understanding of the structure and function of TaMYB29.

MATERIALS AND METHODS

Plant Material

Two wheat (*Triticum aestivum* L.) cultivars, tobacco (*Nicotiana benthamiana*), and *Pst* pathotype CYR32 were used in this study. Wheat AvocetS (AvS) and its near-isogenic line AvS*Yr10*NIL (AvS+*Yr10*) wheat seedlings carrying the *Yr10* resistance gene were grown in a growth chamber at 14°C under a 16 h light/8 h dark photoperiod. *N. benthamiana* was maintained in an artificial climate room with a temperature range of 20 to 22°C, a light intensity of 20,000 Lux, and a 16-h photoperiod.

Pathogen and Inoculation

The *Pst* race CYR32 that is compatible to wheat AvS and incompatible to AvS+*Yr10* was provided by the State Key Laboratory of Crop Stress Biology for Arid Areas, NWAFU, China. The uredospores of the CYR32 pathotype were suspended in isohexadecane (IHD) and sprayed evenly on the first leaves of AvS and AvS+*Yr10* wheat seedlings using a small air pump. After inoculation, these seedlings were maintained for 24 h in a dark chamber with 100% relative humidity. These were subsequently returned to the original photoperiod condition. The seedlings in the control group were treated similarly with IHD containing no uredospores.

RNA Extraction From Wheat Leaves and cDNA Preparation

The wheat leaves were sampled at 0, 12, 24, 48, 72, and 120 h post-inoculation (hpi) and immediately frozen in liquid nitrogen and stored at −80°C before extraction of total RNA. The total RNA of wheat leaves was extracted using the Qiagen RNeasy Plant Mini Kit (Qiagen, Valencia, CA, United States) following the manufacturer's instructions. The quality and concentration of RNA were assessed using a 1.5% agarose gel electrophoresis and $260/280_{abs}$ measurement using a NanoDrop 2000 spectrophotometer (Thermo Fisher Scientific, United States), respectively. Next, cDNAs were synthesized using the RevertAid First Strand cDNA Synthesis Kit (Thermo Fisher Scientific, United States) following the manufacturer's protocol.

Cloning and Sequence Analysis of *TaMYB29* Gene

To clone the *TaMYB29* gene, a pair of primers (M29-F/R) were designed using the Primer 5.0 software. The primers were designed based on the *TaMYB29* sequence released by the Chinese Academy of Agricultural Sciences in 2012 (NCBI GenBank Accession No. JF951912.1); these were largely used to amplify the open reading frame (ORF) of the *TaMYB29* gene. The PCR program was as follows: 3 min at 95°C, followed by 35 cycles of 30 s at 95°C, 30 s at 55°C, and 60 s at 72°C, and finally 10 min at 72°C. The PCR mixture contained the following: 0.125 µl of Takara Ex Taq, 2.5 µl of 10× Ex Tag buffer, 2 µl of dNTP mixture, 2 µl of template, and 1 µl of each primer. Next, the total volume was made up to 20 µl with ddH_2O. The target fragments were inserted into the pGEM-T Easy vector (Promega, Madison, WI, United States) and sequenced. The *TaMYB29* sequence was used to BLAST the related MYB genes at the National Center for Biotechnology Information[1] and the Ensemble plant database at http://plants.ensembl.org/index.html. The DNAman program (Lynnon Biosoft, Quebec, Canada) was used to align all nucleotide sequences of these genes and corresponding deduced protein sequences.

RNA Analysis Using Quantitative Real-Time PCR

To determine the expression profiles of *TaMYB29* after different treatments, a pair of primers (M29-qRT-F/R) were designed. In addition, four pairs of primers were designed to detect the expression patterns of *TaPR1*, *TaPR2*, *TaPR5*, and *TaCAT* genes by quantitative real-time PCR (qRT-PCR). Wheat housekeeping gene *actin* was used as an internal control. All primers used are listed in **Supplementary Table S1**. The qRT-PCRs were performed on a CFX96 Real-Time System (Bio-Rad, Munich, Germany). The reactions were performed in a 20 µl volume containing 10 µl of 2×UltraSYBR mixture, 2 µl of diluted cDNA, 1 µl of each primer, and 6 µl of ddH_2O. The amplification conditions were as follows: a pre-denaturation for 10 min at 95°C, followed by 40 cycles of 15 s at 95°C and 60 s at 60°C. A dissociation curve was generated for every reaction to ensure specific amplification. Each reaction was performed in triplicate, and reactions without templates were used as negative controls. Three independent biological replicates were used for each time point and treatment. The $2^{-\Delta\Delta Ct}$ method was applied to analyze the experimental results (Livak and Schmittgen, 2001).

Determination of Endogenous SA Concentration in Wheat Leaves

To measure the endogenous SA concentration under both compatible and incompatible interactions, the wheat leaves were sampled at 0, 12, 24, 48, 72, and 120 hpi with CYR32 pathotype. These were frozen in liquid nitrogen immediately. The SA

[1]https://www.ncbi.nlm.nih.gov

concentration was analyzed using liquid chromatography-mass spectrometry (LC-MS) on an LC-30A + TripleTOF5600+ machine (AB Sciex, Singapore) according to Wang et al.'s (2017) method. In brief, 200 mg of the sample was ground into a powder in liquid nitrogen and subsequently extracted with 750 µl of MeOH–H_2O–HOAc (90:9:1, v/v/v). The solution was centrifuged at a high speed of 10,000 rpm. Next, the supernatant was collected and dried under nitrogen. The extract was dissolved in 1,000 µl of HPLC-grade MeOH and filtered using a Millex-HV 0.22 µm filter (Millipore, Bedford, United States). Three independent biological replicates were used for each time point.

Expression Profiles of *TaMYB29* Under Hormone Treatments

To analyze the expression profiles of TaMYB29 under different hormone treatments, the one-leaf stage wheat seedlings of AvS+*Yr10* were sprayed with 2 µm methyl jasmonate (MeJA), 2 µm ethylene (ET), 2 µm abscisic acid (ABA), and 20 µm salicylic acid (SA), following Wang et al.'s (2013) method. The mock control seedlings were similarly treated with an equal volume of distilled water. Subsequently, the seedlings were cut with a sterilized scissor for sampling at 0 h, 2 h, 6 h, 12 h, 24 h, and 48 h post-treatment (hpt). The samples were immediately frozen in liquid nitrogen and stored at −80°C. Three independent biological replicates were used for each time point and control.

Subcellular Localization of TaMYB29 Protein

To study the subcellular localization of TaMYB29 protein, a pair of primers (163-M29-F/R) with restriction enzyme *Hin*dIII and *Bam*HI sites were designed. The PCR product of *TaMYB29* was subcloned into the 16318GFP vector. Next, the recombinant plasmid was amplified in *Escherichia coli* strain DH5α and extracted using the OMEGA Plasmid Maxi Kit. The wheat leaves were processed with cellulase R10 (Yakult Honsha) and macerozyme R10 (Yakult Honsha) to isolate protoplasts as previously described (Yoo et al., 2007). The TaMYB29-eGFP fusion vector and only eGFP vector (control) were transformed into the wheat protoplasts separately using PEG4000. The treated wheat protoplasts were maintained in the dark at 23°C for 24 h and subsequently observed under a fluorescence microscope (Olympus Corporation, Tokyo, Japan).

In addition, the gateway cloning technology was used to link the *TaMYB29* gene to the pK7WGF2.0 vector carrying an enhanced green fluorescent protein (eGFP) tag. The pK7-TaMYB29-eGFP and pK7-eGFP vectors served as controls were transformed into the *Agrobacterium* strain GV3101 (pSoup-p19) by electroporation. Strains carrying different recombinant vectors were cultured to an optical density of 0.8 at 600 nm (OD600) and injected into 4-week-old *N. benthamiana* leaves using a 1.0 ml syringe without a needle. The transformed *N. benthamiana* were maintained in a greenhouse at 20 to 22°C, a light intensity of 20,000 Lux, and a 16-h photoperiod. Finally, the fluorescence of eGFP was observed under a laser confocal fluorescence microscope at 48 h post-infiltration.

Verification of Transcription Activation by TaMYB29 Protein

The gene of full-length $TaMYB29_{1–261}$ protein, its N-terminal region $TaMYB29_{1–116}$, and C-terminal region $TaMYB29_{117–261}$ were amplified using three pairs of primers containing *Nde*I and *Eco*RI restriction sites, namely, M29-BD-F/R, M29-BD-F/R_{116}, and M29-BD-F_{117}/R, respectively. The PCR products were purified and linked to the pGBKT7 vectors linearized by restriction endonucleases. The three pGBKT7-*TaMYB29* recombinant plasmids were directly transformed into DH5α *E. coli* strain and amplified. Subsequently, the pGBKT7-*TaMYB29* recombinant plasmids and the pGBKT7 plasmid (negative control) were introduced into the AH109 yeast strain containing the *HIS3*, *ADE2*, *MEL1,* and *lacZ* reporter genes. The transformed yeast strains were plated on a medium lacking tryptophan (SD/-Trp) and incubated at 30°C for 2 to 3 days. The positive clones on the Trp-deficient media were selected and transferred into the yeast peptone dextrose adenine (YPDA) liquid media for culturing. Next, the yeast solutions were diluted to OD_{600} of 1, 10^{-1} 10^{-2}, 10^{-3}, and 10^{-4}. Lastly, these yeast solutions were inoculated into a medium lacking adenine, histidine, and tryptophan (SD-His/-Ade/-Trp) as well as a medium lacking the above three amino acids (SD-His/-Ade/-Trp) and supplemented with X-α-D-galactoside (X-α-Gal). These cultures were incubated at 30°C for 3 to 4 days.

Transient Expression of *TaMYB29* in *Nicotiana benthamiana*

The *TaMYB29* gene was amplified using a pair of primers (PVX-M29-F/R) containing *Sma*I and *Not*I restriction enzyme sites. The PCR product was subcloned into the pMD18-T simple vector. Afterward, the recombinant plasmid was amplified in DH5α *E. coli* strain and digested by *Sma*I and *Not*I restriction enzymes. Subsequently, the gene digestion product was inserted into the PVX vector which carries a 3×HA tag and was linearized by the same restriction enzymes. The PVX-*TaMYB29* construct was transformed into the *Agrobacterium* strain GV3101 (pSoup-p19). Strains were grown in the Luria–Bertani (LB) medium containing 50 mg/ml rifampicin and 25 mg/ml kanamycin at 28°C for 24 h. The bacteria were harvested by centrifugation and resuspended in the acetosyringone (AS) buffer containing 10 mm MES (pH 5.6), 10 mm $MgCl_2$, and 150 µm acetosyringone after being washed with 10 mm $MgCl_2$. Strains carrying different recombinant vectors were adjusted to a density of 0.6 at 600 nm (OD_{600}) with AS buffer and incubated for 2 h in the dark at room temperature before leaf infiltration. These leaves were sampled at 1, 2, and 3 days post-infiltration (dpi) and stained with 3,3′-diaminobenzidine (DAB) or trypan blue (Bai et al., 2012). The PVX-*GFP* construct was used as a control and treated in the same manner. These experiments were repeated at least three times and got the same result.

BSMV-VIGS-Mediated *TaMYB29* Gene Silencing

A conserved region of about 200 bp was selected from the cloned *TaMYB29* sequence to design the primers (M29-vigs-F/R) for silencing the fragments. The PCR product was linked to the BSMV:γ modified vector to construct the

BSMV:γ-*TaMYB29* recombinant plasmid as previously described (Wang et al., 2020a). Next, the positive plasmid was amplified in DH5α *E. coli* strain. A construct carrying only the BSMV genome was used as a negative control and named BSMV:00. A construct carrying a 183-bp *phytoene desaturase* (*PDS*) gene was used as a positive control and named BSMV:*PDS*. The recombinant γ virus vector linearized by *BssH*II and RNAα, RNAγ linearized with *Mlu*I, and RNAβ with *Spe*I were transcribed *in vitro* using the mMessage mMachine T7 *in vitro* transcription kit (Ambion, Austin, TX, United States) following the manufacturer's protocol. The transcription products of BSMV:α, β, γ (or γ-target) were diluted thrice with diethylpyrocarbonate (DEPC) water and mixed in a ratio of 1:1:1. Next, 70 μl of FES buffer which is a kind of inoculation buffer containing a wounding agent was added to every 30 μl of the mixture. The second leaves of AvS and AvS+*Yr10* wheat seedlings were infected with BSMV using the method described by Holzberg et al. (2002). The BSMV-infected wheat seedlings were maintained in a 16 h/8 h photoperiod at 25°C. In addition, the seedlings were mock inoculated with FES buffer devoid of BSMV transcripts. At 10 to 14 days after the virus inoculation, photobleaching was observed on BSMV:PDS seedlings. The third and fourth leaves were further inoculated with uredospores of *Pst* pathotype CYR32. Next, these plants were directly maintained in a growth chamber for 24 h in the dark with 100% relative humidity at 15°C. The leaves were sampled at 0, 24, 48, and 120 hpi for histological changes and analyzed by qRT-PCR.

Histological Study of Fungal Growth and Host Response

Wheat leaves sampled at 0, 24, 48, and 120 hpi in control and silenced plants were observed for ROS accumulation by DAB staining and HR response areas because of the auto-fluorescence of necrotic cells using an Olympus BX-51 fluorescence microscope (Olympus Corp. Tokyo, Japan). Then, the leaf segments were stained with wheat germ agglutinin (WGA) and observed for the infection areas and hyphae development of *Pst* as previously described (Wang et al., 2017). At least 30 infection sites were examined on each of five randomly selected leaf segments per treatment. Infection sites with substomatal vesicles were considered successfully penetrated. Standard deviations were calculated and Tukey's test was performed for statistical analysis using the SPSS software (SPSS, Inc. Chicago, United States).

RESULTS

Sequence Analyses of *TaMYB29* cDNA and Protein

A full-length cDNA fragment was successfully isolated due to its high expression under incompatible interaction of wheat cv. AvS+*Yr10* infected with avirulent *Pst* CYR32. The cDNA sequence displayed 100% identity with the referred *TaMYB29* sequence in the NCBI GenBank (accession no. JF951912.1). In addition, the ORF was cloned using a pair of primers to create a 786-bp fragment. The International Wheat Genomic Sequence Consortium (IWGSC) revealed homologs of *TaMYB29* located on chromosomes 5A, 5B, and 5D in wheat cv. Chinese Spring. The alignment results of these nucleotide sequences also showed a high similarity ranging from 96 to 99%, referred to as *TaMYB29-5A*, *TaMYB29-5B*, and *TaMYB29-5D* (**Supplementary Figure S1**). The *TaMYB29* sequence of AvS+*Yr10* displayed the highest similarity to the nucleotide sequence of the Chinese Spring *TaMYB29-5B*.

The deduced protein of *TaMYB29* had 261 amino acids, with a predicted molecular weight of 29.4 kD and an isoelectric point (pI value) of 9.05. Alignments of all wheat alleles of TaMYB29 with wheat TaMYB4 (AEG64799.1), *Arabidopsis* AtMYB30 (AEE77505.1), and *Arabidopsis* AtMYB4 (AEE86955.1) revealed two highly conserved regions R2 and R3, which contained three uniformly spaced tryptophan residues responsible for the interaction between the MYB protein and specific DNA sequences (**Figure 1**). The second and third tryptophan residues were conserved in all R2R3-MYB protein members, except in R3 repeats, where the first tryptophan was replaced by phenylalanine (Zhang et al., 2012a). These results revealed highly conserved amino acid sequences in these MYB proteins, indicating their similar functions in mediating stress response.

Subcellular Localization of TaMYB29 Protein

To study the subcellular localization of TaMYB29 in plants, the target gene fused with the eGFP vector and only eGFP vector (control) was separately transformed into wheat protoplasts. To avoid the interference of chlorophyll, its distribution was studied individually. After analyzing the fluorescence microscopy observations, the exact localization of TaMYB29-eGFP fusion protein was found to be the nucleus of wheat protoplast, whereas green signals of only eGFP were observed both in the cytoplasm and the nucleus (**Figure 2A**). We subsequently used the leaves of *N. benthamiana* as the transformed material and repeated the subcellular localization experiment and obtained the same results (**Figure 2B**). Therefore, we conclude that TaMYB29 is a nuclear protein.

Transcriptional Activity of TaMYB29 Protein

To identify whether the TaMYB29 protein is a transcriptional activator or repressor, pGBKT7-TaMYB29$_{1–261}$ and its two truncated protein plasmids pGBKT7-TaMYB29$_{1–116}$ and pGBKT7-TaMYB29$_{117–261}$ were transformed into the AH109 yeast strain. In addition, the pGBKT7 plasmid (negative control) was transformed simultaneously. All transformants grew well on a selective synthetic defined (SD) medium lacking tryptophan (SD/-Trp); however, only pGBKT7-TaMYB29$_{1–261}$ and pGBKT7-TaMYB29$_{117–261}$ yeast strains showed growth on the selective medium without tryptophan,

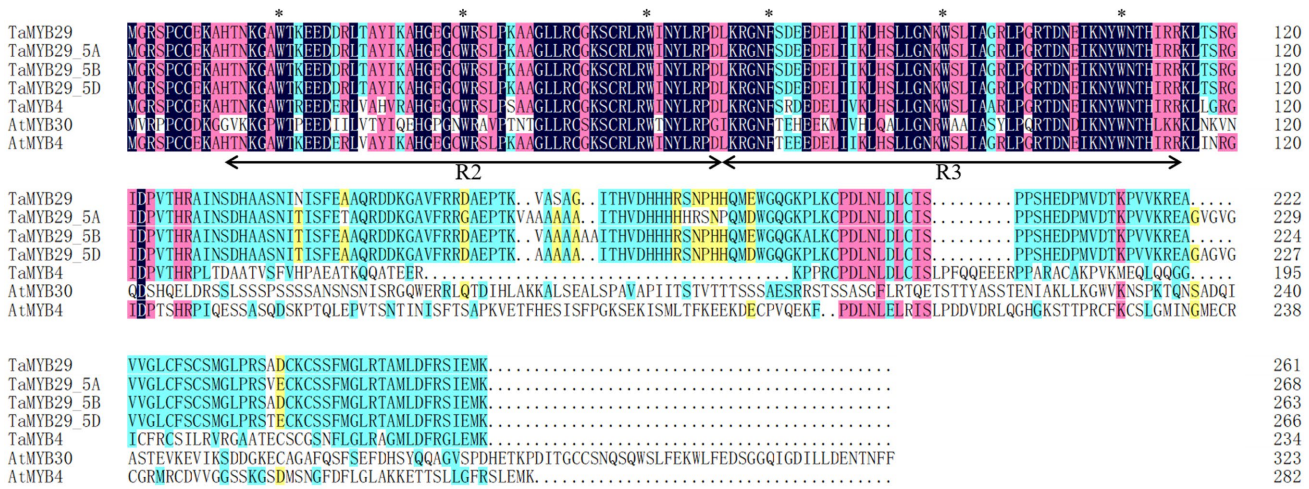

FIGURE 1 | Alignment of the amino acid sequence of TaMYB29 with its homologous sequences. The sequences were aligned with DNAMAN. The identical residues are shaded. The black arrow line shows the MYB-binding domain. The asterisks (*) show typical R2R3-MYB protein contains three regularly spaced tryptophan (W) residues and the first tryptophan residue was replaced by phenylalanine (F) in the R3 repeats.

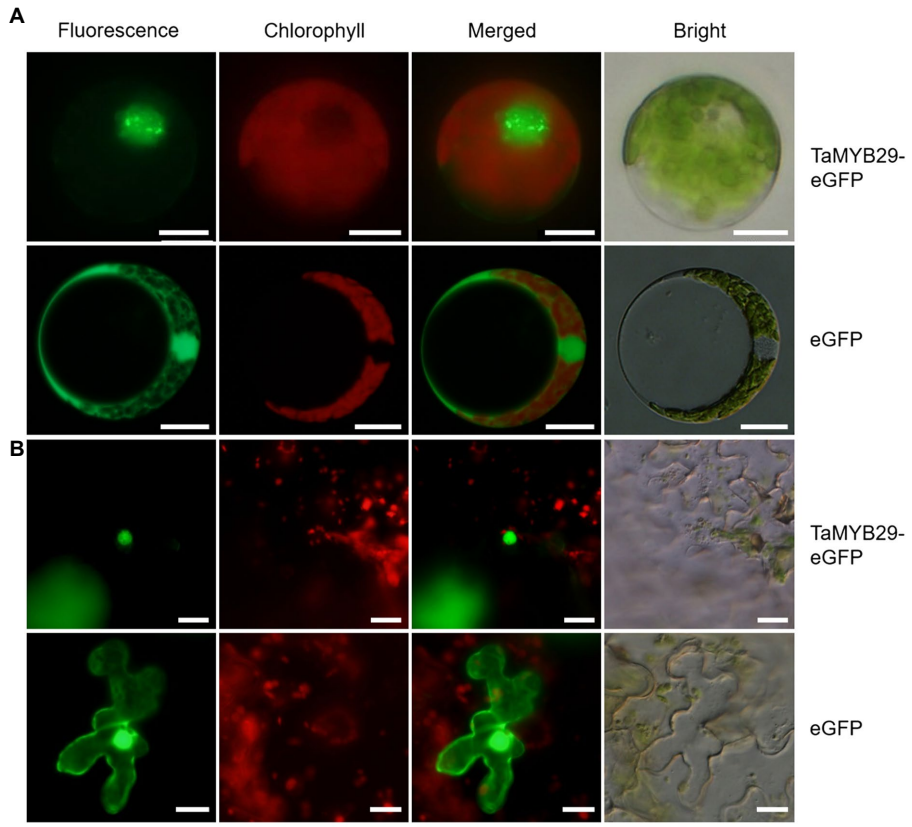

FIGURE 2 | Subcellular localization of TaMYB29 protein. **(A)** TaMYB29-eGFP fusion protein and enhanced green fluorescence protein (eGFP) were expressed in wheat protoplasts; **(B)** TaMYB29-eGFP fusion protein and eGFP protein were expressed in the leaves of *Nicotiana benthamiana*. Bars = 20 μm.

histidine, and adenine (SD-Trp/-His/-Ade). Furthermore, the colonies turned blue on the same medium supplemented with X-α-Gal (SD-Trp/-His/-Ade+X-α-Gal; **Figure 3**). Therefore, we conclude that TaMYB29 functions as a transcriptional activator. What is more, the transactivation domain of TaMYB29 is located in the C-terminal region.

Expression Profile of *TaMYB29* in Response to Exogenous Hormones

To understand the regulation of *TaMYB29* by plant hormones, the AvS+*Yr10* wheat seedling leaves were treated with four different exogenous hormones (SA, ABA, JA, and ET) at the two-leaf stage. The *TaMYB29* transcript levels were detected by qRT-PCR at six different time points (**Figure 4**). Regarding SA treatment, the relative expression of *TaMYB29* showed a 2.59-fold increase at 12 h and a 10-fold increase at 24 h. Eventually, the increase at 48 h was 11 times more than that in the control at 0 h. The *TaMYB29* expression of leaves treated with ABA showed a similar increasing trend. However, the increase was considerably high at 48 h, 50 times as high as that in the control. With respect to JA treatment, the highest level was measured at 12 h, with upregulation recorded from 12 h to 48 h. The upregulation was also observed in ET-treated leaves, especially at 2 h, 12 h, and 24 h. However, the expression peak of *TaMYB29* induced by JA or ET treatment was not as high as that detected with the ABA treatment. These results demonstrate that *TaMYB29* exert an effect in the plant through complex hormone signal pathways.

SA Levels and Expression Profiles of *TaMYB29* and *TaPR1* in Response to *Pst*

To study the expression profile of *TaMYB29* during the interaction between wheat and stripe rust pathogen, the relative expression of *TaMYB29* in the wheat leaves was measured by qRT-PCR at 0, 12, 24, 48, 72, and 120 h in two different wheat cultivars post-inoculation with CYR32 (**Figure 5A**). Wheat AvocetS (AvS), which is susceptible to *Pst* pathotype CYR32, forms a compatible interaction, and its near-isogenic line AvS*Yr10*NIL (AvS+*Yr10*), carrying the *Yr10* resistance gene and highly resistant to CYR32, forms an incompatible interaction. The expression of *TaMYB29* in the leaves of AvS+*Yr10* plants was significantly upregulated at four different time points, except 12 hpi in contrast to the 0 hpi control and peaked at 48 hpi, nearly 3.5 times more than that in the control. However, the expression of *TaMYB29* in the leaves of AvS plants showed an opposite trend, declining slightly until 24 hpi at first. Although the transcript abundance increased slightly at 48 hpi compared with 0 hpi, it decreased to nearly half the level at 0 hpi in the end at 120 hpi. The expression of *TaMYB29* in the incompatible interaction was always higher than that in the compatible interaction at five different time points. These results indicate that TaMYB29 functions during the resistance of wheat against *Pst* infection, especially in the incompatible interaction.

We measured the endogenous levels of SA in both compatible and incompatible interactions at six time points (**Figure 5B**). In the incompatible interaction, the first significant increase in the SA levels appeared at 12 hpi, earlier than the *TaMYB29* expression, and subsequently reduced at 24 and 48 hpi, contrary to the observation in the *TaMYB29* expression compared with the 0 hpi control. The highest SA levels were obtained at 72 hpi. Next, the SA levels rapidly returned to the basal levels at 120 hpi. The SA levels in the compatible interaction presented a similar trend as in the incompatible system although the levels were lower than those in the incompatible system at every time point.

Furthermore, the expression of the wheat *PR* gene *TaPR1* was measured by qRT-PCR (**Figure 5C**). *TaPR1* was upregulated in both interactions during pathogenesis. In the incompatible interaction, the expression of *TaPR1* significantly increased at 24 hpi and reached the 20-fold increase at 48 hpi, and maintained significantly high levels at 72 hpi, which is considerably similar to the expression of *TaMYB29*. Next, it decreased at 120 hpi, different from the expression of *TaMYB29*. In addition, the expression of *TaPR1* in the compatible interaction was slightly upregulated; however, the level was lower as compared with that in the incompatible interaction.

TaMYB29-Induced ROS Accumulation and Pathogen-Independent Cell Death in *Nicotiana benthamiana* Leaves

The recognition of certain molecules released by pathogens triggers plant cell death and a subsequent defense response known as the HR response (Coll et al., 2011). To confirm whether *TaMYB29* can induce ROS and cell death, the HR symptoms were detected in *N. benthamiana* leaves transformed by PVX:*TaMYB29* and PVX:*GFP* constructs. After 1 to 2 days post-infiltration (dpi), the accumulation of ROS was detected successfully with DAB staining (**Figure 6A**). The ROS accumulation in leaf areas infiltrated with PVX:*TaMYB29* was

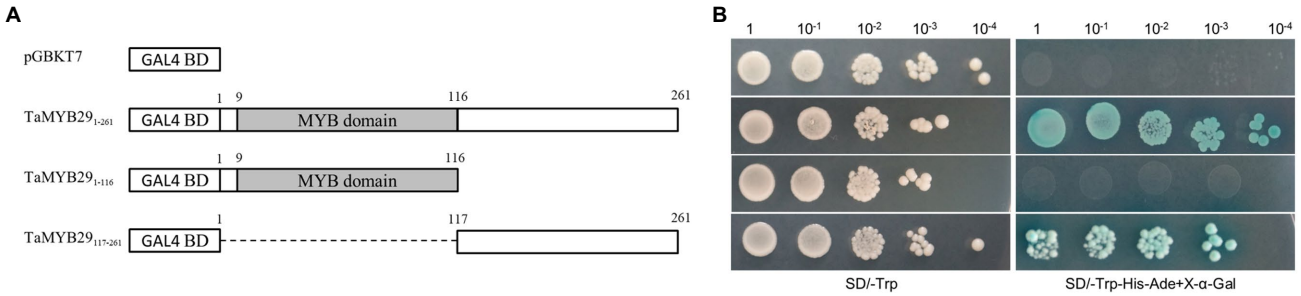

FIGURE 3 | Transcriptional activation activity of the TaMYB29 proteins. **(A)** Constructs of pGBKT7-TaMYB29$_{1–261}$ (full-length) and pGBKT7-TaMYB29$_{1–116}$ (N-terminal region), pGBKT7-TaMYB29$_{117–261}$ (C-terminal region), and pGBKT7 as a control were separately transformed into the yeast strain AH109. **(B)** The diluted yeast solutions were dropped on the SD/-Trp and SD/-Trp-His-Ade+X-α-Gal media, respectively; then, the cultures were incubated at 30°C for 3–4 days.

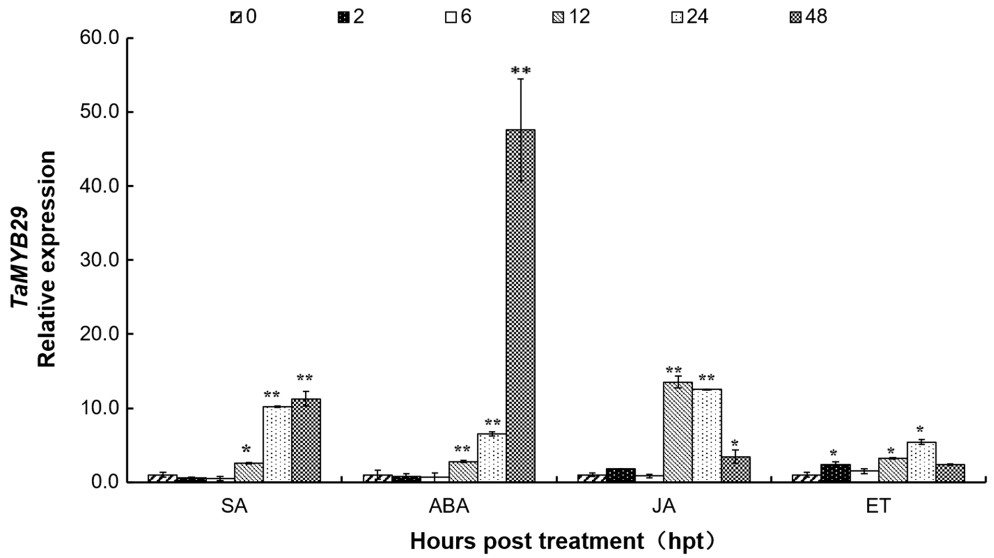

FIGURE 4 | The expression profiles of *TaMYB29* in AvS+*Yr10* wheat leaves in response to exogenous hormones. The wheat leaves were sprayed with SA (salicylic acid), ABA (abscisic acid), JA (methyl jasmonate), and ET (ethylene), respectively and were sampled at 0, 2, 6, 12, 24, and 48 h post-treatment (hpt). Three independent biological replications were performed. Error bars represent standard deviation among three biological replications. Student's *t*-tests were used for the statistical analyses and the asterisks (∗) and (∗∗) indicate a significant difference between that time point and 0 hpt with a value of $p < 0.05$ and 0.01, respectively.

apparent in contrast to that in control PVX:*GFP*. Subsequently, apoptosis was observed using trypan blue staining to further investigate the effects of *TaMYB29* expression during ROS accumulation and pathogen-independent cell death (**Figure 6B**). The *TaMYB29*-induced cell death on *N. benthamiana* leaves was apparent. However, PVX:*GFP* control did not trigger cell death. The results showed that the expression of *TaMYB29* successfully led to ROS accumulation and cell death in contrast to the *GFP* control, indicating that *TaMYB29* played a crucial role in ROS accumulation and pathogen-independent cell death.

TaMYB29 Gene Silencing of Wheat Reduced the Resistance to Stripe Rust

To study the effects of the *TaMYB29* gene during the interaction between wheat and *Pst*, the target gene was silenced using the barley stripe mosaic virus-induced gene silencing (BSMV-VIGS) assay. At the beginning of the knockdown experiment, the *PDS* gene was used to ensure that the VIGS system worked normally and correctly. The photobleaching occurred on BSMV:*PDS* leaves, proving the effectiveness of the VIGS system (**Figure 7A**).

AvS and AvS+*Yr10* wheat seedlings infected with FES buffer (mock), BSMV:00, and BSMV:*TaMYB29* were further inoculated with uredospores of CYR32. Infection types were assessed based on McNeal measurement (Mcneal et al., 1971) to evaluate the differences between the phenotypes of mock, BSMV:00, and BSMV:*TaMYB29*. AvS+*Yr10* displayed a resistant response after inoculation with CYR32 on the mock and BSMV:00 controls, characterized by a large necrosis area at the infection site. While a small number of fungal spores appeared on *TaMYB29*-silenced leaves. These results indicated that the resistance of wheat AvS+*Yr10* with silenced *TaMYB29* gene resulted in a significant decline from highly resistant to moderately susceptible. There was no susceptible phenotype change in *TaMYB29*-silenced AvS wheat compared with the control mock and BSMV:00 (**Figure 7A**). The relative expression of *TaMYB29* was detected by qRT-PCR after *TaMYB29* gene silencing before *Pst* inoculations labeled as 0 hpi, and 24 hpi, and 48 hpi during *Pst* infection. The results showed that the *TaMYB29* transcription level decreased in both AvS+*Yr10* and AvS, which was knocked down up to 86% in incompatible interaction and 55% under compatible interaction compared with BSMV:00 labeled as CK (control check) in **Figure 7B**.

Pathogenesis-related genes are vital for mounting disease resistance responses in plants. *TaPR1*, *TaPR2*, *and TaPR5* have been reported to be involved in systemic acquired resistance (SAR)—a type of plant immunization (Wang et al., 2020b). Therefore, we selected three *PR* genes as defense-related genes to investigate the effects of the knockdown of *TaMYB29* before and during *Pst* inoculation. The results showed that the decline of *TaPR1*, *TaPR2*, and *TaPR5* gene expression in BSMV:*TaMYB29* compared with BSMV:00 was observed at four different time points in the incompatible interaction (**Figure 7C**), proving that the silencing of *TaMYB29* reduced the wheat resistance to disease.

The infection area of *Pst* in *TaMYB29*-silenced AvS+*Yr10* wheat leaves was examined microscopically after inoculation with CYR32. The results showed that the total infection area in *TaMYB29*-silenced leaves was similar to that in BSMV:00 control until 48 hpi. However, significant differences between the two groups were observed at 120 hpi (**Figures 7D,E**).

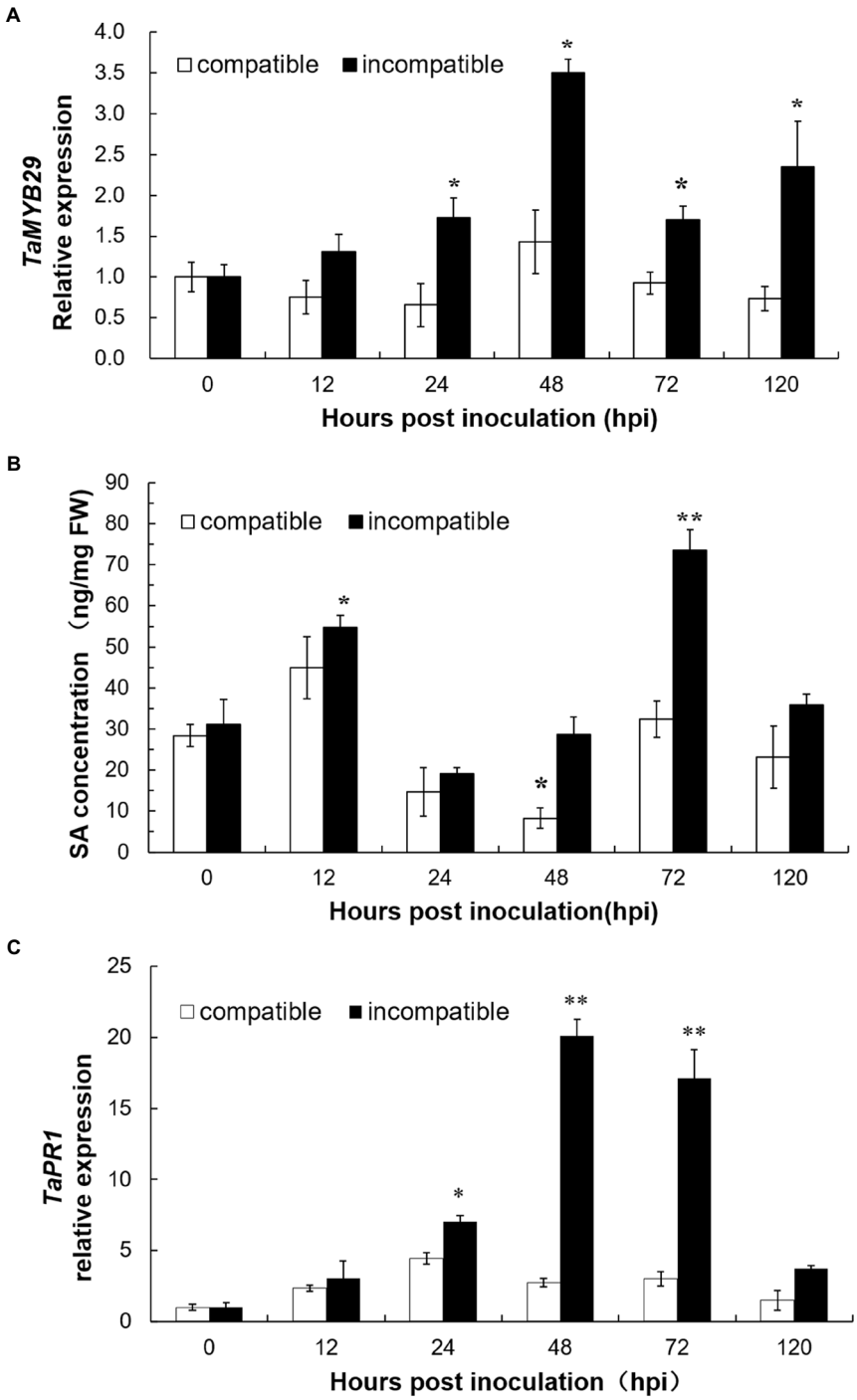

FIGURE 5 | The expression profiles of *TaMYB29* **(A)** and *TaPR1* gene expression **(C)** and salicylic acid (SA) concentration **(B)** in AvS and AvS+*Yr10* wheat leaves during the time course of stripe rust infection. The leaves were sampled at 0, 12, 24, 48, 72, and 120 h post-inoculation (hpi) with three biological experiments replicates. Error bars represent standard deviation among three biological replicates. Student's *t*-tests were used to for the statistical analyses and the asterisks (∗) and (∗∗) indicate a significant difference between the particular time point and 0 hpi with a value of $p < 0.05$ and 0.01.

Furthermore, the hyphae development of *Pst* in BSMV:*TaMYB29* was stronger than that in BSMV:00, especially at 120 hpi (**Figures 7D,E**).

In conclusion, *TaMYB29* knockdown effectively reduced wheat resistance to stripe rust by downregulating the expression of *PR* genes and promoting the development of hyphae.

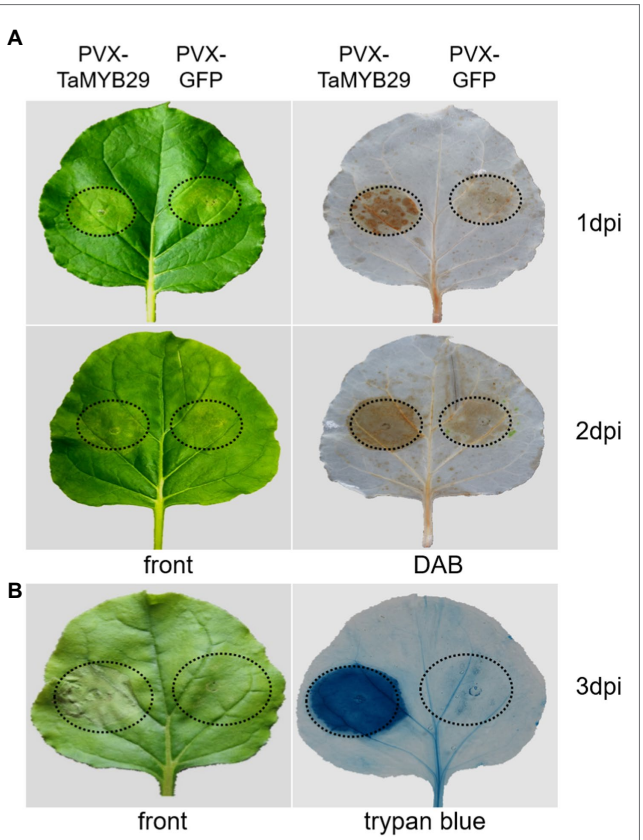

FIGURE 6 | Expression of *TaMYB29*-induced ROS accumulation and pathogen-independent cell death in *N. benthamiana* leaves. **(A)** Symptoms of *N. benthamiana* leaf areas expressing *TaMYB29* or *GFP* gene from 1 to 2 days post-infiltration (dpi). The left and right panels represent the front and after DAB staining, respectively. **(B)** Symptoms of *N. benthamiana* leaf areas expressing *TaMYB29* or *GFP* gene at 3 dpi. The left and right panels represent the front and after trypan blue staining, respectively. These experiments were repeated at least three times and got the same result.

TaMYB29 Was Involved in ROS Accumulation and Hypersensitive Response in Wheat

We observed the accumulation of ROS and cell necrosis of AvS+*Yr10* wheat leaves upon pathogen challenge. The production of H_2O_2 and the necrotic area in BSMV:*TaMYB29* leaves were significantly less than those in BSMV:00 at 48 hpi and 120 hpi, creating a gap of about 2,000 μm^2 at 120 hpi (**Figures 8A,B,D**). In addition, the expression patterns of *TaCAT* (X94352) that can eliminate H_2O_2 as a catalase gene in wheat were detected by qRT-PCR (Coleto et al., 2021). The results showed that the expression of *TaCAT* was significantly upregulated in *TaMYB29*-silenced leaves at 24 hpi, peaked at 48 hpi as compared with control non-*TaMYB29*-silenced leaves (**Figure 8C**), implying that a high expression of *TaCAT* reduced the ROS accumulation in *TaMYB29*-silenced wheat leaves. We hypothesized that the silencing of the *TaMYB29* gene positively regulated the expression of the *TaCAT* gene, eventually decreasing the accumulation of ROS and partially eliminating the HR response in wheat mesophyll cells, thereby weakening the resistance of wheat to stripe rust.

DISCUSSION

We successfully cloned a relatively highly expressed *MYB* gene in response to the *Pst* attack in AvS+*Yr10* wheat leaves. The cDNA sequence showed the same to the *TaMYB29* gene (JF951912.1) searched using the NCBI GenBank database. Three homologous *TaMYB29* genes obtained from the wheat genome database maintained by the IWGSC were located to wheat chromosomes 5A, 5B, and 5D separately. Multiple sequence alignment revealed that the three genes shared 96 to 99% similarity, implying that their co-silencing effectively represented the function of *TaMYB29* genes in wheat. Therefore, we knocked down and measured the expression of three homologs simultaneously and used *TaMYB29* to represent their functions. More in-depth research is required to determine the specific functions of each of the three homologs.

The *MYB* gene superfamily participates in several metabolic reactions in plants (Jin and Martin, 1999). For example, these MYB proteins interact with DNA as transcript factors to regulate the signal network of the defense response. The majority of *MYB* genes belong to the R2R3-MYB superfamily; proteins in this superfamily have R2 and R3 imperfect tandem repeats DNA-binding domains. A comparison of amino acid sequences with the other three MYB family genes of *Arabidopsis* and wheat—all of which function to resist abiotic and biotic stresses—revealed that TaMYB29 also included R2 and R3 conserved domains, suggesting its DNA-binding ability as a transcription factor (**Figure 1**). Its subcellular localization analysis revealed that TaMYB29 is a nuclear protein (**Figure 2**). Transcriptional activation assays in yeast verified the transcriptional activity of TaMYB29 and the necessity of C-terminal 117–261 amino acids for transactivation (**Figure 3**). Based on these results, we speculated that the *TaMYB29* gene functions are similar to those of other resistance-related *MYB* genes previously reported as transcription factors (Morse et al., 2009; Katiyar et al., 2012; Jin et al., 2014).

The genes belonging to the *MYB* superfamily have been implicated in plant resistance against abiotic and biotic stresses (Saha et al., 2016). The expression of the *AtMYB30* gene increased during incompatible interactions between *Arabidopsis* and bacterial pathogens and drought stress (Vailleau et al., 2002). The expression of *AtMYB44* was upregulated following pathogen infection and treatment with defense-related SA phytohormones (Zou et al., 2013). Similarly, the expression of *TiMYB2R-1* was significantly induced following *G. graminis* infection (Liu et al., 2013). The analysis of the expression patterns of 60 wheat *TaMYB* genes under different stress conditions revealed that 32 of them responded to these different stresses (Zhang et al., 2012a). Among these, *TaMYB29* was induced by both high salt and exogenous ABA (Zhang et al., 2012a). We also found that *TaMYB29* was induced by exogenous ABA, a finding same as that of Zhang's study (**Figure 4**). In addition, we found that the transcription of *TaMYB29* was significantly induced and reached the highest

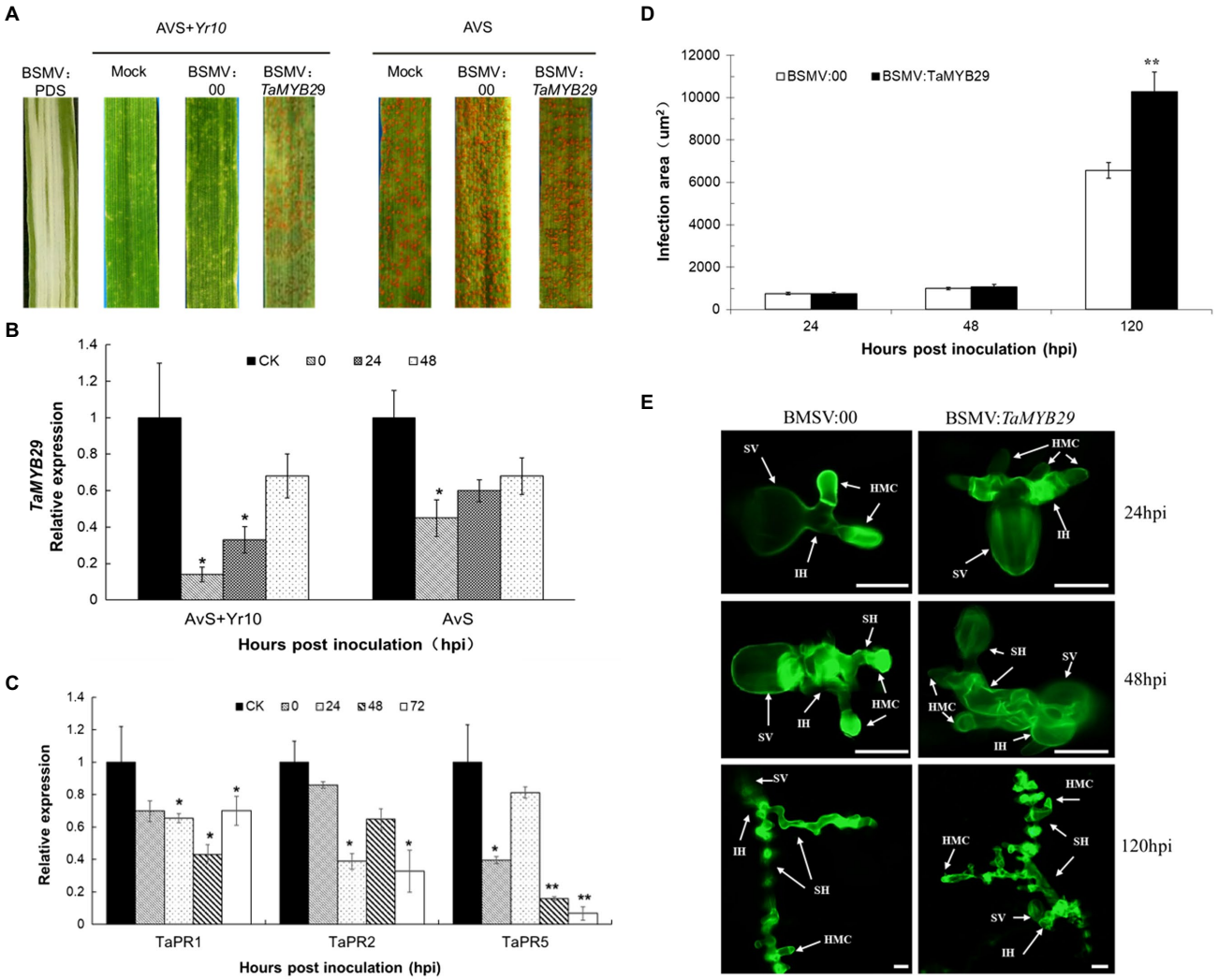

FIGURE 7 | Functional analysis of the *TaMYB29* gene by the BSMV-VIGS assay. **(A)** Infection type of AvS and AvS+*Yr10* wheat leaves to CYR32 after inoculated with BSMV:00 or BSMV:*TaMYB29*. Stripe rust was inoculated 9 days post-BSMV inoculation. Pictures were taken 15 days post-rust inoculation. Mock: wheat leaves inoculated with FES buffer. BSMV:00 means only the BSMV genome; BSMV: *TaMYB29* means a 183-bp fragment of *TaMYB29* was inserted into the BSMV:γ genome. Photobleaching was evident on the leaves infected with BSMV:*PDS* but not on the mock-inoculated leaves. **(B)** Transcriptional level of *TaMYB29* in AvS and AvS+*Yr10* during the course of *Pst* infection at 0, 24, and 48 hpi. CK: wheat leaves treated with BSMV:00. **(C)** Transcriptional level of pathogenesis-related gene *TaPR1*, *TaPR2,* and *TaPR5* in *TaMYB29* silenced AvS+*Yr10* wheat leaves after inoculated with *Pst*. Leaves were sampled at 0, 24 48, and 72 hpi. Three independent biological replications were performed. Error bars represent standard deviation among three biological replicates. Student's *t*-tests were used for the statistical analyses and the asterisks (∗) and (∗∗) indicate a significant difference between that time point and 0 hpi with a value of $p < 0.05$ and 0.01, respectively. **(D,E)** Infection area **(D)** and hyphae development of *Pst* **(E)** in *TaMYB29* knockdown AvS+*Yr10* wheat leaves after infected with CYR32. Wheat leaves were sampled at 24, 48, and 120 hpi and observed microscopically after stained with WGA. SV, substomatal vesicle; IH, initial hyphae; HMC, haustorial mother cell; and SH, secondary hyphae. Bars = 20 μm.

level at 48 h post-rust inoculation in the incompatible system (**Figure 5A**), implicating the involvement of *TaMYB29* in wheat defense response to biotic and abiotic stresses.

Plant hormones are synthesized *de novo* and serve as signal molecules between plants and other surrounding organisms. These are usually conserved in the plant kingdom and can regulate diverse processes including plant growth and development, and responses to abiotic and biotic stresses (Nambara and Wees, 2021). Salicylic acid is a key regulator of plant defense response against living parasitic fungi and the acquisition of SAR pathways. The primary underlying mechanism of SA is to activate the high expression of a series of transcription factors, including DNA-binding proteins containing conserved MYB domains. For example, AtMYB30, AtMYB44, and AtMYB96 participate in the resistance of *Arabidopsis* to *Pseudomonas syringae* pv. *tomato* strain DC3000 *via* the SA signaling pathway (Dong et al., 1999; Vailleau et al., 2002; Seo and Park, 2010). Wheat AvS+*Yr10* containing the stripe rust resistance gene *Yr10* was highly resistant to CYR32 in incompatible interaction. Real-time PCR revealed a rapid induction of *TaMYB29* as early as 12 h post-SA treatment

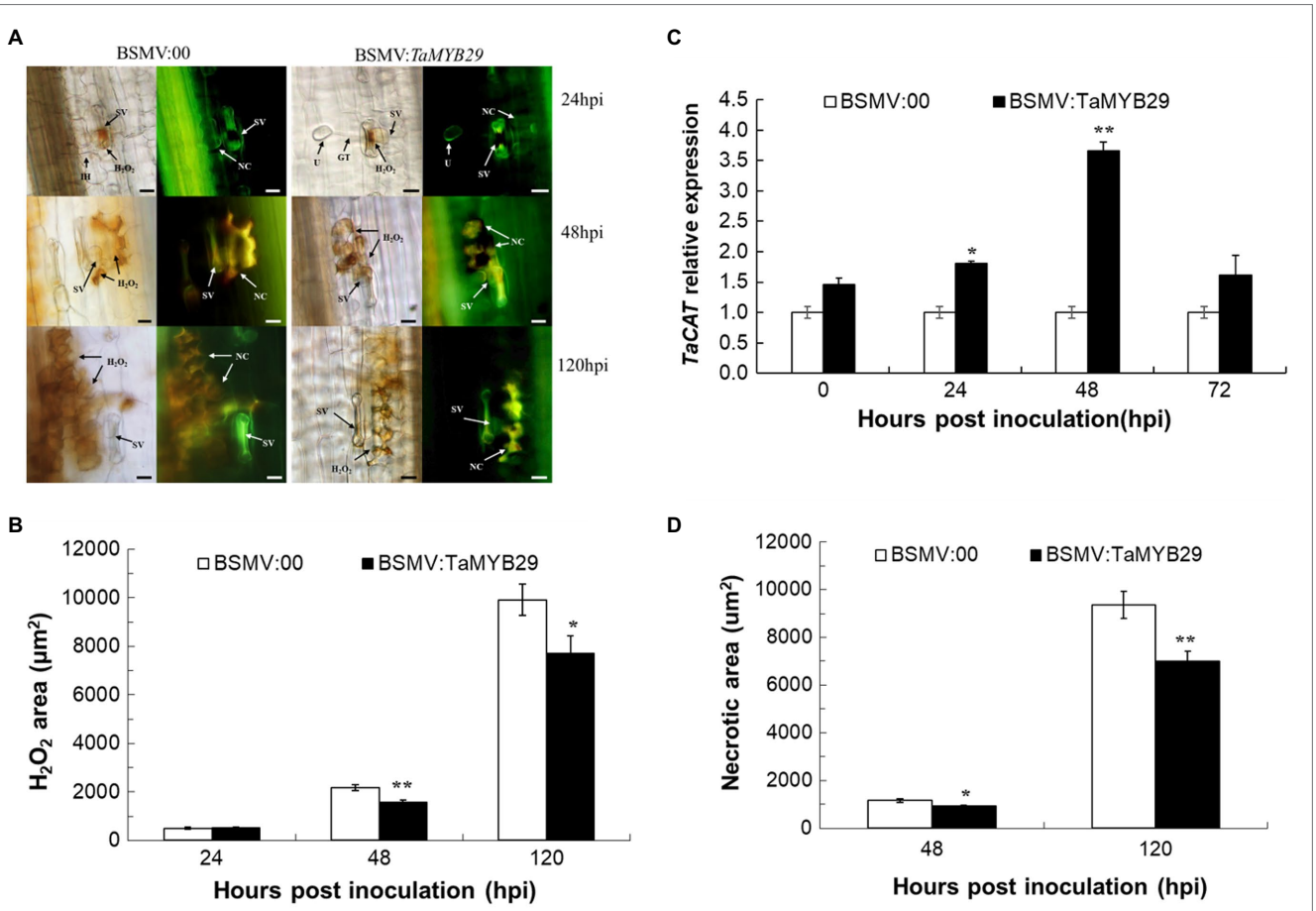

FIGURE 8 | Reactive oxygen accumulation and related gene expression and hypersensitive response in the *TaMYB29* knockdown AvS+*Yr10* wheat leaves. **(A)** The reactive oxygen species and cell necrosis in wheat leaves in response to *Pst* observed under a fluorescence microscope. **(B)** The reactive oxygen species areas were stained with DAB and measured microscopically at 24, 48, and 120 hpi. H_2O_2 accumulation was significantly reduced in *TaMYB29* silenced leaves compared to the control. **(C)** Transcriptional level of ROS-related gene *TaCAT* in AvS+*Yr10* after *TaMYB29*-scilencing at four time points relative to the expression in BSMV:00. **(D)** Cell death was measured microscopically because of the auto-fluorescence of necrotic cells at 48 and 120 hpi. The area of green auto-fluorescence reduced in *TaMYB29*-silenced wheat plant. Pictures were taken under an epifluorescence or light microscopy at 24, 48, and 120 hpi, respectively. BSMV:00 is the control group and BSMV:*TaMYB29* is the experimental group in which *TaMYB29* gene was silenced. U, urediniospore; GT, germ tube; NC, necrotic cell; SV, substomatal vesicle; IH, initial hyphae; HMC, haustorial mother cell; and SH, secondary hyphae. Bars = 20 μm. Error bars represent standard deviation among three biological replications. Student's *t*-tests were used to for the statistical analyses and the asterisks (*) and (**) indicate a significant difference between particular hpi and controls with a value of $p < 0.05$ and 0.01, respectively.

(hpt) in incompatible interaction. The highest 11-fold increase was recorded at 48 hpt (**Figure 4**). In addition, it showed significantly increased endogenous SA levels in AvS+*Yr10* as early as 12 hpi; the second peak appeared at 72 hpi compared to the 0 hpi control (**Figure 5B**). The expression of *TaMYB29* was significantly increased at 24 hpi in the incompatible interaction, which was delayed by 12 h compared to the SA (**Figures 5A,B**). These results suggested that *TaMYB29* functions downstream in the SA biosynthesis pathway to defend against *Pst* in the incompatible interaction.

Crosstalk between defense signaling pathways regulates the defense responses against different types of attackers (Kachroo and Kachroo, 2007; Vlot et al., 2009; Robert-Seilaniantz et al., 2011; Zou et al., 2013). Abscisic acid, an important plant hormone, is involved in plants' response to environmental stresses, such as drought, high salinity, and extreme temperature and plant–pathogen interactions (Popko et al., 2010; Wang et al., 2017). Similarly, JA and ET are primarily involved in the interaction between plants with necrotrophic pathogens and insects as well as in the wounding process (Reymond et al., 2000). We observed that *TaMYB29* was significantly induced after treatment with SA, ABA, JA, and ET exogenous hormones; the highest induced expression was detected at 48 h post-treatment with ABA (**Figure 4**). We previously found that endogenous SA concentration increased post-ABA and JA treatments and improved the wheat defense against stripe rust in Suwon11 (Wang et al., 2017). *AtMYB96*-mediated ABA signals induced pathogen resistance response by promoting SA biosynthesis in *Arabidopsis* (Seo and Park, 2010). *AtMYB44* is involved in both ET- and SA-mediated defense-related signaling pathways to regulate the plant defense response (Zou et al., 2013), implying crosstalks between SA, ABA, JA, and ET in wheat defense response to stripe rust. *TaPIMP1* contributes to biotic and abiotic

stress resistance by regulating defense- and stress-related genes in the ABA–SA signaling pathways in wheat (Zhang et al., 2012b). SA- and JA-mediated plant defense signaling pathways have both synergistic and antagonistic effects. The SA pathway activated by biotrophic pathogen *P. syringae* strongly reduced JA-mediated defenses against the attack of necrotrophic pathogen *A. brassicicola* in *Arabidopsis* (Spoel et al., 2007). On the other hand, co-treatment with low concentrations of SA and JA resulted in a synergistic effect on the transcription of *PR1* in *Arabidopsis* explants (Mur et al., 2006). Exogenous SA and JA could induce the expression of *TaMYB29* in different time points, which indicates that TaMYB29 plays a role in the communication between SA- and JA-mediated resistance signaling pathways (**Figure 4**). Moreover, the transcript of *TaMYB29* is induced both following the treatment with SA, ABA, JA, and ET hormones, and during the defense response against stripe rust (**Figures 4, 5B**). In summary, these results indicate that *TaMYB29* functions in wheat defenses through a complex interaction, including the ABA–SA or JA/ET–SA signaling network.

Increasing evidence shows SA as a crucial signaling molecule in plant defense against pathogens. This defense response usually causes local cell necrosis, namely, HR response and SAR as well as *PR* gene expression (Durrant and Dong, 2004). Pathogenesis-related genes including *PR1*, *PR2*, and *PR5* are induced along with the defense response of plants to pathogens through SA signaling (Vlot et al., 2009). As an indicator gene of SA, the expression of the *PR1* gene was detected during compatible and incompatible interactions. The expression of *PR1* increased significantly at 24 hpi, 48 hpi, and 72 hpi in the incompatible interaction like *TaMYB29*, which was 12 h later than SA (**Figure 5**). Compared with the control, the silencing of *TaMYB29* reduced the expression of three *PR* genes (**Figure 7C**), the production of H_2O_2 (**Figure 8B**), and the HR areas (**Figure 8D**). These findings suggested that *TaMYB29* modulated the defense response in a *PR* gene expression-dependent manner through the signaling molecule SA. During plant defense responses, transcription factors mediate the regulation of the expression of plant host target genes, largely through the specific recognition of cis-promoter elements. Several putative MYB recognition sequences have been found in the promoter region of the *PR1* gene (Abe et al., 1997). The tobacco *MYB1* gene is induced during the HR response and SAR. The MYB1 protein binds to the MYB consensus-binding site in the tobacco *PR1-a* promoter *in vitro* (Yang and Klessig, 1996). In addition, AtMYB44 may regulate the *PR1* gene expression by binding to its promoter region (Zou et al., 2013). Combining the expression of *PR* genes and *TaMYB29* gene in plant defense against stripe rust with the results of *TaMYB29* gene silencing, we hypothesize that TaMYB29 binds to *PR* cis-elements to regulate its expression. However, we cannot exclude the possibility that TaMYB29 indirectly regulates *PR1* expression by regulating other target genes. These results suggest that AvS+*Yr10* defense against *P. striiformis* depends on the expression of *PR* genes *via* the SA signaling pathway.

Yr10 gene encodes for a unique CC-NBS-LRR receptor in wheat cultivar Moro, which provides seedling or all-stage resistance (*R* gene-mediated resistance; Liu et al., 2014). The *R* gene-mediated resistance is characterized by rapid plant cell death at the infection sites, thereby hindering the fungus spread from the infection sites—a process known as plant HR response—and inducing SAR (Heath, 2000; Durrant and Dong, 2004; Ryals et al., 2013). Following the successful recognition of an avirulent gene from the pathogen by the *R* gene, ROS rapidly accumulate and are instantaneously released in a process termed "oxidative burst." This is one of the earliest events of plant defense against pathogens. In our study, the transient overexpression of *TaMYB29* in tobacco caused a rapid ROS increase, consequently inducing cell death at the injection sites (**Figure 6**). Similarly, the overexpression of *AtMYB44* enhanced H_2O_2 accumulation and cell death *via* the SA signaling pathway (Zou et al., 2013). Downregulating the three homologs of *TaMYB29* in AvS+*Yr10* reduced the host resistance to the avirulent *Pst* strain CYR32, whereas no obvious phenotype difference between the *TaMYB29*-silenced AvS plants and controls was observed (**Figure 7A**), suggesting that the *TaMYB29* gene is indispensable for the resistance to *Pst* infection mediated by *Yr10*. In the incompatible interaction, only extremely little accumulation of H_2O_2 in both *TaMYB29*-silenced AvS+*Yr10* plants and the BSMV:00 control was observed at 24 hpi. However, at 48 hpi and 120 hpi, the accumulation of H_2O_2 was reduced significantly in the *TaMYB29*-silenced mesophyll cells in contact with primary hyphae as compared with the control BSMV:00 (**Figures 8A,B**). We hypothesized that *TaMYB29* affected the accumulation of ROS, which was supported by the histological observation and measurement of the production of H_2O_2 after knocking down *TaMYB29* (**Figures 8A,B**). The accumulation of H_2O_2 was only observed in guard cells during the formation of appressorium at 24 hpi (**Figure 8A**), which was about 12 h later than that in Suwon11 inoculated with CYR23 (Wang et al., 2017). These results indicated that the wheat cultivars containing different *R* genes led to varying ROS production in response to different rust isolates. Catalase, a powerful antioxidant enzyme, is an H_2O_2 scavenger. We reported that a 3.66-fold expression of the catalase gene *TaCAT* was induced in *TaMYB29* knocked-down leaves infected with CYR32 compared with the BSMV:00 control at 48 hpi (**Figure 8C**). We speculated the upregulated expression of *TaCAT* as one of the reasons for the reduced ROS accumulation. In addition, the infection area was significantly increased after knocking down *TaMYB29* at 120 hpi in comparison with the BSMV:00 control wheat plants (**Figures 7D,E**). Altogether, *TaMYB29* activated the wheat defense response against *Pst* by modulating H_2O_2 accumulation. During the defense response against pathogens, *TaMYB29* is induced *via* the SA pathway, thus increasing the levels of ROS and the expression of *PR* genes, and eventually generating resistance of wheat containing the *Yr10* disease resistance gene to stripe rust. However, we cannot conclude whether *TaMYB29* is required in all *R* gene-mediated disease resistance pathways, which requires further research. The underlying mechanism of regulation of specific target genes by *TaMYB29* to induce the defense response as a transcription factor requires further research. Finally, the possible use of this gene for breeding disease-resistant plant varieties needs to be assessed.

CONCLUSION

TaMYB29 plays an indispensable role in the wheat response against stripe rust *via* regulating the crosstalk between various signaling pathways. Moreover, our results indicate that *TaMYB29* positively regulates the plant defense response against biological nutritional pathogens by enhancing H_2O_2 accumulation, *PR* gene expression, and cell death *via* the SA signaling pathway.

DATA AVAILABILITY STATEMENT

The original contributions presented in the study are included in the article/**Supplementary Material**, and further inquiries can be directed to the corresponding authors.

AUTHOR CONTRIBUTIONS

XW and ZK conceived the study. XW, XZ, XL, CL, and ZK advised on the experimental design and drafted the manuscript. XW, XZ, XL, QH, DG, CL, ZW, and JC performed experiments and did data analysis. XZ, XL, QH, DG, CL, ZW, and JC interpreted data. XW, XZ, XL, and ZK wrote the manuscript and other authors reviewed and revised the manuscript. All authors contributed to the article and approved the submitted version.

FUNDING

This study was supported by the National Natural Science Foundation of China General Projects (No. 31501619 and No. 32172424), 2021 College Students' innovation and entrepreneurship training program (S202110712787), Natural Science Foundation Research Project of Shaanxi Province (2021JM-095), Shaanxi Innovation Team Project (2018TD-004).

ACKNOWLEDGMENTS

We would like to thank Yi Luo for help on the study and also thank State Key Laboratory of Crop Stress Biology for Arid Areas, Northwest A&F University, China for the equipment support.

SUPPLEMENTARY MATERIAL

The Supplementary Material for this article can be found online at: https://www.frontiersin.org/articles/10.3389/fpls.2021.783388/full#supplementary-material

REFERENCES

Abe, H., Yamaguchi-Shinozaki, K., Urao, T., Iwasaki, T., Hosokawa, D., and Shinozaki, K. (1997). Role of *Arabidopsis* MYC and MYB homologs in drought- and abscisic acid-regulated gene expression. *Plant Cell* 9, 1859–1868. doi: 10.1105/tpc.9.10.1859

Al-Attala, M. N., Wang, X., Abou-Attia, M. A., Duan, X., and Kang, Z. (2014). A novel TaMYB4 transcription factor involved in the defence response against *Puccinia striiformis* f. sp. *tritici* and abiotic stresses. *Plant Mol. Biol.* 84, 589–603. doi: 10.1007/s11103-013-0156-7

Bai, S., Liu, J., Chang, C., Zhang, L., Maekawa, T., Wang, Q., et al. (2012). Structure-function analysis of barley NLR immune receptor MLA10 reveals its cell compartment specific activity in cell death and disease resistance. *PLoS Pathog.* 8:e1002752. doi: 10.1371/journal.ppat.1002752

Cedroni, M. L., Cronn, R. C., Adams, K. L., Wilkins, T. A., and Wendel, J. F. (2003). Evolution and expression of *MYB* genes in diploid and polyploid cotton. *Plant Mol. Biol.* 51, 313–325. doi: 10.1023/A:1022051100610

Chang, C., Yu, D., Jiao, J., Jing, S., Schulze-Lefert, P., and Shen, Q. H. (2013). Barley MLA immune receptors directly interfere with antagonistically acting transcription factors to initiate disease resistance signaling. *Plant Cell* 25, 1158–1173. doi: 10.1105/tpc.113.109942

Chen, W., Wellings, X. M., Kang, Z., and Liu, T. (2014). Wheat stripe (yellow) rust caused by *Puccinia striiformis* f. sp. *tritici*. *Mol. Plant Pathol.* 15, 433–446. doi: 10.1111/mpp.12116

Chini, A., Grant, J. J., Seki, M., Shinozaki, K., and Loake, G. J. (2010). Drought tolerance established by enhanced expression of the CC–NBS–LRR gene, *ADR1*, requires salicylic acid, EDS1 and ABI1. *Plant J.* 38, 810–822. doi: 10.1111/j.1365-313X.2004.02086.x

Coleto, I., Bejarano, I., Marin-Pena, A. J., Medina, J., Rioja, C., Burow, M., et al. (2021). *Arabidopsis thaliana* transcription factors MYB28 and MYB29 shape ammonium stress responses by regulating Fe homeostasis. *New Phytol.* 229, 1021–1035. doi: 10.1111/nph.16918

Coll, N. S., Epple, P., and Dangl, J. L. (2011). Programmed cell death in the plant immune system. *Cell Death Differ.* 18, 1247–1256. doi: 10.1038/cdd.2011.37

De Vos, M., Denekamp, M., Dicke, M., Vuylsteke, M., Van Loon, L., Smeekens, S. C., et al. (2006). The *Arabidopsis thaliana* transcription factor AtMYB102 functions in defense against the insect herbivore *Pieris rapae*. *Plant Signal. Behav.* 1, 305–311. doi: 10.4161/psb.1.6.3512

Ding, Z., Li, S., An, X., Liu, X., Qin, H., and Wang, D. (2009). Transgenic expression of *MYB15* confers enhanced sensitivity to abscisic acid and improved drought tolerance in *Arabidopsis thaliana*. *J. Genet. Genomics* 36, 17–29. doi: 10.1016/S1673-8527(09)60003-5

Dong, H., Delaney, T. P., Bauer, D. W., and Beer, S. V. (1999). Harpin induces disease resistance in *Arabidopsis* through the systemic acquired resistance pathway mediated by salicylic acid and the *NIM1* gene. *Plant J.* 20, 207–215. doi: 10.1046/j.1365-313x.1999.00595.x

Dubos, C., Stracke, R., Grotewold, E., Weisshaar, B., Martin, C., and Lepiniec, L. (2010). MYB transcription factors in *Arabidopsis*. *Trends Plant Sci.* 15, 573–581. doi: 10.1016/j.tplants.2010.06.005

Durrant, W. E., and Dong, X. (2004). Systemic acquired resistance. *Annu. Rev. Phytopathol.* 42, 185–209. doi: 10.1146/annurev.phyto.42.040803.140421

Fujita, M., Fujita, Y., Noutoshi, Y., Takahashi, F., Narusaka, Y., Yamaguchi-Shinozaki, K., et al. (2006). Crosstalk between abiotic and biotic stress responses: a current view from the points of convergence in the stress signaling networks. *Curr. Opin. Plant Biol.* 9, 436–442. doi: 10.1016/j.pbi.2006.05.014

Grant, J. J., Chini, A., Basu, D., and Loake, G. J. (2003). Targeted activation tagging of the *Arabidopsis* NBS-LRR gene, *ADR1*, conveys resistance to virulent pathogens. *Mol. Plant Microbe Interact.* 16, 669–680. doi: 10.1094/MPMI.2003.16.8.669

Heath, M. C. (2000). Hypersensitive response-related death. *Plant Mol. Biol.* 44, 321–334. doi: 10.1023/A:1026592509060

Holzberg, S., Brosio, P., Gross, C., and Pogue, G. P. (2002). Barley stripe mosaicvirus-induced gene silencing in a monocot plant. *Plant J.* 30, 315–327. doi: 10.1046/j.1365-313X.2002.01291.x

Jia, J., Xing, J., Dong, J., Han, J., and Liu, J. (2011). Functional analysis of MYB73 of *Arabidopsis thaliana* against *Bipolaris oryzae*. *Agric. Sci. China* 10, 721–727. doi: 10.1016/S1671-2927(11)60055-2

Jin, H., Cominelli, E., Bailey, P., Parr, A., Mehrtens, F., Jones, J., et al. (2014). Transcriptional repression by AtMYB4 controls production of UV-protecting

sunscreens in *Arabidopsis*. *EMBO J.* 19, 6150–6161. doi: 10.1093/emboj/19.22.6150

Jin, H., and Martin, C. (1999). Multifunctionality and diversity within the plant MYB-gene family. *Plant Mol. Biol.* 41, 577–585. doi: 10.1023/A:1006319732410

Kachroo, A., and Kachroo, P. (2007). Salicylic acid-, jasmonic acid- and ethylene-mediated regulation of plant defense signaling. *Genet. Eng.* 28, 55–83. doi: 10.1007/978-0-387-34504-8_4

Katiyar, A., Smita, S., Lenka, S., Rajwanshi, R., Chinnusamy, V., and Bansal, K. (2012). Genome-wide classification and expression analysis of MYB transcription factor families in rice and *Arabidopsis*. *BMC Genomics* 13:544. doi: 10.1186/1471-2164-13-544

Kranz, H. D., Denekamp, M., Greco, R., Jin, H., Leyva, A., Meissner, R. C., et al. (1998). Towards functional characterisation of the members of the R2R3-MYB gene family from *Arabidopsis thaliana*. *Plant J.* 16, 263–276. doi: 10.1046/j.1365-313x.1998.00278.x

Li, X., Zhao, K., Zhang, X., and Zhou, B. (2017). Expression analysis of poplar MYB transcription factor gene family in response to salt stress. *Bull. Bot. Res.* 37, 424–431. doi: 10.7525/j.issn.1673-5102.2017.03.013

Liu, X., Yang, L., Zhou, X., Zhou, M., Lu, Y., Ma, L., et al. (2013). Transgenic wheat expressing *Thinopyrum intermedium* MYB transcription factor TiMYB2R-1 shows enhanced resistance to the take-all disease. *J. Exp. Bot.* 64, 2243–2253. doi: 10.1093/jxb/ert084

Liu, W., Frick, M., Huel, R., Nykiforuk, C. L., Wang, X., Gaudet, D. A., et al. (2014). The stripe rust resistance gene *Yr10* encodes an evolutionary-conserved and unique CC-NBS-LRR sequence in wheat. *Mol. Plant* 7, 1740–1755. doi: 10.1093/mp/ssu112

Livak, K. J., and Schmittgen, T. D. (2001). Analysis of relative gene expression data using real-time quantitative PCR and the $2^{-\Delta\Delta CT}$ method. *Methods* 25, 402–408. doi: 10.1006/meth.2001.1262

Ma, Q., Wang, C., and Zhu, H. (2011). *TaMYB4* cloned from wheat regulates lignin biosynthesis through negatively controlling the transcripts of both cinnamyl alcohol dehydrogenase and cinnamoyl-CoA reductase genes. *Biochimie* 93, 1179–1186. doi: 10.1016/j.biochi.2011.04.012

Mcneal, F. H., Konzak, C. F., Smith, E. P., Tate, W. S., and Russell, T. S. (1971). *A Uniform System for Recording and Processing Cereal Research Data* (Washington, DC: USDA), 34–121.

Mengiste, T., Chen, X., Salmeron, J., and Dietrich, R. (2003). The BOTRYTIS SUSCEPTIBLE1 gene encodes an R2R3MYB transcription factor protein that is required for biotic and abiotic stress responses in *Arabidopsis*. *Plant Cell* 15, 2551–2565. doi: 10.1105/tpc.014167

Morse, A. M., Whetten, R. W., Dubos, C., and Campbell, M. M. (2009). Post-translational modification of an R2R3-MYB transcription factor by a MAP kinase during xylem development. *New Phytol.* 183, 1001–1013. doi: 10.1111/j.1469-8137.2009.02900.x

Mur, L. A., Kenton, P., Atzorn, R., Miersch, O., and Wasternack, C. (2006). The outcomes of concentration-specific interactions between salicylate and jasmonate signaling include synergy, antagonism, and oxidative stress leading to cell death. *Plant Physiol.* 140, 249–262. doi: 10.1104/pp.105.072348

Nambara, E., and Wees, S. (2021). Plant hormone functions and interactions in biological systems. *Plant J.* 105, 287–289. doi: 10.1111/tpj.15151

Ogata, K., and Nishimura, Y. (1995). Specific DNA recognition by MYB protein. *Tanpakushitsu Kakusan Koso* 40, 1592–1597

Park, R. F., Bariana, H. S., and Wellings, C. R. (2007). Preface to 'global landscapes in cereal rust control'. *Aust. J. Agric. Res.* 58:469. doi: 10.1071/ARv58n6_PR

Paz-Ares, J., Ghosal, D., Wienand, U., Peterson, P. A., and Saedler, H. (1987). The regulatory c1 locus of *Zea mays* encodes a protein with homology to myb proto-oncogene products and with structural similarities to transcriptional activators. *EMBO J.* 6, 3553–3558. doi: 10.1002/j.1460-2075.1987.tb02684.x

Popko, J., Hänsch, R., Mendel, R. R., Polle, A., and Teichmann, T. (2010). The role of abscisic acid and auxin in the response of poplar to abiotic stress. *Plant Biol.* 12, 242–258. doi: 10.1111/j.1438-8677.2009.00305.x

Raffaele, S., Rivas, S., and Roby, D. (2006). An essential role for salicylic acid in AtMYB30-mediated control of the hypersensitive cell death program in *Arabidopsis*. *FEBS Lett.* 580, 3498–3504. doi: 10.1016/j.febslet.2006.05.027

Ramirez, V., Agorio, A., Coego, A., García-Andrade, J., Hernández, M. J., Balaguer, B., et al. (2011). MYB46 modulates disease susceptibility to *Botrytis cinerea* in *Arabidopsis*. *Plant Physiol.* 155, 1920–1935. doi: 10.1104/pp.110.171843

Reymond, P., Weber, H., Damond, M., and Farmer, E. E. (2000). Differential gene expression in response to mechanical wounding and insect feeding in *Arabidopsis*. *Plant Cell* 12, 707–720. doi: 10.1105/tpc.12.5.707

Robert-Seilaniantz, A., Grant, M., and Jones, J. D. (2011). Hormone crosstalk in plant disease and defense: more than just jasmonate-salicylate antagonism. *Annu. Rev. Phytopathol.* 49, 317–343. doi: 10.1146/annurev-phyto-073009-114447

Ryals, J. A., Neuenschwander, U. H., Willits, M. G., Molina, A., and Hunt, M. D. (2013). Systemic acquired resistance. *Plant Physiol.* 1, 179–184. doi: 10.4161/psb.1.4.3221

Saha, G., Park, J. I., Ahmed, N. U., Kayum, M. A., Kang, K. K., and Nou, I. S. (2016). Characterization and expression profiling of MYB transcription factors against stresses and during male organ development in Chinese cabbage (*Brassica rapa* ssp. *pekinensis*). *Plant Physiol. Biochem.* 104, 200–215. doi: 10.1016/j.plaphy.2016.03.021

Seo, P. J., and Park, C. M. (2010). MYB96-mediated abscisic acid signals induce pathogen resistance response by promoting salicylic acid biosynthesis in *Arabidopsis*. *New Phytol.* 186, 471–483. doi: 10.1111/j.1469-8137.2010.03183.x

Shan, T., Hong, Y., Xu, H., Wei, X., and Zhang, Z. (2016). Development and characterization of *TaMYB86*-overexpressing transgenic wheat lines with resistance to common root rot. *Acta Agron. Sin.* 42, 1429–1436. doi: 10.3724/SP.J.1006.2016.01429

Spoel, S. H., Johnson, J. S., and Dong, X. (2007). Regulation of tradeoffs between plant defenses against pathogens with different lifestyles. *Proc. Natl. Acad. Sci. U. S. A.* 104, 18842–18847. doi: 10.1073/pnas.0708139104

Tian, Z., Zhong, H., Shi, R., Sun, L., Fischer, G., and Liang, Z. (2012). Estimating potential yield of wheat production in China based on cross-scale data-model fusion. *Front. Earth Sci.* 6, 364–372. doi: 10.1007/s11707-012-0332-0

Vailleau, F., Daniel, X., Tronchet, M., Montillet, J. L., Triantaphylidès, C., and Roby, D. (2002). A R2R3-MYB gene, *AtMYB30*, acts as a positive regulator of the hypersensitive cell death program in plants in response to pathogen attack. *Proc. Natl. Acad. Sci. U. S. A.* 99, 10179–10184. doi: 10.1073/pnas.152047199

Vlot, A. C., Dempsey, D. A., and Klessig, D. F. (2009). Salicylic acid, a multifaceted hormone to combat disease. *Annu. Rev. Phytopathol.* 47, 177–206. doi: 10.1146/annurev.phyto.050908.135202

Wang, X., Wang, X., Duan, Y., Yin, S., Zhang, H., Huang, L., et al. (2013). *TaAbc1*, a member of Abc1-like family involved in hypersensitive response against the stripe rust fungal pathogen in wheat. *PLoS One* 8:e58969. doi: 10.1371/journal.pone.0058969

Wang, F., Suo, Y., Wei, H., Li, M., Xie, C., Wang, L., et al. (2015). Identification and characterization of 40 isolated *Rehmannia glutinosa* MYB family genes and their expression profiles in response to shading and continuous cropping. *Int. J. Mol. Sci.* 16, 15009–15030. doi: 10.3390/ijms160715009

Wang, X., Wang, Y., Liu, P., Ding, Y., Mu, X., Liu, X., et al. (2017). *TaRar1* is involved in wheat defense against stripe rust pathogen mediated by YrSu. *Front. Plant Sci.* 8:156. doi: 10.3389/fpls.2017.00156

Wang, X., Zhang, H., Nyamesorto, B., Luo, Y., Mu, X., Wang, F., et al. (2020a). A new mode of NPR1 action via an NB-ARC-NPR1 fusion protein negatively regulates the defence response in wheat to stem rust pathogen. *New Phytol.* 228, 959–972. doi: 10.1111/nph.16748

Wang, F., Yuan, S., Wu, W., Yang, Y., Cui, Z., Wang, H., et al. (2020b). TaTLP1 interacts with TaPR1 to contribute to wheat defense responses to leaf rust fungus. *PLoS Genet.* 16:e1008713. doi: 10.1371/journal.pgen.1008713

Yang, Y., and Klessig, D. F. (1996). Isolation and characterization of a tobacco mosaic virus-inducible myb oncogene homolog from tobacco. *Proc. Natl. Acad. Sci. U. S. A.* 93, 14972–14977. doi: 10.1073/pnas.93.25.14972

Yoo, S. D., Cho, Y. H., and Sheen, J. (2007). *Arabidopsis* mesophyll protoplasts: a versatile cell system for transient gene expression analysis. *Nat. Protoc.* 2, 1565–1572. doi: 10.1038/nprot.2007.199

Zhai, Y., Li, P., Mei, Y., Chen, M., Chen, X., Xu, H., et al. (2017). Three *MYB* genes co-regulate the phloem-based defence against English grain aphid in wheat. *J. Exp. Bot.* 68, 4153–4169. doi: 10.1093/jxb/erx204

Zhang, L., Zhao, G., Jia, J., Liu, X., and Kong, X. (2012a). Molecular characterization of 60 isolated wheat MYB genes and analysis of their expression during abiotic stress. *J. Exp. Bot.* 63, 203–214. doi: 10.1093/jxb/err264

Zhang, Z., Liu, X., Wang, X., Zhou, M., Zhou, X., Ye, X., et al. (2012b). An R2R3 MYB transcription factor in wheat, TaPIMP1, mediates host resistance to *Bipolaris sorokiniana* and drought stresses through regulation of defense- and stress-related genes. *New Phytol.* 196, 1155–1170. doi: 10.1111/j.1469-8137.2012.04353.x

Zhang, C., Ma, R., Xu, J., Yan, J., Guo, L., Song, J., et al. (2018). Genome-wide identification and classification of *MYB* superfamily genes in peach. *PLoS One* 13:e0199192. doi: 10.1371/journal.pone.0199192

Zheng, X., Yi, D., Shao, L., and Li, C. (2017). In silico genome-wide identification, phylogeny and expression analysis of the R2R3-MYB gene family in *Medicago truncatula*. *J. Integr. Agric.* 16, 1576–1591. doi: 10.1016/S2095-3119(16)61521-6

Zou, B., Jia, Z., Tian, S., Wang, X., Gou, Z., Lü, B., et al. (2013). AtMYB44 positively modulates disease resistance to *Pseudomonas syringae* through the salicylic acid signalling pathway in *Arabidopsis*. *Funct. Plant Biol.* 40, 304–313. doi: 10.1071/FP12253

Conflict of Interest: The authors declare that the research was conducted in the absence of any commercial or financial relationships that could be construed as a potential conflict of interest.

Publisher's Note: All claims expressed in this article are solely those of the authors and do not necessarily represent those of their affiliated organizations, or those of the publisher, the editors and the reviewers. Any product that may be evaluated in this article, or claim that may be made by its manufacturer, is not guaranteed or endorsed by the publisher.

frontiers in Plant Science

ORIGINAL RESEARCH
published: 23 December 2021
doi: 10.3389/fpls.2021.800077

Silencing of a Wheat Ortholog of Glucan Synthase-Like Gene Reduced Resistance to *Blumeria graminis* f. sp. *tritici*

Peng Cheng, Zihao Wang, Yanyan Ren, Pengfei Jin, Kangjie Ma, Qiang Li and Baotong Wang**

State Key Laboratory of Crop Stress Biology for Arid Areas, College of Plant Protection, Northwest A&F University, Yangling, China

Wheat powdery mildew, caused by the obligate biotrophic ascomycete fungal pathogen *Blumeria graminis* f. sp. *tritici* (*Bgt*), is a major threat to wheat production worldwide. It is known that *Arabidopsis thaliana glucan synthase-like 5* (*AtGSL5*) improves the resistance of wheat to powdery mildew by increasing its anti-penetration abilities. However, the function of glucan synthase-like (*GSL*) orthologs in crop species remains largely unknown. In this study, *TaGSL22*, a novel functional ortholog of *AtGSL5*, was isolated as the only *Bgt*-induced *GSL* gene in wheat. Phylogenetic analysis indicated that *TaGSL22* was conserved within the group of Gramineae and showed a closer relationship to *GSL* orthologs from monocots than to those from dicots. The *TaGSL22* transcript was highest in the wheat leaves, followed by stems then roots. *TaGSL22* was localized in the cell membrane and cytoplasm of wheat protoplasts, as predicted by transmembrane structure analysis. In addition, expression of *TaGSL22* was induced by the plant hormones ethylene (ETH) and salicylic acid (SA), but down-regulated by jasmonate (JA) and abscisic acid (ABA). The transcript level of *TaGSL22* was up-regulated in the incompatible interaction between *Bgt* and wheat, whereas it remained relatively unchanged in the compatible interaction. Knocking down of *TaGSL22* by virus-induced gene silencing (VIGS) induced a higher infection type in the wheat–*Bgt* interaction. The *TaGSL22*-silenced plants exhibited reduced resistance to *Bgt*, accompanied by decreased callose accumulation. Our study shows a conserved function of *GSL* genes in plant immunity associated with penetration resistance, and it indicates that *TaGSL22* can be used to improve papilla composition and enhance resistance to wheat powdery mildew.

Keywords: wheat powdery mildew, BMSV-VIGS, disease resistance, callose, glucan synthase-like, *TaGSL22*

OPEN ACCESS

Edited by:
Guotian Li,
Huazhong Agricultural University, China

Reviewed by:
Heng Ye,
University of Missouri, United States
Li Song,
Yangzhou University, China

****Correspondence:***
Peng Cheng
pengcheng@nwafu.edu.cn
Baotong Wang
wangbt@nwafu.edu.cn

Specialty section:
This article was submitted to Plant Pathogen Interactions, a section of the journal Frontiers in Plant Science

Received: *22 October 2021*
Accepted: *06 December 2021*
Published: *23 December 2021*

Citation:
Cheng P, Wang Z, Ren Y, Jin P, Ma K, Li Q and Wang B (2021) Silencing of a Wheat Ortholog of Glucan Synthase-Like Gene Reduced Resistance to Blumeria graminis f. sp. tritici. Front. Plant Sci. 12:800077. doi: 10.3389/fpls.2021.800077

INTRODUCTION

Wheat is one of the earliest cultivated crops in history. More than 10,000 years ago, humans began to plant *Triticum monococcum* for use as food (Araus et al., 2007). Today it remains the main source of calories and protein globally, and cultivating wheat varieties with high nutrition, yield, and resistance to biotic and abiotic stresses is key to ensuring food security (Mondal et al., 2016).

Wheat powdery mildew is a fungal disease caused by *Blumeria graminis* f. sp. *tritici* (*Bgt*) (Belanger et al., 2003). The disease occurs in all wheat-growing regions in the world, and its distribution is very extensive. The reproduction of *Bgt* mainly depends on the conidia and ascospores of the pathogen, and the disease often occurs in a large area following the spread of airflow. Typically, wheat powdery mildew will cause a 5–19% yield loss of the crop, while in serious epidemic years that number may reach to more than 30%. As incidences of the disease increase, the safety of global wheat production is seriously threatened (Li et al., 2019). Planting disease-resistant wheat cultivars is the most effective and cost-effective strategy for the control of powdery mildew. At present, more than 60 loci of powdery mildew resistance genes have been identified, of which only a few have been cloned successfully, such as *Pm5e* and *Pm41* (Li et al., 2020; Xie et al., 2020). However, because most of these resistance genes are based on a gene-for-gene system and are race-specific, they are at risk of being overcome by new emerging races of the pathogen (McDonald and Linde, 2002). Genes that contribute to disease resistance with a broad spectrum are needed to provide durable resistance.

The cell wall of plants is the first barrier against the invasion of pathogens (Kacprzak et al., 2011). In the resistance of plants to pathogenic fungi and oomycetes, the plant cell wall will self-modify where the pathogens attempt to invade. This results in a complex structure known as a papilla, which is essentially a physical barrier created to slow down or even prevent the invasion of pathogens. The papilla contains a variety of chemical components with clear anti-microbial functions, such as thionins and phenolic compounds (McLusky et al., 1999). Callose, the most prominent component of the papillae, is likely indispensable in papillae disease resistance. The prevention of pathogen invasion has been observed to be associated with the deposit of relatively high amounts of callose at sites of attempted penetration, forming typical papillae (Voigt, 2016).

The glucan synthase-like (*GSL*) gene family exists in many plants and is responsible for the production of callose, which is present not only at sites of pathogen attack and fungal penetration, but also in the pollen cell wall and in callus plugs in wounds (Voigt et al., 2006). For example, Arabidopsis *thaliana glucan synthase-like 5* (*AtGSL5*) (also known as the *powdery mildew resistance gene 4*, *PMR4*) in *Arabidopsis thaliana* is involved in the formation of the callose wall that separates tetrads, making it essential for the formation of pollen (Enns et al., 2005). In addition, *AtGSL5* improves the resistance of *A. thaliana* to powdery mildew by increasing its anti-penetration abilities (Blümke et al., 2013). It was also found that CRISPR/Cas-9-targeted mutagenesis of the *PMR4* gene in tomato plants produced mutants that displayed a reduction (but not a complete loss) of susceptibility to the tomato powdery mildew pathogen *Oidium neolycopersici* (Martinez et al., 2020). The functional ortholog of *AtGSL5* in barley was identified as *HvGSL6*, whose down-regulation led to reduced glucan deposition and increased cell wall penetration by powdery mildew (Chowdhury et al., 2016). In wheat, eight different *TaGSL* genes were identified and ascertained to mediate the synthesis and regulation of callose under different environmental conditions in various tissues (Voigt et al., 2006). Functional analysis of members of the *GSL* gene family in wheat revealed that either *TaGSL8* or *TaGSL10* are involved in plant regeneration, while the *TaGSL3* and *TaGSL8* RNAi transgenic lines showed slightly reduced resistance against *Fusarium graminearum* (Rana et al., 2014). However, the *GSL* genes associated with papillary callose accumulation in common wheat have not been identified, and their organ- and tissue-specific expressions and involvement in disease resistance remain unknown.

A number of plant hormones play critical roles in the defense systems of plants (Shigenaga and Argueso, 2016). For example, salicylic acid (SA) is considered to be an important signaling molecule that induces an immune reaction in plants. It is involved in the hypersensitive response and the systemic acquired resistance response in a plant, both of which can regulate reactive oxygen species and antioxidants to improve plant resistance (Ryals et al., 1994). It has also been reported that the SA pathway in *A. thaliana* is negatively regulated by callose synthase, the loss of which can result in SA-dependent disease resistance to powdery mildew (Nishimura et al., 2003). Jasmonate (JA) is a plant hormone produced by the metabolism of unsaturated fatty acids, and it is involved in the regulation of plant resistance to pathogens, insects, and mechanical damage (Koo and Howe, 2009). In Arabidopsis, *AtGSL5* was found to negatively regulate JA and SA production or signaling to enhance disease resistance to powdery mildew, and the negative regulation of defense signaling by this gene could be independent of callose production (Wawrzynska et al., 2010). Ethylene (ETH) is a gaseous plant hormone derived from methionine, which is abundant in plants. The ETH response factor subfamily plays an important role in the establishment and regulation of defense systems of plants by balancing positive and negative transcriptional regulation (Bari and Jones, 2009). In fact, in most cases, these plant hormones are more effective when they act in relation to each other, making them indispensable members of the plant disease resistance response network. However, the regulatory function of these plant hormones in the defense of common wheat triggered by a *GSL* gene is not clear.

In the present study, the wheat ortholog gene *TaGSL22* of the Arabidopsis gene *AtGSL5* was identified in wheat. Transcript profiling of *TaGSL22* was analyzed in wheat seedlings inoculated with virulent and avirulent *Bgt* races, and in response to various plant hormones. Tissue-specific expression and subcellular localization of TaGSL22 were determined. The BMSV-VIGS technique was performed to demonstrate how *TaGSL22* was involved in callose regulation and disease resistance to *Bgt*. Taken together, our results indicated that the *TaGSL22* gene plays a role in callose synthesis and resistance to *Bgt* in wheat.

MATERIALS AND METHODS

Plant Material and Pathogen Preparation

The common wheat variety *Asosan/8Cc*, which is highly resistant to *Bgt* E09 and susceptible to *Bgt* A13, was used throughout the study. The plants were placed under a transparent cover in a greenhouse with a temperature of 17°C, 75% humidity,

and a 16 h photoperiod of light (18 μmol/m^2/s). Inoculation with *Bgt* was carried out after about 7–10 days, when the wheat seedlings grew to one leaf (Zeng et al., 2010). Before inoculation, the seedlings were misted with water. Fresh conidia were then inoculated on the wheat leaves by the shaking powder method. About 7 days later, when the susceptible control "Jingshuang 16" reached infection type (IT) 4, the ITs of the tested materials were rated using a scale of 0–4 (**Supplementary Table 1**).

Identification and Phylogenetic Analysis of *TaGSL22*

The protein sequence of *AtGSL5* in Arabidopsis was used to search the UniProt protein database for its ortholog gene in wheat. A 423 bp DNA sequence of *TaGSL22* was found in the linked NCBI database using the amino acid sequence of the TaGSL22 protein obtained in the UniProt protein database. Using this sequence, ortholog genes of *TaGSL22* in other plant species were identified by a BlastX search. A phylogenetic tree was constructed with sequences of the seven homologous genes obtained in BlastX using the molecular evolutionary genetic analysis software MEGA7. The signal peptide and transmembrane domain of the protein were predicted by online software TMHMM-2.0, and its subcellular localization was analyzed and predicted by online software cNLS Mapper.

RNA Extraction and Quantitative Real-Time Polymerase Chain Reaction

Samples measuring about 100 mg were collected from leaves, stems, and roots at the seedling stage (7–10 days of growth), then frozen immediately in liquid nitrogen and stored at −80°C for RNA extraction using a plant RNA small extraction kit (Magen, Guangzhou, China). First-strand cDNA was synthesized in accordance with the instructions of the Hiscript III 1st Strand cDNA Synthesis Kit (+gDNA wiper) (Vazyme, Nanjing, China). For quantitative real-time polymerase chain reaction (qRT-PCR) analysis, ChamQ Universal SYBR qPCR Master Mix (Vazyme) was used on a Quant Studio 5 fluorescence quantitative instrument (Thermo Fisher, Waltham, MA, United States). Gene encoding wheat elongation factor (EF-1α) was used as the internal reference gene (**Supplementary Table 1**). After qRT-PCR analysis, the $2^{-\Delta\ \Delta\ CT}$ method was used to calculate the relative expression of the target gene (Livak and Schmittgen, 2001). The experiments consisted of three biological repeats and three technical repeats. The sequences of quantitative primers are shown in **Supplementary Table 2**.

Subcellular Localization of TaGSL22::GFP Fusion Protein

The pJIT163-GFP vector was used to construct a *TaGSL22* expression vector (pJIT163-*TaGSL22*::GFP) for subcellular localization (Wang et al., 2013). Endonuclease *Bam*HI and *Xba*I were used to digest the pJIT163 plasmid, and the reaction was carried out on a Bio-Rad MyCycler PCR (Bio-Rad, Hercules, CA, United States) at 37°C for 4 h. After the reaction was complete, the product was recovered using a Gel Extraction Kit (Omega, Norcross, GA, United States). The *TaGSL22*, along with the recognition sequences and homologous arms, was amplified and ligated with the linear vector using a ClonExpress Ultra One Step Cloning Kit (Vazyme) with two CaMV 35S promoters. The ligated product was then transformed into *E. coli* DH5α and sequenced to confirm the successful construction of the *TaGSL22* expression vector. Wheat protoplasts were prepared using a wheat protoplast preparation and transformation kit (Coolaber, Beijing, China). The protoplasts were observed with a FV3000 confocal laser scanning microscope (Olympus Corp., Tokyo, Japan) using a GFP channel (Alexa Flour 488, green) and an SV2 channel (Alexa Flour 565, red).

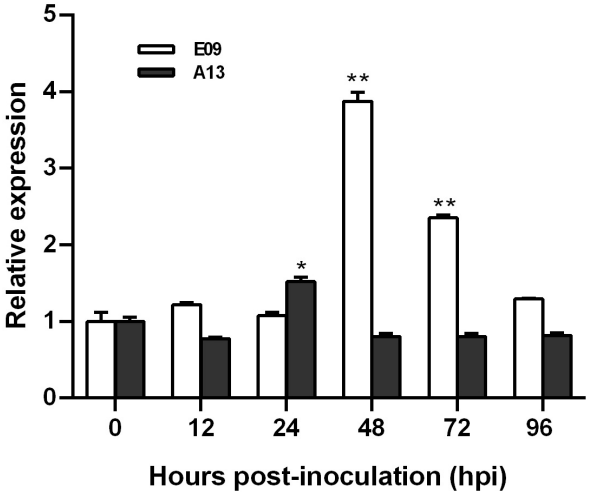

FIGURE 1 | Transcript profiles of *TaGSL22* after inoculation with avirulent (E09) and virulent (A13) *Bgt* races. Relative gene quantification was calculated by the comparative ΔΔCT method. Data were normalized to the expression level of the wheat elongation factor TaEF-1α. * and ** indicate significant differences ($P < 0.05$ and $P < 0.01$) from the mock-inoculated control at 0 hpi using Student's *t*-test. Error bars represent SEM of three biological replicates.

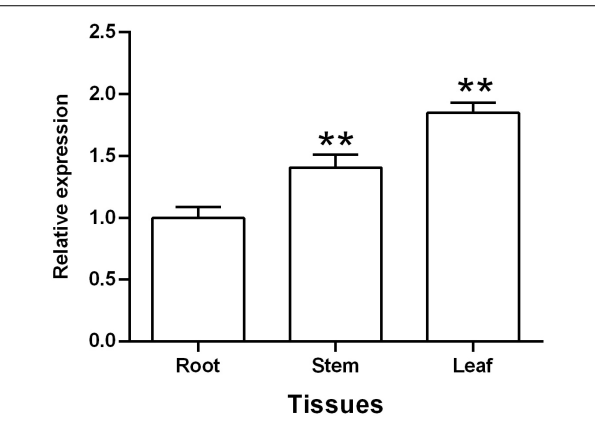

FIGURE 2 | Tissue-specific expression of *TaGSL22*. Relative gene quantification was calculated by the comparative ΔΔCT method. Data were normalized to the expression level of the wheat elongation factor TaEF-1α. ** indicates a significant difference ($P < 0.01$) from the root by Student's *t*-test. Error bars represent SEM of three biological replicates.

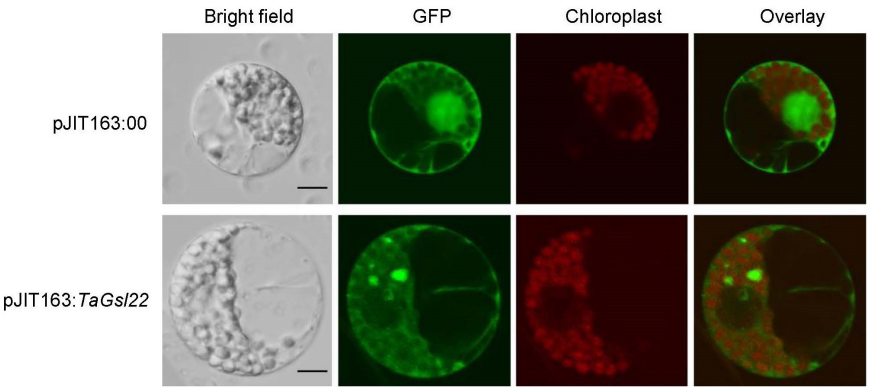

FIGURE 3 | Subcellular localization of the TaGSL22 protein. pJIT163:00, pJIT163 empty plasmid; pJIT163:*TaGSL22*, pJIT163 recombinant plasmid with *TaGSL22*; overlay, superposition of green fluorescent protein (GFP) channel and chloroplast channel; bright field images show the equivalent field observed under white light. Scale bars: 10 μm.

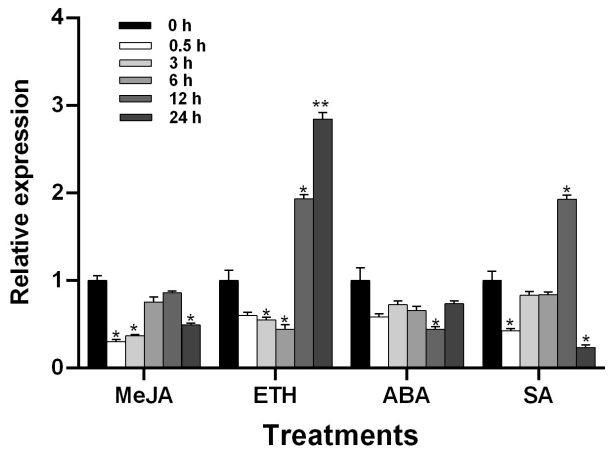

FIGURE 4 | Transcript profiles of *TaGSL22* under different hormone treatments. MeJA, methyl jasmonate; ETH, ethylene; ABA, abscisic acid; SA, salicylic acid. The mock control was treated with water. Data were normalized to the expression level of the wheat elongation factor TaEF-1α. Relative gene quantification was calculated by the comparative ΔΔCT method. * and ** indicate a significant difference ($P < 0.05$ and $P < 0.01$) from the control at 0 hpt using Student's *t*-test. Error bars represent SEM of three biological replicates.

Transcript Profiling of *TaGSL22* Induced by Different Plant Hormones

The seedlings were treated with methyl jasmonate (MeJA) (0.1 mM), ETH (0.2 mM), abscisic acid (ABA) (0.2 mM), and SA (1 mM), respectively. Leaf samples were collected at 0, 0.5, 3, 6, 12, and 24 h after each treatment to conduct qRT-PCR analysis as described above. The mock control was treated with water. Data were normalized to the expression level of the wheat elongation factor TaEF-1α. The transcript level of genes in control plants at time 0 was standardized as 1. The qRT-PCR analysis for each respective experiment was repeated three times.

Production of *TaGSL22*-Silenced Wheat Plants by Virus-Induced Gene Silencing

The viral vectors, including BMSV: α, BMSV: β, BMSV: γ, and BMSV: γ-phytoene desaturase gene (*PDS*), were donated by Professor Jun Guo at Northwest A&F University. The BSMV-VIGS system was performed as previously described (Yuan et al., 2011). *TaGSL22* was connected to BMSV: γ-*PDS* plasmid by homologous recombination to form γ-*TaGSL22* using a ClonExpress Ultra One Step Cloning Kit (Vazyme). BMSV: α and BMSV: γ were digested with endonuclease *Mlu*, BMSV: γ-*PDS* and BMSV: γ-*TaGSL22* were digested with *Bss*HII, BMSV: β was digested with *Spe*I, and the linearized vector was transcribed *in vitro* with an *in vitro* transcription kit (Promega, Madison, WI, United States). The transcripts of linearized plasmids α, β, and γ were mixed with appropriate amounts of 1 × FES buffer (0.1 M glycine, 0.06 M K_2HPO_4, 1% w/v tetrasodium pyrophosphate, 1% w/v bentonite, and 1% w/v celite, pH 8.5) (Pogue et al., 1998). When the seedlings reached the stage of two leaves and one heart, the second leaves were inoculated with the virus, and one pot of seedlings was kept uninoculated to serve as control. The wheat leaves were treated in darkness at 25°C for 24 h. After phenotypic observation, the virus-infected wheat seedlings were selected and inoculated with *Bgt* E09, then transferred to the growth chamber under the same conditions as described above. Samples were taken at 0, 48, and 120 h post infection (hpi) for qRT-PCR, and the silencing efficiency was measured. The primers used are listed in **Supplementary Table 2**.

Histopathological Observation of the Powdery Mildew Pathogen in the *TaGSL22*-Silenced Plant

During virus-induced gene silencing (VIGS), histopathological observation was performed on samples taken at 24, 48, and 96 hpi with *Bgt* E09. The collected leaves were cut with scissors into 2 cm segments and placed in a decolorizing solution of anhydrous ethanol and glacial acetic acid for 2 days. The leaf segments were then transferred into a saturated chloral hydrate solution for transparency, and finally into a 50% glycerol solution. After wheat

germ agglutinin (WGA) staining, the samples were then observed under an Olympus BX53 microscope (Olympus Corp., Tokyo, Japan). Representative colonies from the control and silenced groups were selected for imaging, and the colony areas, number of mycelial branches, and mycelium lengths were recorded.

Microscopic Analysis of Callose Accumulation in the *TaGSL22*-Silenced Plant

During VIGS, freshly cut leaf tissues collected at 24 hpi with *Bgt* E09 were decolorized and washed twice with 50% (v/v) ethanol for 15 min, rinsed with water, then stained with aniline blue solution [67 mM K_2HPO_4, 0.05% (w/v) aniline blue]. The degree of callose deposition was determined in fields of 1 mm^2 using a BX-51 microscope (Olympus Corp., Tokyo, Japan) (Xu et al., 2020). Representative pictures of the callose accumulation in the control and silenced groups, with scale bars measuring 100 μm, were selected for imaging. The average number of callose foci per field of view (1 mm^2) was calculated from 30 fields.

Statistical Analysis

The data processing system SPSS Statistics 25 (IBM, Armonk, NY, United States) was used for statistical analysis. The Student's *t*-test method was used, wherein * and ** represented significant differences at $P < 0.05$ and $P < 0.01$, respectively. Relative gene quantification was calculated by the comparative ΔΔCT method. All experiments were performed and analyzed separately with three biological replicates.

RESULTS

TaGSL22 Gene Was Identified as a Wheat Ortholog of *Arabidopsis thaliana Glucan Synthase-Like 5*

To identify the putative ortholog of *AtGSL5* in common wheat, the UniProt protein database[1] was searched using the amino acid sequence of the *AtGSL5* protein as the query sequence. A wheat ortholog gene with the highest sequence identity, *TaGSL22*, was extracted (UniProtKB: Q4JHU1).

The phylogenetic relationships of *GSL* genes in seven other plant species, *Aegilops tauschii*, *Hordeum vulgare*, *Setaria viridis*, *Zea mays*, *Oryza sativa*, *Gossypium hirsutum*, and *A. thaliana*, were investigated to identify their orthologs. A phylogenetic tree was then constructed using Mega 7 (**Supplementary Figure 1A**). It was inferred that the *GSL* gene was relatively conservative in Gramineae (in the same clade as *Hordeum* and *Aegilops*). The average hydrophobicity of the TaGSL22 protein was 0.289, indicating it was a hydrophobic protein. It was predicted that the TaGSL22 presented in cytoplasm and had transmembrane domains (**Supplementary Figure 1B**). According to the structure analysis, no signal peptide or nuclear localization were predicted.

[1]https://www.uniprot.org/

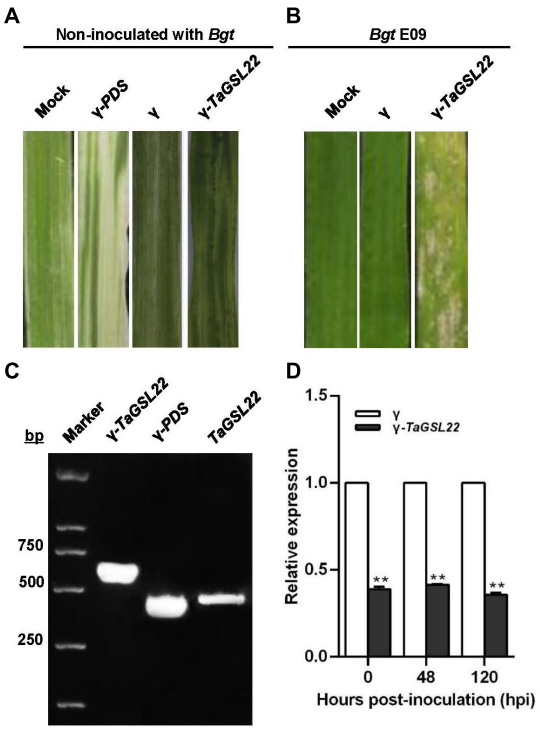

FIGURE 5 | Functional assessment of *TaGSL22* in the wheat–*Bgt* interaction by gene silencing. **(A)** The leaf phenotype of successful virus infection; photographs were captured 12 days post-inoculation (dpi); mock: leaves inoculated with water; γ-*PDS*: transcripts of α, β, γ-*PDS* plasmids inoculated on leaves; γ: transcripts of α, β, γ plasmids inoculated on leaves; γ-*TaGSL22*: transcripts of α, β, γ-*TaGSL22* plasmids inoculated on leaves. **(B)** Disease phenotypes of the leaves pre-inoculated with BSMV: γ then the avirulent E09 *Bgt* race; mock: the leaves were only inoculated with *Bgt*. Photos were taken at 10 dpi. **(C)** PCR amplification of γ-*TaGSL22*, γ-*PDS*, and *TaGSL22* from corresponding leaves. **(D)** Assessment of *TaGSL22* silencing efficiency. Relative gene quantification was calculated by the comparative ΔΔCT method, and data were normalized to the expression level of the wheat elongation factor TaEF-1α. ** indicates a significant difference at $P < 0.01$ from the control group (γ) by Student's *t*-test. Error bars represent SEM for three biological replicates.

TaGSL22 Expression Increased in the Resistance Reaction to *Bgt* E09

To characterize the expression pattern of *TaGSL22* in wheat after a fungal infection, its transcript profiles with races E09 (avirulent) and A13 (virulent) were examined using RT-qPCR (**Figure 1**). Expression levels were recorded in a time course at 12/24 h intervals across the first 96 h after inoculation. It was found that the expression of *TaGSL22* was increased at 48 hpi, and subsequently decreased with *Bgt* E09 infection. The peak at 48 hpi was about 3.8 times that of the control (0 hpi), indicating that gene expression was significantly induced. After 48 h, the expression of *TaGSL22* decreased slowly, but its value was always higher than during the first 24 h. In contrast, inoculation of *Bgt* A13 suppressed the overall expression of the *GSL* gene, except at 24 hpi when a 1.5 times expression was noted. These results

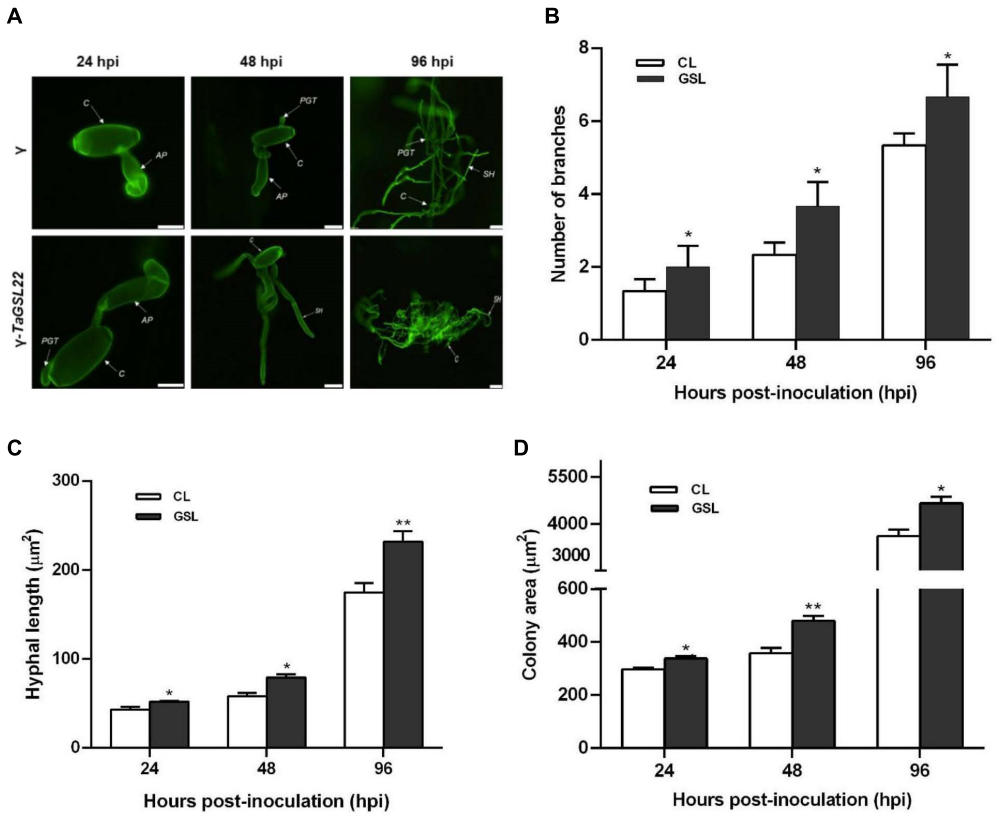

FIGURE 6 | (A) Histopathological observation of *Bgt* infection on leaves after gene silencing. Samples of control plants (γ) and the gene-silenced plants (γ-*TaGSL22*) were taken at 24, 48, and 96 hpi. The fungal structures were stained with wheat germ agglutinin (WGA). C, conidia; AP, appressorium; PGT, primary germ tube; SH, secondary hyphae. Scale bars: 5 μm. **(B)** Number of branches, **(C)** hyphal length, and **(D)** colony area of *Bgt* after gene silencing. The leave samples were collected at 24, 48, and 96 hpi, and all results were obtained from 50 infection sites. CL, control leaf; *GSL*, gene-silenced leaf. Error bars represent SEM of three biological replicates. * and ** represent significant differences at $P < 0.05$ and $P < 0.01$, respectively, from the control by Student's *t*-test.

indicated that *TaGSL22* was highly induced in the wheat powdery mildew resistance response, but not in the susceptible reaction.

Expression of *TaGSL22* Was Highest in Leaves

A qRT-PCR assay was used to assess the expression patterns of *TaGSL22* in different tissues, including root, stem, and leaf. The results showed that *TaGSL22* was detected in all tested plant tissues (**Figure 2**). *TaGSL22* had the highest expression in leaves and the lowest expression in roots. If the expression level in root tissues was defined as 1, then its expression in the stem and leaf tissues were 1.41 and 1.85, respectively.

TaGSL22 Was Localized in the Cell Membrane and Cytoplasm of Wheat

To verify the subcellular localization predicted by the cNLS Mapper online software based on the amino acid sequence of the TaGSL22 protein, the pJIT163 empty plasmid (pJIT163:00) and pJIT163 recombinant plasmid with green fluorescent protein (GFP) fusion (pJIT163:*TaGSL22*) were transformed into wheat protoplasts. It was found that the protoplasts with pJIT163:00 emitted green fluorescence in the cell membrane, cytoplasm, and nucleus under the GFP channel, and under the SV2 channel, red fluorescence was observed only in the region where the organelles were located (**Figure 3**). In the protoplasts transformed with pJIT163:*TaGSL22*, the cell membrane and cytoplasm emitted green fluorescence under the GFP channel. These results suggested that the TaGSL22 protein was located in the cell membrane and cytoplasm, which was consistent with the initial prediction based on the amino acid sequence.

TaGSL22 Was Induced by Plant Hormones Ethylene and Salicylic Acid

To understand the regulatory effect of plant hormones on *TaGSL22* in wheat, the seedlings of variety *Asosan/8Cc* were treated with MeJA (0.1 mM), ETH (0.2 mM), ABA (0.2 mM), and SA (1 mM), respectively (**Figure 4**). After MeJA or ABA treatment, expression of *TaGSL22* was down-regulated. In contrast, the *TaGSL22* transcript level dropped to its minimum at 6 h post treatment (hpt) with ETH, then increased dramatically at 12 hpt until reaching its maximum at 24 hpt, at about 2.8 times that of the control (0 hpt). When treated with SA, expression of the gene decreased initially, then increased gradually to reach its maximum at 12 hpt, then decreased again. It was therefore

inferred that *TaGSL22* may be involved in the ETH- and SA-mediated signaling pathways.

Silencing of *TaGSL22* Reduced Resistance to Powdery Mildew in Wheat

To further assess the function of *TaGSL22* in wheat, the gene was silenced *via* a BSMV-based VIGS approach (Singh et al., 2012). Ten days after inoculation with γ-*PDS* as a control for VIGS, an efficient silencing of the *PDS* gene was indicated by the observation of photobleaching symptoms on the leaves (**Figure 5A**). The leaves inoculated with both the γ virus and the γ-*TaGSL22* virus exhibited chlorotic stripes, and no symptoms were observed on the leaves without virus inoculation. To evaluate the role of *TaGSL22* in resistance against the powdery mildew pathogen *Bgt*, the fourth leaf with evident virus virulence was inoculated with *Bgt* E09 and the disease IT was scored at 10 dpi. The gene-silenced group was found to have significantly more spores on its leaves than on leaves in the control groups (**Figure 5B**).

The involvement of *TaGSL22* in the plant resistance reaction was verified by PCR amplification of γ-*TaGSL22*, γ-*PDS*, and *TaGSL22* from corresponding leaves. qRT-PCR analysis was carried out to determine whether the gene was effectively silenced at the transcript level (**Figure 5C**). At three time points, the endogenous *TaGSL22* transcript levels were significantly reduced in leaves inoculated with the γ-*TaGSL22* virus compared with those in control plants (**Figure 5D**). The results indicated that the wheat resistance to *Bgt* was reduced after down-regulation of *TaGSL22*.

Down-Regulation of *TaGSL22* Led to Significantly More Virulent Fungal Infections

To further clarify the role of *TaGSL22* during the fungal colonization on leaves, samples were taken at three time points and observed under a fluorescence microscope (**Figure 6A**). At 24 hpi, the appressoria were two times longer in the *TaGSL22* down-regulated leaves (γ-*TaGSL22*) compared to those in the control plants (γ). Secondary hypha were observed at 48 hpi in the *TaGSL22*-silenced leaves, while in the control plants, the primary germ tube was only just germinated from the conidium. At 96 hpi, the hypha mass was significantly larger in the gene-silenced plants than in the control plants. The leaves of the gene-silenced group displayed a significant increase in the number of mycelia branches and mycelia lengths compared to those in the control group, and the powdery mildew colony areas were also larger (**Figures 6B–D**). Over time, all three measured parameters increased dramatically at the histological level. A considerably faster growth of the fungus in the *TaGSL22*-silenced plants suggested that down-regulation of *TaGSL22* increased the *Bgt* fungal infection.

Silencing of *TaGSL22* Resulted in Reduced Levels of Callose

In order to determine whether the silencing of the *TaGSL22* gene affected the deposition of callose in epidermal cells during *Bgt* infection, infected wheat leaves were stained with aniline blue to examine callose accumulation (**Figure 7A**). Samples of control plants (wild-type and γ) and the gene-silenced plants (γ-*TaGSL22*) were collected at 24 hpi with *Bgt* E09 and stained, then microscopic observation was carried out. It was observed that the fluorescent signals detected in the gene-silenced plants were significantly reduced compared to signals in the control plants, whereas the wild-type and empty vector plants showed similar intensities of callose accumulation signals (**Figure 7B**).

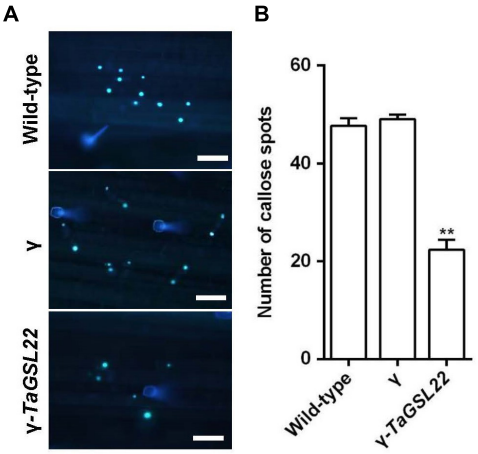

FIGURE 7 | Down-regulation of *TaGSL22* expression reduced the callose deposition in host plant. **(A)** Representative wheat leaves stained with aniline blue for callose deposition (bar = 100 μm). Pictures of control plants (wild-type and γ) and the gene-silenced plants (γ-*TaGSL22*) were taken at 24 hpi with *Bgt* avirulent race E09 at ×10 magnification with an Olympus BX-51 microscope. **(B)** The average number of callose foci per field of view (1 mm^2) was calculated from 30 fields for each sample. Error bars represent SEM of three biological replicates. ** represent significant differences at $P < 0.01$ (Student's *t*-test).

DISCUSSION

Callose Synthase Glucan Synthase-Likes Play Different Roles in Various Plant Species and Tissues

Callose, a β-1,3-glucan, plays critical regulatory roles in plants, such as in sieve tube metabolism and gametophyte development (Legentil et al., 2015; Shi et al., 2015). It has long been observed that the deposition of relatively high amounts of callose and cellulose at sites of attempted penetration induces the formation of effective papillae, preventing the invasion of pathogens (Voigt, 2016). The most prominent cell wall polymer of papillae is β-1,3-glucan callose (Mangin, 1895). It has been reported that callose can enhance the resistance of melon to aphids (Shinoda, 1993), and early callose deposition increased the resistance of Arabidopsis to powdery mildew (Ellinger et al., 2013). Furthermore, overexpression of the Arabidopsis callose synthase gene *AtGSL5* in barley induced penetration resistance to the barley powdery mildew pathogen *Blumeria graminis* f. sp.

hordei (*Bgh*) (Blümke et al., 2013). Silencing of *HvGSL6*, encoding the barley callose synthase that falls into the *AtGSL5* clade, also caused a decline in callose accumulation in powdery mildew-induced papillae and resulted in an increased penetration rate of *Bgh* (Chowdhury et al., 2016).

To date, a number of *TaGSL* genes have been identified in different wheat tissues with various regulatory functions under different environmental conditions (Voigt et al., 2006). *TaGSL8* or *TaGSL10* are involved in plant regeneration, and the knocking down of *TaGSL3* and *TaGSL8* slightly reduced the resistance against *F. graminearum* (Rana et al., 2014). In the present study, phylogenetic analysis revealed that *TaGSL22* had the closest sequence similarity with *AtGSL5*. Transcript profile analysis at different time points revealed a significant up-regulation of the *TaGSL22* gene following infection by *Bgt*. As *AtGSL5* was the only *GSL* induced during pathogen infection (Dong et al., 2008), our results suggested that *TaGSL22* was likely the ortholog of *AtGSL5*. The tissue-specific expression analysis of *TaGSL22* showed that its expression was highest in the leaves compared to the roots and stems, which is consistent with the finding by Voigt et al. (2006). Silencing of *TaGSL22* reduced the accumulation of callose significantly and increased the *Bgt* growth rate. Our study is the first report on the *GSL* genes associated with papillary callose accumulation and powdery mildew resistance in common wheat.

Pathogen-Induced Callose Synthase in Poaceae May Be Involved in Different Plant Defense Regulating Pathways Than Dicots

Unlike in barley and wheat, it was found that silencing the pathogen-induced callose synthase *AtGSL5* in Arabidopsis results in a significant reduction of callose deposition, leading to an unexpected increase in fungal resistance (Jacobs et al., 2003). Similarly, silencing of the callose synthase gene *SlPMR4*, the ortholog of *AtGSL5* in tomato, resulted in increased resistance to the adapted powdery mildew pathogen *O. neolycopersici* (Huibers et al., 2013). Interestingly, the increased resistance in Arabidopsis has previously been explained to result from a hyperactivation of the SA-dependent defense pathway due to the loss of callose (Nishimura et al., 2003). It has also been suggested that SA may be involved in the regulation of stress response genes, since similar results were found in a study of induced plant defense responses against chewing insects in Arabidopsis (Stotz et al., 2000). Although reciprocal phenomena were observed from the down-regulation of *GSL* in Arabidopsis and barley, the function of callose deposition was verified by the overexpression of *AtGSL5* in barley and Arabidopsis, resulting in complete penetration resistance to *Bgh* and *Golovinomyces cichoracearum*, respectively (Blümke et al., 2013; Ellinger et al., 2013). Combining this result with the fact that silencing the *HvGSL6* gene leads to a loss-of-resistance phenotype that is not clouded by an off-target increase in the SA-dependent defense pathway, Chowdhury et al. (2016) proposed that the pathogen-induced callose synthase observed in barley may not be involved in regulating other plant defense pathways, as compared to observations in the dicotyledonous plants Arabidopsis and tomato.

In the present study, it was indicated that the expression of *TaGSL22* increased at 12 hpt with ETH and SA, respectively. Interestingly, reciprocal trends were observed at 24 hpt. While the transcript level of TaGSL22 kept increasing under ETH treatment, the *TaGSL22* expression was suppressed by SA. Considering the loss of callose induced SA-dependent defense pathways in Arabidopsis, further investigation is needed to understand the relationship between *GSL* regulation and SA-dependent defense pathways in wheat and barley.

Utilization of *TaGSL22* in Wheat Resistance Breeding

The nucleotide sequence of *TaGSL22* had the highest similarity with those of *A. tauschii* and *H. vulgare*, indicating that the gene is relatively conservative in Gramineae plants and evolves slowly. This gives new opportunities for investigating orthologous genes in relative species and provides new targets for increasing crop resistance against penetration. Our study identified a novel wheat ortholog gene, *TaGSL22*, that may contribute to improved resistance in wheat breeding. In future studies, we plan to search the wheat whole-genome resequencing database for any natural variations in *TaGSL22* that can be identified for breeding applications. Molecular markers can be developed and tested in a natural wheat accession to verify the association between *Bgt* resistance and the *TaGSL22* allele. The identified polymorphic markers could then be used for marker-assisted selection for introgression of *TaGSL22* in wheat resistance breeding.

It is noteworthy that although *HvGSL6* has been identified in barley and its RNAi transgenic lines resulted in increased penetration by *Bgh* (Chowdhury et al., 2016), studies on the overexpression of *HvGSL6* have not been reported. We are working on developing *TaGSL22* overexpression wheat lines to further investigate its positive regulation of resistance to wheat powdery mildew. However, transgenic crops are not widely accepted for agricultural production. Recently, A donor-DNA-free CRISPR/Cas-based approach was reported to increase expression of target genes by creating structural variations in rice (Lu et al., 2021). This cutting-edge technology knocks out the sequence between the target gene and the promotor of a neighboring high-expressed gene, resulting in gene knock-up by ligating the high-expressed promotor with the coding region of the target gene. It is believed that this advanced gene knock-up technology sheds light on the potential applications of an identified resistance gene in crop resistance enhancement without introducing alien DNA residues by plant transformation.

DATA AVAILABILITY STATEMENT

The datasets presented in this study can be found in online repositories. The names of the repository/repositories and accession number(s) can be found in the article/**Supplementary Material**.

AUTHOR CONTRIBUTIONS

PC and ZW designed the experiments and wrote the manuscript. ZW, YR, and PC performed the experiments. ZW, PC, PJ, KM, and QL analyzed the data. PC acquired the funding. BW supervised the project. All authors read and approved the final manuscript.

FUNDING

This study was financially supported by the grants from the National Natural Science Foundation of China (Grant Nos. 32072410 and 31701745), Key Research and Development Project of Shaanxi Province (Grant No. 2021ZDLNY01-01), Natural Science Basic Research Program of Shaanxi Province (Grant No. 2020JQ-257), and Scientific Startup Foundation for Doctors of Northwest A&F University (Grant No. 2452019582).

ACKNOWLEDGMENTS

We thank Jun Guo, Qiao Wang, and Chang Su for providing reagents, materials, and analysis tools. We also thank reviewers for their constructive comments.

SUPPLEMENTARY MATERIAL

The Supplementary Material for this article can be found online at: https://www.frontiersin.org/articles/10.3389/fpls.2021.800077/full#supplementary-material

REFERENCES

Araus, J. L., Ferrio, J. P., Buxo, R., and Voltas, J. (2007). The historical perspective of dryland agriculture: Lessons learned from 10,000 years of wheat cultivation. *J. Exp. Bot.* 58, 131–145. doi: 10.1093/jxb/erl133

Bari, R., and Jones, J. D. (2009). Role of plant hormones in plant defence responses. *Plant. Mol. Biol.* 69, 473–488. doi: 10.1007/s11103-008-9435-0

Belanger, R. R., Benhamou, N., and Menzies, J. G. (2003). Cytological Evidence of an Active Role of Silicon in Wheat Resistance to Powdery Mildew (*Blumeria graminis* f. sp. *tritici*). *Phytopathology* 93, 402–412. doi: 10.1094/PHYTO.2003.93.4.402

Blümke, A., Somerville, S. C., and Voigt, C. A. (2013). Transient expression of the *Arabidopsis thaliana* callose synthase PMR4 increases penetration resistance to powdery mildew in barley. *Adv. Biosci. Biotechnol.* 4, 810–813. doi: 10.4236/abb.2013.48106

Chowdhury, J., Schober, M. S., Shirley, N. J., Singh, R. R., Jacobs, A. K., Douchkov, D., et al. (2016). Down-regulation of the glucan synthase-like 6 gene (*HvGsl6*) in barley leads to decreased callose accumulation and increased cell wall penetration by *Blumeria graminis* f. sp. *hordei*. *New Phytol.* 212, 434–443. doi: 10.1111/nph.14086

Dong, X., Hong, Z., Chatterjee, J., Kim, S., and Verma, D. P. S. (2008). Expression of callose synthase genes and its connection with Npr1 signaling pathway during pathogen infection. *Planta* 229, 87–98. doi: 10.1007/s00425-008-0812-3

Ellinger, D., Naumann, M., Falter, C., Zwikowics, C., Jamrow, T., Manisseri, C., et al. (2013). Elevated early callose deposition results in complete penetration resistance to powdery mildew in Arabidopsis. *Plant. Physiol.* 161, 1433–1444. doi: 10.1104/pp.112.211011

Enns, L. C., Kanaoka, M. M., Torii, K. U., Comai, L., Okada, K., and Cleland, R. E. (2005). Two callose synthases, GSL1 and GSL5, play an essential and redundant role in plant and pollen development and in fertility. *Plant. Mol. Biol.* 58, 333–349. doi: 10.1007/s11103-005-4526-7

Huibers, R. P., Loonen, A. E., Gao, D., Van den Ackerveken, G., Visser, R. G., and Bai, Y. (2013). Powdery mildew resistance in tomato by impairment of *SlPMR4* and *SlDMR1*. *PLoS One* 8:e67467. doi: 10.1371/journal.pone.0067467

Jacobs, A. K., Lipka, V., Burton, R. A., Panstruga, R., Strizhov, N., Schulze-Lefert, P., et al. (2003). An Arabidopsis callose synthase, GSL5, is required for wound and papillary callose formation. *Plant Cell* 15, 2503–2515. doi: 10.1105/tpc.016097

Kacprzak, P., Macioszek, V. K., and Kononowicz, A. K. (2011). Induced systemic resistance (isr) in the protection of plants against pathogenic fungi. *Postepy. Biol. Komorki.* 38, 129–142.

Koo, A. J., and Howe, G. A. (2009). The wound hormone jasmonate. *Phytochemistry* 70, 1571–1580. doi: 10.1016/j.phytochem.2009.07.018

Legentil, L., Paris, F., Ballet, C., Trouvelot, S., Daire, X., Vetvicka, V., et al. (2015). Molecular interactions of β-(1→ 3)-glucans with their receptors. *Molecules* 20, 9745–9766. doi: 10.3390/molecules20069745

Li, G., Cowger, C., Wang, X., Carver, B. F., and Xu, X. (2019). Characterization of *Pm65*, a new powdery mildew resistance gene on chromosome 2AL of a facultative wheat cultivar. *Theor. Appl. Genet.* 132, 2625–2632. doi: 10.1007/s00122-019-03377-2

Li, M. M., Dong, L. L., Li, B. B., Wang, Z. Z., Xie, J. Z., Qiu, D., et al. (2020). A CNL protein in wild emmer wheat confers powdery mildew resistance. *New Phytol.* 228, 1027–1037. doi: 10.1111/nph.16761

Livak, K. J., and Schmittgen, T. D. (2001). Analysis of Relative Gene Expression Data Using Real-Time Quantitative PCR and the $2^{-\Delta\Delta CT}$ Method. *Methods* 25, 402–408. doi: 10.1006/meth.2001.1262

Lu, Y., Wang, J., Chen, B., et al. (2021). A donor-DNA-free CRISPR/Cas-based approach to gene knock-up in rice. *Nat. Plants* 7, 1445–1452. doi: 10.1038/s41477-021-01019-4

Mangin, L. (1895). Recherches sur les Péronosporées. *Bull. Société d'Hist. Nat. d'Autun* 8, 55–108.

Martinez, M. I. S., Bracuto, V., Koseoglou, E., Appiano, M., Jacobsen, E., Visser, R. G. F., et al. (2020). CRISPR/Cas9-targeted mutagenesis of the tomato susceptibility gene *PMR4* for resistance against powdery mildew. *BMC Plant. Biol.* 20:284–287. doi: 10.1186/s12870-020-02497-y

McDonald, B. A., and Linde, C. (2002). The population genetics of plant pathogens and breeding strategies for durable resistance. *Euphytica* 124, 163–180. doi: 10.1023/A:1015678432355

McLusky, S. R., Bennett, M. H., Beale, M. H., Lewis, M. J., Gaskin, P., and Mansfield, J. W. (1999). Cell wall alterations and localized accumulation of feruloyl-3'-methoxytyramine in onion epidermis at sites of attempted penetration by Botrytis allii are associated with actin polarisation, peroxidase activity and suppression of flavonoid biosynthesis. *Plant. J.* 17, 523–534. doi: 10.1046/j.1365-313X.1999.00403.x

Mondal, S., Singh, R. P., Mason, E. R., Huerta-Espino, J., Autrique, E., and Joshi, A. K. (2016). Grain yield, adaptation and progress in breeding for early-maturing and heat-tolerant wheat lines in South Asia. *Field Crops Res.* 192, 78–85. doi: 10.1016/j.fcr.2016.04.017

Nishimura, M. T., Stein, M., Hou, B. H., Vogel, J. P., Edwards, H., and Somerville, S. C. (2003). Loss of a callose synthase results in salicylic acid-dependent disease resistance. *Science* 301, 969–972. doi: 10.1126/science.1086716

Pogue, G. P., Lindbo, J. A., Dawson, W. O., and Turpen, T. H. (1998). "Tobamovirus transient expression vectors: tools for plant biology and high level expression of foreign proteins in plants," in *Plant Molecular Biology Manual*, eds S. B. Gelvin and R. A. Schilperoot (Dordrecht: Kluwer Academic Publishers), 1–27. doi: 10.1385/0-89603-321-x:1

Rana, I. A., Salomon, S., Schafer, W., and Becker, D. (2014). Downregulation of *Glucan Synthase-Like* (*TaGSL*) genes in wheat leads to inhibition of transgenic plant regeneration. *In Vitro Cell. Dev. Biol. Plant.* 50, 696–706. doi: 10.1007/s11627-014-9636-y

Ryals, J., Uknes, S., and Ward, E. (1994). Systemic Acquired-Resistance. *Plant. Physiol.* 104, 1109–1112. doi: 10.4161/psb.1.4.3221

Shi, X., Sun, X., Zhang, Z., Feng, D., Zhang, Q., Han, L., et al. (2015). GLUCAN SYNTHASE-LIKE 5 (*GSL5*) plays an essential role in male fertility by regulating callose metabolism during microsporogenesis in rice. *Plant. Cell Physiol.* 56, 497–509. doi: 10.1093/pcp/pcu193

Shigenaga, A. M., and Argueso, C. T. (2016). No hormone to rule them all: Interactions of plant hormones during the responses of plants to pathogens. *Semin. Cell Dev. Biol.* 56, 174–189. doi: 10.1016/j.semcdb.2016.06.005

Shinoda, T. (1993). Callose reaction induced in melon leaves by feeding of melon aphid, *Aphis gossypii* Glover as possible aphid-resistant factor. *Jpn. J. Appl. Entomol. Zool.* 37, 145–152. doi: 10.1303/jjaez.37.145

Singh, A., Liang, Y. C., Kumar, P., Jiang, C. Z., and Reid, M. S. (2012). Co-silencing of the Mirabilis antiviral protein (MAP) permits virus-induced gene silencing (VIGS) of other genes in Four O'Clock plants (*Mirabilis jalapa*). *J. Horticult. Sci. Biotechnol.* 87, 334–340. doi: 10.1080/14620316.2012.11512873

Stotz, H. U., Pittendrigh, B. R., Kroymann, J., Weniger, K., Fritsche, J., Bauke, A., et al. (2000). Induced plant defense responses against chewing insects. Ethylene signaling reduces resistance of Arabidopsis against Egyptian cotton worm but not diamondback moth. *Plant. Physiol.* 124, 1007–1018. doi: 10.1104/pp.124.3.1007

Voigt, C. A. (2016). Cellulose/callose glucan networks: The key to powdery mildew resistance in plants? *New Phytol.* 212, 303–305. doi: 10.1111/nph.14198

Voigt, C. A., Schafer, W., and Salomon, S. (2006). A comprehensive view on organ-specific callose synthesis in wheat (*Triticum aestivum* L.): Glucan synthase-like gene expression, callose synthase activity, callose quantification and deposition. *Plant. Physiol. Biochem.* 44, 242–247. doi: 10.1016/j.plaphy.2006.05.001

Wang, X., Bai, J., Liu, H., Sun, Y., Shi, X., and Ren, Z. (2013). Overexpression of a maize transcription factor ZmPHR1 improves shoot inorganic phosphate content and growth of Arabidopsis under low-phosphate conditions. *Plant. Mol. Biol. Rep.* 31, 665–677. doi: 10.1007/s11105-012-0534-3

Wawrzynska, A., Rodibaugh, N. L., and Innes, R. W. (2010). Synergistic activation of defense responses in Arabidopsis by simultaneous loss of the GSL5 callose synthase and the EDR1 protein kinase. *Mol. Plant. Microbe Interact.* 23, 578–584. doi: 10.1094/MPMI-23-5-0578

Xie, J., Guo, G., Wang, Y., Hu, T., Wang, L., Li, J., et al. (2020). A rare single nucleotide variant in *Pm5e* confers powdery mildew resistance in common wheat. *New Phytol.* 228, 1011–1026. doi: 10.1111/nph.16762

Xu, Q., Tang, C. L., Wang, L. K., Zhao, C. C., Kang, Z. S., and Wang, X. J. (2020). Haustoria - arsenals during the interaction between wheat and *Puccinia striiformis* f. sp. *tritici*. *Mol. Plant Pathol.* 21, 83–94.

Yuan, C., Li, C., Yan, L., Jackson, A. O., Liu, Z., Han, C., et al. (2011). A high throughput barley stripe mosaic virus vector for virus induced gene silencing in monocots and dicots. *PLoS One* 6:e26468. doi: 10.1371/journal.pone.0026468

Zeng, X. W., Luo, Y., Zheng, Y. M., Duan, X. Y., and Zhou, Y. L. (2010). Detection of latent infection of wheat leaves caused by *Blumeria graminis* f. sp. *tritici* using nested PCR. *J. Phytopathol.* 158, 227–235. doi: 10.1111/j.1439-0434.2009.01594.x

Conflict of Interest: The authors declare that the research was conducted in the absence of any commercial or financial relationships that could be construed as a potential conflict of interest.

Publisher's Note: All claims expressed in this article are solely those of the authors and do not necessarily represent those of their affiliated organizations, or those of the publisher, the editors and the reviewers. Any product that may be evaluated in this article, or claim that may be made by its manufacturer, is not guaranteed or endorsed by the publisher.

frontiers | Frontiers in Plant Science

ORIGINAL RESEARCH
published: 05 April 2022
doi: 10.3389/fpls.2022.860170

An Aminobutyric Acid Transaminase in *Zea mays* Interacts With *Rhizoctonia solani* Cellulase to Participate in Disease Resistance

*Xiuna Guo, Jinyin Chen, Mengyi Gao and Duochuan Li**

Department of Plant Pathology, Shandong Agricultural University, Taian, China

Corn sheath blight, caused by AG1-IA, a fusion group of *Rhizoctonia solani*, which acts as a kind of necrotrophic fungal pathogen, poses a global threat to the production of *Zea mays*. Although cellulase plays a crucial role in *R. solani* infections, how plants respond to it is still poorly understood. In this study, we identified a gamma-aminobutyric acid transaminase (GABA-T), ZmGABA-T, in *Z. mays* that interacts with a cell wall–degrading enzyme (CWDE), EG1, in the cell membrane, using yeast two-hybrid assay, co-immunoprecipitation (Co-IP), and bimolecular fluorescence complementation assays. We found that the combination of EG1 and ZmGABA-T suppressed the allergic necrosis induced by EG1. We also found that the substrate of GABA-T–GABA, can inhibit the transcription of EG1. Transient expression of ZmGABA-T inhibited *R. solani* infection in *Nicotiana benthamiana*. The homolog in *Oryza sativa*, OsGABA-T, could also interact with EG1 to suppress the allergic necrosis induced by EG1. The OsGABA-T knocked out plants displayed enhanced susceptibility to *R. solani* and showed larger lesions. In conclusion, our results suggest that ZmGABA-T inhibits allergic necrosis induced by EG1 based on the combination with EG1, producing resistance to *R. solani* infection.

Keywords: ***Rhizoctonia solani*** **AG1-IA, EG1, gamma aminobutyric acid transaminase, allergic necrosis, disease resistance**

OPEN ACCESS

Edited by:
Xiaodong Wang,
Agricultural University of Hebei, China

Reviewed by:
Saeed Tarighi,
Ferdowsi University of Mashhad, Iran
Georgios Tzelepis,
Swedish University of Agricultural Sciences, Sweden

****Correspondence:***
Duochuan Li
lidc20@sdau.edu.cn

Specialty section:
This article was submitted to Plant Pathogen Interactions, a section of the journal Frontiers in Plant Science

Received: *22 January 2022*
Accepted: *04 March 2022*
Published: *05 April 2022*

Citation:
Guo X, Chen J, Gao M and Li D (2022) An Aminobutyric Acid Transaminase in Zea mays Interacts With Rhizoctonia solani Cellulase to Participate in Disease Resistance. Front. Plant Sci. 13:860170. doi: 10.3389/fpls.2022.860170

INTRODUCTION

Plants are constantly invaded by pathogens during their development. As a result, both have evolved a complex immune interaction network to fight each other called the "Invasion Model" (Kanyuka and Rudd, 2019). Pathogens are regarded as invasive molecules (IMs), and host receptors are called invasion pattern receptors. IMs are recognized by invasion pattern receptors and respond with apoplast-initiated immune responses and cytosol-initiated immune responses. Pathogen-associated molecular patterns (PAMPs) are typical IMs that induce PAMP-triggered immunity (PTI) *via* pattern recognition receptors (PRRs), leading to the accumulation of reactive oxygen species (ROS), calcium ion (Ca^{2+}) level elevation, the activation of defense-related genes, and hypersensitive responses (HRs) (Dangl and Jones, 2001; Desaki et al., 2006; Boller and Felix, 2009; Zipfel, 2009). Several studies have reported that some CWDEs, such as xyloglucanase (Ma Z. et al., 2015; Gui et al., 2017; Snarr et al., 2017; Mauff et al., 2019; Shen et al., 2020), endopolygalacturonases (Zhang et al., 2014), and cellulase (Ma Y. et al., 2015; Guo et al., 2021) can act as PAMPs and induce PTI, in which their PAMP activities can be independent of their enzymatic activities.

HRs defend against most pathogens, such as pathogenicity in biotrophic and hemibiotrophic fungi, preventing further development in early infection stages. They comprise a powerful protective mechanism for plants (Stergiopoulos and de Wit, 2009). However, some necrotrophic pathogens, such as *Rhizoctonia solani*, have been known to kill plants. Necrotrophic fungi kill host cells and obtain nutrients from dead plant tissues. Successful necrotrophic pathogens rely on the secretion of hydrolytic enzymes to macerate and digest plants for their development (Doehlemann et al., 2017). A large number of genes coding for CWDEs and other hydrolytic enzymes present in the genomes of necrotrophic fungi support this notion (Amselem et al., 2011). However, the infection process of necrotrophic pathogens is complex. The burst of ROS, which probably has multiple functions, mediates the life cycle of necrotrophic pathogens. Although they are considered to be a kind of defense response, they also serve as a virulence factor, at least in necrotrophic interactions (Doehlemann et al., 2017). For example, HRs facilitate the infection of plants by *Botrytis cinerea* (Govrin and Levine, 2000). During *Sclerotinia sclerotiorum* infection, oxalic acid induces increased ROS levels in plants, which correlates to cell death, thereby promoting infection (Kim et al., 2008).

To resist infection by diverse pathogens, plants have evolved various defense mechanisms. Salicylic acid (SA) contributes to plants' resistance to biotrophic and hemibiotrophic pathogens, whereas SA, jasmonate (JA), and ethylene (ET) all promote resistance to necrotrophic fungi (Tsuda et al., 2009). The Arabidopsis Botrytis Susceptible1 Interactor (BOI) aids disease resistance through the suppression of necrotrophic pathogens–induced cell death (Luo et al., 2010). Inhibitors of apoptosis proteins (IAPs) have a similar structure and function as BOI in animals (Vaux and Silke, 2005). Transgenic plants expressing baculovirus IAPs suppress cell death and are resistant to necrotrophic fungi (Dickman et al., 2001). A transcriptional repressor of gibberellin (GA) signaling, DELLA protein, promotes resistance to necrotrophic pathogens by altering the relative strength of SA and JA signaling (Navarro et al., 2008). The Arabidopsis pentatricopeptide repeat protein, peptidoglycan (PGN), regulates the ROS dynamic equilibrium in mitochondria to resist *B. cinerea* infection (Laluk et al., 2011). In contrast, the *Arabidopsis* BOTRYTIS-SUSCEPTIBLE1 (BOS) mutant is more susceptible to necrotrophic fungi (Mengiste et al., 2003).

Rhizoctonia solani acts as a necrotrophic fungus and harms gramineous crops, posing a severe threat to production. Necrotrophic fungi kill host cells and take nutrients from dead plant tissues to complete their life cycle. During this cycle, they secrete various cell necrosis–causing CWDEs and toxins to achieve a successful infection (Oliver and Solomon, 2010). There are many pathogenic factors in *R. solani*, such as the effector AGLIP1, which triggers cell death in plants and promotes disease development by inhibiting PTI, such as protection-related (PR) gene expression in *Arabidopsis thaliana* (Li et al., 2019). The RsRlpA effector is a protease inhibitor promoting the virulence of *R. solani* through suppression of the ROS burst and HR (Charova et al., 2020). The novel effector RsIA_NP8 in *R. solani* AG1-IA induces cell death and triggers defense responses in non-host plants (Wei et al., 2020). However, how plants interact with *R. solani* during the pathogenic infection process is not yet known. In this study, we identified a transaminase ZmGABA-T that interacts with EG1 and suppresses the allergic necrosis induced by it. We also found that the ZmGABA-T is located in the plasma membrane. GABA, the substrate of GABA-T, suppresses the transcription of EG1. Hence, we inferred that the GABA-T participates in the plant disease resistance process.

MATERIALS AND METHODS

Strains and Plasmids

Escherichia coli T1 was used for cloning and nucleotide sequencing. *Pichia pastoris* GS115 and plasmid vector pPIC9K were used for stable expression. *Agrobacterium* GV3101, plasmid vectors pGR106 and pROKII were used for transient expression.

Plant Material and Growth Conditions

Maize (*Zea mays*) plants (Non-gda 108 from Shandong, China, the most widely cultured hybrid in China) and *N. benthamiana* were grown at 25°C with 16 h of light and 8 h of darkness with a relative humidity of 60–70%. *Oryza sativa* (ZH11) and knockout mutants were grown at 28°C during the daytime and 26°C at night with 16 h of light and 8 h of darkness.

Microbial Cultures

Strains of *R. solani* were cultured in PDA medium (200 g potato infusion, 20 g dextrose, and 20 g agar/L). Different GABA concentrations (0, 30, 40, 50, 60, and 70 mM) were added to the PDA medium to explore the effect of concentrated GABA on the transcription of *EG1*.

Agrobacterium tumefaciens–Mediated Transient Expression on *Nicotiana benthamiana*

Agrobacterium tumefaciens-mediated transient expression was performed. Plasmid constructs were introduced into the *A. tumefaciens* strain GV3101. After culturing for 18 h in a liquid Luria Bertani medium at 28°C, the bacterial cells were harvested by centrifugation and resuspended in an infiltration medium (10 mM 2-morpholinoethanesulfonic acid, 10 mM $MgCl_2$, 150 μM acetosyringone, pH 5.6). The optical densities (ODs) of the cell suspensions in the infiltration medium were adjusted to OD_{600} = 0.6 (the final concentration for each strain in a mixture). Thereafter, the cells were incubated for 3 h at room temperature before infiltration into leaves of 4-week-old *N. benthamiana* plants or *Nicotiana tabacum*. The leaves were harvested for protein 48 h after infiltration.

Agrobacterium tumefaciens–Mediated Transient Expression on Onions

Agrobacterium tumefaciens strain GV3101 was cultivated with 200 μM of acetosyringone for 12 h, and the bacterial cells were harvested by centrifugation and resuspended in a Murashige

and Skoog (MS) liquid medium (with 200 μM acetosyringone). The ODs of the cell suspensions in the MS medium (with 200 μM acetosyringone) were adjusted to OD_{600} = 0.6 (the final concentration for each strain in a mixture). The inner epidermis of the onion was torn off and cultured in the MS medium (with 200 μM acetosyringone) for 24 h in the dark. We placed the onion's pre-cultured inner epidermis in the MS liquid medium (with 200 μM acetosyringone) to resuspend the bacteria solution, soaked it for 30 min, picked up a corner of the epidermis, drained the bacteria solution slightly, and reapplied it to the MS medium (with 200 μM acetosyringone), with a photoperiod of 16–18 h, and a total of 48 h at 25°C.

After the co-cultivation, small pieces of the onion's inner epidermis were taken out and washed with sterile water to remove the attached Agrobacterium. The epidermis was spread on a glass slide, observed, and photographed under a scanning microscope (LSM800, Zeiss). The GFP was detected with excitation at 488 nm and emission at 525 nm, and mCherry was detected with excitation at 552 nm and emission at 600 nm.

Reactive Oxygen Species Detection

3,3-Diaminobenzidine (DAB, 5 mg/mL) was used to detect ROS accumulation in *N. benthamiana*. Three days after the infection, leaves immersed in DAB were vacuumed for 30 min and then lighted for 4 h. After that, the liquid was discarded and the leaves were washed with 95% ethanol and boiled in water at 95°C. The system was allowed to stand until all the chlorophyll had dissolved, then the leaves were transferred to 50% ethanol for preservation and photographed.

Protein Extraction and Detection

For enzyme activity determination, proteins expressed by *N. benthamiana* were extracted by phosphate buffer (1 × protein inhibitor cocktail, CWBIO). And for general purposes, proteins were extracted by lysis buffer (NP-40, Beyotime).

Co-immunoprecipitation Assay

Leaves of *N. benthamiana* were co-infiltrated with *A. tumefaciens* carrying ZmGABA-T-HA and EG1-eGFP, OsGABA-T-HA and EG1-eGFP, NtGABA-T-HA and EG1-eGFP, and AtGABA-T-HA and EG1-eGFP. The infiltrated leaves were harvested after 2 days and then ground to powder in liquid nitrogen, and suspended in a lysis buffer (NP-40, Beyotime). Anti-GFP agarose bead suspension (AlpaLife by KanTi) was added to the protein supernatants. The mixture was incubated at 4°C for 8 h with constant end-over-end rotation. Then the beads were rinsed with washing buffer (10 mM Tris-HCl, pH 7.5, 0.5 mM EDTA, 150 mM NaCl), and the anti-GFP agarose mixtures were collected for Western blotting following SDS–PAGE by 2 × SDS loading buffer. Fusion proteins were detected by anti-HA and anti-GFP antibodies, respectively, according to the EasySee Western Blot Kit (Transgene, China) with the Chenpchemi series chemiluminescence/multicolor fluorescence/visible light gel imaging system.

Pull-Down Assay

Recombinant EG1 was purified from *P. pastoris* GS115, AtGABA-T-eGFP and NtGABA-T-eGFP were expressed by transient expression in *N. benthamiana*, and then extracted proteins were collected on anti-GFP beads (AlpaLife by KanTi). The EG1 proteins were mixed with the beads carrying AtGABA-T or NtGABA-T at a final concentration of 10 μM in a buffer (10 mM Tris-HCl, pH 7.5, 0.5 mM EDTA, 150 mM NaCl), and incubated for 1 h at 4°C. Western blotting was then performed as described above.

BiFC Assay and Microscopy

Contrast vectors EG1-cYFP and ZmGABA-T-nYFP were transformed into *A. tumefaciens*. Thereafter, *A. tumefaciens* was infiltrated onto *N. benthamiana* leaves. The leaves were observed under a confocal laser scanning microscope (LSM880, Zeiss) 48 h after the infiltration, and YFP was detected with excitation at 488 nm and emission at 515 nm.

Furthermore, pGR106 carried with EG1-eGFP and mCherry–ZmGABA-T were transformed into *A. tumefaciens*. Thereafter, *A. tumefaciens* were infiltrated onto *N. benthamiana* leaves. After 48 h infiltration. The leaves were observed under a confocal laser scanning microscope (LSM800, Zeiss) 48 h after the infiltration, and mCherry was detected with excitation at 552 nm and emission at 600 nm.

Enzyme Activity Determination

Enzyme activity was measured using the 3,5-dinitrosalicylic acid (DNS) method (Sumner, 1925; Miller, 1959). To explore the influence of ZmGABA-T on EG1 enzyme activity, EG1 expressed by *P. pastoris* GS115 was co-incubated with ZmGABA-T and pGR106 expressed by *N. benthamiana* at 50°C for 30 min. Next, 1% carboxymethylcellulose sodium (CMC–Na) was used as the enzyme substrate, and phosphate buffer (pH 5.0) was used as the buffer system. Then DNS was used to determine glucose content and measure absorbance at OD_{540}.

To understand the effect of GABA concentration on EG1 enzyme activity, GABA concentrations ranging from 30 to 70 mM were added into an enzymatic reaction system. EG1 expressed by *P. pastoris* GS115 was co-incubated with 1% CMC–Na and GABA at 50°C in a phosphate buffer (pH 5.0) for 30 min. Then DNS was used to determine glucose content and absorbance was measured at OD_{540}.

Quantitative PCR

Zea mays leaves injected with purified EG1 expressed by *P. pastoris* GS115 were harvested at different time points and ground in liquid nitrogen for RNA extraction with TRIzol. The first strand of cDNA was synthesized from 1 μg total RNA using TransScript All-in-One First Strand cDNA Synthesis SuperMix (Transgen, China). qRT-PCR was assayed by TransStart Top Green qPCR SuperMix (Transgen, China). Each PCR tube contained 10 μL of Top Green qPCR SuperMix, 25 ng of cDNA, and 0.2 μM of each primer. The thermal cycling conditions were 30 s at 94°C, followed by 40 cycles of 5 s at 94°C and 15 s at 55°C by Roche LightCycler 96.

Rhizoctonia solani was cultured in PDA with different GABA concentrations for 3 days and was collected in liquid nitrogen for RNA extraction and qRT-PCR as described above.

For biomass measurement, total DNA was extracted by the Plant Genomic DNA Kit (TIANGEN, China), and qPCR was assayed by the TransStart Top Green qPCR SuperMix (Transgen, China).

Rice Transformation

CRISPR/Cas9-mediated gene-editing vectors were constructed according to previous reports (Ma et al., 2016). Transgenic experiments were performed using *A. tumefaciens–mediated* callus transformation in the *japonica* variety ZH11.

RESULTS

EG1 Interacts With ZmGABA-T

To find the protein that interacts with EG1 in plants, we identified potential host protein targets using DUAL membrane yeast two-hybrid (Y2H) assays. We independently screened the EG1 forms as baits against a prey library from RNA prepared at 72 h postinoculation of *Z. mays* injected with EG1 protein. A total of 43 positive colonies were captured by the bait EG1 (**Figures 1A,B**).

According to the analysis of results of the 43 positive colonies, we found that the protein that was most likely to interact with EG1 was ZmGABA-T and chose to make it the focus of our study. We linked the EG1 without its signal peptide with a bait construct because the secreted protein EG1 owned the signal peptide. We also connected the ZmGABA-T to the prey construct. Point-to-point verification showed that all transformants grew on the SD/-Trp-Leu, but only yeasts containing both EG1 and ZmGABA-T could grow on the SD/-Trp-Leu-Ade-His media (**Figure 1C**).

To prove that EG1 can interact with ZmGABA-T in plants, co-immunoprecipitation (co-IP) assays were performed by transient expression in *N. benthamiana*. The proteins were pulled down with GFP beads and were all present in the relevant input samples except for ZmGABA-T-HA, which was co-immunoprecipitated in the presence of EG1-eGFP (**Figure 1D**).

Then EG1 and ZmGABA-T were fused to the construct with yellow fluorescent protein (YFP), which was divided into N-terminal and C-terminal to generate EG1-cYFP or ZmGABA-T-nYFP. In addition, the two empty constructs, nYFP and cYFP, were used as a negative control. Co-expression of EG1-cYFP and ZmGABA-T-nYFP in *N. benthamiana* resulted in YFP fluorescence signals located in the cytoplasmic membrane 72 h post-infiltration (hpi). The EG1-cYFP/nYFP and ZmGABA-T-nYFP/cYFP combinations failed to fluoresce, demonstrating that neither EG1 nor ZmGABA-T produced non-specific fluorescence in *N. benthamiana* (**Figure 1E**). All these results indicate that EG1 interacts with ZmGABA-T in plants.

We fused mCherry to the N-terminal of ZmGABA-T, with the transient expression of mCherry–ZmGABA-T in *N. benthamiana*. This resulted in red fluorescence signals in the cytoplasmic membrane 48 hpi. The plasmolysis of the onion epidermal cells returned similar results, the EG1-eGFP colocalized with mCherry–ZmGABA-T in the onions cell membrane (**Figure 2**).

ZmGABA-T and Gamma-Aminobutyric Acid Transaminase Work Together to Suppress Allergic Necrosis Induced by EG1

Five days after the EG1 and ZmGABA-T were co-injected into the *N. benthamiana*, we found that the allergic necrosis caused by EG1 was weakened (**Figure 3A**). The ROS detected by 3,3-di-aminobenzidine (DAB) also showed weakened symptoms (**Figure 3B**).

To explore why the allergic necrosis was suppressed, the EG1 and ZmGABA-T were expressed by yeast and *N. benthamiana*, respectively. Then, proteins were used to detect the enzyme activity by DNS. After enzymatic reaction for 30 min at 50°C, there was no significant difference in the specific vitality of EG1 in the presence of ZmGABA-T. Therefore, we concluded that ZmGABA-T could not affect EG1 enzyme activity (**Figure 3C**).

Then the co-expressed proteins by *N. benthamiana* were extracted. A Western blotting analysis showed that the expression of EG1-eGFP was significantly reduced in the presence of ZmGABA-T–HA (**Figure 1D**). To prove the results, we increased the concentration of ZmGABA-T—-HA gradually and then co-expressed ZmGABA-T–HA and EG1-eGFP in *N. benthamiana*. The result showed that the expression of EG1-eGFP was reduced because of the increased concentration of ZmGABA-T–HA (**Figure 3D**). The above results proved that ZmGABA-T promotes EG1 degradation and suppresses the EG1-induced allergic necrosis in *N. benthamiana*.

γ-Aminobutyric acid (GABA) plays an important role in the metabolism of amino acids (Ludewig et al., 2008). We added different concentrations of GABA to the EG1 enzymatic reaction system and found that GABA did not affect EG1 enzyme activity (**Figure 4A**). Thereafter, we added GABA to the culture medium of *R. solani*, and the transcription of *EG1* was detected by the qPCR. However, we were surprised to see that increased GABA concentration led to decreased *EG1* transcription (**Figure 4B**). Based on this result, we concluded that GABA repressed *EG1* transcription during *R. solani* infection. All these results prove that ZmGABA-T and GABA work together to inhibit allergic necrosis induced by EG1.

ZmGABA-T Suppresses the Infection of *Rhizoctonia solani*

To explore the function of ZmGABA-T, the leaves of *N. benthamiana*, which have transiently expressed ZmGABA-T 36 h after, were inoculated with *R. solani*. Leaves that expressed pGR106 were used as a negative control. Infection lesion sizes were recorded for comparison 4 days after inoculation with *R solani*. We found that, compared with the negative control, leaves that expressed ZmGABA-T showed smaller lesions (**Figures 5A,B**). Measurement of fungal DNA by quantitative PCR was used to quantify fungal colonization of the host tissues. There was a fivefold reduction in the fungal

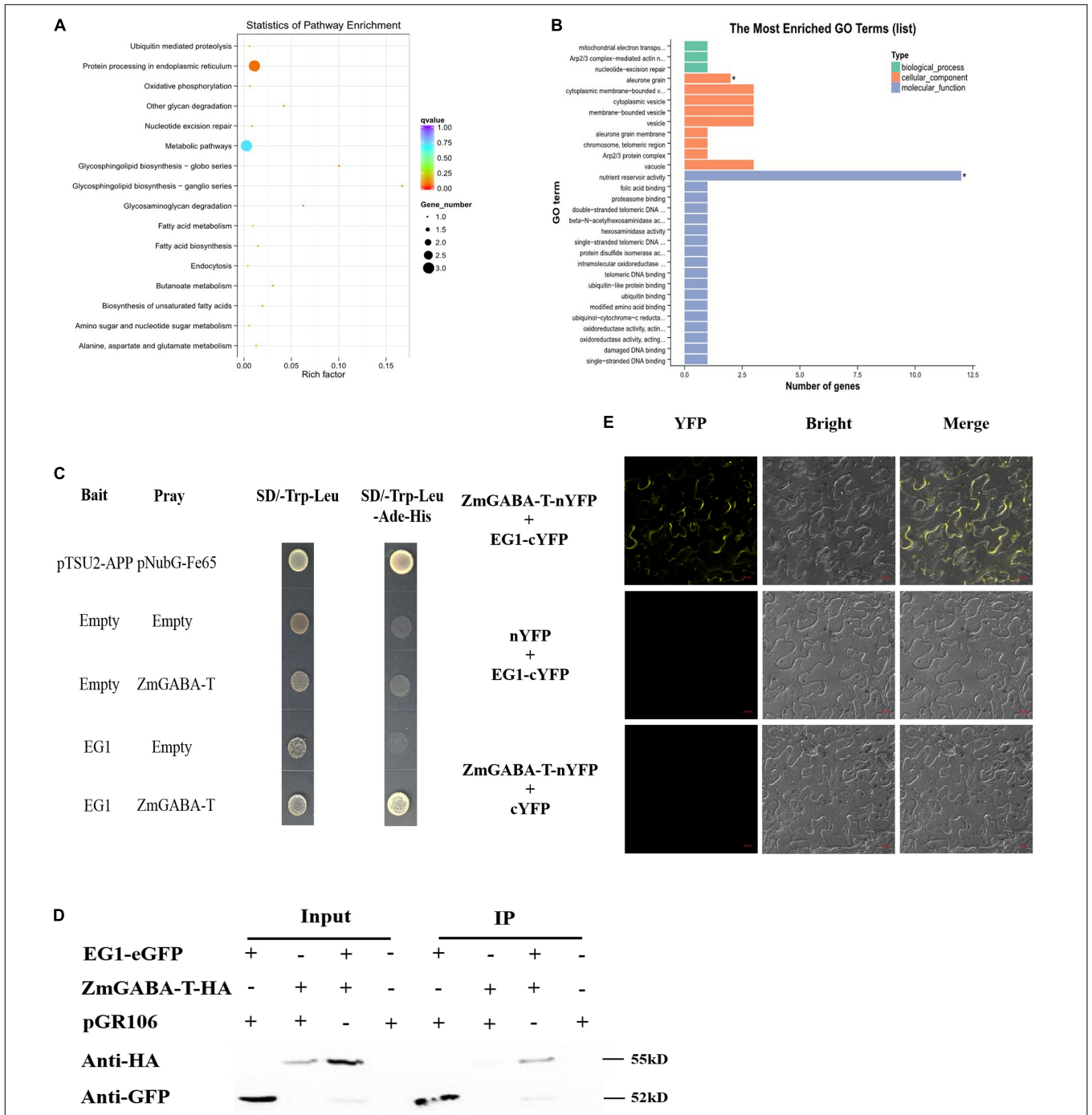

FIGURE 1 | EG1 interacts with ZmGABA-T. **(A)** Biological function pathways of candidate genes. There are 43 genes in total. And all the 43 genes were classified into 16 types according to their functions: Ubiquitin-mediated proteolysis, protein processing in the endoplasmic reticulum, oxidative phosphorylation, other glycan degradation, nucleotide excision repair, metabolic pathways, glycosphingolipid biosynthesis–globo series, ganglio series, glycosaminoglycan degradation, fatty acid metabolism, fatty acid biosynthesis, endocytosis, butanoate metabolism, biosynthesis of unsaturated fatty acids, amino sugar, and nucleotide sugar metabolism, and alanine, aspartate, and glutamate metabolism. **(B)** Gene Ontology (GO) analysis of candidate genes. The function of genes is divided into three parts: Biological process, cellular component, and molecular function. And the genes function of nutrient reservoir activity has the largest number. Enriched P-values less than 0.05 are marked with "*". **(C)** Interactions between EG1 with ZmGABA-T in the DUAL membrane yeast 2 hybrid system. Yeast NMY32 cells cotransformed with bait and prey vectors were grown on QDO (SD/–Ade/–His/–Leu/–Trp) medium. The combination of pTSU2-APP and pNubG-Fe65 was used as a positive control, while the combination of pTSU2-APP and pPR3N was used as the negative control. **(D)** Interactions between EG1 with ZmGABA-T in *Nicotiana benthamiana*. pGR106 carried EG1-EGFP and ZmGABA-T-HA, respectively, were coexpressed in *Nicotiana benthamiana.* Around 48 h after infiltration, immunoprecipitates obtained from whole-cell extracts using anti-GFP trap beads were analyzed by immunoblotting with anti-HA and anti-GFP antibodies. This experiment was repeated three times with the same results. **(E)** BiFC assay in *Nicotiana benthamiana.* Bars = 20 μm.

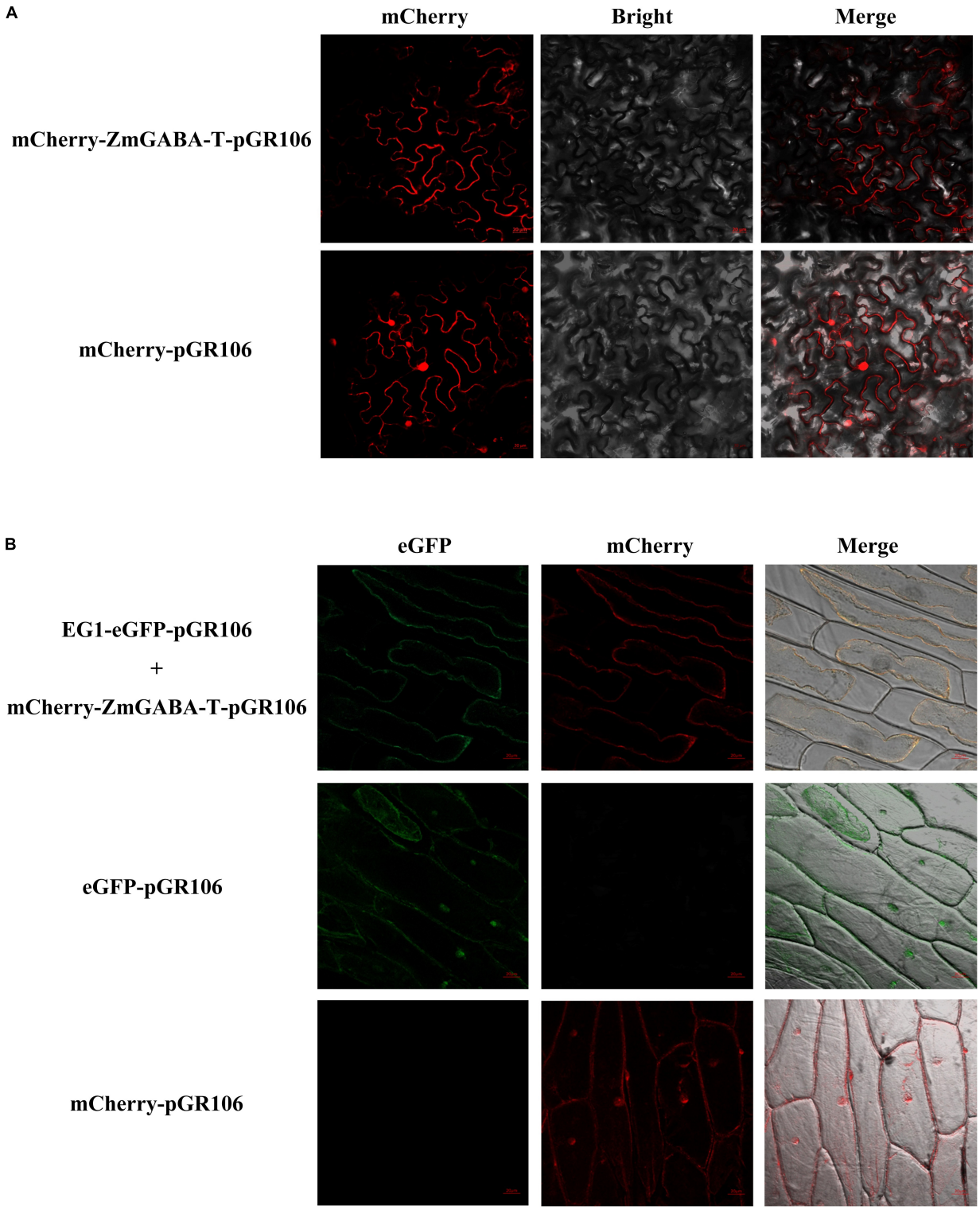

FIGURE 2 | Subcellular localization of ZmGABA-T and EG1 in *Nicotiana benthamiana* and onions. **(A)** Subcellular localization of ZmGABA-T. mCherry fused with ZmGABA-T were transiently expressed by *A. tumefaciens* in *Nicotiana benthamiana* 48 h after infiltration. **(B)** Co-localization of EG1 and ZmGABA-T. For coexpressed, EG1 fused with eGFP and mCherry fused with ZmGABA-T were coexpressed in onions 48 h after infiltration. After 48 h of co-cultivation on MS medium and plasmolysis with 1 M NaCl to induce cytoplasmic separation, both red and green fluorescent signals were found on the cell membrane. The infiltrated *N. benthamiana* leaves and onion's epidermal cells were observed *via* fluorescence microscopy. The eGFP and mCherry were used as check samples. The merged image of two fluorescence signals is shown on the right. Bars = 20 μm.

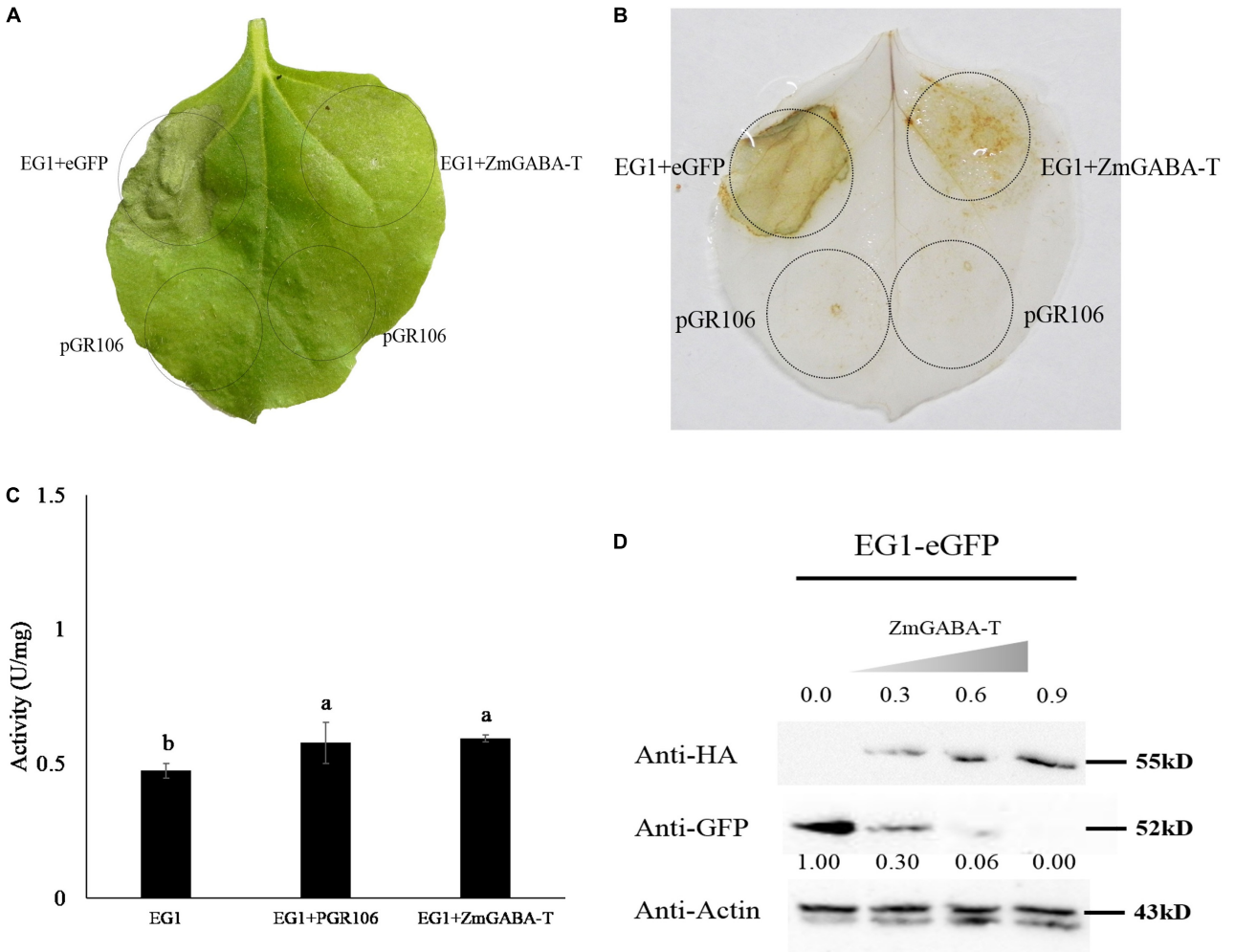

FIGURE 3 | ZmGABA-T suppresses allergic necrosis induced by EG1 according to promoting the degradation of EG1, rather than inhibit the enzyme activity of EG1. **(A)** Transient expression of EG1 and ZmGABA-T in *Nicotiana benthamiana*. Transient expression was operated in *Nicotiana benthamiana* leaves injected with *Agrobacterium* carrying the indicated genes, pGR106, eGFP, EG1, and ZmGABA-T. eGFP and EG1 were coexpressed on the left of the leaf, and ZmGABA-T and EG1 were coexpressed on the right. Experiments were repeated three times at least with similar results. **(B)** ROS detection of EG1 and ZmGABA-T. The transient expression of *Nicotiana benthamiana* leaves inoculated with eGFP and EG1, ZmGABA-T and EG1 were dyed with 5 mg/mL DAB (3,3-diaminobenzidine). Transient expression was assessed in *Nicotiana benthamiana* leaves from 4-week-old plants 5 days after agroinfiltration, and pGR106 empty vector was used as a control. Experiments were repeated three times at least with similar results. **(C)** Enzyme activity determination of EG1 and ZmGABA-T. Co-incubation EG1 (1 μM) expressed by *Pichia pastoris* GS115 with pGR106 and ZmGABA-T expressed by *Nicotiana benthamiana* (2 mg/mL) separately at 50°C for 30 min, then dinitrosalicylic acid (DNS) was used to determine glucose content, and measured absorbance at OD_{540}, thereby calculated enzyme activity of EG1. The results of the experiment were repeated three times at least. Lower-case letters indicate statistically significant differences ($P < 0.05$). **(D)** Co-expression of EG1-eGFP and ZmGABA-T-HA in *Nicotiana benthamiana*. The concentration of inoculation about ZmGABA-T was increased sequentially from OD_{600} = 0 to 0.9, while the concentration of EG1 was OD_{600} = 0.5. The numbers in the first row indicated the inoculation concentration of ZmGABA-T-HA. The numbers in the second row indicated the gray value of EG1. The results of the experiment were repeated three times at least.

colonization of the host in leaves that had transiently expressed ZmGABA-T (**Figure 5C**).

EG1 Interacts With OsGABA-T Specifically

To explore whether EG1 interacts with ZmGABA-T specifically, we compared different kinds of GABA-T around *Z. mays*, *O. sativa*, *Arabidopsis thaliana*, and *N. tabacum* (**Supplementary Figure 1A**), all of which had a Pyridoxal-5′-phosphate–binding domain (Ser/Thr-X-X-Lys). Yeast two-hybrid assay showed that OsGABA-T can interact with EG1. Co-IP proved that OsGABA-T interacts with EG1 weakly in *N. benthamiana* (**Figure 6**), and pull-down assay showed that EG1 interacts with neither AtGABA-T nor NtGABA-T (**Supplementary Figures 1B,C**).

So we continued to explore if OsGABA-T has the same function as ZmGABA-T. Transient expression of OsGABA-T and EG1 showed that the allergic necrosis induced by EG1 was attenuated (**Figure 7A**). The ROS detected by DAB also showed an obvious weakening of the symptoms (**Figure 7B**).

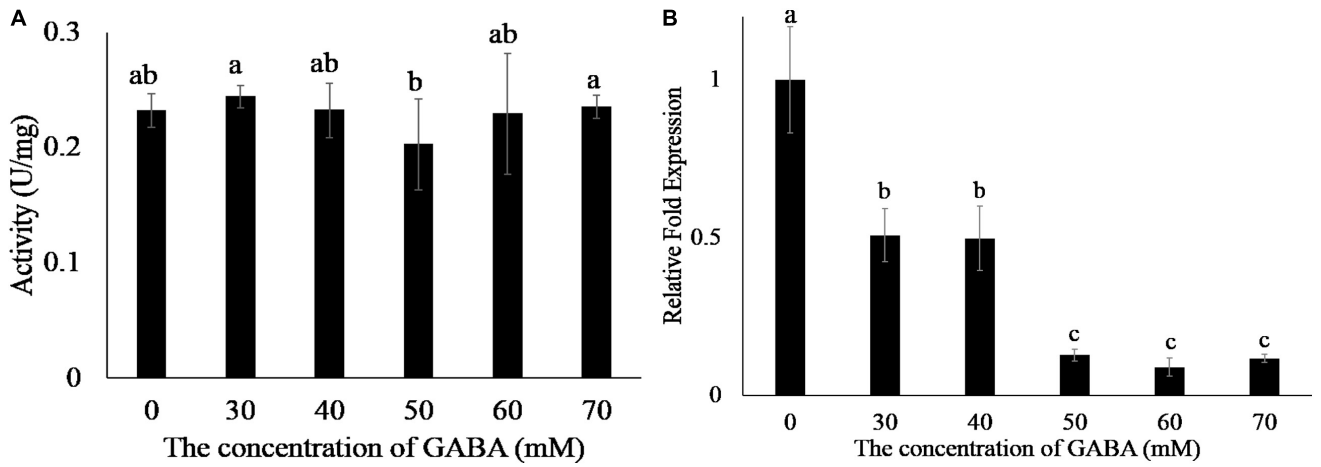

FIGURE 4 | GABA does not affect the enzyme activity of EG1 but suppresses the transcription of *EG1*. **(A)** Enzyme activity determination of EG1 after adding different concentrations of GABA. Different concentrations of GABA were added to the enzymatic reaction system, and DNS was used to detect the content of glucose. The experiments were repeated three times with the same results. Lowercase letters indicate statistically insignificant differences ($P > 0.05$). **(B)** The effect of different concentrations of GABA on the transcription of *EG1*. Different concentrations of GABA were added to the Potato Dextrose Agar (PDA) medium, then *Rhizoctonia solani* was grown on PDA medium with GABA for 3 days. Total RNA was extracted 3 days after training. Then qRT-PCR was used to detect the transcription level of *EG1*. The results of the experiment were repeated three times at least. Lower-case letters indicate statistically significant differences ($P < 0.05$).

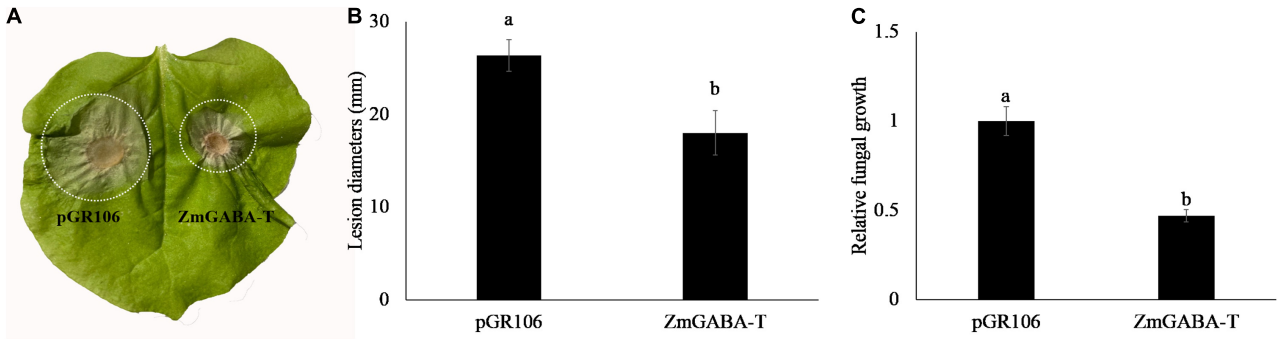

FIGURE 5 | Expression of ZmGABA-T can inhibit *Rhizoctonia solani* infection. **(A)** *Rhizoctonia solani* infection on *Nicotiana benthamiana*. *N. benthamiana* leaves were inoculated by *Rhizoctonia solani* AG1-IA after transient expression of pGR106 vector and ZmGABA-T at 36 h, and photographed at 72 h post-inoculation. **(B)** Lesion diameters of infected *Nicotiana benthamiana* leaves. Lesion diameters were calculated from three independent biological replicates. Error bars represent ± SD of at least six leaves each. Lower-case letters indicate statistically significant differences ($P < 0.05$). **(C)** Quantitative PCR was performed for quantification of relative fungal growth on inoculated leaves $2^{(Ct\_NbActin - Ct\_Rsdna)}$. The values represent the means ± SD of six independent tests. Lower-case letters indicate statistically significant differences ($P < 0.05$).

Knockout of OsGABA-*T* Reduces Rice Resistance to *Rhizoctonia solani*

Two independent transgenic rice lines whose *OsGABA-T* were knocked out by CRISPR (Os-24 and Os-31) were tested for OsGABA-T expression. A cytosine (C) or guanine (G) residue was inserted into the putative U3-gRNA target site, and thymine (T) was inserted into the putative U6a-gRNA target site or a guanine–adenine–adenine (GAA) sequence was lost from the U6a-gRNA target site (**Figure 8A**). Both caused an 80% more reduction in OsGABA-T expression than the non-transformed line ZH11 wild type at 4 weeks (**Figure 8B**). Mutant plants exhibited reduced resistance against *R. solani* (**Figure 8C**). The measurement of fungal DNA by qPCR was used to quantify the fungal colonization of the host tissue. Compared with the wild type, the lesion length of Os-24 and Os-31 were significantly increased (**Figure 8D**). There was a 15-fold increase in the fungal colonization of the host in Os-24 and Os-31 plants (**Figure 8E**). All the results showed that mutant plants increased sensitivity to *R. solani*.

DISCUSSION

The HR refers to cell death induced by pathogenic infections and is a classical indicator of resistance. Cell death has markedly different functions in plant responses to necrotrophs and biotrophs. HR is thought to confine pathogens by abolishing nutrient supply, thereby limiting the growth of pathogens in

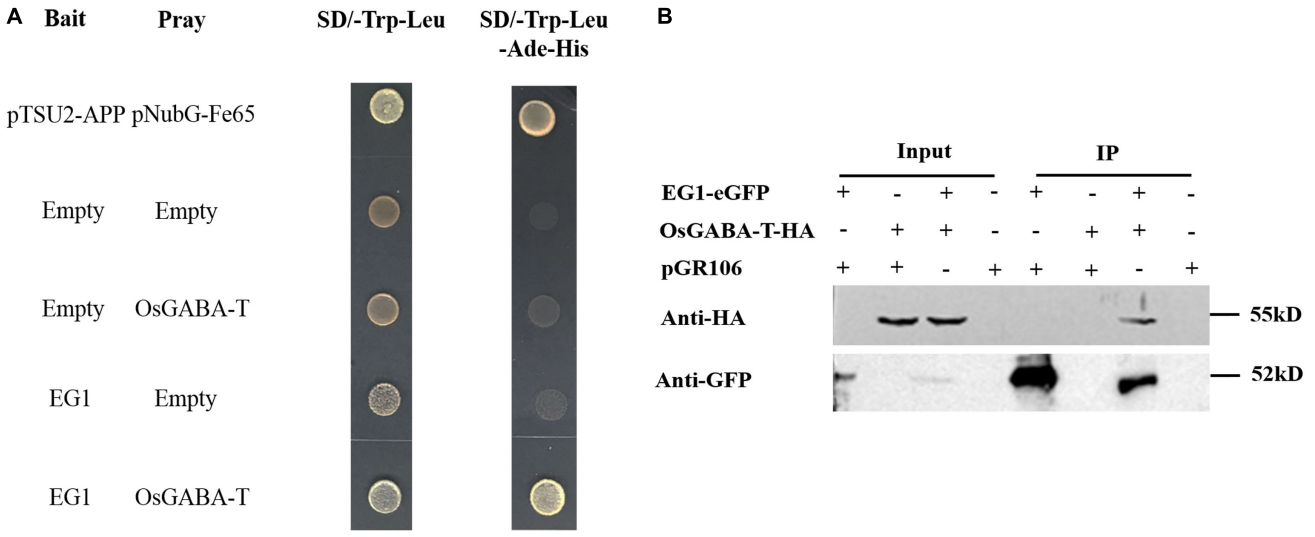

FIGURE 6 | EG1 interacts with OsGABA-T. **(A)** Interactions between EG1 with OsGABA-T in the DUAL membrane yeast 2 hybrid system. Yeast NMY32 cells cotransformed with bait and prey vectors were grown on QDO (SD/–Ade/–His/–Leu/–Trp) medium. The combination of pTSU2-APP and pNubG-Fe65 was used as a positive control, while the combination of pTSU2-APP and pPR3N was used as the negative control. **(B)** Interactions between EG1 with OsGABA-T in *Nicotiana benthamiana*. pGR106 carried EG1-EGFP and OsGABA-T-HA were coexpressed in *Nicotiana benthamiana*; 48 h after infiltration, immunoprecipitates obtained from whole-cell extracts using anti-GFP trap beads were analyzed by immunoblotting with anti-HA and anti-GFP antibodies. This experiment was repeated three times with similar results.

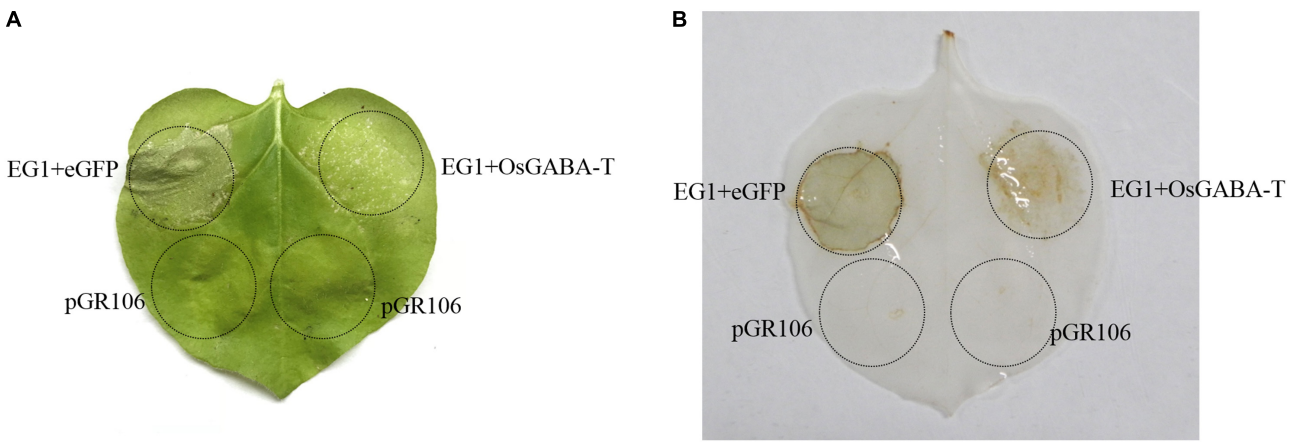

FIGURE 7 | OsGABA-T suppresses allergic necrosis induced by EG1. **(A)** Transient expression of EG1 and OsGABA-T in *Nicotiana benthamiana*. Transient expression was operated in *Nicotiana benthamiana* leaves injected *Agrobacterium* carrying the indicated genes, pGR106, eGFP, EG1, and OsGABA-T. eGFP and EG1 were coexpressed on the left of the leaf, OsGABA-T and EG1 were coexpressed on the right. Experiments were repeated three times at least with similar results. **(B)** ROS detection of EG1 and OsGABA-T. The transient expression of *Nicotiana benthamiana* leaves inoculated with eGFP and EG1, and OsGABA-T and EG1 were dyed with 5 mg/mL 3,3-diaminobenzidine (DAB). Transient expression was assessed in *Nicotiana benthamiana* leaves from 4-week-old plants 5 days after agroinfiltration, and pGR106 empty vector was used as a control. Experiments were repeated three times at least with similar results.

biotrophs (Mengiste, 2012). However, cell death also occurs at the early stage of necrotrophic pathogens infection and promotes further infection (Govrin et al., 2006; van Kan, 2006). Necrotrophic fungi, including *R. solani*, kill the cells and tissues of the host plant and then draw nutrients from them. Successful necrotrophs rely on a large number of hydrolytic enzymes for the maceration and utilization of the plant as their source of nutrition (Doehlemann et al., 2017). As a countermeasure, plants develop surveillance systems to perceive necrotrophic fungi and activate their innate immunity, like the signal of chitin perception, the regulation of mitogen-activated protein kinase, and the modification of histones (McGrath et al., 2005; Veronese et al., 2006; Kemmerling et al., 2007; Berr et al., 2010; Lenz et al., 2011; Li et al., 2012; Zhang et al., 2012). In our previous study, we proved that the cellulase EG1 secreted by *R. solani* can act as a PAMP that participates in plant immune responses (Ma Y. et al., 2015; Guo et al., 2021). In this study, we identified ZmGABA-T, a GABA-T from

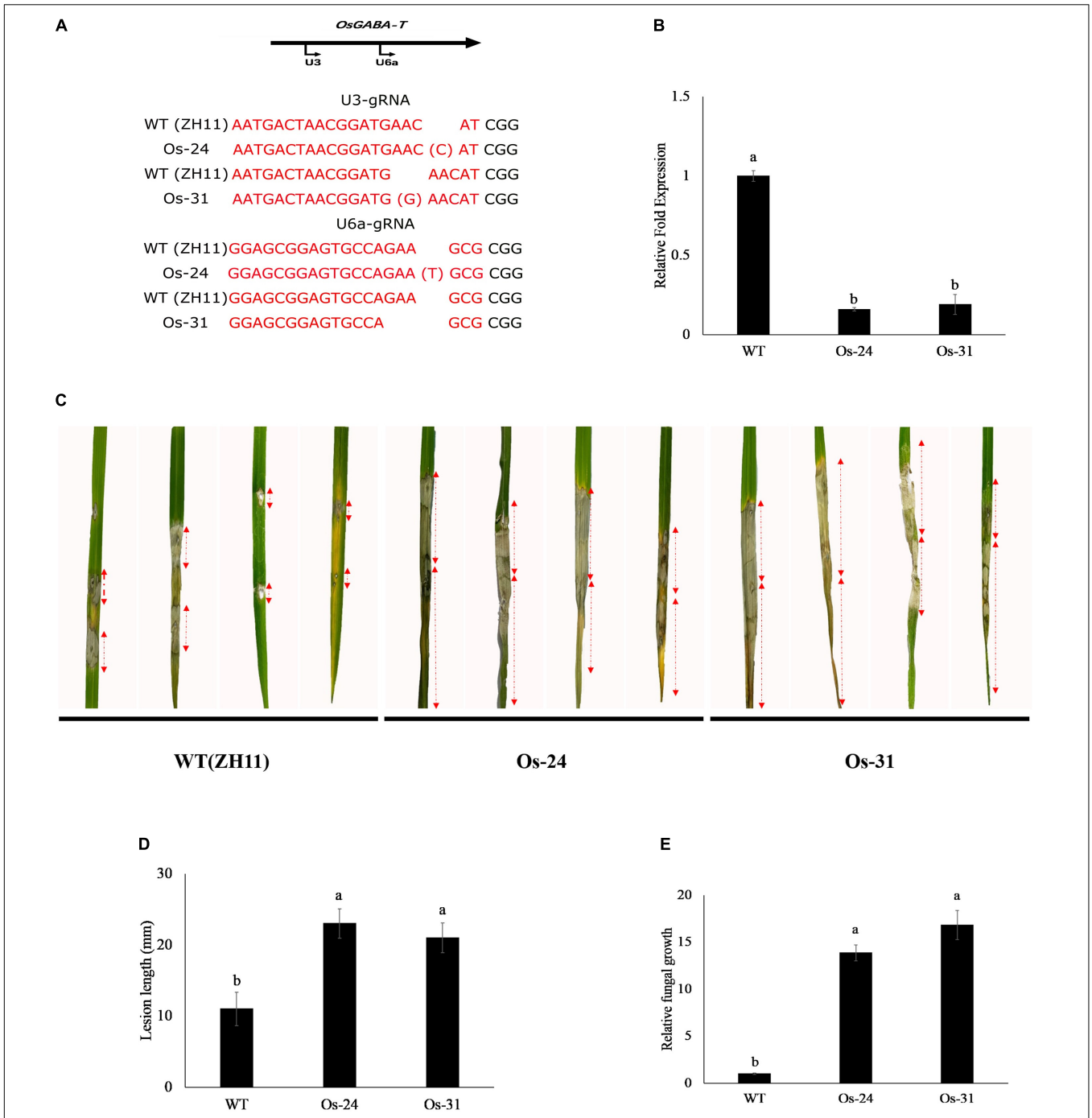

FIGURE 8 | Knockout of *OsGABA-T* reduces rice disease resistance to *Rhizoctonia solani*. **(A)** Sequence of gRNA target of rice. Red color represents the target sequence. **(B)** *OsGABA-T* transcription levels in wild-type ZH11 and *OsGABA-T* knocked out rice lines, Os-24 and Os-31. Error bars represent ± SD of at least three independent tests. Lower-case letters indicate statistically significant differences ($P < 0.05$). **(C)** Inoculation of wild-type ZH11 and *OsGABA-T* knocked out lines Os-24 and Os-31 with *Rhizoctonia solani* AG1-IA. Images were taken 72 h after inoculation. **(D)** Lesion length of infected rice leaves. Lesion length was calculated from three independent biological replicates. And the red arrows indicated lesion length. Error bars represent ± SD of at least six leaves each. Lower-case letters indicate statistically significant differences ($P < 0.05$). **(E)** Quantitative PCR was performed for quantification of relative fungal growth on inoculated leaves $2^{(Ct\_OsUbiq - Ct\_RsDNA)}$. Error bars represent ± SD of 6 independent tests. Lower-case letters indicate statistically significant differences ($P < 0.05$).

Z. mays through Y2H screening, and the interaction between ZmGABA-T and EG1 was verified by Y2H, CoIP, and BiFC assays (**Figure 1**).

GABA-T catalyzes the breakdown of GABA to succinic semialdehyde (SSA), playing a key role in its life cycle and metabolism (Cauwenberghe and Shelp, 1999;

Cauwenberghe et al., 2002). In *A. thaliana*, full-length AtGABA-T contains an N-terminal targeting pre-sequence that is 36 amino acids long and is both sufficient and necessary for targeting enzymes to mitochondria (Clark et al., 2009a). In the tomato plant *Solanum lycopersicum* L., three GABA-Ts owned highly similar sequences in their coding regions, except their N-terminal regions, leading to distinct subcellular localizations in the mitochondrion, plastid, or cytosol (Clark et al., 2009b). In *O. sativa*, four putative GABA-T genes exhibit a high amino acid identity (73–82%), but they differ in length at the N-terminal region, located in different organelles (Shimajiri et al., 2013). Our study revealed that ZmGABA-T in *Z. mays* is located in the cell membrane (**Figure 2A**).

In *A. thaliana* and *Z. mays*, plant elicitor peptides (PEPs) play a key role in plant immunity (Yamaguchi and Huffaker, 2011; Bartels and Boller, 2015). PEPs without N-terminal secretion signals can be released to the extra-plasma by unidentified mechanisms and identified by plant elicitor peptide receptors (PEPRs) on the plasma membrane (Yamaguchi et al., 2006; Yamaguchi et al., 2010; Yamaguchi and Huffaker, 2011). ZmGABA-T also lacks transmembrane structure and does not contain a signal peptide. During the infection of *R. solani*, ZmGABA-T can interact with EG1 in the cell membrane (**Figure 2B**). Therefore, we concluded that an unknown protein can interact with it in cells and anchor it to the cell membrane.

Research has shown that the regulatory actions of GABA-T are closely related to immune responses to pathogens (Wu et al., 2006). Our results showed that the transient expression of GABA-T in *N. benthamiana* decreased the level of ROS triggered by EG1 and further suppressed the allergic necrosis induced by EG1 (**Figures 3A,B**, **7**). In addition, we proved that the reduced allergic necrosis and ROS can be attributed to the promotion of EG1 degradation by ZmGABA-T rather than the inhibition of EG1 activity in *N. benthamiana* (**Figures 3C,D**).

GABA is a four-carbon, ubiquitous, non-proteinogenic amino acid. In animals, it is a signaling molecule that functions as an inhibitory neurotransmitter. In plants, abiotic stress (hypoxia, heat, cold, drought, mechanical wounding) or biotic stress (wounding due to herbivory and infection) results in the rapid accumulation of GABA. In addition, GABA can also act as a signaling molecule in plant defense (Bown and Shelp, 2016). Our results showed that GABA can suppress the transcription of *EG1* while not affecting its enzymatic activity (**Figure 4**). Thus, we conclude that GABA-T and GABA can directly or indirectly inhibit the expression of EG1, and therefore the production of ROS and allergic necrosis.

The transient expression of ZmGABA-T inhibited *R. solani* infection, and the size of lesions and the biomass of pathogenic fungi were reduced (**Figure 5**). When the homologous sequence of ZmGABA-T in *O. sativa* was knocked out, the resistance of knocked out plants to *R. solani* was significantly weakened (**Figure 8**). These results suggest that GABA-T may positively regulate disease resistance against *R. solani* in rice.

In plants, GABA-T is involved in the metabolism of GABA, which is a significant component of the free amino acid pool in most prokaryotic and eukaryotic organisms (Bown, 1997; Shelp et al., 1999). GABA is metabolized mainly *via* the GABA-shunt pathways. GABA production from glutamate is catalyzed by glutamate decarboxylase; whereas GABA-T catalyzes the conversion of GABA to SSA, which is then oxidized to succinate due to succinic semialdehyde dehydrogenase. Thus, the carbon skeleton of GABA enters the tricarboxylic acid cycle (Tuin and Shelp, 1994; Shelp et al., 2012). Other studies have shown that GABA-T (GABA shunt) may play a role in restricting the levels of allergic necrosis during host and pathogen interaction (Wu et al., 2006).

In summary, our study revealed that GABA-T in *Z. mays* can target the CWDE EG1 and act as a positive defense regulator that can suppress the accumulation of ROS and allergic necrosis caused by EG1. Future studies will focus on investigating the protein interactions with ZmGABA-T and the receptor that interacts with EG1 in the plasma membrane.

DATA AVAILABILITY STATEMENT

The datasets presented in this study can be found in online repositories. The names of the repository/repositories and accession number(s) can be found below: Sequence data from this article can be found in the GenBank/EMBL data libraries under the following accession numbers: ZmGABA-T (XM_008670668.1), OsGABA-T (AF297651.1), NtGABA-T (XM_016626518.1), and AtGABA-T (NM_113117.4).

AUTHOR CONTRIBUTIONS

XG and DL designed the experiments, analyzed the data, and contributed to the drafting and revision of the manuscript. XG, JC, MG, and DL performed the experiments. All authors read and approved the final manuscript.

FUNDING

This research was funded by the Ministry of Science and Technology of China (Grant Nos. 2015BAD15B05 and 2012AA10180402) and the National Nature Science Foundation of China (Grant No. 31571949).

ACKNOWLEDGMENTS

We are grateful for funding the work by the Ministry of Science and Technology of China and the National Natural Science Foundation of China.

SUPPLEMENTARY MATERIAL

The Supplementary Material for this article can be found online at: https://www.frontiersin.org/articles/10.3389/fpls.2022.860170/full#supplementary-material

REFERENCES

Amselem, J., Cuomo, C. A., van Kan, J. A., Viaud, M., Benito, E. P., Couloux, A., et al. (2011). Genomic analysis of the necrotrophic fungal pathogens *Sclerotinia sclerotiorum* and *Botrytis cinerea*. *PLoS Genet.* 7:e1002230. doi: 10.1371/journal.pgen.1002230

Bartels, S., and Boller, T. (2015). Quo vadis, Pep? Plant elicitor peptides at the crossroads of immunity, stress, and development. *J. Exp. Bot.* 66, 5183–5193. doi: 10.1093/jxb/erv180

Berr, A., Mccallum, E. J., Alioua, A., Heintz, D., Heitz, T., and Shen, W. H. (2010). *Arabidopsis* histone methyltransferase SET DOMAIN GROUP8 mediates induction of the jasmonate/ethylene pathway genes in plant defense response to necrotrophic fungi. *Plant Physiol.* 154, 1403–1414. doi: 10.1104/pp.110.161497

Boller, T., and Felix, G. (2009). A renaissance of elicitors: perception of microbe-associated molecular patterns and danger signals by pattern-recognition receptors. *Annu. Rev. Plant Biol.* 60, 379–406. doi: 10.1146/annurev.arplant.57.032905.105346

Bown, A. W. (1997). The metabolism and function of γ-aminobutyric acid. *Plant Physiol.* 115, 1–5.

Bown, A. W., and Shelp, B. J. (2016). Plant GABA: not just a metabolite. *Trends Plant Sci.* 21, 811–813. doi: 10.1016/j.tplants.2016.08.001

Cauwenberghe, O., and Shelp, B. J. (1999). Biochemical characterization of partially purified gaba:pyruvate transaminase from *Nicotiana tabacum*. *Phytochemistry* 52, 575–581. doi: 10.1016/s0031-9422(99)00301-5

Cauwenberghe, O. V., Makhmoudova, A., Mclean, M., Clark, S. M., and Shelp, B. J. (2002). Plant pyruvate-dependent gamma-aminobutyrate transaminase: identification of an *Arabidopsis* cDNA and its expression in *Escherichia coli*. *Can. J. Bot.* 80, 933–941. doi: 10.1139/b02-087

Charova, S. N., Dölfors, F., Holmquist, L., Moschou, P. N., Dixelius, C., and Tzelepis, G. (2020). The RsRlpA effector is a protease inhibitor promoting rhizoctonia solani virulence through suppression of the hypersensitive response. *Int. J. Mol. Sci.* 21:8070. doi: 10.3390/ijms21218070

Clark, S. M., Di Leo, R., Dhanoa, P. K., Van Cauwenberghe, O. R., Mullen, R. T., and Shelp, B. J. (2009a). Biochemical characterization, mitochondrial localization, expression, and potential functions for an *Arabidopsis* gamma-aminobutyrate transaminase that utilizes both pyruvate and glyoxylate. *J. Exp. Bot.* 60, 1743–1757. doi: 10.1093/jxb/erp044

Clark, S. M., Di Leo, R., Van Cauwenberghe, O. R., Mullen, R. T., and Shelp, B. J. (2009b). Subcellular localization and expression of multiple tomato gamma-aminobutyrate transaminases that utilize both pyruvate and glyoxylate. *J. Exp. Bot.* 60, 3255–3267. doi: 10.1093/jxb/erp161

Dangl, J. L., and Jones, J. D. (2001). Plant pathogens and integrated defence responses to infection. *Nature* 411, 826–833. doi: 10.1038/35081161

Desaki, Y., Miya, A., Venkatesh, B., Tsuyumu, S., Yamane, H., Kaku, H., et al. (2006). Bacterial lipopolysaccharides induce defense responses associated with programmed cell death in rice cells. *Plant Cell Physiol.* 47, 1530–1540. doi: 10.1093/pcp/pcl019

Dickman, M. B., Park, Y. K., Oltersdorf, T., Li, W., Clemente, T., and French, R. (2001). Abrogation of disease development in plants expressing animal antiapoptotic genes. *Proc. Natl. Acad. Sci. U.S.A.* 98, 6957–6962. doi: 10.1073/pnas.091108998

Doehlemann, G., Ökmen, B., Zhu, W., and Sharon, A. (2017). Plant pathogenic fungi. *Microbiol. Spectr.* 5:23.

Govrin, E. M., and Levine, A. (2000). The hypersensitive response facilitates plant infection by the necrotrophic pathogen *Botrytis cinerea*. *Curr. Biol.* 10, 751–757. doi: 10.1016/s0960-9822(00)00560-1

Govrin, E. M., Rachmilevitch, S., Tiwari, B. S., Solomon, M., and Levine, A. (2006). An Elicitor from *Botrytis cinerea* induces the hypersensitive response in *Arabidopsis thaliana* and other plants and promotes the gray mold disease. *Phytopathology* 96, 299–307. doi: 10.1094/PHYTO-96-0299

Gui, Y. J., Chen, J. Y., Zhang, D. D., Li, N. Y., Li, T. G., Zhang, W. Q., et al. (2017). *Verticillium dahliae* manipulates plant immunity by glycoside hydrolase 12 proteins in conjunction with carbohydrate-binding module 1. *Environ. Microbiol.* 19, 1914–1932. doi: 10.1111/1462-2920.13695

Guo, X., Liu, N., Zhang, Y., and Chen, J. (2021). Pathogen-associated molecular pattern active sites of GH45 endoglucanohydrolase from *Rhizoctonia solani*. *Phytopathology* 112, 355–363. doi: 10.1094/PHYTO-04-21-0164-R

Kanyuka, K., and Rudd, J. J. (2019). Cell surface immune receptors: the guardians of the plant's extracellular spaces. *Curr. Opin. Plant Biol.* 50, 1–8. doi: 10.1016/j.pbi.2019.02.005

Kemmerling, B., Schwedt, A., Rodriguez, P., Mazzotta, S., Frank, M., Qamar, S. A., et al. (2007). The BRI1-associated kinase 1, BAK1, has a brassinolide-independent role in plant cell-death control. *Curr. Biol.* 17, 1116–1122. doi: 10.1016/j.cub.2007.05.046

Kim, K. S., Min, J. Y., and Dickman, M. B. (2008). Oxalic acid is an elicitor of plant programmed cell death during *Sclerotinia sclerotiorum* disease development. *Mol. Plant Microbe Interact.* 21, 605–612. doi: 10.1094/MPMI-21-5-0605

Laluk, K., Abuqamar, S., and Mengiste, T. (2011). The *Arabidopsis* mitochondria-localized pentatricopeptide repeat protein PGN functions in defense against necrotrophic fungi and abiotic stress tolerance. *Plant Physiol.* 156, 2053–2068. doi: 10.1104/pp.111.177501

Lenz, H. D., Haller, E., Melzer, E., Kober, K., and Nürnberger, T. (2011). Autophagy differentially controls plant basal immunity to biotrophic and necrotrophic pathogens. *Plant J.* 66, 818–830. doi: 10.1111/j.1365-313X.2011.04546.x

Li, G., Meng, X., Wang, R., Mao, G., Han, L., Liu, Y., et al. (2012). Dual-level regulation of ACC synthase activity by MPK3/MPK6 cascade and its downstream WRKY transcription factor during ethylene induction in *Arabidopsis*. *PLoS Genet.* 8:e1002767. doi: 10.1371/journal.pgen.1002767

Li, S., Peng, X., Wang, Y., Hua, K., Xing, F., Zheng, Y., et al. (2019). The effector AGLIP1 in *Rhizoctonia solani* AG1 IA triggers cell death in plants and promotes disease development through inhibiting PAMP-triggered immunity in *Arabidopsis thaliana*. *Front. Microbiol.* 10:2228. doi: 10.3389/fmicb.2019.02228

Ludewig, F., Hüser, A., Fromm, H., Beauclair, L., and Bouché, N. (2008). Mutants of GABA transaminase (POP2) suppress the severe phenotype of succinic semialdehyde dehydrogenase (ssadh) mutants in *Arabidopsis*. *PLoS One* 3:e3383. doi: 10.1371/journal.pone.0003383

Luo, H., Laluk, K., Lai, Z., Veronese, P., Song, F., and Mengiste, T. (2010). The *Arabidopsis Botrytis* susceptible1 interactor defines a subclass of RING E3 ligases that regulate pathogen and stress responses. *Plant Physiol.* 154, 1766–1782. doi: 10.1104/pp.110.163915

Ma, X., Zhu, Q., Chen, Y., and Liu, Y. G. (2016). CRISPR/Cas9 platforms for genome editing in plants: developments and applications. *Mol. Plant* 9, 961–974. doi: 10.1016/j.molp.2016.04.009

Ma, Y., Han, C., Chen, J., Li, H., He, K., Liu, A., et al. (2015). Fungal cellulase is an elicitor but its enzymatic activity is not required for its elicitor activity. *Mol. Plant Pathol.* 16, 14–26. doi: 10.1111/mpp.12156

Ma, Z., Song, T., Lin, Z., Ye, W., and Wang, Y. (2015). A *Phytophthora sojae* glycoside hydrolase 12 protein is a major virulence factor during soybean infection and is recognized as a PAMP. *Plant Cell* 27:2057. doi: 10.1105/tpc.15.00390

Mauff, F. L., Bamford, N. C., Alnabelseya, N., Zhang, Y., Baker, P., Robinson, H., et al. (2019). Molecular mechanism of *Aspergillus fumigatus* biofilm disruption by fungal and bacterial glycoside hydrolases. *J. Biol. Chem.* 294, 10760–10772. doi: 10.1074/jbc.RA119.008511

McGrath, K. C., Dombrecht, B., Manners, J. M., Schenk, P. M., Edgar, C. I., Maclean, D. J., et al. (2005). Repressor- and activator-type ethylene response factors functioning in jasmonate signaling and disease resistance identified *via* a genome-wide screen of *Arabidopsis* transcription factor gene expression. *Plant Physiol.* 139, 949–959. doi: 10.1104/pp.105.068544

Mengiste, T. (2012). Plant immunity to necrotrophs. *Annu. Rev. Phytopathol.* 50, 267–294. doi: 10.1146/annurev-phyto-081211-172955

Mengiste, T., Chen, X., Salmeron, J., and Dietrich, R. (2003). The BOTRYTIS SUSCEPTIBLE1 gene encodes an R2R3MYB transcription factor protein that is required for biotic and abiotic stress responses in *Arabidopsis*. *Plant Cell* 15, 2551–2565. doi: 10.1105/tpc.014167

Miller, G. L. (1959). Use of dinitrosalicylic acid reagent for determination of reducing sugar. *Anal. Biochem.* 31, 426–428. doi: 10.1021/ac60147a030

Navarro, L., Bari, R., Achard, P., Lisón, P., Nemri, A., Harberd, N. P., et al. (2008). DELLAs control plant immune responses by modulating the balance of jasmonic acid and salicylic acid signaling. *Curr. Biol.* 18, 650–655. doi: 10.1016/j.cub.2008.03.060

Oliver, R. P., and Solomon, P. S. (2010). New developments in pathogenicity and virulence of necrotrophs. *Curr. Opin. Plant Biol.* 13, 415–419. doi: 10.1016/j.pbi.2010.05.003

Shelp, B. J., Bown, A. W., and Mclean, M. D. (1999). Metabolism and functions of gamma-aminobutyric acid. *Trends Plant Sci.* 4, 446–452. doi: 10.1016/s1360-1385(99)01486-7

Shelp, B. J., Mullen, R. T., and Waller, J. C. (2012). Compartmentation of GABA metabolism raises intriguing questions. *Trends Plant Sci.* 17, 57–59. doi: 10.1016/j.tplants.2011.12.006

Shen, D., Wang, J., Dong, Y., Zhang, M., and Xia, A. (2020). The glycoside hydrolase 18 family chitinases are associated with development and virulence in the mosquito pathogen *Pythium guiyangense*. *Fungal Genet. Biol.* 135:103290. doi: 10.1016/j.fgb.2019.103290

Shimajiri, Y., Ozaki, K., Kainou, K., and Akama, K. (2013). Differential subcellular localization, enzymatic properties and expression patterns of γ-aminobutyric acid transaminases (GABA-Ts) in rice (*Oryza sativa*). *J. Plant Physiol.* 170, 196–201. doi: 10.1016/j.jplph.2012.09.007

Snarr, B. D., Baker, P., Bamford, N. C., Sato, Y., Liu, H., Lehoux, M., et al. (2017). Microbial glycoside hydrolases as antibiofilm agents with cross-kingdom activity. *Proc. Natl. Acad. Sci. U.S.A.* 114, 7124–7129. doi: 10.1073/pnas.1702798114

Stergiopoulos, I., and de Wit, P. J. (2009). Fungal effector proteins. *Annu. Rev. Phytopathol.* 47, 233–263. doi: 10.1146/annurev.phyto.112408.132637

Sumner, J. B. (1925). A more specific reagent for the determination of sugar in urine. *J. Biol. Chem.* 65, 393–395. doi: 10.1016/s0021-9258(18)84848-7

Tsuda, K., Sato, M., Stoddard, T., Glazebrook, J., and Katagiri, F. (2009). Network properties of robust immunity in plants. *PLoS Genet.* 5:e1000772. doi: 10.1371/journal.pgen.1000772

Tuin, L. G., and Shelp, B. J. (1994). In situ [14C]glutamate metabolism by developing soybean cotyledons I. metabolic routes. *J. Plant Physiol.* 143, 1–7. doi: 10.1016/s0176-1617(11)82089-4

van Kan, J. A. (2006). Licensed to kill: the lifestyle of a necrotrophic plant pathogen. *Trends Plant Sci.* 11, 247–253. doi: 10.1016/j.tplants.2006.03.005

Vaux, D. L., and Silke, J. (2005). IAPs, RINGs and ubiquitylation. *Nat. Rev. Mol. Cell Biol.* 6, 287–297. doi: 10.1038/nrm1621

Veronese, P., Nakagami, H., Bluhm, B., Abuqamar, S., Chen, X., Salmeron, J., et al. (2006). The membrane-anchored BOTRYTIS-INDUCED KINASE1 plays distinct roles in *Arabidopsis* resistance to necrotrophic and biotrophic pathogens. *Plant Cell* 18, 257–273. doi: 10.1105/tpc.105.035576

Wei, M., Wang, A., Liu, Y., Ma, L., Niu, X., and Zheng, A. (2020). Identification of the novel effector RsIA_NP8 in *Rhizoctonia solani* AG1 IA that induces cell death and triggers defense responses in non-host plants. *Front. Microbiol.* 11:1115. doi: 10.3389/fmicb.2020.01115

Wu, C., Zhou, S., Zhang, Q., Zhao, W., and Peng, Y. (2006). Molecular cloning and differential expression of an gamma-aminobutyrate transaminase gene, OsGABA-T, in rice (*Oryza sativa*) leaves infected with blast fungus. *J. Plant Res.* 119, 663–669. doi: 10.1007/s10265-006-0018-3

Yamaguchi, Y., and Huffaker, A. (2011). Endogenous peptide elicitors in higher plants. *Curr. Opin. Plant Biol.* 14, 351–357. doi: 10.1016/j.pbi.2011.05.001

Yamaguchi, Y., Huffaker, A., Bryan, A. C., Tax, F. E., and Ryan, C. A. (2010). PEPR2 is a second receptor for the Pep1 and Pep2 peptides and contributes to defense responses in *Arabidopsis*. *Plant Cell* 22, 508–522. doi: 10.1105/tpc.109.068874

Yamaguchi, Y., Pearce, G., and Ryan, C. A. (2006). The cell surface leucine-rich repeat receptor for AtPep1, an endogenous peptide elicitor in *Arabidopsis*, is functional in transgenic tobacco cells. *Proc. Natl. Acad. Sci. U.S.A.* 103, 10104–10109. doi: 10.1073/pnas.0603729103

Zhang, L., Kars, I., Essenstam, B., Liebrand, T. W., Wagemakers, L., Elberse, J., et al. (2014). Fungal endopolygalacturonases are recognized as microbe-associated molecular patterns by the *Arabidopsis* receptor-like protein responsiveness to botrytis polygalacturonases1. *Plant Physiol.* 164, 352–364. doi: 10.1104/pp.113.230698

Zhang, X., Wang, C., Zhang, Y., Sun, Y., and Mou, Z. (2012). The *Arabidopsis* mediator complex subunit16 positively regulates salicylate-mediated systemic acquired resistance and jasmonate/ethylene-induced defense pathways. *Plant Cell* 24, 4294–4309. doi: 10.1105/tpc.112.103317

Zipfel, C. (2009). Early molecular events in PAMP-triggered immunity. *Curr. Opin. Plant Biol.* 12, 414–420. doi: 10.1016/j.pbi.2009.06.003

Conflict of Interest: The authors declare that the research was conducted in the absence of any commercial or financial relationships that could be construed as a potential conflict of interest.

Publisher's Note: All claims expressed in this article are solely those of the authors and do not necessarily represent those of their affiliated organizations, or those of the publisher, the editors and the reviewers. Any product that may be evaluated in this article, or claim that may be made by its manufacturer, is not guaranteed or endorsed by the publisher.

frontiers | Frontiers in Plant Science

ORIGINAL RESEARCH
published: 23 June 2022
doi: 10.3389/fpls.2022.917493

Multi-Omics Analysis Reveals a Regulatory Network of ZmCCT During Maize Resistance to Gibberella Stalk Rot at the Early Stage

Bozeng Tang[1†], Zhaoheng Zhang[1†], Xinyu Zhao[1], Yang Xu[1], Li Wang[1], Xiao-Lin Chen[2] and Weixiang Wang[1*]*

[1] Beijing Key Laboratory of New Technology in Agricultural Application, National Demonstration Center for Experimental Plant Production Education, College of Plant Science and Technology, Beijing University of Agriculture, Beijing, China, [2] State Key Laboratory of Agricultural Microbiology and Provincial Hubei Key Laboratory of Plant Pathology, College of Plant Science and Technology, Huazhong Agricultural University, Wuhan, China

OPEN ACCESS

Edited by:
Xiao-Ren Chen,
Yangzhou University, China

Reviewed by:
Huiquan Liu,
Northwest A&F University, China
Kang Zhang,
Hebei Agricultural University, China
David Sewordor Gaikpa,
University of Hohenheim, Germany

***Correspondence:**
Weixiang Wang
wwxbua@163.com
Xiao-Lin Chen
chenxiaolin@mail.hzau.edu.cn

[†] These authors have contributed equally to this work

Specialty section:
This article was submitted to Plant Pathogen Interactions, a section of the journal Frontiers in Plant Science

Received: 11 April 2022
Accepted: 12 May 2022
Published: 23 June 2022

Citation:
Tang B, Zhang Z, Zhao X, Xu Y, Wang L, Chen X-L and Wang W (2022) Multi-Omics Analysis Reveals a Regulatory Network of ZmCCT During Maize Resistance to Gibberella Stalk Rot at the Early Stage. Front. Plant Sci. 13:917493. doi: 10.3389/fpls.2022.917493

Gibberella stalk rot (GSR) caused by *Fusarium graminearum* is one of the most devastating diseases in maize; however, the regulatory mechanism of resistance to GSR remains largely unknown. We performed a comparative multi-omics analysis to reveal the early-stage resistance of maize to GSR. We inoculated *F. graminearum* to the roots of susceptible (Y331) and resistant (Y331-ΔTE) near-isogenic lines containing GSR-resistant gene *ZmCCT* for multi-omics analysis. Transcriptome detected a rapid reaction that confers resistance at 1–3 hpi as pattern-triggered immunity (PTI) response to GSR. Many key properties were involved in GSR resistance, including genes in photoperiod and hormone pathways of salicylic acid and auxin. The activation of programmed cell death-related genes and a number of metabolic pathways at 6 hpi might be important to prevent further colonization. This is consistent with an integrative analysis of transcriptomics and proteomics that resistant-mediated gene expression reprogramming exhibited a dynamic pattern from 3 to 6 hpi. Further metabolomics analysis revealed that the amount of many chemical compounds was altered in pathways associated with the phenylpropanoid biosynthesis and the phenylalanine metabolism, which may play key roles to confer the GSR resistance. Taken together, we generated a valuable resource to interpret the defense mechanism during early GSR resistance.

Keywords: multi-omics, gibberella stalk rot, *Fusarium graminearum*, plant resistance, transcriptomics, metabolomics, maize disease

HIGHLIGHTS

- Through a multi-omics strategy, this study comprehensively revealed ZmCCT-associated maize defense response to Gibberella stalk rot at the early stage of *Fusarium graminearum* infection.

INTRODUCTION

Gibberella stalk rot (GSR), one of the maize stalk rot diseases, is a severe soil-borne disease in maize (*Zea mays* L.), which has become a major threat to maize production (Jackson-Ziems et al., 2014). GSR is caused by the fungus *Fusarium graminearum*, which severely reduces both the yield and the quality of maize and produces various mycotoxins (Ledencan et al., 2003). In addition to crown rot, root rot, and seedling blight, Fusarium Head Blight is well-known to be caused by *F. graminearum* (Stephens et al., 2008; Wang et al., 2015). As a hemibiotrophic fungal pathogen, *F. graminearum* undergoes a biotrophy phase at the early stage and a necrotrophy phase at the later stage (Glazebrook, 2005). During infection, the hyphae of *F. graminearum* emerge intercellularly at the early stage (before 24 h post-inoculation, hpi), emerge intracellularly and intercellularly in the middle stage (36–48 hpi), and grow rapidly at the later stage (after 72 hpi), when the plant cell structure collapsed and tissue rotted (Glazebrook, 2005; Brown et al., 2010; Kazan et al., 2012).

Plants have evolved a repertoire of molecules to facilitate response to biotic stress mainly via a two-layer innate immunity by detecting pathogen-derived molecules, including pattern-triggered immunity (PTI) and effector-triggered immunity (ETI) (Jones and Dangl, 2006; Ngou et al., 2022). Some studies have focused on plants responding to *F. graminearum* infection, including wheat, barley, and maize. It has been reported that defense-related hormones, reactive oxygen species (ROS), pathogenesis-related (PR) proteins, and cellular detoxification-related proteins are used by plants to restrict *F. graminearum* infection (Dodds and Rathjen, 2010; Ding et al., 2011; Chetouhi et al., 2016). However, the underlying mechanisms of how maize resists *F. graminearum* at different infection stages are also limited. Therefore, it is necessary to make full use of the central resistance genes to understand the regulation mechanism of maize at different *F. graminearum* infection stages. In the past decade, comparative transcriptomic analyses of near-isogenic lines (NILs) that differ by the presence or absence of resistance-related loci have revealed insights into the potential mechanisms of defense response to *F. graminearum* in wheat or maize (Yang et al., 2010; Zhuang et al., 2013; Huang et al., 2016; Liu Y. et al., 2016). These studies identified numerous differentially expressed genes (DEGs) between GSR-resistant (R) and -susceptible (S) maize genotypes to dissect the molecular mechanisms of maize–*Fusarium* interactions by discovering key genes. The single transcriptomic analysis provides a landscape of defense response at a given time point (Ye et al., 2013); however, not all transcriptional changes observed are translated into proteins or metabolites. Therefore, combining transcriptomic data with those proteomic and metabolomic approaches can be used to comprehensively reveal the multilevel landscape of plant defense response and better understand the molecular mechanism of GSR resistance (Zhou et al., 2019; Sun et al., 2021). Recently, an integrative analysis combining transcriptomics and metabolomics showed that *ZmHIR3* controls cell death at the later stage of GSR, probably through the transcriptional regulation of key genes and functional metabolites (Sun et al., 2021).

So far, there are only several genes in maize that provide resistance to GSR, and due to the soil-borne infection pattern of *F. graminearum*, it is hard to effectively control GSR. Therefore, cloning and utilization of the GSR resistance genes became an effective strategy in controlling GSR (Yang et al., 2010; Zhang X. W. et al., 2012; Ye et al., 2013; Ma et al., 2017). The GSR resistance is controlled by quantitative resistance genes, which involve complex regulatory mechanisms. Several quantitative trait loci (QTLs) and relevant genes for GSR resistance were identified in the past two decades, including qRfg1, qRfg2, and qRfg3 (Yang et al., 2010; Zhang D. et al., 2012; Ye et al., 2013; Ma et al., 2017). Among these, qRfg1 is a major GSR resistance locus, and the GSR resistance gene *ZmCCT* was cloned from this locus (Yang et al., 2010; Wang et al., 2017). Although several GSR resistance loci and genes have been reported, the regulatory mechanisms of GSR resistance remain largely unknown. Therefore, it is necessary to make full use of GSR resistance genes to understand the regulation mechanism of maize, especially the key genes, pathways, and regulatory networks at different *F. graminearum* infection stages.

ZmCCT plays a dual function in photoperiod sensitivity and GSR resistance. Compared with the temperate maize, *ZmCCT* expresses much higher in teosinte maize and is responsible for delayed flowering under long days conditions (Yang et al., 2010; Hung et al., 2012). *ZmCCT* plays its role in a tissue-specific pattern that shows strong photoperiod sensitivity in leaves but conferred a stable defense response in roots during *F. graminearum* infection (Wang et al., 2017). This *ZmCCT*-dependent photoperiod sensitivity and GSR resistance could be separated by modifying a polymorphic CACTA-like transposable element (TE1) in its promoter region. The TE1 element in the promoter region of *ZmCCT* dramatically reduced maize flowering time (Yang et al., 2013). It was found that both repressive H3K27me3/H3K9me3 and active H3K4me3 histone marks enriched the non-TE1 *ZmCCT* allele. Upon *F. graminearum* infection, the non-TE1 *ZmCCT* allele functioned as a major epigenetic factor in the regulation of *ZmCCT* expression by a rapid reduction in the H3K27me3/H3K9me3 level and a progressive decrease in H3K4me3 level, which conferred to the GSR resistance (Wang et al., 2017). However, the downstream regulatory mechanisms of *ZmCCT* in photoperiod sensitivity and GSR resistance are still largely unknown.

In this study, we set out to reveal regulatory mechanisms of maize resistance to GSR at the early stage of *F. graminearum* infection. We utilized maize near-isogenic lines, Y331 and Y331-ΔTE, for testing. In Y331, a TE1 element located at the upstream sequence of *ZmCCT* promoter leads to a compromised expression of *ZmCCT* and confers susceptibility to GSR, while in Y331-ΔTE, the TE1 element was removed and confers resistance to GSR. The expression of *ZmCCT* in Y331-ΔTE is transcriptionally induced by *F. graminearum* at 1 to 3 hpi and reduced quickly, suggesting that it plays key roles at the early stage during *F. graminearum* infection. A comparative multi-omics analysis was then performed by using Y331 and Y331-ΔTE to generate RNA-seq, proteomic, and metabolomic data after inoculation with *F. graminearum* at different time points.

The integrative analysis of multi-omics data demonstrated a regulatory network of defense response at the early stage of GSR.

MATERIALS AND METHODS

Plant Materials

The maize (*Zea mays* L.) susceptible near-isogenic line Y331 and resistant near-isogenic line Y331-ΔTE are used as published previously (Wang et al., 2017). Y331 contains a susceptible ZmCCT allele with the insertion of transposon TE in the promoter region. Y331-ΔTE carries a disease-resistant ZmCCT allele which does not contain the transposon insertion.

Inoculation of *Fusarium graminearum*

Fusarium graminearum was cultured at 25°C for 5∼7 days for propagation. The culture medium was cut into small pieces and put into a mung bean soup culture medium. The fungal strain was incubated in dark at 28°C and 200 rpm for 10 days, then the spores were harvested with a double-layer gauze, and the spore concentration was adjusted to 10^7 spores/ml. The root of 2-week-old (one-leaf period) maize seedlings with spore suspension was immersed, shaken for 1 h at 28°C and 200 rpm, and then placed into an incubator to observe the disease state of maize. The root samples infected with *F. graminearum* were collected at different time points (0, 1, 3, 6 or 24 hpi) for RNA-seq, proteomic, and metabolomic analysis.

Microscopic Observation of *Fusarium graminearum* Infection

For visualization of the growth of *F. graminearum* in maize root, the WGA-Alexa Fluor 488 dye (Thermo Fisher Scientific, Waltham, MA, United States) was used to stain the infection hyphae of the fungus. At different time points, the *F. graminearum*-infected maize roots were harvested and gently washed with distilled water, treated with 50% ethanol for 4 h and with 20% KOH at 85°C for 1.5 hs, rinsed thoroughly with distilled water and PBS buffer, and then stained with WGA-Alexa Fluor 488 (1 μg/ml) for 10 min. The stained samples were used to observe the *F. graminearum* infection process under a confocal microscope Leica TCS SP8 (Leica Microsystems, Mannheim, Baden-Württemberg, Germany).

RNA-Seq Analysis

The maize root samples (Y331 and Y331-ΔTE, 2-week-old seedlings) inoculated with *F. graminearum* were collected at 0, 1, 3, and 6 hpi. Three biological replicates were used for assessment. Total RNA from the maize root samples was extracted using TRIzol reagent (Invitrogen, Carlsbad, CA, United States). The mRNA was enriched and purified using poly-T oligo-attached magnetic beads. Then, under elevated temperature, the purified mRNA was fragmented into small pieces using divalent cations. The RNA fragment was copied into the first-strand cDNA using reverse transcriptase and random primers. The second strand cDNA was then synthesized using DNA polymerase I and RNase H. Then, these cDNA fragments added a single "A" base and were connected to the adapter. The product was purified and enriched by PCR amplification. Subsequently, we quantified the PCR yield by a qubit and gathered the samples together to form a single-stranded DNA cycle (ssDNA cycle) so as to obtain the final library. DNA nanoballs (DNB) were generated by single-stranded DNA rings during sequencing by rolling circle replication (RCR) to amplify fluorescence signals. DNB was loaded into the patterned nanoarray, and a 100-bp opposite end reading was taken on the MGI2000 platform for the following data analysis. The MGI2000 platform combines DNA nanosphere-based nanoarrays and step-by-step sequencing using combined probe anchor synthesis sequencing methods (Beijing Genomics Institution, Bejing, China).

The raw reads were assessed using FastQC and trimmed using trimmomatic (Bolger et al., 2014). Using Hisat2 (v.2.2.0) (Kim et al., 2015), the cleaned reads were aligned against the B73 maize reference genome (Ensembl Genomes database) (Schnable et al., 2009). Differentially expressed genes were analyzed by DESeq2 (Love et al., 2014), and the expression with $\log2|FC| > 1$ with less than 0.05 *p*-adjust values was defined as DEGs. Gene Ontology enrichment analysis was performed by AgriGO toolkits (Du et al., 2010) using p-adjust value cutoffs (0.05) for significances. KEGG enrichment of metabolic pathways and Gene Ontology term analysis were analyzed by the R package clusterProfilter v3.16 (Yu et al., 2012). Pathview (Version 3.11) was used to produce detailed mapping for the selected pathways (Luo et al., 2017). For the weighted correlation network analysis (WGCNA) analysis, only genes with at least five reads aligned to the maize genome from all the samples were kept. A total of 24,894 genes were processed as input by WGCNA (Langfelder and Horvath, 2008). The TMM values were obtained after normalization by using raw read counts. The function blockwiseModules was used to produce a network of Pearson's correlation matrix to examine the similarity between genes. A soft power threshold of 12 was chosen because it was the lowest power to obtain the lowest correlation value (0.9) from topology analysis. Module detection was generated by modified settings to minimize the numbers of clusters by using min Modules Size = 100, merge Cut Height = 0.30. For each module, the expression of the hub gene which represents the expression of each module was generated by choosing TopHubInEachModule function.

Data Independent Acquisition Proteomic Analysis

Maize root samples (Y331 and Y331-ΔTE) inoculated with *F. graminearum* were collected at 0, 1, 3, and 6 hpi. Three biological replicates were used for assessment. The total protein was then extracted, 5 times the volume of acetone was added, and placed at –20°C for 2 h. Then, the samples were centrifuged at 25,000 g at 4°C for 20 min, and the supernatant was separated. The resulting particles were air-dried and then 200 μL buffer (7 M urea, 2 m thiourea and 20 mm Tris HCl, pH 8.0) was added to redissolve the particles. Subsequently, 20 μL of 10 mM dithiothreitol was added at 56°C for 1 h, and then, 20 μL of 55 mM iodoacetamide was added for alkylation in the dark at room temperature for 45 min, followed by centrifugation at 4°C and 25,000 *g* for 20 min. The supernatant of protein concentration was determined using Bradford Protein Analytical

Kit (Bio-Rad, Hercules, CA, United States). Around 100 μg of proteins was digested with trypsin using an enzyme-to-protein ratio of 1:40 (v/v). Then, the mixture was incubated at 37°C for 12 h. The peptides were subsequently hydrolyzed and desalted by a Strata X column (Waters, Milford, MA, United States). The peptide solution was lyophilized, and the toxic dissolved peptide was placed at −20°C for use. The sample protein concentration was calculated based on the standard curve using the Bradford quantification method. Every 10 μg of protein solution was mixed with an appropriate amount of loading buffer, heated at 95°C for 5 min, and centrifuged at 25,000 *g* for 5 min, and the supernatant was poured into a well of a 12% SDS polyacrylamide gel. After electrophoresis, the gel was stained with Coomassie brilliant blue and then decolored with a decoloring solution (40% ethanol and 10% acetic acid). For protein enzymatic hydrolysis, 100 μg of protein solution was taken per sample and diluted with 50 mM NH_4HCO_3 by four times the volume. Then, 2.5 μg of Trypsin enzyme was added in the ratio of protein, enzyme = 40:1, and digested for 4 h at 37°C. Trypsin was added one more time in the above ratio and digested for 8 h at 37°C. Enzymatic peptides were desalted using a Strata X column and vacuumed to dryness. For high pH RP separation, all samples were taken at 10 μg, respectively, to mix, and 200 μg mixture was diluted with 2 mL of the mobile phase A (5% ACN pH 9.8) and injected. The Shimadzu LC-20AB HPLC system coupled with a Gemini high pH C18 column (5 μm, 4.6 × 250 mm) was used. The sample was subjected to the column and then eluted at a flow rate of 1 mL/min by gradient: 5% mobile phase B (95% CAN, pH 9.8) for 10 min, 5% to 35% mobile phase B for 40 min, 35% to 95% mobile phase B for 1 min, where flow Phase B lasted for 3 min, and 5% mobile phase B was equilibrated for 10 min. The elution peak was monitored at a wavelength of 214 nm, and the component was collected every minute. Components were combined into a total of 10 fractions, which were then freeze-dried.

Date-dependent acquisition (DDA) fractions and Data Independent Acquisition (DIA) sample analysis were performed using the Nano-Liquid Chromatography-Tandem Mass Spectrometry (nanoLC-MS/MS), which was combined with a Q-Exactive HF mass spectrometer (Thermo Fisher Scientific, Waltham, MA, United States) and an Ultimate 3000 RSLCnano system (Thermo Fisher Scientific, Waltham, MA, United States). A nano-LC column (Thermo Fisher Scientific, Waltham, MA, United States) was packed for peptide separation, at a flow rate of 500 nL/min. For DDA analysis, the peptide was loaded into the C18 trap column (Thermo Fisher Scientific, Waltham, MA, United States) with buffer A (2% ACN, 0.1% FA) for 5 min, then eluted gradient with 5 to 25% buffer B (98% ACN, 0.1% FA) for 155 min, 25–30% buffer B for 10 min, and 30–80% buffer B for 5 min. Quantitation analysis for proteomics, including normalization, data transformation, missing imputation, PCA, missing values detection, and differentially expressed proteins (DEPs), was performed using the DEP package (Zhang et al., 2018). The cutoff to define DEPs (differentially expressed proteins) was set as log2| FC| > 1, and the p-adjust was <0.05. Further enrichment analysis was performed as same in RNA-seq.

Metabolite Profiling

The maize root samples (Y331 and Y331-ΔTE) inoculated with *F. graminearum* were collected at 0 and 24 hpi. Unbiased metabolomic profiles of the maize root samples were performed by using the High Performance Liquid Chromatography-Mass Spectroscopy (HPLC-MS). For each sample, ten biological replicates were used. Around 100 mg of each sample was homogenized in 500 μl of a solvent of acetonitrile-water (7:3) and treated with ultrasonic for 15 min. The mixture was centrifuged at 12,000 rpm at 4°C for 15 min. Prior to liquid chromatographic separation, 200 μl of the supernatant was transferred to a new 1.5 ml polypropylene tube. The LC-MS system operates in a binary gradient solvent mode consisting of 0.1% (v/v) formic acid/water (solvent A) and 0.1% (v/v) formic acid/methanol (solvent B). The C18 columns were used for all subsequent analyses. Sample analysis was carried out in positive electrospray ionization (ESI+) and negative ion (ESI) modes. The column temperature was 45°C with a 5 μl injection volume. The LC-MS data were obtained by using an Agilent 1290 Infinity LC System combined with an Agilent 6530 Accurate-Mass Quadrupole Time-of-Flight (Q-TOF).

For data acquisition, the Agilent MassHunter Workstation QTOF Acquisition software (B.03.01) was used. Raw data files of LC-MS were converted into mzdata format, and data processing was performed by the XCMS toolbox (Tautenhahn et al., 2012). Peak picking was performed by the XCMS software implemented within the R statistical language (v 2.13.1). To identify ion intensities of detected peaks, the retention time (RT)-m/z data pairs were used. The obtained scaled data set was imported into SIMCA-P + 11.0 (Umetrics, Umea, Sweden) for PCA, PLS discriminant analysis (PLS-DA), and orthogonal partial least squares discriminant analysis (OPLS-DA) in order to observe the maximum metabolic changes of each group at all-time points.

Metabolites found to be highly similar were compared to investigate differential alteration in different samples. Differential metabolites were selected when the statistical significance threshold of the variable impact projection (VIP) value obtained from the OPLS-DA model was greater than 1.0 ($p < 0.05$). Based on metabolite abundance, Log2 fold change (FC) was used to show differential metabolites changes. By searching against the online HMDB, METLIN, and KEGG databases with exact molecular mass data from redundant m/z peaks, putative metabolites were determined. Specific metabolites were screened out when the difference between the observed mass and the theoretical mass was less than 10 ppm. To visualize the network of gene ontology terms, Cytoscape 3.8 software with ClueGO plugin was used. For mapping the metabolites and transcript into pathways, Pathview (Version 3.11) was used (Luo et al., 2017).

Hormone Content Determination by Liquid Chromatography With Tandem Mass Spectrometry (LC-MS/MS)

Fresh maize roots inoculated with *F. graminearum* were harvested at 0, 3, and 6 hpi, immediately frozen in liquid nitrogen and ground into powder, and then stored at −80°C until utilization. Around 50 mg of plant powder sample was

dissolved in 1 mL methanol/water/formic acid (15:4:1, V/V/V). For quantification, internal standards were used by adding 10 μL of standard mixed solution (100 ng/mL) into the extract. The mixture was vortexed repeatedly and then centrifuged for 5 min at 4°C (12,000 r/min). The supernatant was transferred for evaporation and dissolved in 100 μL 80% methanol (V/V). Then, the solution was filtered by a 0.22 μm membrane filter for further liquid chromatography with tandem mass spectrometry (LC-MS/MS) analysis using a UPLC-ESI-MS/MS system (UPLC, ExionLC^{TM} AD, AB SCIEX, United States; MS, Applied Biosystems 6500 Triple Quadrupole, Thermo Fisher Scientific, Waltham, MA, United States). The hormone contents were determined by MetWare.[1]

Quantitative Reverse Transcription PCR

Fresh maize roots inoculated with *F. graminearum* were harvested at 0, 1, 3, and 6 hpi for the test. Total RNA was extracted by using TRIzol reagent (Invitrogen, Carlsbad, CA, United States), and genomic DNA was removed by treating with DNaseI (Invitrogen, Carlsbad, CA, United States). Total RNA sample was used for cDNA synthesis by using a reverse transcription system (Promega, Fitchburg, MA, United States). Then, the quantitative reverse transcription PCR (qRT-PCR) analysis was performed by preparing a reaction system with SYBR Green mix (TAKARA, Dalian, China), and the reaction was running on a real-time PCR detection system (Bio-Rad, California, United States). For each gene (*ZmCCT*, flowering genes, and hormone signaling genes), three replicates were performed. The expression of genes were normalized by comparing with an actin encoding gene *ZmActin1*.

RESULTS

Strategy to Investigate Dynamics of Gene Expression Between Y331 and Y331-ΔTE Upon Infection

Previously, a locus encoding *ZmCCT* in maize cultivar Y331 was characterized (**Figure 1A**; Wang et al., 2017). In Y331, the TE1 element located at the upstream sequence of *ZmCCT* promoter leads to compromised transcription of ZmCCT to promote susceptibility to GSR. The non-TE1 ZmCCT allele in another cultivar Y331-ΔTE is transcriptionally induced at 1–3 hpi and reduced at 6 hpi upon infection and confers resistance to the disease in a transient manner (**Figure 1B**). These evidence suggest that *ZmCCT* is vital to control resistant response to GSR. First, we tested the pathogenicity of *F. graminearum* against maize cultivars Y331 and Y331-ΔTE (2-week-old seedlings) (**Figure 1C**), which confirmed that Y331-ΔTE was more resistant than Y331 (**Figure 1C**). Live-cell imaging using time-course inoculation (at 0, 6, 12, 24, and 48 hpi) by using GFP-labeled *F. graminearum* was observed, and we found that invasive growth of the fungus in the tissue of the susceptible cultivar Y331 was growing more rapidly than that in the resistant cultivar Y331-ΔTE (**Figure 1D**).

[1]http://www.metware.cn/

Then, we sought to detect the resistance response by comparing the resistance Y331-ΔTE and susceptible Y331. We deployed the samples of Y331 and Y331-ΔTE inoculated with *F. graminearum* to perform the multi-omic analysis, which were combined with transcriptomic and proteomic analyses at 0, 1, 3, and 6 hpi and metabolomic analysis at 0 and 24 hpi. In total, the analysis collectively characterized 32,741 transcripts, 7715 proteins, and more than 3,660 features as putative metabolite compounds in all the samples (**Figure 1E**).

Severe Transcriptional Profiling Changes Between Y331 and Y331-ΔTE Upon Infection

To discover the defense-related genes in maize conferring resistant response to GSR during the early stages of infection, we compared the transcriptome signatures crossing four key time points (0, 1, 3, and 6 hpi). After determining the reproducibility by principal component analysis (PCA) (**Figure 2A** and **Supplementary Figure 1B**), we compared transcriptional profiling of Y331-ΔTE to Y331 by generating a pairwise comparison for all four time points. We defined 250, 1,198, 1,185, and 146 DEGs ($\log2|FC| > 1$, p-adj < 0.05) at 0, 1, 3, and 6 hpi, respectively (**Supplementary Figure 1D** and **Supplementary Table 1**). This result was consistent with the expression pattern of *ZmCCT* in Y331-ΔTE, as the high number of DEGs occurred at 1 and 3 hpi when *ZmCCT* also showed peak expression. Interestingly, the majority of DEGs detected at each time point specifically occurred at each time point. For instance, 74% of DEGs at 1 hpi were not exhibiting significant variation in any other time point and 76% of DEGs at 3 hpi were not showing significant changes in another group of comparisons. Similar patterns were also exhibited at 0 hpi (44%) and 6 hpi (53%) (**Figure 2B**). This result reflected a rapid reaction triggered as an early response to GSR, and specific variations at 1 and 3 hpi that occurred during defense response would be key factors conferring the resistance.

To further characterize the DEGs, a metabolic pathway enrichment analysis was performed (**Supplementary Figure 1**), which revealed a number of metabolic pathways potentially associated with defense response to GSR (**Supplementary Table 2**). For instance, plant hormone signal transduction, pentose phosphate pathway, alpha-linolenic acid metabolism, and fructose and mannose metabolism were specifically enriched at 1 hpi (**Figure 2C**). DEGs at 3 hpi were specifically enriched in plant-pathogen infection, MAPK signaling pathways, beta-alanine metabolism, biotin metabolism, flavonoid biosynthesis, galactose metabolism, terpenoids biosynthesis, and linoleic acid metabolism (Tang et al., 2021). By connecting multiple metabolic pathways enriched in DEGs, we observed glycolysis/gluconeogenesis, phenylpropanoid biosynthesis, diterpenoid biosynthesis, benzoxazinoid biosynthesis, and alanine, aspartate, and glutamate metabolisms were co-regulated by DEGs at 1 and 3 hpi, indicating that these pathways were probably important to activate defense response in maize at the early stage of infection (**Figure 2C**). Strikingly, only two metabolisms, arginine and proline metabolisms

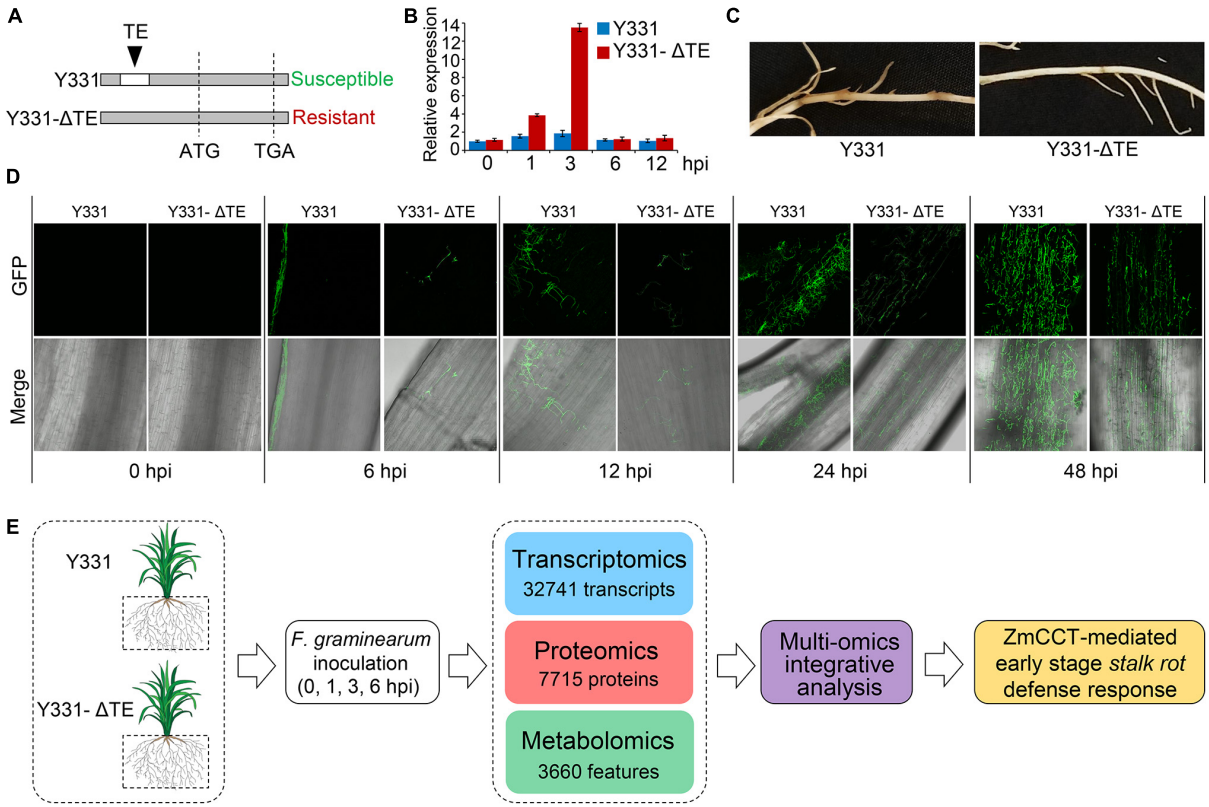

FIGURE 1 | Framework of integrative multi-omic analysis of early-stage defense response to GSR in maize. **(A)** Sketch maps of NILs Y331-ΔTE1 and Y331 at the *ZmCCT* locus. **(B)** Expression profiles of *ZmCCT* in Y331-ΔTE1 and Y331 seedling roots inoculated with *Fusarium graminearum* at different time points. Data were normalized to Y331 at 0 h post-inoculation (hpi). For each sample, the *ZmGAPDH* gene was used as the internal control. Error bars present the ±s.d. of three biological replicates. **(C)** Symptoms of the *F. graminearum*-inoculated maize seedling roots at 72 hpi. **(D)** Growth and distribution of GFP-tagged *F. graminearum* in diseased root tissues of Y331-ΔTE1 and Y331 at different time points. **(E)** Strategy for multiple omics analysis of ZmCCT-mediated defense response in maize.

and glycosaminoglycan degradation, were enriched at 6 hpi, suggesting that ZmCCT-associated resistance to GSR is an early response during infection before 6 hpi. Metabolism of carbon fixation in photosynthetic organisms and pyruvate metabolism were enriched at 0 hpi, suggesting ZmCCT functions in photosynthesis before fungal infection. Gene ontology (GO) enrichment analysis yielded a number of functions such as peroxidase activity and plant-type cell wall, and the response to oxidative stress are enriched in DEGs at 1 hpi. We also discovered that DEGs at 3 hpi were enriched in biological processes associated with nucleosome, MCM complex, nuclear nucleosome, and plasma membrane (**Supplementary Figure 1** and **Supplementary Table 3**).

The top differentially expressed genes were shown in **Supplementary Figure 2**. To validate the DEGs results, we selected seven differentially expressed genes to perform qRT-PCR experiment, which showed a high consistency between RNA-seq and qRT-PCR results (**Supplementary Figure 2**). To get more insights into underlying key properties conferring GSR resistance, we compared the DEGs in our RNA-seq to PTI-induced genes in *Arabidopsis* (Bjornson et al., 2021). In total, 933 maize DEGs were orthologous genes of *Arabidopsis* PTI-responsive genes (**Figure 2D** and **Supplementary Table 4**). Many of these genes were involved in pathways reported as key properties in PTI, such as the MAPK signaling pathway, phenylpropanoid biosynthesis, and glycolysis pathways (**Supplementary Figure 3**). At 3 hpi, we observed the highest number of DEGs during early resistance to GSR. By visualizing the fractions of DEGs at different time points, we observed that a big proportion of DEGs at 3 hpi were also transactionally induced or repressed at 1 hpi, many of which were not transcriptionally induced at 6 hpi (**Figure 2E**). This result demonstrated a set of genes that specifically altered their transcriptional levels upon infection and triggered a transient resistance to stalk rot at 1–3 hpi.

Weighted Correlation Network Analysis Defined Nine Modules as Transcriptional Co-expressed Maize Genes Responding to Gibberella Stalk Rot

To uncover more insights into the underlying resistance mechanism of maize to GSR, we performed WGCNA analysis using all the samples at four time points. Nine different modules were identified by clustering analysis (**Supplementary Table 5**). To elucidate the expression pattern of these modules

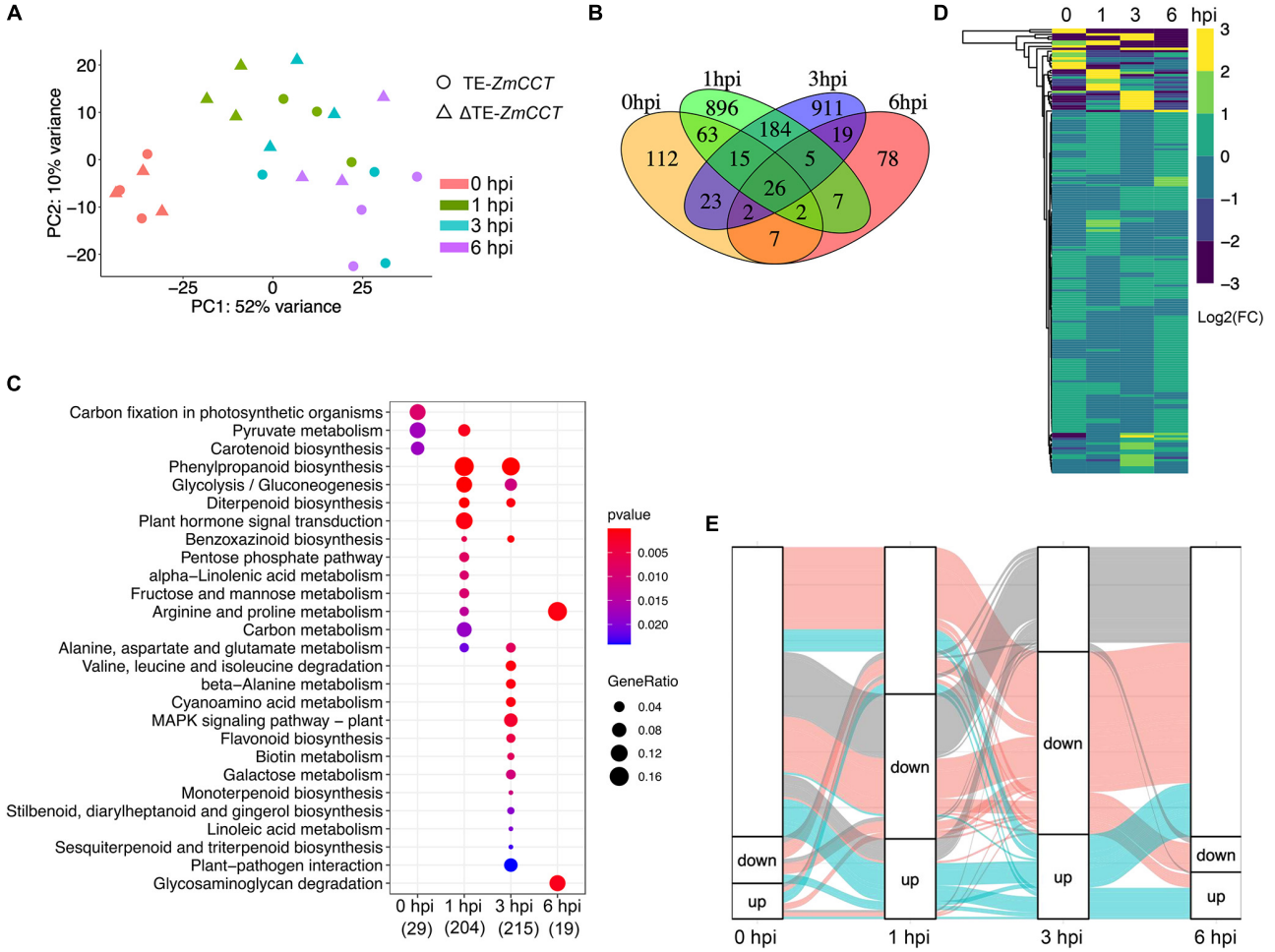

FIGURE 2 | Early-stage resistance to GSR by reprogramming maize transcriptomics. **(A)** The plot showing the principal component analysis (PCA) of maize transcriptomics from Y331-ΔTE and Y331 at four different time points. Normalized reads count was used. **(B)** A Venn diagram showing the numbers of differentially expressed genes (log2| FC| > 1, padj < 0.05) detected in RNA-seq at 0, 1, 3, and 6 hpi. **(C)** The KEGG pathway enrichment analysis using DEGs detected in RNA-seq. **(D)** A heatmap showing relative expression using log2| FC| values from our RNA-seq to demonstrate the expression of ortholog genes between maize and *Arabidopsis*. The *Arabidopsis* RNA-seq data were reported as transcriptionally induced genes responding to fungal elicitor (2021, Nature Plant). **(E)** Alluvial plots of a fraction of a number of differentially expressed genes during infection stages. Each panel shows one time point, and each line represents a different group of DEGs. Red and blue highlight the fractions of DEGs detected at 3 hpi.

of co-expressed genes, we visualized the expression of hub genes, which are the representative ones in each module (**Figure 3A**), and performed metabolic pathway enrichment analysis to determine their functions (**Figure 3B**). This co-expression analysis provided a landscape of dynamic gene expression to illustrate transcriptional divergence in resistant and susceptible maize. In module 1, 7105 genes were transcriptionally co-expressed, which represented about 15% of all genes in the genome of maize. These genes exhibited peak expression at 1 hpi in the resistant cultivar Y331-ΔTE, but a flat pattern in the susceptible cultivar Y331. This result suggests that these genes were transcriptionally induced as a response to GSR. Enrichment analysis indicates that these genes were tightly associated with pathways of the autophagy process, vesicular transport, and endocytosis to facilitate resistant response, and maize modulates a series of pathways associated with secretion and the autophagy process (**Figure 3B**). Similarly, in modules 3, 4, 5, and 8, genes exhibited peak expression at 3 hpi and/or 6 hpi in Y331-ΔTE (**Figure 3A**), suggesting that these genes were co-expressed and induced at these time points to mediate the resistance. These genes were significantly enriched in metabolic pathways of the MAPK signaling pathway and plant hormone signal transduction, which is reported as core components to confer PTI (**Figure 3B**). By contrast, in modules 2, 6, 7, and 9, gene expression shows a reduced pattern in Y331-ΔTE samples at 1, 3, and 6 hpi, indicating that these genes are transcriptionally repressed at these stages. Taken together, the co-expression network analysis demonstrated a sophisticated transcriptomics circuit reprogrammed in Y331-ΔTE and revealed the autophagy process and secretion pathways, MAPK pathways, and plant hormone pathways that were vital in the early-stage response to GSR.

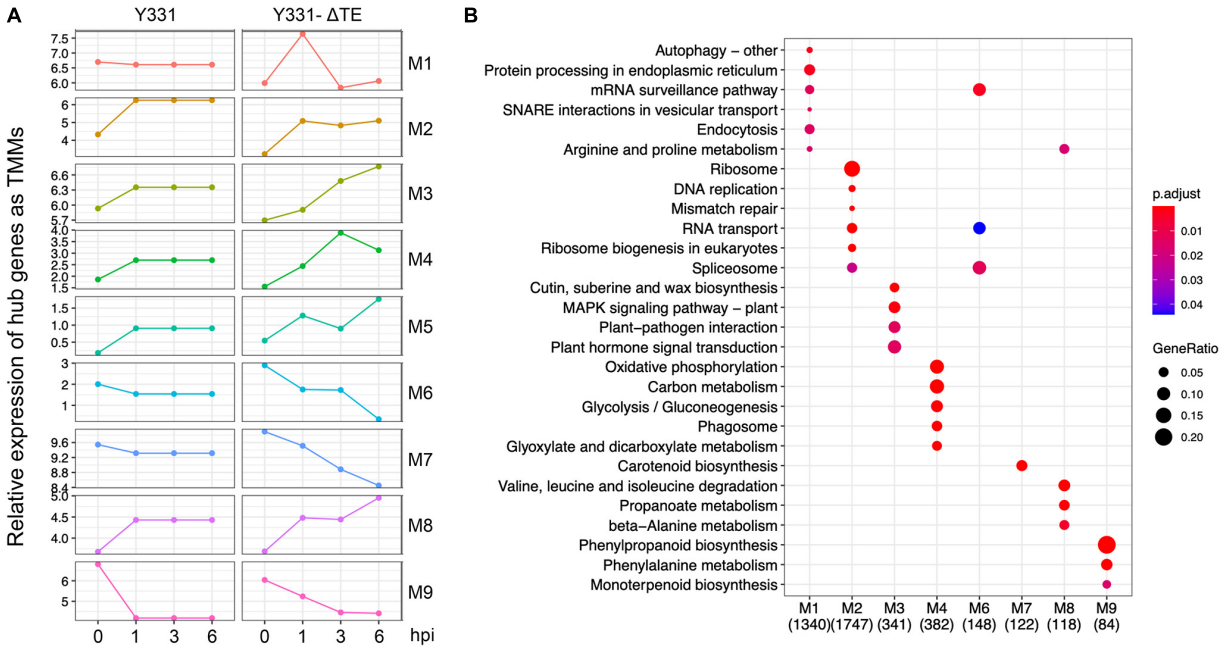

FIGURE 3 | Weighted correlation network analysis (WGCNA) analysis defined nine co-expressed genes as modules during infection stages. **(A)** The plots showing relative expression as TPM values of hub genes representing nine coexpressed genes modules derived from WGCNA analysis using all samples. **(B)** A dot plot showing the significance of KEGG pathways enriched by each coexpression module.

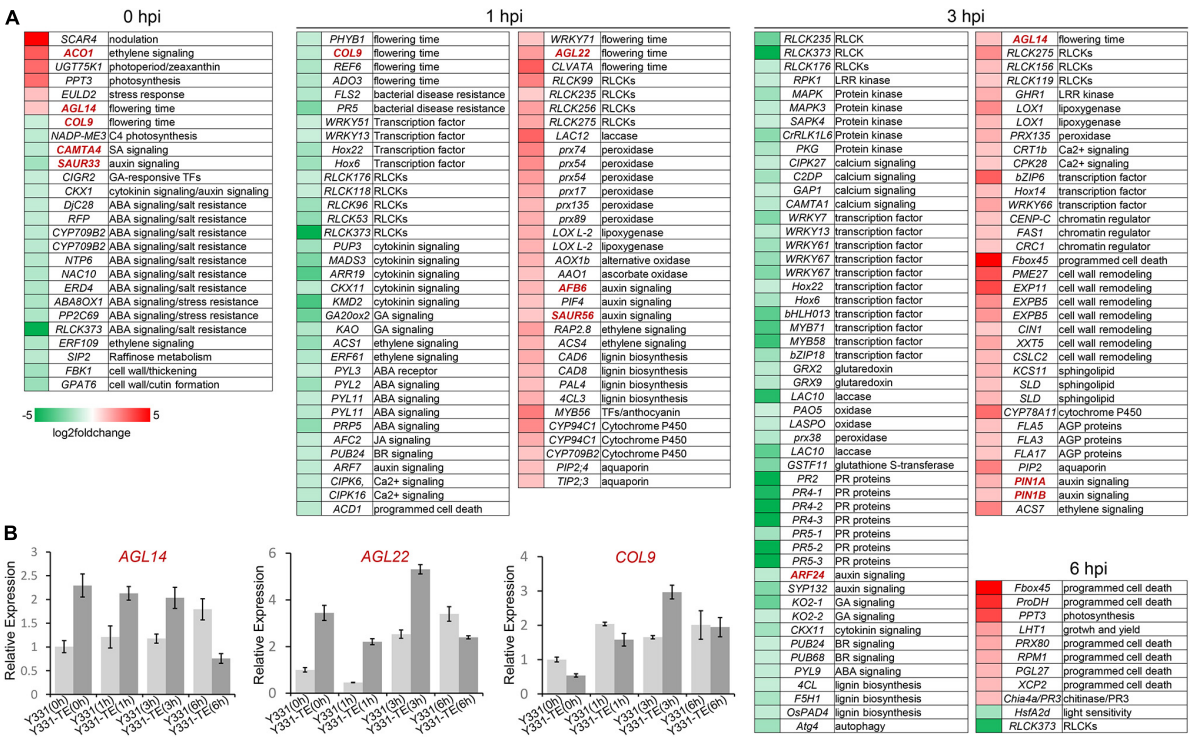

FIGURE 4 | Mapping of differentially expressed genes in maize during different infection stages of *Fusarium graminearum*. **(A)** The heatmaps showed detailed relative expression (log2 fold change) of selected genes related to important functions from RNA-seq. Genes were named according to their *Arabidopsis* or rice orthologs. **(B)** Relative expression of several putative flowering time-related genes in *F. graminearum*-infected maize seedling root at different time points. The β-actin gene *ZmActin* was used as an internal control for normalization. For each gene, the relative enrichment value in Y331-infected seedling root cells at 0 hpi was assigned as 1. Error bars present the ±s.d. of three biological replicates.

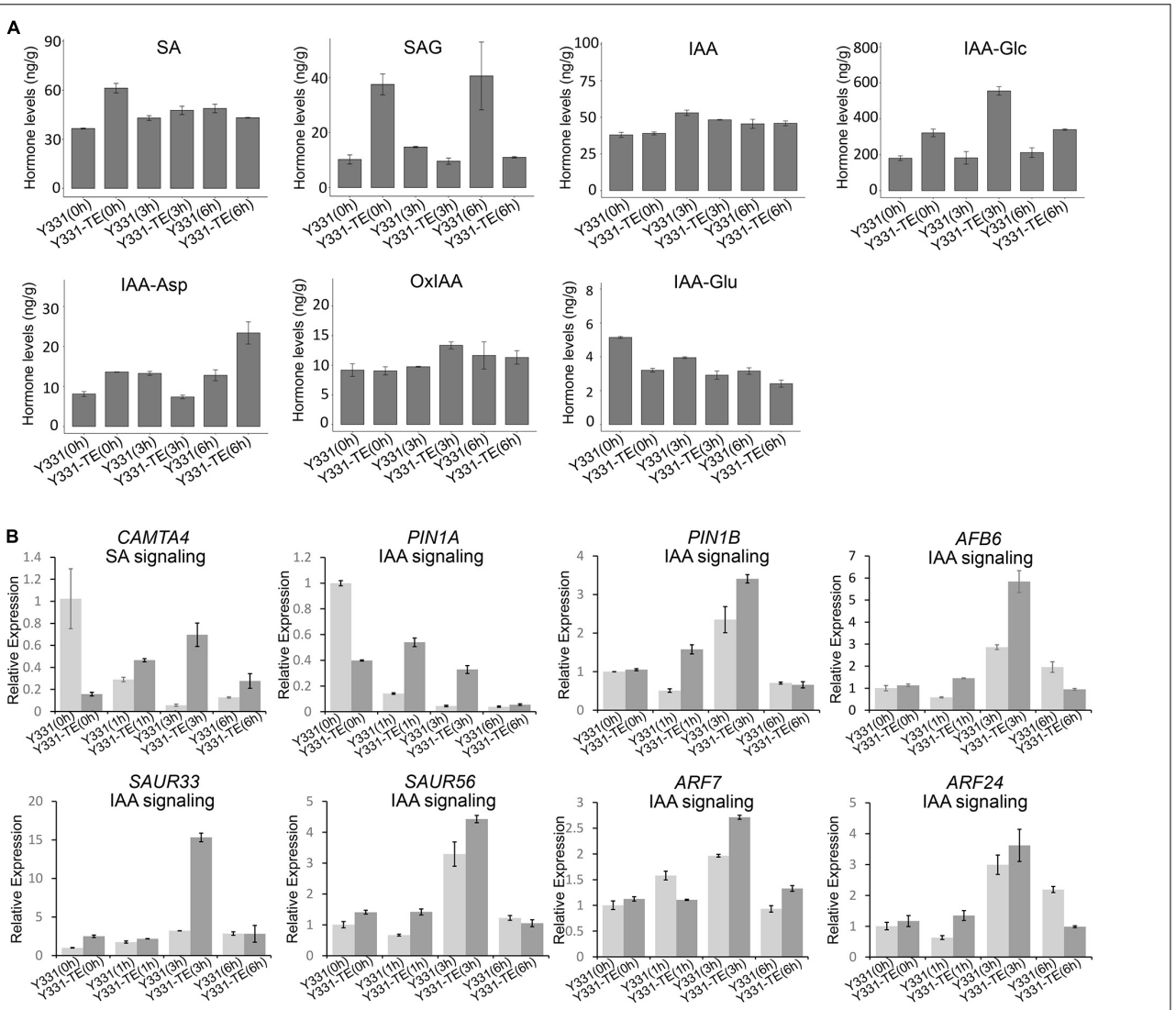

FIGURE 5 | Hormone level changes in Y331-ΔTE and Y331 during infection of *Fusarium graminearum*. **(A)** Determination of endogenous maize hormone contents by LC-MS/MS during *F. graminearum* infection on Y331-ΔTE or Y331 at different time points. SA, salicylic acid; SAG, salicylic acid 2-O-β-glucoside; IAA, indole-3-acetic acid; IAA-Asp, indole-3-acetyl-L-aspartic acid; IAA-Glc, 1-O-indol-3-ylacetylglucose; OxIAA, 2-oxindole-3-acetic acid; IAA-Glu, indole-3-acetyl glutamic acid. **(B)** Relative expression of hormone signaling pathway-related genes in *F. graminearum*-infected maize seedling root at different time points. The β-actin gene *ZmActin* was used as an internal control for normalization. For each gene, the relative enrichment value in Y331-infected seedling root cells at 0 hpi was assigned as 1. Error bars present the ±s.d. of three biological replicates.

ZmCCT Coordinates Different Cellular Processes for Resistance to Stalk Rot Disease in Maize

To widen the analysis and interpret more insights into the resistance mechanism in maize to GSR, we sought to investigate the orthologous genes with known functions by extracting orthologous genes in maize to *Arabidopsis* and rice. Using the RNAseq analysis, DEGs were identified, and using proteomics analysis, DEPs were identified, and the known function of the orthologous genes was identified by mining the published data and reports in *Arabidopsis* and rice genes (**Supplementary Table 6** and **Figure 4A**).

To explore why ZmCCT can coordinate photoperiod and defense response, the known function of genes associated with the photoperiod process were identified. Interestingly, we found four genes significantly induced by *F. graminearum* infection at 1 or 3 hpi are known as key factors regulating flowering development in *Arabidopsis*, *AGL14*, *AGL22*, *WRKY71*, and *CLVATA* (**Figure 4A**). In contrast, several other *Arabidopsis* homologous genes, CONSTANS-like gene *COL9*, phytochrome gene *PHYB1*, histone H3 lysine 27 demethylase gene *REF6* were severely repressed during *F. graminearum* infection at 1 or 3 hpi (**Figure 4A**). The MADS transcription factor AGL14 modulates auxin transport during *Arabidopsis* root development by regulating the expression of *PIN* genes

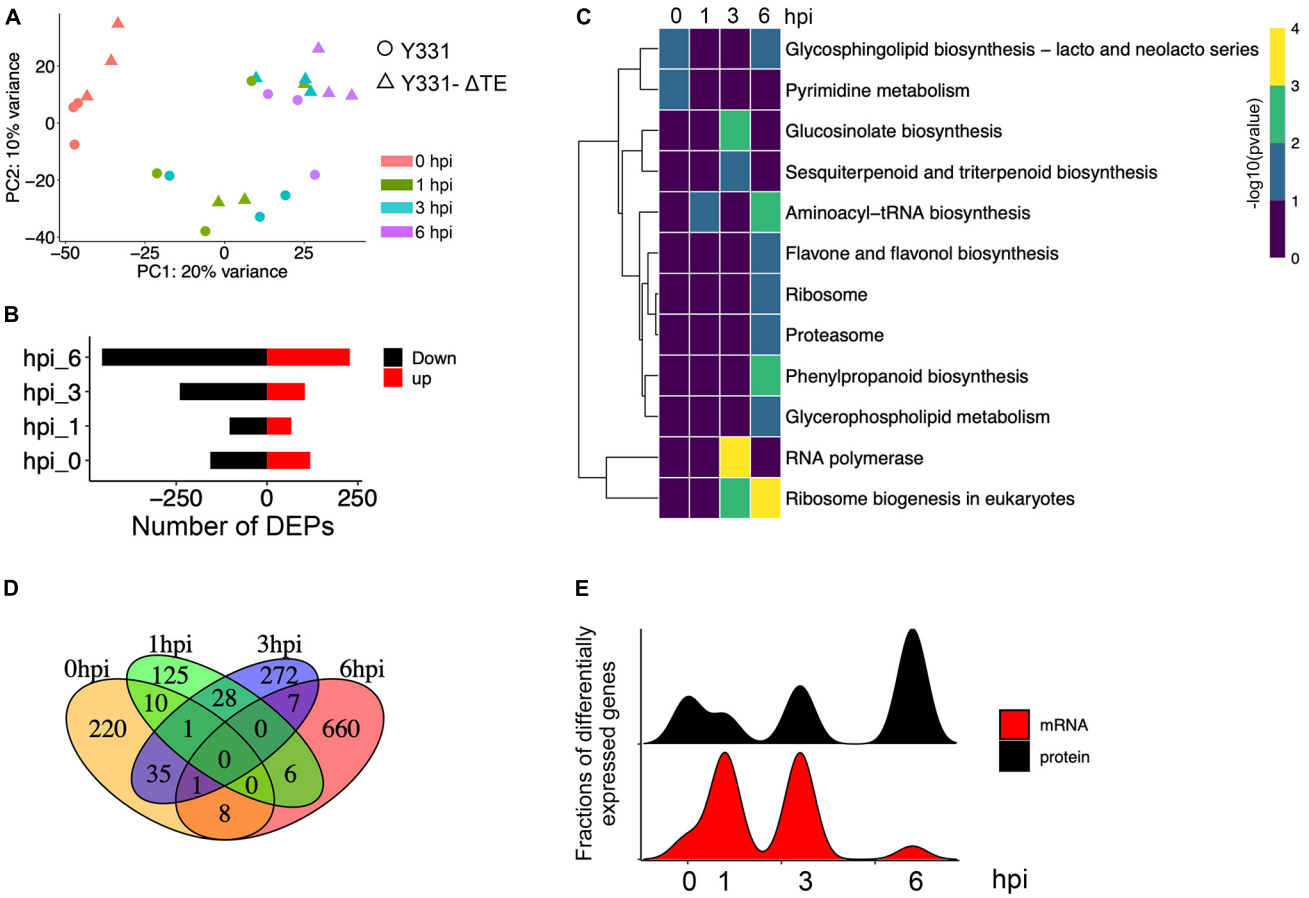

FIGURE 6 | Proteomic analysis revealed a stronger response to infection at the translational level at 6 hpi. **(A)** Principal component analysis of maize proteomics from Y331-ΔTE and Y331 at different time points. **(B)** Barplot showing numbers of DEPs as upregulated and downregulated proteins. **(C)** A dot plot showing the significance of KEGG pathways enriched by DEPs detected in proteomics. **(D)** A Venn diagram showing numbers of differentially expressed proteins when comparing Y331-ΔTE and Y331 at 0, 1 3, and 6 hpi after inoculation. **(E)** Density plot showing the relative fraction of DEGs in RNA-seq, and DEPs in proteomics at four time points.

(Garay-Arroyo et al., 2013). Overexpression of *AGL14* in *Arabidopsis* results in early flowering, suggesting that it also regulates flowering time (Pérez-Ruiz et al., 2015). Another MADS transcription factor, AGL22, is involved in the transition from vegetative state to the flowering stage (Bechtold et al., 2016), and deletion of *AGL22* resulted in early flowering similar to the phenotype of non-functional ZmCCT (Y331) (Gregis et al., 2013). Transcription factor WRKY71 accelerates flowering via the direct activation of the flowering time integrator gene FLOWERING LOCUS T and the floral meristem identity genes LEAFY (Yu et al., 2016). The CLAVATA gene is also reported to modulate flowering time and flower number in chickpeas (Basu et al., 2019). We also identified several genes homologous to *A. thaliana* CONSTANS-like gene *COL9*, phytochrome gene *PHYB1*, histone H3 lysine 27 demethylase gene *REF6* (a relative of early flowering 6), and PAS domain gene *ADO3*, which were severely repressed during *F. graminearum* infection at 1 or 3 hpi (**Figure 4A**). *COL9* delays the flowering time by repressing the Ehd1 pathway in *Oryza sativa* and *A. thaliana* (Cheng and Wang, 2005; Liu H. et al., 2016). *REF6* encodes a Jumonji N/C and zinc finger domain-containing protein that acts as a positive regulator of flowering in an FLC-dependent pathway (Cui et al., 2016). The qRT-PCR experiment confirmed that expression patterns of selected flowering-related genes, *AGL14*, *AGL22*, and *COL9* were consistent with the omics data (**Figure 4B**). Altogether, these data suggested that ZmCCT may be involved in coordinating photoperiod and defense response through key regulatory genes related to flowering.

At 1 and 3 hpi, many known functions of homologous genes of DEGs/DEPs were reported to be involved in PTI response, including genes encoding RLCK kinases (RLCK99, RLCK156, RLCK119, RLCK235, RLCK256, RLCK275, and GHR1), redox proteins (laccase, peroxidase, lipoxygenase, and oxidase), hormone pathway proteins, transcription regulators (WRKY66, Hox14, bZIP6, CENP-C, FAS1, and CRC1), aquaporins, AGPs proteins, lignin biosynthesis proteins, and sphingolipid biosynthesis proteins (**Figure 4A**). Interestingly, expressions of some redox-related genes, protein kinases, calcium signaling pathway proteins, the lignin biosynthesis genes, and several disease resistance proteins (FLS2, PR2, PR4, PR5) were

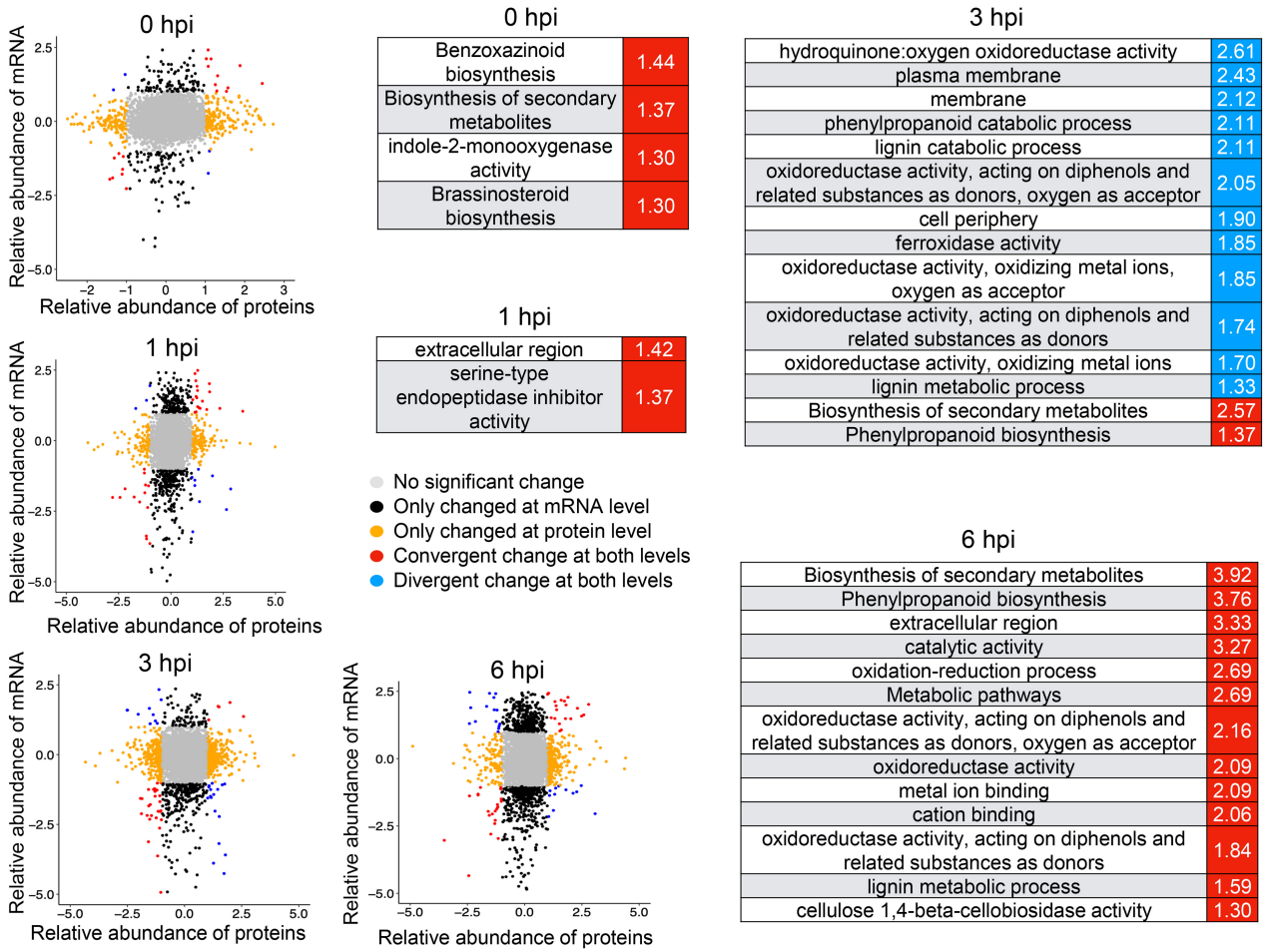

FIGURE 7 | Integrative analysis of RNA-seq and proteomics identified a number of genes co-induced upon resistance to stalk rot disease. The mRNA/protein expression fold changes of samples were calculated by comparing Y331-ΔTE and Y331 at four time points. mRNAs/proteins differentially expressed (| log2[FC]| > 1; *p*-adj < 0.05) in both, either and neither (unchanged) transcriptome and proteome studies were grouped and color-coded. Red and blue represent the Gene Ontology term significantly enriched by co-induced or co-repressed genes at transcriptional and translational levels, respectively.

significantly repressed at 3 hpi, suggesting a weaker PTI response at 3 hpi and a different cellular process comparing to that at 1 hpi.

When inoculated onto susceptible maize cultivar, *F. graminearum* undergoes a biotrophic growth stage at least before 12 hpi (Zhang et al., 2016). Interestingly, some programmed cell death-related genes, including genes homologous to *A. thaliana* ubiquitin E3 ligase component *Fbox45*, proline dehydrogenase *ProDH*, peroxidase *PRX80*, *PGL27*, and xylem cysteine protease *XCP2* (Avci et al., 2008), as well as an R gene *RPM1* (Boyes et al., 1998), were significantly upregulated in Y331-ΔTE at 6 hpi in resistant maize (**Figure 4A**). These data suggested that the Y331-ΔTE resistant line launches a hypersensitive reaction strategy for resistance at 6 hpi. To test this possibility, we stained the *F. graminearum*-infected root seedling cells with Trypan blue, which was commonly used to stain dead cells in plants. At 0, 1, and 3 hpi, none of the *F. graminearum*-infected host cells could be stained to deep blue color, while at 6 hpi, the infected host cells were much easier to be stained to deep blue in Y331-ΔTE but not in Y331 (**Supplementary Figure 4**), suggesting that cell death occurred, which is consistent with the prediction.

Different Hormone Pathways Were Coordinated for Early-Stage Resistance to Gibberella Stalk Rot

Plant defense against microbial attack is regulated by a complex network of hormone signaling pathways (Robert-Seilaniantz et al., 2011). We identified that a large number of DEGs/DEPs were involved in hormone pathways during maize responding to GSR. At 0 hpi before *F. graminearum* infection, many genes involved in hormone signaling pathways were repressed in resistant line Y331-ΔTE (**Figure 4A**). Genes encoding auxin receptor F-box protein AFB6 (Prigge et al., 2016), bHLH transcription factor PIF4 (Choi and Oh, 2016), and small auxin upregulated protein SAUR56 were activated at 1 hpi, while the other two genes encoding *PIN1* (*PIN1A* and *PIN1B*) were activated at 3 hpi (**Figure 4A**). Several other auxin signaling

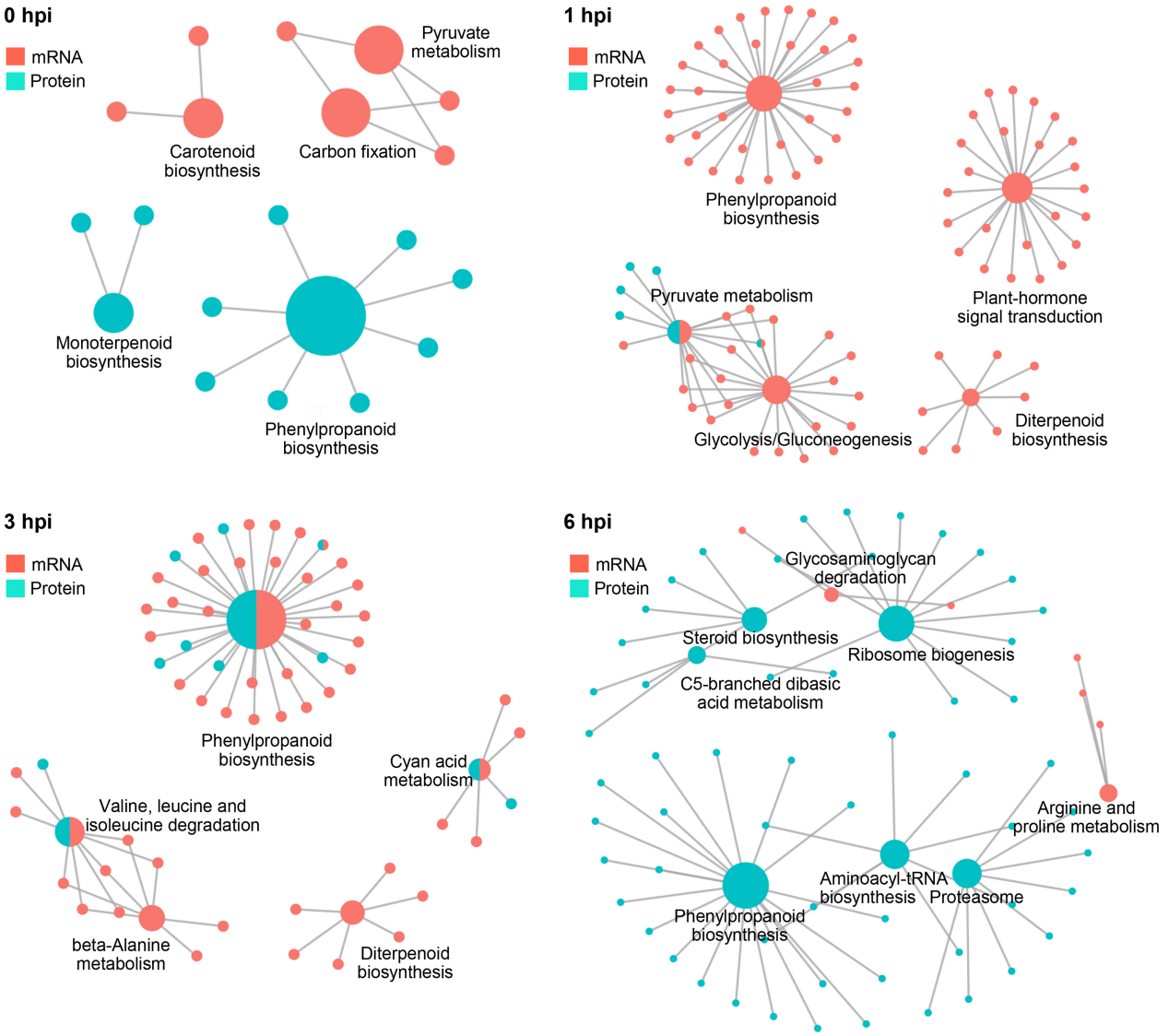

FIGURE 8 | The complex association between enriched KEGG pathways. Plots showing KEGG pathways significantly enriched by DEGs and DEPs detected in RNA-seq and proteomics at 0, 1, 3, and 6 hpi.

pathway genes, auxin response transcription factor genes, *ARF7*, *ARF24*, and syntaxin *SYP132* (Xia et al., 2020) were decreased in Y331-ΔTE at 1 or 3 hpi.

We measured the contents of chemical compounds related to SA and IAA hormones in both Y331 and Y331-ΔTE during *F. graminearum* infection. In non-inoculated roots, the SA level was higher in Y331-ΔTE than in Y331, but there was no evident difference between these two lines upon fungal infection at 3 and 6 hpi (**Figure 5A**). In addition to the regulation at the biosynthesis level, free SA also undergoes chemical modifications, including glycosylation, to form the inactive SA-glucoside (SAG) (Lefevere et al., 2020). At 0 hpi, SAG was also higher in Y331-ΔTE but decreased in both Y331-ΔTE and Y331 at 3 hpi (**Figure 5A**). Interestingly, it was much higher in Y331 at 6 hpi, suggesting that SA could massively exist as an inactive form in Y331 at this time point. We evaluated the expression pattern of *CAMTA4* by qRT-PCR. As a putative repressor of SA biosynthesis, *CAMTA4* was significantly decreased in Y331-ΔTE under the non-treatment condition; coincidently, the SA level was elevated when compared with that in Y331. Upon *F. graminearum* infection at 1 and 3 hpi, the expression level of *CAMTA4* in Y331-ΔTE was increased when compared with that in Y331 but reduced to the level under the non-treatment condition, which was correspondent with the SA signaling pathway (**Figure 5B**).

In general, the IAA levels were slightly elevated during *F. graminearum* infection, but no evident differences were observed between the resistant line Y331-ΔTE and the susceptible line Y331 at 3 and 6 hpi (**Figure 5A**). As a major storage form of auxin in plants, auxin conjugates also play a

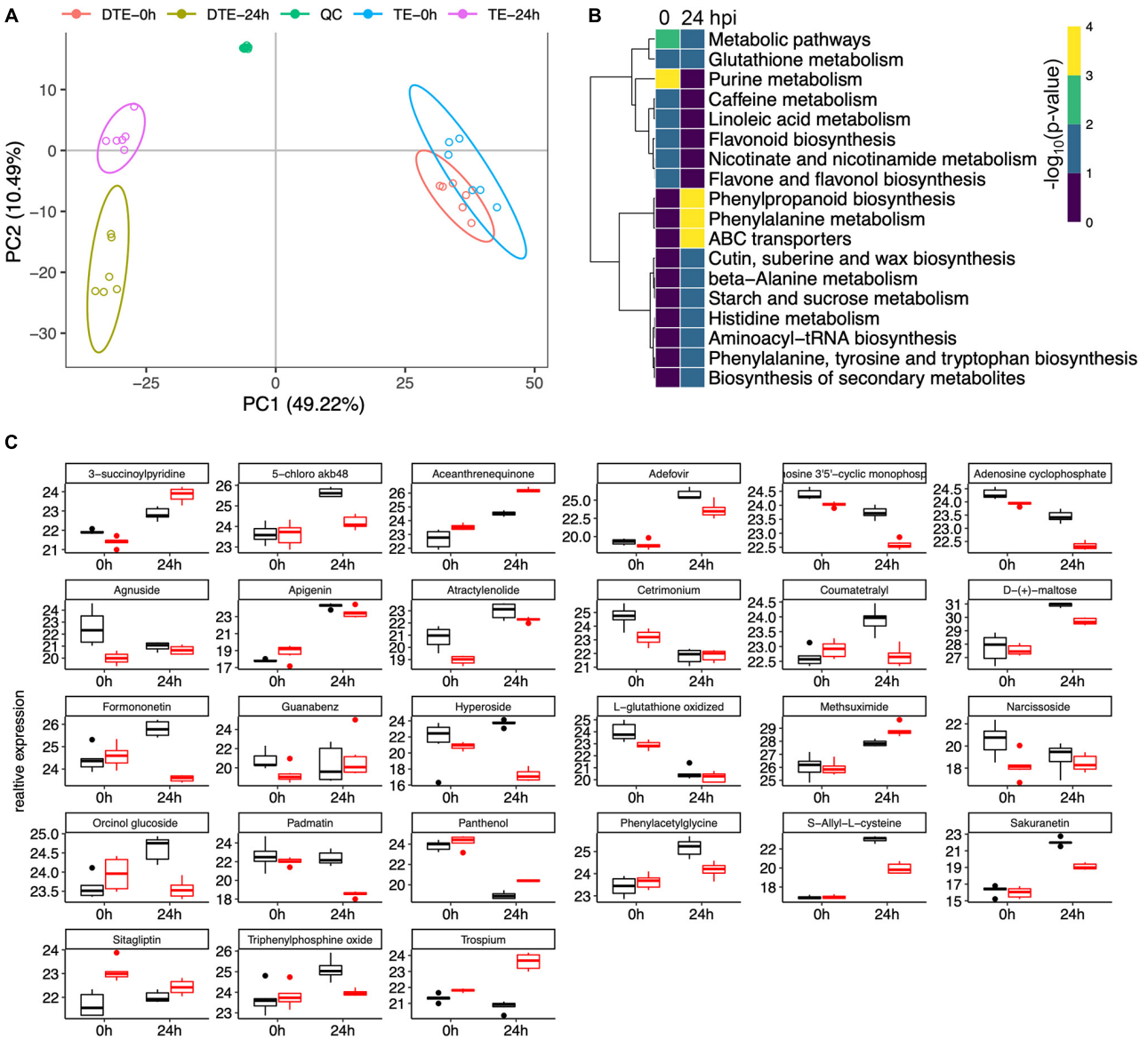

FIGURE 9 | Metabolomic analysis revealed key pathways associated with early-stage resistance to gibberella stalk rot (GSR). **(A)** Principal component analysis to determine the global metabolic variation between Y331-ΔTE and Y331 at 0 and 24 hpi. **(B)** Heatmap showing the significance of metabolic pathways enriched by metabolic compounds detected in comparative metabolomics comparing Y331-ΔTE and Y331. **(C)** Boxplots showing the relative abundance of detected metabolic compounds in comparative metabolomics which are significantly altered between Y331-ΔTE and Y331. Black refers to Y331, and red refers to Y331-TE.

key role in regulating the availability of endogenous-free IAA (Ludwig-Müller, 2011). The mainly detected auxin conjugates in root samples of Y331-ΔTE and Y331 include IAA-Glc, IAA-Asp, OxIAA, and IAA-Glu, among which the content of IAA-Glc accounted for the vast majority (**Figure 5A**). Interestingly, the IAA-Glc level was significantly increased in Y331-ΔTE compared with that in Y331 at each detecting time, suggesting a possible role of ZmCCT in the regulation of IAA-Glc to affect IAA signaling pathway during *F. graminearum* infection. We chose several IAA signaling pathway genes mentioned above to confirm their expression pattern during *F. graminearum* infection (**Figure 4A**). As expected, most of these genes, including *PIN1A*, *PIN1B*, *AFB6*, SAUR33, and SAUR56, ARF7 and ARF24, were activated at 1 or 3 hpi but reduced to the level similar to that of non-treatment condition (**Figure 5B**). These results showed that these IAA signaling pathway genes were affected at the early stage of GSR.

After data normalization, quality control, and the PCA (**Figure 6A** and **Supplementary Figure 5**), comparative proteomic analysis identified 275, 170, 344, and 682 proteins as differentially expressed proteins (DEPs) at 0, 1, 3, and 6 hpi, respectively (**Figure 6B** and **Supplementary Table 7**). These results indicated a rapid increase of proteins at 6 hpi during defense response to GSR (**Supplementary Figure 6**). The GO enrichment analysis indicated that DEPs at 6 hpi

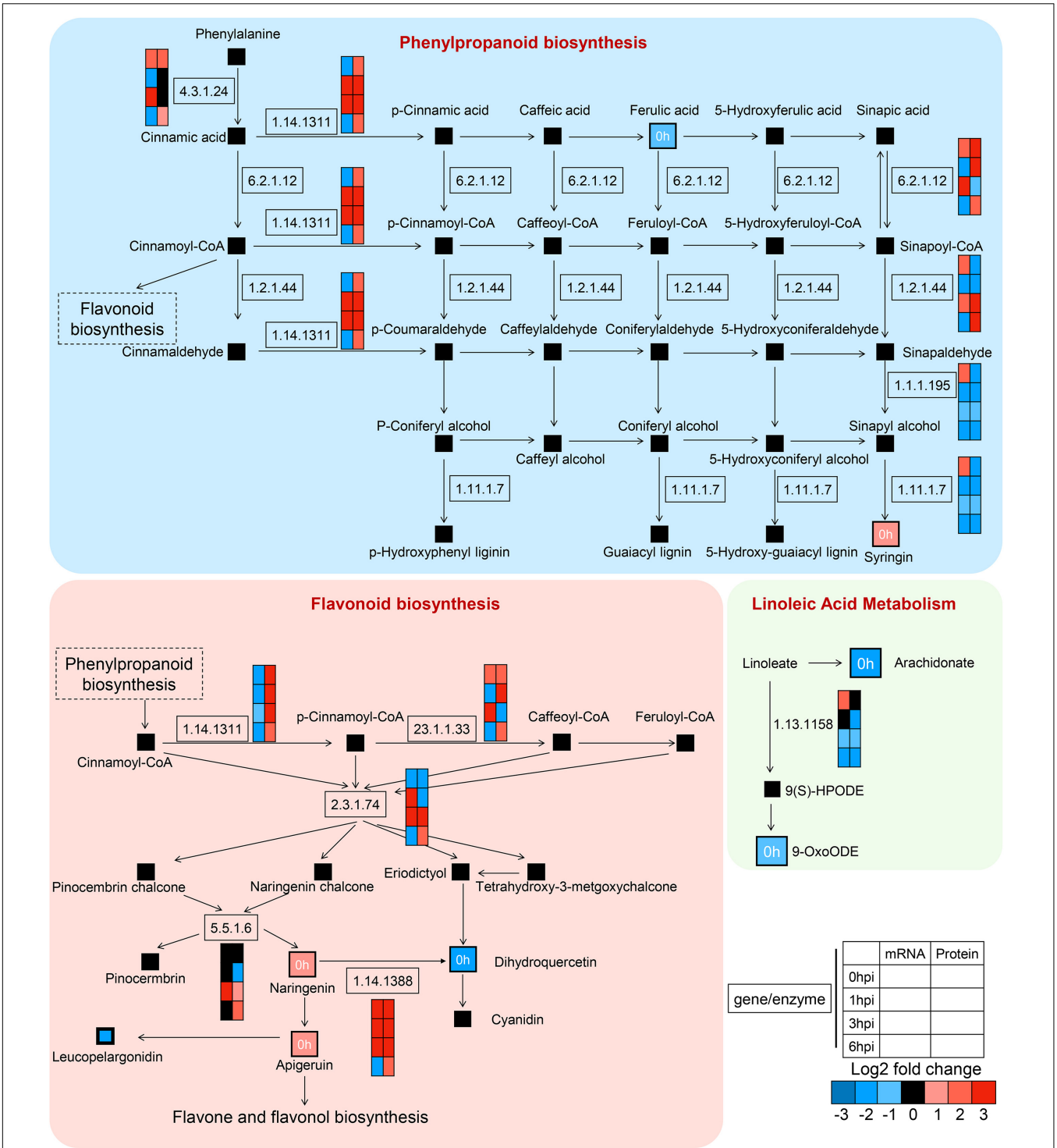

FIGURE 10 | High-resolution mapping of the regulatory network to metabolic pathways. Simplified metabolic flow schemes described changes in metabolites and enriched enzymes associated with transcripts, proteins, phenylpropanoid biosynthesis, flavonoid biosynthesis, and linoleic acid metabolism. The colors indicated rates of upregulation or downregulation of groups of enzymes.

were significantly enriched in terms associated with nucleic acid binding, RNA binding, RNA helicase activity, nuclear transport, and rRNA process (**Supplementary Figure 6**). This result suggested a specific function of DEPs at 6 hpi in RNA process and binding, which may also continue to modulate defense response at 6 hpi (**Supplementary Figures 7A,B**

and **Supplementary Table 8**). We discovered these DEPs are significantly enriched in metabolic pathways in glucosinolate biosynthesis at 3 hpi and phenylpropanoid biosynthesis at 6 hpi (**Figure 6C** and **Supplementary Table 9**). Similar to the result of DEGs, DEPs at four time points were not well-overlapped (**Figure 6D**), suggesting that, at each time point during the early stage, the expression of the specific group of genes were significantly altered at both transcriptional and translational levels. To further integrate RNA-seq and proteomic data, we generated correlation analysis and found an uncorrelated pattern in samples at all four time points, suggesting that the abundance of transcripts and proteins were not equal during defense response (**Supplementary Figure 7**). By comparing the variation patterns of RNA-seq and proteomic analyses, we found that the defense response triggers transcriptional reprogramming at 1 and 3 hpi, but the translational level was most changed at 6 hpi (**Figure 6E**).

Integrative analysis of RNA-seq and proteomics data also defined a set of genes induced at both transcriptional and translational levels (**Figure 7**), among which genes involved in brassinosteroid biosynthesis and benzoxazinmoid biosynthesis were enriched at 0 hpi and genes involved in the phenylpropanoid biosynthesis pathway were enriched at 3 hpi (**Figure 7**). There were more co-induced genes at 6 hpi, which were significantly enriched in phenylpropanoid biosynthesis and the oxidation–reduction process (**Figure 7**), suggesting that these biological processes and pathways might be vital to conferring resistance to GSR. These results highlighted a set of important genes that show convergent patterns at mRNA and protein levels. At the same time, some genes showing divergent patterns at mRNA and protein levels at four time points were also detected (**Figure 7**). Notably, the divergent pattern genes at 3 hpi were significantly enriched in many GO terms, including the lignin catabolic process, cell periphery, and plasma membrane (**Figure 7**), suggesting that a turnover regulatory event occurred in these genes.

Further integrative analysis with metabolic pathways demonstrated a clear dominant regulatory effect in the mRNA level at 1 hpi and in the protein level at 6 hpi (**Figure 8**), suggesting a transient response to stalk rot at a very early stage in the transcriptional level after 1 hpi and in the translational level at 6 hpi. Taken together, the combination of RNA-seq and proteomic analyses demonstrated a distinct responsive pattern in transcriptional and translational levels during early defense response to GSR in maize.

Genome-Wide Metabolomics Analysis Uncovered Key Properties Associated With Defense to Gibberella Stalk Rot

Given that a sophisticated gene expression reprogramming was affected during the resistance to GSR at the early stages of infection, we set up to explore the outcome of these regulatory events. Using genome-wide metabolomics to compare Y331-ΔTE and Y331 samples, after inoculation at 0 and 24 hpi, we profiled 3,660 putative features from all the samples after normalization (**Supplementary Figure 8**). The PCA and clustering analysis demonstrated a distinct metabolomic pattern between Y331-ΔTE and Y331 at 24 hpi (**Figure 9A**). A significantly distinct metabolomic pattern between 0 and 24 hpi was also observed (**Figure 9A**), suggesting a massive metabolic outcome of transcriptional regulation.

Differentially expressed compounds analysis defined 8 and 12 enriched metabolic pathways at 0 and 24 hpi, respectively (**Figure 9B**, **Supplementary Figure 9**, and **Supplementary Tables 10**, **11**). At 24 hpi, the phenylpropanoid biosynthesis, phenylalanine metabolism, and ABC transporters were severely increased (**Figure 9B**), suggesting key roles of these metabolic processes in GSR defense response. Several other metabolic processes, including cutin, suberin, and wax biosynthesis, beta-alanine metabolism, starch and sucrose metabolism, histidine metabolism, aminoacyl-tRNA biosynthesis, phenylalanine, tyrosine, and tryptophan biosynthesis, as well as biosynthesis of secondary metabolites, were also enriched (**Figure 9B**), suggesting that these metabolic processes were also involved in GSR defense response. **Figure 9C** showed a series of detected metabolic compounds in comparative metabolomics which were significantly altered between Y331-ΔTE and Y331.

To demonstrate the regulatory network during early GSR defense response in maize, we mapped the DEGs, DEPs, and altered compounds in phenylpropanoid biosynthesis and flavonoid biosynthesis, which were known to play key roles in plant defense (**Figure 10**). We found severe upregulation in genes at the transcriptional level relevant to enzymatic reactions, such as 23.1.1.133 in flavonoid biosynthesis and 1.14.1311 in phenylpropanoid biosynthesis (**Figure 10**). We detected a concurrent upregulated abundance of gene products at both transcriptional and translational levels in genes associated with enzymatic reaction 1.14.1388 at 0, 1, and 3 hpi, which negatively regulates the abundance of dihydroquercetin. Interestingly, we found that, in the linoleic acid metabolism, genes and proteins associated with enzymatic reaction 1.13.1158 at 1, 3, and 6 hpi were all decreased, suggesting that this metabolic process was negatively associated with ZmCCT upon infection. Taken together, these results demonstrated detailed information on the metabolic processes in maize's early GSR defense.

DISCUSSION

The filamentous fungus *F. graminearum* infects maize as a hemibiotrophic lifestyle to cause GSR. As a consequence of arm racing, maize has evolved complex defense strategies to encounter fungal infection at different cellular levels (Kazan et al., 2012). Given that the maize quantitative resistance gene *ZmCCT* is transcriptionally induced in maize at the early infection stage of *F. graminearum* (1–3 hpi) for defense, it can be used as a key resource to study the regulatory mechanism of maize's early-stage defense response to GSR. We found that, at the early infection stage of *F. graminearum*, maize rapidly launches a massive PTI-mediated defense response pattern. Transcriptional profiling indicates a transit reaction that is served at 1 and 3 hpi. Comparing the gene expression variation patterns in RNA-seq and proteomics, we found that, in Y331-ΔTE, defense

triggers transcriptional reprogram at 1 and 3 hpi but a severe change occurs at the translational level at 6 hpi. Combining with the metabolomic analysis, we discovered some key metabolic pathways that might be important for resistance response to GSR. Our study also suggested that *ZmCCT* fine-tunes the cellular processes between defense and photoperiod response. Altogether, the study produces a great resource to interpret the early defense mechanism during GSR resistance in maize.

Multi-Omic Strategy Provides a Comprehensive Understanding of Gibberella Stalk Rot Resistance

The multi-omic analysis has been used to explore the mechanisms of plant disease resistance (Crandall et al., 2020), which provides more in-depth insights into the molecular mechanism of defense response to the infection of the pathogens. For example, the roles of ZmHIR3 in maize resistance to GSR were revealed by integrative analyses of gene co-expression analysis and metabolites profiling (Sun et al., 2021). Besides, transcriptomic and metabolomic integrative analyses of the resistant and susceptible lines of Fusarium head blight caused by *F. gramineae* was also carried out, which identified that several enzymes and transcription factors were candidate resistance genes (Dhokane et al., 2016). A comparative proteomic analysis revealed ZmWRKY83-mediated GSR resistance (Bai et al., 2021). Combined with DAP-Seq and RNA-Seq analyses, a recent study also showed the regulatory mechanism of ZmCCT in coordinating flowering, stress response, and development (Su et al., 2021). In this study, we combined transcriptomic data with those proteomic and metabolomic approaches to comprehensively reveal a multilevel landscape of maize defense response and better understand the mechanism of GSR resistance at the early biotrophic growth stage during *F. graminearum* infection.

The Resistance Mechanism of Gibberella Stalk Rot in the Early Stage of Infection Is Closely Related to Pattern-Trigged Immunity

Fusarium graminearum possesses a hemibiotrophic lifestyle upon the infection of maize which causes GSR (Glazebrook, 2005; Brown et al., 2010; Kazan et al., 2012). At the early infection stage, *F. graminearum* remains non-symptomatic for a period before the development of a necrotrophic phase (Brown et al., 2010; Kazan et al., 2012). To encounter *F. graminearum* infection, maize have also developed complex defense strategies at both transcriptional and translational levels. Considering that the lifestyles of *F. graminearum* during different phases of disease development are quite different, correspondingly, the host plant also evolves different resistance responses during different infection stages. Previous studies have shown that various plant defense signaling pathways show spatio-temporal dynamics and stage-specific patterns in response to pathogen attacks (Ding et al., 2011; Zhang X. W. et al., 2012; Brown et al., 2017). For example, Ca^{2+} signaling pathway and SA signaling pathway were usually induced at the early infection stage, but JA signaling pathway was usually induced at the late infection stage (Ding et al., 2011). A transcriptomic analysis comparing lines with and without qRfg1 showed that defense-associated genes are quickly induced at the early infection stage of GSR (Yang et al., 2010; Ye et al., 2013; Liu Y. et al., 2016). In this study, the integrative transcriptomic, proteomic, and metabolomic analyses clearly showed the different patterns of DEGs, DEPs, and DAMs, further supporting that early-stage GSR resistance is strongly activated at the early infection stage of *F. graminearum*.

To provide a wider vision of transcriptional profiling associated with GSR resistance in the early stage, we deployed WGCNA to construct co-expression networks, in which a series of genes were identified to be significantly enriched at the early stage of fungal infection, including genes associated with pathways of autophagy process, vesicular transport, and endocytosis. Genes involved in metabolic pathways of MAPK signaling pathway, plant hormone signal transduction, glycolysis, and phagosome were significantly enriched in modules co-expressed and induced at 3 hpi and/or 6 hpi to mediate the resistant (**Figure 3**). More interestingly, most of these genes are reported as core components to confer the PTI-mediated defense Response (**Supplementary Figure 3**). Our result is consistent with a previous study in barley, which showed that the transcriptome analysis of barley revealed that *F. graminearum* infection-induced differential expression of genes was related to the PTI-mediated defense response (Bigeard et al., 2015). Future studies should focus on dissecting the function and molecular mechanisms, including the PTI-related defense response underlying the GSR resistance.

ZmCCT Coordinates Defense and Photoperiod at the Early-Stage Response to Gibberella Stalk Rot

Previous studies have shown that the qRfg1 locus not only increases maize resistance to GSR by activating the expression of defense-related genes but also fine-tunes the metabolic processes to balance defense and growth. Our multi-omic analysis provides a more detailed explanation for important defense-related biological processes in the resistant line Y331-ΔTE (**Figures 2**, **3**). We found in maize that many orthologous rice or *Arabidopsis* genes were reported to be involved in flavonoid, phytoalexin, redox, RLCKs, and WRKY transcription factors, which are also detected as DEGs in our analysis. These results suggest that Y331-ΔTE can counterattack the infection of *F. graminearum* via constitutive resistance.

Pathogen infection activates phytohormone signaling pathways which, in turn, mediates signaling transmission to trigger plant immunity (Bari and Jones, 2009). However, pathogens have evolved effectors as secreted proteins to interfere with plant hormone signaling pathways (Han and Kahmann, 2019). Genes upregulated in Y331-ΔTE is an action as a response to the SA signaling pathway and auxin signaling pathway that is believed to be associated with FHB resistance (Hao et al., 2018), suggesting the role of *ZmCCT* in the constitutive resistance to infection by regulating phytohormones. The

ZmCCT gene seems to contribute to GSR resistance by positively influencing the expression of auxin signaling pathway genes (**Figure 4**). Experimental detection confirmed the elevation of auxin signaling during *F. graminearum* infection in the resistant line Y331-ΔTE. As discussed above, *ZmCCT* functions at the early biotrophic stage; therefore, we speculate that, during GSR resistance, the auxin signaling pathway is affected by ZmCCT for early biotrophic stage resistance and repressed by other regulators (such as ZmHIR3) for late necrotrophic stage resistance. Recently, a transcriptome and oxylipin profiling joint analysis indicated that 9-oxylipins contribute to resistance but JAs facilitate susceptibility during GSR (Wang et al., 2021). Another recent study showed that ZmCOIa and endogenous JA may function as susceptibility factors during GSR (Ma et al., 2021).

ZmCCT is one of the most important genes regulating photoperiod response. The presence of *ZmCCT* blocked the flowering transition of maize seedlings, which was characterized by increased plant height and delayed flowering (Yang et al., 2010). There may be an internal relationship between flowering time and resistance because late flowering is usually related to strong disease resistance (Elzinga et al., 2007). It was found that *ZmCCT* plays its role in a tissue-specific pattern, which shows strong photoperiod sensitivity in leaves, but conferred stable defense response to GSR in roots (Wang et al., 2017). A chromatin remodeling of the *ZmCCT* promoter may be a major epigenetic factor in the regulation of *ZmCCT* expression. It seems reasonable for plants to use such a chromatin-based regulatory mechanism to orchestrate basal and stress-induced gene regulation in a precise and timely manner to balance the trade-offs of growth and pathogen defense. Here, we identified a series of flowering controlling genes that were activated or repressed in Y331-ΔTE, among which, *AGL14*, *AGL22*, and *COL9* were confirmed by the qRT-PCR analysis, suggesting that *ZmCCT* can well balance the flowering-defense balance by coordinating downstream signaling networks. It is interesting to reveal the regulatory mechanisms between *ZmCCT* and these identified flowering controlling genes in the future.

In summary, this study clearly shows that the multi-omic analysis has been very useful in advancing our overall understanding of maize defense response to GSR, which significantly advanced our understanding of this economically important plant–microbe interaction.

DATA AVAILABILITY STATEMENT

The original contributions presented in the study are publicly available. This data can be found here: NCBI, PRJNA757397 and National Genomics Data Center, PRJCA006316.

AUTHOR CONTRIBUTIONS

WW, X-LC, and BT designed the project. ZZ, XZ, YX, and LW performed the experiments. BT and X-LC performed the multi-omic data analysis and interpretation of the results. X-LC, BT, ZZ, and WW wrote the manuscript. All authors contributed to the article and approved the submitted version.

FUNDING

This work was supported by the National Natural Science Foundation of China (Grants 32072365 and 31871909 to X-LC, and 31871638 to WW), the Special Scientific Research Project of Beijing Agriculture University (YQ201603), the Research Fund for Academic Degree and Graduate Education of Beijing University of Agriculture (2019YJS037), the Research Fund of State Key Laboratory for Biology of Plant Diseases and Insect Pests (SKLOF202102), the Opening Project of Beijing Key Laboratory of New Technology in Agricultural Application (kf2020022), and the Fundamental Research Funds for the Central Universities (2021ZKPY007 to X-LC).

ACKNOWLEDGMENTS

We thank Mingliang Xu at China Agricultural University for providing us with maize near-isogenic lines Y331 and Y331-ΔTE.

SUPPLEMENTARY MATERIAL

The Supplementary Material for this article can be found online at: https://www.frontiersin.org/articles/10.3389/fpls.2022.917493/full#supplementary-material

REFERENCES

Avci, U., Earl Petzold, H., Ismail, I. O., Beers, E. P., and Haigler, C. H. (2008). Cysteine proteases XCP1 and XCP2 aid micro-autolysis within the intact central vacuole during xylogenesis in *Arabidopsis* roots. *Plant J.* 56, 303–315. doi: 10.1111/j.1365-313X.2008.03592.x

Bai, H., Si, H., Zang, J., Pang, X., Yu, L., Cao, H., et al. (2021). Comparative proteomic analysis of the defense response to gibberella stalk rot in maize and reveals that ZmWRKY83 is involved in plant disease resistance. *Front. Plant Sci.* 12:694973. doi: 10.3389/fpls.2021.694973

Bari, R., and Jones, J. D. (2009). Role of plant hormones in plant defence responses. *Plant Mol. Biol.* 69, 473–488. doi: 10.1007/s11103-008-9435-0

Basu, U., Narnoliya, L., Srivastava, R., Sharma, A., Bajaj, D., Daware, A., et al. (2019). CLAVATA signaling pathway genes modulating flowering time and flower number in chickpea. *Theor. Appl. Genet.* 132, 2017–2038. doi: 10.1007/s00122-019-03335-y

Bechtold, U., Penfold, C. A., Jenkins, D. J., Legaie, R., Moore, J. D., Lawson, T., et al. (2016). Time-series transcriptomics reveals that agamous-like22 affects primary metabolism and developmental processes in drought-stressed *Arabidopsis*. *Plant Cell* 28, 345–366. doi: 10.1105/tpc.15.00910

Bigeard, J., Colcombet, J., and Hirt, H. (2015). Signaling mechanisms in pattern-triggered immunity (PTI). *Mol. Plant* 8, 521–539. doi: 10.1016/j.molp.2014.12.022

Bjornson, M., Pimprikar, P., Nürnberger, T., and Zipfel, C. (2021). The transcriptional landscape of *Arabidopsis thaliana* pattern-triggered immunity. *Nature Plants* 7, 579–586. doi: 10.1038/s41477-021-00874-5

Bolger, A. M., Lohse, M., and Usadel, B. (2014). Trimmomatic: a flexible trimmer for Illumina sequence data. *Bioinformatics* 30, 2114–2120.

Boyes, D. C., Nam, J., and Dangl, J. L. (1998). The *Arabidopsis* thaliana RPM1 disease resistance gene product is a peripheral plasma membrane protein that is degraded coincident with the hypersensitive response. *Proc. Natl. Acad. Sci. U.S.A.* 95, 15849–15854. doi: 10.1073/pnas.95.26.15849

Brown, N. A., Evans, J., Mead, A., and Hammond-Kosack, K. E. (2017). A spatial temporal analysis of the *Fusarium graminearum* transcriptome during symptomless and symptomatic wheat infection. *Mol. Plant Pathol.* 18, 1295–1312. doi: 10.1111/mpp.12564

Brown, N. A., Urban, M., van de Meene, A. M., and Hammond-Kosack, K. E. (2010). The infection biology of *Fusarium graminearum*: defining the pathways of spikelet-to-spikelet colonisation in wheat ears. *Fungal Biol.* 114, 555–571. doi: 10.1016/j.funbio.2010.04.006

Cheng, X. F., and Wang, Z. Y. (2005). Overexpression of COL9, a CONSTANS-LIKE gene, delays flowering by reducing expression of CO and FT in Arabidopsis thaliana. *Plant J.* 43, 758–768. doi: 10.1111/j.1365-313X.2005.02491.x

Chetouhi, C., Bonhomme, L., Lasserre-Zuber, P., Cambon, F., Pelletier, S., Renou, J.-P., et al. (2016). Transcriptome dynamics of a susceptible wheat upon Fusarium head blight reveals that molecular responses to Fusarium graminearum infection fit over the grain development processes. *Funct. Integr. Genomics* 16, 183–201. doi: 10.1007/s10142-016-0476-1

Choi, H., and Oh, E. (2016). PIF4 integrates multiple environmental and hormonal signals for plant growth regulation in *Arabidopsis*. *Mol. Cell* 39, 587–593. doi: 10.14348/molcells.2016.0126

Crandall, S. G., Gold, K. M., Jiménez-Gasco, M. M., Filgueiras, C. C., and Willett, D. S. (2020). A multi-omics approach to solving problems in plant disease ecology. *PLoS One* 15:e0237975. doi: 10.1371/journal.pone.0237975

Cui, X., Lu, F., Qiu, Q., Zhou, B., Gu, L., Zhang, S., et al. (2016). REF6 recognizes a specific DNA sequence to demethylate H3K27me3 and regulate organ boundary formation in *Arabidopsis*. *Nat. Genet.* 48, 694–699. doi: 10.1038/ng.3556

Dhokane, D., Karre, S., Kushalappa, A. C., and McCartney, C. (2016). Integrated metabolo-transcriptomics reveals *fusarium* head blight candidate resistance genes in wheat QTL-Fhb2. *PLoS One* 11:e0155851. doi: 10.1371/journal.pone.0155851

Ding, L., Xu, H., Yi, H., Yang, L., Kong, Z., Zhang, L., et al. (2011). Resistance to hemi-biotrophic F. graminearum infection is associated with coordinated and ordered expression of diverse defense signaling pathways. *PLoS One* 6:e19008. doi: 10.1371/journal.pone.0019008

Dodds, P. N., and Rathjen, J. P. (2010). Plant immunity: towards an integrated view of plant-pathogen interactions. *Nat. Rev. Genet.* 11, 539–548. doi: 10.1038/nrg2812

Du, Z., Zhou, X., Ling, Y., Zhang, Z., and Su, Z. (2010). agriGO: a GO analysis toolkit for the agricultural community. *Nucleic Acids Res.* 38, W64–W70. doi: 10.1093/nar/gkq310

Elzinga, J. A., Atlan, A., Biere, A., Gigord, L., Weis, A. E., and Bernasconi, G. (2007). Time after time: flowering phenology and biotic interactions. *Trends Ecol. Evol.* 22, 432–439. doi: 10.1016/j.tree.2007.05.006

Garay-Arroyo, A., Ortiz-Moreno, E., de la Paz Sánchez, M., Murphy, A. S., and García-Ponce, B. (2013). The MADS transcription factor XAL2/AGL14 modulates auxin transport during *Arabidopsis* root development by regulating PIN expression. *EMBO J.* 32, 2884–2895. doi: 10.1038/emboj.2013.216

Glazebrook, J. (2005). Contrasting mechanisms of defense against biotrophic and necrotrophic pathogens. *Annu. Rev. Phytopathol.* 43, 205–227. doi: 10.1146/annurev.phyto.43.040204.135923

Gregis, V., Andrés, F., Sessa, A., Guerra, R. F., Simonini, S., Mateos, J. L., et al. (2013). Identification of pathways directly regulated by SHORT VEGETATIVE PHASE during vegetative and reproductive development in *Arabidopsis*. *Genome Biol.* 14:R56. doi: 10.1186/gb-2013-14-6-r56

Han, X., and Kahmann, R. (2019). Manipulation of phytohormone pathways by effectors of filamentous plant pathogens. *Front. Plant Sci.* 10:822. doi: 10.3389/fpls.2019.00822

Hao, Q., Wang, W., Han, X., Wu, J., Lyu, B., Chen, F., et al. (2018). Isochorismate-based salicylic acid biosynthesis confers basal resistance to *Fusarium graminearum* in barley. *Mol. Plant Pathol.* 19, 1995–2010. doi: 10.1111/mpp.12675

Huang, Y., Li, L., Smith, K. P., and Muehlbauer, G. J. (2016). Differential transcriptomic responses to *Fusarium graminearum* infection in two barley quantitative trait loci associated with *Fusarium* head blight resistance. *BMC Genomics* 17:387. doi: 10.1186/s12864-016-2716-0

Hung, H. Y., Shannon, L. M., Tian, F., Bradbury, P. J., Chen, C., Flint-Garcia, S. A., et al. (2012). ZmCCT and the genetic basis of day-length adaptation underlying the postdomestication spread of maize. *Proc. Natl. Acad. Sci. U.S.A.* 109, E1913–E1921. doi: 10.1073/pnas.1203189109

Jackson-Ziems, T., Rees, J., and Harveson, R. (2014). *Common Stalk Rot Diseases Of Corn. University of Nebraska-Lincoln Extension; Extension Sheet EC-1898*. Lincoln, NE: University of Nebraska-Lincoln.

Jones, J. D., and Dangl, J. L. (2006). The plant immune system. *Nature* 444, 323–329.

Kazan, K., Gardiner, D. M., and Manners, J. M. (2012). On the trail of a cereal killer: recent advances in *Fusarium graminearum* pathogenomics and host resistance. *Mol. Plant Pathol.* 13, 399–413. doi: 10.1111/j.1364-3703.2011.00762.x

Kim, D., Langmead, B., and Salzberg, S. L. (2015). HISAT: a fast spliced aligner with low memory requirements. *Nat. Methods* 12, 357–360. doi: 10.1038/nmeth.3317

Langfelder, P., and Horvath, S. (2008). WGCNA: an R package for weighted correlation network analysis. *BMC Bioinformatics* 9:559. doi: 10.1186/1471-2105-9-559

Ledencan, T., Simic, D., Brkic, I., Jambrovic, A., and Zdunic, Z. (2003). Resistance of maize inbreds and, their hybrids to Fusarium stalk rot. *Czech J. Genet. Plant Breed.* 39, 15–20.

Lefevere, H., Bauters, L., and Gheysen, G. (2020). Salicylic acid biosynthesis in plants. *Front. Plant Sci.* 11:338. doi: 10.3389/fpls.2020.00338

Liu, H., Dong, S., Sun, D., Liu, W., Gu, F., Liu, Y., et al. (2016a). CONSTANS-Like 9 (OsCOL9) Interacts with receptor for activated c-kinase 1(OsRACK1) to regulate blast resistance through salicylic acid and ethylene signaling pathways. *PLoS One* 11:e0166249. doi: 10.1371/journal.pone.0166249

Liu, Y., Guo, Y., Ma, C., Zhang, D., Wang, C., Yang, Q., et al. (2016b). Transcriptome analysis of maize resistance to Fusarium graminearum. *BMC Genomics* 17:477. doi: 10.1186/s12864-016-2780-5

Love, M. I., Huber, W., and Anders, S. (2014). Moderated estimation of fold change and dispersion for RNA-seq data with DESeq2. *Genome Biol.* 15:550. doi: 10.1186/s13059-014-0550-8

Ludwig-Müller, J. (2011). Auxin conjugates: their role for plant development and in the evolution of land plants. *J. Exp. Bot.* 62, 1757–1773. doi: 10.1093/jxb/erq412

Luo, W., Pant, G., Bhavnasi, Y. K., Blanchard, S.G. Jr, and Brouwer, C. (2017). Pathview Web: user friendly pathway visualization and data integration. *Nucleic Acids Res.* 45, W501–W508. doi: 10.1093/nar/gkx372

Ma, C., Ma, X., Yao, L., Liu, Y., Du, F., Yang, X., et al. (2017). QRfg3, a novel quantitative resistance locus against Gibberella stalk rot in maize. *Theor. Appl. Genet.* 130, 1723–1734. doi: 10.1007/s00122-017-2921-5

Ma, L., Sun, Y., Ruan, X., Huang, P. C., Wang, S., Li, S., et al. (2021). Genome-wide characterization of jasmonates signaling components reveals the essential role of ZmCOI1a-ZmJAZ15 action module in regulating maize immunity to gibberella stalk rot. *Int. J. Mol. Sci.* 22:870. doi: 10.3390/ijms22020870

Ngou, B., Ding, P., and Jones, J. D. (2022). Thirty years of resistance: zig-zag through the plant immune system. *Plant Cell* 34, 1447–1478. doi: 10.1093/plcell/koac041

Pérez-Ruiz, R. V., García-Ponce, B., Marsch-Martínez, N., Ugartechea-Chirino, Y., Villajuana-Bonequi, M., de Folter, S., et al. (2015). XAANTAL2 (AGL14) is an important component of the complex gene regulatory network that underlies *Arabidopsis* shoot apical meristem transitions. *Mol. Plant* 8, 796–813. doi: 10.1016/j.molp.2015.01.017

Prigge, M. J., Greenham, K., Zhang, Y., Santner, A., Castillejo, C., Mutka, A. M., et al. (2016). The *Arabidopsis* auxin receptor F-box proteins AFB4 and AFB5 are required for response to the synthetic auxin picloram. *G3* 6, 1383–1390. doi: 10.1534/g3.115.025585

Robert-Seilaniantz, A., Grant, M., and Jones, J. D. (2011). Hormone crosstalk in plant disease and defense: more than just jasmonate-salicylate antagonism. *Annu. Rev. Phytopathol.* 49, 317–343. doi: 10.1146/annurev-phyto-073009-114447

Schnable, P. S., Ware, D., Fulton, R. S., Stein, J. C., Wei, F., Pasternak, S., et al. (2009). The B73 maize genome: complexity, diversity, and dynamics. *Science* 326, 1112–1115. doi: 10.1126/science.1178534

Stephens, A. E., Gardiner, D. M., White, R. G., Munn, A. L., and Manners, J. M. (2008). Phases of infection and gene expression of Fusarium graminearum

during crown rot disease of wheat. *Mol. Plant Microbe Interact.* 21, 1571–1581. doi: 10.1094/MPMI-21-12-1571

Su, H., Liang, J., Abou-Elwafa, S. F., Cheng, H., Dou, D., Ren, Z., et al. (2021). ZmCCT regulates photoperiod-dependent flowering and response to stresses in maize. *BMC Plant Biol.* 21:453. doi: 10.1186/s12870-021-03231-y

Sun, Y., Ruan, X., Wang, Q., Zhou, Y., Wang, F., Ma, L., et al. (2021). Integrated gene co-expression analysis and metabolites profiling highlight the important role of ZmHIR3 in maize resistance to *Gibberella* stalk rot. *Front. Plant Sci.* 12:664733. doi: 10.3389/fpls.2021.664733

Tang, B., Liu, C., Li, Z., Zhang, X., Zhou, S., Wang, G. L., et al. (2021). Multilayer regulatory landscape during pattern-triggered immunity in rice. *Plant Biotechnol. J.* 19, 2629–2645. doi: 10.1111/pbi.13688

Tautenhahn, R., Patti, G. J., Rinehart, D., and Siuzdak, G. (2012). XCMS online: a web-based platform to process untargeted metabolomic data. *Anal. Chem.* 84, 5035–5039. doi: 10.1021/ac300698c

Wang, C., Yang, Q., Wang, W., Li, Y., Guo, Y., Zhang, D., et al. (2017). A transposon-directed epigenetic change in ZmCCT underlies quantitative resistance to Gibberella stalk rot in maize. *New Phytol.* 215, 1503–1515. doi: 10.1111/nph.14688

Wang, Q., Sun, Y., Wang, F., Huang, P. C., Wang, Y., Ruan, X., et al. (2021). Transcriptome and oxylipin profiling joint analysis reveals opposite roles of 9-oxylipins and jasmonic acid in maize resistance to *gibberella* stalk rot. *Front. Plant Sci.* 12:699146. doi: 10.3389/fpls.2021.699146

Wang, Q., Vera-Buxa, S., Furch, A., Friedt, W., and Gottwald, S. (2015). Insights into Triticum aestivum seedling root rot caused by Fusarium graminearum. *Mol. Plant Microbe Interact.* 28, 1288–1303. doi: 10.1094/MPMI-07-15-0144-R

Xia, L., Mar Marquès-Bueno, M., and Karnik, R. (2020). Trafficking SNARE SYP132 partakes in auxin-associated root growth. *Plant Physiol.* 182, d1836–d1840. doi: 10.1104/pp.19.01301

Yang, Q., Li, Z., Li, W., Ku, L., Wang, C., Ye, J., et al. (2013). CACTA-like transposable element in ZmCCT attenuated photoperiod sensitivity and accelerated the postdomestication spread of maize. *Proc. Natl. Acad. Sci. U.S.A.* 110, 16969–16974. doi: 10.1073/pnas.1310949110

Yang, Q., Yin, G., Guo, Y., Zhang, D., Chen, S., and Xu, M. (2010). A major QTL for resistance to *Gibberella* stalk rot in maize. *Theor. Appl. Genet.* 121, 673–687. doi: 10.1007/s00122-010-1339-0

Ye, J., Guo, Y., Zhang, D., Zhang, N., Wang, C., and Xu, M. (2013). Cytological and molecular characterization of quantitative trait locus qRfg1, which confers resistance to *Gibberella* stalk rot in maize. *Mol. Plant Microbe Interact.* 26, 1417–1428. doi: 10.1094/MPMI-06-13-0161-R

Yu, G., Wang, L. G., Han, Y., and He, Q. Y. (2012). ClusterProfiler: an R package for comparing biological themes among gene clusters. *OMICS* 16, 284–287.

Yu, Y., Liu, Z., Wang, L., Kim, S. G., Seo, P. J., Qiao, M., et al. (2016). WRKY71 accelerates flowering via the direct activation of FLOWERING LOCUS T and LEAFY in *Arabidopsis thaliana*. *Plant J.* 85, 96–106. doi: 10.1111/tpj.13092

Zhang, D., Liu, Y., Guo, Y., Yang, Q., Ye, J., Chen, S., et al. (2012). Fine-mapping of qRfg2, a QTL for resistance to Gibberella stalk rot in maize. *Theor. Appl. Genet.* 124, 585–596. doi: 10.1007/s00122-011-1731-4

Zhang, X. W., Jia, L. J., Zhang, Y., Jiang, G., Li, X., Zhang, D., et al. (2012). In planta stage-specific fungal gene profiling elucidates the molecular strategies of *Fusarium graminearum* growing inside wheat coleoptiles. *Plant Cell* 24, 5159–5176. doi: 10.1105/tpc.112.105957

Zhang, X., Smits, A. H., van Tilburg, G. B., Ovaa, H., Huber, W., and Vermeulen, M. (2018). Proteome-wide identification of ubiquitin interactions using UbIA-MS. *Nat. Protoc.* 13, 530–550. doi: 10.1038/nprot.2017.147

Zhang, Y., He, J., Jia, L. J., Yuan, T. L., Zhang, D., Guo, Y., et al. (2016). Cellular tracking and gene profiling of Fusarium graminearum during maize stalk rot disease development elucidates its strategies in confronting phosphorus limitation in the host apoplast. *PLoS Pathog.* 12:e1005485. doi: 10.1371/journal.ppat.1005485

Zhou, S., Zhang, Y. K., Kremling, K. A., Ding, Y., Bennett, J. S., Bae, J. S., et al. (2019). Ethylene signaling regulates natural variation in the abundance of antifungal acetylated diferuloylsucroses and *Fusarium graminearum* resistance in maize seedling roots. *New Phytol.* 221, 2096–2111.

Zhuang, Y., Gala, A., and Yen, Y. (2013). Identification of functional genic components of major *fusarium* head blight resistance quantitative trait loci in wheat cultivar Sumai 3. *Mol. Plant Microbe Interact.* 26, 442–450. doi: 10.1094/MPMI-10-12-0235-R

Conflict of Interest: The authors declare that the research was conducted in the absence of any commercial or financial relationships that could be construed as a potential conflict of interest.

Publisher's Note: All claims expressed in this article are solely those of the authors and do not necessarily represent those of their affiliated organizations, or those of the publisher, the editors and the reviewers. Any product that may be evaluated in this article, or claim that may be made by its manufacturer, is not guaranteed or endorsed by the publisher.

frontiers | Frontiers in Plant Science

ORIGINAL RESEARCH
published: 30 June 2022
doi: 10.3389/fpls.2022.926621

The Black Necrotic Lesion Enhanced *Fusarium graminearum* Resistance in Wheat

Lanfei Zhao[1,2†], Peisen Su[1,3†], Bingqian Hou[1†], Hongyan Wu[1], Yanhui Fan[1], Wen Li[1], Jinxiao Zhao[1], Wenyang Ge[1], Shoushen Xu[1], Shiwen Wu[1], Xin Ma[1], Anfei Li[1], Guihua Bai[2,4], Hongwei Wang[1] and Lingrang Kong[1]**

[1] State Key Laboratory of Crop Biology, Shandong Key Laboratory of Crop Biology, College of Agronomy, Shandong Agricultural University, Tai'an, China, [2] Department of Agronomy, Kansas State University, Manhattan, KS, United States, [3] College of Agronomy, Liaocheng University, Liaocheng, China, [4] Hard Winter Wheat Genetics Research Unit, USDA, Manhattan, KS, United States

Fusarium head blight, mainly incited by *Fusarium graminearum*, is a devastating wheat disease worldwide. Diverse Fusarium head blight (FHB) resistant sources have been reported, but the resistance mechanisms of these sources remain to be investigated. FHB-resistant wheat germplasm often shows black necrotic lesions (BNLs) around the infection sites. To determine the relationship between BNL and FHB resistance, leaf tissue of a resistant wheat cultivar Sumai 3 was inoculated with four different *F. graminearum* isolates. Integrated metabolomic and transcriptomic analyses of the inoculated samples suggested that the phytohormone signaling, phenolamine, and flavonoid metabolic pathways played important roles in BNL formation that restricted *F. graminearum* extension. Exogenous application of flavonoid metabolites on wheat detached leaves revealed the possible contribution of flavonoids to BNL formation. Exogenous treatment of either salicylic acid (SA) or methyl jasmonate (MeJA) on wheat spikes significantly reduced the FHB severity. However, exogenous MeJA treatment prevented the BNL formation on the detached leaves of FHB-resistant wheat Sumai 3. SA signaling pathway influenced reactive oxygen species (ROS) burst to enhance BNL formation to reduce FHB severity. Three key genes in SA biosynthesis and signal transduction pathway, *TaICS1*, *TaNPR1,* and *TaNPR3*, positively regulated FHB resistance in wheat. A complex temporal interaction that contributed to wheat FHB resistance was detected between the SA and JA signaling pathways. Knowledge of BNLs extends our understanding of the molecular mechanisms of FHB resistance in wheat and will benefit the genetic improvement of wheat FHB resistance.

Keywords: FHB, black necrotic lesions, metabolomics, transcriptomics, flavonoids, SA, MeJA

OPEN ACCESS

Edited by:
Jianhui Wu,
Northwest A&F University, China

Reviewed by:
Jinhui Li,
Boston University, United States
Guoqiang Li,
Nanjing Agricultural University, China

***Correspondence:**
Hongwei Wang
wanghongwei@sdau.edu.cn
Lingrang Kong
lkong@sdau.edu.cn

† These authors have contributed equally to this work

Specialty section:
This article was submitted to Plant Pathogen Interactions, a section of the journal Frontiers in Plant Science

Received: *22 April 2022*
Accepted: *03 June 2022*
Published: *30 June 2022*

Citation:
Zhao L, Su P, Hou B, Wu H, Fan Y, Li W, Zhao J, Ge W, Xu S, Wu S, Ma X, Li A, Bai G, Wang H and Kong L (2022) The Black Necrotic Lesion Enhanced Fusarium graminearum Resistance in Wheat. Front. Plant Sci. 13:926621. doi: 10.3389/fpls.2022.926621

INTRODUCTION

Plants coexist and coevolve with multiple pathogens. Since plants are immobile organisms and lack mammalian-like adaptive immunity, they have obtained various defense mechanisms including passive and active defense mechanisms during evolution to survive under adverse environments and retain their reproductivity (Abramovitch et al., 2006; Kiraly et al., 2007). The passive

defense mechanisms take advantage of preexisting organization structures (Martin, 1964) and multiple chemical defense mechanisms to produce antimicrobial or toxic secondary metabolites, resistance-related proteins or peptides, and other antimicrobial compounds (Levin, 1976). The active defense mechanisms may include induction of oxidative burst (Lamb and Dixon, 1997), hypersensitive response (HR; Heath, 2000), and systemic acquired resistance (SAR; Ryals et al., 1996). Accumulation of phytoalexin-like compounds and metabolites can be triggered rapidly and directly in response to a pathogen attack (Thomma et al., 1999). The activation timing of the defense reactions and the strength of the defense responses usually play crucial roles in the development of resistance or susceptibility of a host plant (Kiraly et al., 2007; Ding et al., 2011).

Plant pathogens can be broadly divided into biotrophic and necrotrophic pathogens according to their lifestyles. Biotrophic pathogens gain nutrients from living host tissues; whereas necrotrophic pathogens kill host tissues to feed on the remains (Zhang et al., 2013). However, many pathogens are in between hemibiotrophic pathogens, and they can be either biotrophic or necrotrophic, depending on the conditions or the stages of their life cycles. *Fusarium graminearum* is a typical hemibiotrophic pathogen that causes wheat (*Triticum aestivum*) Fusarium head blight (FHB), a devastating wheat disease worldwide (Bai and Shaner, 1994). *F. graminearum* has a biotrophic phase at the early stages of FHB infection and a necrotrophic phase after the tissue death in the infection site (Bai and Shaner, 1994; Sorahinobar et al., 2016), which not only cause significant yield losses but also deteriorate grain quality. During infection, *Fusarium* can produce several types of trichothecene mycotoxins, such as deoxynivalenol (DON) and nivalenol (NIV), and these toxins are detrimental to humans and animals when the toxin-contaminated grains are used as foods and feeds (Bai and Shaner, 1994; Trail, 2009; Wang et al., 2020).

The molecular mechanisms underlying activation of plant defense responses to a hemibiotrophic pathogen are quite different from, even more complicated than, those for a biotrophic or necrotrophic pathogen. With the rapid development in "multi-omic" technologies, transcriptomics, proteomics and metabonomics have been used to elucidate mechanisms of FHB resistance (Wang et al., 2018; Su et al., 2020). Some studies showed that *F. graminearum* activated host defense genes in a similar manner to many other pathogens (Rudd et al., 2001; Kazan et al., 2012). Differentially expressed genes (DEGs) induced by *F. graminearum* infection mainly encode pathogenesis-related (PR) proteins, transporters, primary and secondary metabolisms, UDP-glycosyltransferases, lectins and regulators of oxidative burst, or compounds involved in hormone biosynthesis and signaling, phenylpropanoid biosynthesis, and other related pathways (Golkari et al., 2009; Kazan and Gardiner, 2018). Wang et al. (2018) conducted both transcriptome and hormone profiling and found that salicylic acid (SA) and jasmonic acid (JA) played positive roles in enhancing FHB resistance, and auxin and ABA were often associated with susceptibility; however, ethylene appeared to play dual roles during the *F. graminearum*-wheat interaction (Wang et al., 2018). More recently, Su et al. (2020) identified 789 differentially accumulated metabolites, including flavonoids, phenolamides, tryptamine derivatives, and phytohormones, and revealed altered expression of more than 100 known functional genes that are related to the biosynthesis or regulation in these pathways by analyzing both metabolomic and transcriptomic data (Su et al., 2020).

Although extensive studies have been conducted to reveal FHB resistance mechanisms, the conclusions on the *F. graminearum*-wheat interactions remain equivocal. In *tobacco mosaic virus* (TMV) disease, the local lesion has been considered one of the most notable resistance mechanisms in which the virus remains in a local infection and does not continue to spread to new cells after multiplying in several hundred cells around the entry point of the pathogen (Loebenstein, 2009). In many FHB-resistant lines, black necrotic lesions (BNLs) were observed around the entry sites of *F. graminearum*, with a few hyphae from the BNLs. In this study, we attempted to explore the possible relationship between wheat FHB resistance and BNLs using both metabolomic and transcriptomic approaches.

MATERIALS AND METHODS

Plant Materials and Growth Conditions

The wheat cultivars Sumai 3, Jimai 22 and a set of wheat cultivars and breeding lines with different levels of FHB resistance (Ning 7840, Yangmai 158, Shengxuan 6, Haian 15-19, Am324925, Caizihuang, Guangtoumai, Chimianmai, Ningmai 6, Ningmai 9, Apogee73S2, Mimai, Tutoumai, Chimianmai, Huoshaomai, Zaoshiri, Laomangmai, Wugongmai, Huaiyang 05155, Jinmai 73, Linmai 7, Shannong 664, Yannong 19, Huaimai 33, and Taimai 198 and Apogee) were used in this study. Apogee (FHB susceptible NIL) and Apogee73S2 (FHB-resistant NIL) are two near-isogenic lines (NILs) contrasting in *Fhb1* alleles provided by Dr. David Garvin at USDA-ARS, Plant Science Research Unit, Saint Paul, MN, United States. All wheat seedlings were grown in a greenhouse at 20/25°C with a 16/8 h (light/dark) photoperiod. The wild-type *Nicotiana benthamiana* plants were grown in a growth chamber at 24/20°C with a 14/10 h day/night photoperiod.

Fusarium graminearum Strains

The *F. graminearum* strain PH1-1 maintained in the State Key Laboratory of Crop Biology, Shandong Agricultural University was used as inoculum. The green-fluorescence-protein-labeled *F. graminearum* strain, eGFP-PH-1 obtained from Prof. Jinrong Xu of the Department of Botany and Plant Pathology at Purdue University, West Lafayette, IN, United States was used for tracking the pathogen spread. The *F. graminearum* isolates R40, R64, S52, and S66 were provided by Prof. Yuancun Liang at the Department of Plant Pathology, Shandong Agricultural University which were collected from 15 cities in Shandong Province. The four isolates were selected from the 93 *F. graminearum* based on their virulence to Sumai 3. S52

and S66 were highly virulent, and R40 and R64 were low virulent to Sumai 3.

Evaluation of *F. graminearum* Resistance in Detached Spikes and Leaves

The wheat spikes were inoculated by single-floret inoculation as described by Bai and Shaner (1994) with minor modifications (Kong et al., 2007). Briefly, one basal floret of the middle spike was inoculated with 10 μl of an *F. graminearum* conidia suspension (5–10 × 10^4 conidia mL^{-1}) at anthesis, and then sealed with transparent plastic bags to maintain moisture for 48 h. The number of diseased spikelets and rachises was recorded at 21 DAI.

A detached leaf assay described by Browne and Cooke (2004) was used to screen FHB resistance in wheat with minor modifications. Briefly, wheat seedlings were grown in a growth chamber at 22 and 19°C day/night with 12 h photoperiod and 45–50% relative humidity. A 4.5 cm segment from the mid-section of the first leaf was collected at the two-leaf stage. Each detached leaf segment was injured by punching the center of the leaf segment using a pipette tip and arched in the top of a well in a 96-well plate. The plate was then moved gently to a plastic tray (30 cm × 50 cm × 15 cm) filled with water that submerged both ends of the leaf segment in the water. The tip injured site on the leaf segment was added with 3 μl of a *Fusarium* conidia suspension at 5–10 × 10^4 conidia mL^{-1}. Then, the tray was covered with a transparent plastic wrap to maintain moisture at 25–28°C in a growth chamber for 3 days before the length of saprophytic spots was measured.

Exogenous Hormone Treatment on Detached Spikes

The consistent spikes of FHB susceptible cultivar Jimai 22 were selected at anthesis and cut from the base of the stem. The spikes were treated in a solution containing 2 mM SA or 100 μM MeJA at 0, 12, 24, and 48 HAI of *F. graminearum* PH1-1 using a single floret inoculation. The spikes were covered with thin plastic wrap and then maintained in a 25°C incubator for 2–3 days. Water was used as the negative control. The number of FIR that directly connected to the inoculated spikelet was counted at 4 DAI and DR was recorded at 7 DAI. PSS of the detached spikes was counted at 15 DAI. At least 20 spikes per replication were counted with three replicates in each treatment. Student's *t*-test analysis was used to compare the differences among exogenous hormone treatments, and a significant difference was claimed at $p < 0.05$.

Preparation of Scanning Electron Microscopy

The tissue for scanning electron microscopy was prepared as described by Kang and Buchenauer (2000), with minor modifications. The inoculated rachises of Sumai 3 and Jimai 22 were sampled at 12 DAI with PH1-1. The samples were fixed with 4% (v/v) glutaraldehyde in 50 mM phosphate buffer (PH = 6.8) for 24 h and rinsed for five cycles with phosphate buffer (PH = 6.8) at 20 min per cycle. Subsequently, samples were postfixed in 1% (w/v) osmium tetroxide in 50 mM phosphate buffer (PH = 6.8) overnight at 4°C and rinsed for five cycles with phosphate buffer (pH 6.8) at 20 min per cycle, then rinsed with a graded of ethanol and isopentyl acetate series. After dehydration, the sample was dried, mounted on a stub, sputter coated with gold-palladium, and viewed using a Zeiss 100 scanning electron microscope (JEOL, JSM-6610 LV) operating at 15 kV. Each treatment had three replications.

Transcriptional Profiling

The detached leave segments described previously were used for transcriptional profiling. The first leaves of FHB-resistant wheat cultivar Sumai 3 were inoculated with conidia suspensions of four *F. graminearum* isolates R40, R64, S52, or S66 with different virulence and harvested at 4 DAI. Total RNA samples were isolated using TRIzol reagent (Invitrogen Corporation, Carlsbad, CA, United States) and RNA sequencing was done in the Berry Genomics Corporation Company (Beijing, China) using an Illumina HiSeq^{TM} 2000 sequencer. The sequence reads were aligned to the Chinese Spring reference genome v1.0 (International Wheat Genome Sequencing Consortium [IWGSC], 2018). The differentially expressed genes (DEGs) were analyzed by comparing each treated sample with its mock-inoculated control using the DEGseq R package (Mortazavi et al., 2008). The genes were considered to show a statistically significant difference based on a false discovery rate (FDR) < 0.05. The raw expression values were converted into log2 ratios.

MapMan was specifically designed to cover plant-specific pathways and processes[1]. MapMan pathway analyses were performed using the Log_2 fold change of common DEGs induced by both R40 and R64 (RR) or both S52 and S66 (SS) to determine BNL-related pathways. Custom specific mapping file for the MapMan based on the wheat sequencing output was created using the Mercator pipeline (Lohse et al., 2014)[2]. MapMan v3.5.1R2 (Thimm et al., 2004) was used to visualize expression changes of DEGs to multiple MapMan functional categories.

Metabolomic Analysis

The detached leaf samples were inoculated with an *F. graminearum* conidia suspension as described previously. Leaf tissue was collected including the saprophytic spot and 2–3 mm adjacent leaf tissue at 4 DAI. The samples were prepared and extracted as previously described (Chen et al., 2013) and analyzed using an LC-ESI-MS/MS system (HPLC, Shim-pack UFLC SHIMADZU CBM20A system[3]; MS, Applied Biosystems 4000 Q TRAP[4]). The analytical conditions were as follows: HPLC: column, shim-pack VP-ODS C18 (pore size 5 μm, length 2 mm × 150 mm); solvent system, water (0.04% acetic acid): acetonitrile (0.04% acetic acid); gradient program, 100:0 V/V at 0 min, 5:95 V/V at 20 min, 5:95 V/V at 22 min, 95:5 V/V at 22.1 min, 95:5 V/V at 28.0 min; flow rate, 0.25 ml min^{-1}; temperature, 40°C; and injection volume: 5 μl. The effluent

[1]https://mapman.gabipd.org/mapman

[2]http://mapman.gabipd.org/web/guest/Mercator

[3]www.shimadzu.com.cn/

[4]www.appliedbiosystems.com.cn/

was connected to an ESI-triple quadrupole-linear ion trap (Q TRAP)-MS. Linear Ion Trap (LIT) and triple quadrupole (QQQ) scans were acquired on a triple quadrupole-linear ion trap mass spectrometer (Q TRAP), API 6500 Q TRAP LC/MS/MS System, equipped with an ESI Turbo Ion-Spray interface, operating in a positive ion mode and controlled by Analyst 1.6 software (AB Sciex, Framingham, MA, United States).

Metabolite data were $\log_2$-transformed before statistical analysis to improve normality. To identify the differentially accumulated metabolites induced by different virulent *F. graminearum* isolates, *F. graminearum*-infected samples were compared with the mock-inoculated control (CK). The principal component analysis (PCA) was carried out by SPSS for Windows (Version 25, SPSS Inc., Chicago, IL, United States). Differences in the metabolites between wheat leaves from treated and control samples were determined using Welch's *t*-test ($p < 0.01$) in ZS97 and IRAT10 (Chen et al., 2013). The metabolites were identified as significantly enriched or depleted in content and were set with thresholds of variable importance in fold-change $\geq$1.5 or $\leq$0.5.

Endogenous Salicylic Acid and Jasmonic Acid Content Measurements

To measure endogenous SA and JA content, a central spikelet in a spike of Sumai 3 at anthesis was inoculated with *F. graminearum* PH1-1 using single-floret inoculation (Bai and Shaner, 1994; Kong et al., 2007). The inoculated spikelets were sampled at 0, 12, 24, 48, 72, and 96 HAI to extract and quantify SA and JA using an HPLC-ESI-MS/MS separation (Agilent 1200, Agilent Technologies, Palo Alto, CA, United States) as described by Ding et al. (2011). The standard curves for SA and JA quantification were generated using a series of SA and JA (Sigma, St. Louis, MO, United States) dilutions. All experiments were performed with two biological replicates and three technical replicates.

Identification of Reactive Oxygen Species in Detached Leaves

The ROS levels were measured using the cell-permeable fluorescent dye DCFH-DA (2′,7-dichlorofluorescein diacetate) as described by Tiwari and Kakkar (2009) with minor modification. Briefly, detached leaves were incubated in 5 μM DCFH-DA for 45 min using a pH 7.5 phosphate buffer in the dark at 3 DAI of *F. graminearum*. The samples were rinsed with 70% ethanol and photographed using a BX60 light microscope (Olympus, Japan).

Exogenous Treatments of Metabolites and Hormones on the Detached Leaves

To study the function of metabolites and hormones in FHB resistance, exogenous metabolites and hormones were applied on detached wheat leaves of Jimai 22, Kenong 199, Huaimai 33, and Taimai 198, respectively. The detached leaves were placed separately in a solution containing 2 mM SA, 100 μM MeJA, 50 mM apigenin, neohesperidin, catechin, proanthocyanidins, or spermidine. Water treatment was used as a control. The treated and controlled detached leaves were prepared and inoculated with *F. graminearum* PH1-1 as described previously, then placed in a plastic tray (30 cm × 50 cm × 15 cm) and sealed with transparent plastic wrap to maintain high moisture content for 3 days in a growth chamber set at 25°C. The length of necrotic spots was measured in 20 leaf segments per replicate for three replicates per treatment.

Gene Expression Analysis

The two NILs, Apogee and Apogee73S2, were inoculated with *F. graminearum* PH1-1 (5–10 × 10^4 conidia mL^{-1}) as previously described, and the inoculated spikes were harvested at 0, 12, 24, 48, and 72 HAI to isolate total RNA using TRIzol reagent (TransGen, Beijing, China). The total RNA was then reverse-transcribed into cDNA using a TransScript® One-Step gDNA Removal and cDNA Synthesis Kit (TransGen, Beijing, China) and oligo(dT) primers following the manufacturer's instructions. The expression of targeted genes was profiled using qRT-PCR in a Roche LightCycler® 480 (Roche, Mannheim, Germany). The housekeeping gene β-*Actin* was used as an internal reference. The threshold cycle (CT) values were used to calculate the fold-changes of relative expression accumulation using the formula $2^{-\Delta\Delta CT}$ and standard errors. Each treatment had three biological replicates, and each biological replicate had three technical replicates to reduce the error. All primers used in this study were listed in **Supplementary Table 1**. Student's *t-test* analysis was used to compare the differences in the gene expression levels among different time points.

Functional Evaluation of Key Genes in Salicylic Acid Pathway Using *Barley Stripe Mosaic Virus*-Induced Gene Silencing

Transient silencing of key genes in the SA pathway was carried out using the *barley stripe mosaic virus-induced* gene silencing system (Yuan et al., 2011; Fan et al., 2019). Briefly, the specific short fragments of *TaICS1*, *TaPAL2*, *TaNPR1*, *TaNPR2,* and *TaNPR3* were obtained from the cDNA of Sumai 3 using corresponding primer pairs, respectively (**Supplementary Table 3**). The fragments were cloned into the vector pCa-γbLIC (pCa-γb:target-gene) and transformed into *Agrobacterium EHA105* using the previously described method (Yuan et al., 2011). The *Agrobacterium* mixtures containing equal amounts of pCaBS-α, pCaBS-β, and pCa-γb-target-gene were used to inoculate *N. benthamiana* at the four-leaf stage to generate the recombinant virus initially. At 7–10 DAI, the tobacco leaves with mosaic spots were harvested and ground in the pH 7.2 phosphate buffer saline (PBS) containing 1% celite. The leaf sap was mechanically rub-inoculated onto the flag leaves of Sumai 3 (Fan et al., 2019). The transcript abundances of target genes were detected by semi-quantitative RT-PCR, and 18S rRNA was used as an internal control. Each treatment had three biological replicates, and each biological replicate had three technical replicates. The number of scabbed spikelets was recorded from 7 to 30 DAI with

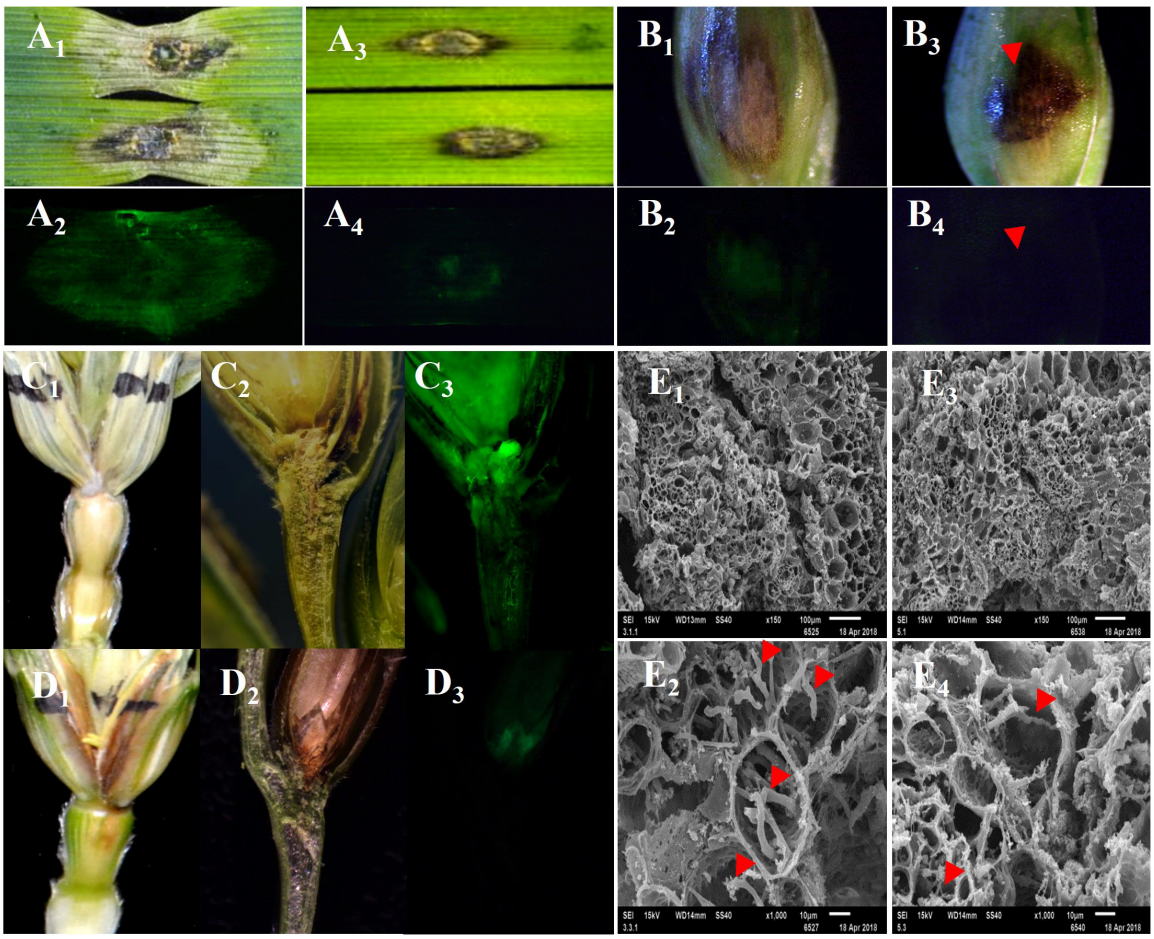

FIGURE 1 | The disease symptoms and movement of *F. graminearum* in detached leaves, glumes, and spikes of susceptible (Jimai 22) and resistant (Sumai 3) plants after infection of *F. graminearum* eGFP-PH-1. The black necrotic lesions (BNLs) were detected in Sumai 3, which effectively limited the size of disease symptoms and hypha spread of *F. graminearum* among tissues. **(A_1,A_2,B_1,B_2,C_1–C_3)** Show detached leaves, glume, and spike of Jimai 22 after infection of *F. graminearum* that were photographed under regular light and green fluorescent light, respectively. **(A_3,A_4,B_3,B_4,D_1–D_3)** Show the detached leaves, glume, and spikes of Sumai 3 after inoculation of *F. graminearum* that were photographed under regular light and green fluorescent light, respectively. **(E_1–E_4)** Show the organizational structure of the nodes which connect the inoculated floret to the rachis of Jimai 22 and Sumai 3, respectively, at 12 DAI under SEM. The red arrows point to hyphae of *F. graminearum* in the rachis.

F. graminearum. Each treatment had three replicates with 10 spikes per replicate.

RESULTS

Black Necrotic Lesion Restricted *F. graminearum* Spread in Wheat

The FHB symptoms on the leaves, glumes, and spikes were significantly different between the FHB-resistant wheat cultivar "Sumai 3" and the susceptible wheat cultivar "Jimai 22" after they were inoculated with different isolates of *F. graminearum*. In Jimai 22, a large water-soaked spot was observed on a detached leaf 4 days after inoculation (DAI), and a dry, chalky spot appeared on the glume at 7 DAI and spread to rachis at 12 DAI (**Figures 1A_1–C_1**). In Sumai 3, however, BNLs appeared on a detached leaf, glume, and rachis (**Figures 1A_3,B_3,D_1**). When these tissues were inoculated with the green fluorescence-labeled *F. graminearum* strain eGFP-PH-1, a large mass of hyphae was observed around the water-soaked spots on the leave, glum and spike of Jimai 22 (**Figures 1A_2,B_2,C_3**), but very few hyphae were observed in BNLs on these tissues of Sumai 3 (**Figures 1A_4,B_4,D_3**). In the longitudinal section of rachis and floret of Jimai 22, hyphae passed the node between floret and rachis and quickly spread to the adjacent rachises (**Figures 1C_2,C_3**); whereas the hyphae mainly appeared on the surface of the inoculated floret and rarely spread to rachis in Sumai 3 (**Figures 1D_2,D_3**). Under scanning electron microscope (SEM), much more hyphae grew in the infected rachis of Jimai 22 than in Sumai 3, and hyphae in the rachis of Sumai 3 were thinner and weaker than in Jimai 22 (**Figures 1E_2,E_4**). These results support that the black substances in BNLs may slow down or inhibit the spread of *F. graminearum* among different wheat tissues.

To investigate the relationship between BNLs and the spread of *F. graminearum* in different wheat tissues, 19 moderately to highly FHB resistant and 8 highly susceptible wheat cultivars were phenotyped for FHB symptoms on spikes at 21 DAI. All the 19 FHB-resistant cultivars showed a lower percentage of symptomatic spikelets in a spike (PSS), ranging from 6.4 to 45.4%, than these susceptible cultivars, ranging from 54.5 to 89.3%, and had obvious BNLs in the inoculated spikelet and sometimes in the adjacent rachis of most FHB-resistant cultivars. Sumai 3 and Ning 7840, with the highest FHB resistance among tested cultivars, showed BNLs on the inoculated spikelets as early as 3 DAI. Only Wugongmai, a moderately resistant cultivar, did not show BNLs even at 21 DAI. All eight susceptible wheat cultivars showed high PSS and chalky-dry symptoms on rachises, except Kenong 199 which showed some black lesions in the inoculated spikelets and neighboring rachises at 10 DAI (**Supplementary Figure 1**). That *F. graminearum* infection-induced BNLs in most FHB-resistant cultivars but not in most susceptible cultivars suggests that BNL may play an important role in wheat resistance to FHB.

Differentially Expressed Genes and Accumulated Substances Induced by *F. graminearum* Isolates With Different Degrees of Virulence

Significantly different symptoms were observed on the detached leaves of Sumai 3 at 4 DAI with the four *F. graminearum* isolates (R40, R64, S52, S66). The mock-inoculated leaves (CK) did not show any symptoms and the isolates R40 and R64 induced small BNLs around the inoculation points on the leaves. However, the isolates S52 and S66 induced large water-soaked spots surrounding inoculation points, therefore, were more virulent than R40 and R64 in Sumai 3 (**Figure 2A**).

To identify DEGs and related pathways induced by *F. graminearum*, comparisons of transcript profiles between the *F. graminearum* isolates S52, S66, R40, and R64 inoculated and mock-inoculated Sumai 3 leaf tissues identified 41,460 unique DEGs, with 20,258 between S52 and CK, 28,101 between S66 and CK, 29,085 between R40 and CK and 23,310 between R64 and CK. Among these, 10,182 genes were differentially expressed in all four isolates, 5,458 genes were differentially expressed in the R40 and R64 (low virulence) inoculated samples (**Supplementary Table 2**), 3,199 genes were differentially expressed in the S52 and S66 (high virulence) inoculated samples (**Supplementary Table 3**), and 11,019 DEGs were uniquely induced by a single isolate including 937 genes induced by S52, 5,021 genes by S66, 3,409 genes by R40 and 1,661 genes by R64 (**Figure 2B**). Among these DEGs, 375 genes induced by both R40 and R64 and 396 by both S52 and S66 were related to the biotic stress pathways. The upregulated DEGs by the two low virulent isolates (R40 and R64) mainly code proteins for phytohormone signaling pathways including auxin, brassinosteroids, abscisic acid (ABA), ethylene (ET), and jasmonic acids (JA) pathways (**Figure 2C**) and some proteins for the redox state, secondary metabolites, cell wall, and abiotic stress pathways in responses to *F. graminearum* infection; however, most S52 and S66 induced DEGs were downregulated in the ET, ABA, and JA pathways (**Figure 2C**), suggesting that phytohormone signaling pathways played an important role in the interaction between *F. graminearum* and wheat.

In Sumai 3, 20 DEGs induced by S52 and S66 and 35 DEGs induced by R40 and R64 were mapped in the secondary metabolism pathways, in particular flavonoids metabolic pathway in which all the five upregulated DEGs (Traescs2D01G530600, Traescs2B01G048400, Traescs2A01G468200, Traescs6B01G056900, Traescs6D01G048400) were induced by R40 and R64, and all the eight downregulated DEGs (Traescs3A01G253800, Traescs3D01G254700, Traescs5A01G475600, Traescs7B01G310900, Traescs7A01G411700, Traescs2D01G512700, Traescs2A01G511300, Traescs7A01G212800) were induced by S52 and S66 (**Figure 2D**). The results suggest that the flavonoids metabolic pathway is differentially regulated between the wheat-low virulent *F. graminearum* interaction system and the wheat-high virulent *F. graminearum* interaction system, which may contribute to the regulation of BNL formation in responses to *F. graminearum* infection.

Metabolomic analyses on the detached leaf tissues of Sumai 3 that were collected 4 DAI by the isolates R40, R64, S52, or S66 identified 789 metabolites with known structures. A total of 206, 198, 215, and 213 metabolites were significantly differentially accumulated in S52, S66, R40, and R64 inoculated samples, respectively (Su et al., 2020). Compared with the mock-inoculated control (CK), 30, 28, 19, and 15 metabolites were specifically accumulated in S52, S66, R40, and R64 inoculated samples, respectively; 23 metabolites were accumulated in both S52 and S66 inoculated samples; 47 metabolites were accumulated in both R40 and R64 inoculated samples; 114 were common metabolites accumulated in all the samples that were inoculated with the four different isolates (**Figure 2E**).

In the R40 and R64 (RR cluster) treated samples and S52 and S66 (SS cluster) treated samples, 81 species of *Fusarium*-induced metabolites were identified and further functionally classified, respectively (**Supplementary Tables 4**, **5**). Based on the structural features of each metabolite, the RR cluster contained 21 categories of metabolites and the SS cluster had 25 categories. Many of the metabolites were amino acid derivatives, flavones, and quinate derivatives, suggesting that both highly and lowly virulent *F. graminearum* isolates induced the accumulation of these metabolites. Since highly virulent isolates did not produce BNL, these metabolites may not be the causal agents for BNL.

In comparison of the metabolite categories between RR and SS clusters, two species of benzoic acid derivatives, four species of carbohydrates, and two species of flavonolignans were identified in the samples only from the RR cluster. In addition, seven species of phenolamides were identified in the samples from the RR cluster with only one of these species from the SS cluster. These results suggest that these metabolites were induced specifically by infection of the high virulent *F. graminearum*, which might result in water-soak spots on wheat. However, one species each of alcohols and polyols, two species of flavanones, four species of flavone C-glycosides, three species of flavonols, two species of isoflavones, and one species of nicotinic acid and its derivatives were identified from low-virulent-isolate-inoculated samples (**Figure 2F**), suggesting that flavonoids and

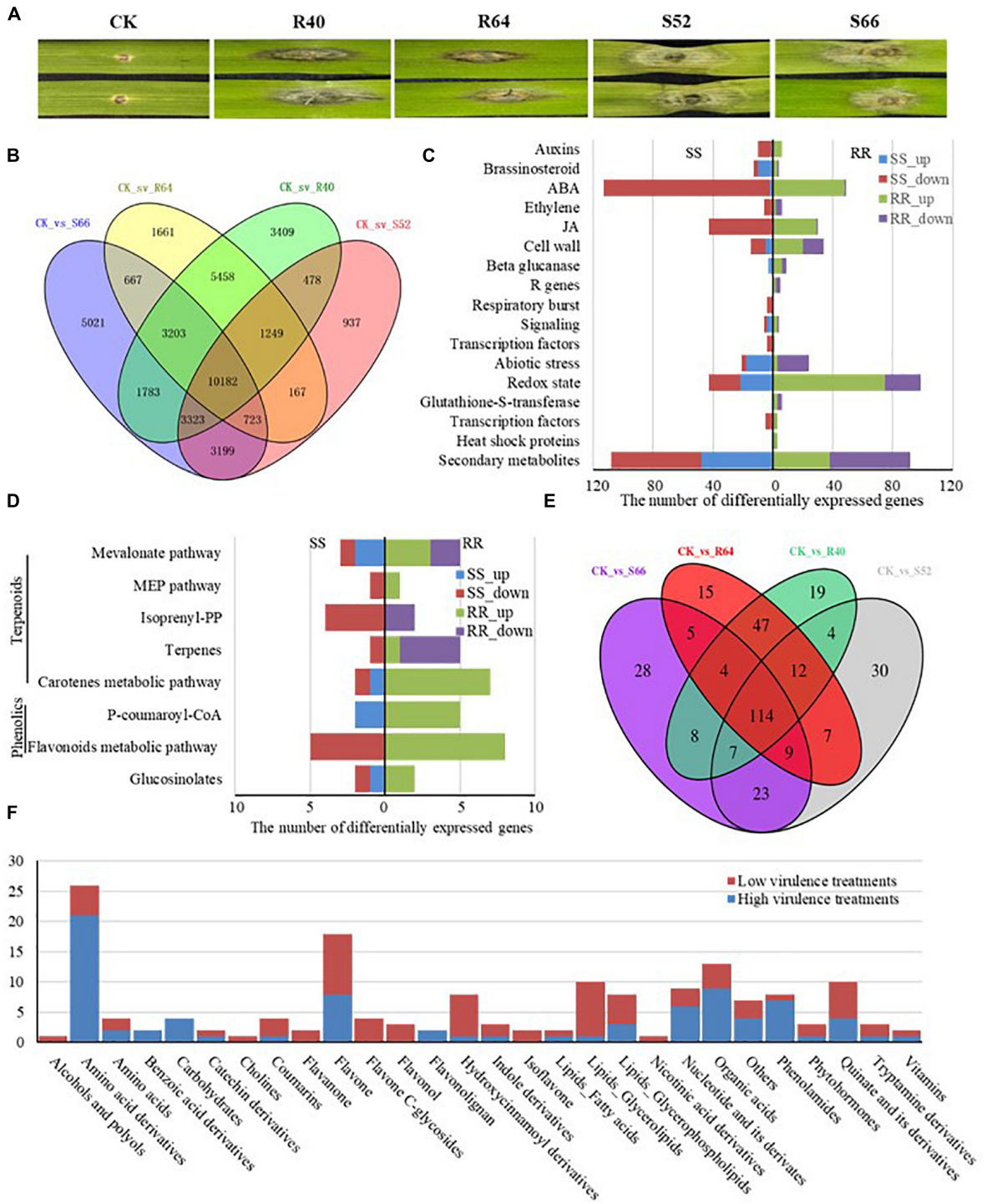

FIGURE 2 | Overview of significantly differentially expressed genes (DEGs) and the accumulated metabolites in detached leaves of Sumai 3 treated with the *F. graminearum* isolates R40, R64, S52, and S66. **(A)** The symptoms on the detached leaves inoculated with H_2O, low virulent isolates (R40 and R64), and high virulent isolates (S52 and S66). **(B)** Venn diagram of significantly DEGs induced by R40, R64, S52, and S66 compared with CK. **(C)** A number of significant DEGs were mapped to the corresponding pathways in biotic stress pathways. **(D)** A number of significant DEGs were mapped to the secondary metabolism pathway. **(E)** A Venn diagram of the different metabolites induced by R40, R64, S52, and S66 compared with CK. **(F)** Number of specific metabolites in different categories after inoculating with high- and low-virulence *F. graminearum*.

its derivatives might contribute significantly to BNL formation in FHB-resistant plants.

Responses of Exogenous Metabolite Treated Wheat Detached Leaves to *F. graminearum* Infection

The leaves were detached from four highly FHB susceptible wheat cultivars (Jimai 22, Kenong 199, Huaimai 33, and Taimai 198) and treated with 50 μM each of apigenin, neohesperidin, catechin, proanthocyanidin, and spermidine, individually. Among these chemicals, apigenin and neohesperidin belong to flavonoids, proanthocyanidin belongs to anthocyanins, catechin belongs to catechin derivatives, and spermidine belongs to phenolamides. All the chemical-treated leaves were then inoculated with the *F. graminearum* PH1-1. Although variation in sizes of BNLs was observed among cultivars within a treatment, obvious variation was observed among treatments. The catechin treatment limited *F. graminearum* spread in detached leaves of all wheat cultivars with the smallest BNLs in Kenong 199. The apigenin and neohesperidin-treated leaves showed moderate BNLs around the *F. graminearum* inoculation sites but had significantly shorter saprophytic spots than negative H_2O control on all four inoculated wheat cultivars at 4 DAI (**Figure 3**). Proanthocyanidins-treated leaves showed a similar phenotype to H_2O treated CK in all cultivars. The spermidine-treated samples showed excessive hypha growth on the saprophytic spots and longer saprophytic spots than H_2O-treated CK in all four cultivars. These results indicated that exogenous application of flavonoids may induce BNLs to restrain fungal growth on wheat leaves.

The Relationship of Salicylic Acid and Jasmonic Acid to Wheat Fusarium Head Blight Resistance

In the susceptible wheat Kenong 199, the mean length of saprophytic spot (0.73 cm) in the H_2O-treated detached leaves was longer than in the SA-treated samples (0.57 cm), but was shorter than methyl jasmonate (MeJA)-treated leaves (0.95 cm) at 4 DAI of *F. graminearum* PH1-1 with obvious BNLs only in the SA-treated samples (**Supplementary Figures 2A,B**). In the resistant cultivar Sumai 3, small BNLs (0.45 and 0.46 cm) were observed in H_2O- and SA-treated leaves, respectively; whereas the MeJA-treated leaves showed serious etiolation with the longest saprophytic spots (1.53 cm) among the six treatment combinations (**Supplementary Figures 2A,C**). These results indicated that exogenous application of SA induced BNLs to restrain fungal growth on wheat leaves; in contrast, JA facilitated the antagonistic interactions between the SA and JA signaling pathways to promote *F. graminearum* growth. In addition, the small BNLs in Sumai 3 showed very strong ROS signals around the edge of the BNL at 4 DAI (**Supplementary Figure 3A**$_2$), but Jimai 22 had relatively large saprophytic spots with very weak ROS signals in the spot (**Supplementary Figure 3B**$_2$), suggesting that ROS burst might contribute to the BNL formation to limit the growth of *F. graminearum*.

Application of exogenous SA at 0, 12, and 24 HAI with PH1-1 restrained the spread of the pathogen from the inoculated spikelet to the adjacent rachis on the detached spikes of Jimai 22 (**Figure 4**). When SA was applied at 0, 12, and 24 HAI, the percentage of the first infected rachis (FIR) was significantly lower (23, 20, and 31%, respectively) than H_2O control (59%) at 4 DAI with PH1-1; however, FIR was similar (55%) to H_2O control when SA was applied at 48 HAI with PH1-1 (**Figure 4G**). The percentage of dead rachises (DR) followed the same pattern as FIR. Also, the percentage of scabbed spikes (PSS) in these SA-treated samples at 0, 12, and 24 HAI with PH1-1 were significantly lower than the H_2O control. However, the SA-treated spikes at 48 HAI with PH1-1 produced higher PSS (65%) than the H_2O control (55%) (**Figure 4I**).

In the MeJA-treated samples, the MeJA slightly aggravated the spread of *F. graminearum* in the spikes that were treated with MeJA at 0, 12, and 24 HAI with PH1-1. However, both FIR and DR of the spikes that were treated with MeJA at 48 HAI were the same as H_2O control (**Figure 4H**). Most MeJA-treated spikes (0, 24, and 48 HAI) had lower PSS than those treated with SA with the lowest PSS for 0 HAI treatment (**Figure 4I**). Therefore, early exogenous application (0–24 HAI) of SA significantly enhanced wheat FHB resistance, while exogenous application of MeJA could effectively slow down the fungal spread within a spike after the initial disease spread to rachises if it is applied within 48 h of FHB infection.

To study the relationship between *F. graminearum* infection and SA or JA content accumulated in the resistant plants, endogenous SA and JA contents were measured in dry spike tissues of Sumai 3 at 0, 12, 24, 48, 72, and 96 after inoculation with *F. graminearum* PH1-1. SA content started with 73.8 ng/mg at 0 HAI, quickly increased to the peak (125.1 ng/mg) at 12 HAI, then quickly dropped to 22.3 ng/mg at 48 HAI (**Supplementary Figure 4**); in contrast, JA content in Sumai 3 started (0 HAI) at low levels of 3–3.9 ng/mg, decreased slowly at 24 HAI, then jumped 12.1 ng/mg at 24 HAI, and reached 15.8 ng/mg at 96 HAI. These data suggested an antagonistic interaction between the SA and JA signaling pathways, and that high SA content in the early stage of the fungal infection is likely associated with FHB resistance.

Expression Patterns of Key Genes for Salicylic Acid Synthesis and Signaling

The expression patterns of genes encoding an isochorismate synthase (*TaICS1*) and a phenylalanine ammonia-lyase (*TaPAL2*) for SA synthesis and *TaNPR1*, *TaNPR2,* and *TaNPR3* for signaling transduction were analyzed using the tissues from two *Fhb1*-near-isogenic lines (NILs), Apogee ($Fhb1^-$) and Apogee73S2 ($Fhb1^+$), collected at 0, 12, 24, 48 and 72 HAI with PH1-1. *TaICS1* expression in the resistant NIL Apogee73S2 was significantly higher than in the susceptible NIL Apogee at all the five-time points, with the peak at 24 HAI (**Figure 5A**). Had non-differential expression of *TaPAL2* between the NILs (**Figure 5B**) suggests *TaPAL2* may not associate with FHB resistance. Therefore, that higher endogenous SA content coincided with the higher

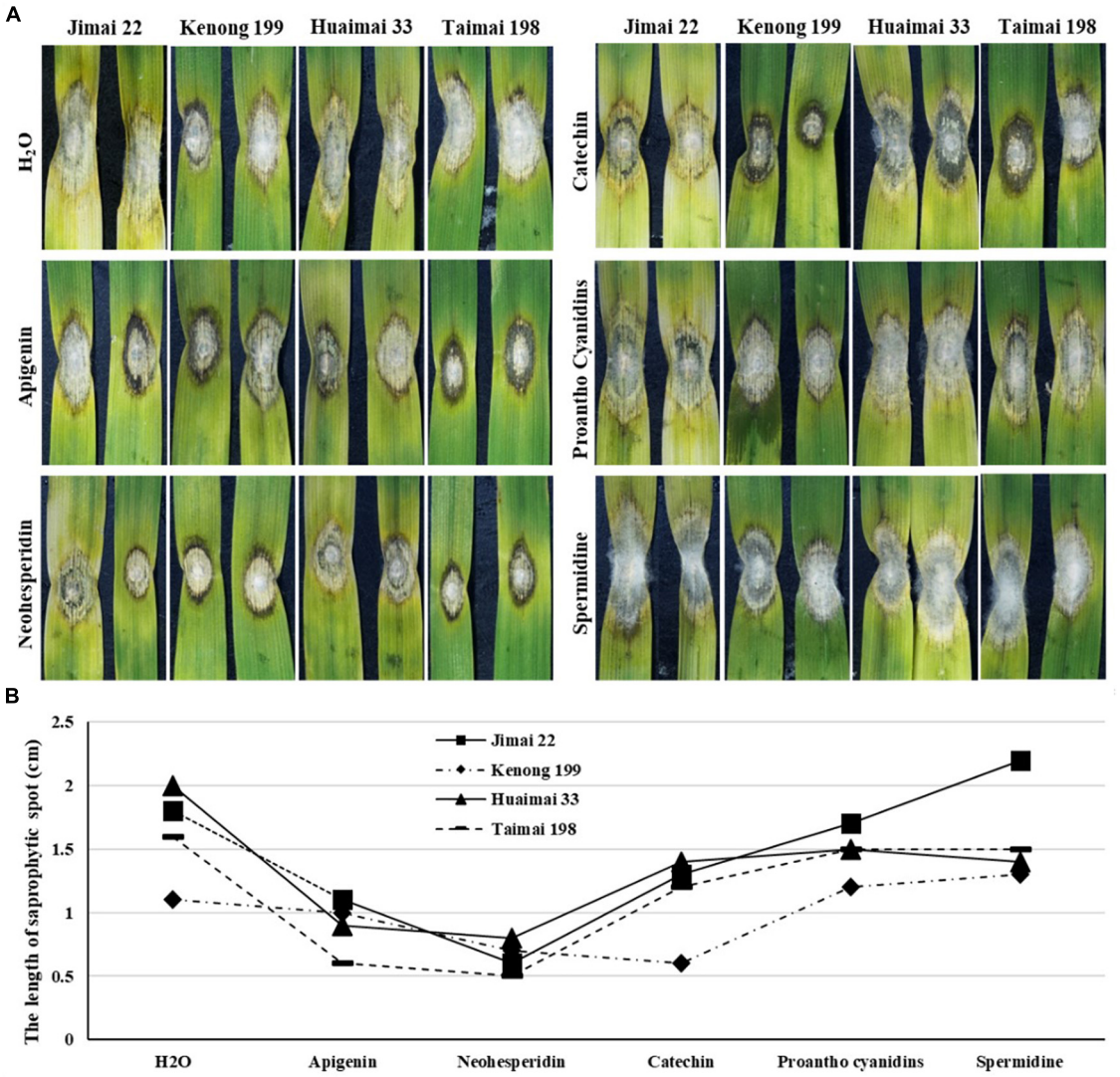

FIGURE 3 | Response to *F. graminearum* PH1-1 infection to exogenous metabolite treatments on the detached leaves of four different wheat cultivars (Jimai 22, Kenong 199, Huaimai 33, and Taimai 198) at 4 DAI. **(A)** Detached wheat leaves were treated with H_2O, 50 μM of apigenin, neohesperidin, catechin, proanthocyanidins, and spermidine after *F. graminearum* inoculation, respectively. **(B)** Length of the saprophytic spots on the detached leaves of Jimai 22, Kenong 199, Huaimai 33, and Taimai 198 at 4 DAI treated with H_2O and 50 μM of apigenin, neohesperidin, catechin, proanthocyanidins, and spermidine, respectively. Each replicate comprised at least 20 detached leaves.

expression of *TaICS1* in the FHB-resistant NIL suggests that the *TaICS1* gene is likely a key gene in the SA synthesis pathway and it may play an important role in wheat FHB resistance.

Among three *TaNPR* genes, *TaNPR1* showed significant differential expression between the two NILs with the peak expression at 12 HAI in Apogee73S2 and at 24 HAI in Apogee (**Figure 5C**). However, *TaNPR2* was not differentially expressed between the NILs at all the time points tested (**Figure 5D**). *TaNPR3* also showed significantly higher expression in Apogee73S2 between 12 and 48 HAI (**Figure 5E**). Taken together, both *TaNPR1* and *TaNPR3* may play important roles in enhancing wheat FHB resistance through SA signal transduction.

Functional Evaluation of Salicylic Acid-Related Key Genes Using *Barley Stripe Mosaic Virus*-Mediated Gene Silencing

Transient gene silencing was successfully used to silence the two genes on the SA synthesis pathway and three genes on SA signaling pathway. The Sumai 3 plants with silenced *TaICS1*, *TaNPR1,* or *TaNPR3* showed significantly higher ($p < 0.05$) FHB severity (∼45%) than those for wild-type and non-silenced controls (10%) at 15 DAI (**Figure 6**). The plants with silenced *TaPAL2* gene had no significant difference in PSS compared to the

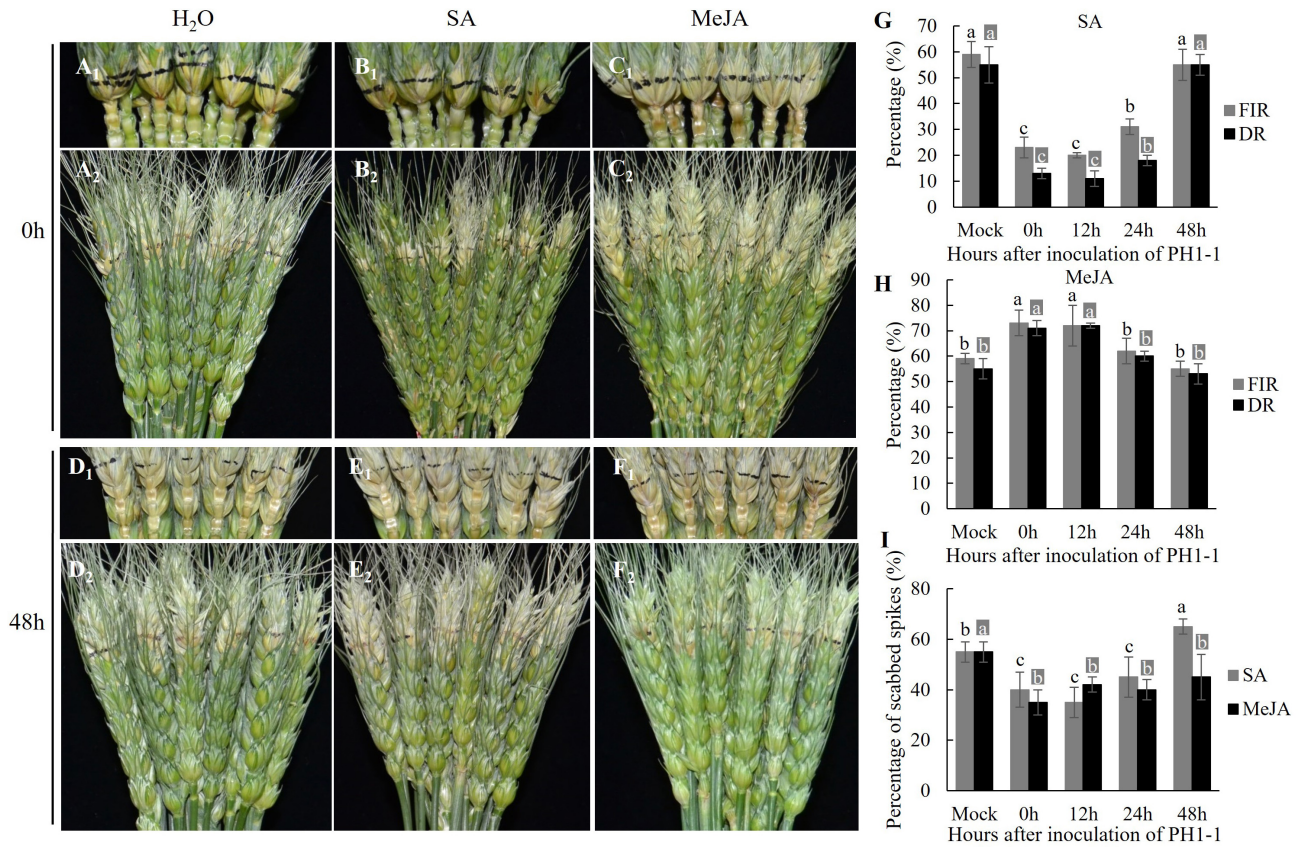

FIGURE 4 | The comparisons of FHB symptoms, first infected rachises (FIR), and dead rachises (DR) on the spikes of Jimai 22 that were applied with exogenous SA and MeJA at 0–48 h after inoculation (HAI) with PH1-1. **(A_1–F_1)** Showed the infected rachises of the inoculated spikes at 7 days after inoculation (DAI) and **(A_2–F_2)** showed the infected spikelets in inoculated spikes at 7 DAI. All these samples were treated with H_2O (Mock), SA, and MeJA, respectively. **(G,H)** Percentage of FIR and DR in the infected spikes of Jimai 22 that were applied with H_2O, SA, and MeJA at 0 h, 12 h, 24 h, and 48 h after PH1-1 inoculation at 4 DAI and 7 DAI, respectively. **(I)** PSS of infected spikes of Jimai 22 at 15 DAI that was applied with H_2O, SA, and MeJA at 0, 12, 24, and 48 HAI of PH1-1. Error bar shows standard deviation. In **(G–I)**, different letters on the top of each bar in the same color (dark or light) indicate significant differences at $p = 0.05$ (LSD) among mean FIR, DR, or PSS at inoculation time points, respectively.

Sumai 3 controls until 10 DAI, and then the PSS in the *TaPAL2*-silenced plants was significantly increased ($p < 0.05$) after 15 DAI and reached 38% at 30 DAI. However, PSS has not changed even 30 DAI in the plants carrying silenced *TaNPR2*. Those results confirmed that *TaICS1* in the SA synthesis pathway and *TaNPR1* and *TaNPR3* in the SA signaling pathway play important roles in wheat FHB resistance.

DISCUSSION

Black Necrotic Lesion Restrained *F. graminearum* Spread in Wheat

The typical early visible FHB symptoms include brownish water-soaked spots on the glume of an inoculated spikelet. With the infection progression, all the infected spikelets may dry up with an appearance similar to ripen spikelets and die quickly. These bleached, premature spikelets due to FHB damage usually mix with green spikelets in a spike in the later grain filling stage in moderately resistant or susceptible cultivars, but the apical part or entire wheat spike may dry up completely as the fungal infection progresses through rachis that cut off the water and nutrient supplies to these apical spikelets in highly susceptible genotypes (Kang and Buchenauer, 2000; Bai et al., 2002). However, in highly resistant genotypes such as Sumai 3, only small BNLs were observed on the initially infected glumes and the majority of the spike remains green till maturity as seen in this study (**Figure 1** and **Supplementary Figure 1**). Holmes (1929) noticed similar local lesions that were induced by TMV. The local lesion has been considered a resistance mechanism that limited the spread of the virus from the initial inoculation point (Loebenstein, 2009). In this study, we observed only a few hyphae around the BNL induced by FHB infection (**Figure 1**) and showed that the BNL was closely associated with ROS burst (**Supplementary Figure 3**), SA pathway, and flavonoids metabolites. The BNLs appeared to be HR-like symptoms that were induced by *F. graminearum*, especially in the FHB-resistant wheat genotypes, and it significantly enhanced the FHB resistance by restraining the growth and spread of the pathogen within wheat tissue. The integrated metabolomic and transcriptomic

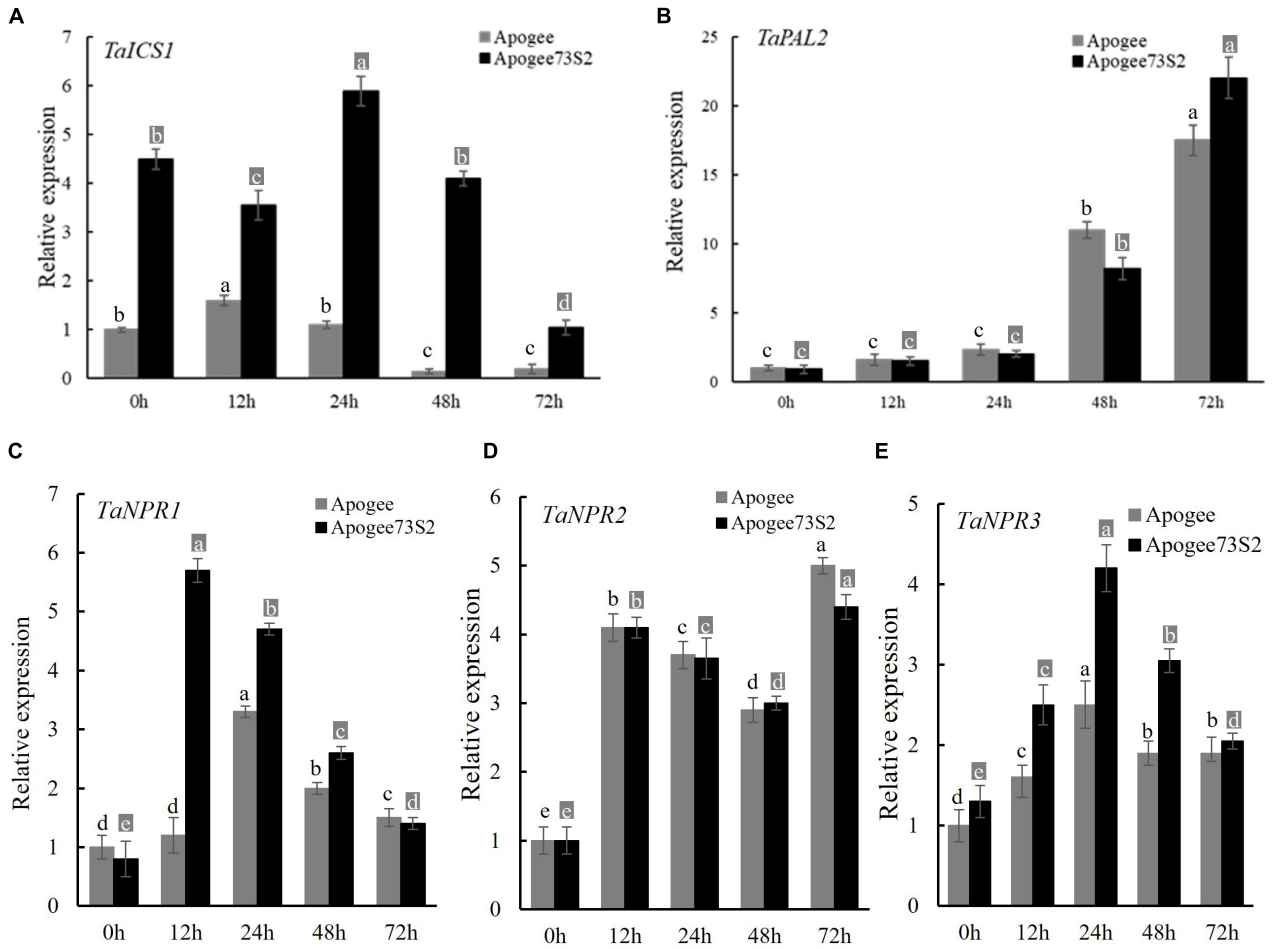

FIGURE 5 | Expression of *TaICS1* **(A)** and *TaPAL2* **(B)** for SA synthesis, and *TaNPR1* **(C)**, *TaNPR2* **(D)**, and *TaNPR3* **(E)** for SA signaling transduction in the spike of the Apogee (Fhb1 susceptible NIL) and Apogee73S2 (Fhb1 resistant NIL) at 0, 12, 24, 48, and 72 h after inoculation with *F. graminearum* PH1-1. Error bar shows standard deviation. Different letters on the top of each bar in the same color (dark or light) indicate significant differences at $p = 0.05$ (LSD) among relative expressions at inoculation time points.

analyses of the inoculated samples in this study suggested that the upregulated DEGs induced by the two low virulent isolates (R40 and R64) mainly encoded proteins for phytohormone signaling pathways and for the redox state, secondary metabolites, cell wall, abiotic stress pathways, and phenolamine and flavonoids metabolic pathways to form BNLs that restricted *F. graminearum* extension (**Figure 2**).

Effect of Salicylic Acid on Wheat Fusarium Head Blight Resistance

Salicylic acid (SA) is a small phenolic compound that regulates plant growth and development (Rivas-San Vicente and Plasencia, 2011); it also serves as a critical signal to activate the expression of disease resistance genes (Delaney et al., 1994; An and Mou, 2011). The SA biosynthesis in *Arabidopsis* is primarily *via* an isochorismate synthase (ICS) pathway. A distinct pathway utilizing phenylalanine ammonia-lyase (PAL) as the substrate may also contribute to SA accumulation (Wildermuth et al., 2001; Dempsey et al., 2011). However, the SA biosynthetic pathway remains largely unknown in *Triticeae*. Hao et al. (2018) cloned an *ICS* gene and seven *PAL* genes from barley (*Hordeum vulgare*) and studied their functions by overexpression and suppression of these genes in barley, and they found that suppression of *ICS* reduced plant FHB resistance, but suppression of *PAL* expression did not. Suppression of *ICS* might result in a reduction in SA accumulation that weakens defense responses during pathogen infection; therefore, they concluded that *ICS* likely played a unique role in barley SA biosynthesis (Hao et al., 2018). In the current study, *TaICS1* and *TaPAL2*, the two key genes for SA synthesis, in resistant cultivar Sumai 3 were transiently silenced by VIGS, and only the *TaICS1* silenced plants significantly increased PSS compared to its wide type genotype at 15 DAI, suggesting that *TaICS1* might play an important role in wheat FHB resistance by regulating SA synthesis pathway in wheat (**Figures 5**, **6**). Interestingly, DEG in SA biosynthesis pathway was not detected in the RNA-seq study where the tissue was collected at 4 DAI, which might be due to the observation that

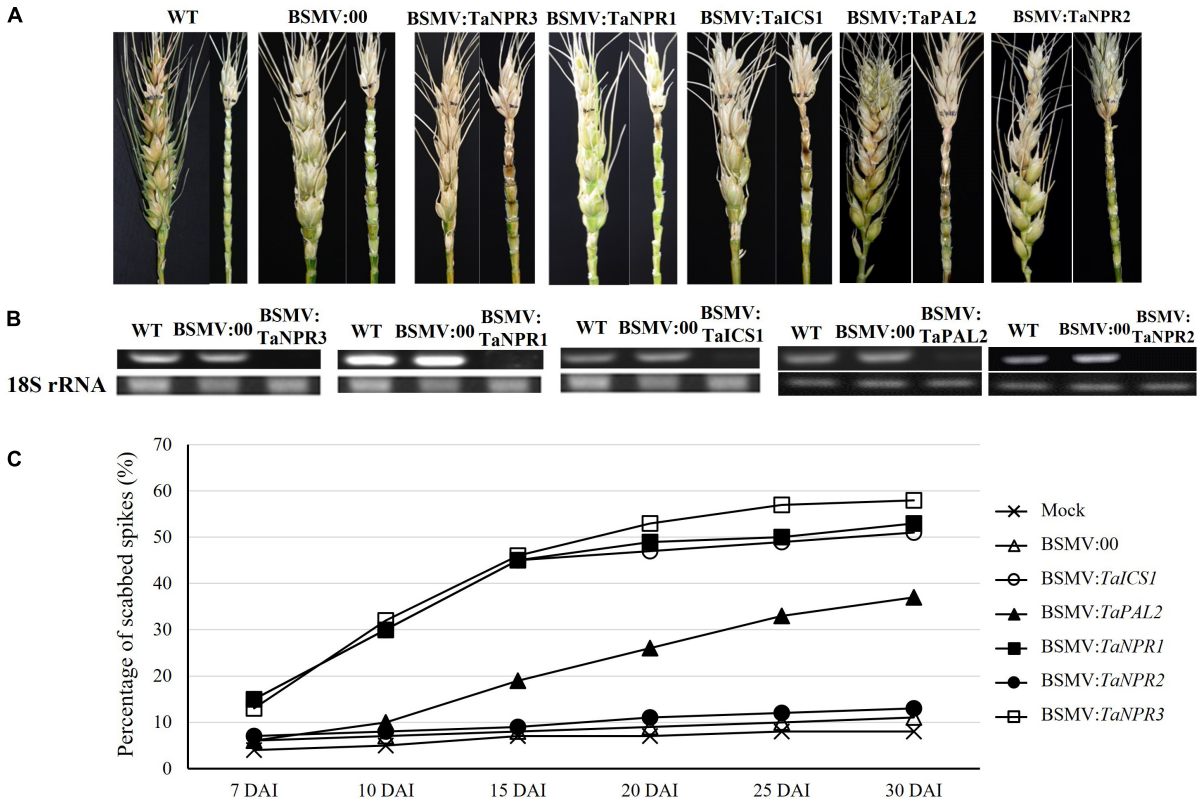

FIGURE 6 | Effects of the five genes in SA pathways and signaling that were silenced by *barley stripe mosaic virus*-mediated gene silencing (BSMV-VIGS) from Sumai 3 on FHB resistance. **(A)** FHB symptoms on wheat spikes with BSMV-VIGS silenced genes. **(B)** Gene expression profiles for the five VIGS-treated genes in wheat spikes were evaluated by semi-quantitative RT-PCR. The wheat *18S rRNA* gene was used for endogenous reference for normalization. Each treatment had three biological replicates, and each biological replicate had three technical replicates. **(C)** The percentage of scabbed spikelets in the spikes with and without VIGS-silenced genes from Sumai 3 at 7, 10, 15, 20, 25, and 30 days after inoculation (DAI). BSMV:00, BSMV with blank vector.

these genes in the SA biosynthesis pathway have been activated at earlier stages of FHB infection. This assumption was supported by the observation that SA content in the Sumai 3's spike tissue increased quickly after inoculation and reached the peak at 12 HAI, which is highly consistent with the gene expression pattern of *TaICS1* (**Figure 5**). Furthermore, we confirm that the *TaICS1* gene plays a major role in wheat SA biosynthesis and high SA content in the early infection stage was highly related to reactive oxygen burst, BNL formation, and FHB resistance (**Supplementary Figure 4**).

In *Arabidopsis*, a non-expression of a pathogenesis-related (PR) gene (*AtNPR1*) is considered a key regulator of SAR, which regulates *PR* gene expression through interaction with the TGACG motif-binding factor family of transcription factors (Zhang et al., 1999; Zhou et al., 2000). Mutants of *AtNPR1* did not respond to various SAR-inducing treatments, showed a low expression of the PR genes, and exhibited higher disease susceptibility (Cao et al., 1997; Dong, 2004; Makandar et al., 2006). In wheat, overexpression of *AtNPR1* and *Secale cereale-NPR1* in an FHB-susceptible wheat cultivar enhanced wheat FHB resistance (Makandar et al., 2006; Yu et al., 2017). However, Gao et al. (2013) reported that the transgenic wheat lines expressing *AtNPR1* were resistant to *Fusarium* in spikes, but highly susceptible at the seedling stage, suggesting that NPR1 may have dual functions in regulating defense responses in plants. In the current study, silencing *TaNPR2*, an *AtNPR1* homolog in wheat, in Sumai 3 did not significantly change FHB resistance, but silencing *TaNPR1* and *TaNPR3* (two *TaNPR1* homologs) in Sumai 3 significantly reduced wheat FHB resistance (**Figure 6**), suggesting different *NPR* functions between wheat and *A. thaliana*. *TaNPR1* and *TaNPR3* genes likely play an important role in SA signal transduction to facilitate wheat responses to FHB infection.

The Effects of Salicylic Acid and Jasmonic Acid Interaction on Wheat Fusarium Head Blight Resistance

Jasmonic acid and SA are two key endogenous phytohormonal signal molecules that regulate plant resistance to diverse pathogens (Makandar et al., 2012; Yang et al., 2015). SA primarily regulates defense mechanisms against biotrophic and hemibiotrophic pathogens, whereas JA primarily contributes to resistance against necrotrophic pathogens, which have been well characterized in *A. thaliana* (Glazebrook, 2005; Koornneef and Pieterse, 2008). For resistance to *F. graminearum*, both SA

and JA may be required for the basal resistance response in *Arabidopsis* (Makandar et al., 2010). However, JA signaling shows dichotomous functions in both *Arabidopsis-F. graminearum* and wheat-*F. graminearum* interactions, in which JA attenuated SA signaling during the early infection stages and promoted defense against *F. graminearum* during the later infection stages (Makandar et al., 2010). JA and its methyl ester, methyl jasmonate (MeJA), and plant lipid derivatives may play a role in plant responses to wound and pathogen attacks. In the current study, the application of exogenous SA and MeJA to detached wheat leaves and spikes induced local or systemic responses and variations in FHB severity in the treated plants. MeJA reduced wheat FHB resistance and inhibited the BNL formation on the detached leaves due to attenuation of SA signaling in resistant wheat Sumai 3 (**Supplementary Figure 2**). Therefore, the SA signaling pathway more likely contributes to the BNL formation.

Furthermore, the detached leaves showed similar responses to early-stage infection by *F. graminearum* and can be used as alternative materials to study the spread of *F. graminearum* in wheat tissue. The current study showed that the effect of interaction between SA and JA on wheat FHB resistance as measured by FIR, DR, and PSS per spike is time-dependent. SA defense against *F. graminearum* infection started in an early stage (within 24 HAI) by inducing a local resistant response; however, the resistance disappeared if SA was applied at a later infection stage (after 48 HAI), probably due to the reactive oxygen burst (Makandar et al., 2012; Sorahinobar et al., 2016). Although the early stage MeJA treatments facilitated the spread of *F. graminearum* to rachises, the application of exogenous MeJA effectively limited the late spread of *F. graminearum* within a spike, resulting in low final PSS in all-time points of MeJA treatments (**Figure 4I**).

Fusarium Head Blight Resistance-Related Metabolites in Wheat

Hamzehzarghani et al. (2005) analyzed the metabolic profiles in spikelets of wheat cultivars, Roblin and Sumai 3, using GC/MS and developed a method to discriminate FHB resistance levels using metabolic profiling (Hamzehzarghani et al., 2005). They found several highly abundant fatty acids, aromatic compounds, p- and m-coumaric acids, myo-inositols and other sugars, and malonic acids in resistant cultivar Sumai 3, but only amino acids, fatty acids, and aromatics in the susceptible cultivar Roblin (Hamzehzarghani et al., 2005). In barley, metabolomics was used to identify the metabolites that are related to FHB resistance. The resistance-related metabolites mainly include phenylpropanoid, flavonoid, fatty acid, and terpenoid metabolic pathways (Bollina et al., 2010). Recently, an integrated analysis of metabolomics and transcriptomics of infected wheat plants identified 789 differentially accumulated metabolites, including flavonoids, phenolamides, tryptamine derivatives, and phytohormones, and revealed altered expression of more than 100 genes that functioned in the biosynthesis or regulation of these pathways (Su et al., 2020). In the current study, a large number of amino acid derivatives, flavones, nucleotide, and its derivatives, and quinate derivatives were detected in both low and high virulent isolates inoculated samples, thus they were most probably induced by *F. graminearum* infection, which is consistent with the previous reports (Hamzehzarghani et al., 2005). Similarly, a large number of flavonoid and terpenoid metabolites were identified from the samples that were inoculated with low virulent *F. graminearum* isolates, which is consistent with Su et al. (2020). Furthermore, flavonoids are widely present in plants and belong to a biologically important and chemically diverse group of secondary metabolites with diverse subgroups (Treutter, 2005, 2006). In the phenolic phytoalexin subgroup, the isoflavonoids, phenylpropanoids, and simple phenolics have been well characterized. In this study, exogenous application of apigenin and neohesperidin on the detached leaves of all selected wheat cultivars reduced *Fusarium* infection and induced BNL surrounding the infection sites; application of proanthocyanidins and spermidine, however, did not improve FHB resistance. Integrated metabolomic and transcriptomic analyses suggest that the flavonoid metabolic pathway might function differently between FHB resistant and susceptible wheat cultivars, and play an important role in the formation of BNLs in resistant genotypes in response to *F. graminearum* infection (**Figure 2**). Although direct evidence for SA to increase the accumulation of flavonoids was not detected in this study, exogenous SA has been known to boost the accumulation of flavonoids in several plant species (Xu et al., 2009; Tounekti et al., 2013). Moreover, SA has been reported to trigger the expression of some core flavonoid biosynthetic genes and lead to the accumulation of flavonoid phytoalexins (Ahuja et al., 2012). In this study, all the five DEGs induced by the low virulent *F. graminearum* isolates were upregulated and all the eight DEGs induced by the high virulent *F. graminearum* isolates were downregulated in the flavonoids metabolic pathway (**Figure 2**), which support roles of flavonoids metabolic pathway in FHB resistance. Further research is needed to determine the effects of SA on the biosynthesis of particular flavonoids, and to establish the relationship between the flavonoids' biosynthetic pathways and specific individual flavonoids leading to FHB resistance.

DATA AVAILABILITY STATEMENT

The datasets presented in this study can be found in online repositories. The names of the repository/repositories and accession number(s) can be found below: https://www.ncbi.nlm.nih.gov/search/all/?term=PRJNA842823. The accession number of the raw data is PRJNA842823.

ETHICS STATEMENT

The authors declare that the experiments comply with the current laws of the country in which they were performed.

AUTHOR CONTRIBUTIONS

LZ, PS, BH, HWW, and LK designed the experiments. LZ, PS, BH, YF, HYW, WL, JZ, WG, and SX performed the experiments. XM, SW, and AL contributed to plant materials. LZ, PS, and GB wrote the manuscript. All authors have read and approved the manuscript.

FUNDING

This is contribution number 22-161-J from the Kansas Agricultural Experiment Station. This project was funded by the National Natural Science Foundation of China (32030081), and U.S. Wheat and Barley Scab Initiative, and National Research Initiative Competitive Grants 2017-67007-25939 from the U.S. Department of Agriculture, National Institute of Food and Agriculture. Mention of trade names or commercial products in this publication is solely for the purpose of providing specific information and does not imply recommendation or endorsement by the USDA. USDA is an equal opportunity provider and employer.

SUPPLEMENTARY MATERIAL

The Supplementary Material for this article can be found online at: https://www.frontiersin.org/articles/10.3389/fpls.2022.926621/full#supplementary-material

REFERENCES

Abramovitch, R. B., Anderson, J. C., and Martin, G. B. (2006). Bacterial elicitation and evasion of plant innate immunity. *Nat. Rev. Mol. Cell Biol.* 7, 601–611. doi: 10.1038/nrm1984

Ahuja, I., Kissen, R., and Bones, A. M. (2012). Phytoalexins in defense against pathogens. *Trends Plant Sci.* 17, 73–90.

An, C., and Mou, Z. (2011). Salicylic acid and its function in plant immunity. *J. Integr. Plant Biol.* 53, 412–428. doi: 10.1111/j.1744-7909.2011.01043.x

Bai, G., and Shaner, G. (1994). Scab of wheat: prospects of control. *Plant Dis.* 78, 760–766. doi: 10.3390/nano10102000

Bai, G.-H., Desjardins, A., and Plattner, R. (2002). Deoxynivalenol-nonproducing *Fusarium graminearum* causes initial infection, but does not cause disease spread in wheat spikes. *Mycopathologia* 153, 91–98. doi: 10.1023/a:1014419323550

Bollina, V., Kumaraswamy, G. K., Kushalappa, A. C., Choo, T. M., Dion, Y., Rioux, S., et al. (2010). Mass spectrometry-based metabolomics application to identify quantitative resistance-related metabolites in barley against *Fusarium* head blight. *Mol. Plant Pathol.* 11, 769–782. doi: 10.1111/j.1364-3703.2010.00643.x

Browne, R., and Cooke, B. (2004). Development and evaluation of an in vitro detached leaf assay forc pre-screening resistance to Fusarium head blight in wheat. *Eur. J. Plant Pathol.* 110, 91–102.

Cao, H., Glazebrook, J., Clarke, J. D., Volko, S., and Dong, X. (1997). The *Arabidopsis* NPR1 gene that controls systemic acquired resistance encodes a novel protein containing ankyrin repeats. *Cell* 88, 57–63. doi: 10.1016/s0092-8674(00)81858-9

Chen, W., Gong, L., Guo, Z., Wang, W., Zhang, H., Liu, X., et al. (2013). A novel integrated method for large-scale detection, identification, and quantification of widely targeted metabolites: application in the study of rice metabolomics. *Mol. Plant* 6, 1769–1780. doi: 10.1093/mp/sst080

Delaney, T. P., Uknes, S., Vernooij, B., Friedrich, L., Weymann, K., Negrotto, D., et al. (1994). A central role of salicylic acid in plant disease resistance. *Science* 266, 1247–1250. doi: 10.1126/science.266.5188.1247

Dempsey, D. M. A., Vlot, A. C., Wildermuth, M. C., and Klessig, D. F. (2011). Salicylic acid biosynthesis and metabolism. *Arabidopsis Book* 9:e0156.

Ding, L., Xu, H., Yi, H., Yang, L., Kong, Z., Zhang, L., et al. (2011). Resistance to hemi-biotrophic *F. graminearum* infection is associated with coordinated and ordered expression of diverse defense signaling pathways. *PLoS One* 6:e19008. doi: 10.1371/journal.pone.0019008

Dong, X. (2004). NPR1, all things considered. *Curr. Opin. Plant Biol.* 7, 547–552. doi: 10.1016/j.pbi.2004.07.005

Fan, Y., Hou, B., Su, P., Wu, H., Wang, G., Kong, L., et al. (2019). Application of virus-induced gene silencing for identification of FHB resistant genes. *J. Integr. Agric.* 18, 2183–2192.

Gao, C. S., Kou, X. J., Li, H. P., Zhang, J. B., Saad, A., and Liao, Y. C. (2013). Inverse effects of *Arabidopsis* NPR1 gene on *fusarium* seedling blight and fusarium head blight in transgenic wheat. *Plant Pathol.* 62, 383–392.

Glazebrook, J. (2005). Contrasting mechanisms of defense against biotrophic and necrotrophic pathogens. *Annu. Rev. Phytopathol.* 43, 205–227. doi: 10.1146/annurev.phyto.43.040204.135923

Golkari, S., Gilbert, J., Ban, T., and Procunier, J. D. (2009). QTL-specific microarray gene expression analysis of wheat resistance to Fusarium head blight in Sumai-3 and two susceptible NILs. *Genome* 52, 409–418. doi: 10.1139/g09-018

Hamzehzarghani, H., Kushalappa, A., Dion, Y., Rioux, S., Comeau, A., Yaylayan, V., et al. (2005). Metabolic profiling and factor analysis to discriminate quantitative resistance in wheat cultivars against fusarium head blight. *Physiol. Mol. Plant Pathol.* 66, 119–133.

Hao, Q., Wang, W., Han, X., Wu, J., Lyu, B., Chen, F., et al. (2018). Isochorismate-based salicylic acid biosynthesis confers basal resistance to *Fusarium graminearum* in barley. *Mol. Plant Pathol.* 19, 1995–2010. doi: 10.1111/mpp.12675

Heath, M. C. (2000). *Hypersensitive Response-Related Death. Programmed cell Death in Higher Plants*. Berlin: Springer, 77–90.

Holmes, F. O. (1929). Local lesions in tobacco mosaic. *Bot. Gaz.* 87, 39–55.

International Wheat Genome Sequencing Consortium [IWGSC] (2018). Shifting the limits in wheat research and breeding using a fully annotated reference genome. *Science* 361:eaar7191. doi: 10.1126/science.aar7191

Kang, Z., and Buchenauer, H. (2000). Cytology and ultrastructure of the infection of wheat spikes by *Fusarium culmorum*. *Mycol. Res.* 104, 1083–1093.

Kazan, K., and Gardiner, D. M. (2018). Transcriptomics of cereal-*Fusarium graminearum* interactions: what we have learned so far. *Mol. Plant Pathol.* 19, 764–778. doi: 10.1111/mpp.12561

Kazan, K., Gardiner, D. M., and Manners, J. M. (2012). On the trail of a cereal killer: recent advances in *Fusarium graminearum* pathogenomics and host resistance. *Mol. Plant Pathol.* 13, 399–413. doi: 10.1111/j.1364-3703.2011.00762.x

Kiraly, L., Barna, B., and Király, Z. (2007). Plant resistance to pathogen infection: forms and mechanisms of innate and acquired resistance. *J. Phytopathol.* 155, 385–396.

Kong, L., Ohm, H. W., and Anderson, J. M. (2007). Expression analysis of defense-related genes in wheat in response to infection by *Fusarium graminearum*. *Genome* 50, 1038–1048. doi: 10.1139/g07-085

Koornneef, A., and Pieterse, C. M. (2008). Cross talk in defense signaling. *Plant Physiol.* 146, 839–844.

Lamb, C., and Dixon, R. A. (1997). The oxidative burst in plant disease resistance. *Annu. Rev. Plant Biol.* 48, 251–275.

Levin, D. A. (1976). The chemical defenses of plants to pathogens and herbivores. *Annu. Rev. Ecol. Syst.* 7, 121–159.

Loebenstein, G. (2009). Local lesions and induced resistance. *Adv. Virus Res.* 75, 73–117.

Lohse, M., Nagel, A., Herter, T., May, P., Schroda, M., Zrenner, R., et al. (2014). *M ercator: a Fast and Simple web Server for Genome Scale Functional Annotation of Plant Sequence data*. Hoboken: Wiley Online Library.

Makandar, R., Essig, J. S., Schapaugh, M. A., Trick, H. N., and Shah, J. (2006). Genetically engineered resistance to Fusarium head blight in wheat

by expression of *Arabidopsis* NPR1. *Mol. Plant Microbe Interact.* 19, 123–129. doi: 10.1094/MPMI-19-0123

Makandar, R., Nalam, V., Chaturvedi, R., Jeannotte, R., Sparks, A. A., and Shah, J. (2010). Involvement of salicylate and jasmonate signaling pathways in *Arabidopsis* interaction with *Fusarium graminearum*. *Mol. Plant Microbe Interact.* 23, 861–870. doi: 10.1094/MPMI-23-7-0861

Makandar, R., Nalam, V. J., Lee, H., Trick, H. N., Dong, Y., and Shah, J. (2012). Salicylic acid regulates basal resistance to Fusarium head blight in wheat. *Mol. Plant Microbe Interact.* 25, 431–439. doi: 10.1094/MPMI-09-11-0232

Martin, J. (1964). Role of cuticle in the defense against plant disease. *Annu. Rev. Phytopathol.* 2, 81–100.

Mortazavi, A., Williams, B. A., McCue, K., Schaeffer, L., and Wold, B. (2008). Mapping and quantifying mammalian transcriptomes by RNA-Seq. *Nat. Methods* 5, 621–628. doi: 10.1038/nmeth.1226

Rivas-San Vicente, M., and Plasencia, J. (2011). Salicylic acid beyond defence: its role in plant growth and development. *J. Exp. Bot.* 62, 3321–3338. doi: 10.1093/jxb/err031

Rudd, J., Horsley, R., McKendry, A., and Elias, E. (2001). Host plant resistance genes for Fusarium head blight: sources, mechanisms, and utility in conventional breeding systems. *Crop Sci.* 41, 620–627.

Ryals, J. A., Neuenschwander, U. H., Willits, M. G., Molina, A., Steiner, H.-Y., and Hunt, M. D. (1996). Systemic acquired resistance. *Plant Cell* 8:1809.

Sorahinobar, M., Niknam, V., Ebrahimzadeh, H., Soltanloo, H., Behmanesh, M., and Enferadi, S. T. (2016). Central role of salicylic acid in resistance of wheat against *Fusarium graminearum*. *J. Plant Growth Regul.* 35, 477–491.

Su, P., Zhao, L., Li, W., Zhao, J., Yan, J., Ma, X., et al. (2020). Integrated metabolo-transcriptomics and functional characterization reveals that the wheat auxin receptor *TIR1* negatively regulates defense against *Fusarium graminearum*. *J. Integr. Plant Biol.* 63, 340–352. doi: 10.1111/jipb.12992

Thimm, O., Bläsing, O., Gibon, Y., Nagel, A., Meyer, S., Krüger, P., et al. (2004). MAPMAN: a user-driven tool to display genomics data sets onto diagrams of metabolic pathways and other biological processes. *Plant J.* 37, 914–939. doi: 10.1111/j.1365-313x.2004.02016.x

Thomma, B. P., Nelissen, I., Eggermont, K., and Broekaert, W. F. (1999). Deficiency in phytoalexin production causes enhanced susceptibility of Arabidopsis thaliana to the fungus *Alternaria brassicicola*. *Plant J.* 19, 163–171.

Tiwari, M., and Kakkar, P. (2009). Plant derived antioxidants-geraniol and camphene protect rat alveolar macrophages against t-BHP induced oxidative stress. *Toxicol. In Vitro* 23, 295–301.

Tounekti, T., Hernández, I., and Munné-Bosch, S. (2013). "Salicylic acid biosynthesis and role in modulating terpenoid and flavonoid metabolism in plant responses to abiotic stress," in *Salicylic Acid*, eds S. Hayat, A. Ahmad, and M. Alyemeni (Dordrecht: Springer), 141–162.

Trail, F. (2009). For blighted waves of grain: *fusarium graminearum* in the postgenomics era. *Plant Physiol.* 149, 103–110. doi: 10.1104/pp.108.129684

Treutter, D. (2005). Significance of flavonoids in plant resistance and enhancement of their biosynthesis. *Plant Biol.* 7, 581–591. doi: 10.1055/s-2005-873009

Treutter, D. (2006). Significance of flavonoids in plant resistance: a review. *Environ. Chem. Lett.* 4:147.

Wang, H., Sun, S., Ge, W., Zhao, L., Hou, B., Wang, K., et al. (2020). Horizontal gene transfer of Fhb7 from fungus underlies Fusarium head blight resistance in wheat. *Science* 368:eaba5435. doi: 10.1126/science.aba5435

Wang, L., Li, Q., Liu, Z., Surendra, A., Pan, Y., Li, Y., et al. (2018). Integrated transcriptome and hormone profiling highlight the role of multiple phytohormone pathways in wheat resistance against fusarium head blight. *PLoS One* 13:e0207036. doi: 10.1371/journal.pone.0207036

Wildermuth, M. C., Dewdney, J., Wu, G., and Ausubel, F. M. (2001). Isochorismate synthase is required to synthesize salicylic acid for plant defence. *Nature* 414, 562–565.

Xu, M., Dong, J., Wang, H., and Huang, L. (2009). Complementary action of jasmonic acid on salicylic acid in mediating fungal elicitor-induced flavonol glycoside accumulation of Ginkgo biloba cells. *Plant Cell Environ.* 32, 960–967. doi: 10.1111/j.1365-3040.2009.01976.x

Yang, Y.-X., Ahammed, G. J., Wu, C., Fan , S-y, and Zhou, Y.-H. (2015). Crosstalk among jasmonate, salicylate and ethylene signaling pathways in plant disease and immune responses. *Curr. Protein Pept. Sci.* 16, 450–461. doi: 10.2174/1389203716666150330141638

Yu, G., Zhang, X., Yao, J., Zhou, M., and Ma, H. (2017). Resistance against Fusarium head blight in transgenic wheat plants expressing the ScNPR1 gene. *J. Phytopathol.* 165, 223–231.

Yuan, C., Li, C., Yan, L., Jackson, A. O., Liu, Z., Han, C., et al. (2011). A high throughput barley stripe mosaic virus vector for virus induced gene silencing in monocots and dicots. *PLoS One* 6:e26468. doi: 10.1371/journal.pone.0026468

Zhang, Y., Fan, W., Kinkema, M., Li, X., and Dong, X. (1999). Interaction of NPR1 with basic leucine zipper protein transcription factors that bind sequences required for salicylic acid induction of the PR-1 gene. *Proc. Natl. Acad. Sci. U.S.A.* 96, 6523–6528. doi: 10.1073/pnas.96.11.6523

Zhang, Y., Lubberstedt, T., and Xu, M. (2013). The genetic and molecular basis of plant resistance to pathogens. *J. Genet. Genomics* 40, 23–35. doi: 10.1016/j.jgg.2012.11.003

Zhou, J.-M., Trifa, Y., Silva, H., Pontier, D., Lam, E., Shah, J., et al. (2000). NPR1 differentially interacts with members of the TGA/OBF family of transcription factors that bind an element of the PR-1 gene required for induction by salicylic acid. *Mol. Plant Microbe Interact.* 13, 191–202. doi: 10.1094/MPMI.2000.13.2.191

Conflict of Interest: The authors declare that the research was conducted in the absence of any commercial or financial relationships that could be construed as a potential conflict of interest.

Publisher's Note: All claims expressed in this article are solely those of the authors and do not necessarily represent those of their affiliated organizations, or those of the publisher, the editors and the reviewers. Any product that may be evaluated in this article, or claim that may be made by its manufacturer, is not guaranteed or endorsed by the publisher.

Advantages of publishing in Frontiers

OPEN ACCESS
Articles are free to read for greatest visibility and readership

FAST PUBLICATION
Around 90 days from submission to decision

HIGH QUALITY PEER-REVIEW
Rigorous, collaborative, and constructive peer-review

TRANSPARENT PEER-REVIEW
Editors and reviewers acknowledged by name on published articles

Frontiers
Avenue du Tribunal-Fédéral 34
1005 Lausanne | Switzerland

Visit us: www.frontiersin.org
Contact us: frontiersin.org/about/contact

REPRODUCIBILITY OF RESEARCH
Support open data and methods to enhance research reproducibility

DIGITAL PUBLISHING
Articles designed for optimal readership across devices

FOLLOW US
@frontiersin

IMPACT METRICS
Advanced article metrics track visibility across digital media

EXTENSIVE PROMOTION
Marketing and promotion of impactful research

LOOP RESEARCH NETWORK
Our network increases your article's readership